



# ***Water chemistry and corrosion control of cladding and primary circuit components***

*Proceedings of a Technical Committee meeting  
held in Hluboka nad Vltavou, Czech Republic,  
28 September – 2 October 1998*



INTERNATIONAL ATOMIC ENERGY AGENCY

**IAEA**

December 1999

**30 - 50**

①

The originating Section of this publication in the IAEA was:

Nuclear Fuel Cycle and Materials Section  
International Atomic Energy Agency  
Wagramer Strasse 5  
P.O. Box 100  
A-1400 Vienna, Austria

The IAEA does not normally maintain stocks of reports in this series. However, electronic copies of these reports can be obtained from:

INIS Clearinghouse  
International Atomic Energy Agency  
Wagramer Strasse 5  
P.O. Box 100  
A-1400 Vienna, Austria

Telephone: (43) 1 2600-22880 or 22866  
Fax: (43) 1 2600-29882  
E-mail: [CHOUSE@IAEA.ORG](mailto:CHOUSE@IAEA.ORG)  
Web site: <http://www.iaea.org/programmes/inis/inis.htm>

Orders should be accompanied by prepayment of 100 Austrian Schillings in the form of a cheque or credit card (MasterCard, VISA).

WATER CHEMISTRY AND CORROSION CONTROL OF  
CLADDING AND PRIMARY CIRCUIT COMPONENTS  
IAEA, VIENNA, 1999  
IAEA-TECDOC-1128  
ISSN 1011-4289

© IAEA, 1999

Printed by the IAEA in Austria  
December 1999

## FOREWORD

Corrosion is the principal life limiting degradation mechanism in nuclear steam supply systems, especially taking into account the trends to increase fuel burnup, thermal rate and cycle length. Primary circuit components of water cooled power reactors have an impact on Zr-based alloys behaviour due to crud (primary circuit corrosion products) formation, transport and deposition on heat transfer surfaces. Crud deposits influence water chemistry, radiation and thermal hydraulic conditions near cladding surface, and by this way-Zr-based alloy corrosion.

During the last decade, significant improvements were achieved in the reduction of the corrosion and dose rates by changing the cladding material for one more resistant to corrosion or by the improvement of water chemistry conditions. However, taking into account the above mentioned tendency for heavier fuel duties, corrosion and water chemistry, control will remain a serious task to work with for nuclear power plant operators and scientists, as well as development of generally accepted corrosion model of Zr-based alloys in a water environment in a new millennium.

Upon the recommendation of the International Working Group on Water Reactor Fuel Performance and Technology, water chemistry and corrosion of cladding and primary circuit components are in the focus of the IAEA activities in the area of fuel technology and performance. At present the IAEA performs two co-ordinated research projects (CRPs): on On-line High Temperature Monitoring of Water Chemistry and Corrosion (WACOL) and on Activity Transport in Primary Circuits. Two CRPs deal with hydrogen and hydride degradation of the Zr-based alloys. A state-of-the-art review entitled: "Waterside Corrosion of Zirconium Alloys in Nuclear Power Plants" was published in 1998. Technical Committee meetings on the subject were held in 1985 (Cadarache, France), 1989 (Portland, USA), 1993 (Řež, Czech Republic).

During the last few years extensive exchange of experience in corrosion and water chemistry control has been carried out between PWR/BWR and WWER specialists which is beneficial to both parties. During this meeting corrosion and water chemistry specialists from countries operating BWRs, PHWRs, PWRs, RBMKs and WWERs exchanged with the recent results on optimization of water chemistry parameters and Zr-based alloys composition to reduce corrosion and dose rates. This publication addresses the engineers and scientists working in the areas of structural materials development, water side corrosion and nuclear power plants chemists.

The 27 papers from 17 countries were grouped into five sessions which covered corrosion experience in nuclear power plants and test facilities, impact of irradiation, water chemistry and material composition on corrosion, crud formation and dose rates, fundamental studies of corrosion and modelling and in situ measurements.

The IAEA wishes to thank the Nuclear Research Institute Řež, plc, Czech Republic, for hosting and J. Kysela of NRI for chairing the meeting and all participants for their contributions to this publication. The IAEA officer responsible for the organization of the meeting was V. Onoufrieu of the Division of the Nuclear Fuel Cycle and Waste Technology.

## *EDITORIAL NOTE*

*In preparing this publication for press, staff of the IAEA have made up the pages from the original manuscripts as submitted by the authors. The views expressed do not necessarily reflect those of the IAEA, the governments of the nominating Member States or the nominating organizations.*

*Throughout the text names of Member States are retained as they were when the text was compiled.*

*The use of particular designations of countries or territories does not imply any judgement by the publisher, the IAEA, as to the legal status of such countries or territories, of their authorities and institutions or of the delimitation of their boundaries.*

*The mention of names of specific companies or products (whether or not indicated as registered) does not imply any intention to infringe proprietary rights, nor should it be construed as an endorsement or recommendation on the part of the IAEA.*

*The authors are responsible for having obtained the necessary permission for the IAEA to reproduce, translate or use material from sources already protected by copyrights.*



## CONTENTS

SUMMARY .....	1
<b>PLANT EXPERIENCE (Session 1)</b>	
Indian experience on corrosion of zirconium based alloys and primary heat transport components.....	11
<i>A.K. Saxena, S.L. Mandowara, M. Das, B.K. Bhasin</i>	
Primary heat transport system chemical control review.....	19
<i>D. Zotica, O. Marciulescu</i>	
Impact of Zr + 2.5% Nb alloy corrosion upon operability of RBMK-1000 fuel channels .....	27
<i>V. Kovyrshin, N. Zaritsky, V. Kolesov</i>	
Influence of hydrazine primary water chemistry on corrosion of fuel cladding and primary circuit components .....	37
<i>V. Iourmanov, V. Pashevich, J. Bogancs, P. Tilky, J. Schunk, T. Pinter</i>	
In-reactor fuel cladding external corrosion measurement process and results .....	65
<i>J. Thomazet, Y. Musante, J. Pigelet</i>	
<b>IRRADIATION EFFECTS, CORROSION TESTING (Session 2)</b>	
Corrosion of Zr-based alloys.....	85
<i>V. Vrtilková, J. Jaroš, J. Čmakal, M. Valach, M. Lahodová</i>	
Study of irradiation effects on the crystallographic nature of zirconia.....	95
<i>F. Gilbert, C. Couvreur, D. Damien, M. Gautier-Soyer, N. Thromat, M.J. Guittet, S. Bouffard, Y. Serruys, E. Elkaim</i>	
Factors affecting out-of-and in-reactor corrosion of Zr claddings of fuel rods .....	103
<i>V.F. Kon'kov, A.V. Nikulina, V.N. Shishov, T.N. Khokhunova, A.E. Novoselov</i>	
Effect of LiOH, NaOH, and KOH on corrosion and oxide microstructure of Zr-based alloys .....	115
<i>Y.H. Jeong, H.G. Kim, Y.H. Jung, H. Ruhmann</i>	
The corrosion behavior of low tin and high tin zirconium based alloys under different lithium hydroxide and boric acid containing environments.....	135
<i>H. Ruhmann, F. Garzarolli, I. Pohlmeyer, H.-J. Sell</i>	
<b>CORROSION LAYERS, CRUD DEPOSITION, ACTIVITY BUILDUP (Session 3)</b>	
SIMS depth profiling analyses on in-reactor corroded Zircaloy cladding specimens.....	151
<i>O. Gebhardt, D. Gavillret, J.Y. Blanc, L. Ottavi, J. Thomazet</i>	
Corrosion behaviour and deposition of crud on Zr-alloys.....	163
<i>A.J.G. Maroto, R. Bordoni, A.M. Olmedo, M. Villegas, M. Chocrón and J. Szpunar</i>	
Investigation of likely causes of white patch formation on irradiated WWER fuel rod claddings .....	179
<i>Yu.K. Bibilashvili, V.P. Velioukhanov, A.Y. Ioltoukhovski, V.P. Pogodin</i>	
Corrosion product deposits on cladding material .....	185
<i>M. Zmitko, J. Kysela, J. Šrank, T. Grygar, J. Šubrt</i>	
Microstructural investigation of Swedish BWR fuel crud .....	195
<i>H.P. Hermansson, J. Chen</i>	
Potential impacts of crud deposits on fuel rod behavior on high powered PWR fuel rods.....	205
<i>W. Wilson, R.J. Comstock</i>	
Characterization of the parameters at the origin of the chemical species hideout process at the fuel rod surface in boiling conditions.....	213
<i>J. Peybernes, Ph. March</i>	

## CORROSION MODELLING (Session 4)

Ammonia role in WWER primary circuit water chemistry optimization .....	225
<i>V.G. Kritskij, P.S. Stjagkin, M.N. Chvedova, A.A. Slobodov</i>	
Modelling of zirconium alloys corrosion in LWRs .....	235
<i>V.G. Kritskij, I.G. Berezina, A.V. Kritskij, P.S. Stjagkin</i>	
Subcooled boiling effect on dissolved gases behaviour .....	243
<i>M. Zmítko, J. Sinkule, V. Linek</i>	
The possible influences of fuel crud build-up and water chemistry on waterside corrosion of zirconium alloys .....	257
<i>J. Chen, B. Rosborg</i>	

## IN SITU MEASUREMENT, LOOP FACILITIES (Session 5)

Shadow corrosion testing in the Inca facility in the Studsvik R2 reactor .....	267
<i>A.C. Nystrand, A. Lassing</i>	
On-line monitoring of resistance of aqueous solutions at high temperature.....	273
<i>Hu Shilin, Zhang Pingzhu, Zhang Weiguo</i>	
Advanced in-situ characterisation of corrosion properties of LWR fuel cladding materials .....	279
<i>E. Arilahti, B. Beverskog, M. Bojinov, L. Hansson-Lyyra, T. Laitinen, J.F.W. Markgraf, P. Moilanen, K. Mäkelä, M. Mäkelä, T. Saario, P. Sirkiä</i>	
Model experiments on simulation of the VVER water-chemical conditions at loop facilities of the MIR reactor .....	287
<i>O.S. Benderskaya, E.A. Zotov, V.A. Kuprienko, V.A. Ovchinnikov</i>	
Loop capabilities in Řež for water chemistry and corrosion control of cladding and in-core components .....	299
<i>J. Kysela, M. Zmítko, J. Šrank, R. Vřolák</i>	
Halden research on Zircaloy cladding corrosion .....	309
<i>T.M. Karlsen, M. McGrath, E. Kolstad</i>	
List of Participants .....	319

## SUMMARY

### BACKGROUND AND INTRODUCTION

At the invitation of the Government of Czech Republic, following a proposal of the International Working Group on Water Reactor Fuel Performance and Technology (IWGFPT), the IAEA convened a Technical Committee meeting on Water Chemistry and Corrosion Control of Cladding and Primary Circuit Components from 28 September to 2 October 1998 in Hluboka nad Vltavou, Czech Republic. 45 specialists from 24 countries and a number of observers from the Czech Republic attended the meeting. Twenty-seven papers were presented at five sessions covering different aspects of corrosion of cladding and coolant circuit components of water cooled power reactors and its interrelation with water chemistry parameters.

At present, different types of water cooled power reactors are in use. These are BWR, CANDU/PHWR, PWR, RBMK and WWER reactors. The common feature of these reactors, even if they differ in characteristics and water coolant technology, is the use of zirconium alloys as a fuel cladding material. For economical reasons utilities and fuel vendor needs are to increase fuel burnup, cycle length and heat rate and, on the other hand, to decrease the radiation field and Zr-based alloy corrosion rate. In this context, Zr-based alloy behaviour includes corrosion, hydrogen uptake, effect of irradiation and high temperature, while water chemistry reflects on the environment, including alkali agents, impurities, etc.

Primary circuit components have an impact on Zr-based alloys behaviour due to crud (primary circuit corrosion products) formation, transport and deposition on heat transfer surfaces. Crud deposits influence water chemistry, radiation and thermal hydraulic conditions near cladding surface, and by this way-Zr-based alloy corrosion.

The performance of Zr-based materials is dependant on the material (alloy composition, fabrication parameters), on the environment and on the operating conditions. Modern materials (alloys) optimized for better corrosion resistance probably seem to be more sensitive to environmental influences than standard alloys. Therefore the influencing parameters generated by the environment have come into the focus of interest. Changes in water chemistry for the purpose of man dose reduction or suppression of corrosion and stress corrosion cracking of steel components, can be detrimental to the corrosion resistance of Zr-based cladding alloys. A broad database is available for standard materials under standard water chemistry conditions but information on the effect of modified water chemistry (increased Li, K, NH<sub>3</sub>, H<sub>2</sub>, N<sub>2</sub>H<sub>4</sub>, <sup>10</sup>B, alternative alkalizes, zinc-injection, noble metal additions or hydrazine ) on standard and advanced Zr-based alloys is rather limited. Crud induced effects on corrosion are of importance and irradiation induced phenomena like shadow corrosion, microstructural changes and radiolysis effects are of interest.

As mentioned above, utilities are switching to longer cycles and extended burnups. The materials have to meet these requirements. Power histories and operating conditions are important with respect to boiling induced deposition which may be the reason for unexpected material behavior. Factors that lead to accelerating corrosion behaviour under different operating conditions are still not well understood. The material behavior under elevated temperature and the metallurgical changes under such conditions are of interest. Secondary degradation mechanisms which determine the behavior of defected fuel rods under operation should be also considered at the meeting.

Experimental results and operating experience contribute new information and are the basis for improved empirical models. However, better mechanistic understanding of these empirical models is necessary to provide physical meaning to them.

## PURPOSE AND AIM OF THE MEETING

So far, key international conferences such as ASTM-Zirconium in Nuclear Industry were focusing on Zr-alloy behaviour on the one side, and BNES and JAIF-Water Chemistry in Nuclear Plants - on water chemistry and plant operation on the other side. The aim of this TCM was to bring together specialists of both fields and to support the exchange of information, experience and discussions in order to achieve the better understanding of Zr-alloy corrosion behaviour under different environmental conditions.

## SESSION 1 - PLANT EXPERIENCE

In this session, a lot of detailed information was presented in 5 papers from six different types of nuclear reactor systems operated in five different countries:

BWRs	in	India
PWRs	in	France (and Germany)
PHWRs	in	India and Romania
WWERs	in	Russia
RBMKs	in	Ukraine.

All papers presented information about the performance of Zr-based alloy used in these reactors in different forms and under operation conditions related to the applied coolant. For some of the materials unexpected corrosion phenomena were reported and very different conclusion were drawn (e.g. nodular corrosion observation on cladding in BWR's operated in India and at RBMK pressure tubes). On one side a need for the development of improved materials was concluded (for the cladding operated in Indian plants), on the other side no real lifetime limiting effects were reported (for corrosion observed at pressure tubes in RBMK).

Activities to establish long life times for Zircaloy and steel components by adapted and improved procedures (hot conditioning in PHWR's) and water chemistry modification (hydrazine water chemistry in WWER's) were reported. In all cases a significant improvement of the performance could be stated.

An unavoidable prerequisite for the documentation of performance improvements is an adequate monitoring of performance parameters during operation. It was demonstrated that a careful measurement of the oxide-scale thickness by a non-destructive eddy current method allows comparison between predicted and actually observed in pile corrosion of commercial and experimental cladding (J. Tomazet et al, Framatome, France). This study showed also the high variability in thickness of in pile corrosion layers developed on cladding manufactured from identical materials depending on locally established thermohydraulic conditions.

In order to allow comparison and quantification of plant performance the evaluation of „reliability factors“, as proposed in joint (VNIIAES, Russian Federation-Paks NPP, Hungary) paper, is highly recommended (on the basis of proposals made by the World Association of Nuclear Operation “WANO”).

Assessments on the reliability of materials in nuclear power plant are only possible, if data are available and accessible . Those data should comprise information on material properties and operation condition. Unexpected phenomena reported and mechanistically explained, as shown in this session, should not be excluded.

## SESSION 2 - IRRADIATION EFFECTS, CORROSION TESTING

Fuel rod cladding operate in extremely heavy conditions: high temperature and irradiation field, corrosion effects of coolant at high temperature, etc.

Systematic laboratory experiments were performed with Zr-based alloys exposed to different water chemistry environments under isothermal, pressurised water reactor simulating conditions.

The investigated materials are zirconium alloys with different tin content (papers by Y.H. Jeong, KAERI, Korea and H. Ruhmann, Siemens/KWU, Germany) and alloys systems Zr-Nb, Zr-Sn-Nb+Fe (papers by V. Vrtilkova, SKODA-UJP, Czech Republic and A.V. Nikulina, VNIINM, Russian Federation). Weight gain increases are followed as a function of exposure time. The experiments confirm the sensitivity of zirconium based alloys to water environments with increasing lithium hydroxide concentrations. Low tin alloys show a decreasing sensitivity with increasing lithium hydroxide content (paper by H. Ruhmann). Additions of boric acid to lithium hydroxide containing water reduce the corrosion rates for low tin and high tin zirconium based alloys.

Impact of lithiated environment on corrosion of zirconium alloys was discussed in details. Excellent corrosion behaviour was observed for the ZIRLO in water environment with higher lithium concentration (360 °C) (V. Vrtilkova). High corrosion properties were revealed by E110 alloy in water contained to 10 ppm Li and by E635 alloy in water contained up to 70 ppm Li and demonstrated the perspective of their use in PWR water chemistry (A.V. Nikulina).

The corrosion rate in alkali hydroxide solutions decreases with the increasing ionic radius of alkali cation (Y.H. Jeong).

The strong acceleration of corrosion in high concentration is mainly controlled by the transformation of oxide microstructure. KOH does not significantly accelerate the hydrogen pickup as well as the corrosion rate of Zircaloy even in high concentration. It is thought that KOH has a potential as an alternative alkali for PWR application with respect to Zircaloy corrosion (Y.H. Jeong).

Impact of actual environmental conditions (irradiation, water chemistry) on corrosion rate was summarized in paper by A.V. Nikulina. Results evidences that E110 and E635 alloys have adequate margins of corrosion resistance of fuel rod claddings at extended burnup (~ 60 MW·day/kg U) under the WWER conditions. Zr-4 has higher propensity for hydrogen up take during operation under WWER and PWR water chemistry conditions compared to E110 and E635. The E110 and E635 alloys exhibited sensitivity to oxygen available in water under irradiation. It is the main factor governing their corrosion behaviour.

Study of ion irradiation on the crystallographic nature of zirconia and its comparison with neutron (PWR) irradiation was presented in paper by G. Gibert et al (CEA/Saclay, France). Examination of fuel rods shows that PWR irradiation produces similar effects to those revealed in the case of ion bombardment. Results of study show that ions irradiation always favours the transformation of a part of monoclinic zirconia into tetragonal zirconia. All changes in crystallographic structure caused by irradiation are particularly harmful for the cohesion of zirconia layer.

### SESSION 3 - CORROSION LAYERS, CRUD DEPOSITION, ACTIVITY BUILDUP

Major emphasis of 7 papers presented at this session was given to crud deposition and activity buildup (presented by V. Veloukhanov, M. Zmitko, H.-P. Hermansson, J. Comstock and J. Pebeyrnes), properties of corrosion layers were also considered, but to a lesser extent (presented by O. Gebhardt and A. J.C. Maroto).

Appearance of white patches on WWER-440 and WWER-1000 fuel rod surfaces (Loviisa, Kozloduy, Khmel'nitskaya NPPs) and major causes of their appearance were discussed in paper presented by V. Veloukhanov (VNIINM, Russian Federation). The thickness of these patches was estimated to 2/3 µm up to 100-200 µm when spalling occurred. No rod failures were observed correlatively with the presence of these patches which could be eliminated by brushing.

Autoclaves tests were performed for reproducing these patches. Autoclave tests with the most probable (F and C) and lesser probable (oil, LiOH, starch, graphite) pollutants permitted to accelerate the corrosion of various claddings and permitted to reproduce patches. It was observed that the E-635 material behaves better than the E-110 material in abnormal water chemistry. Pollutants, in order of crud hazard decreasing, are: fluorine, carbon (for cladding surface) and oxygen, LiOH, starch, graphite, mineral oil (for coolant). Further investigation are necessary for a better understanding of the patches formation and the nature determination of these patches observed after irradiation is strongly recommended.

Results of the experimental programme to study corrosion/crud behaviour of Zr alloy cladding materials at a reactor water loop RVS-3 under severe conditions (outlet temperature-335°C, high flux-100 W/cm<sup>2</sup>, high void boiling fraction-6 %, and high Li/B concentration-5 ppm Li / 600 ppm boron) were reported by M. Zmitko (NRI, Czech Republic). The crud deposition occurred on heated surfaces. It was loose at the bottom region and heavy with "chimney" structure at the upper region (under subcooling boiling). Comprehensive examination techniques were used to study structure and chemical composition of crud deposits. The structure and chemical composition were different from those observed in commercial NPPs. It was proposed that some changes in loop design and operation were to be done to exclude artificial facts dealt with loop operation. New tests are undertaken to verify that these changes will eliminate these phenomena.

Results of investigation of morphology and chemical composition of fuel crud deposits collected from three different Swedish BWRs operated with a HWC (hydrogen water chemistry) or a NWC (normal water chemistry) control were presented by H.-P. Hermansson (Studsvik Material AB, Sweden). Part of the crud on fuel rod surfaces was relatively loosely adhered and can be easily removed. The surface concentration of the crud seemed to be lowest on the top part of the pins. At the bottom of the crud layer, closest to the zirconium oxide, the crud was built up of very well crystallized material and contained mainly iron and nickel. On the outer sublayer of the crud, the structure was finely crystalline or amorphous mainly consisted of iron oxide. Together with XRD (X-ray diffraction) results it is concluded that the outer finely crystalline part consists mainly of hematite and the inner with larger octahedral crystals of nickel spinel. These analyses are a case study of fuel crud collected from BWRs and a larger amount of information is needed to complete the data base in the future.

Results of Westinghouse studies on potential impacts of crud deposits on fuel rod behavior on high powered PWR fuel rods were presented by R.J. Comstock. These studies were initiated due to the fact that high power histories of fuel, high burnup and long cycle management lead more and more to crud deposit on core, Axial Offset Anomalies and increase of radiation crud build up. Observations of crud deposition were made typically in the highest powered assemblies, in the upper spans of the fuel assemblies. Generally, these crud formations occurred under subcooled boiling condition and thickness up to 80 microns approximately was observed.

Crud was scrapped from cladding for evaluation of the thickness and chemical composition. Destruction examinations led to a good agreement between crud thickness and Eddy current measurement (oxide + crud). Metallographic cross-section of rod in crud affected region indicated sometimes acceleration of the cladding corrosion. Degradation of the clad occurred by metal/oxide interface increase or chemical effect under boiling in the crud porosities and correction actions must be taken to avoid the crud formation. The increase of the pH during the cycle, at the beginning of cycle in particular and control of circulating corrosion products are today proposed.

A new techniques, which permits the visualization of the two phase flow regime (bubble formation at the cladding wall), experimental and calculation data were presented by J. Peybernes (CEA/Cadarache). The visualization device has been adapted on the out-of-pile loop REGGAE which allows to simulate the operating conditions of the PWR except irradiation. Thermohydraulic parameters and surface condition effect (roughness, porosity of the cladding surface) on the flow pattern were studied. It was shown that these effects affected strongly the bubble density and the

bubble diameter. Results were in agreement with the proposed model. This techniques could be used for thermohydraulic model improvement (e.g. void fraction measurement) and could be used for a better quantification of the species hideout at the wall. The optical access will allow on the other hand to study other phenomena as crud deposition, spalling, etc.

The results of quantitative analysis of lithium and boron distribution in zirconia, in in-reactor corroded Zr-based alloy samples, using the Secondary Ion Mass Spectrometry (SIMS), were presented by O. Gebhardt et al (PSI, Switzerland). It was observed that both boron and lithium depleted in a zone located at a distance evaluated to 0,8 - 1  $\mu\text{m}$  from the interface metal/oxide. The profiles of boron and lithium showed peaks which are not clearly explained at this moment. The concentration of lithium and boron in the oxide were estimated to 8 to 22 ppm and 75 to 190 ppm respectively but the oxide thickness was limited to 10 micrometers maximum. No conclusion concerning the influence of the cladding material chemical composition and final mechanical/thermal treatment on the penetration of Li and B was done and it was suggested to pursue the investigations. In particular, analyses by line-scan of samples with thicker oxide layer (up to 100 microns) are proposed.

Long-term oxidation kinetics of Zry-4 and Zr-2.5%Nb alloys at different structural conditions have been studied for the temperatures of 265 to 435°C and different environments (primary PHWR coolant conditions, steam at high pressure) and reported by A.J.G. Maroto (CNEA, Argentina). Zry-4 has a cyclic behaviour following a cubic law oxidation. At all temperature, the corrosion rates of Zry-4 specimen were lower than those of the Zr-2.5%Nb coupons. The heat treatment improved the corrosion resistance of Zr-2.5%Nb due to changes in the microstructure of the alloy. It has been shown that the orientation of the crystallite of the zirconia tetragonal phase with respect of the metal surface in Zircaloy-4 is different that the orientation of those crystallite in Zr-2.5%Nb. It was also shown that the compressive stresses affected the corrosion rate.

#### SESSION 4 - CORROSION MODELLING

The session consisted of four papers which dealt with aspects of modelling oxide film growth phenomena near the cladding surface and in the bulk water chemistry.

Rosborg's paper (Studsvik Material AB, Sweden) emphasized the complex situation that exists within the superficial dense oxide, porous oxide and crud layers over the base metal. He alluded to the known effects of water chemistry on corrosion but pointed out that the operating mechanisms are unclear. The effect of crud buildup on corrosion has received little attention in terms of mechanistic understanding and modelling. Possible causes for these effects on the assumption that diffusion of oxygen through the barrier layer was the rate limiting process for the corrosion kinetics were suggested. He suggested that a form of the kinetic equation, similar to that developed for gaseous oxidation might be derived for aqueous corrosion, which implies that the oxide growth is influenced by 3 factors: 1) the chemical potential of oxygen at the metal-oxide and oxide-water interfaces, 2) diffusivity of oxygen vacancies in the dense layer and 3) concentration of the impurity cations which substitute for zirconium in the dense layer. He reviewed how these factors may be influenced by water chemistry and crud layers. Suggested possibilities included oxide phase stability, impurity cations originating from the crud as well as the alloy, oxide morphology of the dense layer, alteration of local radiolytic processes, enhanced grain boundary diffusion and others. He emphasized that the complexity of the corrosion process is that a number of these individual processes occur simultaneously and the relative importance of each may change as the oxide film grows.

Kritskij (VNIPIET, Russian Federation) discussed the influence of  $\text{NH}_3$  on the solution pH, and hence the crud solubility in various mixtures of  $\text{H}_3\text{BO}_3$ , and KOH. He found that:

- 1) at constant  $[\text{H}_3\text{BO}_3]$ , the influence of  $\text{NH}_3$  on increasing the  $\text{pH}_T$  was greatest when the  $[\text{KOH}]$  was low,
- 2) for co-ordinated water chemistry (WWER),  $[\text{NH}_3]$  up to 54 ppm had *no effect* on  $\text{pH}_T$ , thus magnetite solubility under normal operating conditions,

- 3) however, under shutdown conditions at low temperature,  $\text{NH}_3$  had a *significant effect* on  $\text{pH}_T$  increases, thus reducing magnetite solubility,
- 4) “updated” water chemistry regime was calculated to be worse than the “co-ordinated” regime with regards to magnetite solubility and dose rate since the  $\text{pH}_T$  (average) is higher into the alkaline regime and further removed from the optimum  $\text{pH}_T$  for magnetite solubility,
- 5) during power adjustments, large amounts of  $\text{H}_3\text{BO}_3$  are introduced that results in increased activity from the large swings in  $\text{pH}_T$  due to delays in introducing KOH. The  $\text{pH}_T$  swings are more severe in the “updated” water chemistry regime because of the higher allowable alkali contents. However, if  $[\text{NH}_3]$  is high it can compensate for this because it is most effective at the lower temperatures. This thus explains the reduction in dose rates observed with increasing  $[\text{NH}_3]$  in operating power plants

As a result of these modelling efforts and calculations, it is recommended that 1)  $\text{H}_3\text{BO}_3/\text{KOH}$  mixtures be injected during power adjustments (shutdowns), 2) maintain  $[\text{NH}_3]$  at its upper limit, and 3) use  $\text{H}_3\text{BO}_3$  enriched in  $^{10}\text{B}$  would be beneficial.

This work is a good example of how modelling calculations can impact on understanding in-reactor phenomena and assist in suggesting improved operational procedures.

Kritskij, in his another paper, described an extension of his earlier corrosion model originally proposed at the 1993 meeting. The original model was for Zr - 1%Nb cladding and contained two components of corrosion growth - a thermal component and a radiation component. Mechanistically, the model for post-transition oxide growth is based on an oxide dissolution mechanism. A similar dependence on  $\text{pH}_T$  for the corrosion rate and the total solubilities of  $\text{Zr}(\text{OH})_3^+$  and  $\text{Zr}(\text{OH})_5^-$  provide some support for the dissolution based model. An extension to this model now includes components that account for alloy composition and water chemistry conditions. These components are based on the free energy of mixed oxide formation due to alloying elements and the ion hydration energies for the various coolant additives (impurities). A new generalized corrosion equation is proposed. The equation predicts uniform and nodular corrosion of E110 alloy in LWR and it is suggested that with the new generalized form it may be possible to predict corrosion of zirconium alloys in general.

Kritskij also described a model for estimating the number of fuel failures in WWERs and concluded that fuel failure rates are dependent on iron oxide deposition on the cladding and local vapour content of coolant. This stresses the need for optimal water chemistry in operating reactors.

Modelling analyses of the sub-cooled boiling process with respect to dissolved gas behaviour (i.e. gas stripping into the steam phase) was described by M. Zmiko (NRI, Rez, Czech Republic). Using a steady-state equilibria approach, there is no driving force for significant gas depletion and effects are only significant at large void fractions. Using the dynamic approach, the effect is still small for conditions of non-developed subcooled boiling, due to limited gas diffusion rate into the bubbles. But for developed subcooled boiling, where you have periodical bubble formation and continual gas diffusion, one can get significant local depletion of gases (e.g.  $\text{H}_2$ ) in the liquid layer surrounding the bubble, although it is time and space dependent. Modelling of water radiolysis at elevated temperature ( $250^\circ\text{C}$ ) resulted in a  $[\text{H}]$  critical of  $\sim 7$  ml/kg which was required for complete suppression of radiolysis under PWR conditions. This result was consistent but somewhat conservative compared to lower values reported in experiments.

The underlying message here from this work is that under boiling conditions one needs to be aware of depletion phenomena which could lead to radiolytically produced oxidizing species locally. The next obvious question then is can we go one step further and attempt to model radiolytic processes in porous oxides where we have relatively large surface areas?



In general, all papers certainly emphasized the complexity of the processes we are trying to model but also demonstrated that progress was being made towards taking a more fundamental approach in the modelling area, both for oxide growth and water chemistry.

## SESSION 5 - IN SITU MEASUREMENTS, LOOP FACILITIES

At session 5, experimental techniques (on-line monitor to determine electrical resistance of aqueous solution at elevated temperatures, CIAE, Beijing, China; thin layer electrode (TLE), a new in-situ techniques for characterization of Zr alloy corrosion resistance developed by VTT, Helsinki, Finland) and facilities (INCA-loop for water chemistry and materials research in the Studsvik R2 reactor, Studsvik Materials AB, Sweden; five high pressure loops modelling PWR, WWER and BWR water environment in the LVR-15 reactor, NRI, Rez, Czech Republic; PVK-2 loop modelling WWER water chemistry environment in the MIR reactor, NIAR, Dimitrovgrad, Russian Federation; and PWR loop system for in-core modelling of Zr alloy corrosion in the Halden reactor, OECD HRP, Halden, Norway) were presented. However, some results from cladding behaviour were also given.

### In situ measurements:

New methods are proposed. At this meeting methods for on time high temperature conductivity measurements, in situ characterization of oxide films (a series of methods), and in situ diameter measurements to follow oxide growth and crud build-ups were treated or mentioned. Some of the proposed methods may be of interest for the IAEA WACOL Co-ordinated Research Project. Some of the methods may be used for in core studies. Before their merits and reliability need to be carefully verified, and sufficient experience has to be achieved. Unnecessary mistakes and failures could be a burden for future development. The methods for in situ characterization of oxide films offers interesting experimental possibilities, perhaps primarily to increase the fundamental understanding rather than elucidate differences in actual behaviour of different materials.

### Loop facilities:

Experimental reactors are available and primary circuit components studies, at this meeting loop facilities from reactors in Norway, Russia, Sweden and the Czech Republic were presented. Loop facilities exist for studies of the influences of different water chemistries.

A trend is obvious: If we in the past „more or less“ studied the effect of irradiation and water chemistry separately, the present demand and future need are to simulate the actual experiments sufficiently well.

The awareness of the need for careful water chemistry control is present and increasing. Work to improve the water chemistry monitoring and follow-up is in progress at the different test reactors.

## SUMMARY OF PANEL DISCUSSION

### General Comments

Corrosion is the principal life-limiting degradation mechanism in nuclear steam supply systems, especially, taking into account the trends to increase fuel burnup, thermal rate and cycle length. Until now there is no generally accepted corrosion model of Zr-based alloys in a water environment because of multiple influencing factors. Ability of the “break point” in the kinetics of Zr-based alloy corrosion does not allow to extrapolate the results of short term tests on actual time of their operation in a power reactor. Appearance of nodular type corrosion on rod claddings also hampers the creation of common corrosion model.

This is why the major tool to forecast corrosion behaviour of Zr-based alloys is to bring to the light the impact of individual factors or their combination on corrosion process in experiments carried

out in autoclaves, loops and in reactors. In general, water corrosion of Zr-based alloys is defined by the aggregate of internal (structure and chemical composition) and external (irradiation, water chemistry, thermal hydraulics, etc.) factors.

As mentioned above, empirical (and semi-empirical) models are limited when predictions outside the current reactor operating regimes are required. It was also generally accepted that any model must have the correct physical form. It was emphasized that an understanding of processes occurring in the superficial crud layer, porous layer, and barrier layer and the influence of any irradiation induced microstructural changes in the underlying metal substrate on these processes was essential. In particular, since the oxide films are for the most part essentially porous and since the controlling processes take place deep within the pores near the dense layer at the metal-oxide interface, the focus should be on understanding the mechanisms of localized processes occurring in these regions.

#### **Areas of Further Concern:**

##### ***-In- and out-of-pile corrosion data:***

- to improve the knowledge on interrelation between corrosion behaviour of different Zr alloy cladding materials in water power reactors and measured water chemistry parameters (hydroxides, boron, hydrogen, oxygen, etc.);
- to pay special attention to unexpected material behaviour, or environmental excursions which are responsible for this behaviour;
- to define correlation of fuel rod cladding corrosion tests in- and out-of -pile.

##### ***-Crud, corrosion layers:***

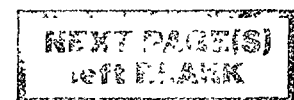
- to study the role of structure changes, oxide film morphology and changes of environment by radiolysis in oxidation kinetics;
- to define influence of oxide structure and porosity and different boiling conditions on corrosion process of Zr-based alloys.

##### ***-Modelling:***

- to build mechanistically based components into current semi-empirical models to improve predictive capabilities outside the range of current operating conditions. This should be an on-going process as our mechanistic understanding improves.
- the focus should be on understanding the localized water chemistry conditions which exist in the porous oxide layer next to the dense layer, and how this impacts the corrosion processes involved.

## PLANT EXPERIENCE

(Session 1)



# INDIAN EXPERIENCE ON CORROSION OF ZIRCONIUM BASED ALLOYS AND PRIMARY HEAT TRANSPORT COMPONENTS

A.K. SAXENA, S.L. MANDOWARA, M. DAS, B.K. BHASIN  
Nuclear Power Corporation of India Ltd,  
Vikram Sarabhai Bhavan, Anushaktinagar,  
Mumbai, India



## Abstract

This paper describes the Indian experience in the areas of Corrosion of Zirconium based alloys and primary heat transport components. It also covers the recent developments on corrosion studies and passivation method for primary heat transport components against corrosion. Chemistry control requirements of the coolant in the PHWR and their surveillance frequency have also been mentioned.

## 1. INTRODUCTION

The nuclear power plants in India are designed, constructed and operated by Nuclear Power Corporation. Presently, 8 units of 220 MWe PHWRs and 2 units of 160 MWe BWRs are in operation and 4 more units of 220 MWe PHWRs are under construction as shown in Table I.

TABLE I. LIST OF OPERATING POWER STATIONS . AND PROJECTS UNDER CONSTRUCTION

Type of Reactor	Plant	Power Rating	City, State
<b>Operating Stations</b>			
BWR	TAPS-1	160 MWe	Tarapur, Maharashtra
	TAPS-2	160 MWe	Tarapur, Maharashtra
PHWR	RAPS-1	150 MWe	Kota, Rajasthan
	RAPS-2	200 MWe	Kota, Rajasthan
	MAPS-1	220 MWe	Kalpakkam, Tamil Nadu
	MAPS-2	220 MWe	Kalpakkam, Tamil Nadu
	NAPS-1	220 MWe	Narora, Uttar Pradesh
	NAPS-2	220 MWe	Narora, Uttar Pradesh
	KAPS-1	220 MWe	Kakrapar, Karnataka
	KAPS-2	220 MWe	Kakrapar, Karnataka
<b>Under Construction</b>			
PHWR	KAIGA-1	220 MWe	Kaiga, Gujarat
	KAIGA-2	220 MWe	Kaiga, Gujarat
	RAPP-3	220 MWe	Kota, Rajasthan
	RAPP-4	220 MWe	Kota, Rajasthan

The studies on the development of zirconium based alloys, characterisation of their properties, fabrication routes of the alloys and evaluation of corrosion resistance have perhaps the longest period of 35 years of documentation.

Zircoloy-2 / Zircoloy-4 is used as cladding material for the fuel elements and other in-core components such as calandria tubes, flow tubes and guide tubes. The choice of zircoloy-2 / zircoloy-4 as cladding material is mainly due to its low absorption cross-section for neutrons, good corrosion resistance and adequate mechanical strength at the temperature of operation. Zr-2.5Nb alloy is used as a coolant tube material due to higher strength, superior creep resistance, adequate corrosion resistance and low hydrogen pick-up under irradiated conditions.

Pressurised heavy water reactors use large surface area of carbon steel alloy in the primary heat transport system (PHT). To reduce the corrosion rate, the passivation is being done by hot conditioning of the PHT main circuit and by controlling the coolant chemistry.

## 2. CORROSION BEHAVIOUR OF FUEL CLADDING

Zircoloy-2 / Zircoloy-4 is used as cladding material in the fuel elements. This cladding material is required to operate for a period of about three years in the reactor operating conditions. The integrity of the cladding depends on the nature and extent of its interaction with the high pressure and high temperature coolant water on one side and with the irradiation  $\text{UO}_2$  fuel on the other side. Enhanced corrosion of zircoloy is observed on the external surface while attack by corrosive fission products may occur at the inner surface of the cladding tube at higher burn-up. The study conducted through the post irradiation examination (PIE) of irradiated fuel elements which has provided very useful information on the water side and fuel side corrosion of the cladding.

### 2.1. Water-side Corrosion

A detailed study of water-side corrosion of zircoloy-2 cladding in TAPS fuel elements have been carried out. Two types of corrosion have been observed :

- (1) Uniform corrosion observed as a thin oxide layer on the cladding surface.
- (2) Localised accelerated nodular corrosion appearing as white pimples on the cladding surface of the fuel cladding.

#### 2.1.1. Uniform corrosion

Uniform corrosion was studied in 12 fuel rods of TAPS. The oxide layer thickness was measured on metallographically prepared samples and corrosion enhancement factor was determined by comparing the measured values with the expected out-of-pile corrosion. Figure 1 shows the plot of measured oxide layer thickness as a function of dwell time. Oxide growth calculated from out-of-pile corrosion correlation for reactor operating temperature is also shown for comparison. The figure shows a clear enhancement of corrosion in reactor condition. Enhancement factor was found to be 3.

#### 2.1.2. Nodular corrosion

Nodular Corrosion was examined in 18 fuel rods, only 3 fuel rods had shown nodular corrosion. The main findings related to nodular corrosion are as follows :

- (1) Corrosion nodular had thickness in the range of 15-55 microns and diameters in the range of 200-500 microns.

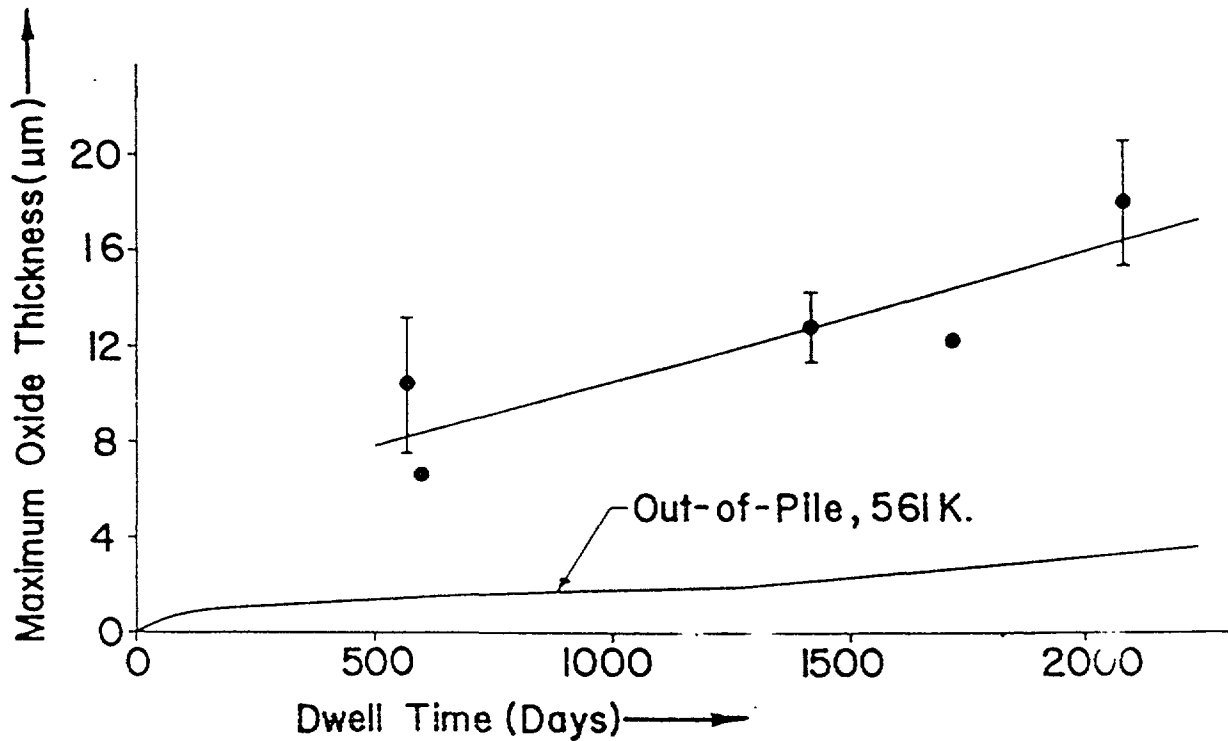


FIG. 1. Variation of the oxide thickness on the zircaloy cladding with the dwell time of the fuel element.

- (2) Nodular concentration on the cladding surface followed the axial fuel burn-up profile.
- (3) Spacer grid locations showed very high concentration of nodules, resulting in formation of a white oxide band at these locations.
- (4) A linear correlation was found between the nodule thickness and fuel burn-up.

## 2.2. Fuel-side corrosion

Two main types of effects were observed on the inside surface of the cladding during metallographic examination of samples taken from failed and unfailed fuel rods :

- (1) Oxidation of cladding giving a thin oxide layer.
- (2) Presence of a fuel cladding interactive layer.

Samples taken from high burn-up (= 30,000 MWD/MTU) fuel rods showed presence of bonding layer in the fuel clad gap. The thickness of such layers was about 20 microns in high burn-up unfailed rods but much higher in the failed rods.

## 3. RECENT DEVELOPMENTS ON CORROSION STUDIES

The corrosion of zirconium alloys for fuel cladding was studied and reviewed with the following objectives : (1) Improved performance during extended burn-up with higher operating temperatures (2) Improvement in fabrication procedures (3) To modify the chemical composition / structure of zircalloys with respect to distribution of alloying elements and control of impurities.

The following are the salient features

- For BWRs, nodular corrosion could be one of the life limiting factors under extended burn-up conditions. Nodular corrosion was not generally observed for Zr-Nb alloys.
- In case of Zircoloy-4, it was recognised that a dispersion of coarser particles would be beneficial for improving the corrosion resistance. To improve upon the corrosion resistance of zircoloy-4 is achieved by specifically reducing the impurity element levels of nitrogen, oxygen, carbon and silicon than the allowable limits and keeping the tin content at a level of 1.35% as against the normal 1.5% tin in conventional zircoloy-4. It was seen that the corrosion rates were significantly less than the conventional zircoloy-4.

#### 4 CORROSION CONTROL OF PRIMARY HEAT TRANSPORT COMPONENTS IN PHWRs BY HOT CONDITIONING

Pressurised heavy water reactors use large surface area of carbon steel alloy in the primary heat transport system (PHT). Passivation of the surfaces of the PHT components and chemistry control of the coolant are required to check the corrosion rate. Passivation of the PHT components surfaces are being done by Hot Conditioning of the PHT System with deoxygenated light water at temperature of about 250 °C during commissioning stage. As a result of Hot Conditioning, a protective magnetite film on the surfaces of carbon steel is formed essentially to guard this material from corrosion.

##### 4.1. Hot conditioning of KAPS-2

Presently KAPS-2 is the youngest PHWR in India. Hot conditioning of PHT system of KAPS-2 began at a PHT temperature of 185 °C and further raised to 250 °C by running all the four primary circulating pumps (PCPs). The temperature of the system continued to increase and stabilised at an average temperature of  $260 \pm 5$  °C throughout the hot conditioning period. Throughout the hot conditioning period the chemistry was maintained well within specifications as shown in Table II.

TABLE-II. REACTOR COOLANT CHEMISTRY DURING HOT CONDITIONING

PARAMETER	VALUE
pH at 25°C	10.5
Specific conductivity at 25°C in micro-siemens/cm	75
Dissolved oxygen in ppb	< 4
Hydrazine in mg/litre	0.11
Iron in mg/litre	0.06
Copper in mg/litre	< 0.01
Nickel in mg/litre	0.03
Chloride in mg/litre	< 0.05

When coolant temperature reached to 185 °C i.e. zero time of hot conditioning, crud content reduced to 3.25 mg/litre once the temperature stabilised. Crud content steadily decreased to less than 0.005 mg/litre and remained almost same till the end of hot conditioning.

#### 4.2. Evaluation of hot conditioning

As per the plan the stringers from either side or both the autoclaves were removed by valving out the respective autoclaves. After removal of stringers, autoclaves were valved in again and flow adjusted to an average value of 38-40 litre/minute.

The coupons from stringers were evaluated on the regular basis during hot conditioning for the thickness of magnetite coating formed on the carbon steel test coupons surfaces. The results of hot conditioning evaluation are shown in Table III.

TABLE III. EVALUATION RESULTS

Cumulative Hours from Zero Time	Thickness of Magnetite Coating in microns.
20	0.28
44	0.46
68	0.53
92	0.68
116	0.70 (*)
140	0.70

(\*) Hot conditioning declared terminated

It is observed that with the progress of hot conditioning the thickness as evaluated was found to increase progressively. The uniform, adherent magnetite coating with the full surface area coverage and steady value of 0.7 microns of magnetite thickness was achieved within 116 hours.

To preserve good magnetite coating formed due to hot conditioning, it is necessary to maintain chemistry control of the coolant. Technical specifications requirements and their surveillance frequency are listed in Table IV for chemistry control of PHT coolant.



TABLE-IV. CHEMISTRY CONTROL OF PHT AND SURVEILLANCE  
FREQUENCY AS PER TECHNICAL SPECIFICATIONS OF MAJOR  
PARAMETERS

Parameter	Sampling Frequency	Range/ Limit	Remarks
pH	1/Day	9.0 - 10.5	Adjusted with lithium hydroxide (LiOH). This is the optimum pH range for least corrosion of the carbon steel in the system.
Specific Conductivity 25°C	3/Week	30 micro-siemens/cm	This limit takes into account limit by the concentration of lithium hydroxide (LiOH) maintained in the coolant for keeping its pH within specified limits.
Chloride	3/Week	0.3 ppm	To minimise possible stress corrosion attack.
Ammonia	3/Week	0.5 ppm	To minimise corrosion of monel boiler tubes in the presence of oxygen.
Crude	1/Week	0.1 ppm	Circulating crud gets activated in the core. It will get deposited on the fuel bundles and on the PHT system surface. The later leads to higher radiation fields in shut down and accessible areas and the former affects heat transfer efficiency.
Dissolved Oxygen	3/Week	10 micro-grams/litre	Higher concentration of oxygen damages the protective magnetite layer and increases the corrosion rate of monel boiler tubes.
Dissolved Deuterium	1/Week	3-10 ml/litre of D <sub>2</sub> O at STP	To maintain the equilibrium concentration of dissolved oxygen within specifications.
Iodine-131	1/Shift	100 micro-curies/litre	Iodine - 131 activity in the coolant indicates the presence of defects or failure in the fuel cladding.

## 5. CONCLUSION

In the last two decades, Indian PHWRs have not experienced any failure of fuel cladding and PHT components due to corrosion. However, there are some incidents of fuel cladding failures in the BWRs due to corrosion. Considering the importance of the corrosion problems, a high pressure and high temperature loop is being commissioned to study the corrosion behaviour of various materials in depth.

## REFERENCES

- [1] GADIYAR, H.S., Proceedings of symposium on "Zirconium Alloys for Reactor Components", organised by Department of Atomic Energy, BARC, Mumbai (1991).
- [2] SAH, D.N., Proceedings of symposium on "Zirconium Alloys for Reactor Components", organised by Department of Atomic Energy, BARC, Mumbai (1991).
- [3] KAPS-2 Commissioning Report on PHT System Hot Conditioning, Report (K - II - CR -33000 - 7 - R - 0), NPC, Mumbai (1993).
- [4] SAXENA, A.K., DAS, M., BHASIN, B.K., "Indian Pressurised Heavy Water Reactor Fuels - licensing requirements", 5th International CANDU Fuel Conference, Toronto, Canada, CNS (1997) 18.
- [6] DAS, M., BHARADWAJ, S.A., PRASAD, P.N., "Fuel Performance Experience in Indian Pressurised Heavy Water Reactor", Proceedings of 3rd International Conference on CANDU Fuel, Chalk River, Canada, CNS (1992) 130.
- [7] Technical Specifications for KAPS Operation, NPC, Mumbai (1991).
- [8] "Code of Practice on Design for Safety in Pressurised Heavy Water Based Nuclear Power Plants", AERB Safety Code, Report AERB/SC/D (1989).
- [9] DAS, M., DESAI, P.B., "Ballooning and Rapture Behaviour of PHWR Fuel Cladding", Proceedings of 3rd International Conference on CANDU Fuel, Chalk River, Canada, CNS, (1992) 260.

**NEXT PAGE(S)  
left BLANK**



D. ZOTICA, O. MARCIULESCU  
Chemical Department/ Production Division,  
Cernavoda Nuclear Power Plant,  
Romania

### **Abstract**

Following the experience of other nuclear stations, at Cernavoda Nuclear Power Plant (NPP) has been established a chemical control program with the main objective to ensure that degradation of materials by fluid contact is minimised and that the design life of the plant will be achieved or exceeded. Chemical Control Program is equally applied to nuclear and conventional NPP Systems. One of the most important plant system is Primary Heat Transport (PHT) System considering its role in active zone cooling and heat transfer to steam generators. Chemical control of PHT System is directed to keep chemical parameters within specified limits in order to minimise corrosion of equipment and related piping, to control the corrosion rate and impurities concentration, such as corrosion and fission products and to minimise activity transport and heat transfer surfaces fouling.

## **1. INTRODUCTION**

Cernavoda NPP is a heavy water moderated and cooled CANDU 6 PHW reactor using natural uranium as fuel. It is located on the right bank of the Danube river, 180 km East from Bucharest. Unit #1 was declared on commercial operation by December 2nd 1996.

This paper describes the experience to date in chemical control of Primary Heat Transport System with background from commissioning phases.

## **2. PHT SYSTEM GENERAL PRESENTATION**

The system is arranged in two separate loops, which are normally tied together each loop serving 190 fuel channels, and comprises two boilers, two circulating pumps, two reactor inlet headers, two reactor outlet headers and necessary interconnecting piping. The general arrangement of PHT System is shown in Figure 1 [1].

To assist in monitoring and optimisation of chemistry control and to give warning of serious corrosion and/or activity transport conditions, one Autoclave System is provided. The Autoclave System consists of four autoclave circuits, one from the reactor outlet header to the boilers and one from the circulating pump discharge to the reactor inlet header on each of the two reactor loops as shown in Figure 2 [2].

Standard coupons are 30 mm by 15 mm with a thickness between 1 and 1.5 mm. Each autoclave contains 6 hanger bars. The first four hanger bars of each autoclave carry Heat Transport System (HTS) materials as follows: Incoloy 800 (tubing of steam generators and heat exchanger), carbon steel ASTM A106 Grade B (piping, headers, feeders, heat exchanger shell), Zr-2.5 Nb (pressure tubes), Zircalloy 4 (fuel cladding), stainless steel Type 403 (End fittings).

## **3. PHT HOT CONDITIONING**

The Heat Transport System hot conditioning of Cernavoda NPP Unit 1 was a two step process (at 150(C and 250(C) using the dilithiated salt of ethylene diamine tetraacetic ( $\text{Li}_2\text{EDTA}$ ) in light water.

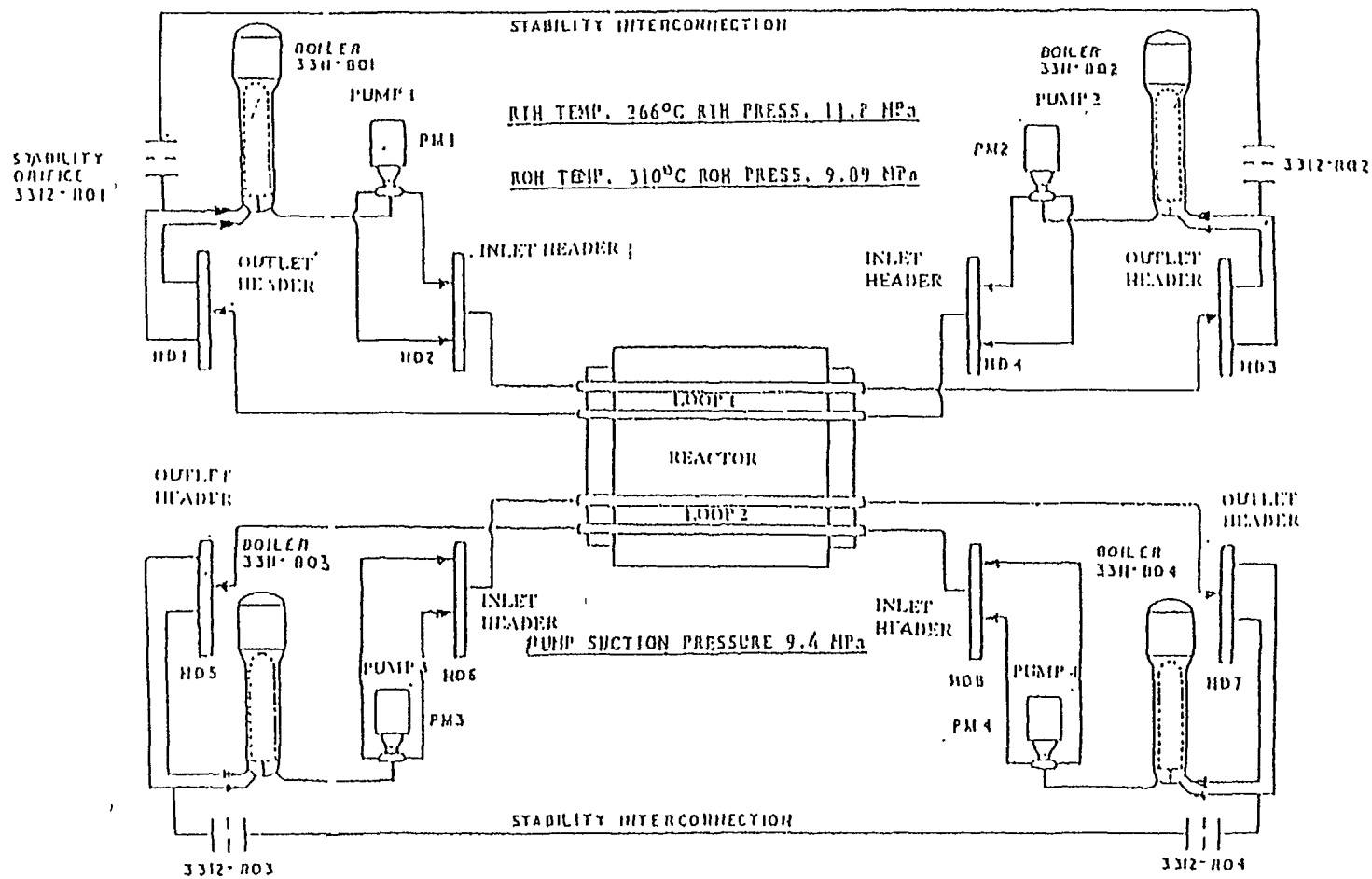


FIG. 1. Main heat transport system diagram.

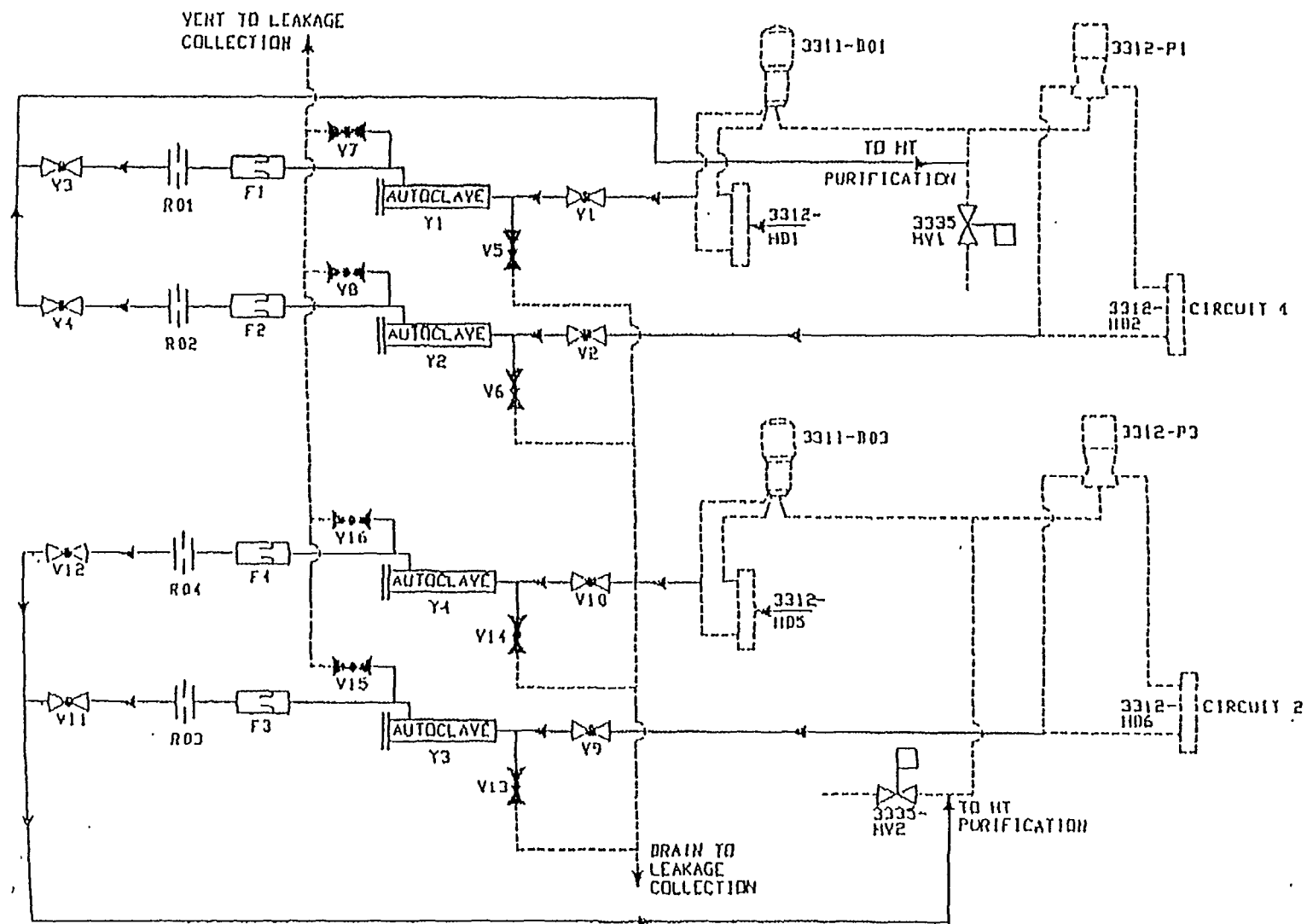


FIG. 2. HT autoclave system diagram.

The process removed 86 g of zinc and 153 of phosphate. Examination of HTS autoclaves corrosion coupons indicated that a protective magnetite layer of 3.78 g/m<sup>2</sup> had been generated on the carbon steel surfaces [3]. Later visual examination of system components confirmed the presence of an adherent/protective magnetite layer

#### 4. PHT HOT PERFORMANCE

The initial HTS chemistry conditions for hot performance were:

pH:	10 – 10.5
Hydrazine	20 mg/kg
Suspended solids:	<0.02 mg/kg

A cleaning step to reduce suspended solids concentration to less than 0.020 mg/kg as a prerequisite to initiate raising HTS temperature was carried out without difficulties, only two mechanical filters being changed after all four pumps started

Ammonia resulted by hydrazine decomposition was removed using D<sup>+</sup>/OD<sup>-</sup> form IRN 150 available in one of the two purification system IX column when hot performance started and by D<sup>+</sup> form IRN 77 subsequently. Two loads (1080 L each) of IRN 77 were necessary throughout hot performance to remove ammonia and maintain pH [4].

Once hot performance tests were finished, IX column containing mixed bed resin form IRN 150 was taken out of service to leave a residual ammonia concentration of 50 mg/kg giving a pH of 10.5 and final hydrazine addition was performed to lay up the HT System with 20 mg N<sub>2</sub>H<sub>4</sub>/kg. For the period between hot performance and power increase only hydrazine 35% was added to the system to control dissolved oxygen.

#### 5 PHT POWER INCREASE

Cernavoda NPP Unit 1 reactor became critical for the first time by April 16th 1996. Before power increase, ammonia was removed from the system and successive LiOH additions were performed until the cation component of mixed bed resin contained in one IX purification column has been lithiated. In the mean time, hydrogen addition replace hydrazine in oxygen control.

Autoclave coupons have been analysed at the end of commissioning phase (loss of class IV test) as well as during commissioning (hot conditioning and hot performance). The result concluded that no significant corrosion process occurred during commissioning [5].

#### 6. PHT STEADY STATE OPERATION

Chemical Control and Diagnostic Parameters for actual steady state operation are summarized in Tables I and II [6].

Chemistry control of the PHT System and Auxiliaries is required to:

- (1) Minimise the corrosion of system components;
- (2) Limit the production rate of radioactive corrosion products;
- (3) Minimise the fouling of the heat transfer surfaces by controlling the crud movement and removal;
- (4) Maintain heat transport storage tank cover gas deuterium and oxygen concentration below explosive limits.

TABLE I. CHEMICAL CONTROL PARAMETERS SPECIFICATION

Parameter	Sample Origin	Specification	Desired Value
pH	Main System IX outlet	10.2- 10.8 N/A	10.2 – 10.4 (IX inlet
Dissolved D2 (ml./kg)	Main System	3 – 10	5
Chloride (mg/kg)	Main System IX Outlet	$\leq 0.2$ <IX inlet	ALARA ALARA
I-131 (MBq/kg)	Main System IX Outlet	<500 <IX inlet	ALARA ALARA
D2 (% by vol.)	Storage tank cover gas	$\leq 2$	ALARA
O2 (% by vol.)	Storage tank cover gas	$\leq 1$	ALARA
N2 (% by vol.)	Storage tank cover gas	$\leq 6$	ALARA

TABLE II. DIAGNOSTIC PARAMETERS SPECIFICATION

Parameters	Sample Origin	Specification	Desired Value
Lithium (mg/kg)	Main System	0.5 – 1.1	0.5
Conductivity ((S/cm)	Main System	8 – 25	8 – 20
Fluoride (mg/kg)	Main System IX outlet	<0.1 <IX inlet	ALARA ALARA
Suspended Solids (mg/kg)	Main System Gland Seal	<0.1 <0.010	ALARA ALARA
Total Organic Carbon (mg/kg)	Main System	$\leq 1.0$	ALARA
Radionuclide Gama Scan (MBq/l)	Main System IX outlet	0.1 <IX inlet	ALARA ALARA

The corrosion of the system components is minimized by selecting and then controlling a set of chemical parameters which together reduce the aggressiveness of the coolant agent to the specific materials used in the system. The aggressiveness of PHT System water is reduced by controlling.

## Dissolved oxygen content

The corrosion rates of zirconium alloys and carbon steel are significantly enhanced in the presence of dissolved oxygen. The operating objective is to maintain the concentration of dissolved oxygen below 10(g/kg D<sub>2</sub>O). A small excess of dissolved deuterium (or hydrogen) in the PHT System water creates the necessary environment to minimize the net production of free oxygen by radiolytic reaction. Too high a concentration of dissolved deuterium should be avoided to minimize any potential for increased deuterium pick-up by pressure tubes. A concentration of dissolved deuterium less than critical deuterium concentration (the concentration above which the dissolved deuterium must be maintained to ensure that oxygen is not produced) should be also avoided to minimize corrosion process.

## pH

There is a narrow band of pH values, i.e. 10.2 – 10.4 within which to optimally operate the PHT System. The lower end of the specification has been associated with fouling of the core by magnetite deposition. The upper limit of the specification is influenced by the issues of flow accelerated corrosion of the outlet feeder pipes and reactor inlet header temperature rise due to magnetite deposition in the steam generators.

At Cernavoda NPP, one main issue for PHT Chemistry Control is to reduce pH from actual values, 10.5 – 10.6, to optimum range, 10.2 – 10.4.

First attempt to reduce pH value from 10.5 – 10.6 to 10.2 – 10.4 was by addition of same quantities of D<sup>+</sup>/OD form IRN150 to Li<sup>+</sup>/OD form IRN 154 currently used for PHT purification when resin was changed.

As shown in Figure 3, the solution has a limited application, within few weeks, the pH being back to 10.5 – 10.6. Currently we are looking for other solutions to be applied in order to give the possibility to control pH in optimum range.

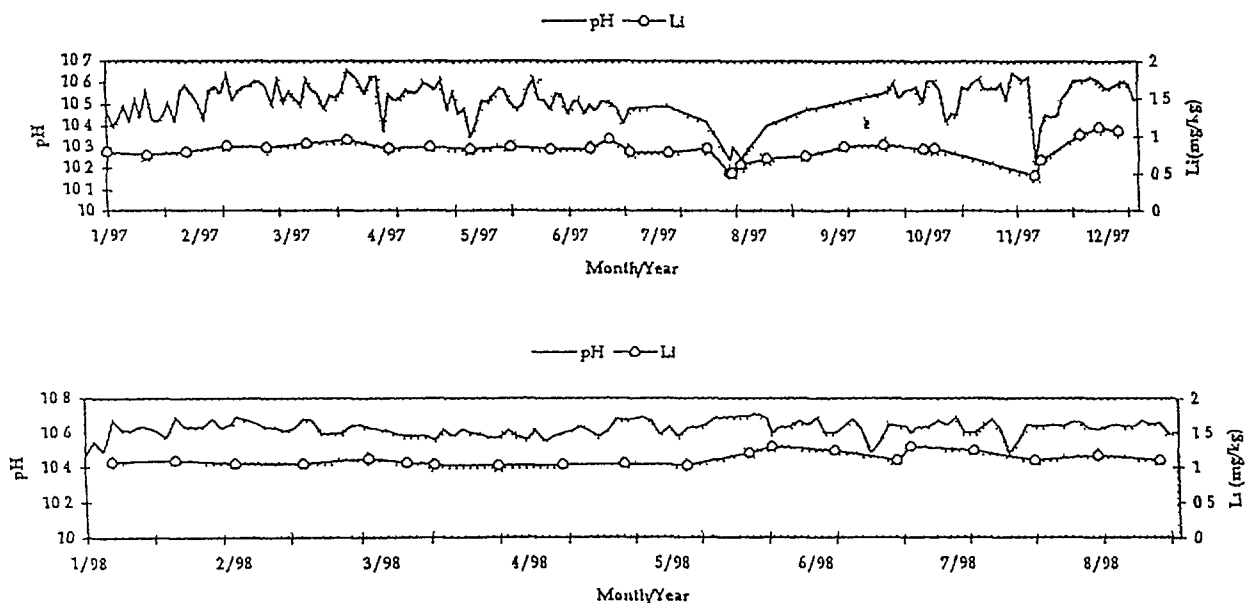


FIG 3 Main heat transport pH and lithium control (loop 1)



Radioactive crud:

The production rate of radioactive materials is minimized by:

- operating with a low concentration of dissolved oxygen which is maintained by hydrogen addition to the PHT water;
- continuous steady state operation with no thermal, hydraulic or chemical transients;
- operating at pH value above 10.2;
- operating with a minimum number of defective fuel bundles.

Fission products:

The reduction of fission product concentration in the PHT System is achieved by:

- location and rapid removal of defective fuel bundles;
- purification by ion exchange.

## 7. CONCLUSIONS

Major areas of concerns for PHT System:

- Hydriding/corrosion of zirconium alloys which compromises the integrity of the pressure tube and fuel bundles.
- Corrosion of the steam generators tubing leading to leaks in the secondary side.
- Activity transport producing elevated radiation fields from PHT System components.

Objectives for PHT System:

- Determine crud transport and composition.
- Identify main sources of crud and possibilities of mediation.
- Minimize flow-assisted corrosion.
- Minimize personnel dose during maintenance.
- Minimize radioactive waste quantities.

Maximize lifetime and thermal performance.

Optimize pH and oxygen control.

## REFERENCES

- [1] DRAGOMIRESCU, C., Main Heat Transport System Training Manual, RENEL (1997).
- [2] GROZA, M., Autoclave System Training Manual, RENEL (1997).
- [3] AGATIELLO, O.E., Heat Transport System Hot Performance Chemistry Control, Report No. 1-CR-78200-CH-01-FINAL, Cernavoda NPP (1994).
- [4] AGATIELLO, O.E., Heat Transport System Hot Performance Chemistry Control, Report No. 1-CR-78200-CH-02-FINAL, Cernavoda NPP (1995).

[5] TOADER, M., Nota Tehnica – Analiza cupoanelor extrase din autoclavele Y1, Y2, Y3, Y4 dupa testul de clasa 4 de la U1/FCNE, Cernavoda NPP (1995).

[6] MARCIULESCU, O., Operating Manual – Primary Heat Transport System Chemistry Control, Cernavoda NPP (1997) 5–10.



## IMPACT OF Zr + 2.5% Nb ALLOY CORROSION UPON OPERABILITY OF RBMK-1000 FUEL CHANNELS

V. KOVYRSHIN, N. ZARITSKY

State Scientific and Technical Center on  
Nuclear and Radiation Safety,  
Kyiv

V. KOLESOV

Chernobyl Nuclear Power Plant,  
Chernobyl

Ukraine

### Abstract

The basic components of RBMK-1000 core (fuel channels, bimetal adapters, claddings of fuel elements, etc.) are of zirconium alloys. Their corrosion is one of factors influencing upon fuel channels operability. Dynamics of channel tubes nodular corrosion development is presented by the results of in-reactor investigation at ChNPP. Radiation-induced mechanism of corrosion damage of tubes surface in contact with coolant was formulated and substantiated by data of post-reactor studies. Within the certain time period of operation corrosion of zirconium alloy of lower bimetal adapter along with removal from there of corrosion products are predominant within the whole process of reactor elements corrosion. The experimental and calculating method was proposed and substantiated to predict time duration up to loss of fuel channels leak tightness. The approaches were generalized to control state of fuel channels material to assess their operability under operation of RBMK-1000 reactors.

### 1. INTRODUCTION

Fuel channels (FC) of RBMK-1000 are made of Zr+2.5%Nb alloy and being of length about 7 m. Besides, contact with coolant by Zr+2.5%Nb alloy occurs at the sections of upper and lower bimetal adapters outside core. Operability of FC elements is in considerable extent being identified by zirconium alloy corrosion level.

During fabrication process there is black color protecting oxide layer being formed of about 1 mcm ( $10^{-6}$  m) thickness. Control over corrosion state of FC is being performed during operational process under periodical in-reactor investigation of surface and by results of post-reactor study. As it comes from [1], state of FC zirconium tubes surface after operation during 10 years is being described by availability of uniform gray color oxide films of thickness up to 10 mcm. Systematic visual in-reactor observation of FC at Chornobyl NPP (ChNPP) power units from the beginning of operation allowed to trace dynamics of tubes surface and adapter zirconium parts state changing.

### 2. NODULAR CORROSION OF CHANNEL TUBES

#### 2.1. Data of in-reactor investigation

During initial period of operation inner surface of tubes retains its protecting layer unaffected, while then it underwent changes of so called nodular corrosion features. It is being registered under TV-inspection after about 400 effective days of operation (on reaching of maximum fluence value –  $7 \times 10^{24} \text{ n m}^{-2}$ ) as separate bright convex “points” of size from about 100 mcm through white (or gray) spots of (1-2) mm diameter.

Creation of initial nodules is being observed firstly in central part of channel tubes at 2...3 m length, i.e. within area of maximum density of neutron flux. As time passes, superficial damage expands over end sections in compliance with the curve presented in Fig.1 being limited by height of

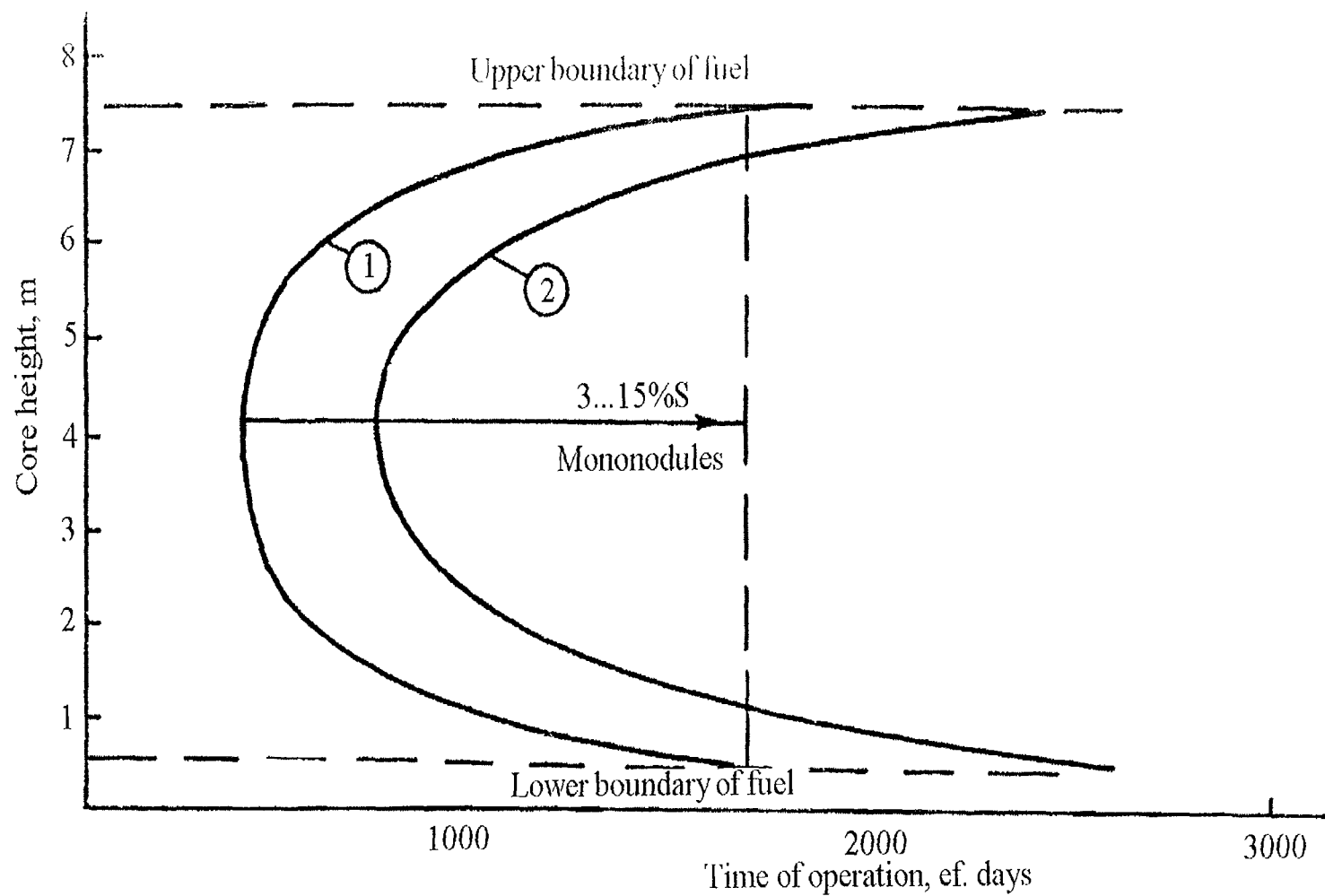


FIG. 1. Temporal dependence of nodular corrosion growing along RBMK-1000 channel tubes height: 1 - boundary of mononodules appearing; 2 - boundary of polynodules unsealing.

fuel assembly column. Unsealing of separate nodules (after about 700 effective days of operation) is being registered by dependence 2 (see Fig.1) similar to 1 one of their creation Process of nodules nucleation at surface covered with protecting oxide film lasts during period of 1500-1800 effective days, while the area they occupy is of 3...15 % of the whole channel surface S (see Fig 1) Merging of corrosion centers (areas) up to complete whitening of surface is being observed in separate tubes under fluence value of about  $4.5 \times 10^{25} \text{ n m}^{-2}$  (see Fig.2) Broad time period of dependence between channel tubes surface corrosion damage and operation duration (fluence) seen in Fig 2 was stipulated by irregularity of the process growing across surface as well as quality of inspection records collecting and processing.

It should be noted that obvious traces of nodular corrosion were absent in FC without fuel assemblies or in those containing additional absorbers (at least, during the period up to 10 years of operation).

## 2.2. Model of radiation induced mechanism of nodular corrosion

The zirconium alloys nodular corrosion (NC) issue is of practical interest as to operability of reactor structural elements aspect due to availability of experimental data on local corrosion damage of depth up to  $5 \times 10^{-4} \dots 10^{-3} \text{ m}$ . There were data obtained by Russian and foreign authors on NC issue reviewed in a number of papers issued by the Nuclear Research Institute (NRI) of Ukrainian National Academy of Sciences (Kyiv) (see, for example, [2]) This analysis showed that NC mechanisms were not identified unambiguously, depend upon many factors and can be sufficiently different for zirconium alloys with niobium and zircalloys. Also, post-reactor testing of RBMK-1000 reactor channel tube specimens was performed in this Institute which results are presented below.

On a basis of literature data and observation results analysis as to kinetics of channel tubes NC growing within RBMK-1000 reactors the general conclusions were made as follows:

- NC is being implemented only at inner surface in contact with coolant,
- Its growing rate depends upon neutron flux density and, probably, spectrum of fast neutrons,
- Level of corrosion damage is being identified by stress-strained state of material along with structural factors,
- Corrosion process grows by electrochemical mechanism and is being controlled by complex inter-relation between above mentioned factors as well as water and chemical regime in reactor.

Post-reactor testing of inner tubes surface after about 800 effective days of operation performed at NRI confirmed availability of nodules (see Fig.3a) of size up to  $2 \times 10^{-3} \text{ m}$  (that is consistent with intra-reactor control data, see Figs 1,2) It is possible to assess dynamics of corrosion damage growing process by the below listed results as follows:

- At the same time with nodules some corrosion centers of (20...80)  $\mu\text{m}$  size and below are being observed (Fig.3b),
- After growing up to the state shown in Fig.3c centers are already objects being registered with the use of intra-reactor control means,
- Results presented in Fig.3b,c show that creation of nodules of (1.. 2) mm size (polynodules) occurs by corrosion merging of small micronodules.

Careful layer-by-layer investigation of separate mononodules or those included into corrosion centers showed that mononodule nucleus differs from the matrix material and oxide layer produced and constitutes separate particles or plain aggregates of the 2<sup>nd</sup>-phase precipitation (see Fig.4,a,b) which were identified as zirconium carbides ZrC, intermetallic compounds (such as Fe<sub>3</sub>Zr), etc There is a picture of matrix material cracking around carbide particle shown in Fig 4c. Such destruction is, most likely, consequence of high local stresses relaxation which, in turn, is the result of

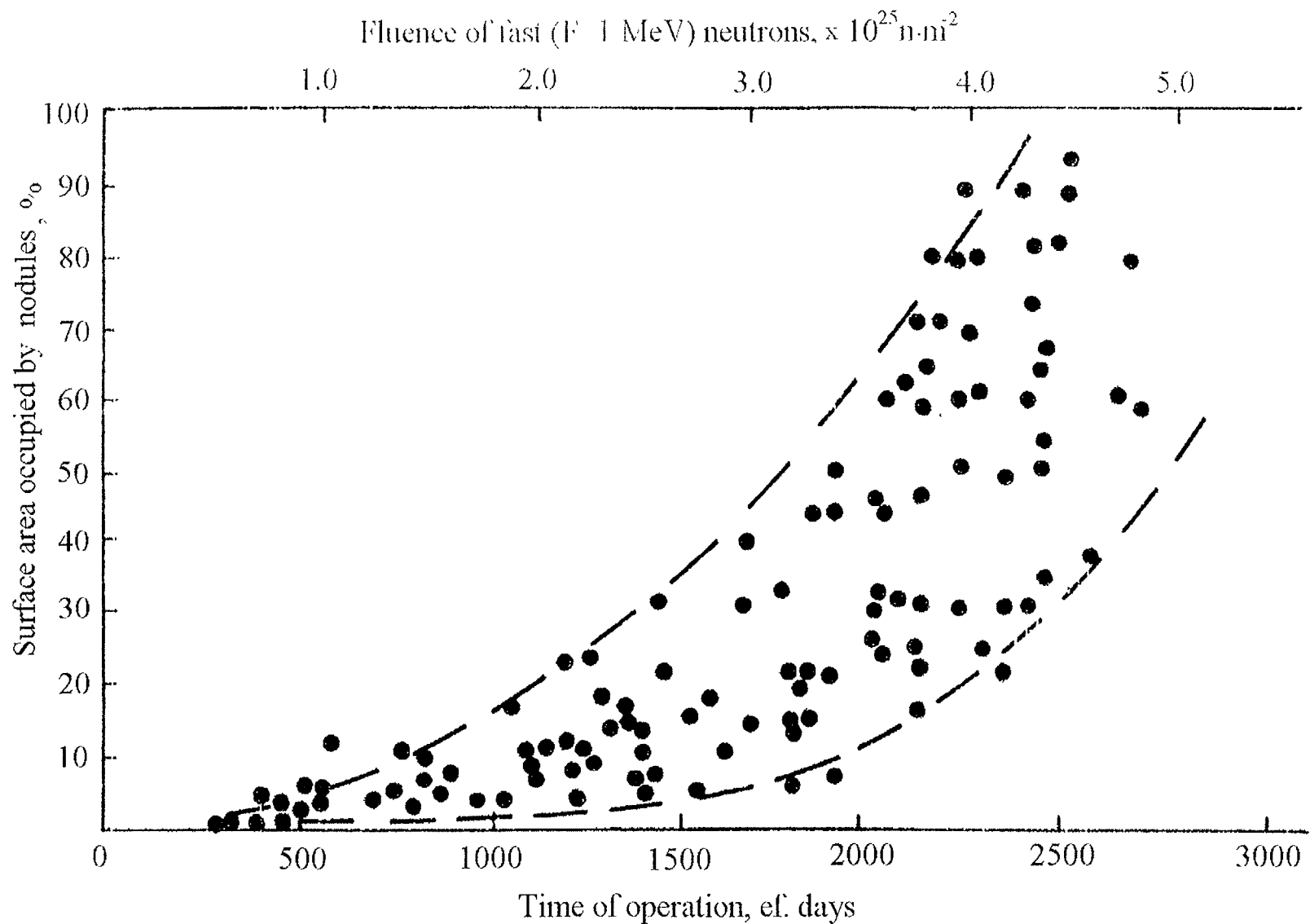
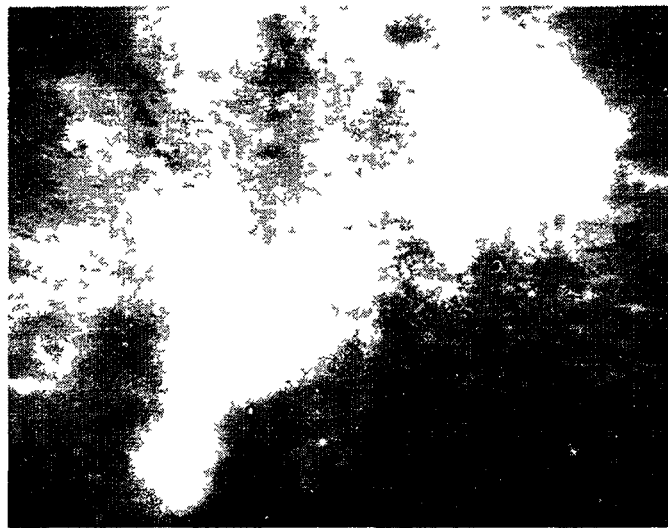


FIG. 2 Temporal dependence of RBMK-1000 channel tubes nodular damage (fraction of oxidized surface)



**a**

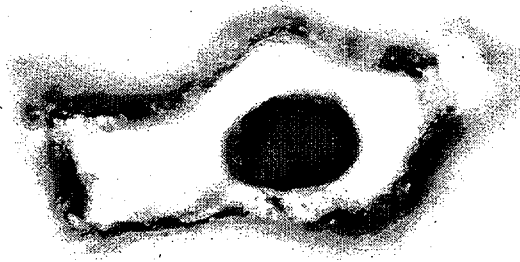


**b**

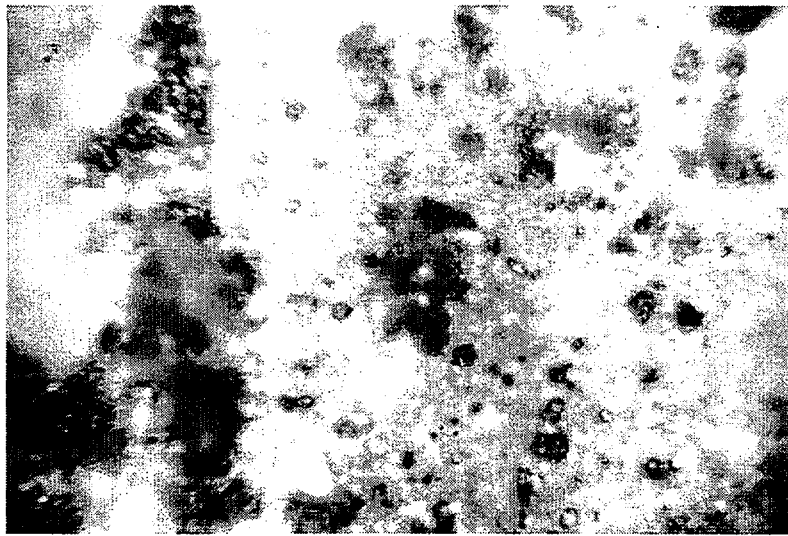


**c**

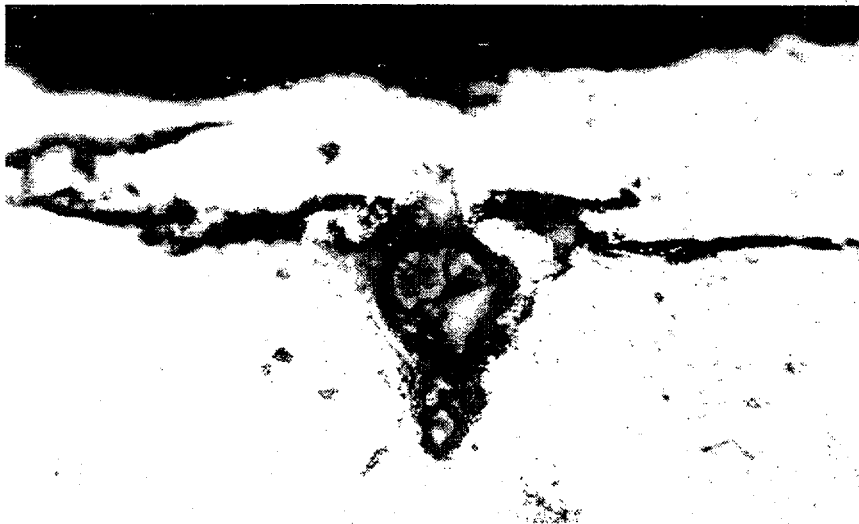
*FIG 3 Nodular corrosion of RBMK-1000 channel tubes inner surface  
Magnification ~ 15(a) 500 (b c)*



**a**



**b**



**c**

FIG.4. The 2<sup>nd</sup> phase precipitation within structure of zirconium alloy of channel tubes:  
*a* - separate particle ZrC at bottom of nodule;  
*b* - fine dispersed aggregates of carbides at bottom;  
*c* - cracking of tubes material near particle ZrC close to surface. Magnitication 500 (*a*),  
 1000 (*b,c*).



secondary inclusions radiation swelling. Analysis of technological residual stresses state within channel tubes material along with the results of material scientific and X-ray diffraction analysis allowed to formulate and substantiate radiation induced mechanism of channel tubes corrosion damage process as follows:

- (1) Zirconium alloy contains the 2<sup>nd</sup>-phase inclusions of amount sufficient for local hydride formation under operational conditions. Increasing of alloy volume by some 13 % in the points of hydrides precipitation is as such being a damage that sufficiently reduces plasticity of material.
- (2) Radiation swelling and corrosion-radiation processes which occur within the 2<sup>nd</sup>-phase precipitation structure lead to appearance of additional local stresses and more intense hydrogenation and embrittlement of zirconium alloy.
- (3) After the certain period of operation the level of stretching stresses in material and at boundary with protective oxide layer is being formed that is sufficient to start with creation of nodules, their subsequent growing, creation of polynodules and areas of complete oxidization.
- (4) Incubation period before initial nodules will appear along with dynamics of nodular corrosion development process are being under control of operational (such as neutrons spectrum and distribution, water and chemical regime, etc.) and engineering factors (such as alloy contamination, level of residual stresses, etc.) taken in totality.

The nodular corrosion model contains availability of the 2<sup>nd</sup>-phase precipitation's and their radiation damage as initial prerequisites to its occurrence and growing. Apparently, the cases of deep (up to  $0,7 \times 10^{-3}$  m) local damage of FC surface after operation during 15 years (see [1]; as well the latest results obtained at NRI on studying of the ChNPP unit 3 FC) was stipulated by prolonged chains of the 2<sup>nd</sup>-phase impurities. This model is valid, first of all, for regular technology of RBMK-1000 channel tubes and their operation conditions.

Model of corrosion-hydride damage of RBMK-1000 channel tubes (up to through defects) is also substantiated with taking into account of increased contamination of alloy with the 2<sup>nd</sup>-phase precipitation [3]. They observed abnormal level of nodular and general corrosion around of through defect at inner surface of tube.

For the other alloys and manufacturing processes under changing of coolant parameters and radiation load during corrosion damaging appropriate adjustment will be introduced.

### 3. CORROSION DAMAGE OF OTHER FC ELEMENTS AND FUEL ASSEMBLY CLADDINGS

At the same time with control over state of channel tubes inner surface there were systematic visual observations arranged at ChNPP site as to kinetics of lower and upper adapter zirconium parts (nipples) oxidization. Initial state of adapters zirconium part material is result of high temperature diffusion welding with the part of stainless austenitic steel OX18H10T. The quite certain regularity of corrosion damage was established along the adapters length.

Initial stage of corrosion is being described by creation of light (as compared with black protective film) oxide layer of some millimeters width from joint "steel – alloy Zr+2.5%Nb". Each stage of corrosion process (appearance of initial oxide ring; oxidization by height of 20...30 mm; complete oxidization of nipple surface; crumbling of oxide film) is located within the certain temporal interval that depends upon individual properties of FC as well as, probably, water and chemical regimes of operation, etc. The main conclusions were made as follows from results of visual observation of adapter nipple surfaces corrosion:

- Sufficient difference was identified between rates of corrosion process growing at upper and lower adapters,
- By period of about 700 effective days oxidization is being completed at the whole nipple surface of lower adapter, and oxidization (peeling) of oxide film starts,

- Process of upper adapter nipple surface oxidization is less intense as compared with lower one, lasts during at least 2100 effective days; at that time peeling of oxide surface does not occur.
- Total surface area of fuel elements (alloy Zr+1.0%Nb) within RBMK-1000 core is as twice as that of Zr+2.5%Nb alloy. However, it was substantiated by experiment that contribution from claddings corrosion for some 2. 4 years of their operation into total corrosion of core zirconium material is insufficient. High corrosion resistance of Zr+1.0%Nb alloy is one of the arguments in favor of fuel assemblies made in Russia using in 5-year fuel cycles [4]

#### 4. PREDICTION OF RBMK-1000 FC OPERABILITY

Circuit of multiple enforced circulation in RBMK type reactors is being addressed as that consisting of two main parts of no principle difference as to sources of corrosion products supply into coolant. Elements of core made of zirconium alloys are being constantly activated under operation of reactor being source of  $^{95}\text{Zr}$  radionuclide direct ingress into the circuit. Under prediction of lower adapters operability [5] the results were used of generalized analysis of experimental facts along with calculated assessments as to preferential corrosion loss of low adapter nipple material by about 2200 effective days of operation. The results of FC elements from Chernobyl and Kursk NPP post-reactor studies showed [5] that intense corrosion of zirconium alloy in lower adapters is initial prerequisite (the 1<sup>st</sup> stage) of their corrosion damage. In some cases the 2<sup>nd</sup> stage is being implemented: accelerated growing of corrosion along boundary of diffusion welding by height of the 1<sup>st</sup> zirconium tooth followed by subsequent through destruction of steel part of adapter by mechanism of intercrystalline corrosion.

Availability of two temporal periods as to corrosion of Zr+2.5%Nb in RBMK-1000 FC was experimentally substantiated, and the maximum value of lower adapters corrosion damage was established by the results of post-reactor studies. The methods were proposed and substantiated to identify relative corrosion rate by direct in-service sampling of corrosion products under reloading of reactor fuel assemblies. Rate of adapter zirconium alloy corrosion was identified by ratio between activity of  $^{95}\text{Zr}$  radionuclide within sample and that of one of the general corrosion product radionuclides having similar half-decay period (for instance,  $^{58}\text{Co}$ ) Products of the circuit steel part corrosion come into core with coolant, being precipitated onto surface, activated, participate in mass exchange. Under substantiated conditions their activity is being used to standardize rate of zirconium alloy corrosion, to develop corrosion dependencies and predict FC elements operability.

#### 5. CONCLUSION

RBMK fuel channels corrosion is one of the components of NPP equipment structural material aging process as well as its operability prediction. In compliance with the current approaches to the aging problem [3], there are two periods occur by the period of failures rate increasing due to aging as follows:

- Initial period of “rejection” when the defects and failures are being implemented stipulated by deficiencies of designing and manufacturing process,
- Period of normal operation.

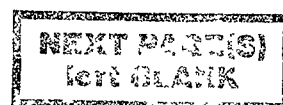
From this point of view period of fuel channels operation before about 2200 effective days should be addressed as “rejection” period. It refers both to lower adapters along with the method to predict their operability based upon observation of FC elements corrosion [5] already implemented in practice and to channel tubes integrity [3].

During normal operation period the other damage mechanisms of their own peculiarities and needing additional study and analysis and begin to reveal themselves [5]. Nodular corrosion moves into stage of total oxidization of channel tubes surface, and consequently – increased hydrogenation

of the whole material . At this stage the priority of intra-reactor control means grows that shall to confirm operability of FC elements by absence of impermissible defects and deviation of structural parameters from maximum permissible values stated in the regulation [6]. Since general corrosion leads to reduction of wall thickness, to control this parameter is of particular attention at NPP with RBMK. At the same time, data of intra-reactor control are consistent with the results of FC material post-reactor studying. Experience gained during operation of units with RBMK-1000 in Ukraine and Russia showed that identifying factor as to operability of fuel channels by about 20 years of operation is not corrosion damage, hydrogenation and degradation of physical and mechanical properties of FC material but exhaustion of gas gap "channel-graphite" [7].

## REFERENCES

- [1] PLATONOV, P., et al., "The RBMK reactors channel tubes corrosion", Workshop on RBMK Fuel Channel Integrity, Internal Report RBMK-SC-039 (Kaunas, Lithuania, 13-17 May 1996), reproduced by the IAEA, Vienna IAEA (1996) 11 (in Russian).
- [2] KARASEV, V., et al., "The nodular corrosion Zr-tubes progressing under neutrons exposure", Voprosy atomnoj nauki i tekhniki, ser.: Radiation damage physics and radiation technology, Is. 1(4), 2(5), Kharkov, KhPTI (1989) 29-37 (in Russian).
- [3] ZARITSKY, N., et al., "On the matter of the RBMK-1000 channel tubes integrity", Internal Report RBMK-SC-039, Vienna IAEA (1996) 7 (in Russian).
- [4] BIBILASHVILI, Yu., ONOUFRIEV, V., "The fuel operation experience on WWER-reactors of Russian NPP'S", the lecture presented at the IAEA Training Courses on WWER Fuel (Russia, Obninsk, June 5-23, 1995) 37 (in Russian.).
- [5] ZARITSKY, N., et al., "The approaches to the steel-Zr transition joints fuel channels of RBMK-1000 operability assessment", Internal Report RBMK-SC-039, Vienna IAEA (1996) 5 (in Russian).
- [6] RESEARCH AND DEVELOPMENT INSTITUTE OF POWER ENGINEERING (RDIPE) OF THE RUSSIAN FEDERATION, Regulation on operational control of the fuel channels, CPS channels and graphite stack of Chornobyl NPP, RDIPE, Moscow (1994) (in Russian).
- [7] INTERNATIONAL ATOMIC ENERGY AGENCY, Internal Report on Workshop on RBMK Fuel Channel Integrity, Internal Report RBMK-SC-039 (Kaunas, Lithuania, 13-17 May 1996), reproduced by the IAEA, Vienna IAEA (1996).



# INFLUENCE OF HYDRAZINE PRIMARY WATER CHEMISTRY ON CORROSION OF FUEL CLADDING AND PRIMARY CIRCUIT COMPONENTS

V. IOURMANOV

Radiation Protection and Chemistry Department,  
VNIIAES, Moscow, Russian Federation



XA9953290

V. PASHEVICH

International Information Academy,  
Russian Federation

J. BOGANCS, P. TILKY, J. SCHUNK, T. PINTER

Paks Nuclear Power Plant Ltd,  
Hungary

## Abstract

Earlier at Paks 1-4 NPP standard ammonia chemistry was in use. The following station performance indicators were improved when hydrazine primary water chemistry was introduced:

- occupational radiation exposures of personnel,
- gamma-radiation dose rates near primary system components during refuelling and maintenance outages.

The reduction of radiation exposures and radiation fields were achieved without significant expenses. Recent results of experimental studies allowed to explain the mechanism of hydrazine dosing influence on:

- corrosion rate of structure materials in primary coolant,
- behaviour of soluble and insoluble corrosion products including long-life corrosion-induced radionuclides in primary system during steady-state and transient operation modes,
- radiolytic generation of oxydising radiolytic products in core and its corrosion activity in primary system,
- radiation situation during refuelling and maintenance outages,
- foreign material degradation and removal (including corrosion active oxidant species) from primary system during abnormal events.

Operational experience and experimental data have shown that hydrazine primary water chemistry allows to reduce corrosion wear and thereby makes it possible to extend the life-time of plant components in primary system.

## 1. INTRODUCTION

At VVER plants a low alkaline reducing primary water chemistry with a boric control is used. Potassium hydroxide is used for chemical neutralization of the acid properties of boric acid. Dosing of ammonia or hydrazine into primary feed water is used for maintaining the required hydrogen concentration and for removing dissolved oxygen. Hydrazine dosing is mainly aimed at reducing the accumulation of radioactive deposits of corrosion products on the inner surfaces of equipment and pipelines of the primary circuit, which will improve the radiation situation and reduce radiation exposure of personnel.

The collective operational exposure of operation and maintenance personnel increases gradually in the course of operational time of power units due to both necessary increase of maintenance work in ageing plants and the increase of radioactive surface contamination of equipment to be serviced. Possible ways for reduction of the collective dose exposure are the use of expensive robotics or/and carrying out chemical decontamination. The main disadvantages of the last method are production of large volume of radioactive waste and accelerated recontamination on surfaces of primary systems during following operation period. According to the results of investigations the corrosion of constructional materials in primary systems produces radionuclides giving the highest contribution in radiation dose exposures.

The primary water chemistry improvement has been used to reduce corrosion processes as well as activation and migration of corrosion products at power units 1-4 of Paks Nuclear Power Plant.

## 2. THE IMPACT OF HYDRAZINE PRIMARY WATER CHEMISTRY ON RADIOACTIVE CONTAMINATION OF PRIMARY SYSTEM, DOSE RATES AND PERSONNEL EXPOSURES

### 2.1. General Description of Primary Water Chemistry

At NPP Paks the hydrazine primary water chemistry has been introduced since 1991 to reduce both radioactive contamination of primary system components and occupational exposures of personnel. These tasks were reached at Paks 1-4 NPP mainly owing to the influence of hydrazine on corrosion control of fuel cladding and primary circuit components during plant power operation.

In 1991 hydrazine primary water chemistry was introduced at the most contaminated unit 2 after six years operation using the standard ammonia primary water chemistry. After receiving positive results at unit 2 the hydrazine primary water chemistry was also introduced at units 1, 3 and 4.

Operational experience with primary hydrazine water chemistry at VVER type units of Paks NPP was presented and discussed by plant chemists during previous international conferences [1-5, 6-7, 9, 11-12, 14-15]. The obvious advantages of primary hydrazine water chemistry were proved by plant operational data. Nevertheless some deficiencies in comparative analysis of operational data, lack of theoretical explanations of hydrazine influence on corrosion process and behaviour of produced radioactive corrosion products were noted during previous discussions.

Taking into account the above mentioned circumstances this report contains:

- analysis of operational data of primary hydrazine water chemistry of Paks 3-4 NPP between 1995-1998 on the base of new statistic data processing procedure
- new experimental and operational data were gained to analyse hydrazine influence on corrosion process and behaviour of produced radioactive corrosion products.

The 3-year operational data of Paks 3-4 NPP with primary hydrazine water chemistry (1995-1998) were compared with similar data during previous 3-year operation period (1993-1995) using standard ammonia water chemistry in order to provide representative comparative analysis. The proposed statistic data processing procedure allows avoiding significant influence of operation data fluctuation on average values due to calculations for 3-year period. The primary hydrazine water chemistry has been introduced at both units (3 and 4) since refuelling outages in 1995. To this moment the operational personnel has 2-4 year experience of primary hydrazine water chemistry at units 1 and 2. As a result more stable primary hydrazine water chemistry has been regularly maintained at units 3 and 4 in 1995-1998 compared to initial period of primary hydrazine water chemistry introduction at power units 2 and 1. The most important fact that there were not any significant abnormal events in primary systems during last 6 fuel cycles of unit 3 and 4 comparatively to operational history of power unit 2 [2, 16].

During the first 3 years operational period of power units 3 and 4 with hydrazine water chemistry special attention has been paid to compare radiometric measurements carried out at the same places and equipment with the same conditions disregarding other operational and maintenance points.

### 2.2. Corrosion products activities in primary coolant

The processing of primary coolant radiochemical control data showed that the activity values of insoluble corrosion products increased up to 3-4 times of the values measured during operation with standard ammonia water chemistry but later a gradual decrease reaching one third part of the original value was observed [1]. The results of special investigations performed by Veszprem University during 1996-1998 manifested effect of hydrazine water chemistry on the change of activities of

corrosion origin radionuclides in primary coolant during operational period of units 1-4. The activity of both soluble and particulate (larger than 0.45 micrometer) corrosion products in primary coolant was generally increasing during operation of unit 1-4 with standard ammonia water chemistry. On the contrary to the above mentioned the activity of corrosion products in primary coolant was generally reduced during following power operation with hydrazine primary water chemistry. The data presented in Fig. 1-2 are given for illustration of these facts. This behaviour of corrosion products may be explained by both reducing of general corrosion rate of stainless steel in primary system and redistribution between different forms of corrosion products including complexes of metals with ammonia and hydrazine in case of reducing primary water chemistry conditions.

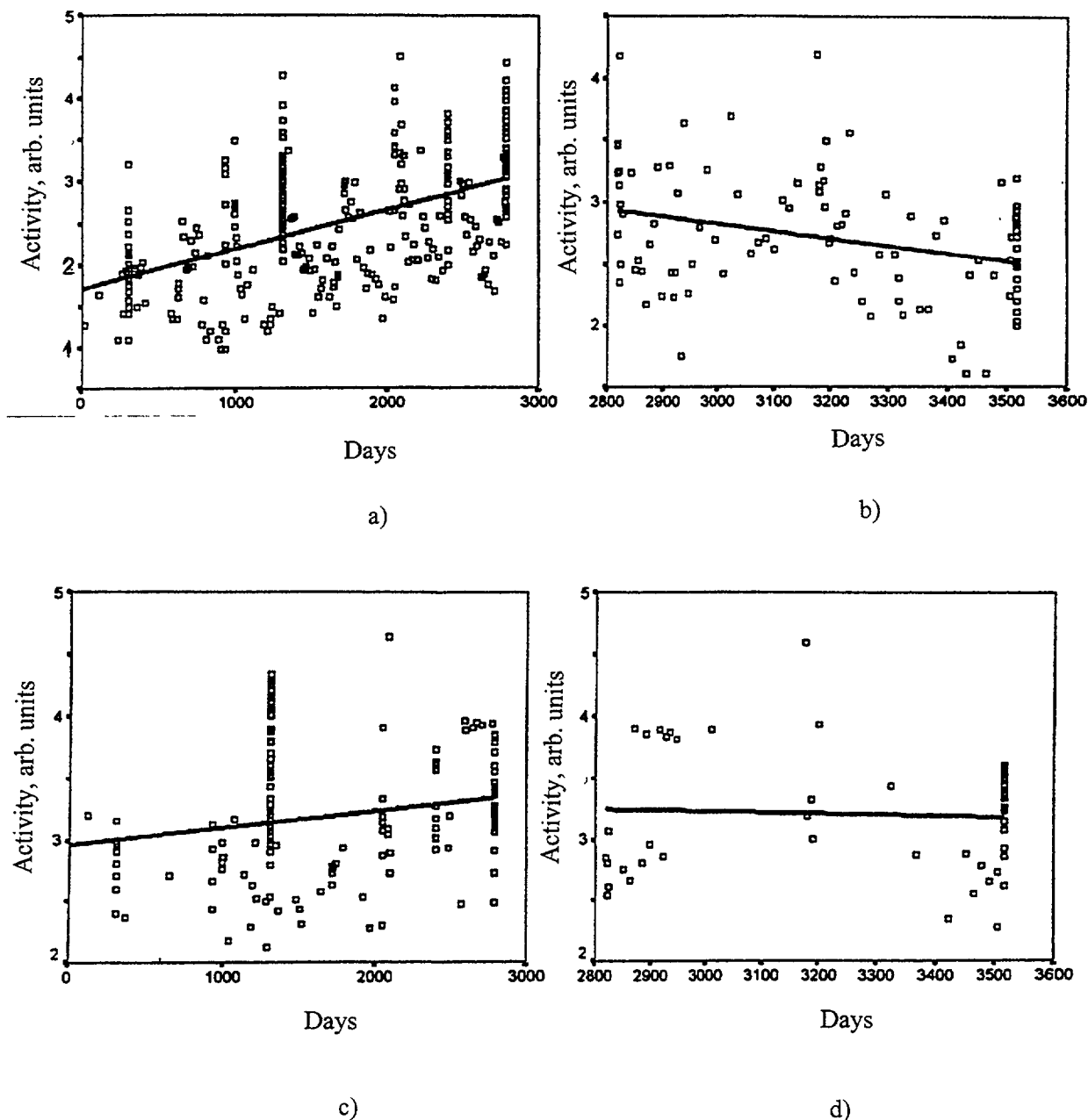


Fig. 1. Trend of Co-60 activity (arbitrary units) in primary coolant of Paks NPP, Unit 4 during operation with ammonia (a, c) and hydrazine (b, d) water chemistry - for particulate ( $\geq 0.45 \mu\text{m}$ -a, b) and soluble and colloid forms ( $\leq 0.45 \mu\text{m}$ -c, d).

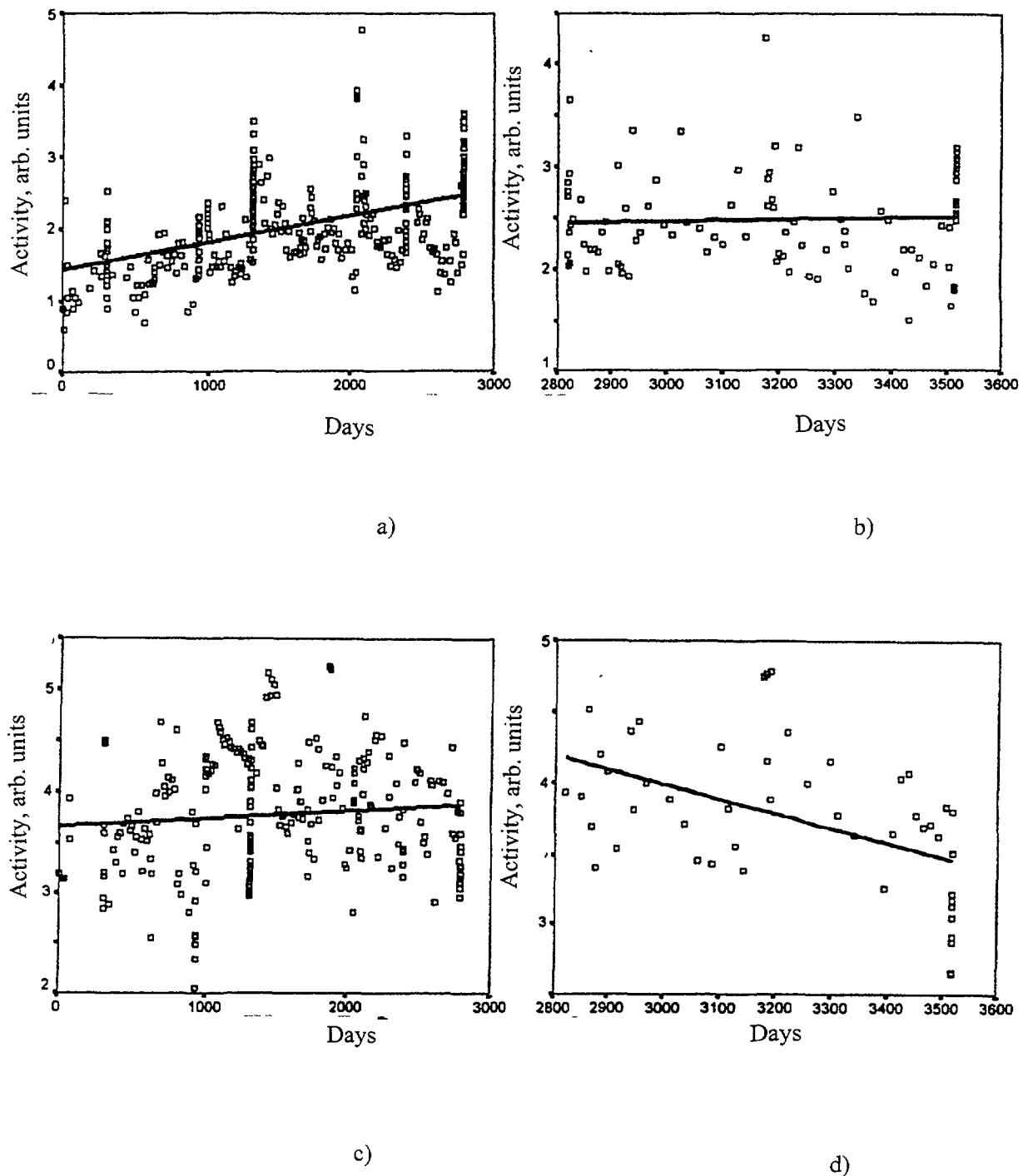


Fig. 2. Trend of Ag-110m activity (arbitrary units) in primary coolant of Paks NPP, Unit 4 during operation with ammonia (a, c) and hydrazine (b, d) water chemistry - for particulate ( $\geq 0.45 \mu\text{m}$ -a, b) and soluble and colloid forms ( $\leq 0.45 \mu\text{m}$ -c, d).

The experts from AEA Winfrith concluded that the lowest radioactivity of primary coolant amongst similar values measured at different WWER plants have been determined at Unit 2 of Paks NPP [1, 2]. It was also pointed out by them that during transient operation (i.e. shut-down, start-up) the lowest increase in corrosion product concentration could be determined after introducing the hydrazine water chemistry [1, 2].

### 2.3. Surface contamination

The primary system surfaces outside the core will also be contaminated by radionuclides transported by primary coolant. This contamination is monitored every year by in-situ gamma spectrometry at selected 4 points of main circulating loops (2 in cold and 2 in hot leg). During the 3-year periods before and after the hydrazine water chemistry introduction the surface contamination of primary equipment was measured by electrochemical and scrub sampling followed by the in-situ gamma spectrometry. Results of the above measurements are presented in Table 2. and Figures 3-4. indicating a characteristic decrease in surface contamination after the hydrazine water chemistry introduction. The highest decrease of surface contamination due to the hydrazine water chemistry introduction was determined in steam generator (SG) and on different parts of main circulating pumps (MCP).

### 2.4. Radiation dose rates

As a consequence of change in radioactive contamination of surfaces in primary system components, the gamma radiation dose rate values measured surrounding the primary equipment has also been changed after the hydrazine water chemistry introduction. The prediction and reduction of dose rate values are necessary for planning and reduction of personnel occupation exposures.

The average (3 year before and after the hydrazine water chemistry introduction) dose rate values surroundings the main circulating loops of units 3 and 4 measured by Health-Physics Section of Paks NPP as well as reference points for radiometric measurements in primary system equipment (main circulating loops, steam generators, main circulating pumps) are shown on Figures 5-6 and Tables 1 and 3. In addition it can also be well seen that at Unit 1 dose rate values after its 6<sup>th</sup> hydrazine water chemistry cycle did not exceed the values measured during last ammonia cycle. The increase of dose rates at unit 2 at 1996-1997 was related to the foreign material ingress into the primary circuit during its 12<sup>th</sup> campaign. Results of Units 3-4 show unambiguous decrease and dose rate values are very low even in international comparison.

In order to evaluate the effect of hydrazine water chemistry, the dose rate values are also measured at those places where in-situ gamma spectrometric determinations were carried out and compared to those values calculated from the measured isotope composition. The calculated and measured values show good agreement [1, 4-6]. The values calculated from in-situ measurements reflect the water chemistry effects.

The operational data unambiguously express that after introducing hydrazine water chemistry the re-contamination of surfaces following a chemical decontamination is very low or even in comparison with this effect in case of ammonia water chemistry.

### 2.5. Collective dose exposure

As a consequence of dose rate reduction dose exposures during maintenance work have also decreased due to introduction of hydrazine water chemistry. Assuming that maintenance tasks are growing as the function of age of the units it can be said that the origin of collective dose exposure reduction given on Figure 7 was due to the change in primary water chemistry. The extent of dose rate reduction was between 22-55%. The highest percent was registered in surrounding the equipment having high dose rate values. The average dose exposure reduction was reached as high as 25-35% taking into consideration the amount of work carried out on different equipment.

The maximum saving in collective dose was calculated as the difference between the real values and that of expected without introducing hydrazine primary water chemistry. Calculating the minimal saving our intention was to take into account the effect of differences in the amount of maintenance works carried out. So, the base of our calculation was the real collective dose exposure during the



TABLE I. GAMMA-DOSE RATES ( $\mu\text{Gy/h}$ ) DETERMINED AT IN-SITU MEASURING POINTS OF MAIN CIRCULATING LOOPS OF UNIT 4 USING FAG-TYPE INSTRUMENT

Years	Water chemistry	Measuring point / Dose rate			
		1	2	3	4
93-95	NH <sub>3</sub>	183	220	517	534
96-98	N <sub>2</sub> H <sub>4</sub>	117	148	370	295

TABLE II. RADIOACTIVE CONTAMINATION OF PRIMARY SURFACE OF UNIT 4 MAIN CIRCULATING LOOPS GIVEN AS AVERAGE VALUES FOR THE LAST 3 YEAR PERIODS WITH AMMONIA AND HYDRAZINE WATER CHEMISTRY

Water chemistry	Loop	Isotope, kBq/cm <sup>2</sup>					
		Cr-51	Fe-59	Co-58	Mn-54	Co-60	Ag-110m
NH <sub>3</sub>	Cold	42	6.7	24	6.5	42	2.2
N <sub>2</sub> H <sub>4</sub>		26	1.8	7.5	3.5	37	1.8
NH <sub>3</sub>	Hot	16	1.3	6.8	4.7	9.3	0.9
N <sub>2</sub> H <sub>4</sub>		10	1	5.5	3	8.8	1

TABLE III. GAMMA-DOSE RATES ( $\mu\text{Gy/h}$ ) MEASURED AROUND PRIMARY MAIN EQUIPMENT OF UNIT 4, AND GIVEN AS AVERAGE VALUE FOR THE LAST 3 YEAR PERIODS WITH AMMONIA AND HYDRAZINE WATER CHEMISTRY

Water chemistry	Loop	Isotope, kBq/cm <sup>2</sup>					
		Cr-51	Fe-59	Co-58	Mn-54	Co-60	Ag-110m
NH <sub>3</sub>	Cold	42	6.7	24	6.5	42	2.2
N <sub>2</sub> H <sub>4</sub>		26	1.8	7.5	3.5	37	1.8
NH <sub>3</sub>	Hot	16	1.3	6.8	4.7	9.3	0.9
N <sub>2</sub> H <sub>4</sub>		10	1	5.5	3	8.8	1

maintenance work and the saving in collective dose exposure was estimated being proportional to 30% of average dose rate reduction.

Economical benefit for introducing hydrazine primary water chemistry was calculated on the base of financial regulations at Paks NPP, according to which 1 man-mSv saving in dose exposure is equal to \$500. The overall costs of hydrazine hydrate consumption for primary water chemistry (about \$8000 per year) is 6 times higher than the cost of ammonia consumption during standard primary water chemistry. The financial benefit calculated with the above mentioned data is equal \$50000 for the cleanest power units 3 and 4.

The collective dose of personnel related to electrical energy production gradually increased from the value of 1,3 man-Sv/GW in 1984 up to 2,6 man-Sv/GW in 1991. Beginning from 1992 it has been decreasing again down to 1,3 man-Sv/GW in 1997.

TABLE IV. FUEL PERFORMANCE IN DIFFERENT TYPES OF POWER REACTORS AT THE BEGINNING OF 90's ACCORDING TO STATISTICS OF PLANT OPERATORS

Plant operator/Fuel vendor/plant producer	Reactor type	Number of units	Typical failure rate for fuel rods before 1990, %	Typical failure rate for fuel rods, beginning of 90s, %
USA/ ABB, B&W, Siemens, Westinghouse, GE, Siemens	PWR	114	0.012 (1986)	0.005
	BWR		0.013 (1986)	0.0015
Siemens	PWR+BWR	30+15		0.001
ABB Atom	PWR+BWR	6+16		0.006
France/Fragema	PWR	50		0.0015
Canada	CANDU			≤0.1 (for FA)
Former Soviet Union/Eastern Europe	RBMK-1000	13		0.05
	RBMK-1500	2		0.02
	WWER-440	26	2-6 % for FA (70s)	0.007
	WWER-1000	17		0.008
Paks NPP:	WWER-440	4	0.0065 (1983-96)	
Unit 1			0.0052	
Unit 2			0.0051	
Unit 3			0.0089	
Unit 4			0.0068	

### 3. PECULIARITY OF HYDRAZINE PRIMARY WATER CHEMISTRY DURING ABNORMAL EVENTS RELATED WITH FOREIGN MATERIAL INGRESSES

Regulatory bodies, operating organizations and fuel manufacturers have been recently concerned about a relative growth of the number of abnormal events at NPPs, associated with foreign material ingress into the primary systems. In July 1995 INPO published a report covering similar events at 12 NPPs, in April 1997 and August 1998 an expert group of the IAEA made an analysis of more than 100 events of this type, in 1997 VNIAES prepared a report with the analysis of 15 similar events at VVER and RBMK plants. The danger of these abnormal events is related with a wide spectrum of possible negative effects for plant safety protective barriers, such as fuel claddings and primary systems. Foreign material can lead to disturbances in operation of control rod system, deterioration of radiation situation and erosion-corrosion failures of fuel cladding, primary equipment and pipelines. The study of abnormal events revealed additional problems to be handled by primary water chemistry, including the removal of corrosion-dangerous contamination and/or the introduction of neutralizing reagents.

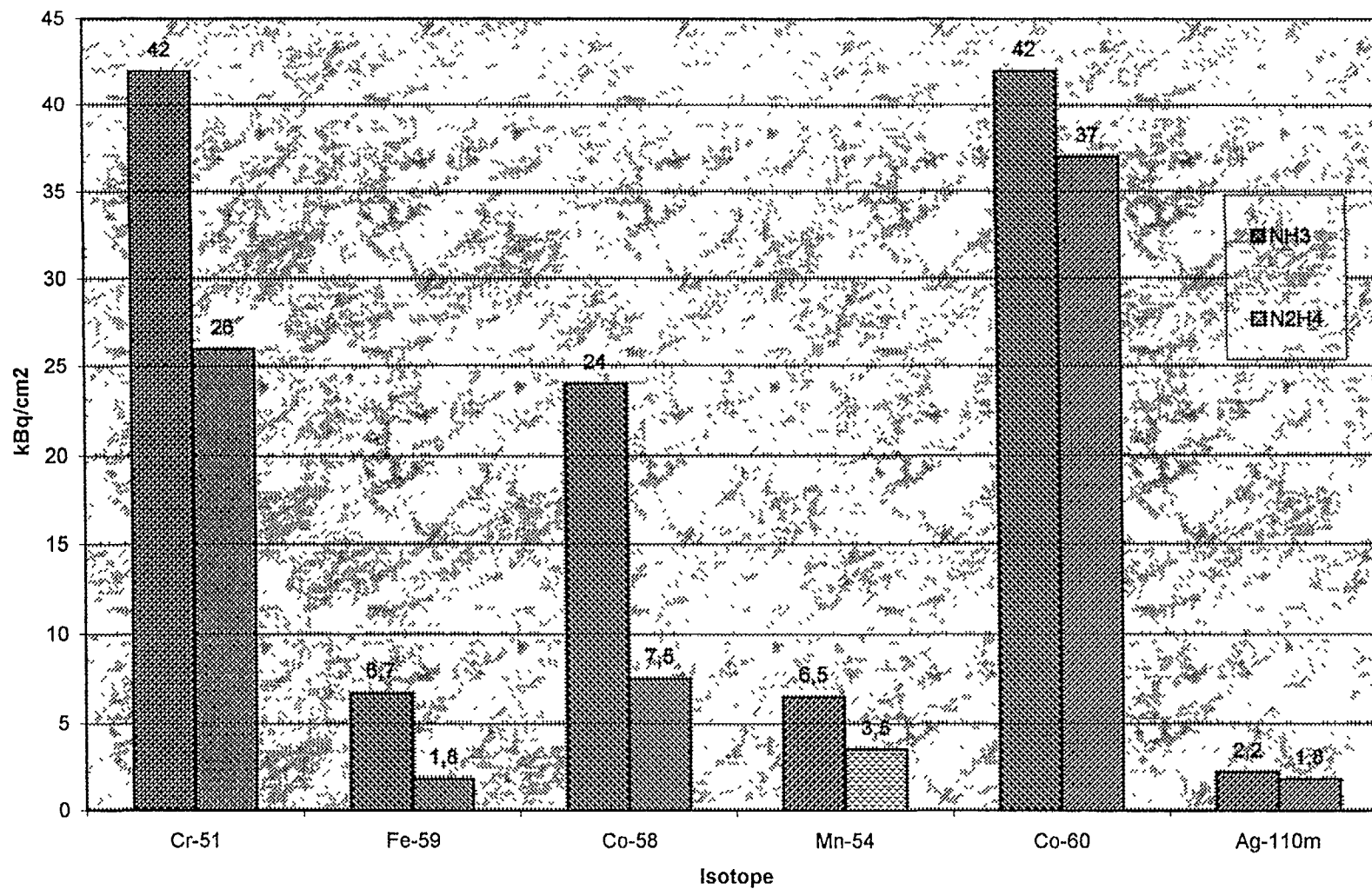


Fig 3. Comparison of an average 3-year surface contamination in reference points near cold legs of main circulation loops at Paks NPP, Unit 4 for ammonia and hydrazine water chemistry

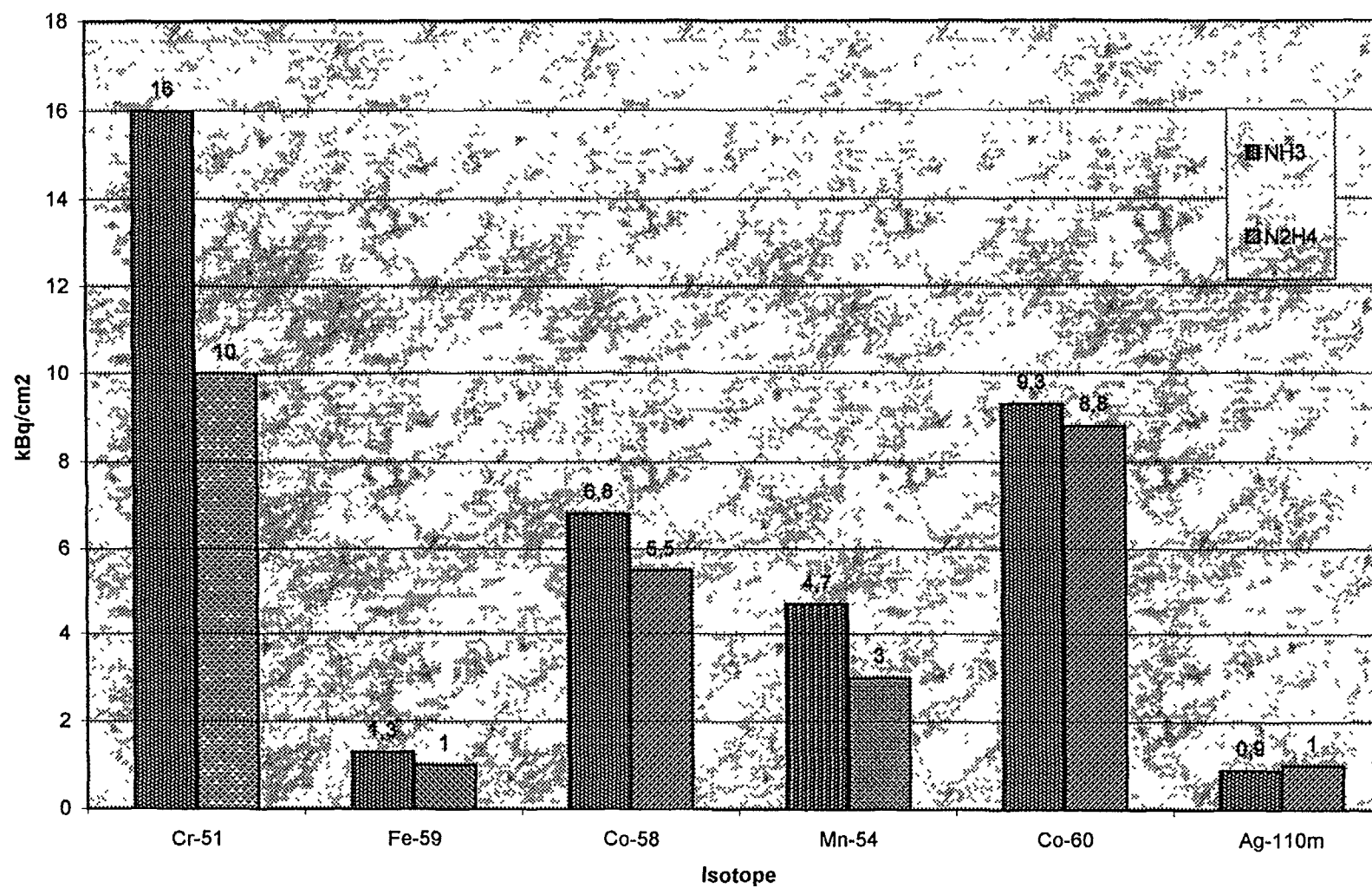


Fig. 4. Comparison of an average 3-year surface contamination in reference points near hot legs of main circulation loops at Paks NPP, Unit 4 for ammonia and hydrazine water chemistry

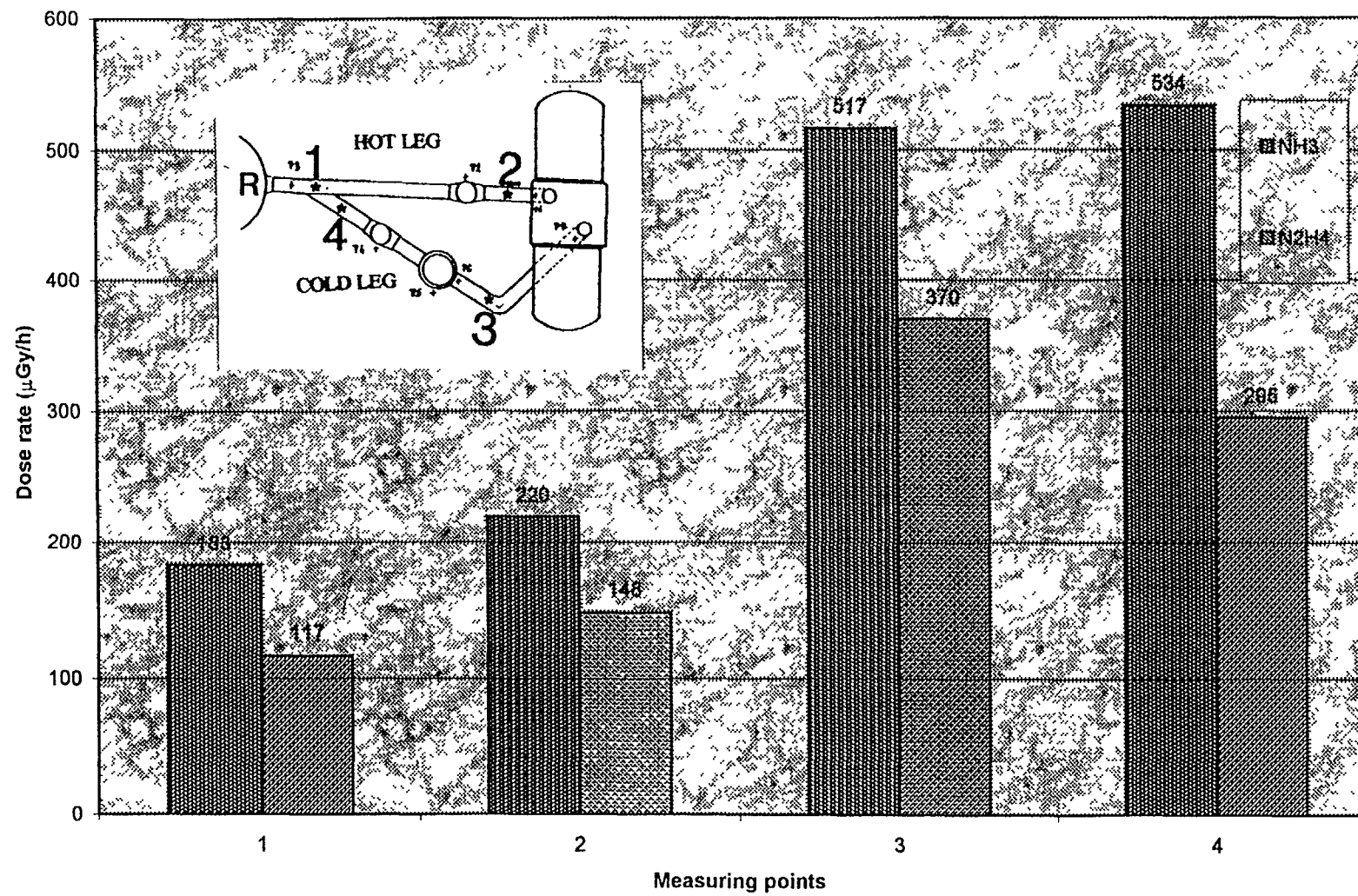


Fig. 5. Comparison of an average 3-year dose rate in reference points near main circulation loop at Paks NPP, Unit 4 for ammonia and hydrazine water chemistry.

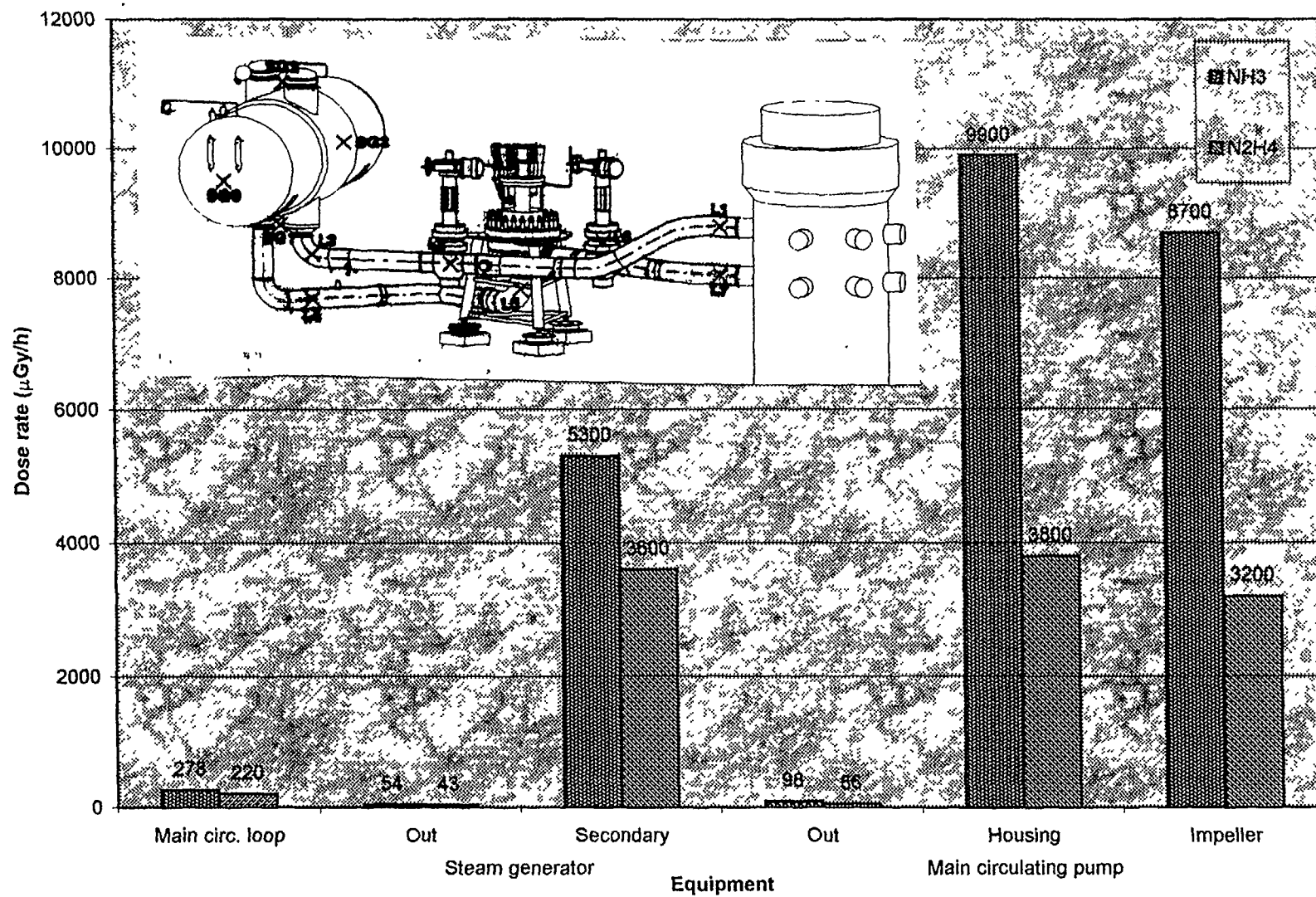


Fig. 6. Comparison of an average 3-year dose rate in reference points near main primary system equipment at Paks NPP, Unit 4 for ammonia and hydrazine water chemistry

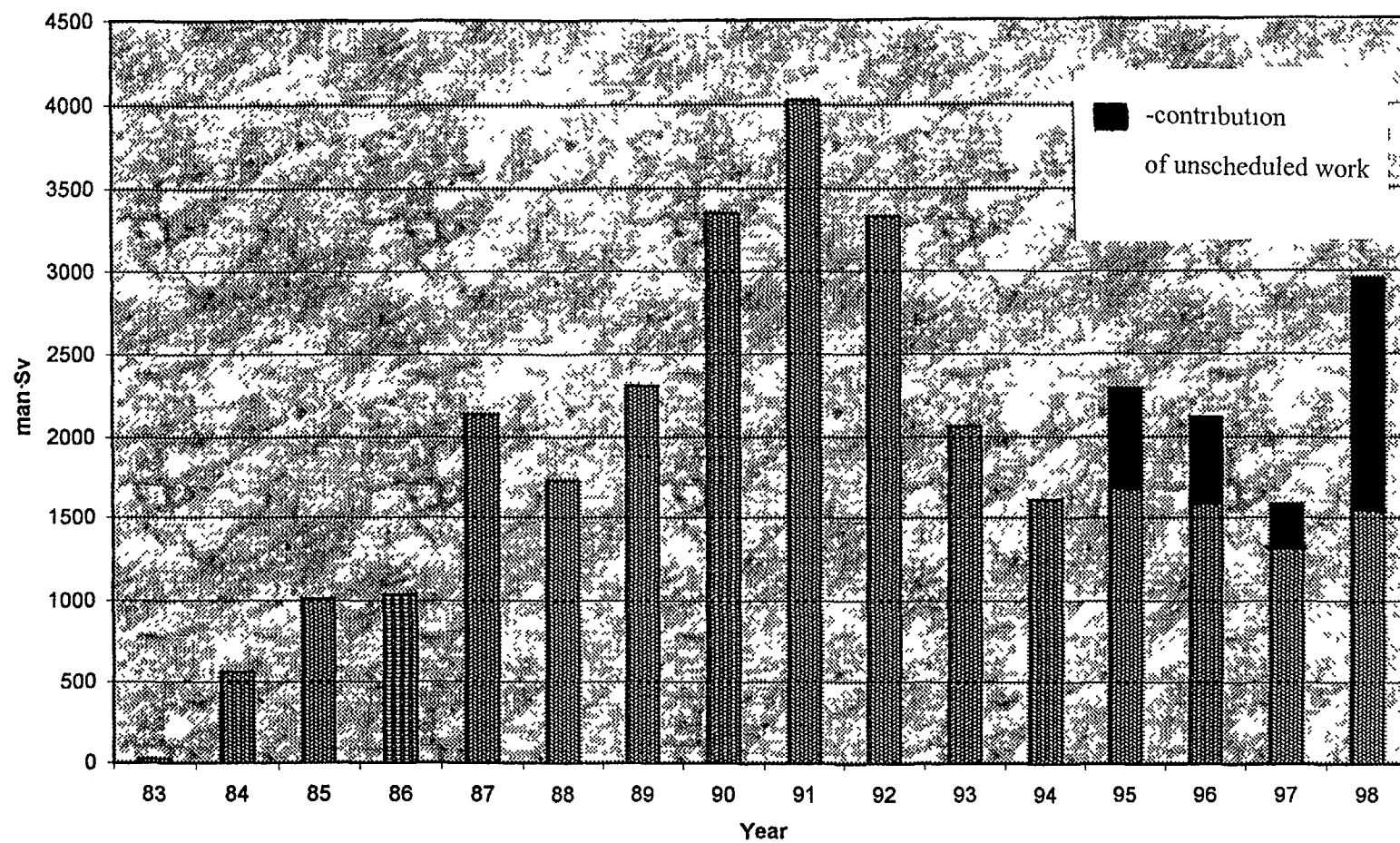


Fig. 7. Trend of occupational exposures at Paks NPP



A comparative analysis of disturbances observed at plants due to ingress of foreign materials and substances into the primary systems has shown the principal advantage of hydrazine water chemistry in comparison with the standard ammonia water chemistry at VVER. Moreover, the dosing of hydrazine-hydrate into the coolant of the primary circuit was successfully used for solution of serious operating problems, as proved by a number of events.

During power operation of the VVER-1000 "A" about 3 m<sup>3</sup> of a 5% nitric acid ingress into the primary coolant was observed. The coolant pH value has decreased to 2.1, coolant samples demonstrated the bursts of iron and zirconium concentrations up to 0.67 ppm and 26 ppb respectively, which indicated a destruction of the protective oxide films of fuel claddings and primary equipment. A "radiation-chemical burning out" of nitric acid at the working parameters by means of dosing of hydrazine-hydrate into the coolant before unit shut-down was used to minimize corrosive action of nitric acid on the primary circuit surfaces as well as to avoid possibility of dangerous alkaline corrosion of zirconium and additional loading on the fuel claddings under conditions of increased corrosive aggressiveness of the coolant.

In addition, the reduction of both the temperature and the ionizing radiation would result in a sharp decrease of the rate of radiolytic decomposition of nitric acid, thus, it can lead to long-term corrosive action of an acid medium on the surfaces of fuel claddings and primary equipment. To prevent local chloride cracking of austenitic steel and corrosion of fuel claddings under conditions of a low pH value, it is necessary to reduce oxygen concentration below an operating level 5 ppb. The presence of nitrate-ions in the coolant (0.3 ppm) representing an efficient acceptor of hydrated electrons, as well as the reduction of pH value to 2.1 resulted in amplification of radiolysis of the water coolant with an increase of the radiolytic yield of oxygen, that intensifies corrosion processes. Thus, the dosing of hydrazine into the primary circuit but not of ammonia or potassium hydroxide, has ensured the fastest decomposition of nitric acid.

At WWER power unit "B" being operating at nominal power, the increase of oxygen concentration up to 20-100 ppb was periodically observed in the primary coolant despite the presence of dissolved hydrogen in the sufficient concentration. The cause for absence or a sharp decrease of the radiolytical binding rate of oxygen and, as a consequence, the increase of oxygen concentration in the coolant in periods of the considered disturbances of primary water chemistry during the reactor power operation was the ingress of nitrate-ion of 1 ppm in the primary coolant, which is representing the efficient acceptors of reducing radicals (atomic hydrogen and hydrated electron). In this case, the molar concentration of nitrate-ion in the coolant was exceeding the oxygen concentration approximately 36 times. The rate constants of interaction of oxygen and nitrate-ion with the reducing radicals are of a similar order, therefore, in a situation under consideration the rate of radiolytical binding of oxygen was reduced by tens of times because of the presence of nitrate-ion, which is more efficient acceptor of reducing radicals than oxygen. On the base of the above mentioned facts, a hydrazine dosing was used into non-deaerated diluted solutions of ammonia, potassium hydroxide in a required amount in accordance with the oxygen concentration.

Thus, the dosing of hydrazine-hydrate into the primary circuit, for instance, when conducting the hydrazine water chemistry prevent the development of dangerous processes of the corrosive cracking of austenitic steel and nodular corrosion of the zirconium alloy at typical disturbances of the water chemistry.

Some of the WWER-1000 units used periodical hydrazine treatment of the primary circuit surfaces with hydrazine concentration in primary coolant up to 5-20 ppb. Due to performing this treatment, it became possible to wash out deposits from the primary circuit surfaces and thereby to reduce considerably the extent of their roughness, including the fuel assemblies guide channels, that explained the possibility for achieving the improvement of control rod system operation. The comparative studies, confirmed the "slimeless" properties of hydrazine water chemistry. In



comparison with the standard ammonia chemistry a considerably smaller stationary level of the surface contamination by corrosion product deposits and consequently, a smaller roughness can be achieved.

The abnormal events of power operation of reactors under conditions of the throwing of a considerable mass of foreign metal articles previously was noted at two WWER power units. In the first of the stated cases due to damage of the MCP, about 30 kg of metal fragments and about 8 kg of graphite-fluoroplastic moulding material of the MCP seals got into the primary circuit. In the process of the operation neptunium has appeared in the coolant. During the testing after the first fuel cycle 6 gas-leak fuel assemblies (FAs) were detected and after the second and the third fuel campaign - 1 and 3 failed FAs respectively. According to the results of post-reactor studies of these FAs ingress of organics into the coolant was a cause of nodular corrosion of the fuel element claddings. In the second case under consideration the MCP heat barrier was damaged with a release of about 86 kg of small metal chip into the primary circuit. The rise of fission product activity in the coolant indicated the appearance of gas-leak claddings of fuel elements, apparently due to the increased thermal stresses.

It was studied how the permanent hydrazine dosing into the coolant influenced the contamination of primary circuit surfaces when a repair plug was left in the "hot" collector of a steam generator at unit 2 of Paks NPP [2]. The increased concentration of corrosion products in the coolant during the 12-th fuel campaign in comparison with the previous one was stipulated not so much by the corrosive wear of the repair plug, but by washing out the corrosion product deposits from the circuit inner surfaces by small particles of the collapsed repair plug which were circulating in the primary circuit.

The circulation of the smallest particles of the repair plug fragments in the primary circuit could assist to washing out of the radioactive deposits from inner surfaces of the primary circuit into the coolant flow, however, under conditions of hydrazine primary water chemistry in contrary to a standard ammonia-potassium water chemistry negative intensive re-deposition of radioactive contamination into out-of-core parts did not appeared. The presented data allow to assume not only the strengthening of protective properties of the oxide films on the primary circuit inner surfaces after the hydrazine water chemistry implementation but a change of the mechanism of activity mass-transfer from the reactor to out-of-core parts, as well.

The comparative analysis of operation data of Paks NPP during the 12-th fuel cycle of unit 2 does not indicate sharp deterioration of the fuel reliability. According to the analysis of operating data, probably only one gas-leak FA appeared in the core by the beginning of 1996, which was developing during this campaign.

The use of hydrazine water chemistry in the primary circuit results not only in the improvement of radiation situation on the equipment in the periods of repair and refueling outages but also ensures a considerable reduction of negative consequences in case of possible abnormal events with foreign material ingress into the primary systems.

#### 4. FUEL RELIABILITY INDICATOR

More than 50 reactor-year operating experience have been accumulated at the Paks NPP. During this period fuel performance was carefully controlled by in-core measurements monitoring the fission radionuclide activities of the primary coolant as well as by occasionally performed sipping tests during reactor outages.

The influence of primary water chemistry on corrosion resistance of fuel claddings can be directly studied during post-reactor investigations in hot cells. Post-reactor inspections of irradiated fuel

assemblies were not carried out at Paks NPP. As a result only operational data of fuel integrity control during reactor operation can be used for fuel performance evaluation at Paks NPP.

Automatic equipment has been developed and since 1996 installed at Paks NPP for continuous measurement of the radioiodine isotopes. This system provides information about the activity levels of 5 iodine isotopes 131-135. These isotopes can be regarded as representatives of the fission products and may be good indicators of the fuel elements tightness. Special software and hardware are used in this system to receive correct data and to avoid malfunctions or false information. The radioiodine analyzer operating at Paks NPP continuously provides activities of 5 iodine nuclides in every 15 minutes. These continuously produced data are very useful on the contrary to data of the laboratory manual analysis. This system as a controller of the fuel element cladding tightness is a useful tool in nuclear reactor safety [11].

A relatively simple method has been developed for characterization of fuel performance during reactor operation by analyzing both volatile and non-volatile radionuclides (iodine, cesium and transuranes) in the primary coolant. The method includes calculation the number of defected elements on the base of the EPRI recommendations and the standard leak parameters empirically determined by Russian experts for WWER-440 reactors. The method is comparatively evaluated. According to the in-core measurements of fuel performance the calculated failure rate on fuel element basis at Paks NPP was 0.007%. The calculated results of failure rates at Paks NPP are summarized in Table 4 and compared with the published experience of other Plants and fuel vendors [12].

There are some reasons for fuel clad failures, which should be taken into account using non-direct method of fuel performance evaluation. Some of them are connected with:

- design (oblateness of fuel element claddings and compacting of fuel tablets, fretting-corrosion of fuel rods, growing and winding of fuel rods in assemblies, etc.),
- fabrication (internal local hydrogenation, enriching mistakes and filling a fuel element with fuel tablets, defects of welding),
- operation (waterside corrosion of fuel claddings).

As a result only good fuel performance guarantee absence of corrosion failures and fabrication or design deficiencies.

Since beginning of 1990<sup>th</sup> the World Association of Nuclear Operators (WANO) developed and implemented NPP Performance Indicator Program. WANO members worldwide collect and report data on the 10 WANO performance indicators. Some of these WANO Performance Indicators are related to water chemistry (Chemistry Index) and its influence on fuel reliability (Fuel Reliability Indicator), on radiation situation and occupational exposures of personnel (Collective Radiation Exposure), on radioactive waste accumulation (Volume of Low-Level Solid Radioactive Waste) [15].

The purpose of the chemistry performance indicator is to monitor operational chemistry control effectiveness. The indicator is based on concentrations of important impurities and corrosion products in selected plant systems by reactor or steam generator blow down water. In BWRs, the focus is on the control of the reactor coolant chemistry and in PWRs and gas cooled reactors, the secondary system chemistry. The chemistry indicator combines several key chemistry parameters into a single indicator that can be used as an overview of the relative effectiveness of plant operational chemistry control.

The purpose of the collective radiation exposure indicator is to monitor efforts to minimize total radiation exposure at each facility and in the worldwide nuclear industry as a whole. This parameter is a measure of the effectiveness of radiological protection programs in minimizing radiation exposure to plant workers.

The purpose of the volume of solid radioactive waste indicator is to monitor progress toward reducing the volume of waste destined for disposal. Reducing the volume of waste will decrease storage, transportation, and disposal needs, and will improve public perception of the environmental impact of nuclear power. This indicator is defined as the volume of solid radioactive waste that has been processed and is in final ready for disposal, during a given period.

The fuel reliability indicator characterises the integrity of fuel. The purpose of the fuel reliability indicator is to monitor industry progress in achieving and maintaining high fuel integrity, and to foster a healthy respect for preservation of fuel integrity. Failed fuel represents a breach in the initial barrier preventing off-site release of fission products. Failed fuel also has a detrimental effect on operating cost and performance, and increases the radiological hazard to plant workers. The fuel reliability indicator provides a general measure of the extent to which the reactor coolant activity is increased as a result of fuel defects. A reactor core containing one or more defects is likely to produce indicator values (under steady-state conditions) greater than 19 Bq/g for PWRs and WWERs. It is recognised that some breaches in fuel cladding are only apparent by short duration activity spikes following significant power changes. A minor breach of this type does not increase indicator values significantly, has little impact on plant operation, and does not measurably increase worker radiation exposure. For this indicator, fuel reliability is inferred from fission product activities present in the reactor coolant. Due to design differences, this indicator is calculated differently for different reactor types.

In case of Pressurized Water Reactors (PWRs) including WWERs this indicator relates to the steady-state primary coolant iodine-131 activity (Bq/g) and adjusted to surface uranium pollution (the uranium tramp) and normalized to a designed value of purification rate of primary coolant clean-up system equipped with anion-exchangers or mixed bed demineralizers. The fuel indicator data of WWER plant and some of PWR plant during last years are summarized in Table 5. Lower value of fuel indicator or corrected I-131 activity indicates fewer fuel defects. The Paks NPP's fuel indicator data are typically better than the world wide median values for all PWR and WWER units excepting 1995. The presented data show that during 1991-1996 Paks NPP had a better values of fuel performance indicator than the worldwide median values and most of the WWER plants excepting 1995 - Figures 8-11.

The reason of extremal values of this indicator in 1995 was an abnormal event at power unit 2 related to foreign material ingress into primary system. On Unit 2 in 1996 during the refuelling outage large amount of foreign material pieces were found in primary system. The pieces were originated from a temporary protecting cover that had been left in the header of a steam generator. It is assumed that after the cleaning of primary system part of foreign material remained in the system and when circulating with the coolant flow mechanically eroded the protective magnetite layer on the system surfaces.

The consequences of this problem appeared later. At Paks NPP on Unit 2 during the 14-th fuel cycle asymmetry of the fuel assembly outlet temperature field was discovered. The asymmetry was caused by clogging of several fuel assemblies due to build-up of deposit of corrosion products. The erosion caused by foreign material in the system and the chemical effect of decontamination resulted in damage of the protective layers on the inside surfaces of primary circuit and consequently intrusion of corrosion products into primary coolant. The high concentration of corrosion products led to crud build-up in the fuel assemblies and to partial clogging.

The decontamination carried out during outage (1-2-3 cycles in steam generators No1-2-3 respectively) also chemically contributed to the removal of protective layer from the surfaces. As a result the accelerated dissolution of cleaned surfaces of stainless steel tubing bundle in steam generators was initiated. Due to erosion and dissolution during the last two fuel cycles big amount of corrosion products was transferring in the reactor. During the outage part of loose deposit fell out from the fuel assemblies into the reactor and the refuelling pool and part remained inside the assemblies. These loose corrosion products following the last outage when the main coolant pumps

TABLE V. FUEL RELIABILITY INDICATOR OF NPPs WITH WWER AND PWR REACTORS (STEADY-STATE I-131 ACTIVITY IN PRIMARY COOLANT IN Bq/g CORRECTED FOR URANIUM TRAMP CONTRIBUTION AND NORMALIZED TO COMMON PURIFICATION RATE)

		1991	1992	1993	1994	1995	1996	Average
NPP	Kola1	2237	4932	4544	1220	5830	3708	3745.00
and	Kola2	7322	3991	6509	1862	3560	2063	4218.00
Power	Kola3	88	474	197	570	464	166	326.00
Units	Kola4	139	162	286	122	142	108	160.00
VVER	NV3	19	13	127	629	267	1916	495.00
440	NV4	1109	70	37	38	33	285	262.00
NPP	NV5	84	26	121	42	125	176	96.00
and	Bal1	30	0.7	40	132	32	35	45.00
Power	Bal2	34	50	256	41	21	182	97.00
Units	Bal3	265	233	289	1.3	1.5	29	153.00
VVER	Bal4				3.7	27	50	26.00
1000	Kal1	58	294	356	108	44	11	145.00
	Kal2	7.5	5.6	184	168	56	44	78.00
Russian	Mean	1819	1607	1950	740	1716	1374	1534.00
VVER-440	Median	624	318	242	600	365	1101	542.00
Russian	Mean	80	102	225	71	44	75	99.00
VVER-1000	Median	46	38	220	42	32	44	70.00
Russian	Mean	949	854	1087	380	815	675	794.00
VVER	Median	86	116	227	122	56	166	129.00
Worldwide	Mean	130	320	120	120	140	130	160.00
PWRs	Median	22	27	4.3	2.2	2	1.2	9.80
	Units	207	222	221	230	236	236	
Ukraine	Median	180	180	14	25	47	64	85.00
	Units	4	12	12	12	12	12	
Bulgaria	Median	0.037	400	120	190	11	64	131.00
	Units	4	3	4	6	6	6	
Czech	Median	0.7	7.4	24	39	2.4	3.2	13.00
	Units	4	4	4	4	4	4	
Slovakia	Median	3.6	2.8	0.7	0.74	0.11	0.32	6.70
	Units	4	4	4	4	4	4	
Paks	Median	18	12	1.2	2.3	7.9	3.30	7.50
	Units	4	4	4	4	4	4	
Finland	Median			0.26	0.037	340	0.22	85.00
	Units			2	2	2	2	
USA	Median	50	40	4.1	4.7	2	0.81	17.00
	Units	74	73	69	71	72	70	
France	Median	16	24	5.2	0.037	1.5	0.81	7.90
	Units	54	49	51	53	53	54	
Germany	Median	2.8	7.8	11	3.1	0.41	0.7	4.30
	Units	11	10	7	9	9	9	
Spain	Median	120	120	37	18	8.9	26	55.00
	Units	7	7	7	6	6	6	
Belgium	Median	40	1.6	1.7	1.6	1.1	5	8.50
	Units	7	7	7	7	7	7	
Japan	Median	0.78	0.78	0.67	0.63	0.52	0.59	0.66
	Units	17	18	18	20	21	22	
Korea	Median	140	27	5.2	0.037	2.6	2.1	30.00
	Units	7	7	8	8	8	8	

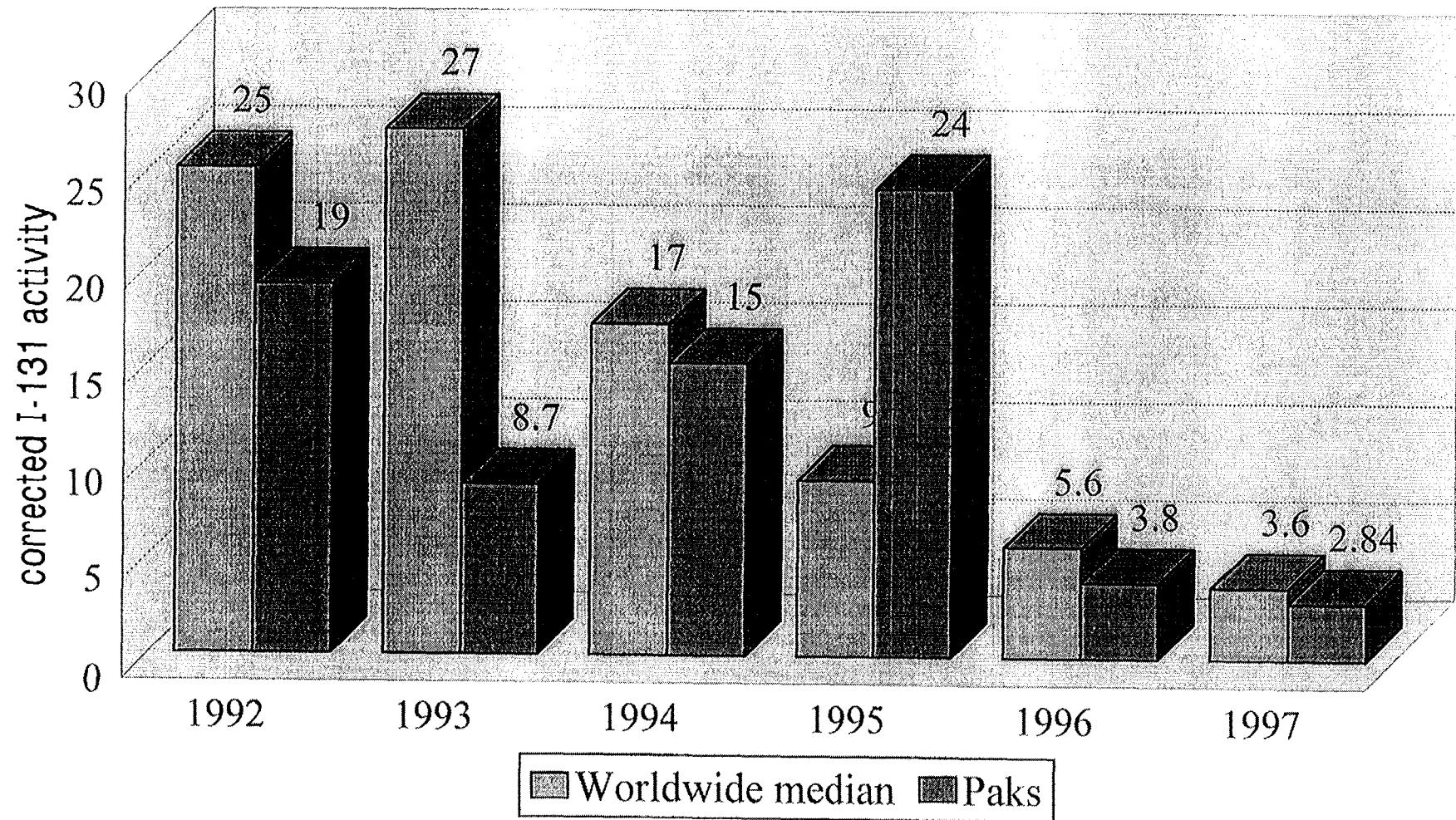


Fig. 8. Fuel reliability indicator for average values for PWRs worldwide and Paks NPP.

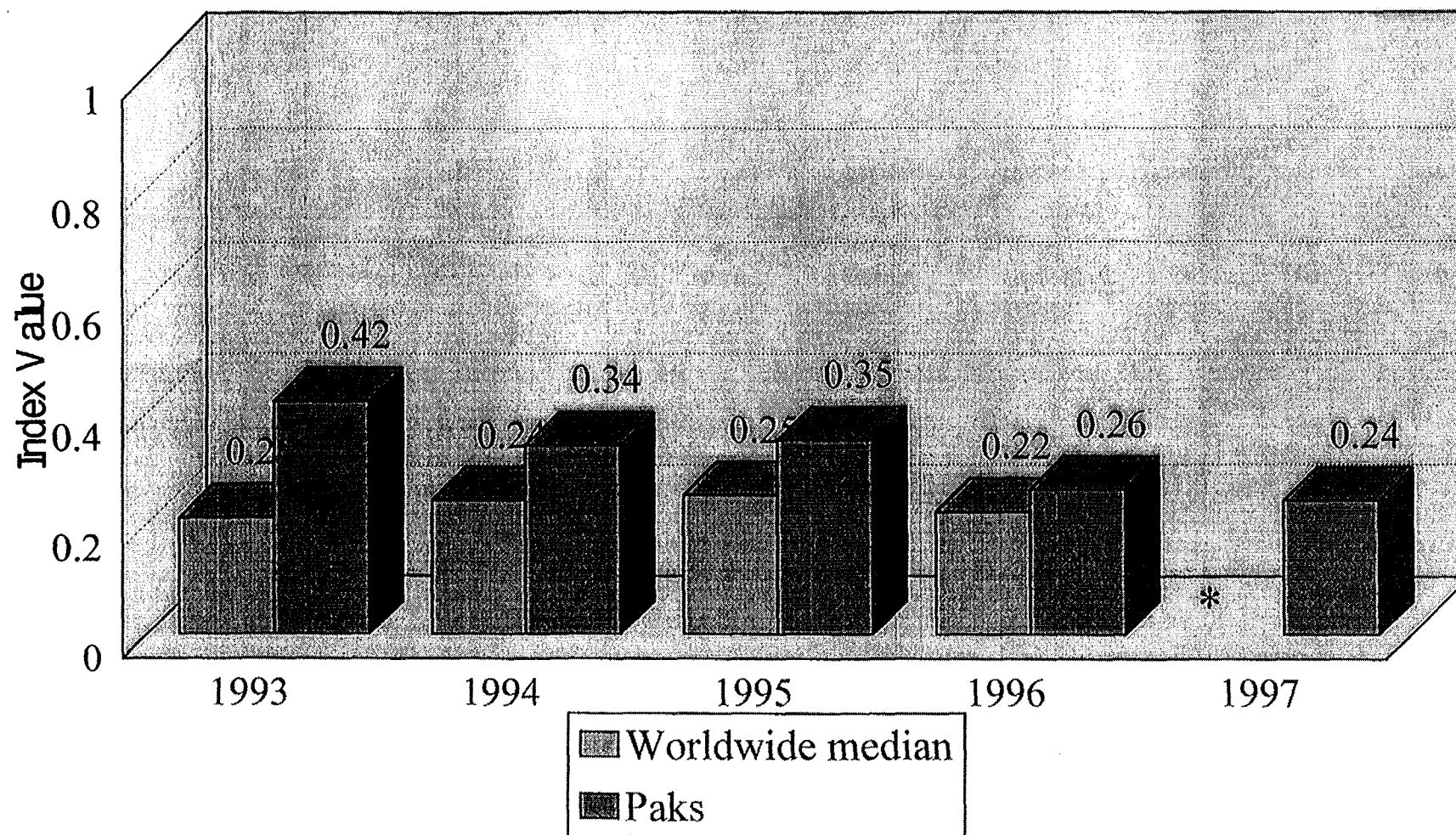


Fig. 9. Chemistry index, trend of average values for PWRs worldwide and Paks NPP (PWR chemistry index at 1997 is not presented because of the changes in its calculation).

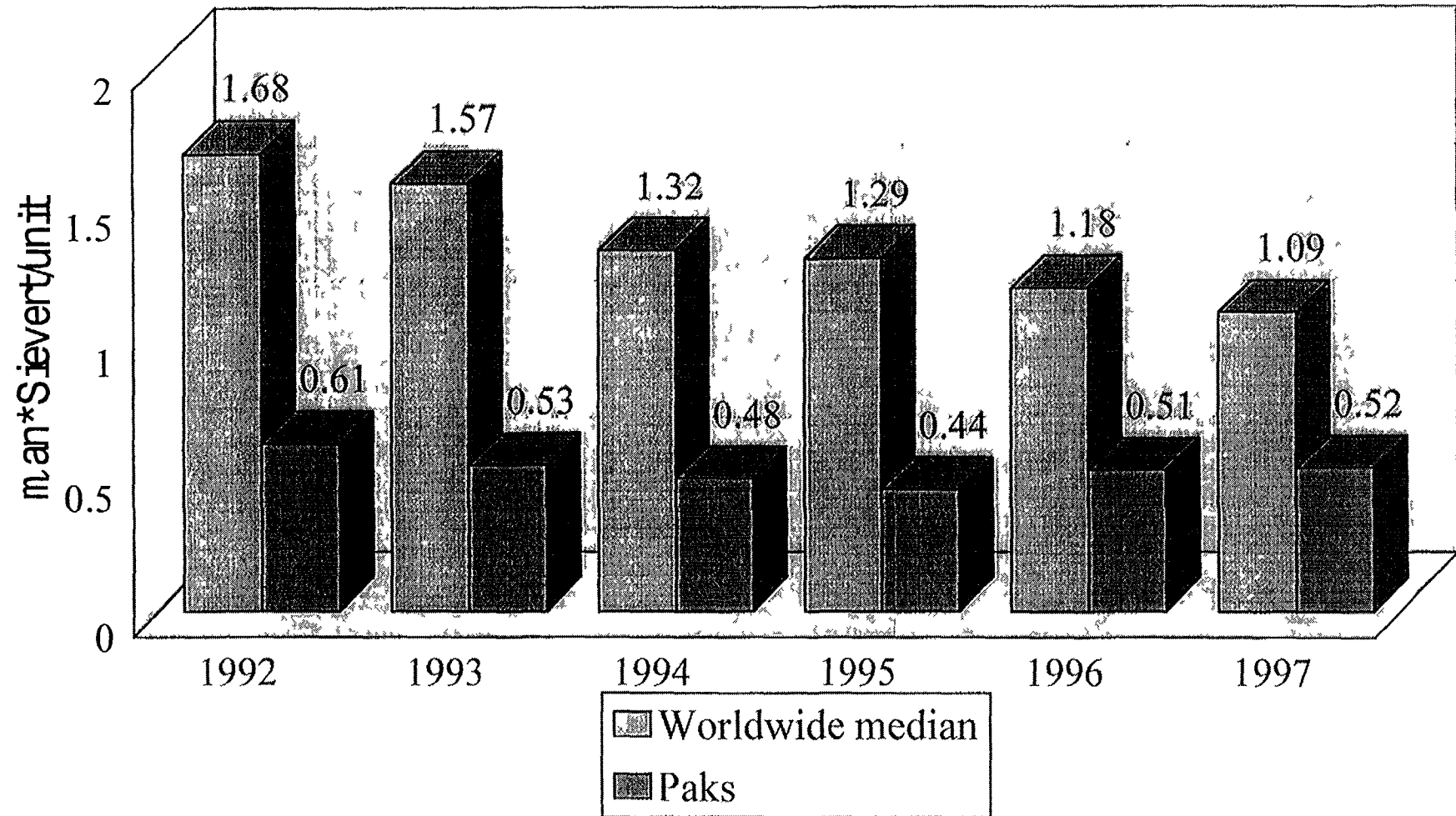


Fig 10 Collective radiation exposure, trend of worldwide and Paks NPP average values



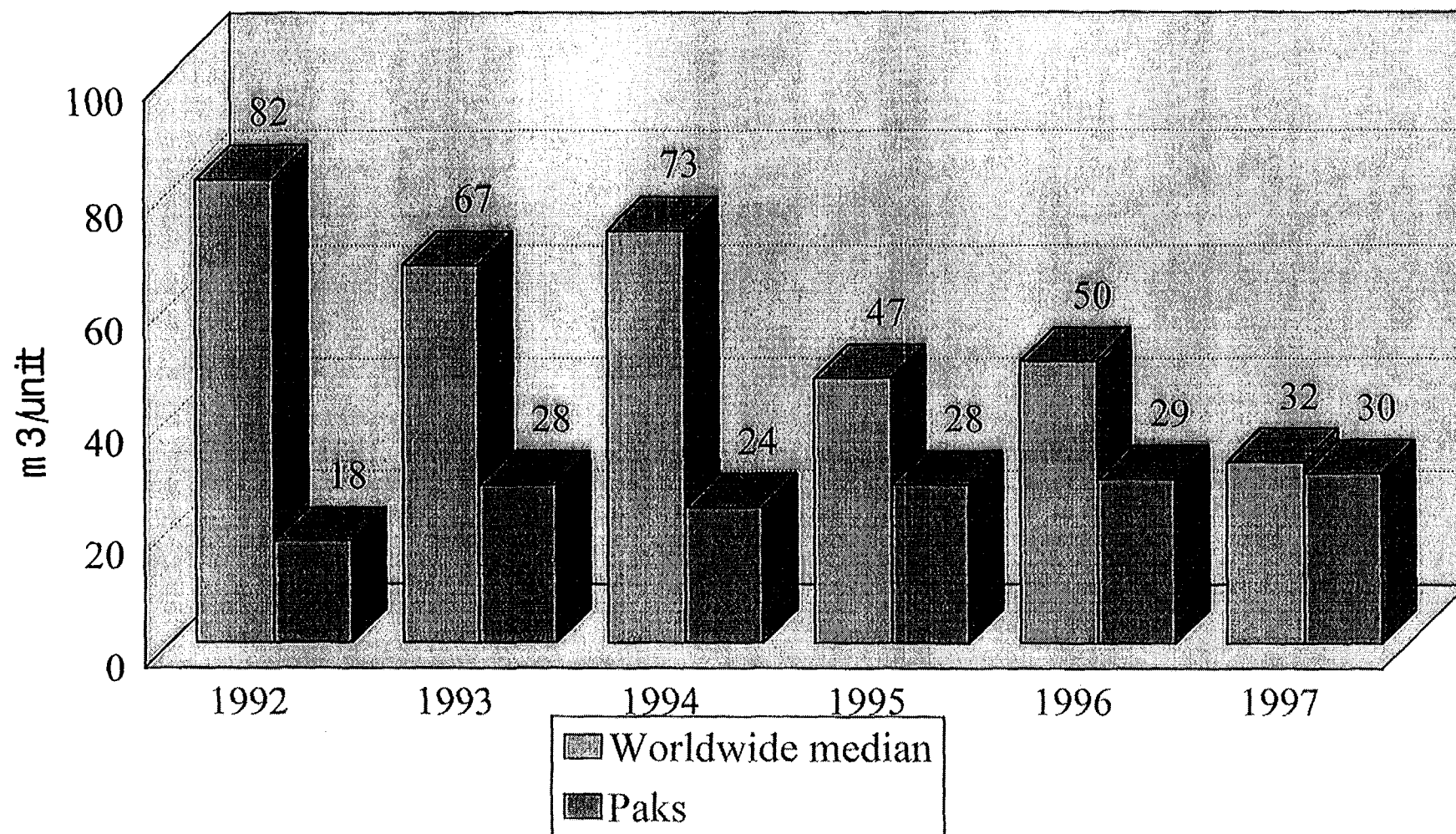


Fig. 11. Volume of low-level solid waste, trend of worldwide and Paks NPP average values.



were started clogged several fuel assemblies. The settlement of these products was uneven but generally their concentration was higher on the side of loops 2 and 3. The clogging of the fuel assemblies by these products and the growing crud due to precipitation of corrosion products from saturated solution by crystallization caused asymmetry in the core.

The unit was shut down for the annual refuelling outage five month earlier than it was scheduled. The core was totally unloaded. The reactor was restarted following the outage with all the fuel assemblies replaced instead of the usual 1/3 of the core replacement.

The following corrective measures were implemented at some NPPs to improve fuel reliability:

- optimization of primary water chemistry and chemistry control;
- increase of efficiency of primary coolant clean-up system;
- implementation of foreign material exclusion program;
- modification of fuel assembly design to avoid fretting and debris failures;
- development of new corrosion resistant structure materials for fuel assembly.

## 5. CORROSION CONTROL OF PRIMARY SYSTEM COMPONENTS USING CORROSION INDICATORS

The influence of primary water chemistry on corrosion processes at NPPs may be directly studied using corrosion test samples immersed and exposed in coolant. The corrosion control on the base of laboratory measurements of corrosion products in samples of primary coolant could not provide representative results due to significant fluctuations of corrosion products concentrations or activities in samples of primary coolant. The corrosion control of primary equipment from different structure materials on the base of corrosion test samples has been carried out at Kola NPP since commissioning. The corrosion samples were delivered to plant by manufacturers of main equipment. The corrosion test samples are made from main structure materials of primary system (carbon steel of reactor pressure vessel, stainless steel of primary pipes and tubes of steam generators, etc.).

The corrosion test samples were installed in vapor, liquid and intermediate phases of coolant in pressurize. In accordance with corrosion test program during outages with inspections of pressurize internals after definite exposition the corrosion test samples are extracted and processed in chemical laboratory. The extracted specimens are processed on the base of special technique to measure types of corrosion and corrosion wear. The corrosion test data are used to calculate the rates of general and localized corrosion rate. It should be noted that since 1980 the hydrazine primary water chemistry has been used at all units of Kola NPP. The measured rate of general corrosion in dependence with duration of exposition is presented on Figure 12. Experimental data show that the rate of general corrosion of austenitic steel type 0.08%C18%Cr10%Ni0.6%Ti (O8X18H10T) is continuously reduced during exposition in liquid coolant phase to 0.02-0.05 mg/(m<sup>2</sup>\*h) after 7-8 years of operation. The results of these investigations can explain the lower doze rate and lower accumulation of radioactive corrosion products on surfaces of primary equipment in case of hydrazine primary water chemistry compared to standard ammonia primary water chemistry. As usual simulation codes based on rate of general corrosion of austenitic steel about 0.10-0.25 mg/(m<sup>2</sup>\*h) have a good agreement with experimental data for plants which used standard ammonia primary water chemistry.

Positive influence of hydrazine primary water chemistry on corrosion of austenitic steel compared to standard and high-alkaline ammonia primary water chemistry was shown earlier during comparative corrosion tests in experimental loop of Nuclear Research Institute in Rez (Czech Republic), but the differences (1.25/1.62-1.40 mg/(m<sup>2</sup>\*h) were not significant due to small duration of runs (up to 1500 hours) [13].

The presented data show that lower value of general corrosion rate for austenitic stainless steels can explain lower doze rate and lower accumulation of radioactive corrosion products on primary

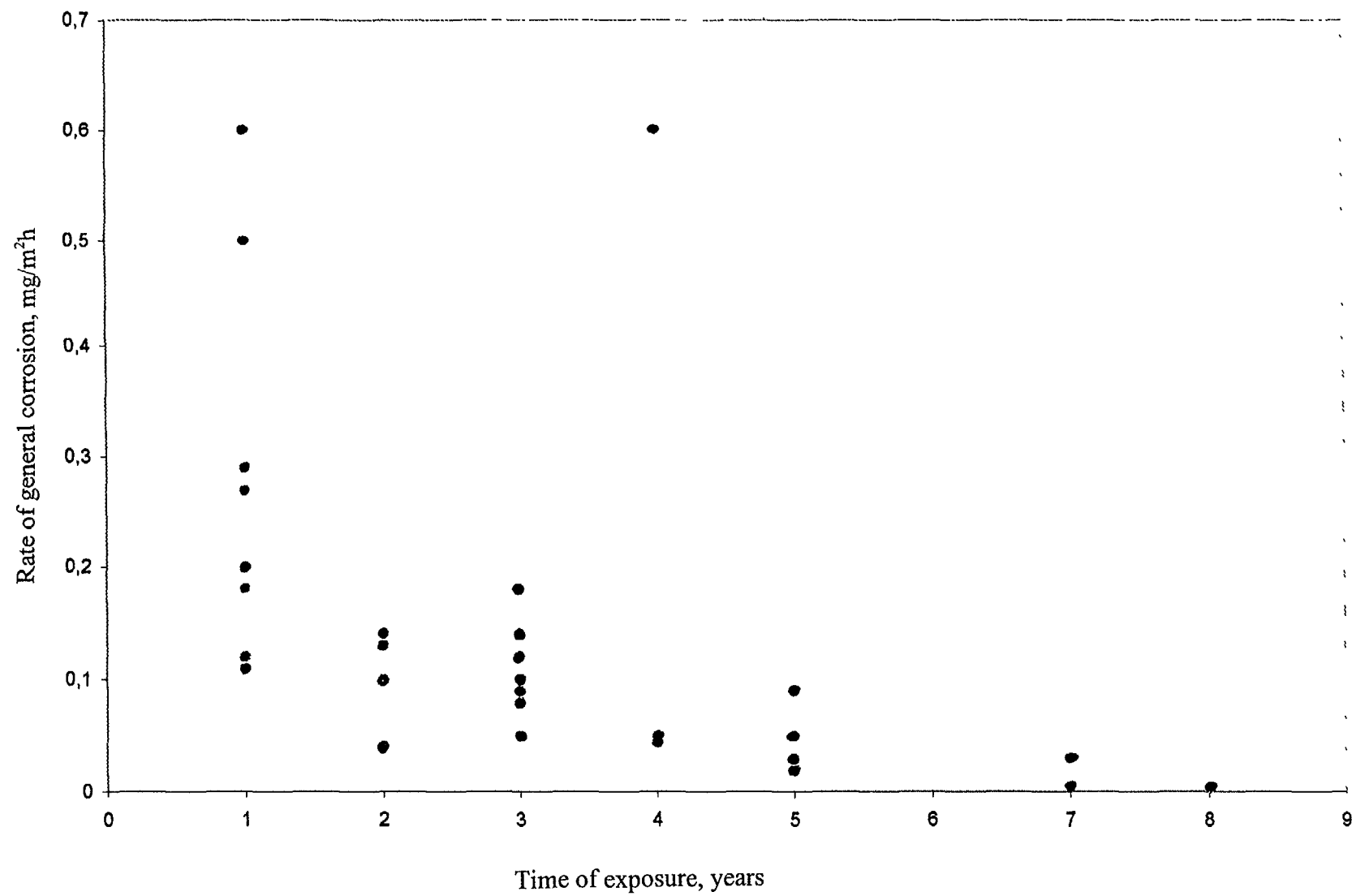


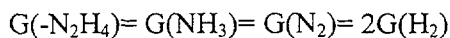
Fig. 12. Rate of general corrosion of austenitic steel in primary system in case of hydrazine water chemistry.

equipment in case of hydrazine primary water chemistry compared to standard ammonia primary water chemistry.

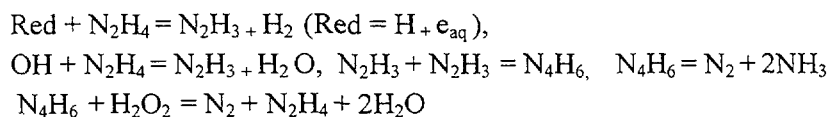
The life-time of primary equipment made of austenitic stainless steels is limited by localized types of corrosion processes. The most important type of localized corrosion of austenitic stainless steels in primary systems is stress corrosion cracking. Generally the rate of cracks depends from different factors, including composition and structure of metal, level of stress, temperature, chemical composition of corrosion medium, etc. The influence of water chemistry on stress corrosion cracking is determinate mainly by concentrations both corrosion active anions (chlorides, sulfates, fluorides, etc.) and oxidant species (first of all - dissolved oxygen). The main task of hydrazine treatment is to reduce the concentration of dissolved oxygen. Besides, recent investigations of radiolytic processes in WWER shown that hydrazine treatment reduces concentration of extremely active oxidant species (such as hydrogen peroxide, hydroperoxide-radical, etc.). Thus implementation of hydrazine primary water chemistry instead of standard ammonia primary water chemistry can provide reduction of oxidant induced localized corrosion of austenitic steel in primary system. As a result the life-time extension of primary equipment made of austenitic stainless steels may be anticipated due to hydrazine treatment of primary coolant.

## 6. HYDRAZINE DOSING IMPACT ON OXIDISING RADIOLYTIC SPECIES PRODUCTION

The primary coolant chemical monitoring data processing of Paks NPP as well as radiation-chemical modeling with the use of MORAVA-H2 programs package have confirmed the previous assumption on the influence of hydrazine on stationary levels of oxidizing radiolytic products in the coolant [10]. Now due to lack of detailed description of the mechanism for the radiolysis of water solution of hydrazine, it is assumed that the decomposition occurs via multiple intermediate radical-like particles which contain 1-4 N atoms. Their kinetic properties depend substantially on pH value of the solution. Irradiation of deaerated water solutions of hydrazine decomposes it to form of ammonia, nitrogen, and hydrogen as final products in the ratio:



Adding the final molecular decomposition products (ammonia and hydrogen) to the initial water solutions of hydrazine does not have a noticeable effect, but concentrations of the radiolysis products during research are usually greater by 3 orders of magnitude than the hydrazine concentration under VVER operation conditions. Hydrazine decomposition increases sharply when oxygen is introduced into alkaline hydrazine solution with pH value above 8. Introducing of hydrogen peroxide into hydrazine solution has a noticeable effect on the radiolysis. Dewhurst and Burton [12] explained effect of hydrogen peroxide on the radiolysis of hydrazine at room temperature by simple mechanism, which includes the following reactions:



Last reaction is important from the viewpoint of explaining of the effect of hydrazine on the primary coolant composition in VVER. It can be assumed that acceptance of hydrogen peroxide by intermediate dimer  $N_4H_6$  (an ammonium precursor during the radiolysis of oxygen-free solutions of hydrazine) should lower the concentration of hydrogen peroxide (as oxidizer) on the one hand, while the reproduction of hydrazine when the dimer interact with hydrogen peroxide should slow the radiolytic decomposition of hydrazine on the other.

Special research was performed on the behavior of hydrazine in the primary system of NPP with WWER-440. The data of primary coolant chemical control for power operation of Paks NPP unit

were processed. The initial data of primary chemistry control included concentrations of ammonia, hydrazine, and hydrogen. Unfortunately, it is only known about the oxygen concentration that it was almost always less than 10 ppb, that is sensitivity of applied analytic technique; therefore nothing definite can be said on how hydrazine affects the oxydizer concentration.

The material balance for hydrazine and its radiolysis products was examined in order to check the validity of the original data for steady-state operation of reactor on rated power, i.e., that the parameters of primary system and the concentrations of chemicals in coolant and makeup water were stable and equal to the average values. Operational experience shows that the ammonia concentration in the makeup water is roughly equal to the ammonia concentration in the primary coolant flow. Consequently, the hydrazine concentration in the makeup water should be roughly equal to the concentration of hydrogen in the coolant (in a molar scale). The average hydrazine concentration in the makeup water (about 30 nml/kg) should correspond to 4 ppm (45 nml/kg) of hydrogen, which agrees with the measured values.

The rate constant for hydrazine decomposition was calculated in the stationary approximation. In this case, the change in the hydrazine mass in the primary loop is described by the differential equation:

$$dM_1/dt = Q \cdot C_m - Q \cdot C_1 + dM_d/dt = 0$$

where  $M_1$  is the mass of hydrazine in the primary system,

$M_d$  is the mass of decomposed hydrazine,

$C_m$  is the hydrazine concentration in the makeup water,

$C_1$  is the hydrazine in the coolant of the primary loop,

$Q$  is the makeup water flow rate.

Hydrazine decomposition proceeds according to an exponential law:  $dC/dt = -kC$ . This allows to calculate the decomposition rate constant:

$$k = (Q/M) \cdot (C_m - C_1) / C_1 = (Q/M) \cdot (C_m / C_1),$$

where  $M$  is the mass the coolant in the primary system.

The following WWER-440 parameters were used in the calculation:

mass of primary coolant - 140 tons,  $C_m$  - 30 ppm, and  $C_1$  - 30 ppb, makeup water rate - 8 tons/h, roughly 1 ton/h goes into the sealing line in the main circulating pump, and the rest is fed to the primary loops. On the base of these data the decomposition rate constant is equal to  $k = 0.015 \text{ s}^{-1}$ , which corresponds to a half-decomposition period of 50 s for hydrazine.

Obviously, the longer the time required for the decomposition (reactions) for any compound, the more the process is affected by other factors (reactor power, the makeup water flow rate, the concentrations of ammonia and hydrazine, etc.). As a result, the decomposition product concentrations become less obvious functions of the concentration of the compound that is decomposing. The decomposition for hydrazine-hydrogen takes longer than the ammonia-hydrogen, which in turn takes longer than for hydrazine-ammonia. This supports the idea that hydrazine is a direct source of ammonia and an indirect source of hydrogen, i.e. the decomposition follows to two stages

first stage       $\text{N}_2\text{H}_4 \rightarrow \text{NH}_3 + \text{N}_2$

second stage     $\text{NH}_3 \rightarrow \text{H}_2 + \text{N}_2$

Probably the first stage of this process is both thermally activated and radiolytic, while the second is only radiolytic.

A second possible mechanism is the radiolytic process



in which hydrogen forms directly from hydrazine, but this process plays a secondary role [10]. Support for this conclusion comes from a calculation of the stationary relationship of the concentrations of ammonia vs. hydrogen in the coolant when the reactor operates under rated power. The calculation was done using the MORAVA-H2 program package, which was developed to model the primary coolant in WWERs. This package was verified using the monitored coolant composition at WWER with standard ammonia chemistry and used to co calculate hydrazine water chemistry.

The MORAVA-H2 code gives a satisfactory quantitative description of the behaviour of the hydrazine water chemistry during WWER operation, and if the hydrazine is replaced by an equivalent amount of ammonia and nitrogen.

The result of the analysis lead to the conclusion that the concentration of oxydizers (oxygen or hydrogen peroxide) is lower in coolant using hydrazine water chemistry, as opposed to standard ammonia water chemistry. The oxygen concentration is lower because it is thermally bound to hydrazine (as indicated by small but detectable hydrazine concentrations in the coolant). The hydrogen peroxide concentrations is lower (without hydrazine its concentration is 1.5 ppb) because its accelerated decomposition in presence of hydrazine.

All this ideas can be desputed or confirmed qualitatively and quantitatively either:

- after these parameters and real hydrazine concentrations in primary coolant are correlated analytically in an operating unit with hydrazine added to the coolant, or
- after experimental research on simulation equipment with similar irradiation conditions, thermophysical parameters, surface to volume rations, construction materials, and coolant properties.

## CONCLUSIONS

1. During the control measurements of hydrazine water chemistry it was concluded that the corrosion products concentration following a short increase stabilises at a level lower than during ammonia cycle.
2. In case of transient operation with hydrazine water chemistry the increase of insoluble corrosion products is lower than with ammonia water chemistry.
3. Radioactive surface contamination and dose rate values of different primary equipment decreased unambiguously both in case of high and low original levels, but of course in a different extent.
4. The volume of the liquid radioactive waste can be reduced by postponement of chemical decontamination.
5. Using hydrazine water chemistry the re-contamination by radioactive isotopes is very slow in comparison with the effect following a chemical decontamination or even with the ammonia water chemistry.
6. There is a significant financial benefit of using hydrazine water chemistry through the savings of collective dose exposures.

7. Recent results of experimental studies allowed to explain the mechanism of hydrazine dosing influence on:

- corrosion rate of structure materials in primary coolant,
- behaviour of soluble and insoluble corrosion products including long-life corrosion-induced radionuclides in primary system during steady-state and transient operation modes,
- radiolytic generation of oxydising radiolytic products in core and its corrosion activity in primary system,
- radiation situation forming during refuelling and maintenance outages,
- degradation and removal of foreign materials (including corrosion active oxidant species) from primary system during abnormal events.

8. Operational experience and experimental data showed that hydrazine primary water chemistry allows to reduce corrosion wear and thereby makes it possible to extend the life-time of plant components in primary system.

## REFERENCES

- [1]. BAJARI, M. et al., "Operational experiences with primary hydrazine water chemistry at VVER type units of Paks NPP Ltd", Primary and Secondary Side Water Chemistry of Nuclear Power Plants (Proc. 3-rd Int. Seminar Balatonfüred, Hungary, 16-20 September), NPP Paks (1997) Bogancs 1.
- [2]. IOURMANOV, V. et al., "Peculiarity of primary hydrazine water chemistry during abnormal events related with foreign material ingress", Primary and Secondary Side Water Chemistry of Nuclear Power Plants (Proc. 3-rd Int. Seminar Balatonfüred, Hungary, 16-20 September 1997), NPP Paks (1997) Yurmanov 1.
- [3]. BRIDGE, D.A. et al., "The measurements of corrosion product levels in the primary coolant at Paks Units 1 and 2 using transition metal ion-chromatography", Primary and Secondary Side Water Chemistry of Nuclear Power Plants (Proc. 1-st Int. Seminar Balatonfüred, Hungary, 28 April-03 May 1992), NPP Paks (1992) Bridge 1.
- [4]. SCHUNK, J. et al., "Elemental and radiochemical measurements carried out on primary coolant at WWER-440 PWRs Paks 1 and 2 in Hungary during steady full-power operation and at end-of-cycle shutdown", Water Chemistry of Nuclear Reactor Systems (Proc. 6-th Int. Conference, Bournemouth, UK, 12-15 October 1992) BNES (1992) 123.
- [5]. SCHUNK, J. et al., "Experiences with hydrazine water chemistry in the primary coolant of WWER-440 Reactors", Primary and Secondary Side Water Chemistry of Nuclear Power Plants (Proc. 1-st Int. Seminar Balatonfüred, Hungary, 28 April-03 May 1992), NPP Paks (1992) Schunk 1.
- [6]. BOGANCS, J. et al., Assessing hydrazine water chemistry for WWER-440s - into extra time, Nuclear Engineering International (February 1993) 50-53.
- [7]. BAJARI, M. et al., "Modified primary water chemistry at Paks Nuclear Power Plant", on Primary and Secondary Side Water Chemistry of Nuclear Power Plants (Proc. 2-nd Int. Seminar Balatonfüred, Hungary, 19-23 September 1995), NPP Paks (1995) Bogancs 1.
- [8]. PASHEVICH, V. et al., P. Experience of VVER-400 Units at Paks NPS Using Hydrazine Water Chemistry, Thermal Engineering, **43**, 8 (1996) 639-643.
- [9]. BURCLOVA, J., "Standard and Hydrazine Water Chemistry in Primary Circuit of VVER-440 Units", Water Chemistry of Nuclear Reactor Systems (Proc. 6-th Int. Conference, Bournemouth, UK, 12-15 October 1992) BNES (1992) 145.
- [10]. ARKHIPOV, O.P. et al., "Thermal and radiation characteristics of hydrazine in the primary loop of NPP with the VVER Reactors", Atomic Energy, **82** 2 (February 1997) 92-98.

- [11]. ERDOS, E. et al, "Results of the on-line Radioiodine Measurements in the Primary Coolant of NPP Paks at block 3", Primary and Secondary Side Water Chemistry of Nuclear Power Plants (Proc. 3-rd Int. Seminar Balatonfüred, Hungary, 16-20 September 1997), NPP Paks (1997) Erdos 1.
- [12]. VAJDA, N. et al, "Fuel Performance Under Normal Operating Conditions at Paks NPP", Primary and Secondary Side Water Chemistry of Nuclear Power Plants (Proc. 3-rd Int. Seminar Balatonfüred, Hungary, 16-20 September 1997), NPP Paks (1997) Vajda 1.
- [13]. KYSELA, J. et al., "Austenitic steel corrosion outside the core in VVERs", Coolant Technology of Water Cooled Reactors (Proc. CRP), IAEA TECDOC-667 Vienna (1992) 25.
- [14]. MAKAI, J. et al, "Development of Full System Contamination Technology at Paks NPP", Primary and Secondary Side Water Chemistry of Nuclear Power Plants Proc. 3<sup>rd</sup> Int. Seminar, September 16-20, 1997, Balatonfüred, Hungary) Paks NPP (1997) Makai 1.
- [15]. NANIAS, M., "WANO Resources For You", Primary and Secondary Side Water Chemistry of Nuclear Power Plants (Proc. 3-rd Int. Seminar Balatonfüred, Hungary, 16-20 September 1997), NPP Paks (1997) Nantias 1.



## IN-REACTOR FUEL CLADDING EXTERNAL CORROSION MEASUREMENT PROCESS AND RESULTS

J. THOMAZET, Y. MUSANTE, J. PIGELET

Framatome Nuclear Fuel,  
Lyon, France

### REFERENCES

#### Abstract

Analysis of the zirconium alloy cladding behaviour calls for an on-site corrosion measurement device. In the 80's, a FISCHER probe was used and allowed oxide layer measurements to be taken along the outer generating lines of the peripheral fuel rods.

In order to allow measurements on inner rods, a thin Eddy current probe called SABRE was developed by FRAMATOME. The SABRE is a blade equipped with two E.C coils is moved through the assembly rows. A spring allows the measurement coil to be clamped on each of the generating lines of the scanned rods. By inserting this blade on all four assembly faces, measurements can also be performed along several generating lines of the same rod. Standard rings are fitted on the device and allow on-line calibration for each measured row.

Signal acquisition and processing are performed by LAGOS, a dedicated software program developed by FRAMATOME.

The measurements are generally taken at the cycle outage, in the spent fuel pool. On average, data acquisition calls for one shift per assembly (eight hours): this corresponds to more than 2500 measurement points. These measurements are processed statistically by the utility program SAN REMO.

All the results are collected in a database for subsequent behaviour analysis: examples of investigated parameters are the thermal/hydraulic conditions of the reactors, the irradiation history, the cladding material, the water chemistry. This analysis can be made easier by comparing the behaviour measurement and prediction by means of the COROS-2 corrosion code.

### 1. INTRODUCTION

The increase in fuel performance has become an unavoidable economic reality. In the early eighties, management was on an annual basis, discharge burnup in the order of 35 GWd/tU and the thermal hydraulic conditions of the first PWR plants built in France were not very severe (the first reactors of the standard Framatome 900 MWe series).

As the proportion of nuclear-generated electricity became greater, grid follow operation was set up, and new, more efficient reactors were built in France (P4/P'4 and more recently the N4). In other countries, new high-performance reactors were also commissioned: the 3-loop / 1000 MWe in Belgium, the Pre-Convoys and Convoys in Germany, the M30 in China, etc.

More efficient forms of fuel management are proposed in parallel, such as long cycles, the use of MOX and low leak management, all associated with higher burnup rates, sometimes even with increases in reactor power, after steam generator replacement, for example.

From the single-product situation it was in yesterday, Framatome must today offer different types of products which must meet with irradiation conditions that are perpetually changing. The cladding material has also changed: Zircaloy-4 standard, followed by optimized Zircaloy-4 and now the advanced alloy M5 is proposed.

External corrosion is one of the parameters which must be monitored by setting up fuel monitoring programmes. To do this, Framatome has developed a tool for measuring the oxide layer on



most fuel rods in the assemblies and several generating lines per rod, which, unlike conventional measuring using an external probe, makes it possible to take thermal hydraulic conditions inside the bundle into account. This tool, named "SABRE", is presented below. The methodology for measuring and analyzing is then presented, together with some typical results for fuel behaviour according to irradiation conditions.

## **2. PRESENTATION OF THE SABRE TOOL**

The general layout drawings are presented in Fig. 1 and 2.

### **2.1. Reminder of specification**

Oxide measurement was, until 1993, made with a FISCHER probe on the outer generating line of the peripheral fuel rods. The results, obtained in a hot cell on extracted rods, showed a variation in the thickness of the zirconia over all generating lines. Knowledge of this azimuthal variation could not be used easily to extrapolate the results to internal rods from measurements made on the outer generating line because of the uncertainty surrounding the thermal hydraulic conditions around the edge of the assembly. It was therefore necessary to develop a procedure by which oxide measurements could be made inside the assembly without having to extract the rods [1].

### **2.2. Design of the SABRE**

This is made up of a blade comprising a measurement coil mounted on a spring and a reference coil. The SABRE moves through the assembly in order to measure all the rods in a row, while the spring ensures that the measurement coil is placed on these rods. A cable roughly twenty meters long, integrated into the SABRE, links the two coils to the eddy current measurement device.

### **2.3. The equipment**

This consists of a data acquisition channel, a carrier and its instrumentation and control (I&C). The carrier, fitted on to the site fresh fuel elevator, is made up of an X-Y cross -movement table to cover all the rods in the assembly.

The acquisition channel is made up of an ELOTEST Eddy current device and a PC fitted with an acquisition board and its LAGOS software. This data acquisition and processing software was developed by Framatome for oxide measurement. I&C enables the X-Y table to be remote-driven under water via a camera, while managing the safety devices related to movement of the instrumentation.

### **2.4. Measurement principle**

When there is a variation in impedance of the measurement coil, a differential voltage appears at the terminals of the eddy current measurement bridge, excited by a sinusoidal voltage. From this voltage, once amplified, the X and Y components of the vector representing the voltage in the impedance plane are extracted.

### **2.5. Data acquisition method**

Calibration was carried out in two stages, the first of which involved establishing, by use of oxide thickness standards (Mylar), a correspondence law ( $\mu\text{m}/\text{millivolts}$ ) obtained by a polynomial regression of order 2 from the voltage read on the Eddy current device and the thickness to be measured. The second stage involved measuring the cladding thickness of cladded rings. These rings are made by projecting alumina on sections of rod cladding of the same type as those to be measured. These rings, mounted on a standard holder, are used to carry out in-line calibration for each row measured.

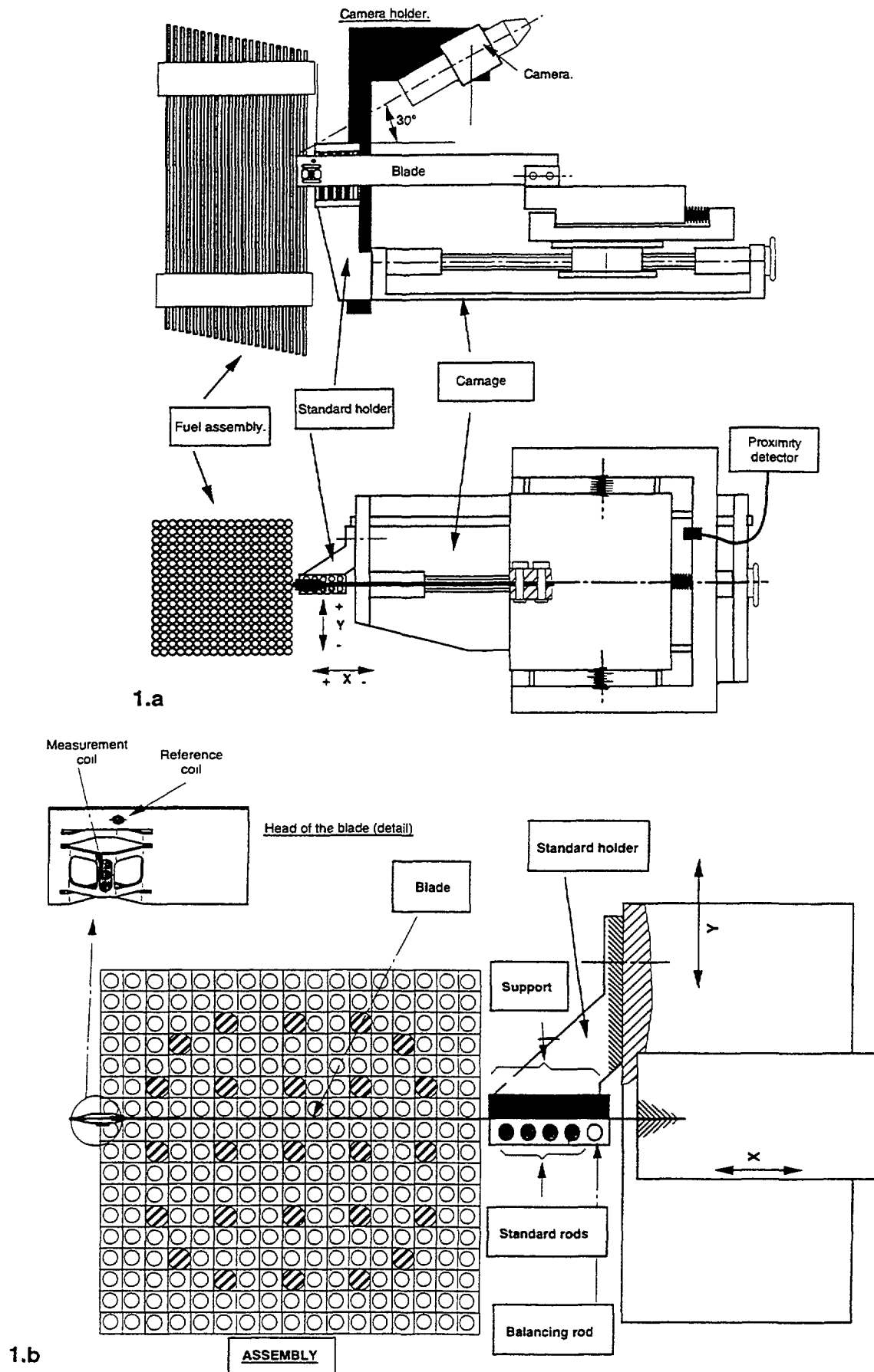
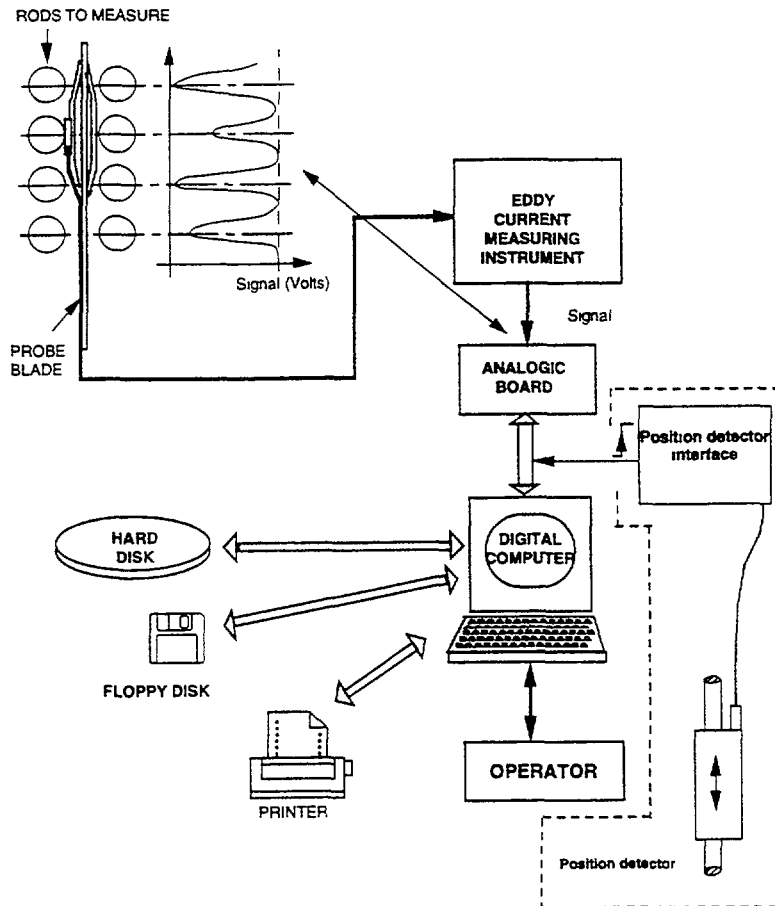


Figure 1 - General Layout : Drawings of the "Sabre"



**Figure 2 - Principle of the data acquisition**

Each row of rods is measured by inserting the sabre until the last rod of the row is detected. The sabre is then withdrawn with acquisition thereby ensuring two measurement points per rod, corresponding to the points of tangency of the generating lines viewed by the measurement coil as it passes. These tangency points are detected and their x,y co-ordinates acquired by the LAGOS software. The second measurement is used to validate.

For each change of row, the table moves the SABRE and the standard holder so that at each measurement of a row of rods, the SABRE scans the standard and the fuel rods in line. The change of altitude is made by the fuel elevator.

Acquisition filters are applied in real time on the standard rings and the rods by the LAGOS software to validate the results.

## **2.6. Efficiency**

The measurement uncertainty for rods is  $\pm 5\mu\text{m}$  for a measurement range of 0 to 150  $\mu\text{m}$ .

### 3. INSPECTION PROGRAMME

#### 3.1. Visual examination

Before making any measurements with the SABRE device, a visual examination of the four faces and ends of the assembly is performed. This examination has two purposes:

- a) To check that the assembly is mechanically reliable and that no debris is present in the tube bundle (preliminary examination). If there is, then this object is removed using an appropriate tool before the inspection.
- b) To observe any cladding areas which might have a special appearance: sudden change of colour, deposits etc. (detailed examination). These areas, once identified, can later be analysed using the SABRE device.

The visual examination is performed by half-face, overlapping the central rod. So for a 17 x 17 assembly, nine rods are viewed.

The detailed examination is made using a camera provided with a lens for viewing the rod throughout the field of observation.

The visual examination, which can be made in colour or in black and white is recorded in full on videotape. The recordings can be accompanied by audio commentaries and text insets as the operator desires. Paper printouts of the recorded image can be made instantaneously during the on-site examination.

#### 3.2. Measurement of the zirconia layer using the SABRE device

The measurements made using the SABRE device involve scanning the rows of rods located at different altitudes between the assembly grids and possibly between the end grids and nozzles. The device provides access to practically all internal rods.

The measurements can be made on any type of PWR fuel :  $\text{UO}_2$ , MOX, REPU etc. and on the five types of geometry currently irradiated: 14 x 14, 15 x 15, 16 x 16, 17 x 17 and 18 x 18. As an example, Fig. 3 shows the positions of the measurements made at a given axial position. Fig. 4 illustrates the thicknesses of oxide measured at this axial position. The values given on these figures are the average of thicknesses in microns of oxide measured on the four generating lines of the rods. Measurement accuracy, evaluated at  $\pm 5$  microns makes it possible to bring out, on the same level, variations in this thickness within the assembly.

##### 3.2.1. Making the measurements

As a result of the temperature increase between the bottom and top of the rods, the cladding is not uniformly oxidized. The thickness of zirconia is at a maximum between grids 6 and 7 for a 12 Ft fuel, and 8 and 9 for a 14 Ft fuel (grids are numbered from the lower nozzle).

By using SABRE, it is possible to establish a cladding oxidation profile by making measurements at different axial positions. In order not to unduly lengthen the acquisition time, these measurements are distributed over the grids at a rate of one level every grid span, except the one corresponding to the expected maximum where the measurements are made over three levels or more.

At each level, it is possible to define the number of rows to be scanned.

The number of rows and levels to be explored depends on the purpose for which the measurement programme is written. If it is desired to know the general oxidation of the cladding of a

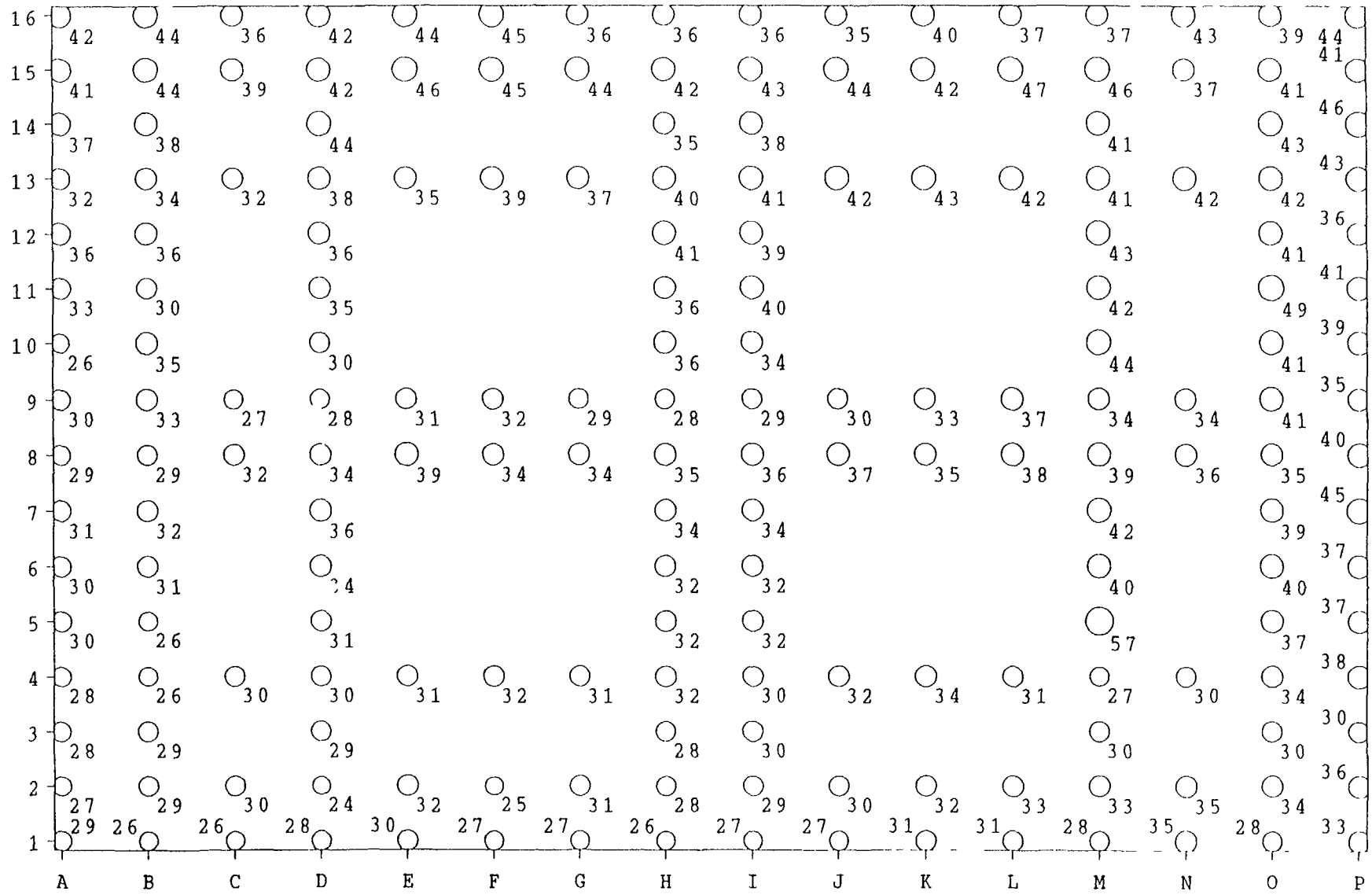


Figure 3 - INDIVIDUAL OXIDE THICKNESS (maximum azimuthal average)

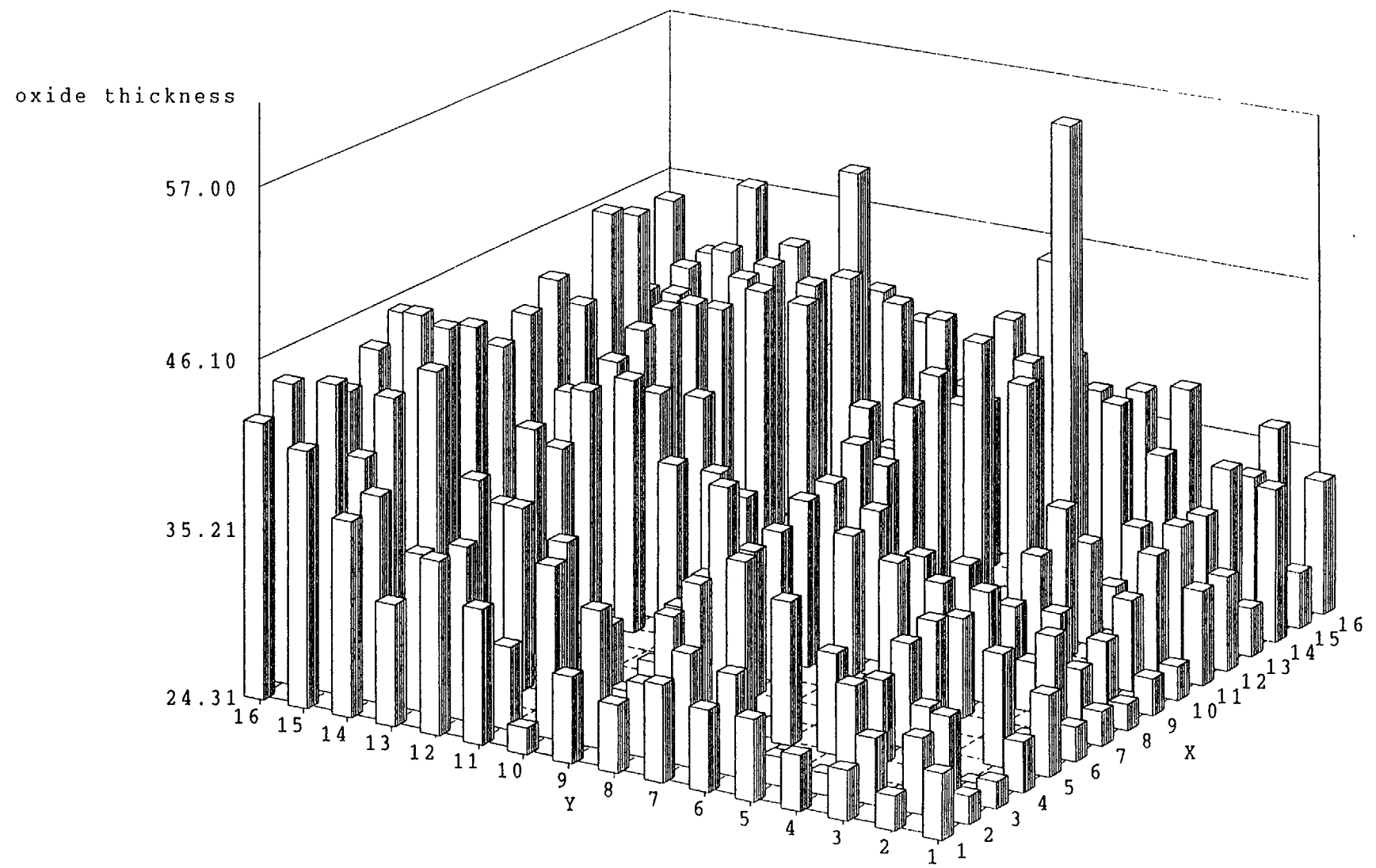


Figure 4 MA (IMUM AZIMUTHAL AVERAGE OF OXIDE THICKNESS : distribution in the F/A

fuel, the standard programme generally deals with nine rows at grid span 8-9 and five rows at grid spans 2-3 to 7-8. This choice is the result of a compromise between the representative nature of the measurements and the time required to perform them on site. If one is more interested, or only interested, in the cladding of certain fuel rods, the corresponding rows only may be selected.

Identification of the levels and rows selected is processed automatically by the LAGOS software, the operator being present to check correct positioning of the SABRE using a control camera.

In certain R&D programmes, rods are extracted after one or more irradiation cycles for in-depth inspection in the hot cell. One of these inspections is measurement of the layer of external zirconia on the cladding, made using an Eddy current device with a FISCHER probe. This measurement, also accurate to  $\pm 5$  microns, enables comparison to be made with results obtained on site using the SABRE. In all cases studied, measurement by FISCHER probe confirms, to the degree of accuracy of the methods used, the results acquired by the SABRE.

Typical time of a standard examination requires about 8 hours per assembly.

### *3.2.2. Processing the results*

Once the data are acquired they can undergo initial processing on site. After being sent by computer network to the Fuel Department at FRAMATOME, these data can be analysed using specially developed statistical methods.

Data are first processed using the Framatome OXY software. This involves drawing up, at all measurement levels, a mapping of the assembly in which the averages of the Forward / Back values for oxide thickness are noted for each rod generating line measured, and plotting the histogram of the distribution of these measurements (Fig. 5).

The second processing operation uses the SAN REMO statistical processing software. This software, which uses the SAS utility, can process the data in a number of ways. Given the very large number of measurement points provided by the SABRE device, it is possible to undertake a statistical analysis, the results of which are significant of the generic behaviour of the cladding with respect to oxidation. This large number of values also makes it possible to test the quality of each measurement by comparing the differences between the "forward" and "back" values obtained as the SABRE passes. An example of a frequency histogram is given in figure (6). In this figure it can be seen that the distribution of Forward/Back differences is centred on the interval 0-1 micron and that deviations are generally within the measurement accuracy ( $\pm 5$  microns).

In certain cases, thick layers of oxide lead to spalling. This gives large Forward/Back differences which then need special analysis.

The measurements thus processed can be used directly for fundamental studies on the performance of cladding materials when subjected to radiation and for qualifying prediction models of oxidation kinetics by comparing the measured with the predicted values.

### **3.3. Comparison between measured and predicted values**

From rod by rod neutronic data and thermal hydraulic conditions, the thickness reduction measured at the peak level is analysed compared to the prediction calculated with the corrosion model COROS 02.

The COROS 02 model describes the two phases of the cladding external oxidation with

:

- a law of the cubic Arrhenius type for the pre-transition phase;
- a law of the linear Arrhenius type for the post-transition phase.

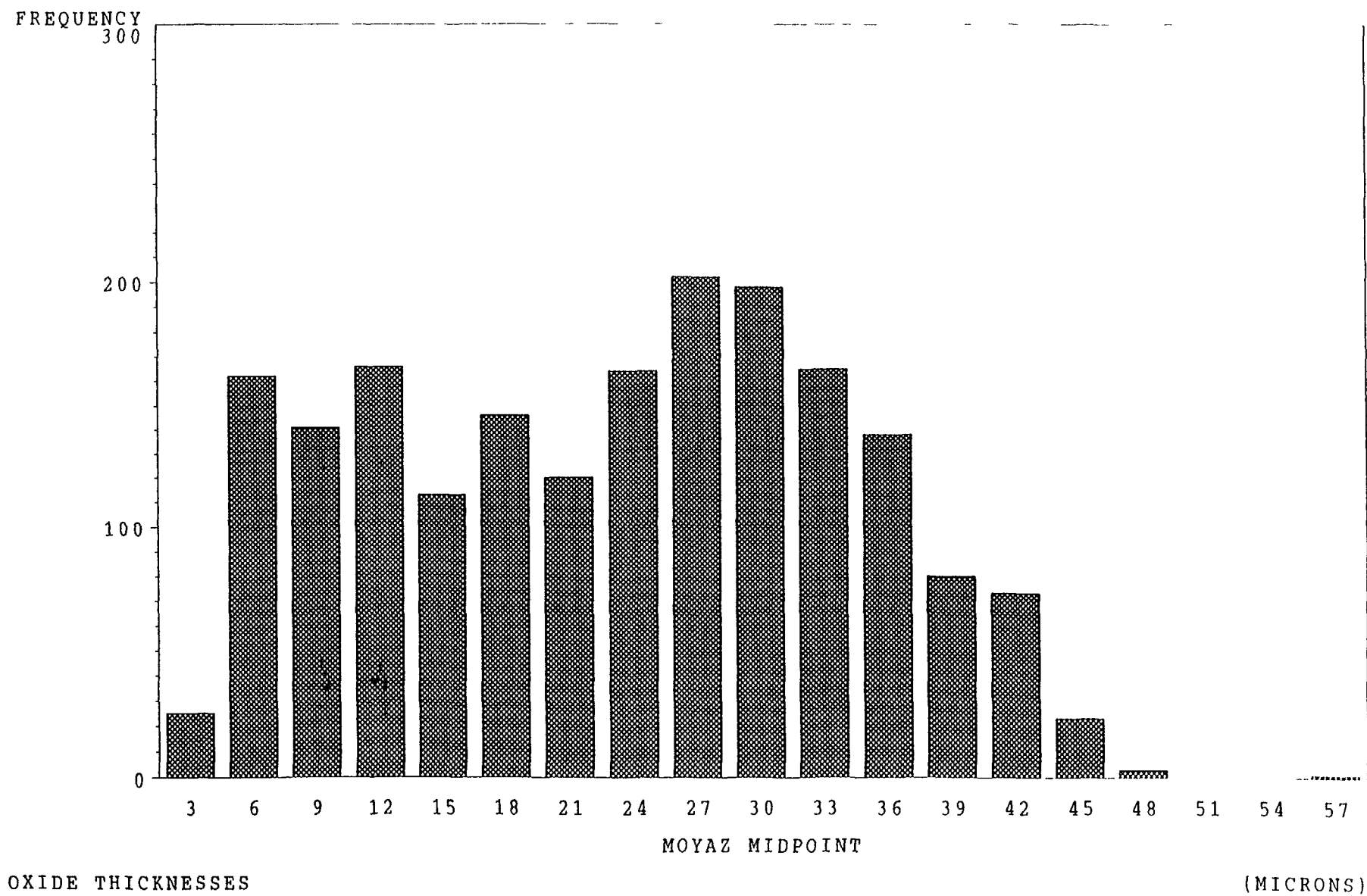


Figure 5 - OXIDE THICKNESS FREQUENCY HISTOGRAM



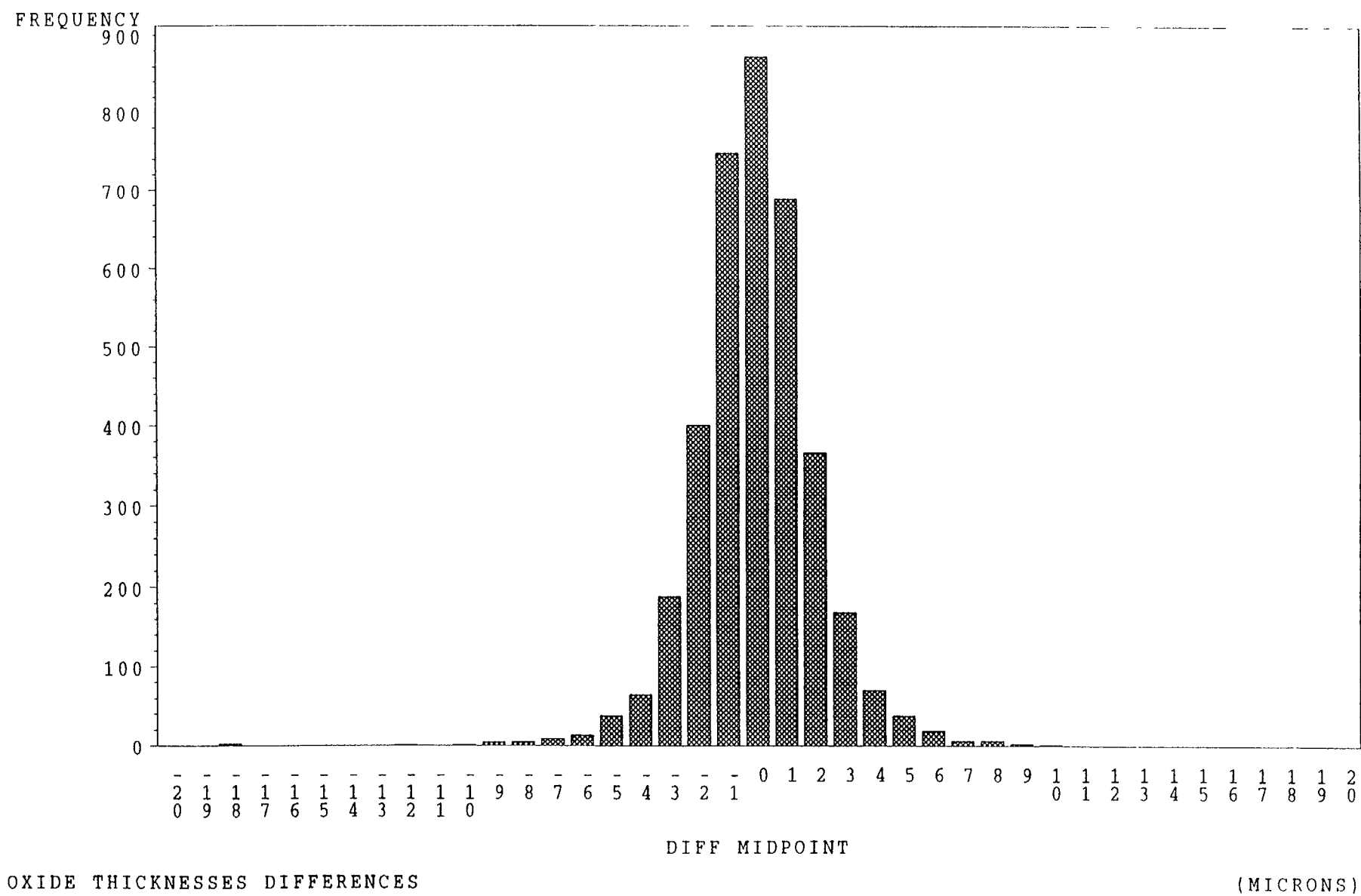


Figure 6 - DISTRIBUTION OF FORWARD/BACK DIFFERENCES OF OXIDE THICKNESSES

This model was fitted from several benchmarking rods which were chosen from different reactors and different irradiation conditions for supplying the best estimate peak external oxidation level at different axial positions (each rod was axially split into 30 increments). This model was then applied to the extensive experience available which corresponds to more than 6000 fuel rods measured on site with the results collected in a database.

A typical example of comparison between measured thicknesses and predicted thicknesses, after one to three cycles of irradiation at the peak, is shown in Fig. 7. In this example the cladding seems to behave better than predicted.

Currently, the dispersal of measurement results accelerates with burnup, which is not found by the model, even though the latter takes the real individual rod power histories into account. A thermal hydraulic analysis in 3D does not explain every time the individual measurements.

Typically, 5 to 6 values of the radial power distributions per rod and per cycle and 2 or 3 axial power distributions per cycle are sufficient for this comparison. Additional data may be required for further investigations.

#### **4. EXPERIENCE FEEDBACK**

Experience feedback from using the SABRE which has been acquired by Framatome is very large. It is illustrated below by a few examples in which certain variables influencing the corrosion behaviour of the cladding (such as the thermal hydraulic conditions of the reactors, the type of cladding, the study of local measurements on internal rods and the chemistry of the primary coolant) will be assessed.

##### **4.1. Impact of the thermal hydraulic conditions of the reactors**

As corrosion of zirconium alloys is thermally activated, it is in those reactors which have the highest metal/oxide interface temperatures that corrosion will be the highest. Table 1 shows the thermal hydraulic conditions of two very different reactors in which experience has been acquired : a Pre-Convoy type reactor and a 900 MWe reactor.

An illustration is presented by the following experiment in the two types of reactor: standard 900 MWe Framatome type reactor and Pre-Convoy type. There are, in fact, many specific features within a reactor type from the same origin which complicate the analyses: for example, the 900 or 1000 MWe reactors are very severe with the fuel after SG replacement since their core power has been increased.

For a given management and with comparable burnup, the Pre-Convoy reactor has higher liquid temperatures at the core inlet and outlet and a greater and more severe average linear power than the 900 MWe reactor.

In this example, the cycles are annual and the cladding material is AFA2G. The layers of zirconia at the axial position where corrosion is greatest are illustrated in Fig. 8.

This result shows that for a burnup in the order of 40 GWd/tU the corrosion may be 30 to 40 percent higher in the Pre-Convoy reactor than in the 900 MWe reactor.

##### **4.2. Impact of the cladding material**

The high burnup rates aimed at and the severe irradiation conditions in which the fuel is loaded have obliged the fuel suppliers to improve the efficiency of the cladding. Framatome today proposes the M5 alloy [2].

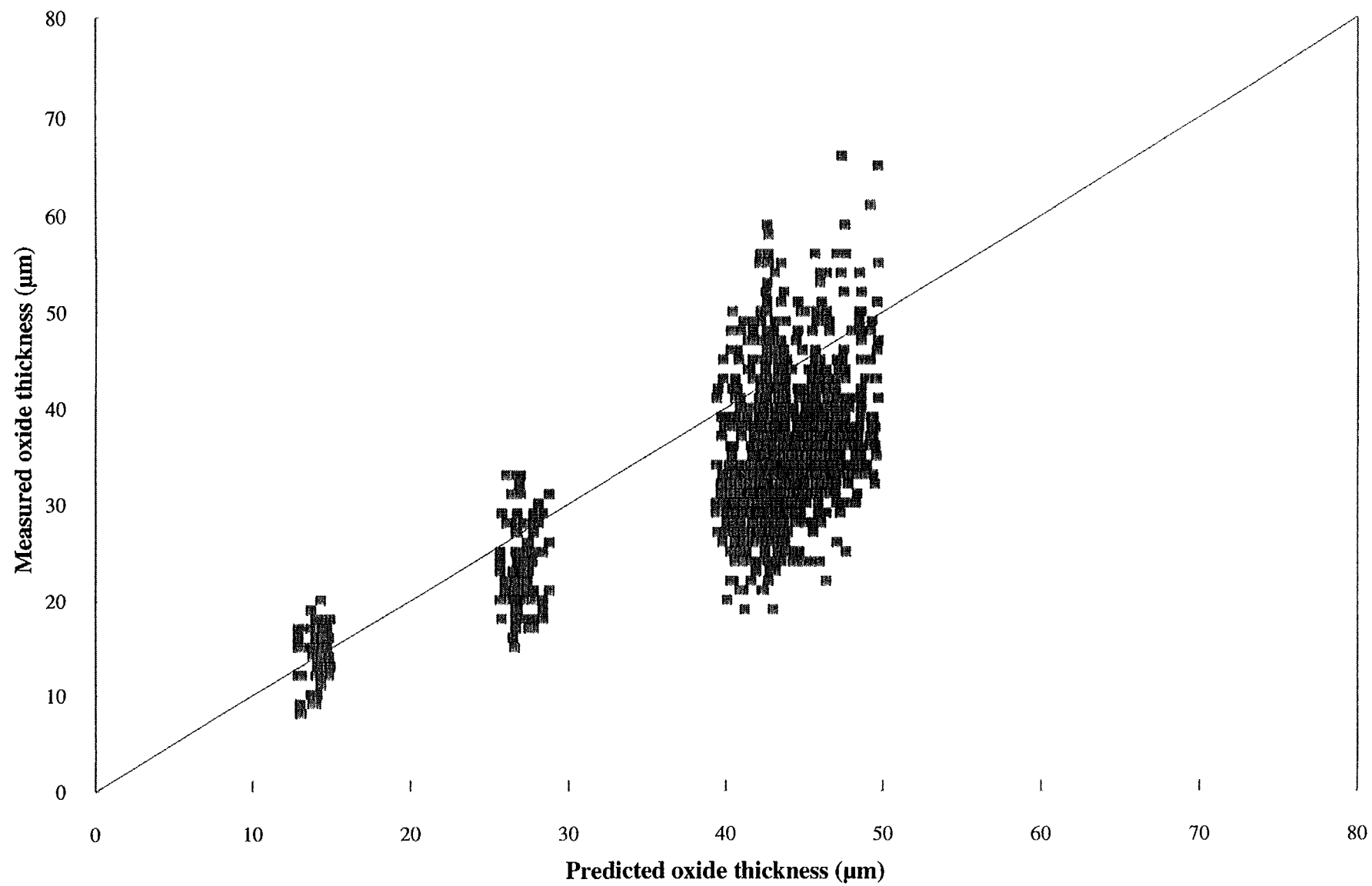


Figure 7 - AFA 2G MEASURED/PREDICTED COMPARISON

TABLE I. THERMAL HYDRAULIC CONDITIONS OF REP 900 AND PRE-CONVOY REACTORS

REACTORS		REP 900	PRE-CONVOY
NOMINAL CORE POWER	(MWt)	2775	3765
ACTIVE CORE LENGHT	(m)	3.65	3.9
GEOMETRY		17x17	16x16
INLET TEMPERATURE	(°C)	284.7	291.3
OUTLET TEMPERATURE	(°C)	321.9	325.2
AVERAGE LINEAR POWER	(kW/m)	17.8	21.1
COOLANT MASS FLOW	(kg/m <sup>2</sup> .s)	2632.3	3314.6

The entire PWR 900 experience feedback on M5 and AFA2G alloys is illustrated in Fig. 9. The measurements were obtained on internal and peripheral rods up to average rod burnup rates of between 50 and 60 GWd/tU.

The results show the large gain obtained by M5 alloy comparatively to the Zircaloy-4.

#### 4.3. Local measurement on internal rods

It has previously been shown that the zirconia thicknesses taken into account in the analyses performed are the maximum thicknesses of the azimuthal averages at the grid span under consideration.

The SABRE provides information on the local thickness, since it is possible to measure the thickness over several generating lines of a number of rods.

Local thickness and the thicknesses of the corresponding azimuthal averages were compared at span 6 of a 17 x 17 assembly, after 1 to 4 cycles of a yearly quarter core management. The alloy studied is AFA2G and a SAN REMO processing case carried out.

Figure 10 represents the relationship between local thickness and the azimuthal average thickness of four generating lines as a function of the azimuthal average thickness.

Each measurement is rounded off to the nearest micron. For thin oxide layers, the local value may apparently be up to 50% higher than average, but in reality the uncertainty of the measurement underestimates this value, which tends, when the measurement uncertainty becomes negligible with regard to the real thickness, to become 15% on average and 25% for the maximum oxide thickness.

The differences in thickness between the generating lines are essentially due to the hydraulic conditions of the channels. The most unfavourable case is when the generating line measured is located opposite a guide tube, since the latter locally increases the neutronic moderation.

#### 4.4. Impact of primary coolant chemistry

For the same management, the chemical specifications of the primary coolant are relatively similar for all PWR utilities (for WWER's, a boric acid/potassium hydroxide/ammonia chemistry

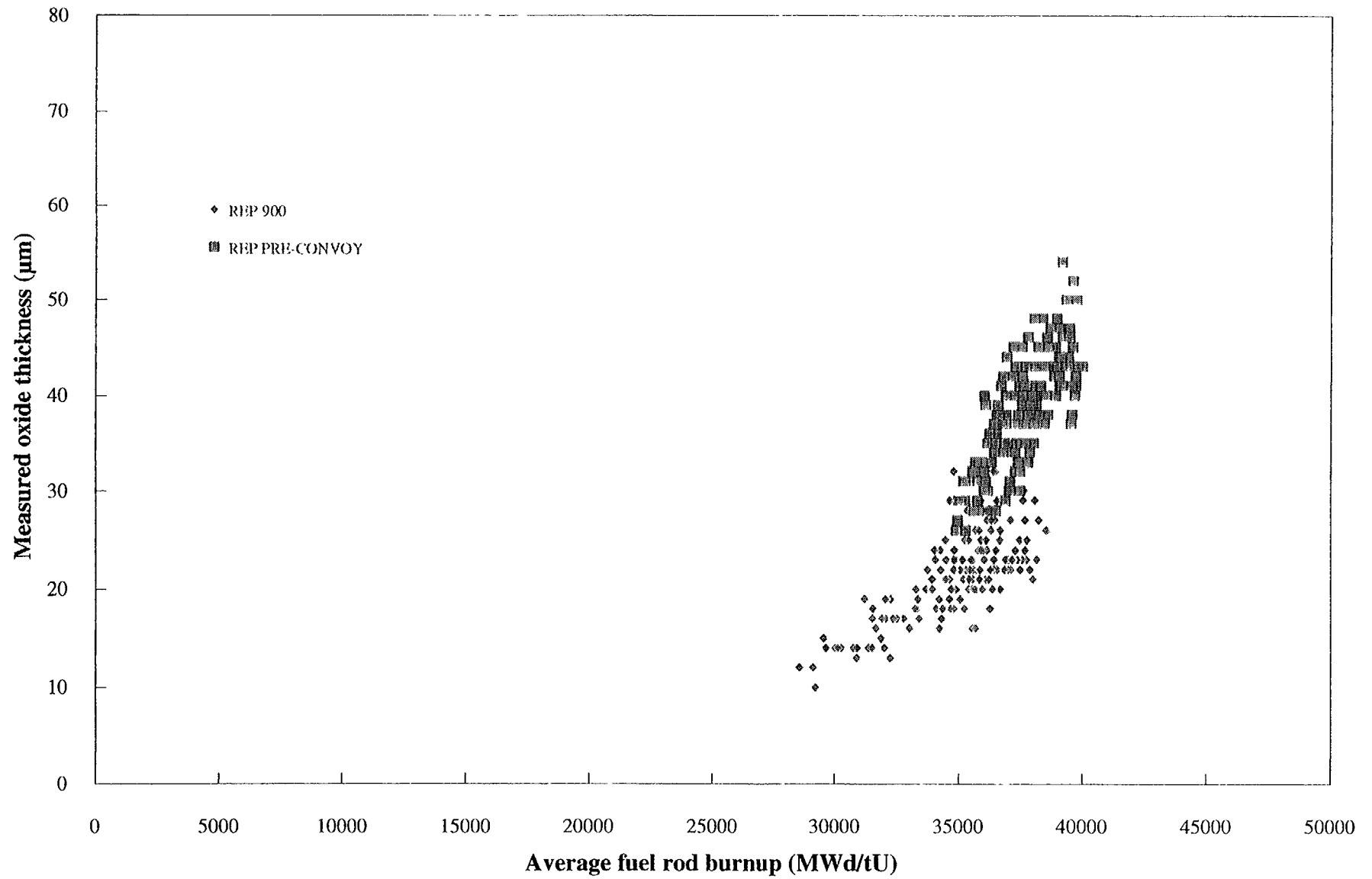


Figure 8 - THERMOHYDRAULICS EFFECT

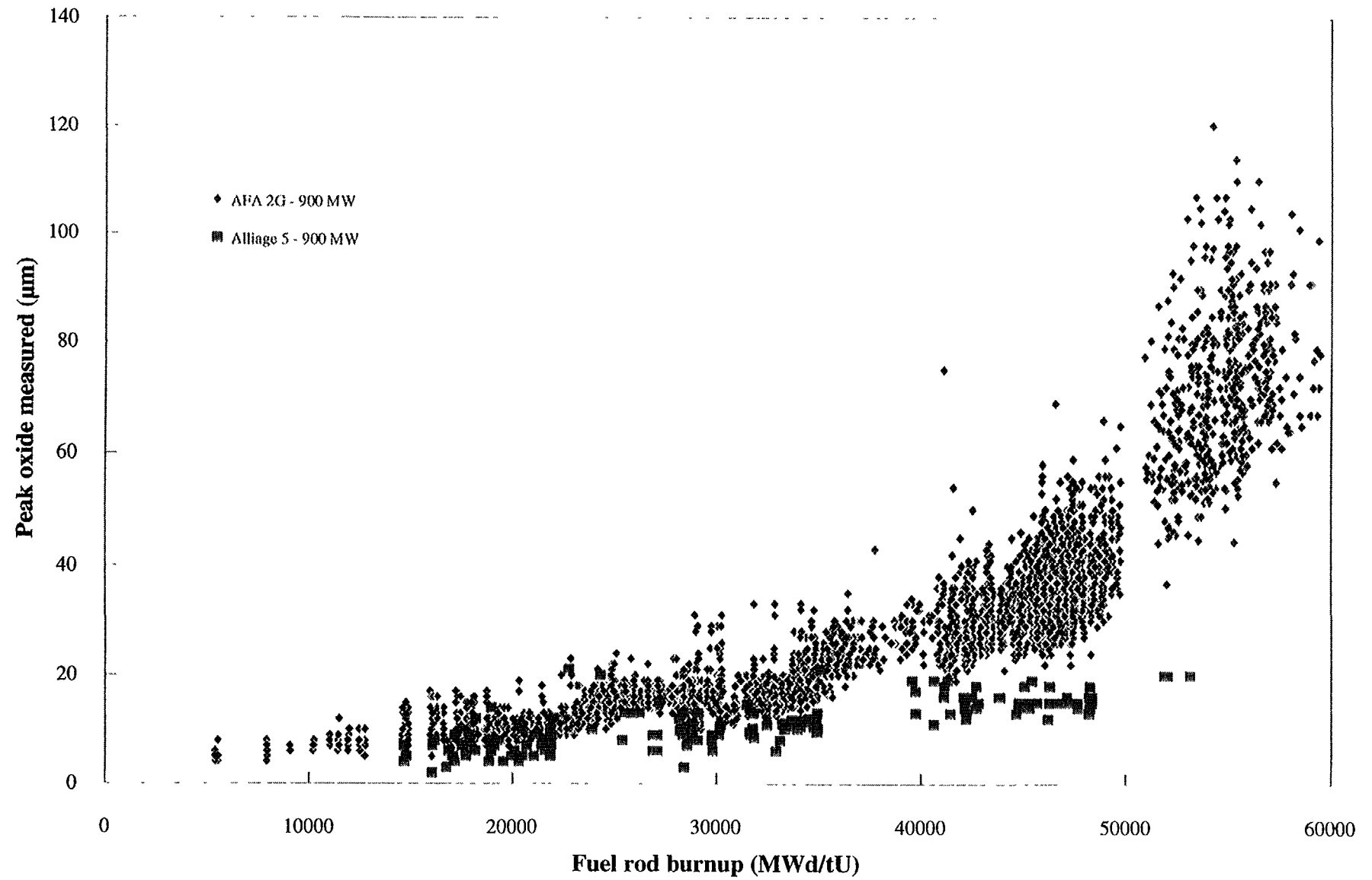


Figure 9 - COMPARISON OF CLADDING MATERIALS

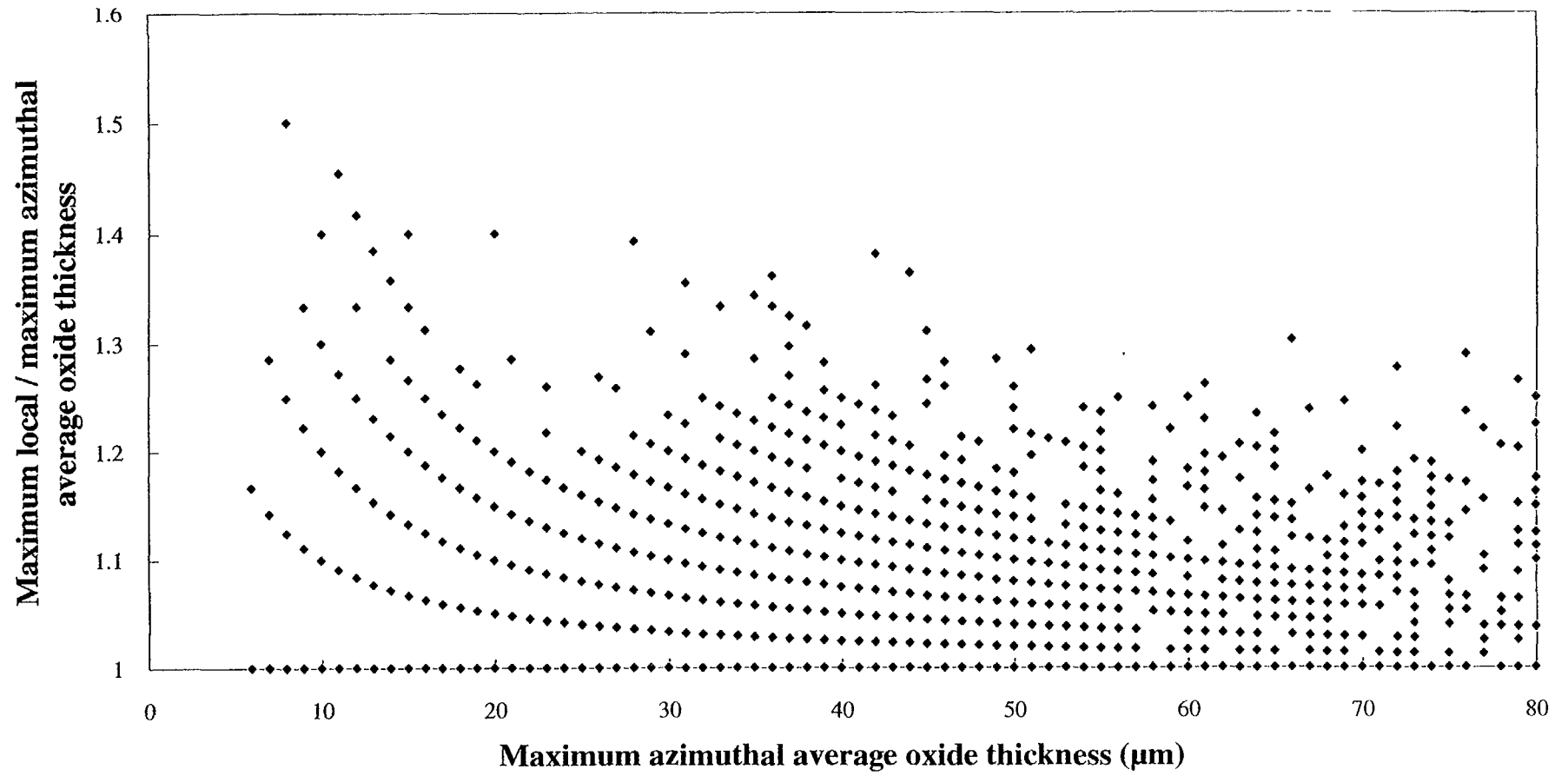


Figure 10 - ANALYSIS OF THE AZIMUTHAL VARIATION OF OXIDE LAYERS

replaces the boric acid/lithium hydroxide/hydrogen chemistry of the PWR's). Generally speaking, the EPRI Guidelines have become the international reference base for PWR utilities [3].

However, there are some specific features related to fuel management for which special chemistry conditions have been studied :

- Load follow operation generates movements of makeup water in the primary circuit which are much greater than base load operation, during the course of successive dilutions and borations of the coolant. This leads to a cumulated introduction of impurities, including oxygen, and to greater difficulties in maintaining, at any instant, the lithium and the hydrogen in the specified concentration ranges.
- During stretch-out operation, very low boric acid concentrations in the primary coolant are frequently attained (<1ppm) with concentrations of lithium hydroxide at the bottom of the specification range (0.4 - 0.6 ppm). This situation is a special one, since the fuel then operates in a lithium hydroxide environment without boron.
- The increase of the cycle length and MOX management requires a higher concentration of boric acid at the start of the cycle. To ensure optimum pH from the start of the cycle (pH at 300° greater than 6.9 at start of cycle and pH 7.2 as soon as possible), an increase in the concentration of lithium from 2.2 to 3.5 ppm expressed as lithium is aimed for.

A special test has been begun in two 1300 MWe reactors, during which corrosion measurements will be made on characterized assemblies comprising AFA2G cladding and cladding made from advanced alloys, all coming from the same cladding manufacturing batches. These will be irradiated in parallel in different chemical conditions.

This test, referred to as the DUO test, is described in [4] and [5]. The SABRE tool has been proposed to analyse the behaviour of claddings at the end of each irradiation cycle.

The full procedure described above should be used to analyse the results of the DUO test.

## 5. CONCLUSION

Behaviour with respect to external corrosion is an important property of fuel since it has become a limiting factor with the increase in burnup and the severity of irradiation conditions.

In order to better characterize the rods with regard to this property, it has become necessary to measure the oxidation of the internal rods of the assembly, it being no longer sufficient simply to take measurements on the external generating line of the peripheral rods.

In order not to have to dismantle the assemblies and extract the internal rods, Framatome has developed the SABRE tool. This tool, which measures the layers of oxide using the Eddy current principle, penetrates inside the assembly between the rows of rods on each face and measures the layers of zirconia on several generating lines of most of the assembly rods. The results, fed into a corrosion database, are compared to prediction to provide better quantification of parameters. The large number of measurements for each assembly measured has justified the parallel development of signal processing systems. Some examples of measurement campaigns carried out in PWR reactors illustrated the possibilities of this tool.

## REFERENCES

- [1] M.MOREL, J.THOMAZET, A.NETTER, G.KOPFF, "Technique and method for upgrading corrosion performance through Framatome fuel experience feedback", Light Water Reactor Fuel Performance (Proc. 1994 Int. Topical Mtg West Palm Beach, Fl., USA, 1994), ANS (1994) 296.



- [2] J.P.MARDON, D.CHARQUET, J.SENEVAT, "Influence of composition and process on out-of-pile and in-pile properties of M5 alloy", Zry in Nuclear Industry (Proc. Int. Conf., Toronto, Canada, 1998) ASTM (in press).
- [3] ELECTRIC POWER RESEARCH INSTITUTE, PWR Primary Water Chemistry Guidelines, Report TR-105714, Palo Alto, Cal., USA (Nov.1995).
- [4] J.C.ROBIN et al, "Modified lithium for extended fuel cycles", Water Chemistry in Nuclear Power Systems (Proc. 7<sup>th</sup> Int. Conf., Bournemouth, UK, 13-17 October 1996) BNES (1996) vol. 2 466.
- [5] J.L.BRETELLE et al., "Extended fuel cycle: the DUO experiment", Water Chemistry in Nuclear Power Plants (Proc. 1998 JAIF Int. Conf., Kashiwazaki, Japan, 1998) JAIF (1998) 170.

# IRRADIATION EFFECTS, CORROSION TESTING

(Session 2)

NEXT PAGE(S)  
104 BLANK

V. VRTÍLKOVÁ, J. JAROS, J. ČMAKAL  
ŠKODA-ÚJP,  
Prague

M. VALACH, M. LAHODOVÁ  
NRI Rez.

Czech Republic

## Abstract

This paper includes continuous results of long-time corrosion tests of Zr alloys, being a part of the "Corrosion of Zr alloys" project (in the frame of CEZ, Czech republic).

The results confirm a poor corrosion resistance of Zr1Nb alloys in a water environment exhibiting a higher Li concentration, a poor corrosion resistance of Zry-4 type alloys in a steam environment at temperatures exceeding 450 °C. On the other hand the results confirm very good corrosion properties of Zr1Nb in steam, Zry-4 Improved in 400 °C steam and ZIRLO alloy in a 360 °C higher Li water environment.

## 1. INTRODUCTION

Corrosion problems of Zr alloys in Czech Republic were studied previously on Zr1Nb cladding tubes used in VVER type nuclear power plants. It was shown that under VVER coolant conditions this alloy exhibits both a good corrosion and hydriding resistance and the radiation does not influence the corrosion rate. Having terminated detailed long-time corrosion tests our attention was paid to the oxidation and creep behaviour of Zr1Nb cladding tubes at high temperatures [1].

Based on the decision that Zry-4 clad fuel elements will be used in the Nuclear Power Plant Temelín, that it will be possible to effect non-destructive post-irradiation oxide thickness measurements and that an irradiation corrosion experiment in the NRI Rez corrosion loop is in preparation, it was evident that for evaluating the results it would be useful to study in more detail the corrosion resistance of these alloys together with a conventional Zry-4 alloy and with perspective alloys such as ZIRLO.

A long-time capacity demanding program of corrosion tests with a 5 year maximum exposure time was proposed. The corrosion conditions were chosen so as to show both pros and cons of particular alloys. The advantage of these tests consists in the fact that all alloys are exposed to identical conditions. The specimens selected for destructive testing are replaced by fresh ones and a constant number of specimens is maintained in the autoclave. In the MS Access program of ALEF Ltd. a CORROSION data base was proposed enabling to record data on specimens (dimensions, initial weight, weight after individual exposures, hydrogen content, specimen position on the rack etc), to evaluate the corrosion history of particular specimens, corrosion rate and average weight gains, to record the temperature history of the test, visual inspection of specimens, to print the forms for weighing and further evaluating etc, serving in this way for a rapid orientation in the results. At present, the data base contains 30 000 data.

Another part of the program consists in a systematic research of corrosion layers of these alloys aimed at the investigation of the development of porosity using the EIS method and a high-pressure mercury porosimetry, the development of stress in oxide and metal using X-ray tensometry, the development of morphology of oxide inner and outer surfaces incl. the oxide cracking using SEM and AFM methods,

the development of a fraction of tetragonal oxide using Raman spectrometry and changes in chemical composition of corrosion layers using ESCA (SIMS) method.

In this program part, the methodics were developed and the research was started. We suppose the results will be stored within the data base. In this paper only some results will be stated.

## 2. EXPERIMENTAL CONDITIONS

For corrosion testing, we used 3 cm long specimens, made of reactor grade cladding tubes in Zr1Nb, Zry-4 Improved (with a lower Sn content), Zry-4 conventional and ZIRLO. The specimens were degreased only (not pickled).

The corrosion tests were performed in LAM 104 and LAM 304 autoclaves (4 litres). Tests in oxygenated water (43 ppm oxygen) were performed in on open loop. The flow of the corrosion medium was provided by a LCP 3001 high-pressure chromatographic pump (600 ml/h).

The autoclave average temperature was  $\pm 3$  °C relative to the nominal temperature.

The absorbed hydrogen in the alloy was determined using the Exhalograph device. Oxide thickness measuring and hydride character studying was made using a Nikon metallographic microscope with a LUCIE image analyzer.

The corrosion tests were performed in a 360 °C water environment with additions imitating the VVER 1000 coolant, with 70 ppm Li, with 43 ppm O<sub>2</sub> and in 400, 425 and 450 °C steam.

## 3. RESULTS

Initially, a black, bright and adhesive oxide formed on all specimens. This oxide was turning light (or spalled) in dependence on the exposure time and environment. Nodular corrosion was observed on Zr1Nb in 70 ppm Li 360 °C water after a 105 d exposure, on conventional Zry-4 in 400 °C steam after 126 days and on Zry-4 Improved in 450 °C steam after 21 days (see Fig. 1).

The oxidation kinetics of the alloys studied in VVER water environment, in water with 70 ppm Li and in 400 °C steam is illustrated in Fig. 2. The results confirm the data of other authors [2 -3].

In Fig. 3 is shown the output of the CORROSION data base documenting the characteristic differences in the course of specimen corrosion on Zr1Nb (see Fig. 3a) and other alloys (see Fig. 3b) in VVER water.

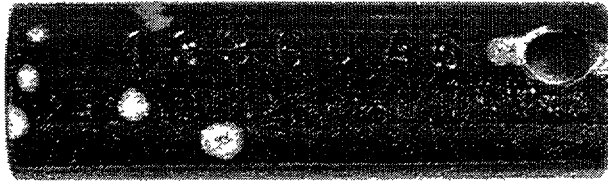
Fig. 4 Similarly documents the differences between the Zr1Nb alloy and the other alloys in dependence of the percentage of hydrogen versus the weight gain.

Fig. 5 documents the morphology of Zr1Nb alloy hydrides in dependence on the hydrogen content. In Fig. 5c a radial distribution of hydrides is illustrated which was observed after tests in Li - containing water. The stress needed to provoke such a distribution is probably caused by a non-uniform oxide thickness on both the outer and the inner tube wall.

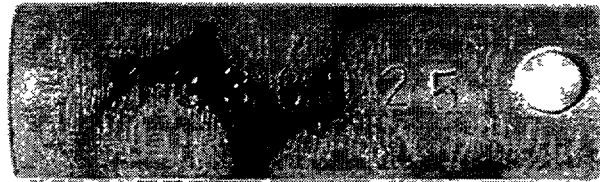
Fig. 6 documents the morphology of hydrides on Zry-4 and ZIRLO alloys, exhibiting predominantly a tangential orientation and being not so massive as for the Zr1Nb alloy.

Fig. 7 illustrates the oxidation kinetics of two ZIRLO alloy specimens as well as the oxide character of these specimens (oxide sublayers related to jumps in the kinetic curve).

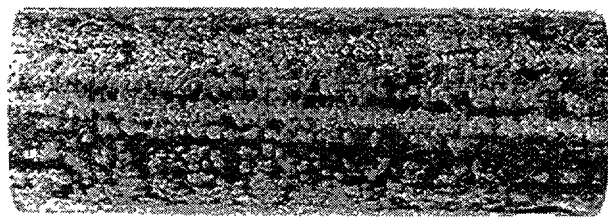
The above mentioned results are consistent with the literature data [2-3]. This is an important presumption for further detailed studies of corrosion properties using special methods mentioned at the beginning.



Zr1Nb  
water 360°C  
+ 70 ppm Li  
105 days



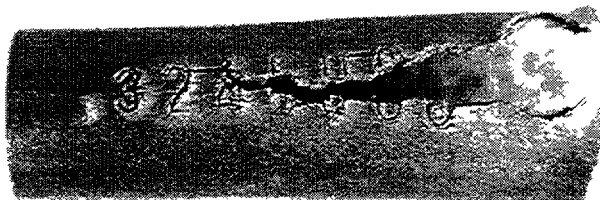
Zr1Nb  
water 360°C  
+ 70 ppm Li  
126 days



Zry-4 conventional  
steam 400°C  
126 days



Zry-4 conventional  
steam 450°C  
3 days



Zry-4 improved  
steam 450°C  
21 days

*FIG. 1 . Nodular corrosion was observed on all alloys except ZIRLO.  
The indicated exposure times represented the first occurrence of the nodules*

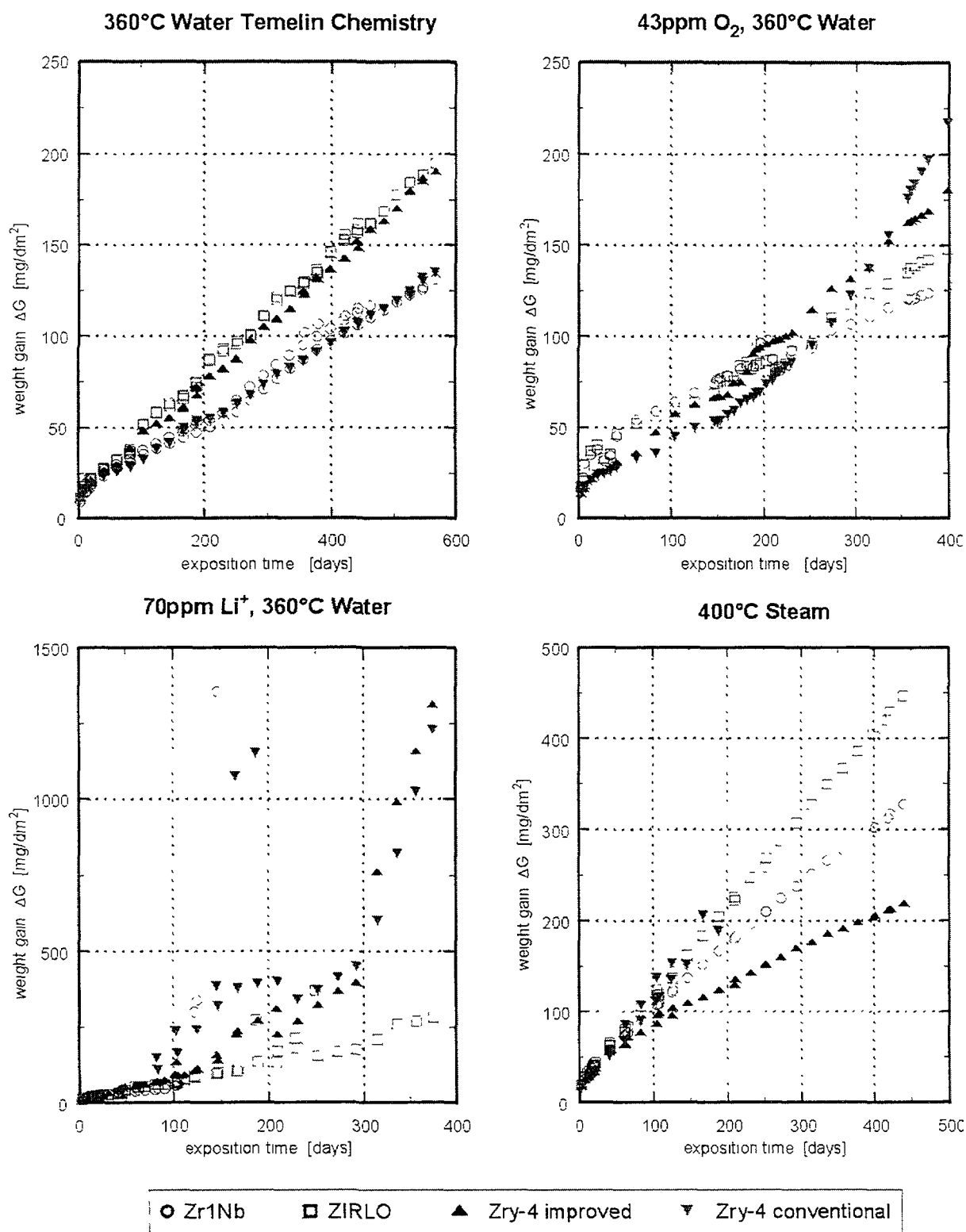
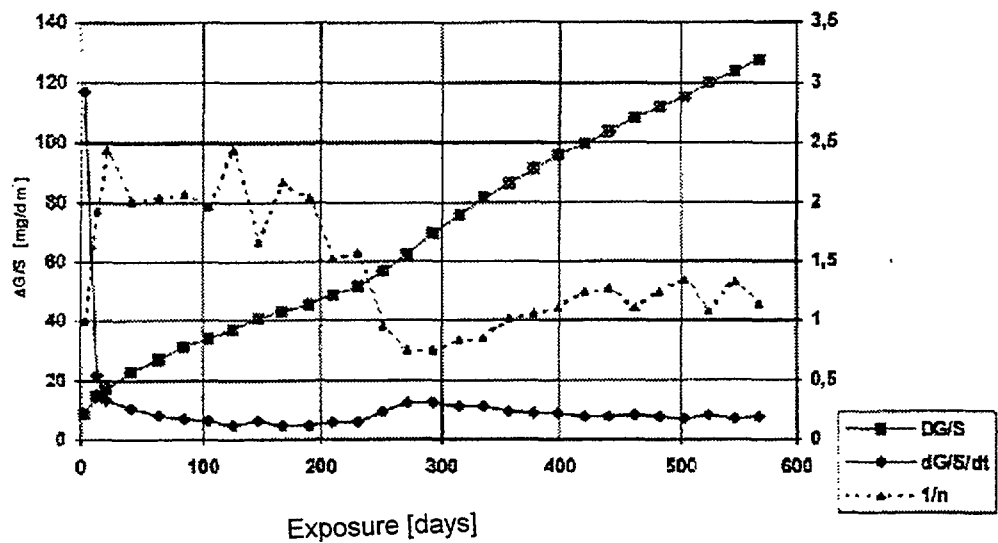
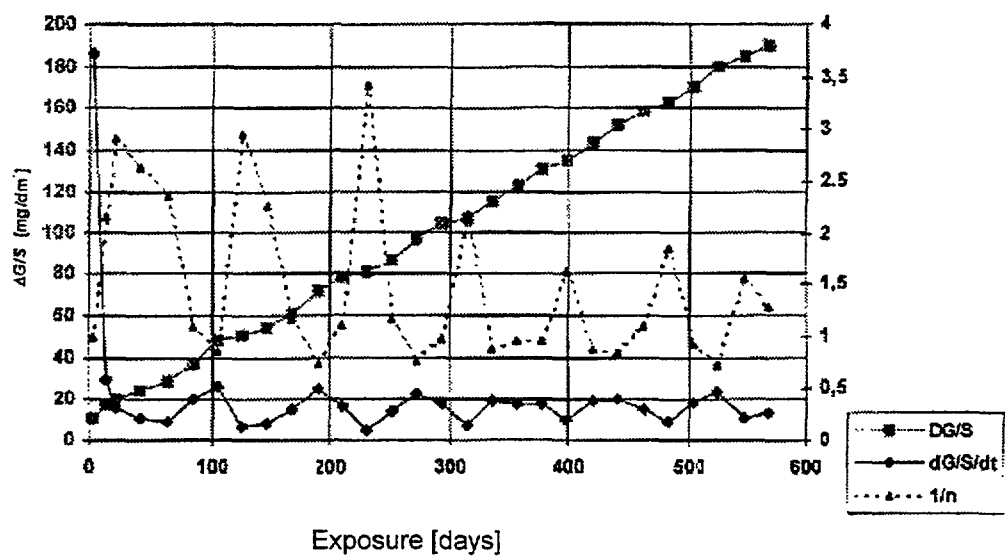


FIG. 2. Corrosion kinetics of the studied Zr-alloys in different environments

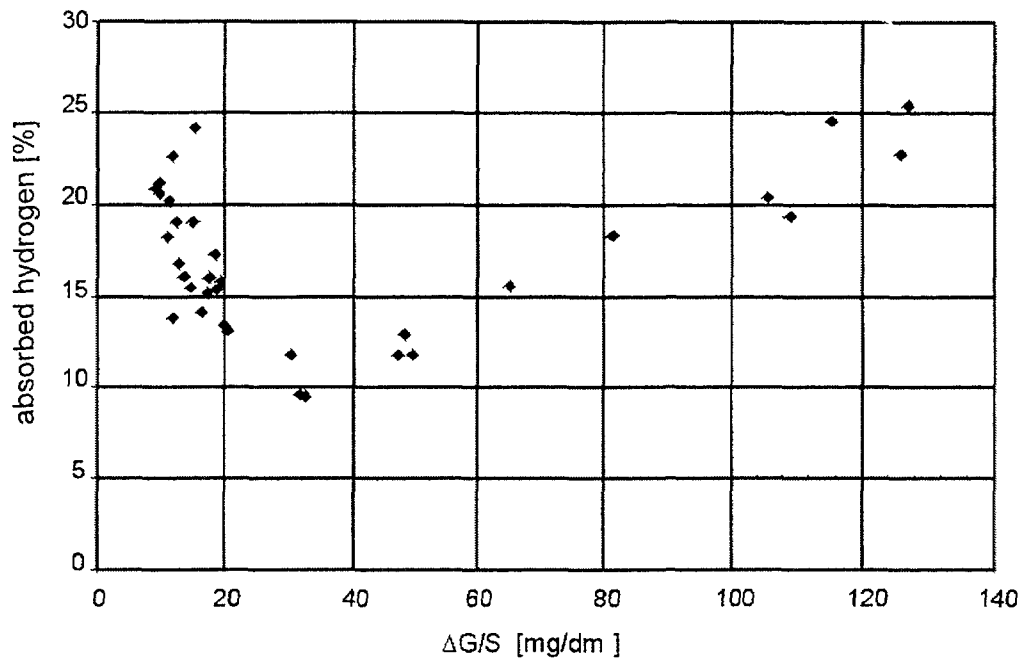


a) Corrosion kinetics of Zr1Nb alloy

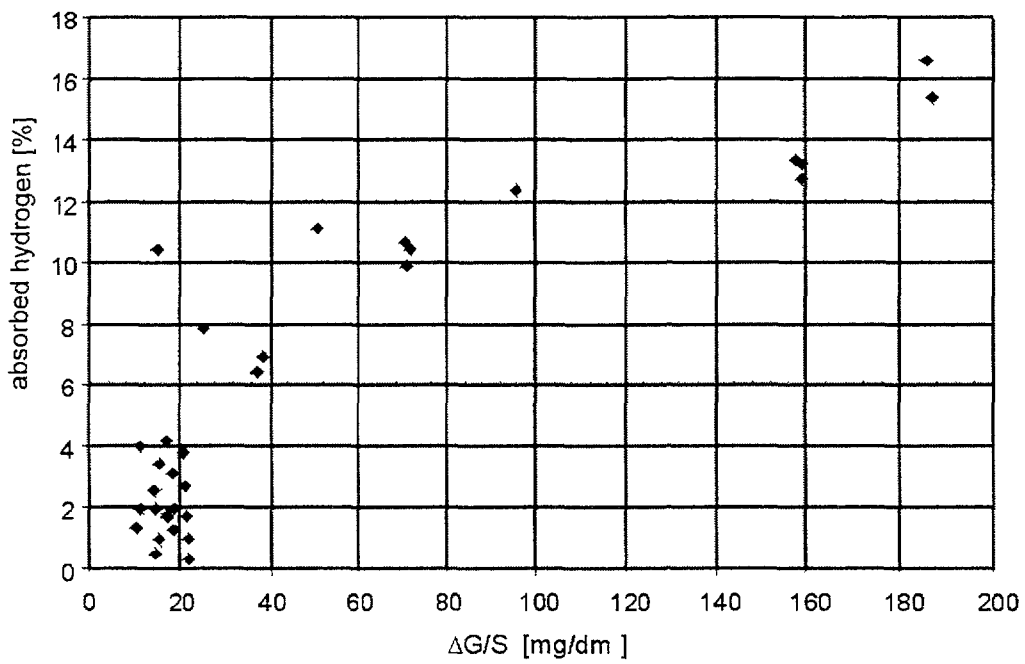


b) Corrosion kinetics of Zry-4 Improved alloy

FIG. 3. Example of the output from database "KOROZE"



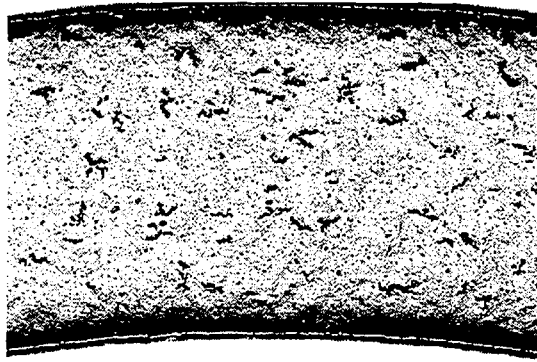
a) Percentage of the absorbed hydrogen versus weight gain for Zr1Nb



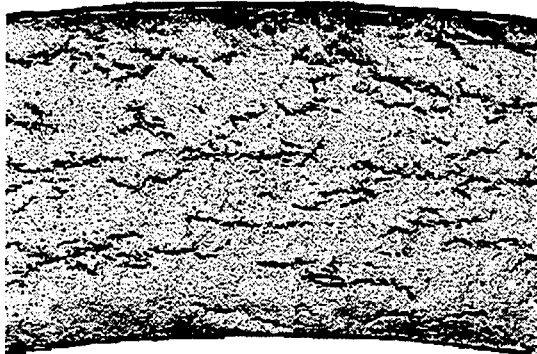
b) Percentage of the absorbed hydrogen versus weight gain for Zr $\gamma$ -4 Improved

FIG 4 Example of the output from the database "KOROZE"

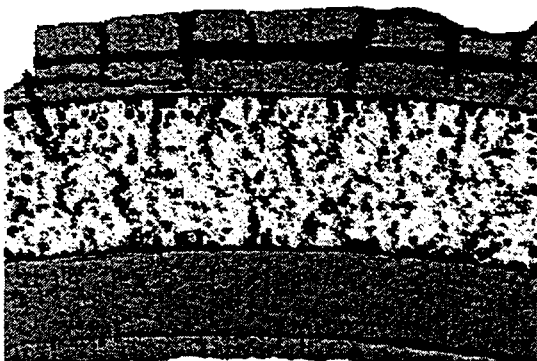




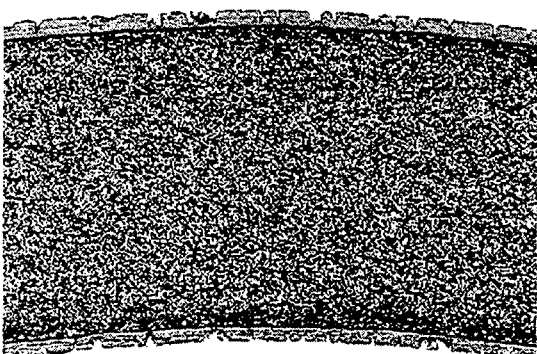
a) 27,5 ppm  $H_2$



b) 158,5 ppm  $H_2$

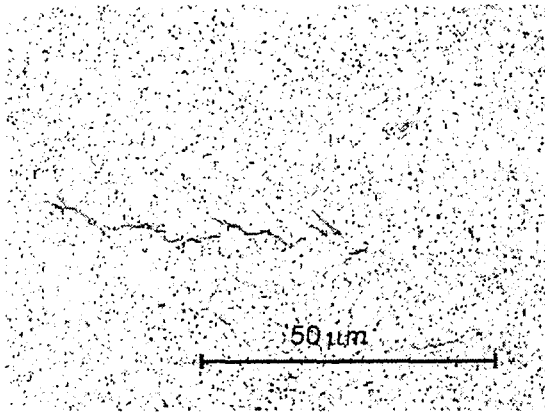


d) 630 ppm  $H_2$

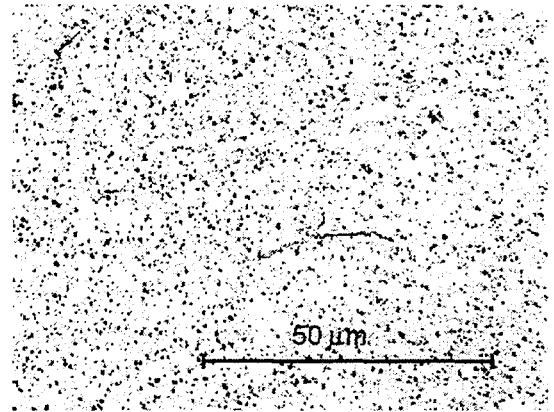


d) 1600 ppm  $H_2$

*FIG. 5. Characteristic morphology and distribution of hydrides in Zr1Nb.*



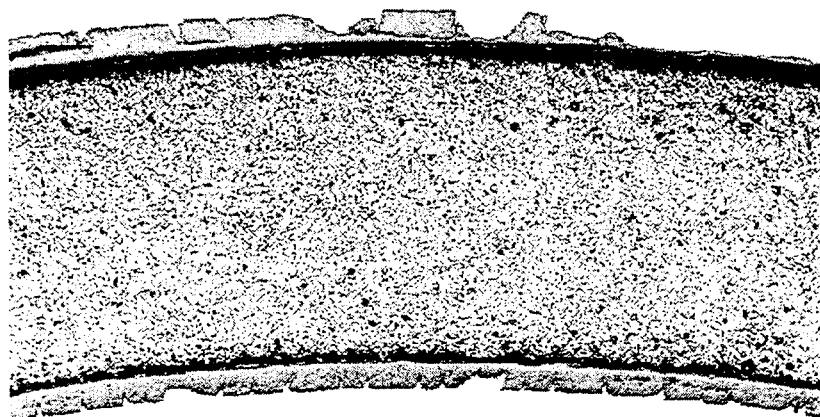
a) 59 ppm  $H_2$



b) 21 ppm  $H_2$



c) 178 ppm  $H_2$



d) 1915 ppm  $H_2$

FIG. 6. Characteristic morphology and distribution of hydrides in both Zr-4 and ZIRLO

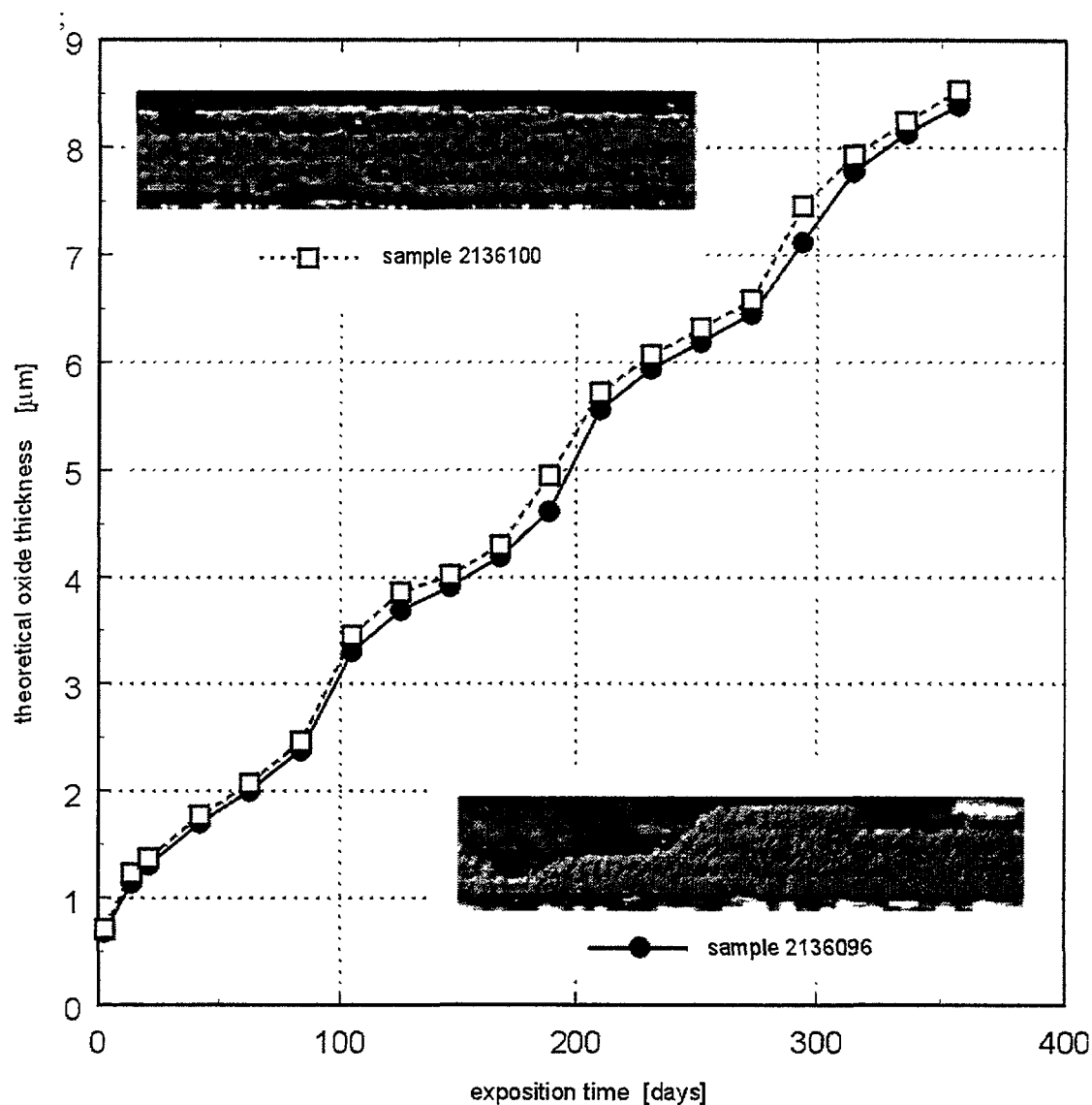


FIG. 7. Example of an oxidation kinetics of ZIRLO in 360°C VVER water

#### 4. REFERENCES

- [1] VRTÍLKOVÁ V., VALACH M. MOLIN L.: "Oxigen and hydriding properties of Zr1Nb cladding material in composition with Zircalloys", Influence of Water Chemistry on Fuel Cladding Behaviour (Proc. TC Mtg Rez, Czech Republic, 1993), Vienna IAEA-TECDOC-927 (1997) 227-251
- [2] SABOL, G.P., COMSTOCK, R.J., WEINER, R.A., LAROUERE, P., and STANUTZ, R.N., "In-Reactor Corrosion Performance of ZIRLO and Zircaloy-4," Zirconium in the Nuclear Industry (Proc Tenth Int. Symp., West Conshohocken, PA, USA, 1994) ASTM STP 1245, A.M. Garde and E.R. Bradley, EDS., American Society for Testing and Materials, 724-744.
- [3] INTERNATIONAL ATOMIC ENERGY AGENCY, "Waterside Corrosion of Zr Alloys in Nuclear Power Plants", IAEA-TECDOC-996, Vienna (1998).

NEXT PAGE(S)  
left in AIAA

F. GIBERT, C. COUVREUR, D. DAMIEN, M. GAUTIER-SOYER,  
N. THROMAT, M.J. GUITTET  
Centre d'études Nucleaires de Saclay,  
Gif-Sur-Yvette

S. BOUFFARD  
DRECAM/CIRIL, BP  
Caen

Y. SERRUYS  
Centre d'études Nucleaires de Saclay,  
Gif-Sur-Yvette

E. ELKAÏM  
Université Paris Sud,  
Orsay

France

## Abstract

PWR irradiation has a specific effect on the Zircaloy 4 oxidation kinetics and increases strongly corrosion for high burn-ups. As zirconia layer is the first barrier against metal oxidation, we focused our study on the crystallographic characterization of non-radioactive zirconia samples irradiated by low and high energy heavy ions and on radioactive samples coming from PWR rod claddings. We first studied the impact of ionic irradiation on pure, powdery, monoclinic zirconia, using  $Kr^{n+}$  and  $Ar^{n+}$  ions of high energy (respectively 170 MeV and 190 MeV). Then, we studied the impact of high and low energy  $Ar^{n+}$  ions (respectively 80 MeV and 4 MeV) on zirconia samples formed on Zircaloy 4 plates by water corrosion (10 days, 400°C, 10.3 MPa). As means of characterization, we mainly used X-ray diffraction with a powerful exploitation method : the Rietveld, Full Pattern Matching, method. In the case of non-radioactive samples, we also used Raman microscopy for local examinations. By and large, the obtained results demonstrate that ionic irradiation always favors the transformation of a fraction of monoclinic zirconia into tetragonal zirconia. This transformation is correlated to a stress field creation and to changes in cell parameters. The observations of fuel rod claddings show that PWR irradiation leads to similar effects. Especially, we evidenced the presence of tetragonal zirconia in the whole external oxide layer, which is fully different from the case of corresponding non-irradiated samples. The internal zirconia layer, which in addition undergoes fission product bombardment, is totally constituted of tetragonal zirconia. All the crystallographic transformations ascribable to irradiation are detrimental to zirconia layer cohesion. As a matter of fact, changes in cell volumes or in stresses will cause sooner or later cracks or material decohesion. Therefore, the diffusion of oxidizing species and so, corrosion, must be accelerated.

## 1. INTRODUCTION

It has been demonstrated that PWR irradiation has a specific effect on the oxidation kinetics of Zircaloy-4 and that it significantly rises corrosion at high burnups, hence the current fuel rod lifetime of about three years [1,2]. In an attempt to understand irradiation role, three main parameters have to be taken into account : the effect of irradiation on the metal (reaction place), the effect of irradiation on the coolant (oxidizing species formation place) and the effect of irradiation on the zirconia (oxidizing species diffusion place). As zirconia is the first barrier against metal oxidation, we chose to concentrate on this third aspect by characterizing the crystal structure of non-radioactive zirconia samples irradiated by low or high energy heavy ions, and of radioactive samples taken from PWR reactors [3]. The aim of ionic irradiation is not so much to accurately simulate PWR radiation

but to precise the consequences of different kinds of interaction on the crystal structure of zirconia and their consistency with observations made on PWR samples.

## 2. EXPERIMENTAL TECHNIQUES

### 2.1. Heavy ions irradiation

The choice of using heavy ions was motivated by different reasons. For one, heavy ions can be used to induce defaults production, either by collisions cascades with a number of displacements per atom (dpa) comparable to neutrons in the case of low energy ions (a few MeV) or by a mechanism due to intense electronic excitations in the case of high energy ions (some tens or hundreds of MeV). For another, once they have been bombarded, the samples are only very slightly radioactive and can be handled safely outside hot laboratories, which, of course, is not the case of PWR spent fuel rod claddings.

In an attempt to determine the influence of Zircaloy (presence of a metal substrate and alloying elements Fe, Cr and Sn) on the behavior of zirconia, two kinds of sample were used: first, pellets obtained by sintering of pure, powdered commercial zirconia (monoclinic structure) and second, previously-oxidized plates of Zircaloy-4 (H<sub>2</sub>O, 400°C, 10.3 MPa, 10 days) with a 1 µm thick zirconia layer containing a small proportion of tetragonal phase [4, 5].

Note : in normal pressure and temperature conditions, the monoclinic phase is the stable phase of zirconia.

The low-energy bombardment was carried out at the *Commissariat à l'Energie Atomique (CEA)* in Saclay in the *Service de Recherche en Métallurgie Physique* using a Van de Graaff generator. The particles used were argon ions with a total energy of 4 MeV. The high-energy bombardment was carried out in Caen using the *Grand Accélérateur National d'Ions Lourds (GANIL)*. The particles used were either krypton or argon ions with an energy level between 80 and 180 MeV.

So that both irradiation operations could be compared, the TRIM software was used to estimate, for each, the contribution of elastic interactions through the nuclear stopping power and of the corresponding dpa, as well as the contribution of inelastic interactions through the electronic stopping power and of the deposited dose (see Table 1). The oxygen and zirconium displacement energy threshold was taken as being 20 eV. In the case of oxidized plates, the penetration distance of the particles in zirconia is far greater than the thickness of the layer (~1µm) for high-energy ions (> 10 µm) and slightly greater for low-energy ions (~ 1.5 µm).

TABLE I. CHARACTERISTICS OF ION BOMBARDMENTS

Sample	Type of irradiation	Maximum fluence (ions/cm <sup>2</sup> )	Nuclear stopping power (keV/µm)	dpa	Electronic stopping power (MeV/µm)	Deposited electronic energy (eV/µm <sup>3</sup> )
Commercial zirconia 1	Kr 170 MeV	1 x 10 <sup>14</sup>	37	3.5 x 10 <sup>-3</sup>	19	1.9 x 10 <sup>13</sup>
Commercial zirconia 2	Ar 190 MeV	1 x 10 <sup>14</sup>	5	4 x 10 <sup>-4</sup>	6.5	6.5 x 10 <sup>12</sup>
Thermal zirconia 1	Ar 80 MeV	1.7 x 10 <sup>15</sup>	10	1.6 x 10 <sup>-2</sup>	8.2	1.4 x 10 <sup>14</sup>
Thermal zirconia 2	Ar 4 MeV	4 x 10 <sup>15</sup>	256	1.2	2.7	1.4 x 10 <sup>14</sup>

Samples were systematically analyzed by X-ray diffraction either *in situ* in GANIL (INEL CPS 120 diffractometer) or, after being bombarded, in the *Laboratoire pour l'Utilisation du Rayonnement Electromagnetique (LURE)* in Orsay, so that advantage could be taken of the resolution provided by synchrotron radiation. Some samples were also characterized by X-Ray Photoelectron Spectroscopy (XPS) in the *Service de Recherche sur les Surfaces et l'Irradiation de la Matière (SRSIM)* at Saclay and by Raman scattering in our own laboratory.

## 2.2. PWR irradiation

In this case, the nature of radiation is more complex because of its multiplicity (neutrons, gamma rays etc.). The fuel rods we chose to analyze operated between 1 and 5 cycles and different positions in the rod length were studied (Spans 2, 4 and 6) so that the change in the crystal structure of the outer zirconia could be monitored as a function of both irradiation and oxidation level. In these conditions, the thickness of the zirconia layer varied between 3  $\mu\text{m}$  and 80  $\mu\text{m}$ , depending on the sample. The nature of the inner zirconia was also studied.

Sample characterization was carried out at Saclay in the SEMI/LECM using equipment installed in hot cells specially adapted to highly-radioactive samples. X-ray diffraction measurements were taken using a Siemens D500 diffractometer.

## 3. RESULTS

### 3.1. Bombardment with ions

#### 3.1.1. Commercial zirconia

Two commercial zirconia pellets were bombarded with 170 MeV krypton ions or with 190 MeV argon ions.

Figures 1 and 2 show that irradiation with krypton ions causes the almost total transformation of monoclinic zirconia into tetragonal zirconia. As a break in the evolution of all crystallographic parameters is observed when the phase transformation took place, the mechanism might involve a threshold phenomena. This transformation is accompanied by an increase of the monoclinic phase cell volume and a decrease of the tetragonal phase cell volume. Rietveld analysis [6] of the diffraction spectra revealed an increase of the microstresses in the monoclinic phase after transformation. It should be noted that the surface color of the zirconia changed from white to brown.

On the other hand, argon ions do not appear to cause any perceptible change in the crystal structure, nor did the color change. Only a large, solid background in the Raman spectra, caused by produced defaults, attested irradiation.

All these observations allow us to imagine a mechanism where, in the early stages, irradiation disorganized the monoclinic phase, leading to a reduction of the size of the coherent domains and a swelling of the cell. Then, once this disorder has exceeded a particular threshold, probably corresponding to an adequate recovery of the ions trace, the structure reorganizes itself to form the metastable phase closest to this state : the tetragonal phase. In the case of argon ions, it seems that the threshold has not been reached due to the fact that the nuclear and the electronic stopping power of argon ions are respectively 7 and 3 times lower than those of krypton ions.

#### 3.1.2. Thermal zirconia

A first series of Zircaloy-4 plates was bombarded in GANIL with 80 MeV argon ions. These ions caused partial transformation of the zirconia (ranging from 15% to around 30%) from the monoclinic to the tetragonal phase (see Figures 3 and 4). It should be noted that in view of the thin oxide layer, tetragonal zirconia was already present before irradiation. Irradiation also caused a decrease of the cell volume of each phase (Figure 5). Rietveld analysis revealed that these evolutions

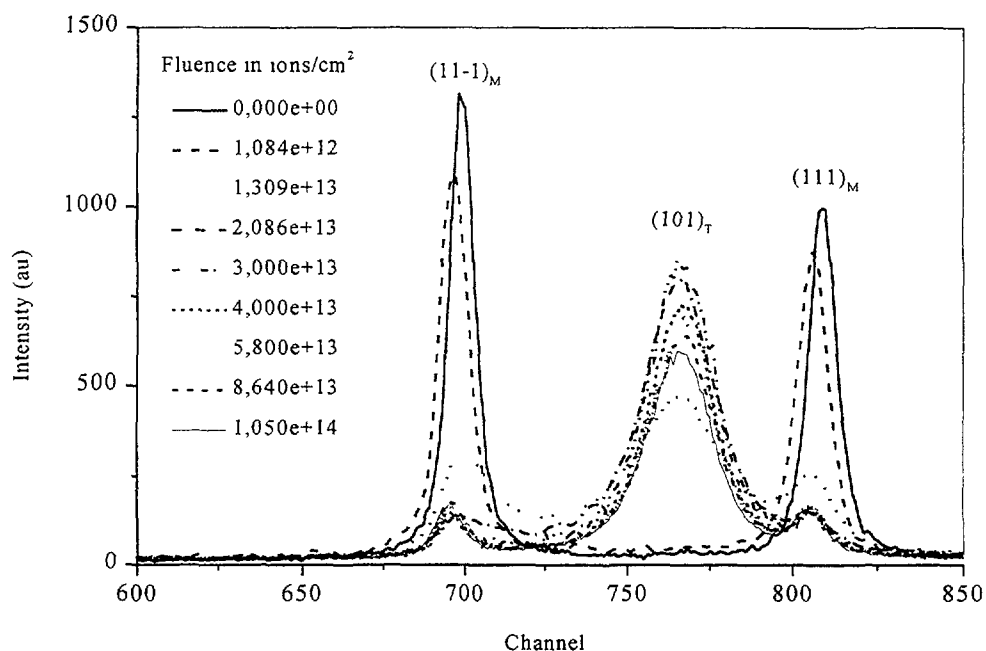


FIG. 1. Effect of bombardment with 170 MeV Kr ions  
Monoclinic  $\text{ZrO}_2 \rightarrow$  Tetragonal  $\text{ZrO}_2$  transformation

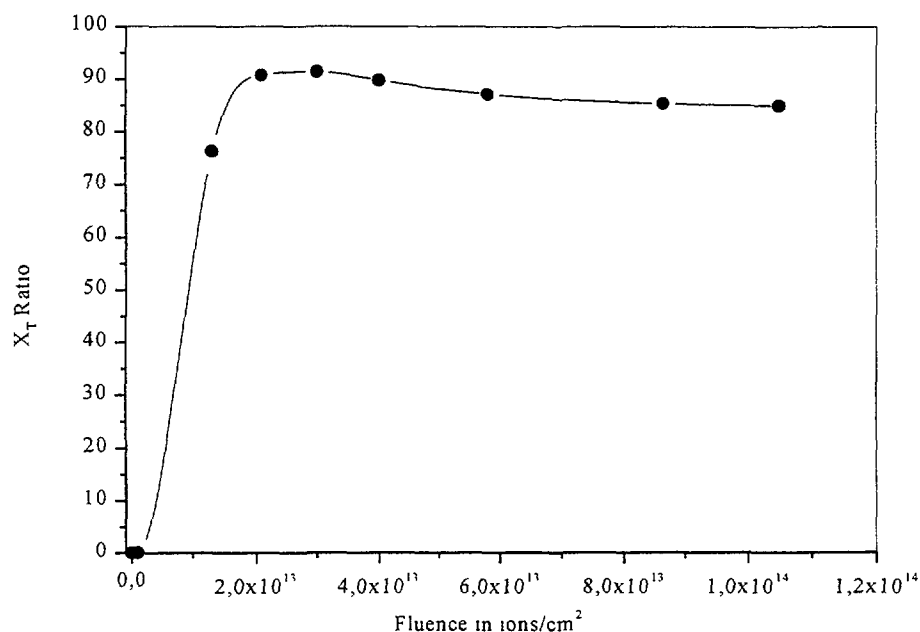


FIG. 2. Change in tetragonal phase content ( $X_T$ ) in zirconia bombarded  
with 170 MeV Kr ions as a function of ionic fluence

were accompanied by an increase of the size of the coherent domains and of the microstresses. Finally, examination by XPS of the irradiated sample with the highest fluence revealed the presence of  $\text{Zr}^{n+}$  ions where  $n < 4$ , mainly  $\text{Zr}^+$  ions. This implies that although the changes in crystal structure were quite different from those observed in commercial zirconia, electron faults are still involved. So, the observed difference can certainly be attributed more to the nature of the samples (existence or not of Zircaloy substrate, stress field, particle size, alloying elements, etc.) than to irradiation conditions.

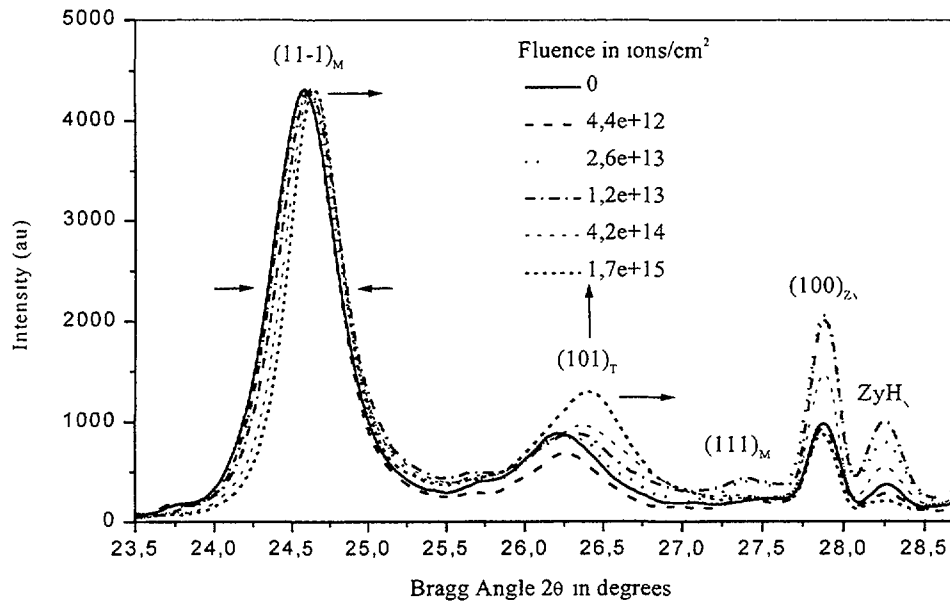


FIG. 3. Effect of bombardment with 80 MeV Ar ions on thermal zirconia  
Monoclinic  $\text{ZrO}_2 \rightarrow$  Tetragonal  $\text{ZrO}_2$  transformation

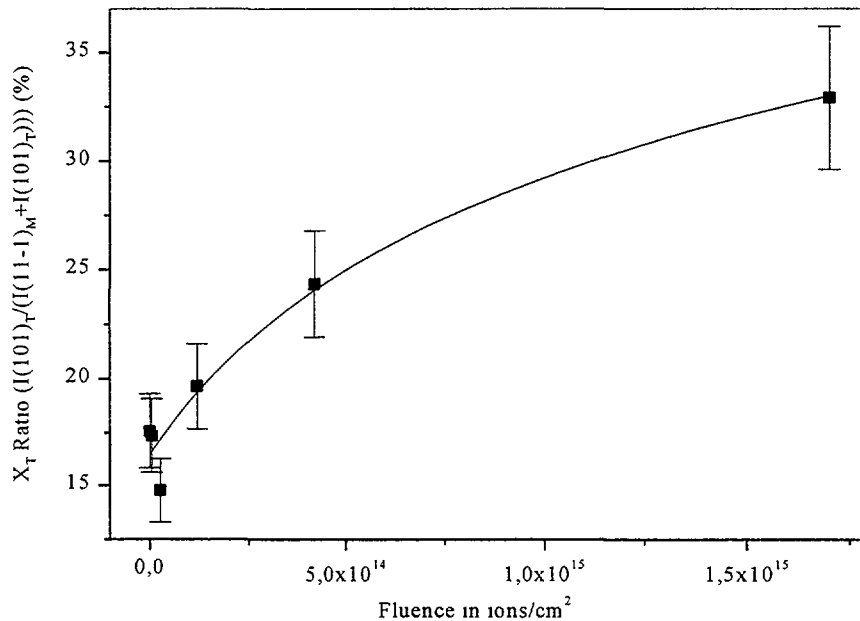


FIG. 4. Effect of bombardment with 80 MeV Ar ions on thermal zirconia  
Change in tetragonal phase content ( $X_T$ ) as a function of ionic fluence

Another sample was bombarded with 4 MeV argon ions. This sample was only characterized after irradiation since the facility had no equipment for *in situ* characterization. As in the case of high-energy irradiation, an increase of tetragonal phase content was observed (Figure 6). On the other hand, the crystallographic parameters were less affected, particularly as far as the monoclinic phase was concerned. The microstresses seemed to have slightly decreased in the monoclinic phase but the appearance of the sample surface tended to imply that part of these microstresses had been released. The change in the width of the tetragonal phase diffraction peak (101) seemed to indicate a crystallite growth.



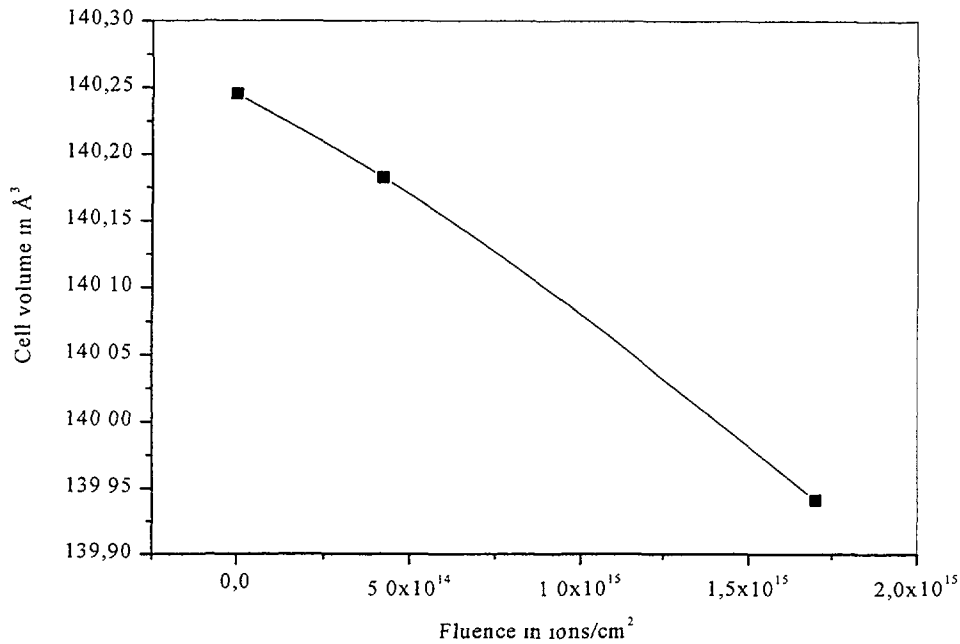


FIG 5 Effect of bombardment with 80 MeV Ar ions on thermal zirconia  
Change in crystalline monoclinic zirconia cell volume as a function of ionic fluence

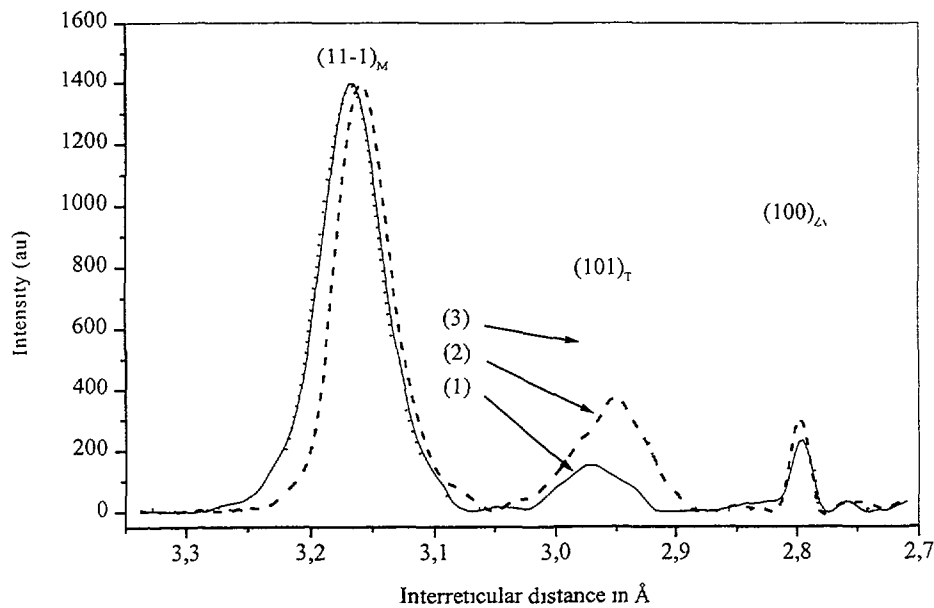


FIG 6 Transformation of monoclinic zirconia into tetragonal zirconia  
Comparison between non-irradiated thermal zirconia (1), thermal zirconia bombarded with 80 MeV Ar,  $1,7 \times 10^{15}$  ions/cm² (2) and thermal zircon bombarded with 4 MeV Ar ions,  $5 \times 10^{15}$  ions/cm² (3)

### 3.2. PWR irradiation

#### 3 2 1 Examination of outer zirconia layer

X-ray diffraction measurements were made using K $\alpha$  copper wavelength (1,54061 Å). In these conditions, the diffraction signal corresponds to the first ten outer microns of the zirconia layer. In other words, with the exception of fuel rods irradiated during 1 cycle, the metal/oxide interface is not reached. Moreover, the cylindrical geometry of the samples was not ideal and was not conducive to take full advantage of Rietveld analysis (inaccurate calculation of parameters and microstresses effects or particles size).

The obtained results show first of all that the tetragonal phase is always present, regardless of the number of cycles and as a result, is always very far from the Zy/ZrO<sub>2</sub> interface, unlike out-of-pile formed zirconia. The proportion of tetragonal phase is at most equal to 28% and seems to be fairly disparate overall. Although the lattice parameters could not be accurately measured, the displacement of diffraction peaks  $(11-1)_M$ ,  $(111)_M$  and  $(101)_T$  tends to reveal that both cell volumes contract under irradiation (Figures 7 and 8).

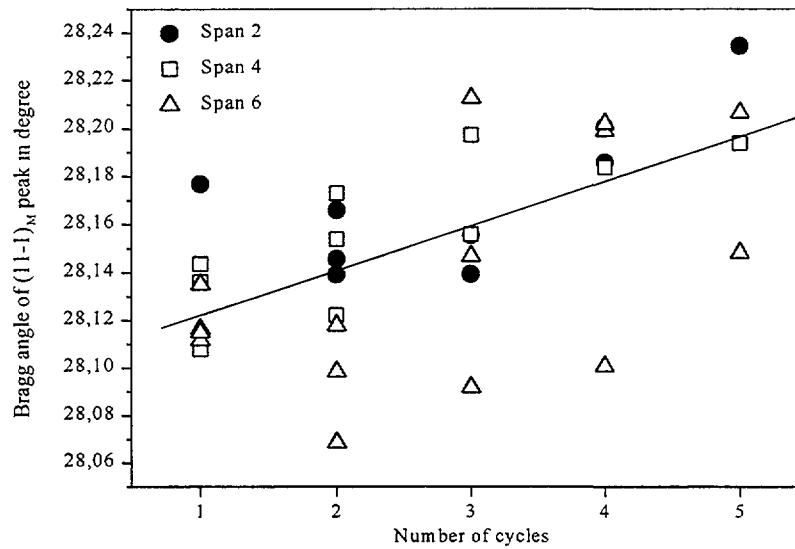


FIG. 7. PWR samples. Change in angular position of monoclinic zirconia  $(11-1)$  diffraction peak as a function of number of cycles

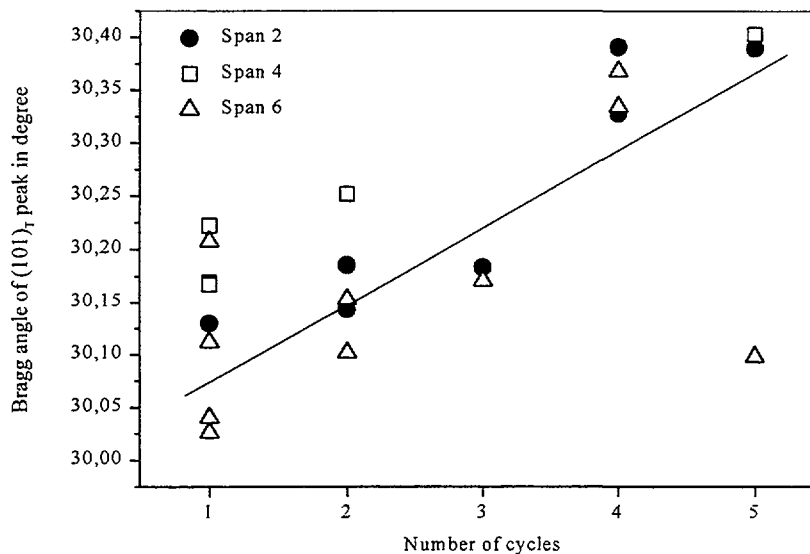


FIG. 8. PWR samples. Change in angular position of tetragonal zirconia  $(101)$  diffraction peak as a function of number of cycles

Moreover, if samples with equivalent zirconia thickness are compared for different irradiation factors (for example, a 3-cycle, span 6 sample compared with a 5-cycle span 2 sample), a decrease of the monoclinic phase cell volume is observed, along with a slight increase of tetragonal phase content, depending on the irradiation level; as it was the case for high energy ions irradiation of thermal zirconia.

### 3.2.2. Examination of inner zirconia layer

Unlike the outer zirconia, the inner zirconia layer is formed under neutron and gamma ray irradiation, as well as fission fragments bombardment.

Only one cladding sample from span 6 of a 3-cycle fuel rod was examined. The sample was cut in two lengthways, the fuel was removed and one of the half-shells was flattened mechanically. In the analyzed area, the thickness of the zirconia was constant at around 8  $\mu\text{m}$ .

The results obtained by X-ray diffraction clearly show that in these conditions, inner zirconia is entirely constituted of tetragonal phase.

## 4. CONCLUSION

The aim of this work was to underline the effects of different kinds of irradiation (ions and neutrons) on the crystallographic structure of zirconia (sintered or thermal zirconia). Generally speaking, the obtained results show that ions irradiation always favors the transformation of a part of monoclinic zirconia into tetragonal zirconia. This transformation is accompanied by the formation of stress fields correlated with changes in crystalline cell volumes. Examination of fuel rods shows that PWR irradiation produces similar effects to those revealed in the case of ion bombardment. One of the most important facts to emerge is that the tetragonal phase is present throughout the thickness of the outer zirconia layer, which is fundamentally different from what is observed on unirradiated samples. The inner zirconia layer, which is also bombarded by fission fragments, is entirely constituted of tetragonal zirconia. All these changes in crystallographic structure caused by irradiation are particularly harmful for the cohesion of the zirconia layer. Thus, variations in crystalline volumes and state of the stresses must lead sooner or later to cracking or material decohesion. As a result, diffusion of oxidizing species and so corrosion have to be accelerated.

## REFERENCES

- [1] INTERNATIONAL ATOMIC ENERGY AGENCY, "Corrosion of zirconium alloys in nuclear power plants", IAEA – TECDOC – 684 (1993).
- [2] INTERNATIONAL ATOMIC ENERGY AGENCY, "Waterside corrosion of zirconium alloys in nuclear power plants", IAEA – TECDOC – 996 (1998).
- [3] GIBERT, C., "Influence de l'irradiation et de la présence de lithium sur la nature cristallographique de la zircone dans le cadre de l'étude de la corrosion du Zircaloy-4 en milieu REP", Thèse de doctorat de l'Ecole Centrale Paris, France (1998).
- [4] GODLEWSKI, J., "Oxydation d'alliages de zirconium en vapeur d'eau. Influence de la zircone tétragonale sur le mécanisme de croissance de l'oxyde", Thèse de doctorat UTC (Compiègne), France (1992).
- [5] BARBERIS, P., "Zirconia powders and Zircaloy oxide films : tetragonal phase evolution during 400°C autoclave tests", Journal of Nuclear Materials, 226 (1995) 34-43.
- [6] RIETVELD, H.M., "A profile refinement method for nuclear and magnetic structure", J. Appl. Cryst. 2 (1969) 65.

V.F. KON'KOV, A.V. NIKULINA, V.N. SHISHOV, T.N. KHOKHUNOVA  
State Science Centre, VNIINM,  
Moscow

A.E. NOVOSELOV  
State Science Centre R.F,  
Dimitrovgrad, Ul'yansovsk reg.,  
Russian Federation

### **Abstract**

Results are generalized that were acquired from studying corrosion behaviour of E110 and E635 cladding under research reactor and commercial WWER conditions. The role was assessed that is played by surface boiling, heat flux and neutron irradiation in the mode of corrosion damage of E110 and E635 alloys. The results of out-of-pile tests are analyzed, i.e., the influence of environment, Li concentration of water, conditions of water and its content of oxygen.

### **INTRODUCTION**

Corrosion of zirconium components in water cooled reactor is a dangerous phenomenon capable of limiting substantially their service life. Until now there has been no generally accepted theory or model of aqueous corrosion of Zr materials due to the influence produced by numerous effects. The "breakaway" available in the kinetics of Zr-alloy corrosion does not allow a long-term extrapolation of the results of short time testing. The elaboration of a single corrosion model to predict the corrosion behaviour of Zr components is also made difficult by the fact that under specific reactor conditions some Zr alloys are subject to deep and surface corrosion damages of a nodular type to from a "pseudouniform" oxide film.

Therefore, in terms of the choice of materials and the operation of components the main instrument in predicting the corrosion behaviour of Zr alloys consists in revealing individual factors or their combination that influence corrosion processes in autoclaves, loops or directly in reactors. Generally, the in-pile corrosion of Zr items is defined by a set of internal (chemical composition and a structure of material) and external (irradiation conditions, water chemistry, heat transfer etc.) conditions.

This paper discusses the results of studying some factors influencing the corrosion behaviour of E110 and E635 alloys. Some experiments were carried out using Zr-4.

#### **1. IN-PILE CORROSION OF ZR-ALLOYS E110 AND E635. INFLUENCE OF VARIOUS FACTORS ON CORROSION**

The corrosion resistance of E110 and E635 fuel rod claddings and coupons was studied under neutron irradiation in WWER and loops simulating the reactor conditions. The influence of the neutron exposure, heat transfer and surface boiling on corrosion is assessed. The fuel rod claddings and coupons in recrystallized condition were used.

##### **1.1. Corrosion of fuel rod claddings under VVER conditions.**

In a WWER reactor fuel rod claddings and other FA components operate in ammonia-potassium-boron water chemistry at a temperature of 320-350°C (Tables I, II).

The results of the analysis of fuel rod cladding corrosion in WWER-440 and WWER-1000 as well as in loops evidence that under the conditions specified for WWER the E110 alloy is highly corrosion resistant (the oxide film  $\leq 16 \mu\text{m}$ ,  $\text{H}_2 \leq 90 \text{ ppm}$ ) at the average fuel burn-up  $\sim 70 \text{ MW}\cdot\text{day/kg U}$  and the testing time  $< 40$  thousand hours (Fig. 1).

TABLE 1. WATER-CHEMISTRY IN COMMERCIAL VVER-1000 AND RESEARCH REACTORS

Water chemistry parameter	VVER-1000	
	Commercial (Specification)	Research
<i>pH (25°C)</i>	5.7 - 10.2	6.0 - 10.2
<i>Chlorides and fluorides (Cl<sup>-</sup> + F<sup>-</sup>), ppm</i>	≤ 0.1	0 - 0.17
<i>Iron (Fe), ppm</i>	≤ 0.2	0 - 0.3
<i>Copper (Cu), ppm</i>	≤ 0.02	0 - 0.075
<i>Oxygen (O), ppm</i>	≤ 0.005	0.005 - 0.02
<i>Hydrogen (H), ppm</i>	-2.7 - 5.4	0.8 - 6.7
<i>Potassium+Lithium+Sodium (K<sup>+</sup> + Li<sup>+</sup> + Na<sup>+</sup>), m-mol/l</i>	0.05 - 0.45	0 - 0.47
<i>Ammonia (NH<sub>3</sub>), ppm</i>	≥ 5.0	0.5 - 45.0
<i>Boron, ppm</i>	0 - 2160	5.0 - 871.0

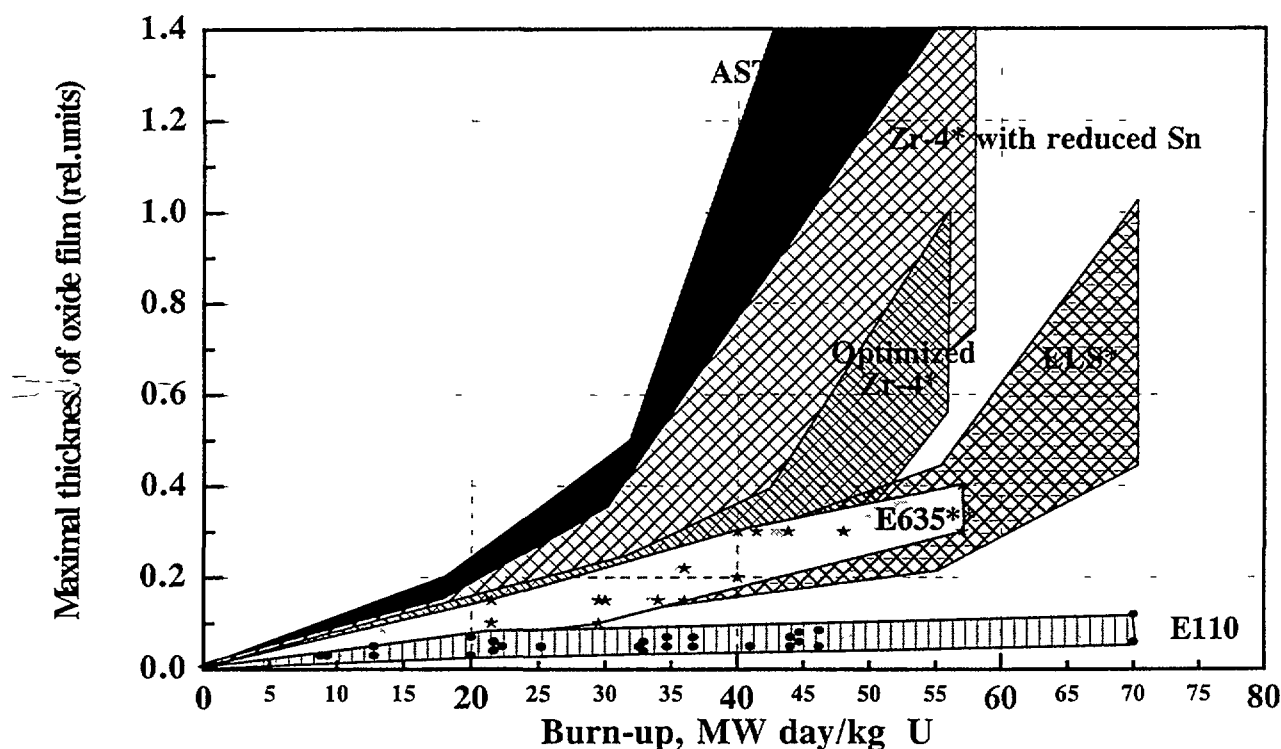
TABLE II. EXPERIMENTAL FA TESTS UNDER VVER-1000 CONDITIONS IN RESEARCH REACTORS

Testing conditions	Parameters	
	Research reactors	Commercial VVER-1000 (3 year cycle)
<i>Time of on-power operation, days</i>	252 - 992	875
<i>Burn-up, MW day/kg U</i>		
<i>average</i>	19.2 - 48.0	43.0
<i>maximum</i>	21.5 - 57.0	54.0
<i>Coolant pressure, MPa</i>	12.5 - 15.7	15.7
<i>Coolant temperature, °C</i>		
<i>inlet</i>	285 - 290	290
<i>outlet</i>	310 - 315	320
<i>Maximum temperature at cladding outer surface, °C</i>	330 - 350	352
<i>Heat flux, MW/m<sup>2</sup></i>		
<i>average</i>	1.05 - 1.70	0.60
<i>maximum</i>	1.20 - 2.00	1.60
<i>Fluence, 10<sup>21</sup>cm<sup>-2</sup> (E≥0.1 MeV)</i>	1.5 - 8.0	10
<i>Coolant condition</i>	Pressurized water, surface boiling	Pressurized water

A weak nodular type corrosion was only observed in single cases [1, 2]. In comparison with the E110 alloy E635 claddings of lead fuel rods research reactor tested under more rigid conditions than those specified for VVER, specifically, with up to 0.02 ppm oxygen available in the coolant and long-term surface boiling are subject to corrosion to develop thicker oxide films <40 µm at the average fuel burn-up ~55 MW·day/kg U. However, the oxide was always uniform without indications of nodular corrosion and the hydrogen content of the claddings did not exceed 200 ppm [3]. At extended burn-up of 55 MW day/kgU the E110 and E635 alloys did not reveal “transitions” (accelerated corrosion) that are typical of Zr-4 alloys.

## 1.2. Influence of surface boiling on fuel rod corrosion

Under surface boiling at the 0.02 ppm oxygen content of the coolant E110 fuel rod claddings reveal dark coloured very thin oxide films along with nodules - light coloured oxide. As the fuel



\*) According to the data submitted by A. Seibold, E. Ortied to the conference on structural material for PWR, Karlsruhe, Germany.

\*\*) Corrosion of fuel cladding under VVER conditions (experimental reactor, surface boiling, oxygen concentration  $\leq 0.02$  ppm).

Fig. 1. Corrosion of Zr claddings under PWR and WWER conditions.

burn-up increases the nodule thickness growth proceeds at the rate almost order of magnitude higher than the growth rate of the uniform oxide (Fig. 2). Also the propagation of the nodules at the cladding surface is increased. Under the above conditions the E635 fuel rod cladding corroded to form only a dark uniform oxide.

### 1.3. Influence of heat flux on fuel rod claddings

In the reactor loop tests the lead highest heat density fuel rods were subjected to surface boiling. At different points along the fuel rods the heat flux density reached  $0.6\div 2.2$  MW/m<sup>2</sup> while the surface temperature could exceed the coolant boiling temperature depending on the heat flux. Under those conditions the E110 alloy shows a clear-cut dependence of the maximum corrosion damage on the heat flux density (Fig. 3). The heat flux density as increased from 0.6 to 1.1 MW/m<sup>2</sup> weakly affects the corrosion rate, however, with a further increase of the flux a "breakaway" takes place after which the corrosion rate is sharply increased. The heat flux density of  $\sim 1.1$  MW/m<sup>2</sup> is likely to be a threshold for the VVER-1000 conditions after which the surface boiling may take place and nodular corrosion may develop at the surface of E110 claddings. No nodular corrosion took place when the heat flux was below the threshold value.

In commercial WWERs where the heat flux was within 0.3-1.1 MW/m<sup>2</sup> the E110 claddings were subject to corrosion to form always uniform thin oxide films.

The corrosion of the lead E635 fuel rod claddings is less dependent on the heat flux density compared to that of the E110 alloy which is likely to explain the absence of the nodular corrosion of that alloy (Fig. 4).

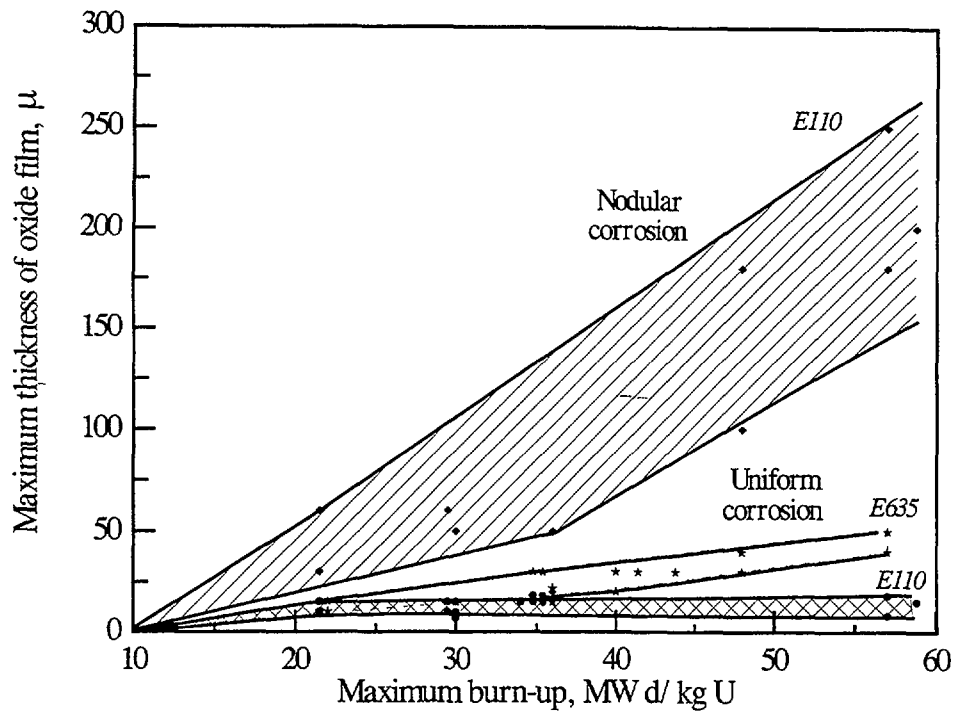


Fig. 2. Research reactor corrosion of E635 and E110 alloy claddings of fuel rods under VVER-1000 conditions (surface boiling, oxygen concentration of water  $\leq 0.02$  ppm).

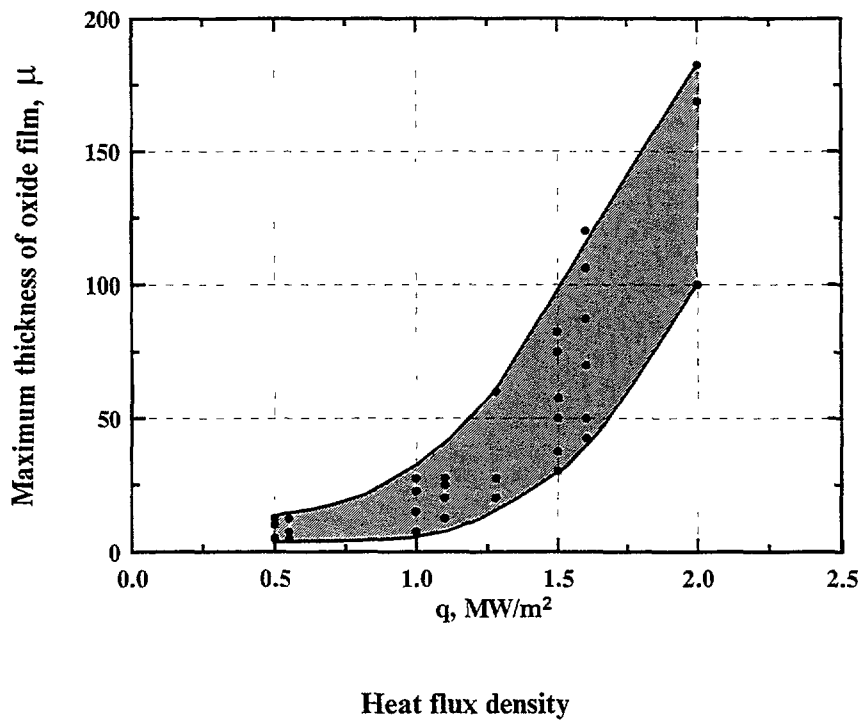


Fig. 3. Maximum oxide thickness on E110 claddings vs heat flux density after 18000h operation on power under WWER conditions.

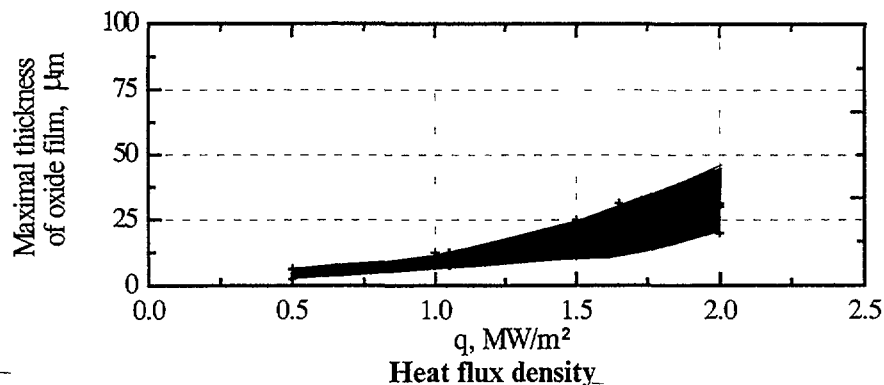


Fig. 4. Maximum oxide thickness on E635 claddings vs heat flux density after 12000 h operation on power under WWER conditions.

#### 1.4. Influence of neutron exposure on corrosion of fuel rod claddings

The analysis and comparison between the results of E110 fuel rod clads testing in commercial VVER reactors and in autoclaves containing deaerated water at 350°C during a long period of time did not show any noticeable effect of the neutron exposure on the E110 alloy corrosion (Fig. 5).

Similarly, no noticeable corrosion effect of the neutron exposure was detected in the E635 alloy the data on which refer for the most part to the tests in high (<2-20 ppm) oxygen water and coolant (Fig. 6). Upon surface boiling 0.02 ppm oxygen contained by the water coolant is transferred to the vapour phase where its concentration is ~100 times higher than in the water [4].

The corrosion of this alloy is more substantially affected by the oxygen available in the water (in out- of and in-pile tests). However, the corrosion effect of oxygen is much lower for E635 compared to E110. The long-term autoclave tests in deaerated water and individual thickness measurement of the oxides on the claddings of lead fuel rods tested under the VVER conditions at the oxygen content of  $\leq 0.005$  ppm did not reveal any noticeable influence of the neutron exposure on the corrosion of E635 alloy as well.

## 2. OUT- OF- PILE CORROSION OF ZIRCONIUM ALLOYS

Investigations of the specific features inherent in the corrosion behaviour of Zr materials and studies into factors influencing their corrosion are carried on to a greater extent out-of-pile, namely, in autoclaves or loops. The results of the investigations have been used to establish the

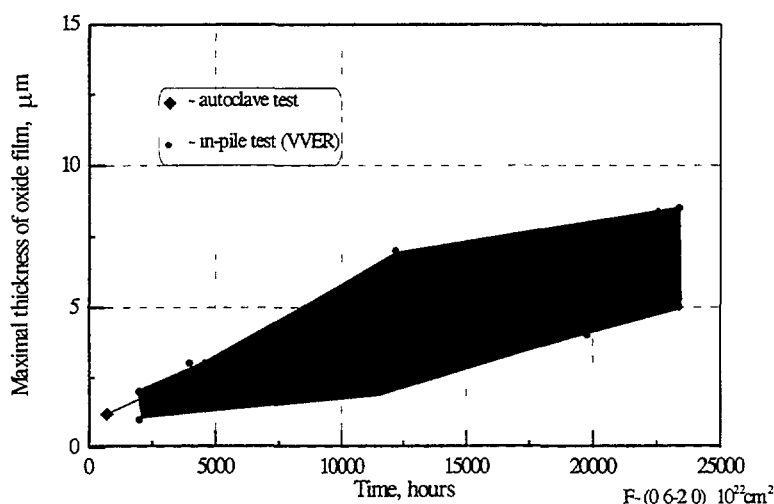


Fig. 5. In- and out-of-pile (350°C, 16,8 MPa) corrosion of E110 alloy claddings.



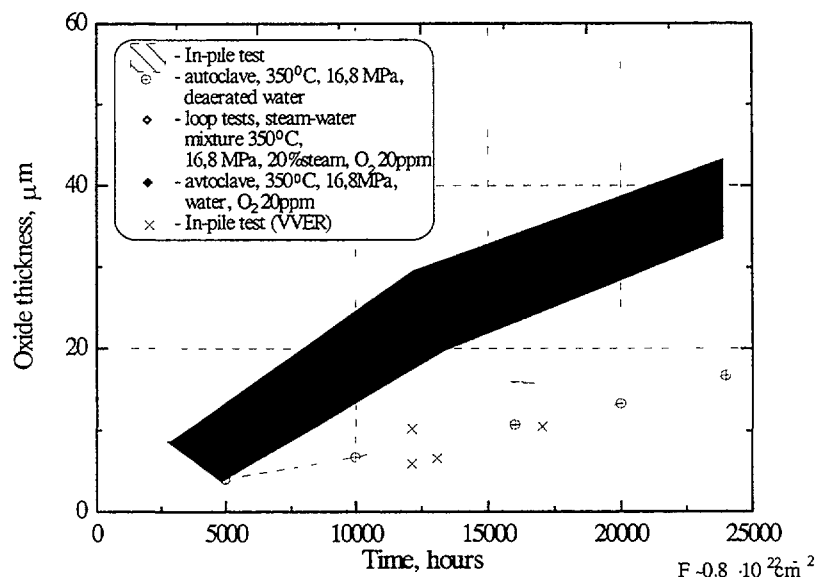


Fig. 6. In- and out-of-pile corrosion of E635 alloy claddings.

chemical composition of the materials and the structure of the items to be loaded into reactors as well as to validate their reliability under various reactor conditions, primarily, the water chemistry.

## 2.1. Zr-alloy corrosion in water of various compositions

The autoclave conditions reproduced the WWER water chemistry having the ammonia-potassium-boron composition and the PWR one having the lithium-boron composition (Table III) [5].

TABLE III. WATER CHEMISTRY IN AUTOCLAVE TESTS OF ZR MATERIALS

Reactor	Water-chemistry , ppm	pH
<i>VVER</i>	K (KOH) - 30 NH <sub>3</sub> (NH <sub>4</sub> OH) - 50 B (H <sub>3</sub> BO <sub>3</sub> ) - 8000	~ 7.0
<i>PWR</i>	Li (LiOH) - 3 B (H <sub>3</sub> BO <sub>3</sub> ) - 6000	7.0 - 7.5

At 360°C and 18.6 MPa specimens of E110, E635 and Zr-4 cladding tubes as commercially supplied were tested in water of various compositions. During the 300 day autoclave testing all the three alloys were subject to corrosion to form dark-coloured oxide films at about the same weight gain (60-80 mg/dm<sup>2</sup>) which corresponds to the oxide thickness of 4-5  $\mu\text{m}$  (Fig. 7). No substantial distinction in the corrosion of the material was observed in water having different compositions. However, in all the tests Zr-4 showed the highest hydrogen uptake (Table IV).

After the 300 day autoclave tests the thickness of the oxide developed on the coupons is comparable to that on fuel rod claddings tested under the WWER conditions during the same period of time.

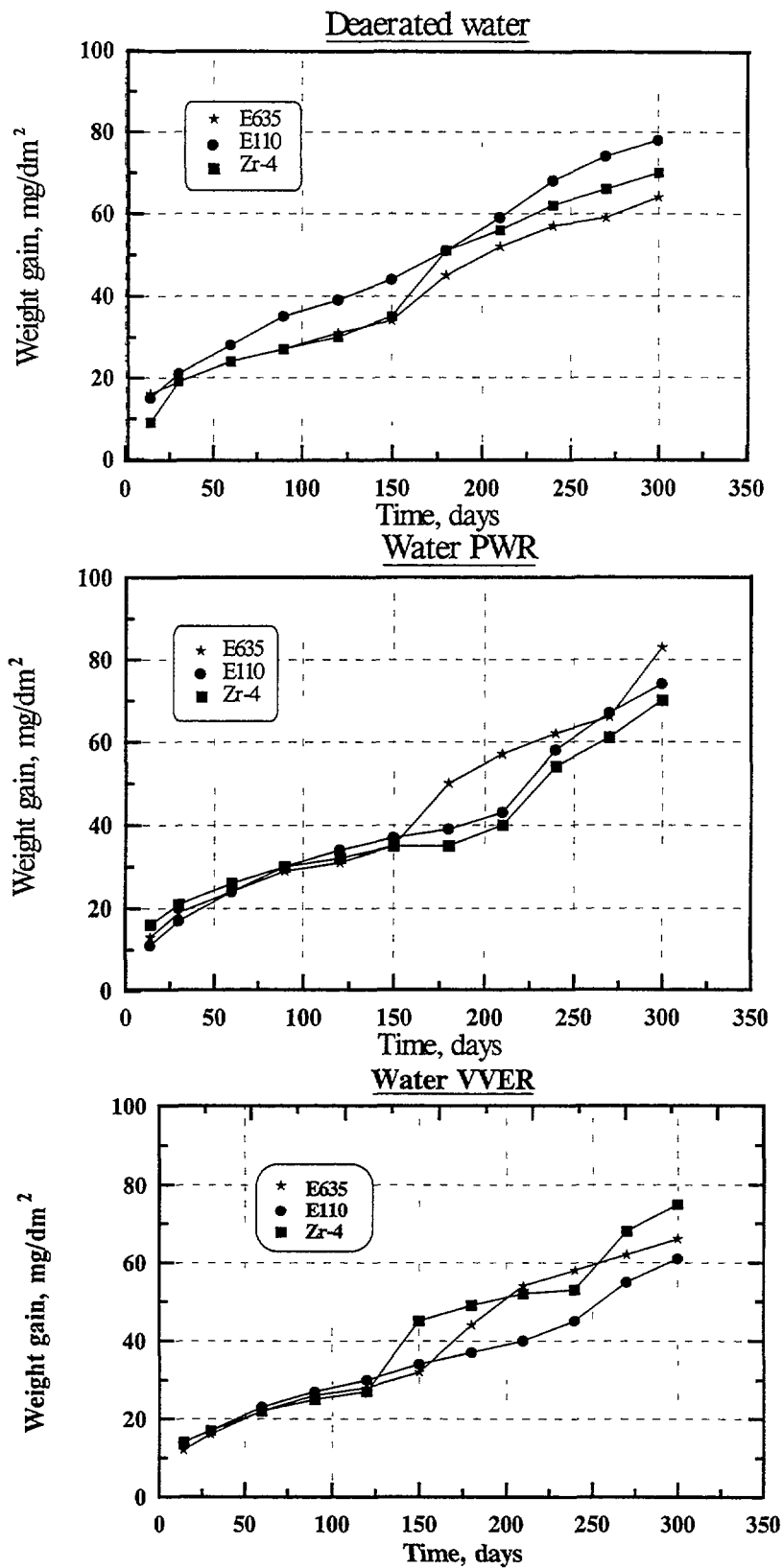


Fig. 7. Autoclave corrosion of alloys at 360°C, 18.6 Mpa.

TABLE IV. HYDROGEN CONTENT (% WT.) OF AUTOCLAVE TESTED ALLOYS

Alloy	360°C, 300 days		
	Deaerated water	Water PWR	Water VVER
E635	0.004	0.006	0.003
E110	0.003	0.003	0.002
Zr-4	0.009	0.015	0.009

The autoclave tests of the materials are in progress to acquire a large array of statistical data for a longer exposure time.

## 2.2. Corrosion of Zr alloys in lithiated water

The influence effected by the lithium content of water on the corrosion of E110, E635 and Zr-4 was studied in autoclave tests. The tests for up to 300 days were carried out at 360°C and 18.6 MPa in water containing 3, 10, 30 and 70 ppm Li. The generalized data on the corrosion behaviour (oxidation, hydrogen uptake) of the alloys in Li containing water are given in Fig. 8.

After 300 days in water at the lithium content <3 ppm all three alloys had a similar corrosion resistance. However, with the Li content increased to 10 ppm the corrosion of E110 and Zr-4 is accelerated which is evidenced by the oxide thickness and the hydrogen uptake.

With a subsequent increase of the lithium content of the water the corrosion behaviour of the alloys becomes drastically different. The E110 alloy reveals a strong dependence of the oxidation extent on the Li content of the water and, correspondingly, a higher hydrogen uptake.

Compared to the E110 alloy the extent of Zr-4 oxidation is slightly less dependent on the Li content of the water. However, in this case Zr-4 picks up very much hydrogen. Compared to E110 or Zr-4 the E635 alloy demonstrated a substantially lower sensitivity to the Li content of the water. At all the concentrations of Li its corrosion resistance is high and is attended by a low uptake of hydrogen.

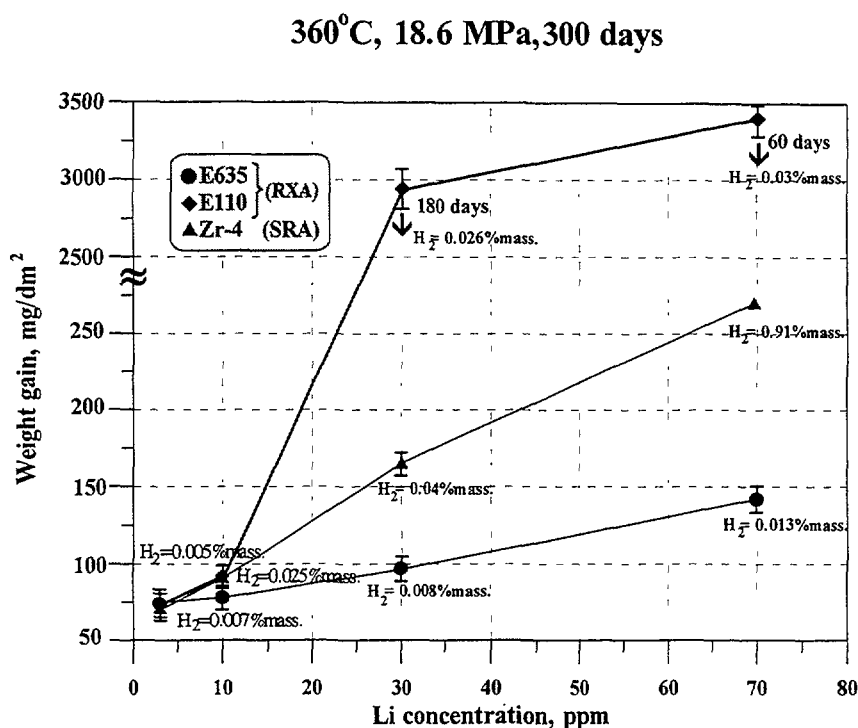


Fig. 8. Corrosion and hydrogen uptake (% wt.) of alloys in autoclaves containing water with Li additives.

### 2.3. Influence of water condition on corrosion of alloys

The influence of the water condition on the behaviour of the E110 and E635 alloys was studied in terms of the off-normal WWER conditions. The investigations were carried on in deaerated water and steam at 350°C for 200 days. The influence of the environmental conditions on the corrosion of the alloys is insignificant. The aggressiveness of steam in comparison with water showed up as ~5 mg/dm<sup>2</sup> higher weight gains of the alloys which corresponds to a ~0,3µm increase of the oxide thickness (Fig. 9).

### 2.4. Influence of oxygen content

To assess the influence of oxygen on E110 and E635 alloy corrosion autoclave tests were carried out in deaerated water and water containing ~20ppm O<sub>2</sub> at 350°C (Fig. 10). The results of the tests evidence that ~20 ppm oxygen available in water has an unfavourable effect on the corrosion of both the alloys.

From the comparison with the data on the effect of neutron exposure (Figs. 6, 2) the conclusion may be drawn that the aggravation of the E635 alloy corrosion under irradiation compared to that in deaerated water at 350°C is explained by the high content of oxygen available in the environment independent of its condition.

The higher oxygen content of water attended by boiling initiates E110 alloy nodular corrosion to the extent much higher than the E635 alloy corrosion.

Without boiling the behaviour of the E110 alloy is assumed to be governed by the oxygen available in water with the influence of irradiation typical of WWER being slight.

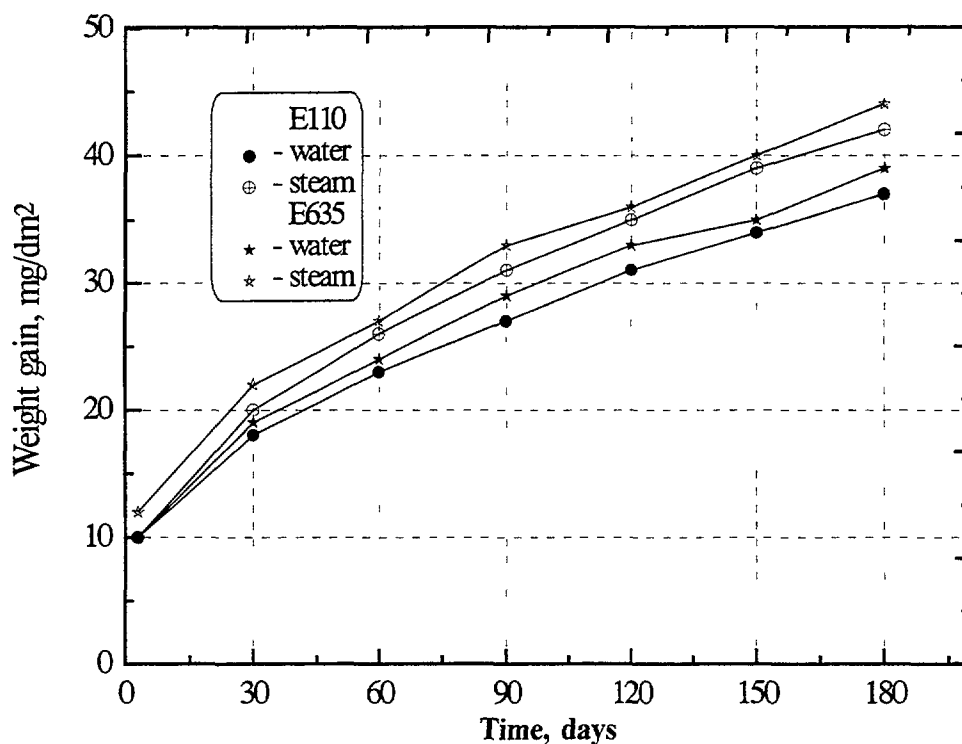


Fig. 9. Influence of water condition on corrosion of alloys at 350°C.

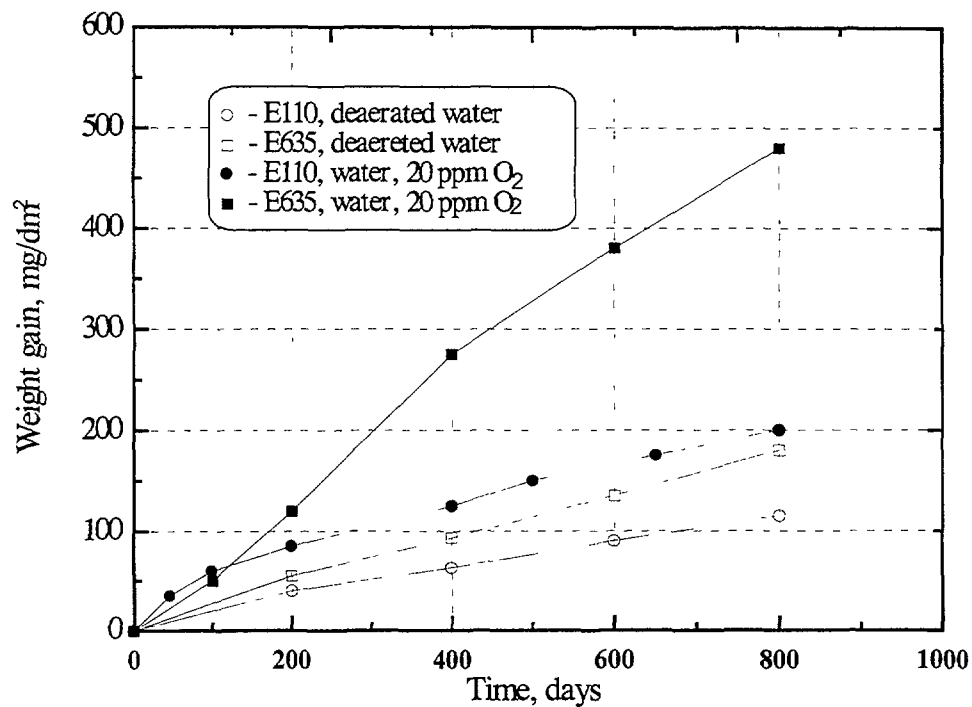


Fig. 10. Influence of oxygen content in water on corrosion of E110 and E635 alloys at 350°C.

## CONCLUSIONS

The analysis of the results evidences that E110 and E635 alloys have adequate reserves of corrosion properties to be used as fuel rod claddings to extended burn-up (~60 MW day/kg U) under the WWER stipulated conditions.

Zr-4 has higher propensity for hydrogen uptake during operation under VVER and PWR water chemistry conditions compared to E110 and E635.

The high corrosion properties revealed by E110 in water containing up to 10 ppm Li and by E635 up to 70 ppm Li make them usable in PWR.

The E110 and E635 alloys exhibited sensitivity to oxygen available in water which under irradiation is the main factor governing their corrosion behaviour.

As distinct from E635 the E110 alloy proved to be prone to nodular corrosion in water under surface boiling; its corrosion being directly related to the heat flux.

The implemented investigations demonstrate that along with the in-pile studies the autoclave tests generate much useful information.

## REFERENCES

1. M. SOLONIN, YU.BIBILASHVILI, A. IOLTUKHOVSKY et al., "WWER fuel performance and material development for extended burnup in Russia", WWER Reactor Fuel Performance, Modeling and Experimental Support (Proc. 2<sup>nd</sup> Int. Seminar Sandanski, Bulgaria, 21-25 April, 1997), Institute for Nuclear Research and Nuclear Energy, Sofia, Bulgaria (1997) 48.

2. NIKULINA A.V., YU.BIBILASHVILI, PEREGUD M.M. et al, "E110 Alloy Cladding Tube Properties and their Interrelation with Alloy Structure-Phase Condition and Impurity Content", Zr in the Nuclear Industry (Proc. 12 Int. Symposium Toronto, 1998), ASTM STP1354, ASTM (in press).
3. NIKULINA A.V., MARKELOV V.A., PEREGUD M.M. et. al, "Zirconium Alloy E635 as a Material for Fuel Rod Cladding and Other Components of VVER and RBMK Cores", Zirconium in the Nuclear Industry (Proc. 11 Int. Symposium, Garmisch-Partenkirchen, Germany, 11-14 Sep. 1996), ASTM STP 1295, ASTM (1997) 785-804.
4. FRANKLIN D., CHE-YU LI, "Effect of Heat Flux and Irradiation induced Changes in Water Chemistry on Zircaloy Nodular Oxidation", Zirconium in the Nuclear Industry (Proc.7 Int. Symposium Philadelphia, 1987), ASTM STP 939, (1988) 206-223.
5. F.GARZAROLLI, Y BROY, R.A. BUSCH, "Comparison of the Long Time Corrosion Behavior of Certain Zr Alloys in PWR, BWR and Laboratory Test", Zirconium in the Nuclear Industry (Proc. 11 Int. Symposium, Garmisch-Partenkirchen, Germany, 11-14 Sep. 1996), ASTM STP 1295, ASTM (1997) 850-863.

NEXT PAGE(S)  
left 15' 44X



## EFFECT OF LiOH, NaOH, AND KOH ON CORROSION AND OXIDE MICROSTRUCTURE OF Zr-BASED ALLOYS

Y.H. JEONG, H.G. KIM, Y.H. JUNG  
Korea Atomic Energy Research Institute,  
Taejeon, Republic of Korea

H. RUHMANN  
Siemens AG, Power Generation Group (KWU),  
Erlangen, Germany

### Abstract

Long-term corrosion test, SIMS analysis, and TEM microstructural study were carried out to investigate the corrosion characteristics and mechanism of Zr alloys in alkali hydroxides. The corrosion tests were performed in solutions of LiOH, NaOH, KOH, RbOH, and CsOH at 350°C for 500 days. SIMS analysis was performed for the specimens prepared to have an equal oxide thickness. TEM studies on the specimens with an equal oxide thickness in various solutions in both pre- and post-transition regimes were also conducted.

The corrosion rate in alkali hydroxide solutions was observed to decrease as the ionic radius of alkali cation was increased. The penetration depth of cation into the oxide decreases with increasing the ionic radius of cation. Even though the oxide thickness was equal, the different oxide morphologies were observed in specimens. Namely, in LiOH solution the oxide morphology was transformed early from columnar to equiaxed structure. However, in KOH solution the columnar structure was maintained up to post-transition regime. Based on the corrosion test, SIMS analysis, and microstructural study, the cation is considered to control the corrosion in an alkali hydroxide solution and its effect is dependent on the concentration of alkali and the oxide thickness. The slight acceleration of the corrosion rate at a low concentration is thought to be caused by cation incorporation into oxide while the significant acceleration at a high concentration is due to the transformation of oxide microstructure that would be induced by cation incorporation. KOH was shown not to affect significantly the corrosion and the hydrogen pickup of Zircaloy. Therefore, it has a potential for PWR application only from the point of view of Zircaloy corrosion.

### 1. Introduction

LiOH, which is added to control the pH of primary coolant in LWR, has been known to accelerate the corrosion of nuclear fuel cladding. The effect of LiOH on the Zircaloy corrosion has been previously studied by many researchers [1-10]. The Li incorporation into oxide [3,11], the modification of oxide nucleation or growth [12], and the dissolution and reprecipitation of oxide [10] were suggested to be the reasons for the accelerated corrosion in LiOH solution. The content of penetrated  $\text{Li}^+$  into oxide was recently measured by SIMS [13-16], and LiOH was suggested to affect the barrier layer of oxide. TEM studies on the oxide were also conducted to investigate the effect of LiOH on the oxide microstructure [13].

Meanwhile, KOH is currently used as a pH controller with other alkali hydroxides in WWER reactors. It was reported that KOH showed high compatibility with Zr-1Nb alloy in in-reactor[17] and the less corrosive characteristic to Zircaloy than LiOH based on the out-of-pile loop test[14]. However, there have been no reports concerning the effect of KOH on Zircaloy corrosion in Western PWR reactors.

In the previous research [11], the corrosion of Zr alloys was investigated in various alkali hydroxide solutions, and the cation incorporation into oxide was suggested to play an important role on the corrosion acceleration. But, only pre-transition corrosion characteristics could be studied for corrosion resistant Zr alloys like Zircaloy due to relatively short exposure time. As a result, the effect of alkali hydroxide on Zircaloy corrosion was not clearly evaluated in the previous study. Therefore, in this study, the corrosion characteristics in equimolar LiOH, NaOH, KOH, RbOH, and CsOH solutions in post-transition as well as pre-transition regime were investigated from long-term corrosion tests (500 days). For the better understanding of cation incorporation, SIMS analysis was performed to observe how  $\text{Li}^+$ ,  $\text{Na}^+$ ,  $\text{K}^+$  cation penetrate into the oxide. TEM studies on the oxide were also conducted to investigate the oxide microstructure change induced by the cation incorporation and its effect on corrosion.

## 2. Experimental Procedure

In this study, two kinds of Zr alloys, that is, Zircaloy-4 and Zr-Sn-Nb alloy, were used for corrosion tests. The chemical compositions of Zircaloy-4 and Zr-Sn-Nb alloys were 1.51wt%Sn, 0.22wt%Fe, and 0.11wt%Cr and 0.8wt%Sn, 0.8wt%Nb, and transition metal (TRM:0.3wt%), respectively. The material condition of both alloys was fully recrystallized. The specimens were chemically polished using a pickling solution before the corrosion test. The corrosion tests were conducted in aqueous alkali solutions in the static autoclave at 350°C under the pressure of 17 MPa. Corrosion resistance was evaluated by measuring the weight gain during the test. According to the literature survey, it is still controversial which one, anion or cation, plays an important role on the corrosion of Zircaloy in alkali solutions. Therefore, the corrosion tests were performed in LiOH, NaOH, KOH, RbOH, and CsOH solutions of 4.3mmol and 32.5mmol with equimolar  $\text{M}^+$  and  $\text{OH}^-$ , where 4.3 mmol corresponds to 30 ppm Li, 99 ppm Na, 169 ppm K, 360 ppm Rb, and 574 ppm Cs and 32.5 mmol corresponds to 220 ppm Li, 724 ppm Na, 1231 ppm K, 2692 ppm Rb, and 4186 ppm Cs.

The penetrations of  $\text{Li}^+$ ,  $\text{Na}^+$ , and  $\text{K}^+$  into the oxides formed in LiOH, NaOH, and KOH solutions were investigated by SIMS analysis to clarify the relationship between cation radius and cation incorporation. Cameca-ims 4f SIMS was used for the analysis of the cation in the oxide. Primary ion beam of  $\text{O}^{2+}$  was used because the sensitivity is improved for the secondary ion detection of  $\text{Li}^+$ ,  $\text{Na}^+$ , and  $\text{K}^+$ . The acceleration voltage of 10 kV,



primary ion beam current of 200 mA, and sputtered area of 150 by 150  $\mu\text{m}$  were selected. Gold coating was applied on the specimen surface with 300Å thickness to reduce the charge effect of Zircornia and an electron gun was used to eliminate the stored charge during the analysis. In SIMS depth analysis, secondary ion counts were indicated as a function of sputtering time. The crater depth was measured by surface roughness tester ( $\alpha$ -step 300) to convert sputtering time into oxide depth. Oxide thickness was also measured by metallography, and the depth measured by the roughness tester was calibrated. Secondary ion counts were converted into the function of oxide depth based on those measurements.

TEM studies on the oxide formed in LiOH, NaOH, and KOH and SEM studies at the metal/oxide interface were carried out. To accurately investigate the characteristics of oxides formed in various solutions, the specimens with an equal oxide thickness should be prepared. If autoclave tests are conducted for a constant exposure time, the different oxide thickness is obtained in each solution due to the different corrosion rates. Therefore, in this study, the different exposure time was applied for each sample depending on solutions to obtain the corroded specimens with the weight gain of 25  $\text{mg}/\text{dm}^2$  in pre-transition regime and the weight gain of 60  $\text{mg}/\text{dm}^2$  in post-transition regime. TEM specimens for the observation of oxide microstructures were prepared in a sequence of cutting, grinding, and polishing. Finally thin foil was prepared by Ar ion milling.

The morphologies of oxide at the oxide-metal interface after the corrosion tests were observed using scanning electron microscope (SEM) after dissolving completely the metal part with a mixing solution of 10% HF, 45%  $\text{HNO}_3$ , and 45%  $\text{H}_2\text{O}$ . The amounts of hydrogen pickup in the corroded specimens were also quantitatively analyzed by using the hot extraction method and hydrogen analyzer (LECO Co.). Before hydrogen analysis of corroded specimens, the oxide films were removed by sand blasting.

### 3. Results

#### 3.1. Long-term corrosion in LiOH, NaOH, KOH, RbOH, and CsOH solutions

Fig.1 to 5 shows the corrosion behaviors of Zr-based alloys in LiOH, NaOH, KOH, RbOH, and CsOH solutions at 350°C for 500 days. In the previous study[11], the corrosion evaluation of Zircaloy in alkali hydroxide was not clearly performed due to the short exposure time of 150 days. However, in the long-term corrosion test in this study, Zr alloys showed the corrosion behavior in the post-transition regime in all test conditions. As shown in Fig.1, in 4.3 mmol (30 ppm Li) LiOH solution, the Zircaloy showed the transition of corrosion rate at 100 days, and then its weight gain increased gradually with increasing exposure time. The Nb containing alloy, which is only a testing alloy, showed the early

transition of the corrosion rate at 50 days compared to Zircaloy. In 32.5 mmol (220 ppm Li) LiOH solution, the both alloy exhibited the early transition and the significant acceleration of corrosion rate. This result is consistent with those by other investigators showing the accelerated corrosion in high concentration of LiOH.

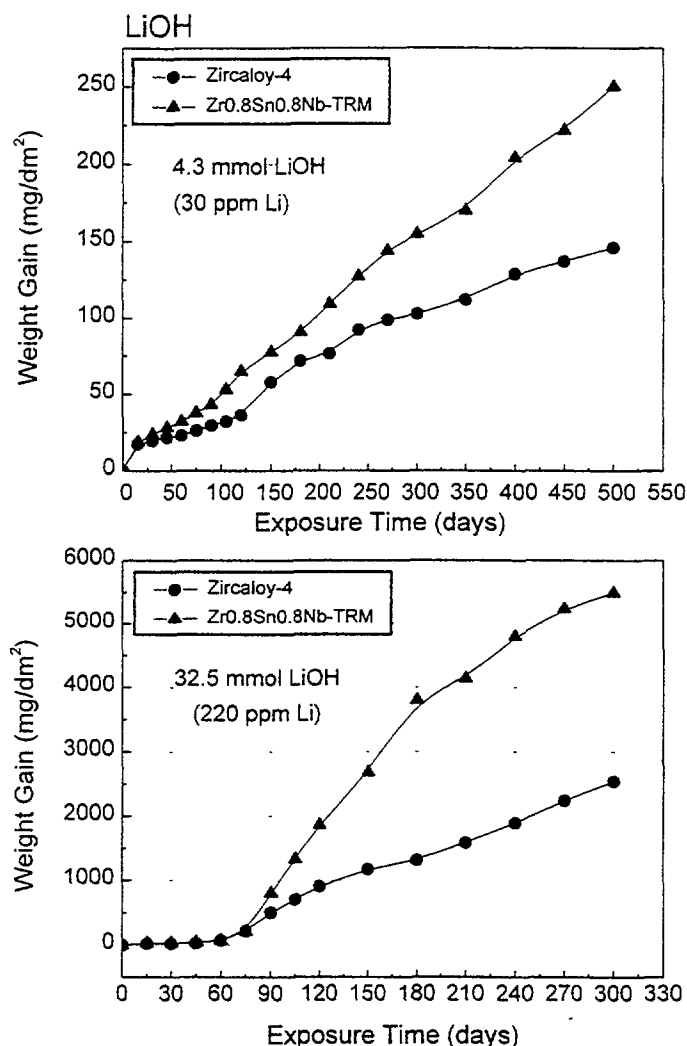


Fig.1 Corrosion behavior of Zr alloys in LiOH solutions at 350°C

The corrosion behavior in 4.3 mmol NaOH solution is similar to that in 4.3 mmol LiOH solution as shown in Fig. 2. However, the corrosion behavior in 32.5 mmol NaOH solution is quite different to that in 32.5 mmol LiOH solution. The Nb containing alloy in 32.5 mmol NaOH showed the oxide spalling at 200 day exposure time with weight gain of 150 mg/dm<sup>2</sup>. This oxide spalling was not observed on the sample corroded in 32.5 mmol LiOH solution even if its weight gain significantly increased up to 5500 mg/dm<sup>2</sup>.

The corrosion behaviors in KOH (Fig.3), RbOH (Fig.4), and CsOH (Fig.5) were similar to that in NaOH regardless of the alloy composition and the concentration of alkali solution.

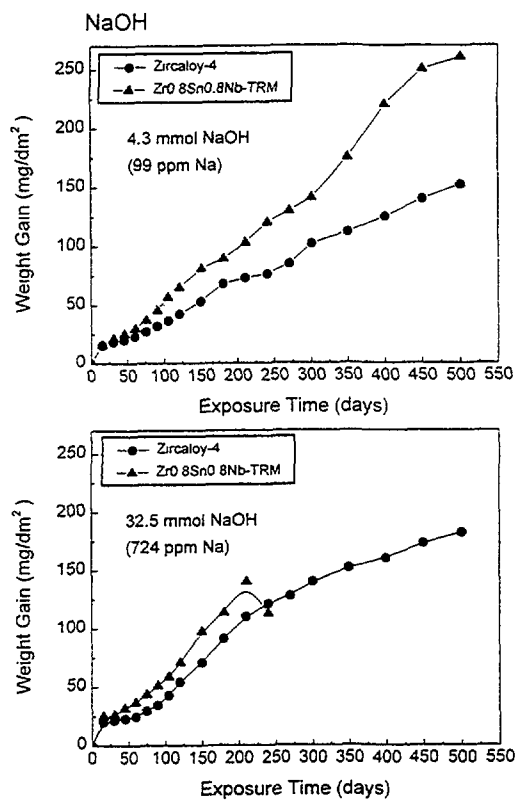


Fig.2 Corrosion behavior of Zr alloys in NaOH solution at 350°C

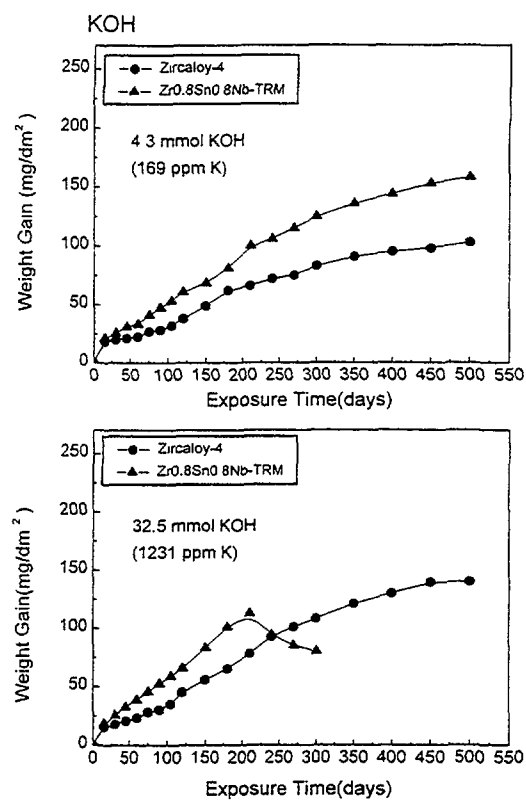


Fig.3 Corrosion behavior of Zr alloys in KOH solution at 350°C

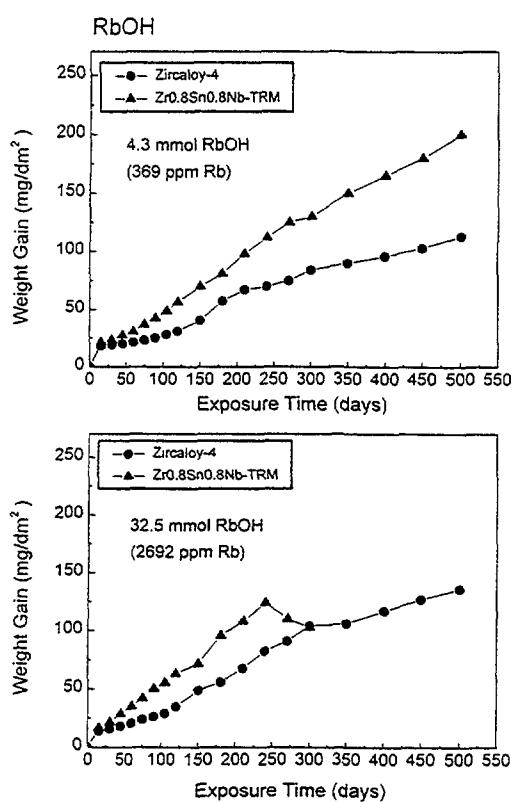


Fig.4 Corrosion behavior of Zr alloys in RbOH solution at 350°C

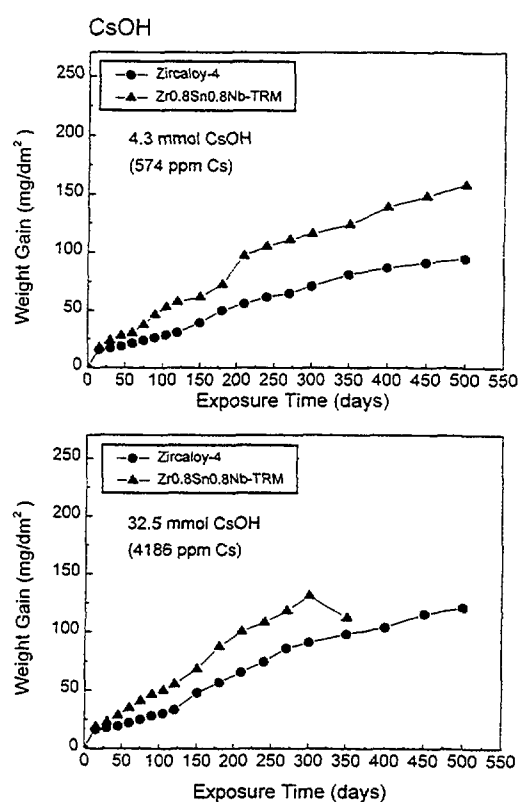


Fig.5 Corrosion behavior of Zr alloys in CsOH solution at 350°C

The oxide spalling of Nb containing alloy was also observed in KOH, RbOH, and CsOH with weight gain between 100 and 150 mg/dm<sup>2</sup>. It is not clear whether the oxide spalling occurred only in Nb-containing alloys or in low corrosion resistant alloys. However, based on the Russian corrosion data showing the compatibility between KOH and Zr-1Nb cladding [17], it is considered that alkali hydroxides except LiOH can easily induce the oxide spalling in the low corrosion resistant alloys.

Fig.6 shows the weight gain after 500 days corrosion test as a function of ionic radius of alkali cation. In the concentration of 4.3 mmol, the weight gain decreased gradually with increasing the ionic radius of alkali cation up to 300 day. In the long-term test (500days), this trend is slightly changed in KOH and RbOH showing the fluctuation of corrosion rate, which would be caused by the reduced stability of oxide in NaOH and RbOH than in LiOH solution. In high concentration (32.5 mmol) of alkali hydroxide, the corrosion rate is

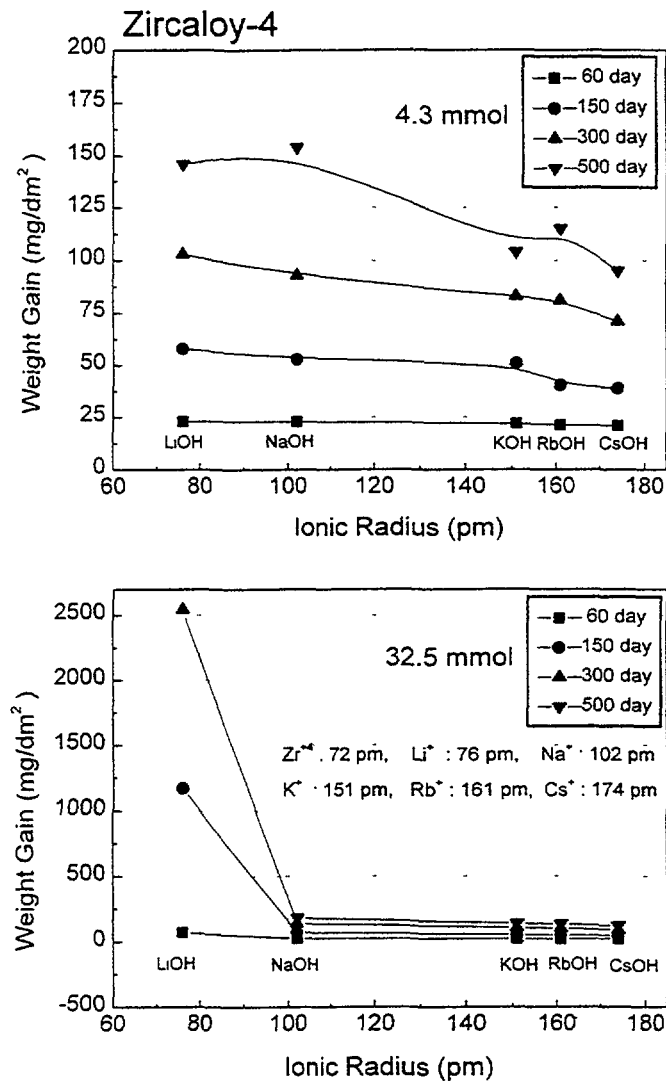


Fig.6 Weight gain of Zircaloy-4 as a function of alkali hydroxide cation

significantly accelerated in LiOH, where the ionic radius of  $\text{Li}^+$  is similar to that of  $\text{Zr}^{4+}$  in the oxide. But the corrosion rate is not significantly accelerated in NaOH, KOH, and CsOH solutions, where there is a big difference of ionic radius between cation and  $\text{Zr}^{4+}$  in the oxide. This means that there is a close relationship between the ionic radius of cation and the corrosion rate.

Fig. 7 shows the variation of hydrogen pickup fraction with the ionic radius. As the ionic radius of the alkali metal increases, the hydrogen pickup fraction decreases regardless of the concentration of alkali hydroxide. The hydrogen pickup fractions in high concentration of LiOH and NaOH increased compared to those in the low concentration. However, the hydrogen pickup fractions in the cases of KOH, RbOH, and CsOH solutions are almost the same showing about 15 % in both transition regimes. It means that the amounts of the hydrogen pickup and the hydrogen pickup fractions become high when the cation in an aqueous alkali hydroxide has a similar size to that of  $\text{Zr}^{4+}$ . Garzarolli [12] reported that the allotropic transformation of the oxide could be enhanced due to the mineralizing effect by the absorbed hydrogen during the corrosion, which results in accelerating the corrosion

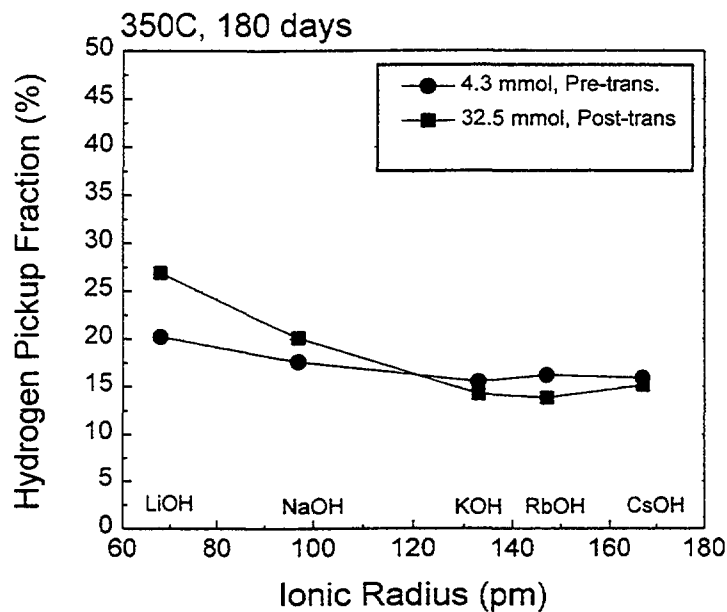


Fig.7 Hydrogen pickup fraction of Zircaloy-4 in equimolar alkali hydroxide solution

### 3.2. Cation content in the oxide by chemical analysis and SIMS

The cation contents in the oxide were measured by SIMS and chemical analysis. Fig.8 shows the cation contents in the oxide by chemical analysis with a variation of weight gain as a function of ionic radius of cation in 4.3 mal solutions. The cation contents decreased gradually with increasing the ionic radius from  $\text{Li}^+$  to  $\text{Cs}^+$ . This variation of cation content is

consistent with that of weight gain. Therefore, it can be thought that the corrosion in low concentration of alkali hydroxides would be controlled by the cation incorporation into the oxide. However, in the high concentration of alkali hydroxides, the variation of cation content in the oxide showing a slight decrease between LiOH and NaOH is inconsistent with that of weight gain showing a rapid decrease. Therefore, it is thought that the strong acceleration of corrosion rate in high concentration of LiOH would be controlled not only by the cation incorporation but also by other factor like oxide microstructure.

Fig. 9 shows the oxide thickness formed in 32.5 mmol LiOH, NaOH, and KOH for 300days. The oxide thickness in LiOH, NaOH, and KOH was about 150, 9, and 6 $\mu$ m, respectively. These samples were used for SIMS analysis.

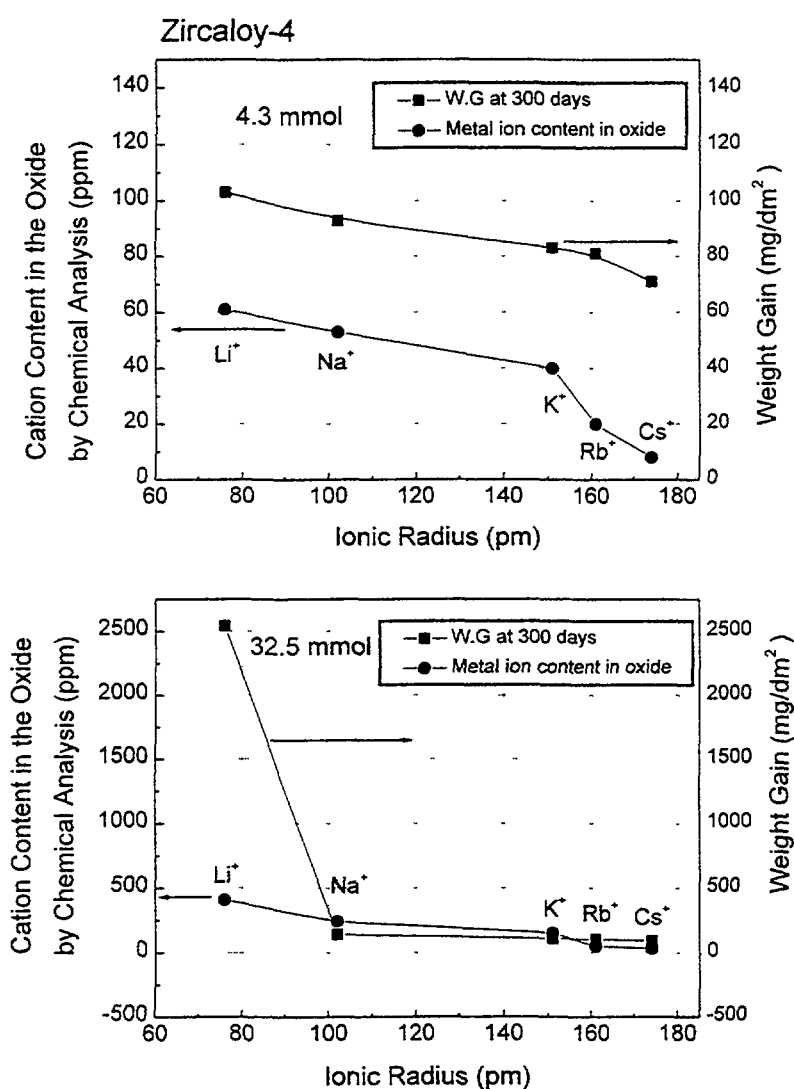
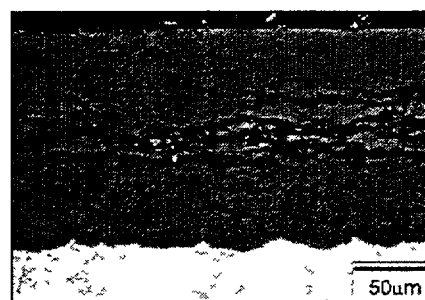
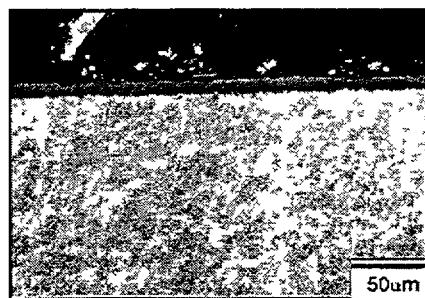


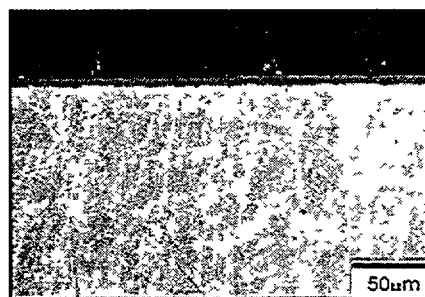
Fig.8 Variation of cation content in the oxide by chemical analysis with increasing the ionic radius of alkali hydroxide cation



(a) LiOH



(b) NaOH



(c) KOH

Fig.9 Oxide Thickness of Zircaloy-4 corroded in 32.5 mmol LiOH, NaOH, and KOH for 300days

Fig.10 shows the depth profile of  $\text{Li}^+$ ,  $\text{Na}^+$ , and  $\text{K}^+$  by SIMS analysis on the oxide formed in high concentration of alkali hydroxide as a function of distance from the oxide surface. The  $\text{Li}^+$  profile rapidly decreased from the oxide surface to  $1\mu\text{m}$ , and then maintained constant up to long distance. The oxide thickness in LiOH solution was too thick to measure the  $\text{Li}^+$  profile at metal-oxide interface. The  $\text{Na}^+$  profile by SIMS shows rapid decrease from surface to  $0.5\mu\text{m}$ , flat concentration to  $3\mu\text{m}$ , and rapid decrease again. On the oxide formed in KOH solution, the content of  $\text{K}^+$  ion continuously decreased up to  $2\mu\text{m}$  without a flat region. The penetration depth of cation decreased in order of  $\text{Li}^+$ ,  $\text{Na}^+$ , and  $\text{K}^+$  ion. However, the fraction of penetration depth from total layer was not clearly evaluated because each oxide thickness was quite different in the corroded samples used for SIMS analysis.

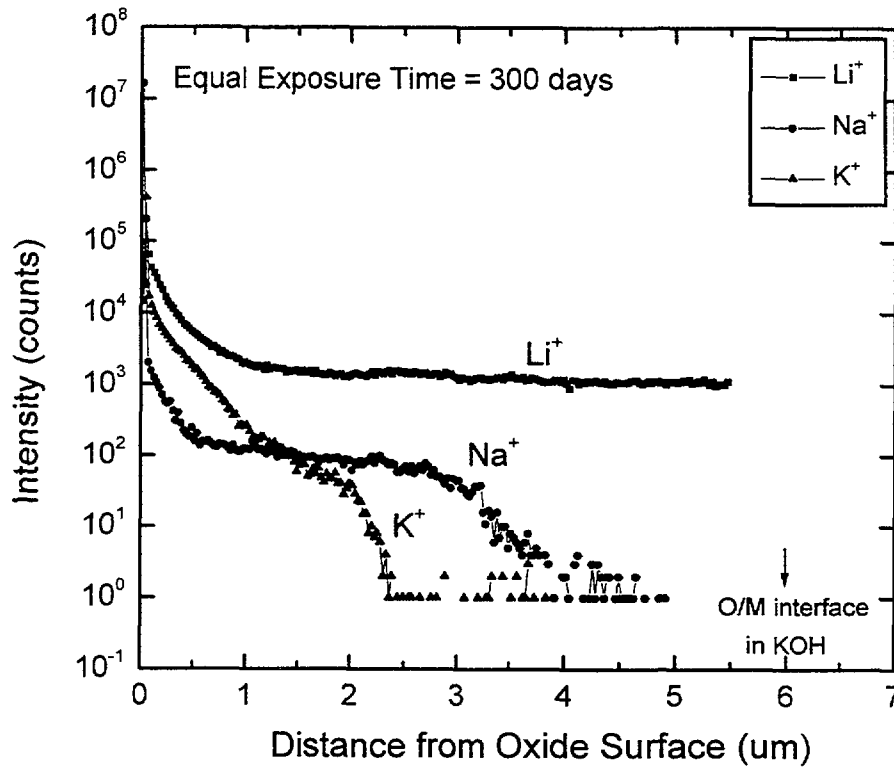
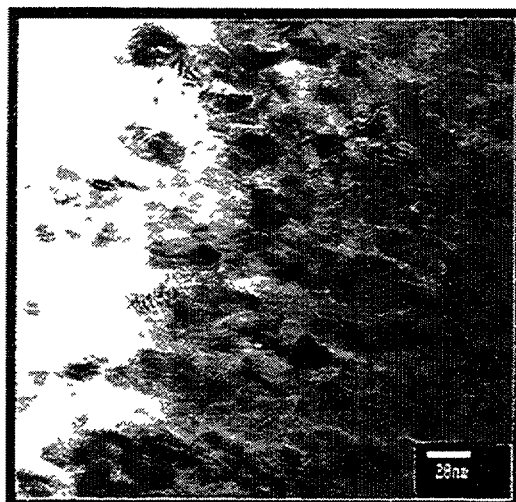


Fig.10 SIMS depth profile of  $\text{Li}^+$ ,  $\text{Na}^+$ , and  $\text{K}^+$  in the oxide formed during long-term autoclave test in 32.5 mmol alkali hydroxide solution

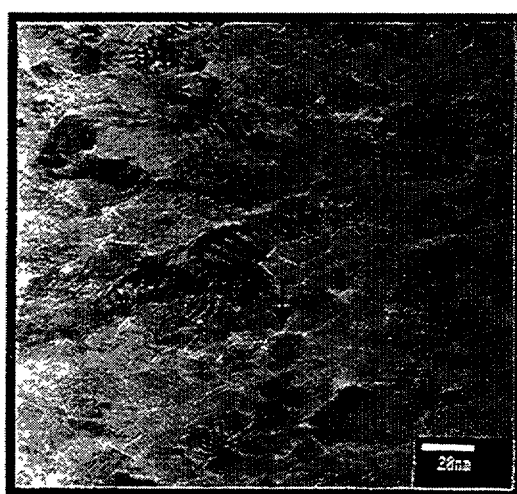
### 3.3. TEM and SEM microstructure of the oxide formed in LiOH, NaOH, and KOH

The TEM observation was performed on the oxide formed in LiOH solution as shown in Fig.11. The oxide in the pre-transition regime as well as the post-transition regime is composed of equiaxed structure. This structure is also observed at the metal-oxide interface of oxide grown in both regimes. Other investigators [13,18] reported that the oxide structures were transformed from the columnar grains in pre-transition regime to the equiaxed grains in post-transition regime. However, in this study the columnar grain was not observed even in pre-transition region, which means that the columnar grain was not formed or not maintained for such exposure time due to the high corrosion rate in LiOH solution even if it was formed. The grain sizes of oxides are measured as 15-20 nm in pre-transition regime (Fig.11-a) and 20-25 nm in post-transition regime (Fig.11-b). Many white grain boundaries are observed in the oxides formed in pre-transition as well as in post-transition regime. It was reported by Pêcheur[13] and Beie[19] that the white grain boundaries would be open grain boundaries or pores which indicates the weak intergranular cohesion.





(a)



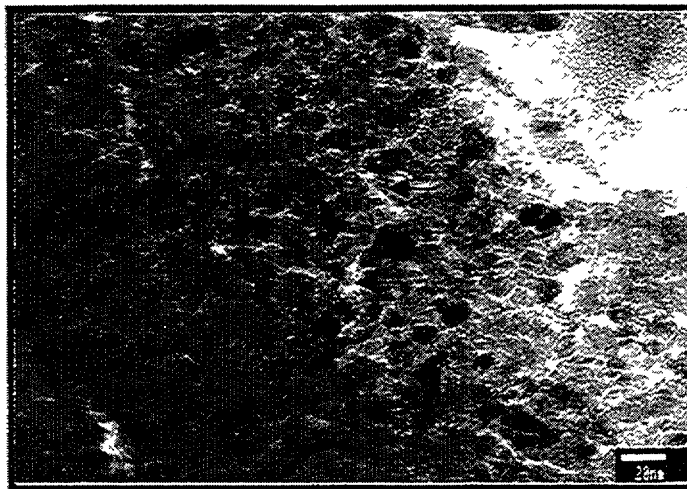
(b)

Fig.11 Cross-sectional TEM micrographs of Zircaloy oxide grown in LiOH solution (a) pre-transition ( $25\text{mg/dm}^2$ ) (b) post-transition ( $60\text{mg/dm}^2$ )

Fig.12 shows the TEM micrographs on the oxide formed in NaOH solution. In pre-transition regime the columnar grains with the length of 150-200 nm and the width of 15-20 nm are observed. Even if the corroded samples have an equal oxide thickness in LiOH and NaOH, the columnar grains are observed only in the oxide formed in NaOH solution. The preservation of the columnar grains in NaOH solution would be related to the low corrosion rate in NaOH solution as compared with that in LiOH solution. Nevertheless, in post-transition regime the columnar grains are transformed into the small equiaxed grains with the grain size of 15-20 nm including the many open grain boundaries or pores.



(a)

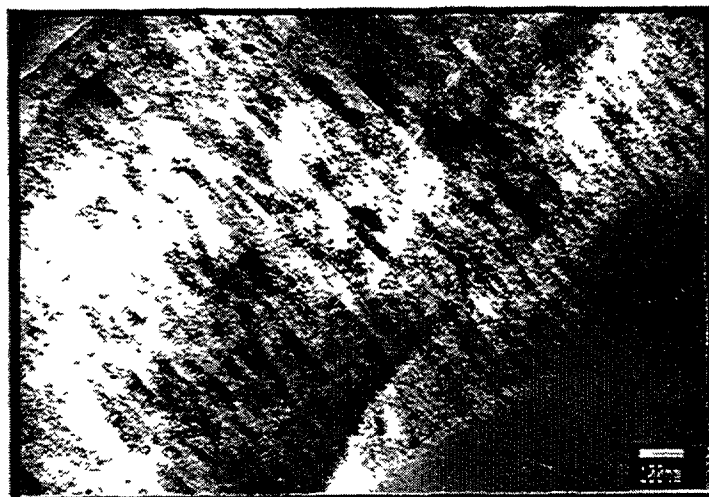


(b)

Fig.12 Cross-sectional TEM micrographs of Zircaloy oxide grown in NaOH solution (a) pre-transition ( $25\text{mg/dm}^2$ ) (b) post-transition ( $60\text{mg/dm}^2$ )

The TEM microstructures of the oxide formed in KOH solution are shown in Fig.13. The oxide formed in pre-transition regime is mostly composed of the columnar grains. This means that the oxide formed in KOH solution is more protective and stable than those formed in LiOH and NaOH solutions.

The SEM micrographs at the metal-oxide interface of the Zircaloy-4 sheet corroded in LiOH, NaOH, and KOH solutions were shown in Fig.14. The oxide morphologies grown in the post-transition regime of LiOH solution represent the shape of ice columns having the different orientation of the oxide growth and the different growth rate of the oxide with varying the grain orientation of metal. It is observed that the oxide morphologies at the



(a)



(b)

Fig.13 Cross-sectional TEM micrographs of Zircaloy oxide grown in KOH solution (a) pre-transition (25mg/dm<sup>2</sup>) (b) post-transition(60mg/dm<sup>2</sup>)

metal-oxide interface are different from grain to grain of the zirconium matrix. It is also observed that the corrosion rate at the grain boundary of zirconium matrix is much faster than that at the interior of the zirconium matrix grain. In the long-term corrosion test for 200 days in LiOH solution, the ice columnar oxides are transformed into the cauliflower morphologies containing the numerous open pores and cracks between the lump-type oxides. The oxides formed in post-transition regime of NaOH solution show the remarkable difference in the oxide morphology with varying the grain orientation of zirconium metal. The width of ice columnar oxides in NaOH solution is much narrower than that in LiOH solution. After a long-term corrosion test for 200 days in a NaOH solution, the ice columnar oxides are mainly transformed into the lump-type oxides but still remained with small fraction. In particular, the cauliflower morphologies of oxides are not observed even after a

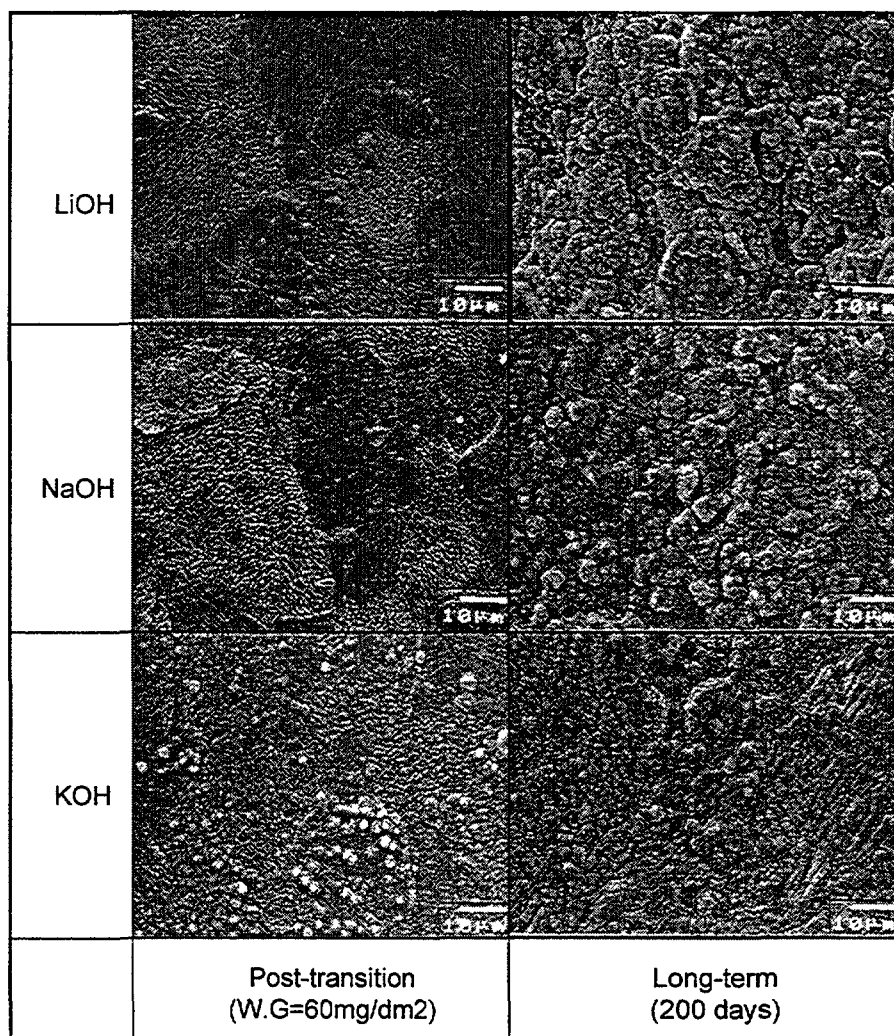


Fig.14 SEM micrographs at metal-oxide interface of Zircaloy-4 in LiOH, NaOH, and KOH solution

long-term corrosion test in NaOH solution. In KOH solution, the process of oxide development is quite different from those in LiOH and NaOH solution. The numerous small round-type oxides, instead of ice columnar oxides, are formed in the post-transition regime. After a long-term corrosion test in KOH solution, the round-type oxide is replaced by the mixed oxides of a columnar-type in a major portion and round-type in a minor portion.

#### 4. Discussion

Based on the corrosion characteristics, the SIMS analysis, and the oxide microstructure, the discussion is classified into the two mechanistic aspects; one is related to the slight enhancement in low concentration and in pre-transition regime of high concentration, and the other the significant enhancement in high concentration.

The corrosion result in low concentration (4.3mmol) of alkali hydroxide shows that the corrosion rate decreases gradually with an increasing ionic radius of alkali cation. This

phenomenon would be caused by the difference of ionic radius between cation and  $\text{Zr}^{4+}$ . It would be easy to substitute  $\text{Li}^+$  for  $\text{Zr}^{4+}$  in the oxide layer due to the similar ionic radii ( $\text{Li}^+ = 76 \text{ pm}$  and  $\text{Zr}^{4+} = 72 \text{ pm}$ ) whereas it be very difficult for  $\text{Na}^+$ ,  $\text{K}^+$ ,  $\text{Cs}^+$ , and  $\text{Rb}^+$  to do due to the big difference of ionic radius between cation and  $\text{Zr}^{4+}$ . Also, it can be said that the slight enhancement of corrosion rate in  $\text{LiOH}$  solution is induced owing to the easy substitution of  $\text{Li}^+$  for  $\text{Zr}^{4+}$  in the oxide layer, indicating the formation of many anion vacancies, by the similar size of their ionic radii. This hypothesis is supported by the variation of cation concentrations measured in this study, namely, the gradual decrease of cation concentration with an increasing ionic radius of cation. Therefore, the slight enhancement of corrosion rate in low concentration of  $\text{LiOH}$  would be controlled by  $\text{Li}^+$  incorporation into the oxide. However, the significant acceleration that occurred in the long-term corrosion test of more than 500days in low concentration can not be explained by this hypothesis. Other factors like oxide characteristics may affect the significant acceleration of corrosion.

It was observed from the corrosion tests in equimolar alkali hydroxides that the corrosion rate of Zircaloy-4 was dependent on the alkali hydroxide. Therefore, the effect of  $\text{OH}^-$  ion in the aqueous solution on the corrosion could be excluded by the equimolar  $\text{M}^+$  and  $\text{OH}^-$  condition used in this study. It could be suggested that the corrosion of the Zircaloy-4 in alkali hydroxide solutions be accelerated by the existence of metallic ion, not by the  $\text{OH}^-$  ion (or pH).

Regarding the corrosion behaviors in high concentration of alkali hydroxide, in the pre-transition region, the corrosion behaviors showed the gradual decrease with increasing the ionic radius. The SIMS analysis on the samples showed that the penetration depth decreased and the ratio of barrier layer to total layer increased with increasing the ionic radius of cation. Even in high concentration of alkali hydroxide, the corrosion behavior in pre-transition regime is well consistent with the depth of the barrier layer in the oxides formed in  $\text{LiOH}$ ,  $\text{NaOH}$ , and  $\text{KOH}$  solution. Therefore, it is thought that the corrosion in pre-transition regime of high concentration would be controlled by the cation incorporation. In the post-transition regime of high concentration, it was observed that corrosion rate was significantly accelerated in only  $\text{LiOH}$  but slightly in other alkali hydroxides. The cation concentration in the oxide by chemical analysis decreased gradually with increasing the ionic radius. Therefore, the cation concentration in the oxide is not clearly consistent with the corrosion behaviors in alkali hydroxide solutions. In SIMS analysis on the thick oxide formed in  $\text{LiOH}$ ,  $\text{NaOH}$ , and  $\text{KOH}$  solution for 300days, it was observed that  $\text{Li}^+$  could be penetrated to the very long distance but  $\text{Na}^+$  and  $\text{K}^+$  up to only 3 and 2  $\mu\text{m}$ , respectively. Therefore, from the corrosion behavior in high concentration and the cation content by SIMS and chemical analysis, it is considered that the strong acceleration of the corrosion rate in high concentration would be caused by not only cation incorporation but also other factors.

It was investigated from the TEM study on oxide that, even if they have an equal oxide thickness, the oxide morphologies are quite different depending on the alkali hydroxide. In LiOH solution the equiaxed structure was formed in both regimes of pre-and post-transition, in NaOH solution the columnar structure in pre-transition and the equiaxed structure in post-transition regime, and in KOH solution the columnar structure in both transition regimes. From the above results, it is thought that the cation in alkali hydroxide can affect the oxide characteristics including morphology, growth mechanism, and spalling of oxide. In a high concentration of alkali hydroxide solution, LiOH accelerates the corrosion due to the early transformation of oxide morphology from columnar to equiaxed structure. On the other hand, KOH is effective to maintain stable oxide morphology. Therefore, the strong acceleration of corrosion in high concentration of LiOH is mainly caused by the transformation of the oxide microstructure, which would be resulted from the cation incorporation in the oxide. However, it is not clear in this study how the cation incorporation induces the transformation of oxide microstructure.

KOH, which is being used as a pH controller with other alkali hydroxide in WWER reactor, does not significantly accelerate the corrosion and the hydrogen pickup of Zircaloy. Thus, KOH has a potential as an alternative alkali hydroxide for PWR reactors. However, the systematic study to use the KOH for PWR reactor is necessary because, according to Henzel's paper [20], KOH may induce the stress corrosion cracking in other primary components.

## 5. Conclusions

The results from the long-term corrosion test, SIMS analysis, and oxide study lead to the following conclusions;

1. The corrosion rate in alkali hydroxide solutions decrease with the increasing ionic radius of alkali cation. The cation would control the corrosion in alkali hydroxides with equimolar  $M^+$  and  $OH^-$ . The effect of cation on the corrosion is dependent on the alkali concentration and the oxide thickness.
  - The slight enhancement of corrosion in low concentration is controlled by the cation incorporation into oxide, which results in the increase of anion vacancy and the decrease of the barrier layer.
  - The strong acceleration of corrosion in high concentration is mainly controlled by the transformation of oxide microstructure, which would be caused by the cation incorporation into oxide.
2. KOH does not significantly accelerate the hydrogen pickup as well as the corrosion rate of Zircaloy even in a high concentration. It is thought that KOH has a potential as an alternative alkali for PWR application with respect to Zircaloy corrosion.

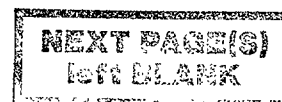
## REFERENCES

- [1] F.GARZAROLLI, J.POHLMEYER, S.TRAPP-PRITSCHING, H.G.WELDINGER,  
"Influence of various additions to water on Zircaloy-4 corrosion in autoclave tests at 350°C", Fundamental Aspects of Corrosion on Zirconium Base Alloys (Proc. Mtg Portland, Oregon, USA, 1989), Rep. IWGFPT/34, IAEA (1990) 65.
- [2] S.G.MCDONALD, G.P.SABAL AND K.D.SHEPPARD, "The effect of lithium hydroxide on the corrosion behaviour of Zircaloy-4", Zirconium in Nuclear Industry (Proc. 6<sup>th</sup> Int. Symposium, Vancouver, BC, Canada, 1984), ASTM, ASTM STP 824 (1984) 519.
- [3] E.HILLNER AND J.N.CHIRIGOS, "The effect of lithium hydroxide and related solutions on the corrosion rate of Zircaloy-2 in 680°F water", US Report WAPD-TM-307, Bettis Atomic Power Laboratory, W. Mifflin, PA (1967).
- [4] R.A.PERKINS AND R.A.BUSCH, "Corrosion of Zircaloy-4 cladding", Environmental Degradation of Materials in Nuclear Reactor Systems (Proc. 4<sup>th</sup> Int. Symposium Jekyll Island, GA, USA, 1990, ASTM, ASTM STP 1132 (1991) 595
- [5] I.L.BRAMWELL, P.D.PARSONS, AND D.R.TICE, "Corrosion of Zircaloy-4 PWR fuel cladding in lithiated and borated water environments", Zirconium in Nuclear Industry (Proc. 9<sup>th</sup> Int. Symposium, Kobe, Japan, 1990), ASTM, ASTM STP 1132 (1991) 628.
- [6] N. RAMASUBRAMANIAN AND P.V.BALAKRISHNAN, "Aqueous chemistry of lithium hydroxide and boric acid and corrosion of Zircaloy-4 and Zr-2.5%Nb", Zirconium in Nuclear Industry (Proc. 9<sup>th</sup> Int. Symposium, Kobe, Japan, 1990), ASTM, ASTM STP 1132 (1991) 628.
- [7] N.RAMASUBRAMANIAN, N.PRECOANIN, AND V.C.LING, " Lithium uptake and the accelerated corrosion of zirconium alloys", Zirconium in Nuclear Industry (Proc. 8<sup>th</sup> Int. Symposium, San Diego, USA, 1988), ASTM, ASTM STP 1023 (1989) 187.
- [8] N.RAMASUBRAMANIAN, "Lithium uptake and corrosion of zirconium alloys in aqueous lithium hydroxide solutions", Zirconium in Nuclear Industry (Proc. 9<sup>th</sup> Int. Symposium, Kobe, Japan, 1990), ASTM, ASTM STP 1132 (1991) 613.
- [9] B.COX AND C.WU, "Dissolution of zirconium oxide film in 300°C LiOH", J. Nucl. Mater. **199** (1993) 272.

- [10] B.COX, M. UNGURELU, Y.M.WONG, AND C.WU, "Mechanism of LiOH and H<sub>3</sub>BO<sub>3</sub> repair of ZrO<sub>2</sub> film", Zirconium in Nuclear Industry (Proc. 11<sup>th</sup> Int. Symposium Germany, 1995), ASTM, ASTM STP 1295 (1996) 114.
- [11] Y.H.JEONG, H.RUHMANN AND F. GARZAROLLI, IAEA-TECDOC-972, "Influence of alkali metal hydroxides on corrosion of zirconium-based alloys" (Proc. Mtg Rez, Czech Republic, 1993), IAEA-TECDOC-927 (1997) 161.
- [12] F.GARZAROLLI, H.SEIDEL, R.TRICOT, AND J.P.GROS, "Oxide growth mechanism on zirconium alloys", Zirconium in Nuclear Industry (Proc. 9<sup>th</sup> Int. Symposium, Kobe, Japan, 1990), ASTM, ASTM STP 1132 (1991) 395.
- [13] D.PÊCHEUR, J.GODLEWSKI, P.BILLOT, AND J.THOMAZET, "Microstructure of oxide films formed during the waterside corrosion of the Zircaloy-4 cladding into lithuated environment", Zirconium in Nuclear Industry (Proc. 11<sup>th</sup> Int. Symposium Germany, 1995), ASTM, ASTM STP 1295 (1996) 94.
- [14] D.PECHEUR, A.GIORDANO, E.PICARD, PH.BILLOT, AND J.THOMAZET, "Effect of elevated lithium on the waterside corrosion of Zircaloy-4: experimental and predictive study", Influence of Water Chemistry on Fuel Cladding Behavior (Proc. Mtg Rez, Czech Republic, 4-8 October, 1993), IAEA-TECDOC\_927 (1997) 111.
- [15] D.PECHEUR, J.GODLEWSKI, J.PEYBERNES, L.FAYETTE, M.NOE, A.FRICHET, AND O.KERREC, "Contribution to the understanding of the effect of the water chemistry on the oxidation kinetics of Zircaloy-4 cladding", Zirconium in the Nuclear Industry, (Proc. 12<sup>th</sup> Int. Symposium Toronto, Canada, 1998), ASTM, ASTM STP1354 (in press).
- [16] T.KIDO, S.WADA, T.TAKARASHI, H.UCHIDA, I.KOMINE, AND Y.INOUE, "Behaviour of lithium and boron in irradiated and unirradiated oxides formed on Zircaloy-4 claddings", Zirconium in the Nuclear Industry, (Proc. 12<sup>th</sup> Int. Symposium Toronto, Canada, 1998), ASTM, ASTM STP1354 (in press).
- [17] J.KYSELA, M.ZMITKO, AND V. VRTILKOVA, "VVER water chemistry related to fuel cladding behaviour" (Proc. Mtg Rez, 1993), IAEA-TECDOC-972 (1997) 473.



- [18] H.ANADA AND K.TAKEDA, "Microstructure of oxides on Zircaloy-4, 1.0Nb Zircaloy-4, and Zircaloy-2 formed in 10.3 Mpa steam at 673 K", Zirconium in Nuclear Industry (Proc. 11<sup>th</sup> Int. Symposium Germany, 1995), ASTM, ASTM STP 1295 (1996) 35.
- [19] H.J.BEIE, A.MITWALSKY, F.GARZAROLLI, H.RUHMANN, AND H.J.SELL, "Examination of the corrosion mechanism of zirconium alloys", Zirconium in Nuclear Industry (Proc. 10<sup>th</sup> Int. Symposium, Baltimore, MD, USA, 1993), ASTM, ASTM STP 1245 (1994) 615-643.
- [20] N.HENZEL, "Alternative water chemistry for the primary loop of PWR plants", Influence of Water Chemistry on Fuel Cladding Behaviour ( Proc. Mtg Rez, 1993), IAEA, IAEA-TECDOC-972 (1997) 421.



# THE CORROSION BEHAVIOR OF LOW TIN AND HIGH TIN ZIRCONIUM BASED ALLOYS UNDER DIFFERENT LITHIUM HYDROXIDE AND BORIC ACID CONTAINING ENVIRONMENTS.

H. RUHMANN, F. GARZAROLLI, I. POHLMAYER, H.-J. SELL  
Siemens AG, Power Generation (KWU),  
Erlangen, Germany



XA9953296

## Abstract

Systematic laboratory experiments were performed with zirconium based alloys exposed to different lithium hydroxide and boric acid containing water chemistry environments under isothermal, pressurized water reactor simulating conditions. The investigated materials are zirconium alloys with different tin content. The samples were exposed to water with different lithium and boric acid concentrations in an static autoclave operated at 350 °C and 17 MPa. Weight gain increases are followed as a function of exposure time. These data are evaluated with respect to late corrosion rate, time to transition and weight gain at transition. The experiments confirm the sensitivity of zirconium based alloys to water environments with increasing lithium hydroxide concentrations. Low tin alloys show a increasing sensitivity with increasing lithium hydroxide content. The onset of enhanced, respectively accelerated corrosion depends on the lithium concentration. If boric acid is added to lithium hydroxide containing solutions a dramatic reduction of the corrosion rate is observed. Corrosion rate measured under these conditions are comparable to pure water corrosion. This effect is mostly independent from the tin content of the investigated alloy. The data is interpreted with respect to water chemistry aspects and brought into correlation to the in reactor situation.

## 1. INTRODUCTION

The optimization of the corrosion behavior of zirconium based alloys has taken into account all border conditions of the in reactor environment. Therefore, the behavior of the materials has not only to be considered under pure water conditions, temperature and pressures, but also in environments which are similar to real reactor operation. Especially coolant additives like lithium hydroxide and boric acid are chemical species which may play here an important role on the corrosion behavior of zirconium based alloys used for cladding and structural components of fuel assemblies. Lithium hydroxide is used in Western pressurized water reactors (at concentrations from 2 - 4 ppm) as an alkalizer to establish a pH that takes care for optimized SCC behavior of loop components and provides in that way low radiation levels (man dose rates). Boron (as boron acid) is applied for reactivity control in concentrations, at the beginning of the cycle, around 1000 ppm. Zirconium based alloys show a increased corrosion sensitivity to lithium hydroxide containing environments above concentration around 30 ppm Li. This has been demonstrated by many investigations since the classical work from Hillner [1], Coriou [2] and Kass [3]. Not as well systematically investigated is the effect of boric acid on the enhanced Li-induced corrosion of zirconium based alloys. First observations of an amelioration effect on corrosion induced by boric acid additions to lithium hydroxide solutions have been mentioned by Tice [4], Garzarolli [5] and Bramwell [6]. Recently published papers shed light mainly onto the properties of corrosion layers and mechanistic aspects [7 - 10].

The objective of this study is primarily not to contribute to mechanistic explanations of the metallurgical and physicochemical aspects being responsible for the corrosion behavior of zirconium based alloys in lithium hydroxide and boric acid containing water. The target is to quantify influencing alloy parameters by a systematic corrosion experiment, and the sensitivity to different lithium and boron containing corrosive media under pressurized water reactor simulating conditions.

## 2. EXPERIMENTAL

### 2.1 Materials

The investigation was carried out with cladding material originating from one prematerial supplier and one ingot with two different values for only one alloy component, the content of tin. The

tin content of the two variants was selected according to the range of commercially applied Zircaloy-type alloys. The lower end of this range is represented by an alloy with nominally 0.5 weight % tin, the upper end by an alloy with a tin content of 1.6 weight % Sn, near the upper end of ASTM specification for Zry-4. The compositions of the investigated cladding materials are given in Table I.

TABLE I. ALLOY COMPOSITION FOR THE TEST MATERIALS USED IN THE INVESTIGATION

Material designation	Sn %	Fe %	Cr %	O ppm	C ppm	Si ppm
ELS 0.6 Sn	0.57	0.218	0.103	1233	87	30
Zry-4 1.6 Sn	1.58	0.218	0.103	1233	87	30

The corrosion samples were taken from cladding tubes with 10.75 OD and 0.73 mm wall thickness. Short rings with a length of 15 mm were cut for the tests. All samples have been pickled in standard etching solution prior to autoclave testing.

## 2.2 Corrosion testing

All corrosion tests were performed in small 0.1 L volume stainless steel static autoclaves operated at 350 °C and 17 MPa. No special inert gas purging was applied before closing the autoclaves. In comparable experiments no influence of remaining air on corrosion was reported by Perkins [12]. For the corrosion tests different compositions of the corrosive medium were prepared from deionized water and additions of high purity commercial LiOH hemihydrate and Boric acid. To avoid cross contamination the same autoclave was exclusively used for one water chemistry. The compositions of the solutions, applied for the corrosion tests, are given in Table II. The concentration of lithium hydroxide and boric acid is expressed as ppm Li and ppm B respectively. The lithium hydroxide concentrations were selected to cover the range of enhanced corrosion (70 ppm Li) to values which are reported to induce accelerated corrosion, if cumulated in porous corrosion layers [10] (700 ppm Li). The concentrations of boron acid additions were selected to cover the range of concentrations commonly occurring in pressurized water reactor coolant.

The test runs were interrupted at different time intervals depending on the aggressiveness of the different solutions, and specific weight gains were calculated from measured weight increase and the surface of the specimen before corrosion.

TABLE II. COMPOSITIONS OF THE CORROSIVE MEDIA USED FOR CORROSION TESTING

Water compositions tested	LiOH ppm Li	in B(OH) <sub>3</sub> ppm B	in pH at 350 °C calculated
0/0	0	0	6.2
70/0	70	0	10.1
70/100	70	100	10.1
70/1000	70	1000	9.5
300/0	300	0	10.6
300/100	300	100	10.5
300/1000	300	1000	10.1
700/0	700	0	10.8
700/100	700	100	10.7
700/1000	700	1000	10.4

### 3. RESULTS

#### 3.1 Corrosion behavior of Zry-4 1.6 Sn

##### 3.1.1 Influence of lithium hydroxide on corrosion

Weight gains as function of exposure for Zry-4 1.6 Sn cladding in water containing different concentrations of lithium hydroxide without boric acid additions are presented in Fig. 1. In comparison to lithium free conditions an significant increase of corrosion is observed with increasing lithium hydroxide concentration.

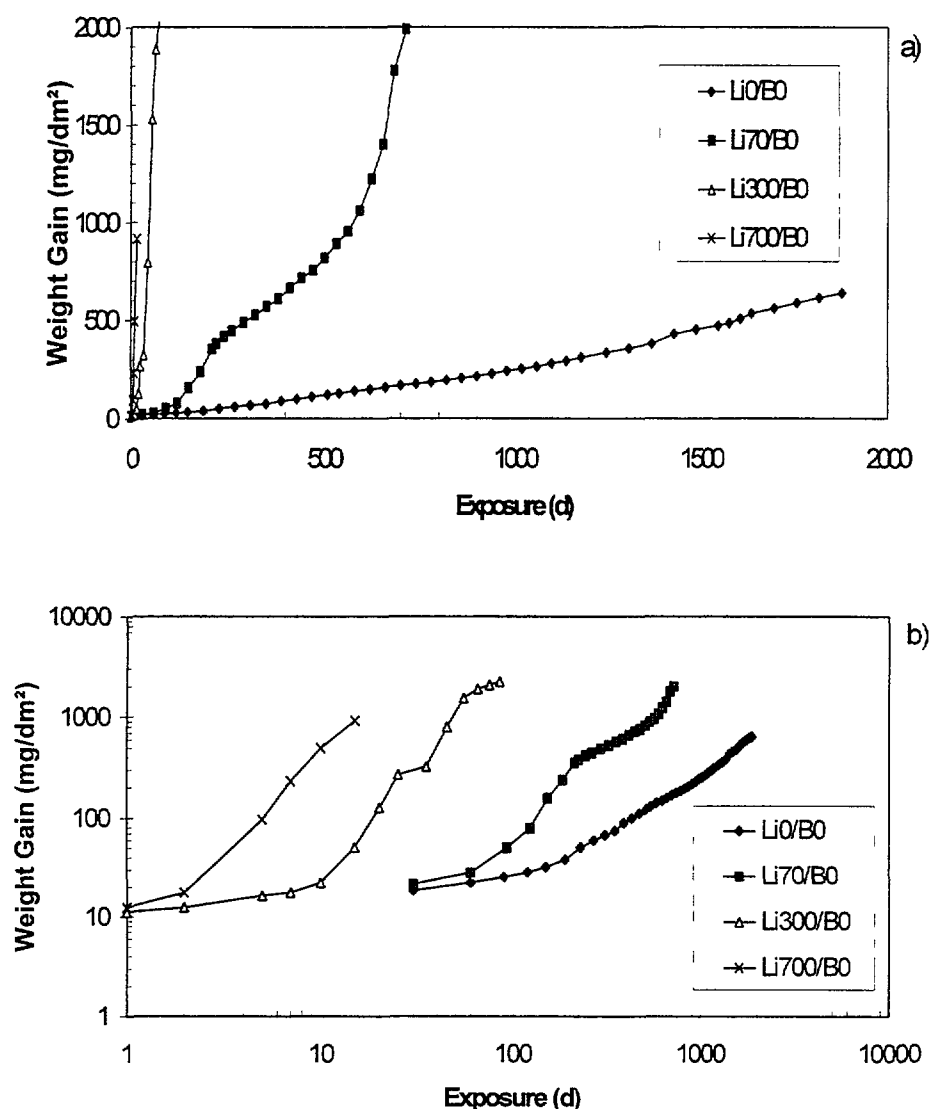


FIG. 1 Corrosion behavior of Zry-4 1.6 Sn in environments with different lithium hydroxide concentrations, a) linear scale, b) double logarithmic scale. Test conditions: 350 °C, 17 MPa.

Corrosion kinetics are obviously different depending on the lithium concentration in the water. The classical behavior with a nonlinear pretransition regime and linear increase of the weight gain after transition is observed only for lithium free environments. An addition of 70 ppm Li (as LiOH) changes the kinetics significantly. After an intermediate period between 200 and 500 days exposure increased corrosion is observed switching at a second kinetic transition to accelerated corrosion. Exclusively accelerated corrosion is found for higher lithium concentrations (300 ppm Li and 700 ppm Li) starting nearly just from the beginning of the experiment. The logarithmic plot of the

weight gains, as shown in Fig. 1 b, reveals the onset point of enhanced and accelerated corrosion and indicates by different slopes of the curves also deviations from linear corrosion kinetics. A slope of  $m = 1$  indicating linear kinetics is observed only for pure water corrosion. Slope exponents for Li containing water lie between 2.1 and 5.5. As an first order approximation late linear corrosion rates were determined graphically for further evaluation. The determined kinetic parameters: linear corrosion rate, time to transition and weight gain at transition are compiled in Table III. It has to be noted that the term transition has an generalized meaning: it stands, besides the classical transformation, also for a transition to enhanced or accelerated corrosion. The distinction can easily be made, as will be explained later, by the measured corrosion rate.

### 3.1.2 Influence of boric acid additions to lithium hydroxide containing water on corrosion

Corrosion experiments were performed at three levels of lithium hydroxide (70 ppm (a), 300 ppm (b) and 700 ppm Li (c)) with additions of boric acid at two different concentrations (100 ppm B and 1000 ppm, refer to Table II). The results are shown in Fig. 1 a - c. An addition of boric acid which corresponds to 100 ppm B influences corrosion sensitivity significantly. Only in the case of additions to water containing 700 ppm Li, enhanced corrosion is observed (Fig. 2 c) in all other cases accelerated corrosion is found. For 1000 ppm B additions low, pure water type corrosion is found up to 220 days exposure but for further exposure times an transition to accelerated can not be excluded. The kinetic data for the effect of boric acid additions evaluated from these measurements are compiled in Tab. III.

TABLE III Results of the corrosion experiments performed at 350 °C, 17 MPa under different water environments. (Abbreviations: WG = weight gain, tr = transition).

Li/B (ppm/ppm)	ELS 0.6 Sn			Zry-4 1.6 Sn		
	corrosion rate (mg/dm <sup>2</sup> d-1)	time to tr (d)	WG at tr (mg/dm <sup>2</sup> )	corrosion rate (mg/dm <sup>2</sup> d-1)	time to tr (d)	WG at tr (mg/dm <sup>2</sup> )
0/0	0.2	200	30	0.5	150	28
70/0	11.5	120	30	10.0	80	25
300/0	84.1	8	20	60.8	12	20
700/0	147.6	1	20	121.6	2	15
70/0	11.5	120	30	10.0	80	25
70/100	0.5	150	38	0.6	190	70
70/1000	0.2	n d	n.d	0.5	n d	n d
300/0	84.1	8	20	60.8	12	20
300/100	0.7	100	30	1.5	40	30
300/1000	0.3	200	48	1.2	n d	n d
700/0	147.6	1	20	121.6	2	15
700/100	22.1	80	35	3.5	40	30
700/1000	0.3	120	32	0.7	60	24

n d = not discernible

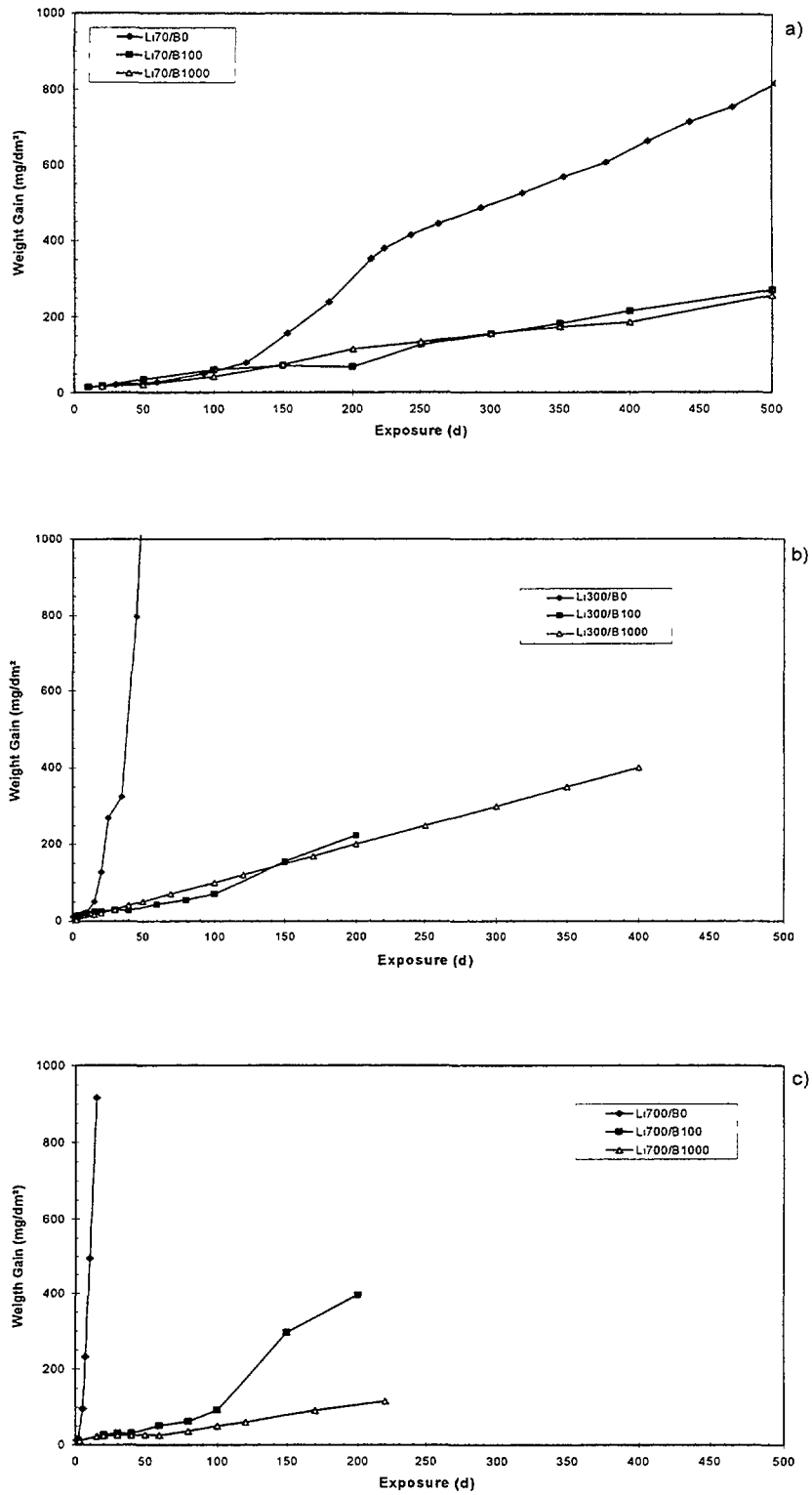


FIG. 2 Corrosion behavior of Zry-4 1.6 Sn in environments with different concentrations of lithium hydroxide and boric acid, a) boric acid additions at 70 ppm Li, b) boric acid additions at 300 ppm Li, c) boric acid additions at 700 ppm Li. Test conditions: 350 °C, 17 MPa.

### 3.2 Corrosion behavior of ELS 0.6 Sn

#### 3.2.1 Influence of lithium hydroxide on corrosion

Analogous corrosion testing, as described for Zry-4 1.6 Sn alloy, was performed with a zirconium based alloy which differs only in the tin content. The corresponding results for ELS 0.6 Sn materials are presented in Fig. 3 a - b.

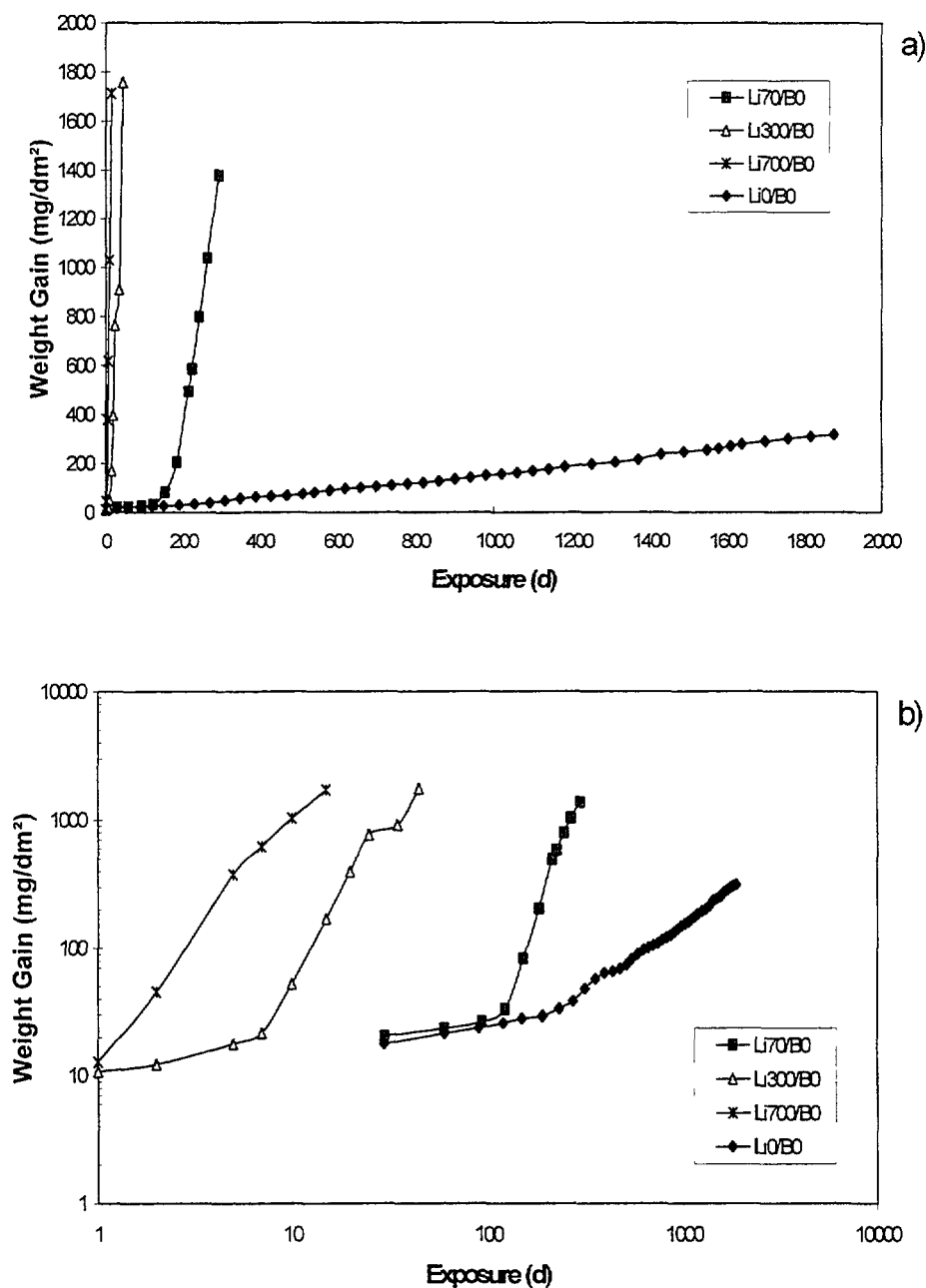


FIG. 3 Corrosion behavior of ELS 0.6 Sn in environments with different lithium hydroxide concentrations, a) linear scale, b) double logarithmic scale . Test conditions: 350 °C, 17 MPa.

At the first glance very similar results as found for the high tin alloy are obtained. But a significant difference to the corrosion behavior of Zry-4 1.6 Sn is the onset of accelerated corrosion already for lithium hydroxide concentration in the water corresponding to 70 ppm Li. A quantification by the determination of the kinetic data allows to identify further differences in the corrosion behavior . This data is included in Tab. III.

### 3.2.2 Influence of boric acid additions to lithium hydroxide containing water on corrosion

Similar, as found for the high tin alloy, a strong influence of boric acid additions to lithium hydroxide containing solutions on the corrosion is found also for the low tin material. This is demonstrated by weight gain curves presented in Fig. 4 a - c . Also for ELS 0.6 Sn the corrosion is effectively reduced to lower values by an addition of only 100 ppm B (as boric acid). Only at the highest Li level in the water (at 700 ppm Li, Fig. 4 c) an addition of 100 ppm B cannot suppress accelerated corrosion. Unfortunately the exposure was terminated after 210 days therefore the question whether a later transition to increased corrosion occurs in at high boron acid addition cannot be answered from this experiment. The kinetic parameters for the effect of boric acid on corrosion derived from the weight gain curves of the low tin material are included in Tab. III.

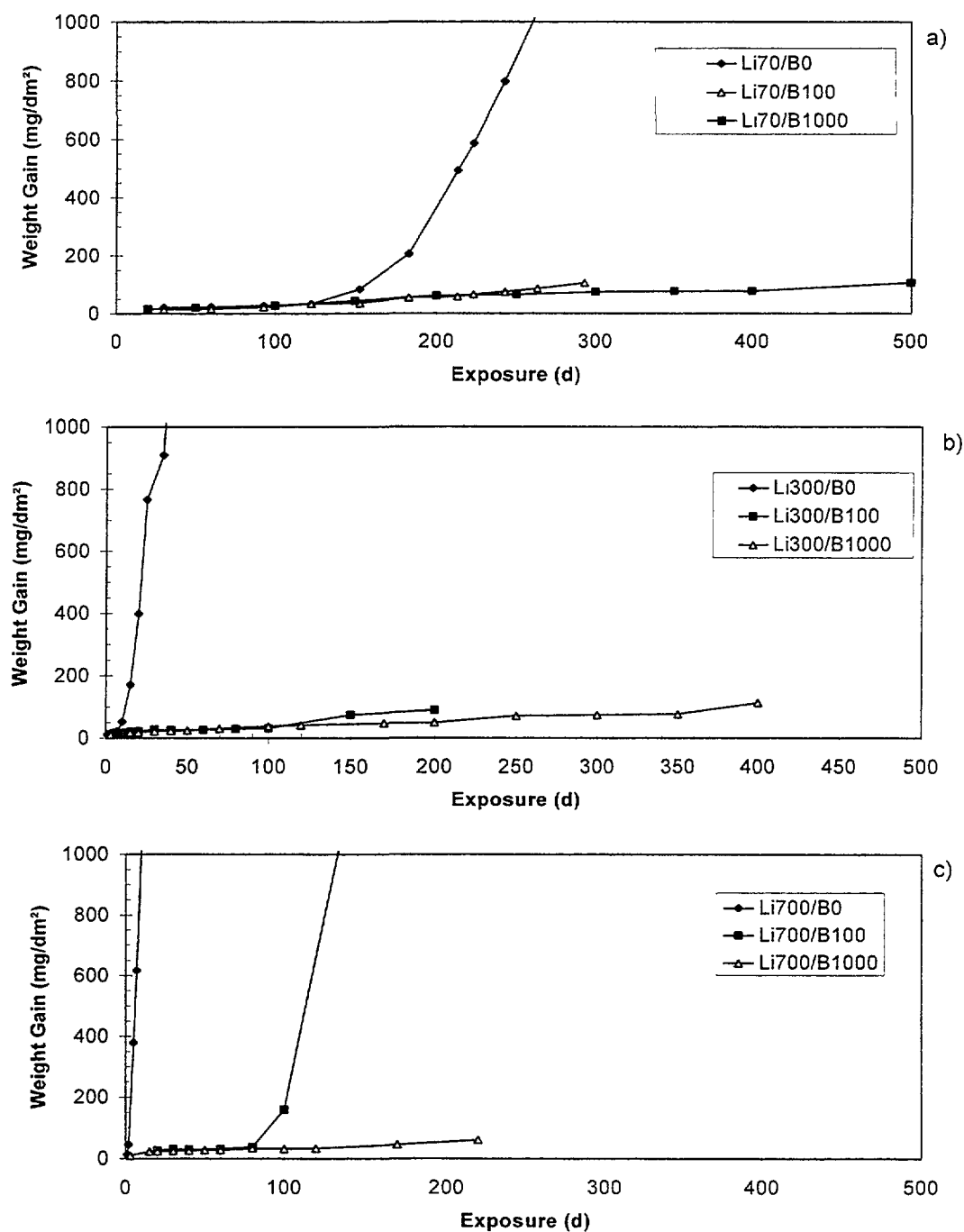


FIG. 4 Corrosion behavior of ELS 0.6 Sn in environments with different concentrations of lithium hydroxide and boric acid, a) boric acid additions at 70 ppm Li, b) boric acid additions at 300 ppm Li, c) boric acid additions at 700 ppm Li . Test conditions: static autoclave at 350 °C, 17 MPa.



## 4. DISCUSSION

### 4.1 Effect of tin content on corrosion resistance in lithium containing environments

The influence of lithium hydroxide on corrosion for the investigated high tin and low tin zirconium based alloys is shown in Fig. 5. Linear corrosion rates are plotted versus the concentration of lithium hydroxide (expressed as ppm Li) present in the water applied for the corrosion experiment.

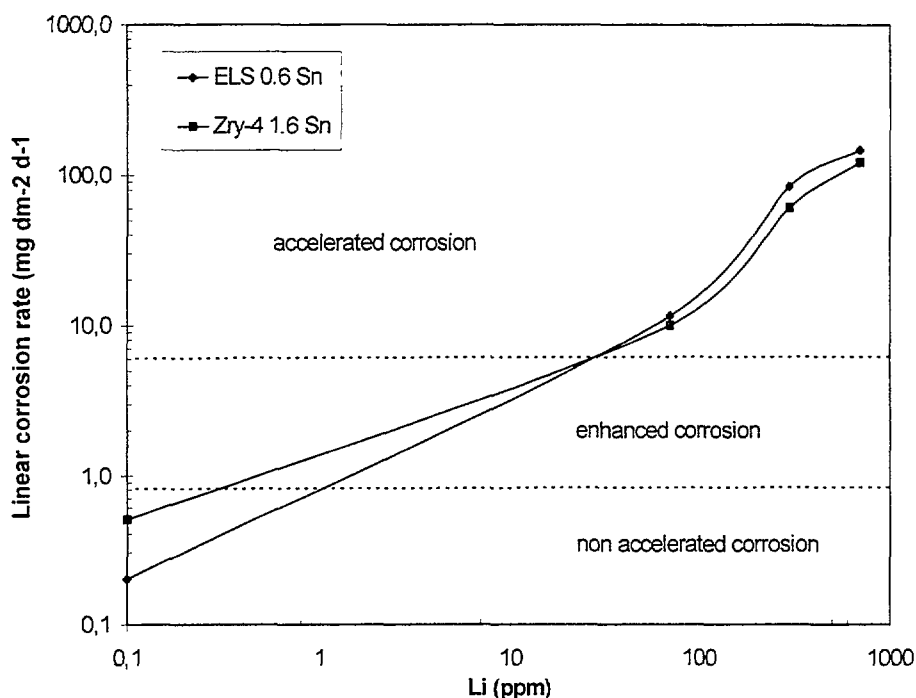


FIG. 5 Linear corrosion rates vs. Li concentration for zirconium based alloys with different tin content. Test conditions: static autoclave, 350 °C, 17 MPa.

The diagram clearly evaluates lower corrosion rates for the low tin alloy at zero-level lithium hydroxide. With increasing lithium concentration in the water the corrosion rate increases and after 30 ppm Li low tin and high tin alloy show an equal corrosion rate of  $6 \text{ mg} \cdot \text{dm}^{-2} \cdot \text{d}^{-1}$ . A further increase of lithium hydroxide in the water induces higher corrosion rates for the low tin alloy variant. The intersection point coincides with the onset of accelerated corrosion independently of the tin content. Enhanced lithium induced corrosion has to be attributed obviously to corrosion rates from 0.4 to  $6 \text{ mg} \cdot \text{dm}^{-2} \cdot \text{d}^{-1}$ . The onset of enhanced corrosion in lithium hydroxide containing water has been reported earlier for lithium hydroxide concentrations above 30 ppm Li [13]. The results of this work allow to differentiate between enhancement and acceleration. It confirms also the fact, that for high lithium concentration, which are supposed to occur in porous corrosion layers, low tin alloys show a degradation of their excellent corrosion behavior observed under low level lithium hydroxide containing environments.

### 4.2 Effect of lithium concentration on the transition and the weight gain at transition

As already qualitatively discussed (see section 3.1.1 and 3.2.1) the exposure time at which the corrosion kinetics changes significantly depends on the concentration of lithium hydroxide and the tin content of the alloy. This observation is quantified in Fig. 6 a - b.

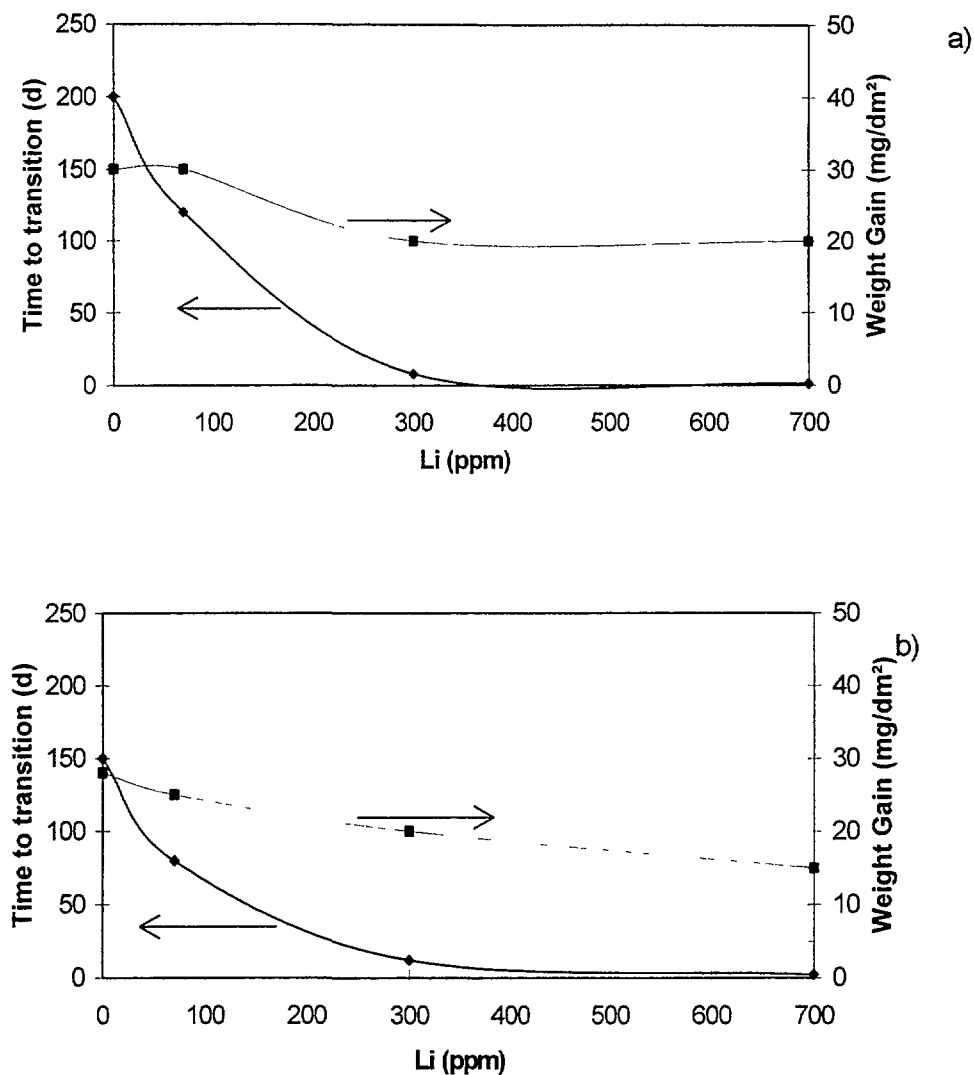


FIG. 6 Time to transition and weight gain at transition for the corrosion of zirconium based alloys in water with increasing lithium content, a) alloy ELS 0.6 Sn, b) alloy Zry-4 1.6 Sn. Test conditions: static autoclave, 350 °C, 17 MPa.

A strong decrease of the transition point is observed for lithium concentrations below 300 ppm Li. This behavior is comparable for low tin and high tin alloys but the value from which the decrease starts (Li = 0 ppm) depends on tin content. Significant higher transition times are found for the low tin alloy. This finding is in accordance to the good corrosion behavior of low tin alloys in low lithium water conditions. Weight gains at the transition point are plotted also in the diagram. With decreasing time to transition an decrease of the weight gain at transition is observed. This indicates that with increasing lithium content the kinetic change occurs at lower oxide scale thickness. These findings are in agreement to results of Pêcheur [11] which show an decreasing barrier layer thickness for corrosion layers grown under lithium containing conditions. The addition of boric acid has an influence on the transition and the weight gain at transition. As can be concluded from Tab. III at constant lithium concentration boric acid additions tend to prolong the pretransition regime (shift the transition to higher values) with an slightly increasing weight gain at transition. As understood as typically in 300 ppm Li water with additions of boric acid an increase of the transition from originally 8 d in boric acid free water to 200 d at 1000 ppm B are observed, whereas the weight gains at transition increase from 20 to 48 mg/dm<sup>2</sup> respectively.

### 4.3 Effect of boric acid additions on corrosion rates

The strong ameliorating effect of boric acid on corrosion of zirconium based alloys in lithium hydroxide containing water is demonstrated in Fig. 7 a - b. Linear corrosion rates for low tin and high tin alloys are plotted versus additions of boric acid to lithium containing water. Obviously, depending on the level of lithium hydroxide, an addition of boric acid reduces the corrosion rate significantly. Only in the case of high lithium (700 ppm Li) an addition of 100 ppm B is not enough to reduce the corrosion rate below  $10 \text{ mg} \cdot \text{dm}^{-2} \cdot \text{d}^{-1}$  and suppress accelerated corrosion. At low lithium level corrosion rates similar to pure water corrosion are observed. No strong dependency of the tin content on this ameliorating effect of boric acid is visible.

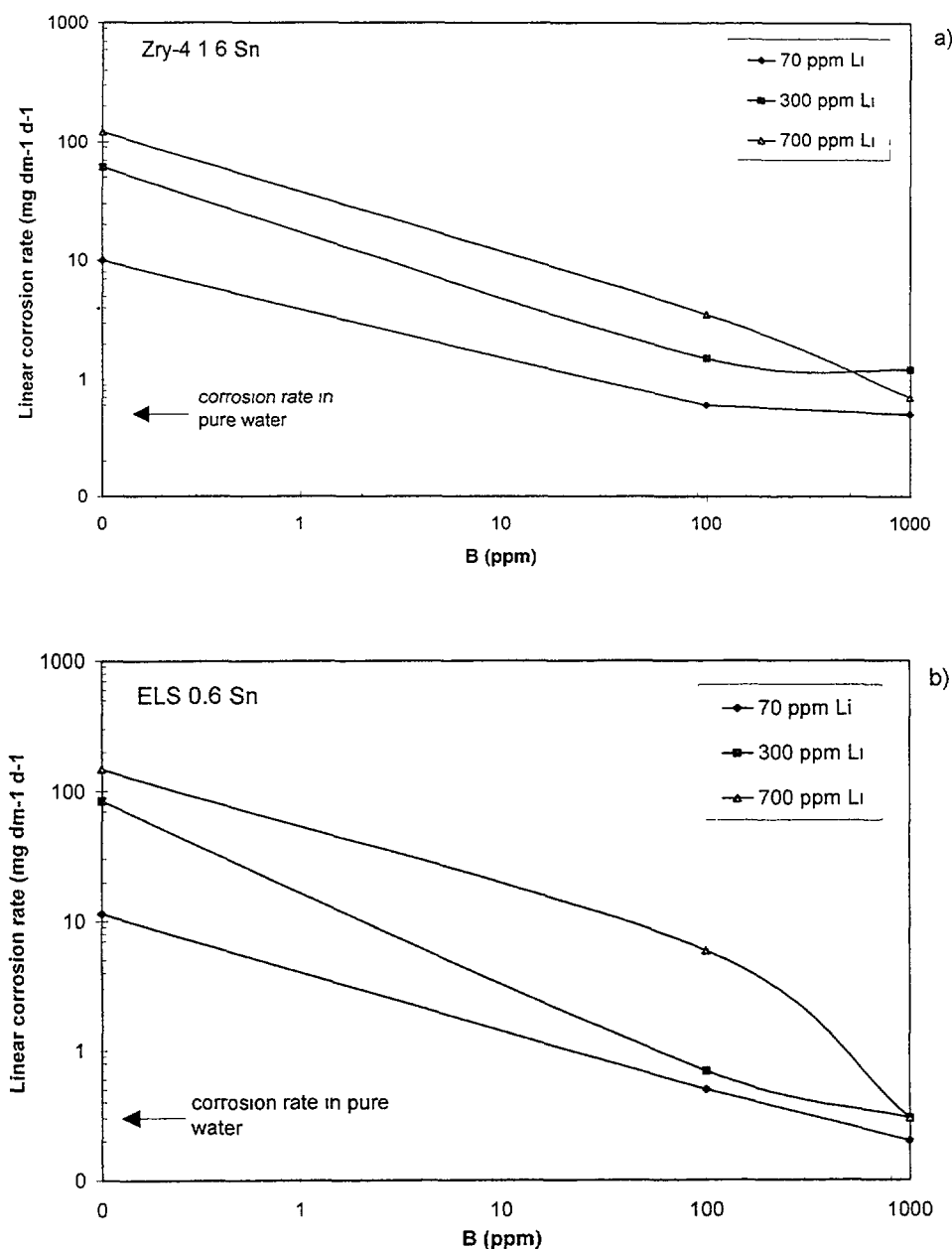


FIG. 7 Influence of boric acid additions to lithium hydroxide containing water on the corrosion of zirconium based alloys, a) alloy Zry-4 1.6 Sn, b) alloy ELS 0.6 Sn. Test conditions: static autoclave, 350 °C, 17 MPa.

#### 4.4 Water chemistry aspects

To understand the strong influence of boric acid in lithium hydroxide containing solutions some water chemistry related aspect shall be discussed. The following statements can be made:

- Corrosion increases with increasing concentration of lithium hydroxide and depends on  $\text{Li}^+$  and  $\text{OH}^-$  simultaneously present in the corrosive environment at the metal oxide interface.
- Corrosion decreases with increasing concentration of boric acid in lithium hydroxide containing environments. Boric acid keeps the  $\text{OH}^-$  concentration more or less constant (borate buffer, compare pH values in table II calculated for different lithium hydroxide levels at constant boric acid concentration). As a second effect increasing boric acid has an influence on the dissociation of lithium hydroxide present in solution. Increasing concentrations increase the concentration of  $\text{Li}^+$  as shown in Fig. 8 (data from [7]).
- The ratio of  $\text{OH}^-/\text{Li}^+$  for the actual concentrations of  $\text{Li}^+$  and  $\text{OH}^-$  present in the corrosive environment changes much less than the corrosion rates (on the basis of published data [7]).

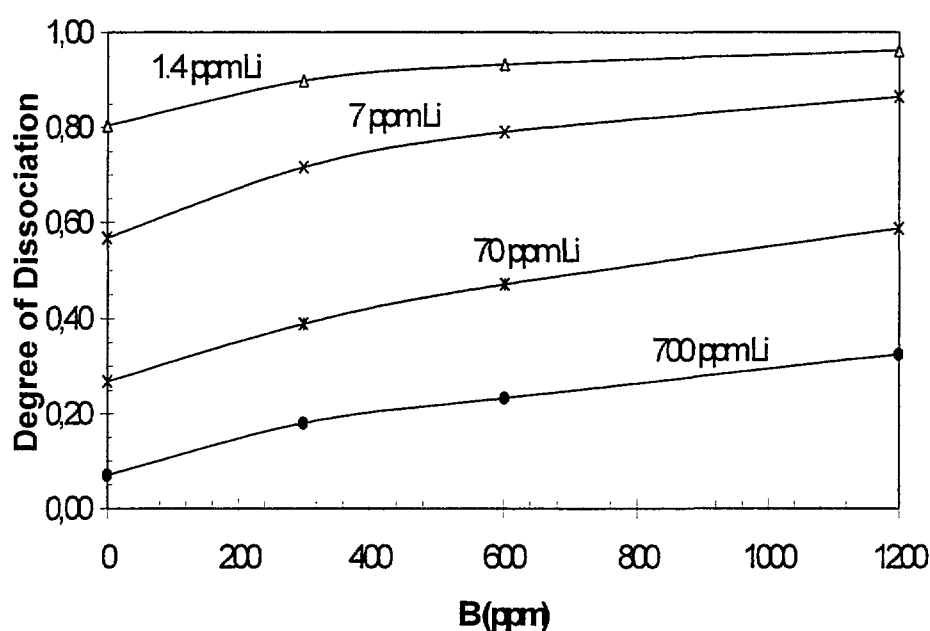


FIG. 8 Degree of dissociation of lithium hydroxide in solutions with different boric acid concentrations at 360 °C [7].

The conclusion from this findings is that not the concentration of  $\text{Li}^+$  and  $\text{B}(\text{OH})_4^-$  in the solution but the concentration at the interface is rate determining. Therefore transportation processes to the metal oxide interface play an important role for the kinetic control of the corrosion reaction.

#### 4.5 Mechanistic aspects

Under isothermal conditions lithium hydroxide decreases, above a certain concentration level, the corrosion resistance of zirconium based alloys drastically. As shown the transition in corrosion kinetics is shifted to lower values (which is connected with porosity formation in the oxide layer) and a higher post transition corrosion rate is observed. Often, especially in those cases where the initial post transition is only moderately increased, a second rate transition to accelerated corrosion is observed later at a higher oxide layer thickness. Chemical analysis of corrosion layers have shown that lithium is incorporated into the oxide scale. The lithium content increases with increasing lithium

hydroxide-concentration in the environment [5] and at similar lithium hydroxide level with decreasing resistance to lithium induced corrosion (e.g. for alloys with decreasing Sn content at constant Fe+Cr content below 0.3%). Fig. 9 shows results from several different Zr-alloys tested in 70 ppm Li at 350 °C. Lots with high corrosion rates under these conditions obviously show higher lithium concentrations in the oxide than corrosion resistant materials. The diagram also reveals that combinations of lithium hydroxide and boric acid result in very low incorporated lithium concentrations. Obviously boric acid inhibits the incorporation of lithium into the oxide.

The following mechanistic explanations for the effect of lithium induced corrosion have been discussed in literature:

1. At high pH the tetragonal fraction of the oxide layer is dissolved which results in a less protective porous oxide layer [10]. A higher sensitivity of Zircaloy-type alloys with extra low tin and zirconium based alloys with high tin content. However just the opposite has been found by Beie [14].

2. Another explanation is that lithium incorporation causes a less protective equiaxed grain oxide structure by lowering the surface energy [11, 15, 16]. The obvious beneficial effect of tin for the corrosion in lithium hydroxide containing environments could be explained in a similar way as its influence on the brake-away corrosion in binary Zr-Sn alloys. Post brake-away corrosion layers are characterized very likely by equiaxed grain structure. The role of tin is, obviously, to reduce the tendency to equiaxed oxidized grain formation. It was pointed out by Garzarolli [15] that monovalent elements like F, Li, and H, which are known to induce increased corrosion, decrease the surface energy of zirconium oxide and facilitate recrystallization.

Boric acid added to solutions with high concentrations of lithium hydroxide increases, as shown, the time to transition. However, time to transition in lithium hydroxide and boric acid mixtures remains shorter than in pure water, at least at the higher lithium hydroxide concentrations. Furthermore the post transition corrosion rate is much less increased by lithium hydroxide if boric acid is present in the environment. Fig. 9 indicates, that boric acid reduces the lithium uptake by the oxide layer significantly. At longer exposure times a second transition to a much more increased corrosion has been observed at least at the highest lithium hydroxide concentrations investigated at lower boron acid additions. At higher boric acid levels it is not clear whether a second rate transition occurs at higher exposure times due to a too short duration of the tests. In pure water a not very pronounced second rate transition can be observed below 1000 day exposure for the two particular investigated alloys.

The mechanistic action of boric acid is even less understood. Cox [10] assumes that boric acid precipitates within oxide pores and keeps lithium hydroxide out by clogging the transportation way. An other possibility is, that boric acid suppresses the tendency to form equiaxed oxide grains. Studies on the effect of boric acid on corrosion of Zr alloys in water have shown that the brake away corrosion of pure zirconium is suppressed by boric acid additions whereas no much effect was observed in case of more corrosion resistant alloys, which are expected to form columnar oxide grains [16]. Probably surface layers of borates (boric acid has a strong complex forming activity) increase the surface energy of formed oxide grains and impedes a continuous crystallization of new grains at the metal oxide interface and prefers the growth of a more protective non equiaxed (columnar) grain structure.

Effects of lithium hydroxide and boric acid on the mode of crystallization of zirconium oxide would imply a migration through pores and grain boundary diffusion down to the metal oxide interface. It has been shown by SIMS examinations of oxide layers [11, 17], that increased corrosion occurs only when Li is present at the interface. Migration and grain boundary diffusion to the metal - oxide interface decreases with increasing oxide layer thickness very likely faster in case of the larger borate anion than for the smaller lithium cation. Thus, it can well be expected, that the beneficial

effect of B is reduced for increasing oxide layer increases. This was observed in the test with 700 ppm Li and 100 ppm B.

#### 4.6 Relevance of the findings for the in reactor behavior

Under non isothermal conditions as cladding is operated in the reactor an enhancement of lithium hydroxide on the surface of the cladding is anticipated, especially under boiling conditions. This leads to lithium concentration which may be detrimental to corrosion. This is literally the reason for taking into account the sensitivity to lithium containing environments for material optimization. This investigation shows a strong beneficial effect of boric acid. Boric acid is also available in the coolant of pressurized water reactors. Under these circumstances (2 ppm Li, 1000 ppm B) a lithium induced corrosion at low oxide thickness with low porosity is not expected for zirconium alloy cladding. At high oxide thickness and high heat flux a locally increase of lithium hydroxide and boric acid concentration has to be anticipated. The different chemical properties of lithium hydroxide and boric acid in water can result in different concentration enhancement of lithium hydroxide and boric acid. Under such conditions a lithium induced accelerated corrosion can not be excluded.

#### 5. CONCLUSIONS

From this isothermal corrosion study with zirconium based alloy with different tin content performed at 350 °C, 17 MPa water with different lithium hydroxide and boric acid containing environments the following conclusions are drawn:

1. The corrosion rate depends on the lithium hydroxide concentration. Enhanced corrosion is observed above 30 ppm Li, accelerated corrosion occurs above 70 ppm Li.
2. The beneficial effect of low tin on corrosion is reduced with increasing lithium hydroxide concentrations, inversely, at high lithium hydroxide concentration higher tin contents seem to be beneficial.
3. Additions of boric acid to lithium hydroxide containing water reduce the corrosion rates for low tin and high tin zirconium based alloys. At 70 ppm Li and more than 100 ppm B present, corrosion rates similar to pure water corrosion are observed.
4. Boric acid additions reduce the incorporation of lithium into the corrosion layers.

#### REFERENCES

- [1] HILLNER, E. and CHIRIGOS, J. N., "The effect of lithium hydroxide and related solutions on the corrosion rate of Zircaloy-2", Bettis Atomic Power Laboratory, Report WAPD-TM-307 (1962).
- [2] CORIOU, H., GRALL, L., MEUNIER, J., PELRAS, M. and WILLERMOZ, H., "Influence de cyclage thermique sur la corrosion du Zircaloy-2 dans l'eau ou la vapeur a 360oC et sur l'absorption de l'hydrogene par le metal", Journal of Nucl. Materials, Vol. 7 (1962) 320 - 327.
- [3] KASS, S., "The development of Zircaloys", Corrosion, Vol. 25, No. 1, 1969, pp. 30 - 46.
- [4] TICE, D. R. HUDDART, G., and BRAMWELL, I. L., in Materials for Nuclear Reactor Core Applications (Proc. British Nuclear Energy Society Conference, Bristol, UK, October 1987), BNES (1987) 57.

- [5] GARZAROLLI, F. et al., "Influence of various additions to water on Zircaloy-4 corrosion in autoclave tests at 350°C, Fundamental Aspects of Corrosion of Zirconium-Base Alloys in Water Reactor Environments (Proc. Mtg Portland, OR, Sept. 1989), Rep. IWGFPT/34, IAEA, Vienna (1990) 65 - 72.
- [6] BRAMWELL, I. L., PARSONS, P. D. and TICE, D. R., in Zirconium in the Nuclear Industry (Proc. 9<sup>th</sup> Int. Symposium Kobe, Japan, 1990), ASTM, ASTM STP1132 (1991) 628 -642.
- [7] RAMASUBRAMANIAN, N. and BALAKRISHNAN, P. V., "Aqueous chemistry of lithium hydroxide and boric acid and corrosion of Zircaloy-4 and Zr-2.5Nb alloys", Zirconium in the Nuclear Industry (Proc. Tenth Int. Symposium, Baltimore, MD, USA, 1993), ASTM, ASTM STP 1245 (1994) 378 - 399 .
- [8] HAN, J. H. and RHEEM, K. S., Journal of Nuclear Materials, 217, 1994, pp. 197 - 199.
- [9] COX, B. and WU, C., "Cathodic polarization of corroding Zircaloy-4", Journal of Nucl. Materials, 224 (1995) 169 - 178.
- [10] COX, B., UNGURELU, M. WONG, Y.-M. and WU, C., "Mechanisms of LiOH degradation and H<sub>3</sub>BO<sub>3</sub> repair of ZrO<sub>2</sub> film, Zirconium in the Nuclear Industry (Proc. Eleventh Int. Symposium, Germany, 1995), ASTM, ASTM STP 1295 (1996) 114 - 136.
- [11] PÊCHEUR, D., GODLEWSKI, J., BILLOT, Ph., and THOMAZET, J., "Microstructure of oxide films formed during the waterside corrosion of the Zircaloy-4 cladding in lithiated environment", Zirconium in the Nuclear Industry (Proc. Eleventh Int. Symposium, Germany, 1995) ASTM, ASTM STP 1295 (1996), 94 - 113.
- [12] PERKINS, R. A. and BUSCH, R., "Corrosion of Zircaloy-4 fuel cladding", Environmental Degradation of Materials in Nuclear Reactor Systems - Water Reactors (Proc. 4<sup>th</sup> Int. Symp. Jekyll Island, GA, 1989), NACE, Houston, Texas (1991) 10-15.
- [13] JEONG, Y. H., RUHMANN, H. and GARZAROLLI, F., "Influence of alkali metal hydroxides on corrosion of Zr-based alloys", Influence of Water Chemistry on Fuel Cladding Behavior (proc. TCM Rez, 1993), IAEA-TECDOC-927 (1997) 161.
- [14] BEIE, H.-J. et al, "Examination of the corrosion mechanism of Zirconium alloys", Zirconium in the Nuclear Industry (Proc. Tenth Int. Symposium Baltimore, MD, USA, 1993), ASTM, ASTM STP 1245 (1994) 615 - 643.
- [15] GARZAROLLI, F. et al., "Oxide growth mechanisms on Zr alloys", Zirconium in the Nuclear Industry (Proc. Ninth Int. Symposium, 1990, Kobe, Japan) ASTM STP 1132 (1991) 395 - 415.
- [16] BRITTON, C. F. and WANKLYN, "The corrosion of zirconium and its alloys, Part III. The influence of of the environment on oxidation", UK Rep. AERE-4130, UKAEA, AERE, Harwell, Berks. (1962).
- [17] PÊCHEUR, D., et al., "Contribution to the understanding of the effect of the water chemistry on the oxidation kinetics of Zircaloy-4 cladding", Zirconium in the Nuclear Industry (Proc. Twelfth Int. Symposium Toronto, Canada, 1998), ASTM, ASTM STP 1354 (in press).

**CORROSION LAYERS, CRUD DEPOSITION, ACTIVITY BUILDUP**  
**(Session 3)**

**NEXT PAGE(S)**  
**left blank**



O. GEBHARDT, D. GAVILLRET  
Paul Scherrer Institute, Villigen, Switzerland

J.Y. BLANC  
Commissariat à l'Energie Atomique, Gif-sur-Yvette, France

L. OTTAVI  
Electricite de France, Villeurbanne, France

J. THOMAZET  
Framatome, Lyon, France

### **Abstract**

The influence of the water components lithium and boron on the uniform corrosion process of in-reactor (PWR) corroded Zircaloy claddings of different material composition has been studied. Small pieces of in-reactor corroded cladding specimens were studied by scanning electron microscopy (SEM) and secondary ion mass spectrometry (SIMS). SEM investigations exhibit the local oxide thickness and structure of the oxides. Claddings which are quite different in their corrosion rate show clear differences in a multiple layer structure of the oxide. The ion microprobe ATOMIKA 4000 was used for SIMS depth profiling to investigate oxide layers with thickness  $< 15 \mu\text{m}$ . For quantitative analysis of lithium and boron special ion implanted standard specimens were investigated. The SIMS profiles exhibit a multiple peak structure of lithium and boron. A thin oxide layer close to the oxide/ metal interface is nearly depleted by lithium and boron. Thus, a compact oxide layer close to the oxide/ metal interface can be assumed. The quantitative amount of lithium and boron was determined by peak value quantification. Specimens of different material show clear differences in the amount of lithium and boron in their oxide layers. These differences are discussed relating to the different compositions of the cladding materials.

## **1. INTRODUCTION**

Zirconium based alloys are commonly used as cladding materials for fuel rods in nuclear water reactors [1-2]. The reactor water chemistry is an important factor that influences the corrosion rate . at the water side surface of the claddings. In most cases, up to 3 wt ppm of LiOH and 150 wt ppm  $\text{H}_3\text{BO}_3$  are added to the reactor water for pH control. It is known from corrosion experiments in autoclaves that lithium ions at a concentration higher than 70 wt ppm in the autoclave water are the cause for an acceleration of the cladding corrosion. The reason for this acceleration is not fully clear yet. It has been assumed that the acceleration of corrosion is related to the special chemical behaviour of lithium ions. These ions can deteriorate the protective dense oxide layer close to the oxide/ metal interface [3].

To understand the in-reactor corrosion process the quantitative amount of lithium and boron ions in the oxide layer of claddings must be known. SIMS depth profiling techniques allow the measurement of the very low concentration of ions in oxide layers with high depth resolution. However, the application of this technique is limited to thin oxide layers  $< 15 \mu\text{m}$  [4]. In this paper, results of quantitative SIMS depth profiling analyses obtained from in-reactor formed corrosion layers on Zircaloy claddings are discussed.

## **2. PARAMETERS OF THE CLADDING SPECIMENS AND PREPARATION OF SAMPLES**

### **2.1. Parameters of the cladding specimens and the standards**

The irradiated cladding specimens arise from the French CHINON B3 nuclear power reactor. The parameters of the irradiated cladding specimen are listed in Table I. In order to quantify the amount of lithium and boron in the oxide layer of the in-reactor corroded specimens two standard specimens were investigated. The zirconium oxide layer on the surface of these specimens is implanted with lithium and boron ions (see Table II). The standard specimens were corroded under PWR conditions in lithium and boron enriched water. Therefore, these specimens contain additional lithium and boron their oxide layers.

Table I. LIST OF PARAMETERS OF THE IN-REACTOR CORRODED CLADDING SPECIMENS

Specimen/ No. of reactor cycles	Alloy Treatment	Position along the rod/ mm Local burnup/ MWd/ tU <sup>1</sup>
YDV/2	Zr - 0.5 Sn - 0.5 Nb - Fe - Cr Recrystallized	660-667 23646
YDW/3	Zr - 0.5 Sn- Fe- V Recrystallized	1260-1267 35950
YDX/3	Zr - 1.0 Nb Recrystallized	1260-1267 35082
YDY/3	Zircaloy-4 Stress relieved	1260-1267 34948
YDZ/3	Zr - 0.5 Sn - Fe - Cr Stress relieved	1260-1267 34929

<sup>1</sup> the indicated values are given before stretch-out operation to be representative of a nominal power in the rod.

Table II. LIST OF PARAMETERS OF ION IMPLANTED STANDARD SPECIMENS

Specimen	Ion density/atcm <sup>-2</sup> Ion dose/ atcm <sup>-3</sup>	Concentration at peak level/ wt ppm	Ion energy/ keV// Implantation depth/ nm
E12E (Li)	4.05x10 <sup>15</sup> / 2x10 <sup>20</sup>	145	190 // 573.6
E11C (B)	2.1x10 <sup>15</sup> / 9x10 <sup>19</sup>	333	190// 354.2

## 2.2. Preparation of samples

The in-reactor corroded specimens were mechanically cleaned to remove the nuclear fuel and to avoid  $\alpha$ -contamination. The cladding rings were cut into small pieces (about 3x2 mm). The remaining dose rate of these small specimens was in the range of 90 to 400  $\mu$ Sv/ h. Only a very low  $\alpha$ -contamination (about 50 cps) was found on their surface.

For scanning electron microscopy (SEM), small pieces of the in-reactor corroded specimens were prepared in form of cross-sections showing the oxide and the metal. Two pieces embedded in epoxy resin (see Fig. 1a) were mechanically polished to get a smooth surface. A platinum layer of about 50 nm thickness was sputtered on the sample surface to prevent electrostatic charging during the electron bombardment. For secondary ion mass spectrometry (SIMS), small pieces of cladding material were mounted on a special SIMS specimen holder using an electrically conductive resin (see Fig. 1b). Analyses by stereo-microscopy show that the surfaces of the in-reactor corroded specimens are deeply scratched in axial direction. These scratches were probably mechanically produced during handling of the rods. However, some areas of the oxide layer of these specimens appeared to be sufficiently smooth for small area SIMS analyses.

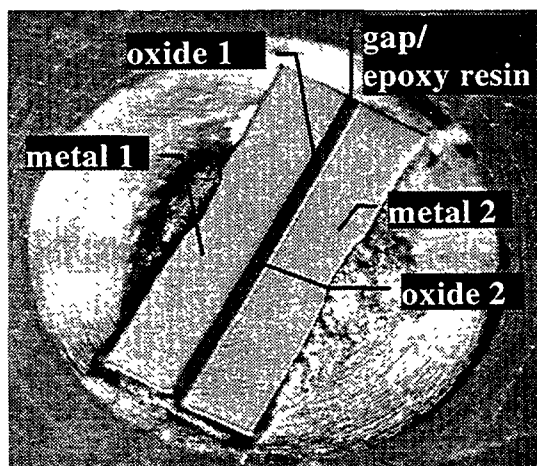


FIG. 1a. Zircaloy cladding specimen prepared for SEM analyses.

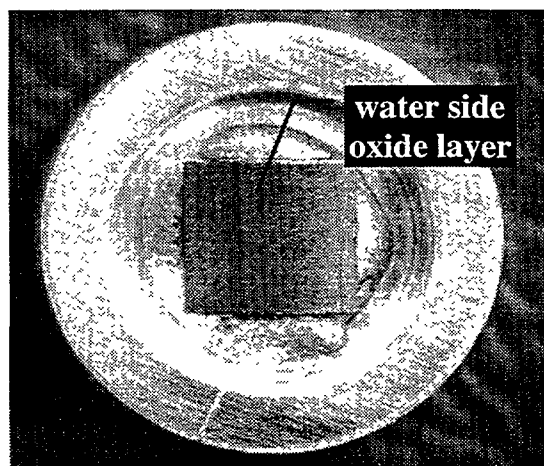


FIG. 1b. Zircaloy cladding specimen prepared for SIMS depth profiling analyses.

### 3. ANALYSES BY SCANNING ELECTRON MICROSCOPY (SEM)

The analyses were performed using a Zeiss DSM 962 digital scanning microscope (see Figs. 2a-e). The images show a layered structure of the oxide but the visible number of these layers does not always correspond to the number of reactor cycles. The physical origin of this layered structure is not clear yet. The oxide layers show strong local variations in their thickness (up to  $\pm 1\mu\text{m}$ ). Nevertheless, an average thickness of the oxide layer can be determined by the microscopic scale and the results can be used to calibrate the erosion rate of SIMS depth profiling in the oxide layer (see Table III).

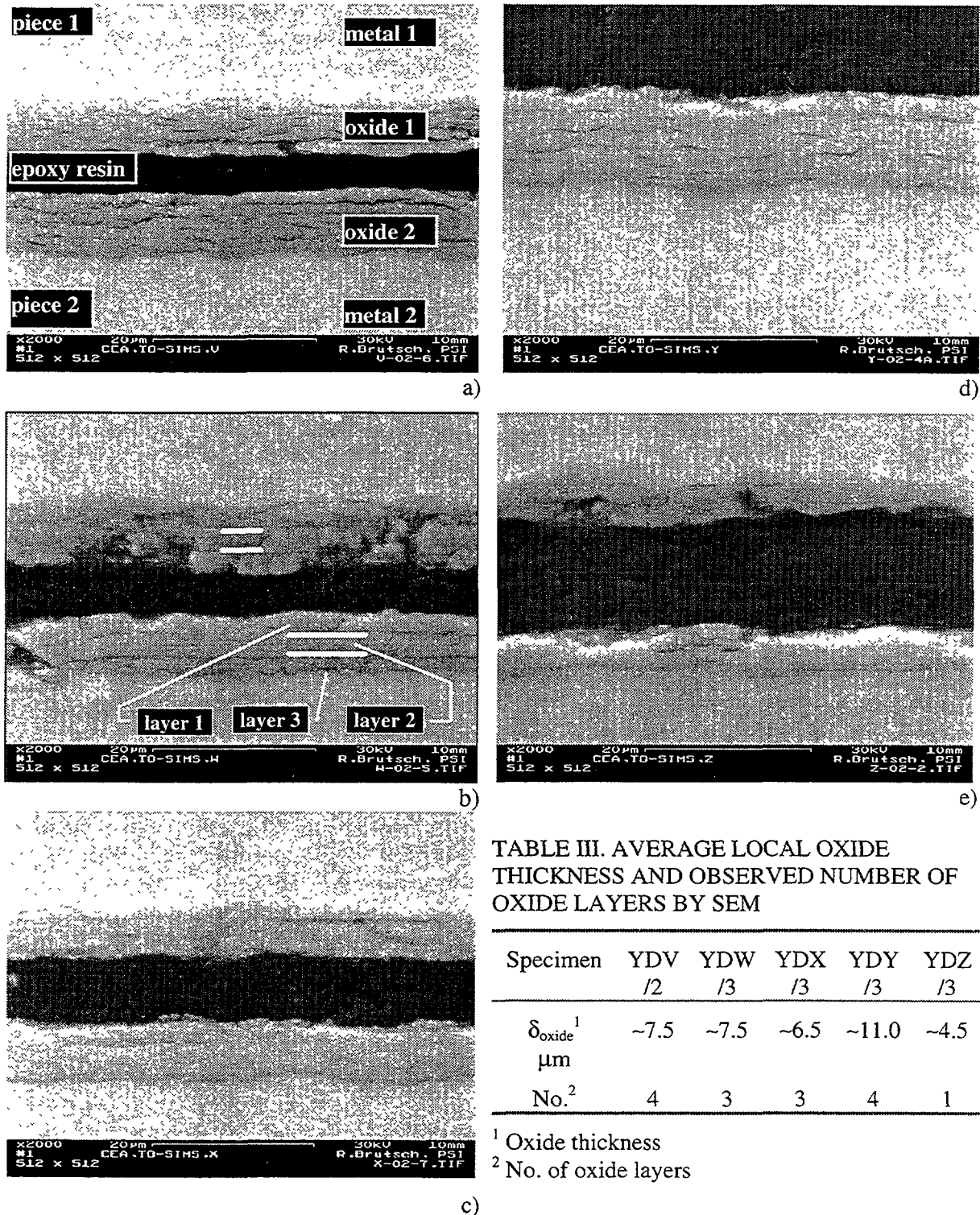


FIG. 2a-e. SEM image of the oxide/ metal interface of the in-reactor corroded cladding specimens. Bar=20 μm. a) YDV/2, b) YDW/3, c) YDX/3, d) YDY/3, e) YDZ/3.

#### 4. ANALYSES BY SECONDARY ION MASS SPECTROMETRY (SIMS)

SIMS depth profiling measurements were performed using the quadrupole based ion microprobe ATOMIKA 4000. The ion source was operated with oxygen enriched in O-18 to 95%. Bombardment was carried out with micro-focused beams of mass filtered ( $^{18}\text{O}$ ) $_2^+$  ions striking the samples with 15 keV at near-normal incidence ( $\approx 5^\circ$  off normal). The current density in the focused spots was about  $0.2 \text{ A/cm}^2$ . Beam current and spot size for depth profiling analysis was about 20 to 100 nA into  $\approx 2\text{--}8 \text{ }\mu\text{m}$ . The small diameter of the primary ion beam enables to operate with a small scan size of  $30 \times 30 \text{ }\mu\text{m}^2$ . Additionally, electronic gates for signal processing were used to increase the dynamic range and to eliminate signal perturbation from the edges of the sputter crater. Comparison of the primary ion charge during bombardment of the insulating zirconium oxide was accomplished by simultaneous bombardment with 4 keV electrons incident at  $50^\circ$  to the surface normal. All species were detected as positive secondary ions.

The use of O-18 has two advantages. (1) Owing to the large free enthalpy for  $\text{ZrO}_2$  formation [5], the metallic regions of the samples can be expected to become highly oxidised as a result of oxygen implantation. This supposition is supported by a comparison of sputtering yields observed under oxygen and neon ion impact [6]. The difference in ionisation probability for emission from the metal and oxide should thus be reduced to a minimum. (2) Bombardment with O-18 primary ions provides means for distinguishing between the metal and the oxide [4]. In fact, the only  $\text{O}^+$  and  $\text{ZrO}^+$  secondary ions that can be observed from the metal are those containing O-18. By contrast, both O-16 and O-18 contribute to the signal of oxygen carrying ions emitted from zirconium oxide.

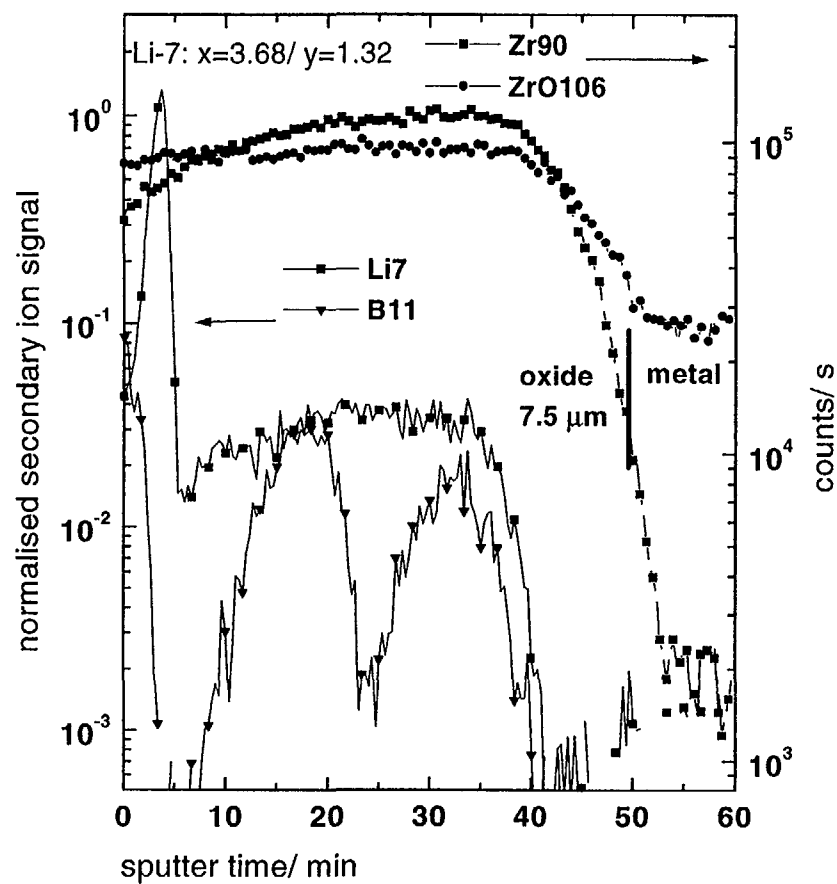
#### 5. EXPERIMENTAL RESULTS OF SIMS DEPTH PROFILING

In order to take account of small variations relating to the measurement conditions during depth profiling, the count rates for lithium and boron were normalised with the count rate of the Zr-90 isotope. The position of the oxide/ metal interface is indicated by the point of inflection of ZrO-106 signal which decreases rapidly close to this interface. The signal level finally achieved in the metal amounts to about 0.5% of the total ZrO signal in the oxide. This relatively high residual ZrO-106 signal appears to be related to the rather high operating pressure in the SIMS. Nevertheless, the rapid drop of the ZrO-106 signal can be used to determine the location of the oxide/ metal interface [4]. The normalised Li-7, B-10 and B-11 signals are presented (left axis) where the original signals of Zr-90 and ZrO-106 (right axis) are fitted to the dynamic range of Li-7.

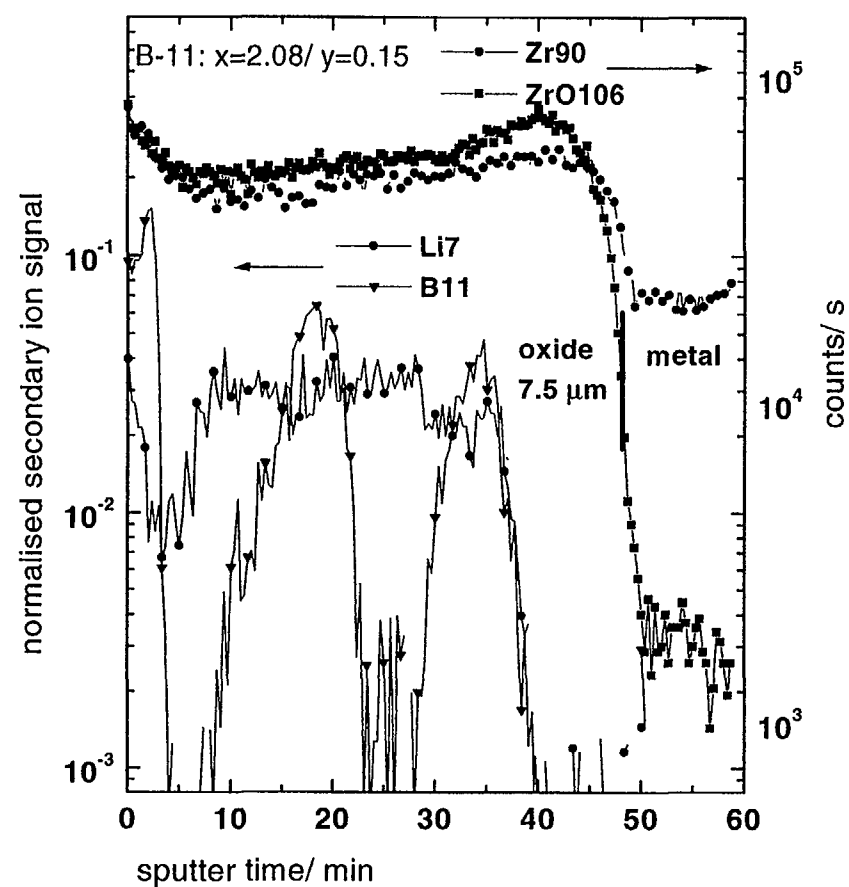
**Standard E12E (Li):** The peak value of Li-7 ( $y=1.32$ ) was found near the surface of the specimen at 3.68 min of sputter time (see Fig. 3a). Outside of the implantation profile the ground level of lithium covers a range of  $y \approx 0.02$  to  $0.04$ . At a sputter time of about 40 min the Li-7 signal drops down to the background level ( $y < 0.001$ ). The oxide layer of the standard specimen contains also boron isotopes (B-11) that exhibits three peaks. The maximum of boron was measured directly at the surface of the specimen ( $y \approx 0.02$ ).

**Standard E11C (B):** The peak value of B-11 ( $y=0.15$ ) was found near the surface of the specimen (see Fig. 3b). Besides the implantation profile the B-11 signal shows two other peaks of relatively high level. As shown in Fig. 3a peaks of comparable level were also observed in specimen E12E(Li). The oxide layer of this standard contains also lithium at a relatively constant level ( $y \approx 0.02\text{--}0.04$ ).

**In-reactor corroded specimens:** For the in-reactor corroded specimens the Li-7 signal shows a peak structure in the first third of the oxide layer. Specimens YDV/2 and YDX/3 show only 1 peak whereas specimens YDW/3, YDY/3 and YDZ/3 exhibit 2 peaks of the Li-7 signal. The B-10 and B-11 signals exhibit a peak value directly at the sample surface (see Figs. 4a-e). The peak structure for the B-10 and B-11 signals is more structured. Specimens YDV/2 and YDX/3 exhibit a multiple peak structure in the bulk of the oxide whereas specimens YDW/3, YDY/3 and YDZ/3 show 3 or 2 individual peaks. The signals of Li-7, B-10 and B-11 decrease rapidly to the background level ( $y < 0.001$ ) before the oxide/ metal interface is reached.

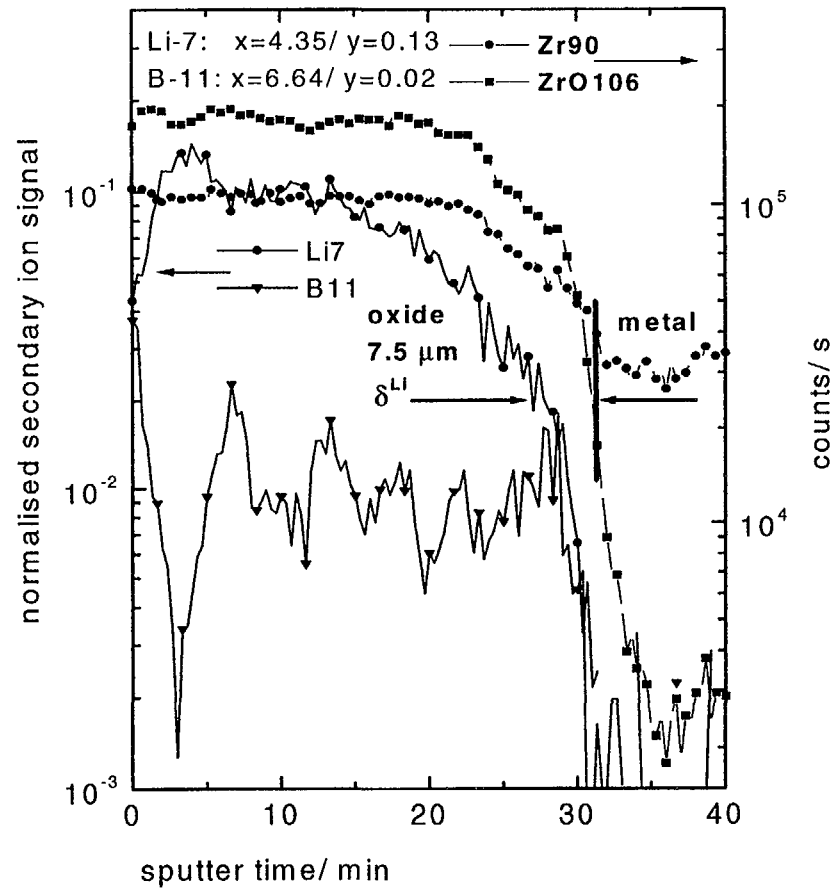


a)

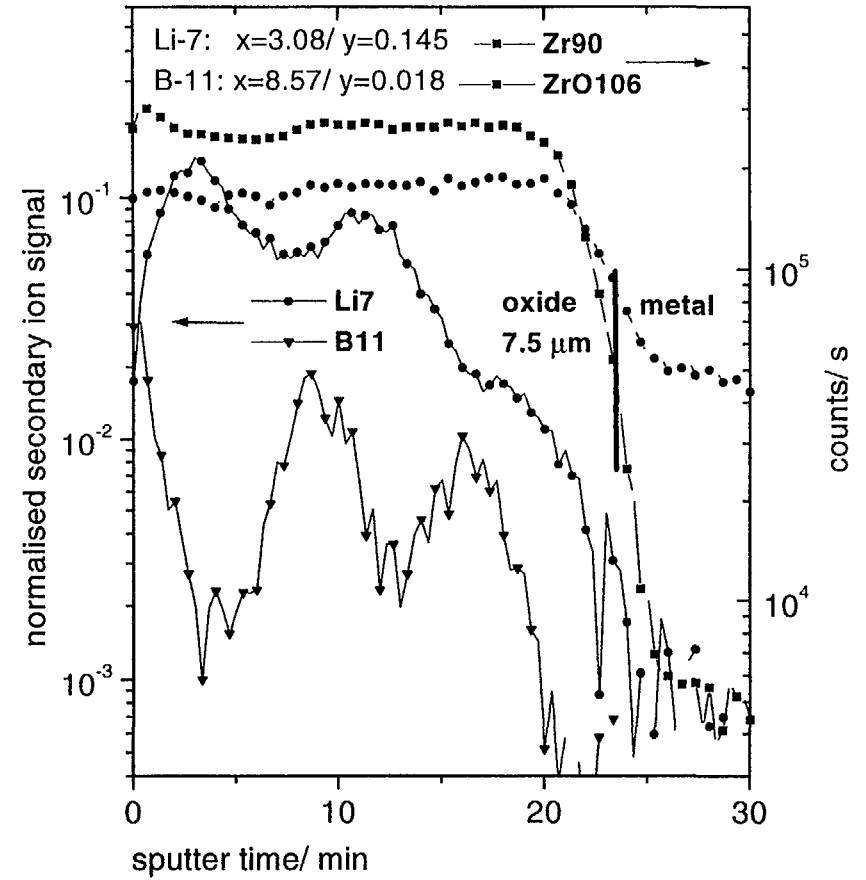


b)

FIG. 3a-b. Standards a) E12E (Li) and b) E11C(B) - Secondary ion signals of Li-7, B-10 and B-11 normalised to the signals of Zr-90 (left axis) and original count rates of Zr-90 and ZrO-106 (right axis).

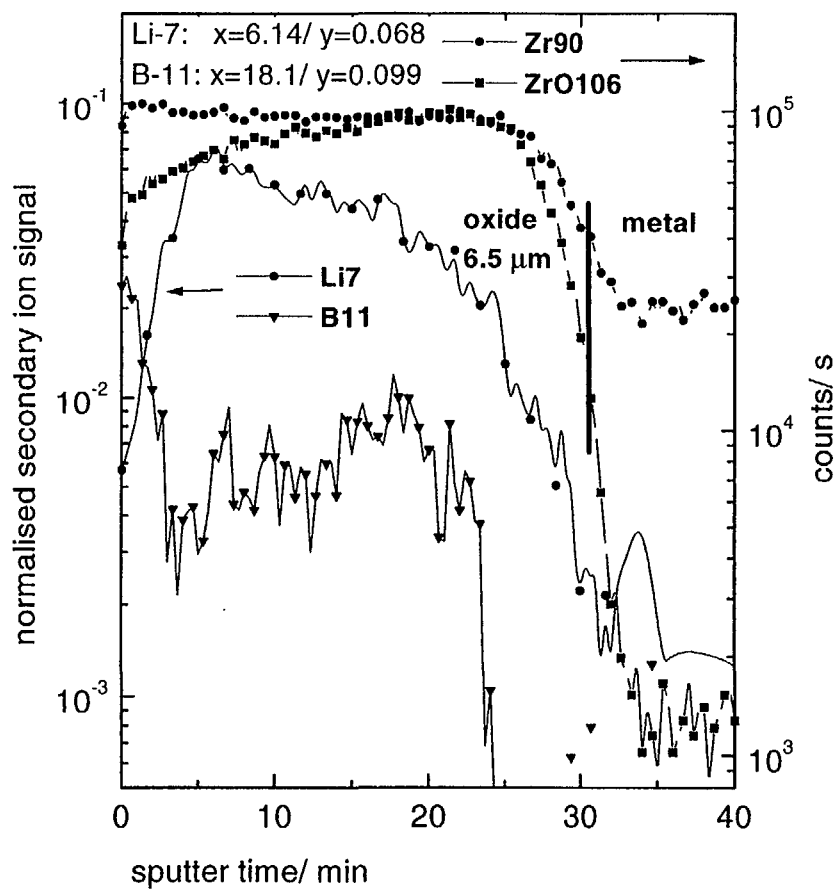


a)

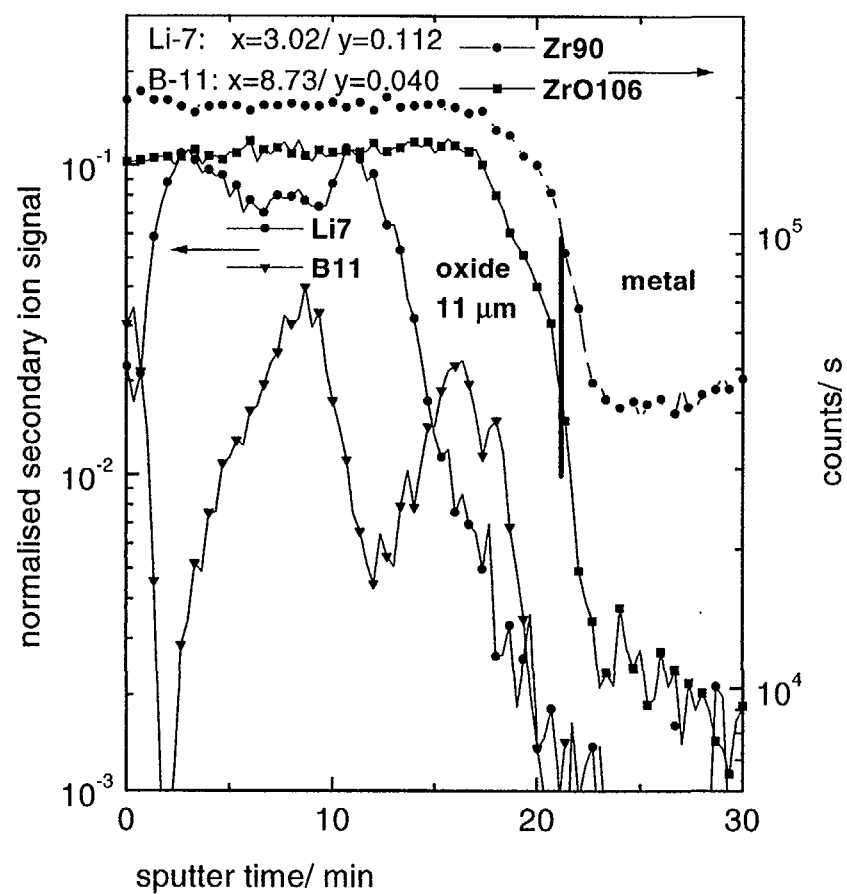


b)

FIG. 4a-b. In-reactor corroded specimens a) YDV/2 and b) YDW/3. - Secondary ion signals of Li-7, B-10 and B-11 normalised to the signals of Zr-90 (left axis) and original count rates of Zr-90 and ZrO-106 (right axis).



c)



d)

FIG. 4c-d. In-reactor corroded specimens c) YDX/3 and d) YDY/3. - Secondary ion signals of Li-7, B-10 and B-11 normalised to the signals of Zr-90 (left axis) and original count rates of Zr-90 and ZrO-106 (right axis).

## 6. ANALYSIS OF EXPERIMENTAL RESULTS AND DISCUSSION

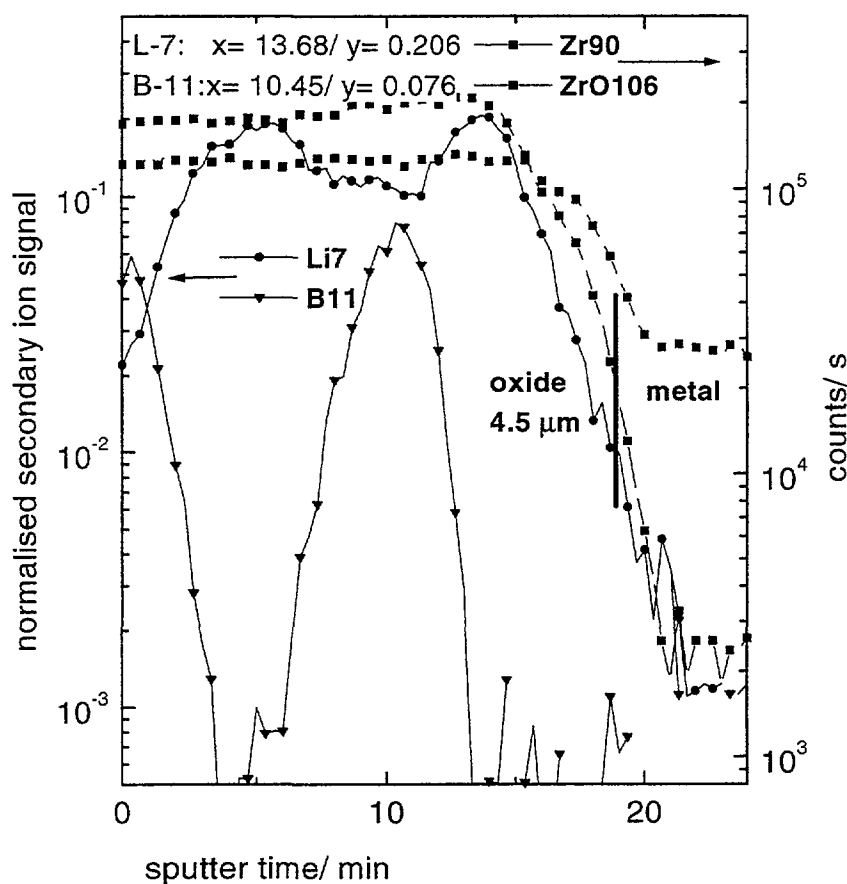
### 6.1. Depth distribution of lithium and boron

If the Li-7, B-11 and the ZrO-106 profiles are compared, the Li-7 and the B-11 signals decrease by more than a factor 50 to 100 in passing from the oxide to the metal. A closer inspection of the data shows that the lithium fall-off occurs in the oxide slightly before the interface. This finding suggests that a thin oxide layer, impermeable for lithium ions, exists on the oxide side of the interface. Studies performed by electrochemical impedance spectroscopy support the hypothesis of an impermeable barrier oxide [7-9]. The thickness of the barrier oxide can be estimated from the SIMS depth profiles.

The distribution of boron in the oxide layers shows strong variations. Therefore, the existence of a boron depleted zone can not be assumed. In Table IV the results of an estimation of the thickness  $\delta^{\text{Li}}$  of the lithium depleted zone close to the oxide/metal interface are listed.

TABLE IV. THICKNESS  $\delta^{\text{Li}}$  OF THE LITHIUM DEPLETED ZONE

Specimen	YDV/2	YDW/3	YDX/3	YDY/3	YDZ/3
$\delta^{\text{Li}}$ / nm	620	940	414	2300	250



e)

FIG. 4e. In-reactor corroded specimen e) YDZ/3. - Secondary ion signals of Li-7, B-10 and B-11 normalised to the signals of Zr-90 (left axis) and original count rates of Zr-90 and ZrO-106 (right axis).



## 6.2. Quantitative analysis of lithium and boron

The peak values of the Zr-90 normalised count rates of lithium and boron from SIMS depth profiling and the peak concentration values of the standard specimens E12E(Li) and E11C(B) due to ion implantation (see Figs. 3a-b and Table II) are used to define a concentration scale in wt ppm.

**Standard E12E(Li):** The normalised signal height of the ground level of Li-7 about  $y \approx 0.02$  to 0.04 but the exact value of the ground level at the depth of the implantation peak can not be directly obtained. From linear extrapolation to the implantation peak a value of about 0.01 can be evaluated. For comparison it can be assumed that both standard corroded under identical conditions. Standard E11C(B) exhibits a normalised Li-7 count rate of about 0.01 at a sputter time of 3.68 min. Therefore, only a very small correction for the ground level of lithium is necessary. Hence, a normalised count rate of  $y = 1.32$  corresponds to 145 wt ppm of lithium at the peak value of implantation.

**Standard E11C(B):** Two additional peaks of the B-11 signal appear in the spectrum which are due to the autoclave corrosion. Because of this multiple peak structure a linear extrapolation from the signal curve is not possible and the ground level of boron at the depth of the implantation peak can not be evaluated. Standard E12E(Li) exhibits about  $y = 0.012$  for the normalised B-11 signal after 2.35 min of sputter time. These value has been subtracted from the total peak signal to consider the ground level of B-11 in specimen E11C(B). Thus, a normalised count rate of  $y = 0.14$  corresponds to 333 wt ppm of boron at the peak value of implantation.

**In-reactor and corroded specimens:** The results of peak value quantification are summarised in Table V. The in-reactor corroded specimens generally show a maximum of Li-7 concentration in the outer third of the oxide layer. Then, for specimens YDV/ 2 and YDX/ 3 a more or less linear decrease of Li-7 concentration was found. In contrast to this behaviour, specimens YDW/ 3, YDY/ 3 and YDZ/ 3 exhibit a double-peak structure with peaks of lower level in the centre of the oxide layer. Except of specimen YDZ/ 3 the specimens show the highest concentration of B-11 directly at the waterside surface.

Within the oxide layer smaller peaks (specimens YDZ/3, YDW/3, and YDY/3) or only strong signal variations (specimens YDV/2, YDX/3) are observed. Obviously, the peak structure of lithium and boron in the oxide layer of specimens YDV/2 and YDX/3 differs considerably from the one observed in the other specimens. It can be noted that these specimens contain a small percentage of niobium. This fact could be linked to the different Li and B distribution. The highest concentration of lithium (15 to 22 wt ppm) was found in the oxide layers of specimens YDV/2, YDW/3 and YDZ/3. The highest concentration of boron was found in specimen YDZ/3 (190 wt ppm). These specimens can be classified within the low-Sn alloy family.

TABLE V. RESULTS OF PEAK VALUE QUANTIFICATION

Specimen	Li-7/ wt ppm number of peaks	B-11/ wt ppm number of peaks
YDV/2/ Zr-0.5Sn-0.5Nb-Fe-Cr recrystallized	~15 1 peak	~90 (*)
YDW3/ Zr-0.5Sn-Fe-V recrystallized	~15.5 2 peaks	~75 3 peaks
YDX/3/ Zr-1.0Nb recrystallized	~7.8 1 peak	~7.8 1 peak
YDY/3/ Zircaloy-4 stress relieved	~12.5 2 peaks	~95 3 peaks
YDZ/3/ Zr-0.5Sn-Fe-Cr stress relieved	~22.5 2 peaks	~190 2 peaks

\*) multiple peak structure

## 7. CONCLUSIONS

- (1) Peak values of ion implantation profiles from standard specimens can be used for calculation of concentration profiles of lithium and boron in-reactor corroded specimens. However, the ground level of lithium and boron outside of the implantation peaks has to be subtracted from the peak values.
- (2) The sharp decrease of the ZrO-106 signal can be used to determine the location of the oxide/ metal interface. The specimens exhibit a lithium and boron depleted zone close to the oxide/ metal interface which could be linked to the presence of a compact oxide layer (barrier layer) close to the oxide/ metal interface. The thickness of the lithium depleted zone covers a range of about 250 nm to about 2300 nm.
- (3) The maximum concentrations of lithium and boron were found in the outer (waterside) third of the oxide layer. The boron peaks are generally at positions of minimum lithium signal but not all specimen show clear individual peaks.
- (4) The lithium concentration in the oxide layer of the in-reactor corroded specimens covers a range of 8 to 23 wt ppm. The highest concentration of lithium (15 to 23 wt ppm) was measured in the oxides of specimens which can be included in the low tin alloy family. The boron concentration in the oxides of the in-reactor corroded specimens is included in the range of 60 to 190 wt ppm.

## REFERENCES

- [1] C. LEMAIGNAN AND A.T. MOTTA, *Material Science and Technology*, Vol. 10 B, Chapter 7, "Zirconium in Nuclear Applications", ed. R.W. Cahn, P. Haasen and E.J. Kramer, Part II: Nuclear Materials, VCH Verlagsgesellschaft mbH, Weinheim, Germany 1994.
- [2] INTERNATIONAL ATOMIC ENERGY AGENCY, *Corrosion of Zirconium Alloys in Nuclear Power Plants*, IAEA TECDOC-684, Vienna (1993).
- [3] H. G. WEIDINGER, H. RUHMANN, G. CHELIOTIS, M. MAGUIRE AND T.L. LAU, "Corrosion-electrochemical properties of Zirconium intermetallics", *Zirconium in the Nuclear Industry* (Proc. 9<sup>th</sup> Int. Symp. Kobe, Japan, 1990), ASTM, ASTM-STP 1132 (1991) 499.
- [4] O. GEBHARDT, E.T. AERNE, M. MARTIN AND K. WITTMAACK, "SIMS depth profile and line scan analyses at the metal/oxide interface of corrosion films on zirconium based alloys", *Secondary Ion Mass Spectrometry, SIMS X* (Proc. 10th International Conference, Münster, October 1-6, 1995), ed. by A Benninghoven et al., Wiley, Chichester (1997) 869-872.
- [5] E. HECHTL AND J. BOHDANSKY, "Sputtering of titanium and zirconium by fusion", *J. Nucl. Mater.* **133&134**, 301 (1985).
- [6] Y. HOMMA AND K. WITTMAACK, "„Effect of matrix composition and impact angle on the fractional ion yield of Be<sup>+</sup> sputtered from oxygen-bombarded silicon and compound semiconductors“, *Appl. Phys. A50* (1990) 417.
- [7] O. GEBHARDT, M. GEHRINGER, TH. GRABER AND A. HERMANN, „Investigation of corrosion films on zirconium based alloys by electrochemical and microscopic methods“, *Electrochemical Methods in Corrosion Research, EMCR'94* (Proc. 5th Int. Symp. Lisboa, September 5-8, 1994), Materials Science Forum, Trans Tech Publications Ltd, Switzerland, (1995) 192-194, 587-598.

- [8] O. GEBHARDT, "Microscopic and electrochemical impedance spectroscopy analyses of Zircaloy oxide films formed in highly concentrated LiOH solution", Electrochemical Impedance Spectroscopy, EIS'3 (Proc. 3rd Int. Conf. Nieuwpoort, May 7-12, 1995), Electrochimica Acta **38** (1993) 633.
- [9] O. GEBHARDT, A. HERMANN, G. BART, H. BLANK, F. GARZAROLLI AND I.L.F. RAY, "Investigation of in-pile grown corrosion films on zirconium-based alloys", Zirconium in Nuclear Industry (Proc. 11<sup>th</sup> Intern. Symposium, Germany, 1995), ASTM, ASTM-STP 1295 (1996) 218-242.

NEXT PAGE(S)  
lost BLANK



## **CORROSION BEHAVIOUR AND DEPOSITION OF CRUD ON Zr-ALLOYS**

A.J.G. MAROTO, R. BORDONI, A.M. OLMEDO, M. VILLEGAS, M. CHOCRÓN  
Unidad de Actividad Química,  
Comisión Nacional de Energía Atómica,  
Buenos Aires, Argentina

J. SZPUNAR  
Department of Metallurgical Engineering,  
McGill University,  
St. Montreal, Quebec, Canada

### **Abstract**

The results from the long term corrosion surveillance of Zr-alloys samples located out of pile in the primary heat transfer system of a PHWR with standard water chemistry show that, up to 3400 days, the mean value of the oxide thickness obtained for Zr-2.5Nb and Zry-4 samples exposed at 305°C is in good agreement with the values reported in the literature. The amount of crud deposited on the corrosion samples was calculated at every inspection of the long term surveillance programme. The corrosion behaviour of these alloys is also studied in static autoclaves with lithiated heavy water. The effect on Zr-alloys of a change in chemistry resulting from the degradation of mixed resins in the primary heat transfer system was investigated in additional tests in static autoclaves up to 120 days at 400°C comparing the results with those from the corrosion samples inserted in the autoclave facilities of the plant.

### **1. INTRODUCTION**

Zirconium alloys are critical structural materials for in-core components of nuclear reactors, either as Zry-4 fuel channels, or as Zr-2.5Nb pressure tubes. These components should ideally retain their integrity during the entire lifetime of the plant, around 30 EFY (effective full power years). Corrosion resistance is one of the main concerns related to these alloys, therefore Argentina continues with the research programme to correlate their long term in- and out-reactor corrosion.

The corrosion behaviour of Zr-alloys depends upon variables concerning the material itself (chemical composition, microstructure) and many others related to the environment in which they are immersed. The compressive stresses that arise in the oxide during the corrosion process have been depicted as a relevant factor in the oxidation kinetics. This presentation describes some results from the out of pile test programme for a range of temperatures between 265 and 435°C, including the effect of stresses on the corrosion rate that was investigated through a carefully designed experiment. The influence of a change in water chemistry due to the degradation of mixed resins in the primary circuit was also studied with a simulation test reproducing the actual incident and from the results of the corrosion test samples located in the autoclaves of the plant.

### **2. EXPERIMENTAL**

Samples of Zr-2.5Nb were machined from pressure tube material which was extruded at 820-850°C, cold-worked 20-30 %, then stress relieved in steam 24 h at 400°C. A batch of samples was heat treated at 500°C for 10 h (TT) before oxidation. Samples of Zry-4 came from a fully recrystallized sheet. Both materials and their chemical composition have already been described [1]. All specimens

were ground and pickled prior to the autoclave tests, following the ASTM G2-88 standard procedure, save the coupons used for the determination of the influence of stresses in the corrosion rate. These specimens were ground down to 1200 emery paper.

Long term (*ca* 3400 full power days ) corrosion tests were carried out in the autoclaves located out of core in the Embalse Nuclear Power Plant at 265 and 305°C,  $p_{H_2O} = 10.2-10.8$  (LiOD) and hydrogen content 3-10 cm<sup>3</sup>/kg D<sub>2</sub>O. Complementary, accelerated tests were performed in static autoclaves at 350, 315 and 265°C in lithiated heavy water simulating primary coolant and at 400 and 435°C in degassed steam at high pressure (10.5 MPa). Corrosion rates were measured from the weight-gain of the samples.

The oxide topography at the outer interface was studied by optical microscopy and scanning electron microscopy (SEM). X-ray Diffraction (XRD), with Cu K $\alpha$  radiation, was used to determine the oxide composition and AC impedance measurements of the samples were performed to provide information on the oxide structure. Both techniques and the procedures involved have been described in details in a previous paper [1].

### 3. CORROSION KINETICS

The corrosion of Zry-4 in steam at 435°C shows a cyclic behaviour, as indicated in Figure 1. This kind of behaviour was also found at other temperatures, Gohr *et al* [2] have shown that the cyclic behaviour occurs without thermal cycling.

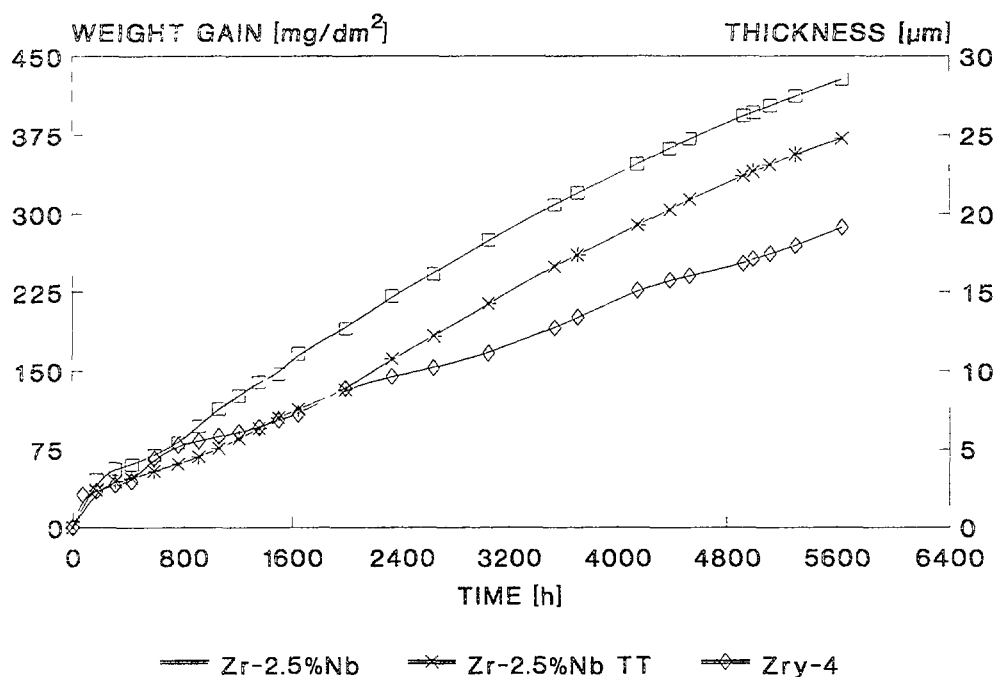


Figure 1: Corrosion Kinetics for Zry-4, Zr-2.5Nb and Zr-2.5Nb TT at 435 °C in steam.

The kinetic law that describes these cycles is:

$$W^3 = k_{pr} t$$

The usual interpretation of the cubic kinetics implies a variable diffusion coefficient  $D$  across the oxide film as the thickness grows. The thicker the film, the more impervious it becomes to diffusion of the oxidizing species.

Figure 1 shows that the second cycle starts in the transition after 500 h, oxide thickness 3.2  $\mu\text{m}$ , and it lasts approximately up to 1350 h reaching 6.4  $\mu\text{m}$  of oxide thickness. The cycles are afterwards almost annealed out and the corrosion rate approaches a constant value of  $1.08 \pm 0.02 \text{ mg/dm}^2\cdot\text{d}$ . Zr-2.5Nb, whether heat-treated (TT) or not, follows a two-stage oxidation kinetics; a parabolic pre-transition rate and a linear post-transition stage, the same behaviour was observed at other temperatures. The transition point occurs at about 600 h of exposure for both batches, corresponding to an oxide thickness of 3.6  $\mu\text{m}$  (TT) and 4.6  $\mu\text{m}$  respectively. Although both lots deviate from the parabolic behaviour, the deviation is far less pronounced than the cyclic features of the Zry-4 oxidation [3]. The parabolic pre-transition behaviour is attributed to control by diffusion of the oxidant through the oxide layer, with a constant diffusion coefficient.

The heat treatment improves the corrosion resistance of Zr-2.5Nb, due to changes in the microstructure of the alloy. During the heat treatment, the metastable  $\beta$ -Zr phase decomposes leading to a smaller volume fraction of the total  $\beta$ -phase. In the  $\alpha$ -Zr grains, supersaturated in Nb, a reduction in Nb concentration in the matrix might occur by the formation of  $\beta$ -Nb precipitates. Both processes would induce a more stabilized microstructure which increases the corrosion-resistance [3-6]. These changes are also induced by the temperature of the test during the corrosion tests as was shown in previous work [7,1].

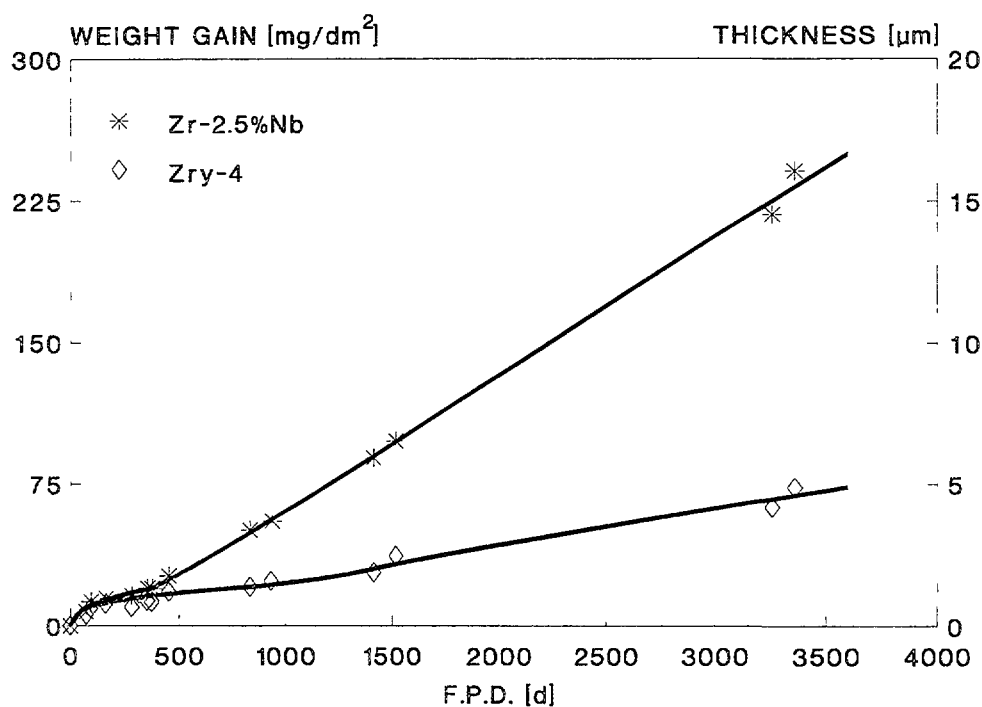


Figure 2: Corrosion kinetics for Zry-4 and Zr-2.5Nb at 305 °C in Embalse's autoclaves

Figure 2 presents the kinetic data obtained at 305°C from the samples inserted in the hot leg autoclaves from both loops of the primary heat transfer system of Embalse after 3400 full power days. The trend in the corrosion of Zr-2.5Nb is similar to that observed at 435°C, with a transition point at about 400 days. The post-transition rate is 0.067 mg/dm<sup>2</sup>.d (1.6 µm/year), in agreement with 0.5–1.6 µm/year reported by Warr *et al* [8] from pressure tubes with 13.4 full power years at 290°C and the values of 1.2–2.3 µm/year obtained by Warr *et al* [9] in out of pile tests at 310°C. The Zry-4 samples have a transition point at around 800 days and the post-transition rate is 0.55 µm/year. The out-of-pile tests indicate that for all temperatures the corrosion rate of the Zry-4 specimens is lower than those of the Zr-2.5Nb coupons and that Zry-4 shows cyclic-kinetics while Zr-2.5Nb has a two stage or parabolic kinetics [10,11].

The deposition of crud was calculated from the samples of Zr-alloys inserted in the hot (305°C) and cold (265°C) leg autoclaves. Table I presents the results of loose and adherent oxide measured in samples of Zry-4 in the autoclaves of one of the loops of the primary circuit.

TABLE I: Loose and adherent crud on Zry-4 specimens

Temperature	Adherent crud (mg/dm <sup>2</sup> )	Loose crud (mg/dm <sup>2</sup> )	Total crud (mg/dm <sup>2</sup> )
305°C	0.3	0.7	1.0
265°C	0.9	0.5	1.4

The values of crud thus obtained are in agreement with the recent theories that explain the mechanism of generation of corrosion products in CANDU reactors with carbon steel feeders and the deposition of these corrosion products in the steam generators according to the related literature [12,13]. As is predicted, specimens in the cold leg autoclave have larger deposits since the coolant is probably still supersaturated in iron respect the solubility value and present a larger percentage (64%) of adherent crud deposited on the surface. The coupons inserted in the hot leg autoclave show smaller values of total deposit and a smaller percentage of adherent crud (30%), this difference can be attributed to the presence of particulate matter that is formed by erosion of crystals recently precipitated.

Table II shows a comparison between the results of crud found on samples from the hot leg autoclaves of the two loops of the primary system.

TABLE II: Comparison between hot leg autoclaves of both loops of the primary system

Loop	Loose crud (mg/dm <sup>2</sup> )	Adherent crud (mg/dm <sup>2</sup> )	Total crud (mg/dm <sup>2</sup> )
1	0.7	0.3	1.0
2	2.0	1.1	3.1

The difference in the samples of both loops is due to an asymmetry in the behaviour of the purification system that has already been observed in previous experiments.

## 4. MICROSTRUCTURE

### 4.1. Impedance measurements

AC impedance measurements of the oxide layers grown at 435°C were performed in 1M H<sub>2</sub>SO<sub>4</sub> solution. The response of the samples changes with autoclave exposure time. At short exposure times, the response is purely capacitive, and at longer times the data indicate an RC equivalent circuit.

Figure 3 presents the time dependence of the total oxide film, the average thickness of the dense oxide layer as calculated from AC impedance measurements and the corrosion rate for Zry-4 at 435°C.

The total oxide layer is composed by two separate layers and this double layer starts at the very beginning of growth of the oxide film. During the first cycle the oxide film and the dense oxide layer grow while the corrosion rate decreases. At the transition point, the thickness of the protective layer decreases and the corrosion rate increases accordingly. When the second cycle begins, the oxide thickness and the dense oxide layer increase once again, the corrosion rate diminishes and the pattern of the first cycle is repeated. The decrease of the dense oxide layer thickness during the transitions implies that part of it has become porous so that the oxidant penetrates the pores reducing the length of the diffusion paths in the oxide for the oxidizing species. Consequently, the corrosion rate should increase. Once the dense layer starts to grow again, the corrosion rate should decrease.

The pattern followed by Zr-2.5Nb showed that the dense layer thickness grew up to the transition where it decreased analogously to Zry-4. From then on, it was nearly constant and the corrosion rate changed accordingly, as a function of the thickness of the dense layer.

Changes in thickness of the dense layer with a trend similar to that observed in this work have been reported by Bossis *et al* [14] on Zry-4 samples oxidized at 415°C in steam and by Pecheur *et al* [15] using the SIMS technique to determine the thickness of the barrier layer in oxide films grown on Zry-4 in autoclave tests at 360°C with different lithium content.

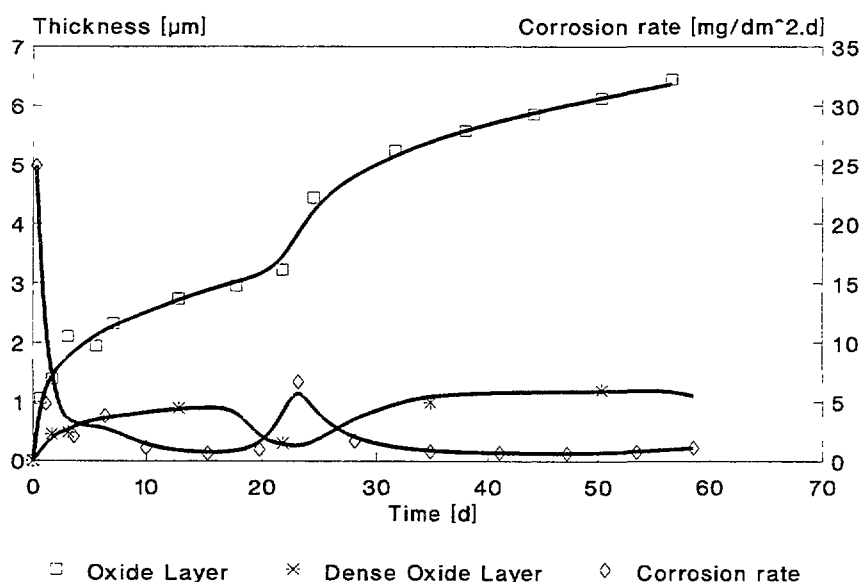


Figure 3: Time dependence of the total oxide layer, average thickness of the dense oxide film and corrosion rate for Zry-4 at 435°C.



#### 4.2. X-ray analysis

X-ray diffraction analysis was performed without removing the oxide layer from the samples. The structure of the films was studied in a powder diffractometer using a  $\theta$  -  $2\theta$  scan by reflection X-ray diffraction and a thin film texture diffractometer described in [16].

The films grown in Zry-4 and Zr-2.5Nb were mainly formed by monoclinic  $\text{ZrO}_2$ , although a small fraction of tetragonal phase was detected, with the conventional reflection X-ray diffraction technique, by a weak peak corresponding to the  $111_t$  reflection, in a fraction varying with the oxide layer thickness. The existence of the tetragonal phase has been described in the literature as a relevant factor in the corrosion mechanism of Zr-alloys [17].

Figure 4 shows a comparison between the spectra of an oxide film of 48  $\mu\text{m}$  grown on Zr-2.5Nb coupons and that of the  $\text{ZrO}_2$  powder, composed by random oriented crystallites. The results clearly indicate the absence of the  $111_m$  peak in the spectrum of the oxide layer and the greater intensity of the  $002_m$ ,  $10\bar{2}_m$ ,  $20\bar{2}_m$  and  $10\bar{4}_m$  peaks of the oxide film as compared with the same ones in the powder spectrum. This is a consequence of the texture of the oxide film, that should be related with the orientation of the base material and the stresses developed in the oxide.

The difference in the detection of the  $111_t$  reflection observed for the Zry-4 and Zr-2.5Nb samples with the conventional technique show that the orientation of the crystallites of the tetragonal phase with respect to the metal surface is different in both alloys. Also, the existence of texture in these oxide films may result in an overestimation or sub-estimation of the tetragonal volume fraction when computed by the conventional X-ray diffraction technique that does not take into account the texture of the oxide as was already reported [16].

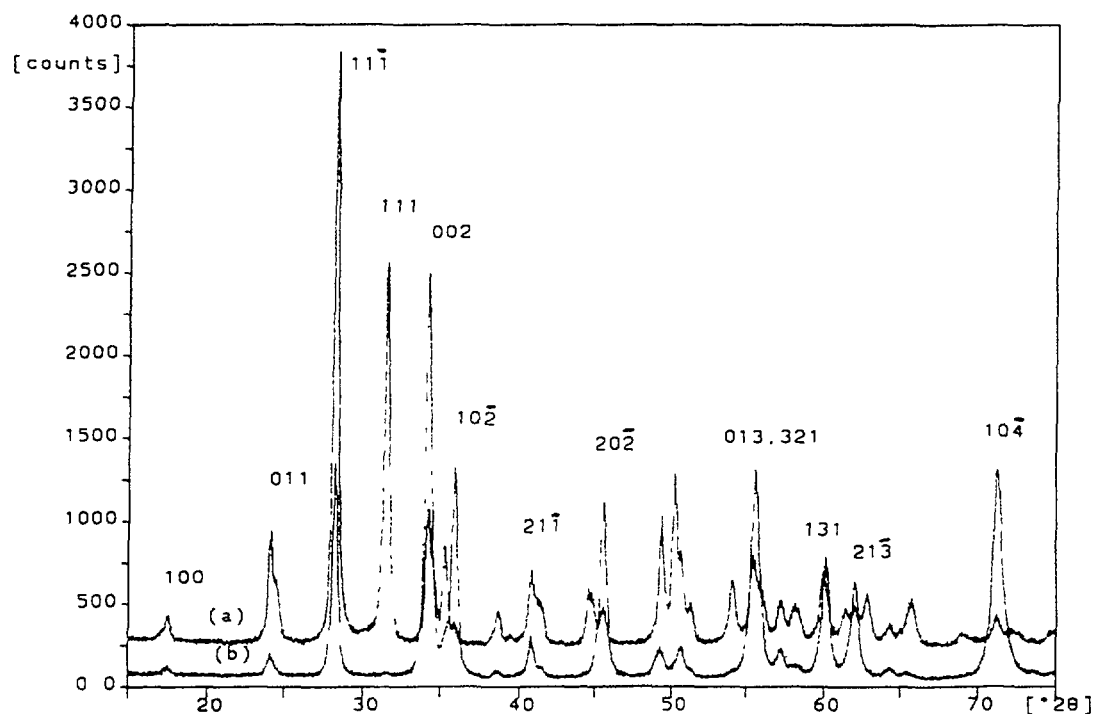


Figure 4: X-ray diffractograms of (a) monoclinic  $\text{ZrO}_2$  powder (b) oxide film of 48  $\mu\text{m}$  thickness grown on Zr-2.5Nb

Table III shows the differences in the values of the tetragonal volume fraction calculated using the conventional X-ray technique with those obtained using a thin film texture diffractometer.

TABLE III: Tetragonal volume fraction vs oxide thickness of films grown in lithiated heavy water at 350°C

% Tetragonal Phase			
Material	Thickness ( $\mu\text{m}$ )	Method A	Method B
Zry-4	0.7	13.36	21.0
Zry-4	1.7	7.85	9.8 – 10.3
Zry-4	2.0	7.16	9.6 – 12.8
Zry-4	2.3	7.86	13.8
Zr-2.5Nb	0.7	7.91	n.d.
Zr-2.5Nb	1.7	5.16	2.8
Zr-2.5Nb	2.7	3.95	1.8 – 2.5
Zr-2.5Nb	3.5	3.12	1.5 – 2.7
Zr-2.5Nb	4.4	3.13	1.5 – 1.7

n.d. : not detected

Method A: Thin film texture diffractometer

Method B: Conventional X-ray diffraction technique

Similar results of a decrease in the tetragonal volume fraction with increasing oxide thickness have been reported either for Zry-4 [1,18-20] or for Zr-2.5Nb [16].

## 5. INFLUENCE OF STRESSES IN THE CORROSION RATE

As the oxide grows on the base metal, the difference in volume between them gives rise to compressive stresses in the oxide. Godlewski *et al* [17] have related the stresses in the oxide film with its stability by measuring the relationship of the stress distribution and the amount of the tetragonal  $\text{ZrO}_2$  phase in the film. In order to assess the influence of the stresses in the corrosion rate, the following experiment was carried out with fully recrystallized Zry-4 sheet.

The samples were oxidized in steam at 400°C. After 19 days of exposure, the kinetic constants **k** and **n** of the oxidation process were calculated. Two samples were removed from the autoclave and mounted on a flat surface for the removal of the oxide film and part of the base metal from one side of the sample. When the samples were dismounted, the specimens bent under the influence of the residual stresses in the remaining oxide. The change in curvature was measured and the stresses were calculated using the procedure described by Bradhurst and Heuer [21]. The other samples were also mounted and dismounted to reproduce the procedure. Figure 5 shows the flow diagram of the experiment.

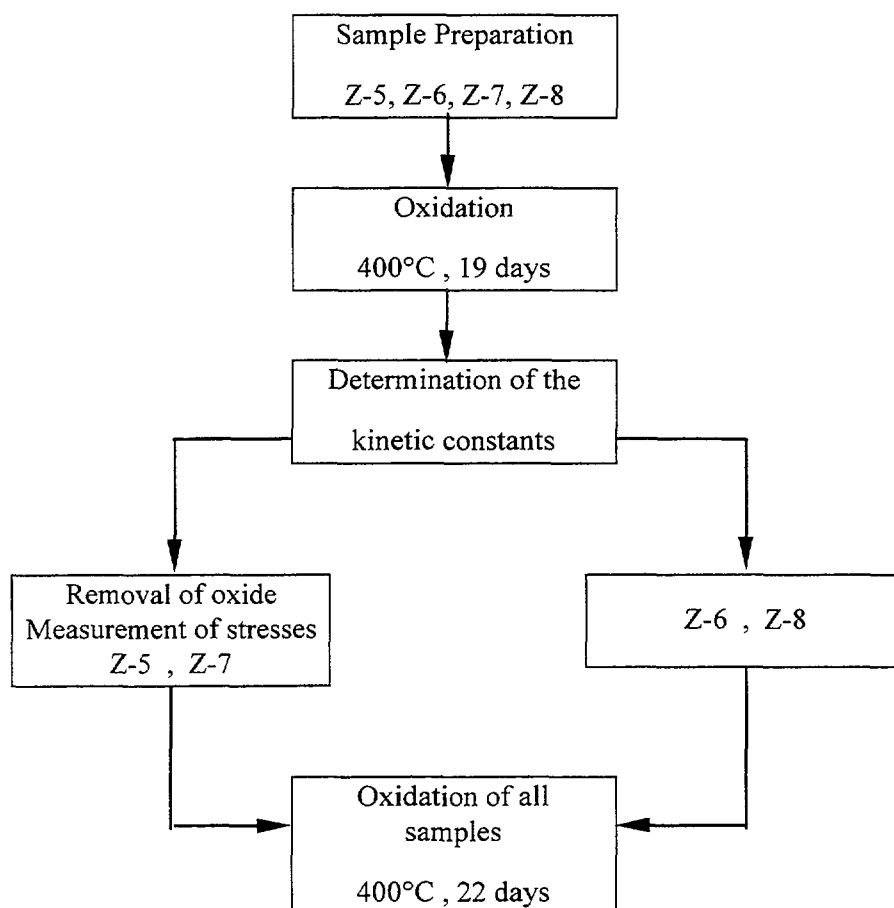


Figure 5 Flow diagram of the experiment

The kinetic constants were obtained from the data collected during the first 19 days of oxidation. The **k** values are close to 12 mg/dm<sup>2</sup> d<sup>n</sup> and **n** is close to 0.35. The values of **n** indicate that the corrosion kinetics of Zry-4 is cubic as is reported in the literature [3,22-24]. The calculated values of the stresses were around 400 MPa, comparable to those obtained by Garzarolli *et al* [19]. All samples were reinserted in the autoclave for another 22 days.

In order to detect if the corrosion kinetics are modified due to the stress relaxation, the measured weight-gains and corrosion rates were compared with the calculated ones for both sets of samples using the values of **k** and **n** determined from the first 19 days of oxidation.

Figure 6 shows the calculated and the experimental values of the weight gain and corrosion rate for Z-5, sample with removal of oxide and metal, and for Z-8, sample without removal. Figure 7 presents the same data for samples Z-7 and Z-6. Both figures indicate that the kinetic constants calculated with weight-gains up to 19 days provide a good prediction of the subsequent oxidation of samples Z-6 and Z-8. This good prediction implicates that the experimental weight-gains and corrosion rate of Z-5 and Z-7 should agree with those calculated if the relaxation of the stresses in the oxide does not affect the corrosion rate. However, there is a difference between both sets of values.

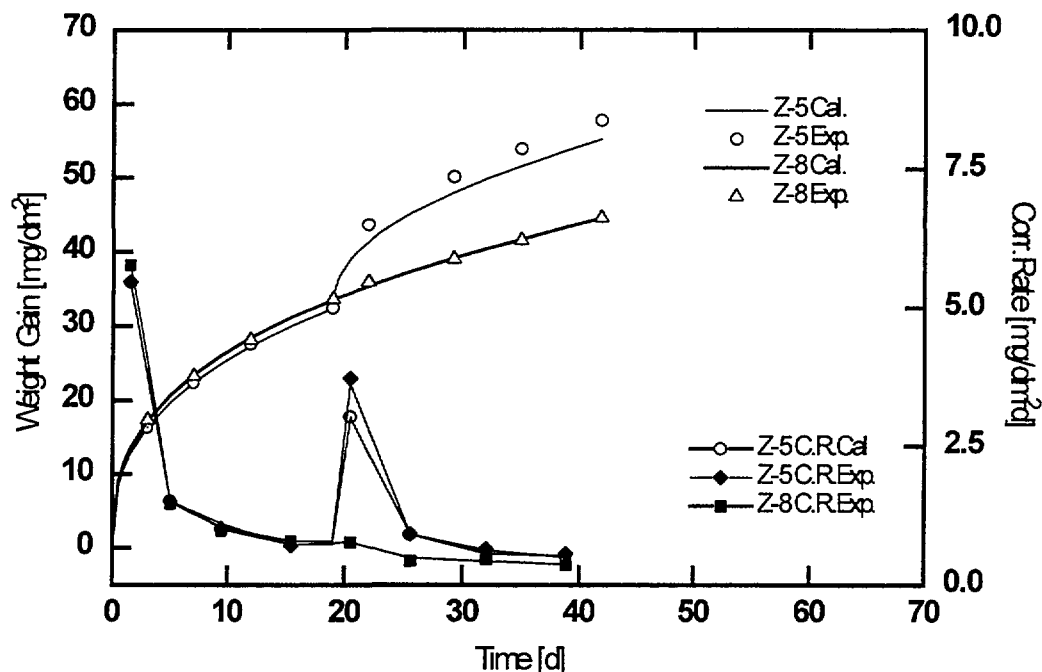


Figure 6 : Calculated and measured weight-gain and corrosion rate of Z-5 and Z-8

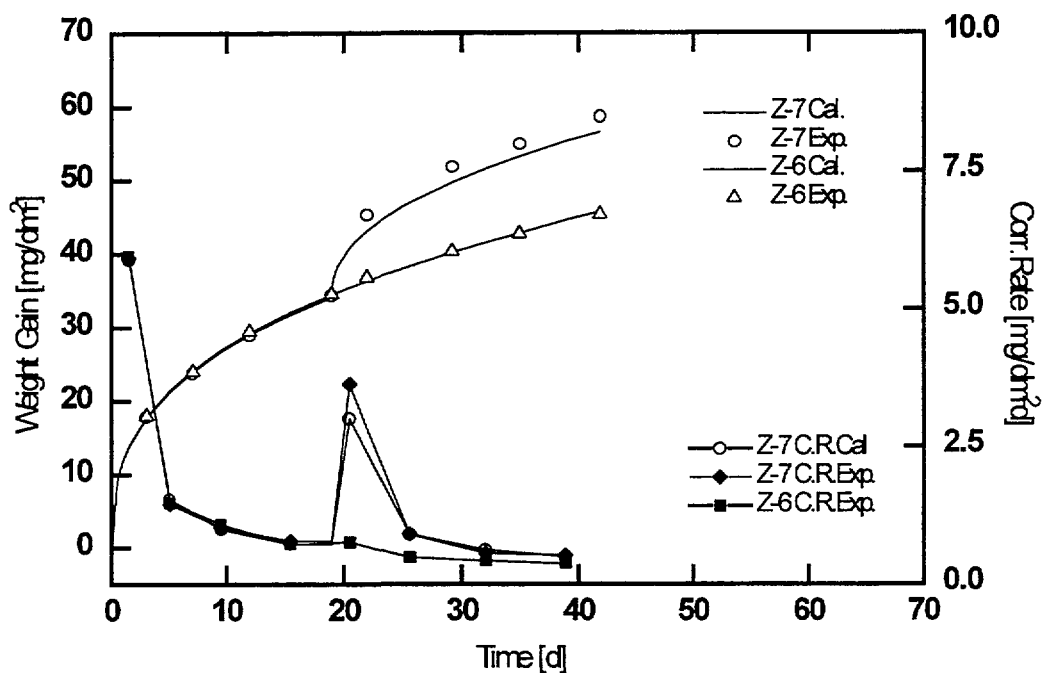


Figure 7: Calculated and measured weight-gain and corrosion rate of Z-7 and Z-6.

This can only be attributed to the relaxation of stresses in the oxide remaining on the samples where one side was polished. Since the surface finish is identical to the initial one of the samples, the increase in corrosion rate is related to the side where the oxide was not removed. Knights and Perkins [25] reported a similar effect at 400°C in a different kind of test. Both figures also show that the difference between the calculated and the experimental weight-gain measured is established during the first three days of oxidation after the removal of oxide and metal. This fact would imply that the stresses have been reestablished with the growth of the very thin layer at the metal/oxide interface. Godleswski *et al* [17] have reported that the compressive stresses are very high in a narrow zone near the metal/oxide interface. These tests are under progress including Zr-2.5Nb samples and testing of both alloys at 350°C.

To ensure that differences in thickness between the specimens with and without removal of oxide and metal have no influence in the corrosion kinetics, specimens cut from the same sheet were ground to different thicknesses using the same surface finish as in the coupons used for the determination of the influence of stresses in the corrosion kinetic. These specimens were also tested at 400°C in steam in order to determine their corrosion kinetics.

Figure 8 shows the oxidation kinetics for the samples of different thicknesses. These results show that for a range of thickness between 1.25 and 0.15 mm, there are no differences in corrosion behaviour between them. For this range of thickness and our test conditions, the difference in thickness does not affect the corrosion kinetics.

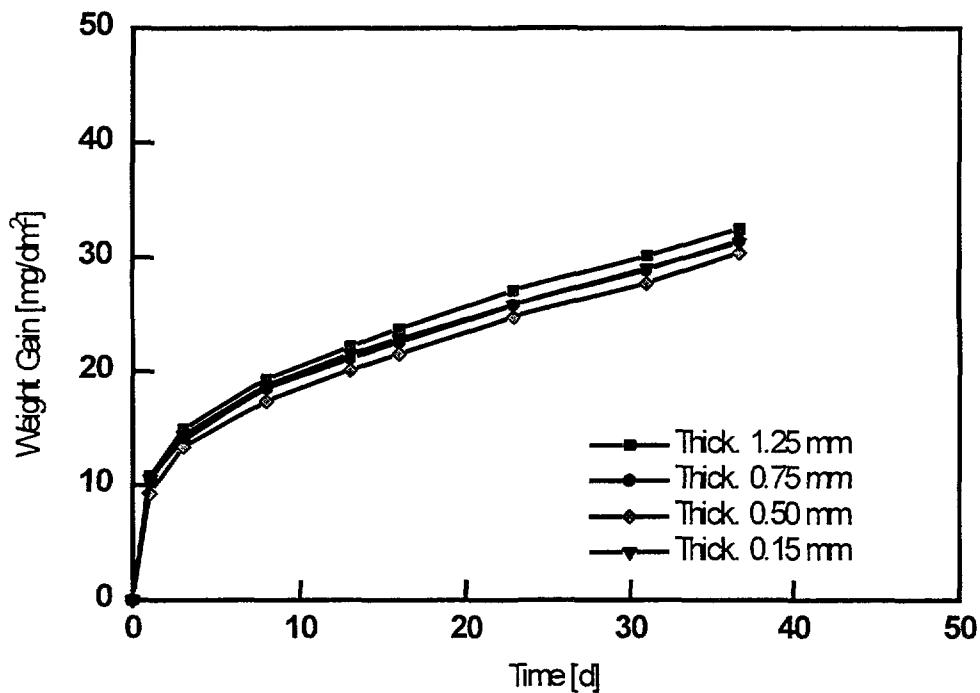


Figure 8 : Corrosion kinetics in steam at 400 °C for coupons with different thicknesses

## 6. EFFECT OF RESIN DEGRADATION ON THE CORROSION RATE OF ZR-2.5NB.

In May 1988, 1000 l of mixed resins entered the primary coolant system of the Embalse NPP. The station was running during six hours before the shut down. The decrease of temperature of the primary system was 3°C per minute. The influence of the resin ingress was evaluated through the behaviour of the corrosion coupons inserted in the Embalse autoclaves and through simulation tests performed in static autoclaves.

### 6.1. Coupons inserted in Embalse's Autoclaves

Zry-4 and Zr-2.5Nb coupons were inserted in October 1986 in the Embalse autoclaves and were inspected after the resin ingress and during further inspections in order to assess the corrosion behaviour of the coupons that were exposed to the degradation products of the resins. The corrosion test samples of Zry-4, also from a fully recrystallized sheet, are labelled as Zry-4 (B).

Table IV shows the cumulative weight gains of the Zry-4 (B) and Zr-2.5Nb coupons after successive inspections. The results indicate that the Zry-4 (B) specimens inserted in the 265°C autoclave, are in the pre-transition stage after 3800 full power days as would be expected at this temperature. The Zry-4 (B) coupons from the 305°C autoclave are in the post-transition stage and the post-transition corrosion rate is 0.7 µm/year. The Zr-2.5 Nb specimens located in the 305°C autoclave have a post-transition corrosion rate of 1.9 µm/year, analogous to the value of 1.6 µm/year for the specimens inserted in these autoclaves after the resin ingress that was reported in the previous part of this work. A comparison with values reported in the literature is also presented in the Table. All coupons were coated with a black oxide and no evidence of damage was seen by optical microscopy.

TABLE IV: Weight-gain and post-transition corrosion rate of coupons from Embalse's autoclaves

Autoclave Temp.	Material	Insertion Date	May-88 mg/dm <sup>2</sup>	Jun-88 mg/dm <sup>2</sup>	May-89 mg/dm <sup>2</sup>	Sep-89 mg/dm <sup>2</sup>	May-91 mg/dm <sup>2</sup>	Apr-93 mg/dm <sup>2</sup>	Post-trans. Corr. Rate µm/year
265°C	Zry-4 (B)	Oct-86	9		10	11	14	16	Pre-trans.
305°C	Zry-4 (B)	Oct-86			26	31	47	61	0.7
	Garzarolli <sup>22</sup>								1.2
	Hillner <sup>23</sup>								1.0
305°C	Zr-2.5Nb	Oct-86		36	63	71			1.9
305°C	Zr-2.5Nb	May-88							1.6
~ 290°C	Warr <sup>8</sup>								0.5-1.6
310°C	Warr <sup>9</sup>								1.2-2.3

## 6.2. Simulation Test

A test simulating the ingress of mixed resin to the primary circuit of Embalse was performed at 400°C in steam with Zr-2.5Nb pressure tube material.

Two batches of samples were machined from pressure tube material, the lot identified as PT was in the as received condition and the lot identified as TT was heat treated 10 h at 500°C. This heat treatment was performed in order to obtain a microstructure similar to that of the irradiated material. All samples were ground and pickled and half of the samples were pre-filmed during 3 days in steam in a static autoclave at 400°C. Some specimens from the four lots were chosen to be used as reference samples.

Next, a simulation test of the ingress of mixed resin to the primary circuit of Embalse was done with all samples, either pre-filmed or not, with and without heat treatment. The test was performed at 300°C in lithiated water,  $\text{pH}_{25^\circ\text{C}} = 10.5$ , with 16 cc of mixed resin / l  $\text{H}_2\text{O}$ , during 7 h. All samples, including the reference ones, were then oxidized in static autoclaves in steam at 400°C. Figure 9 shows the flow diagram of the test.

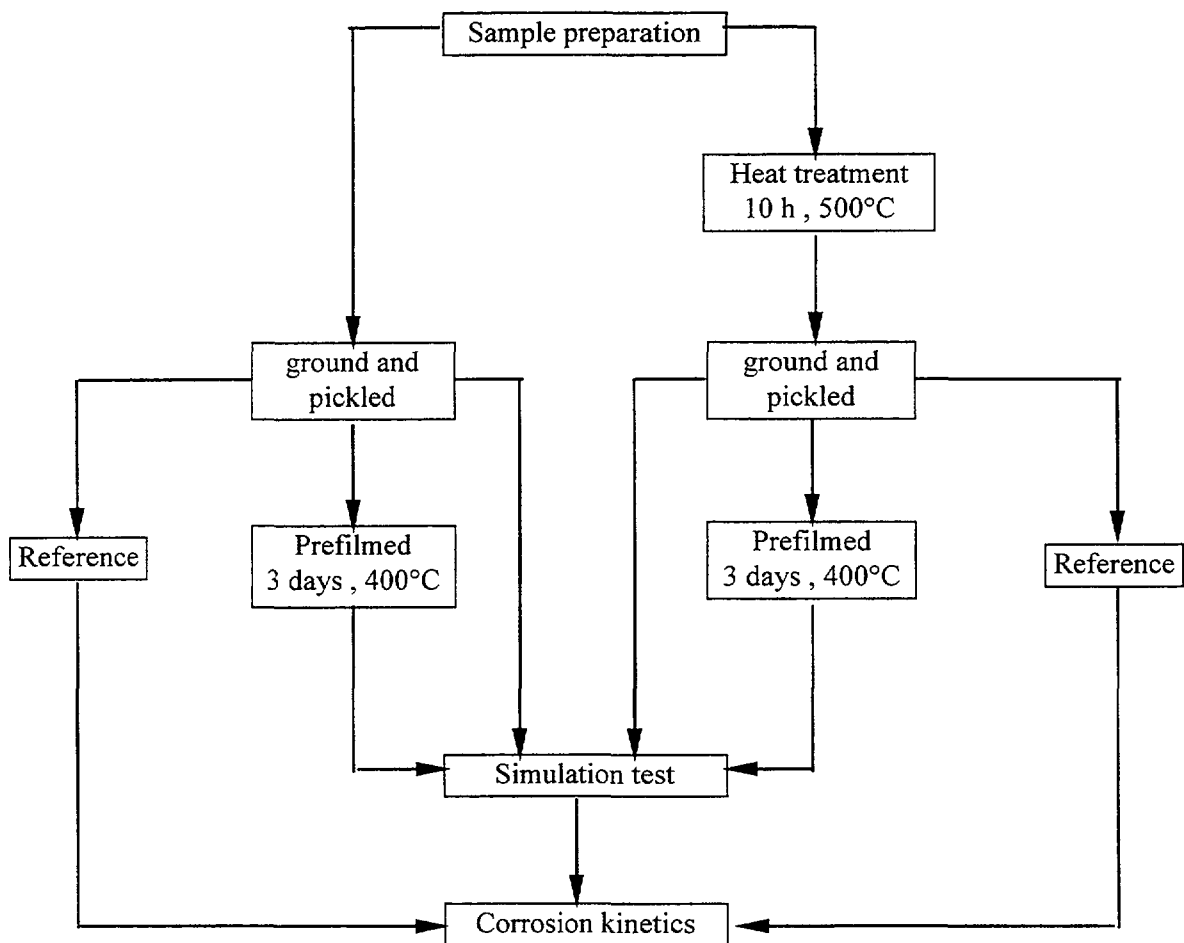


Figure 9 : Flow diagram of the experiment

Figure 10 shows the corrosion kinetics followed by the three kind of samples during 120 days. All specimens are in the post-transition stage, that began at approximately 75 days. No difference of behaviour is found between the two batches and the reference specimens which means that the degradation of the resins did not affect the corrosion behaviour of pressure tube material.

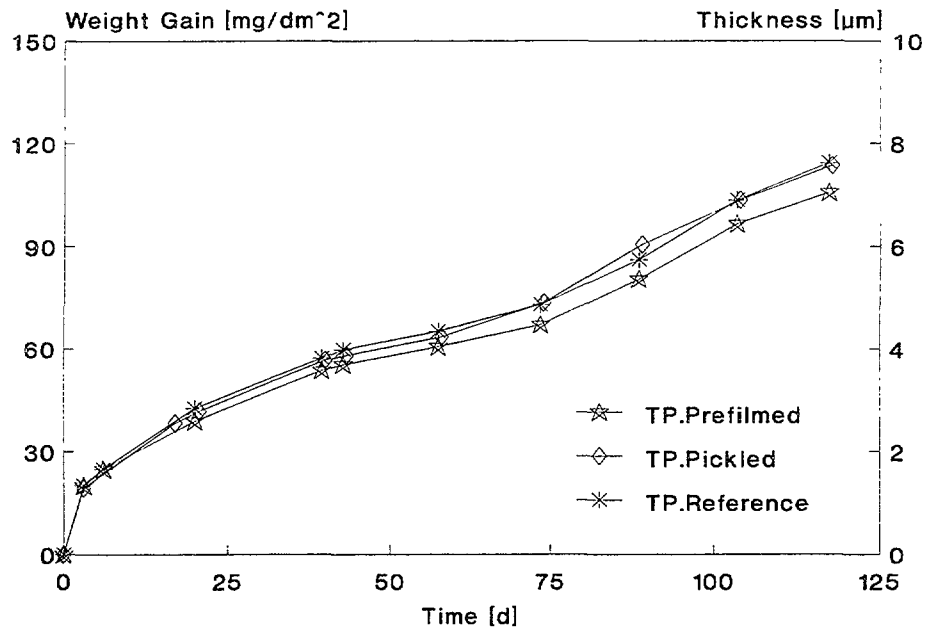


Figure 10 : Corrosion kinetics in steam at 400°C of samples without heat treatment.

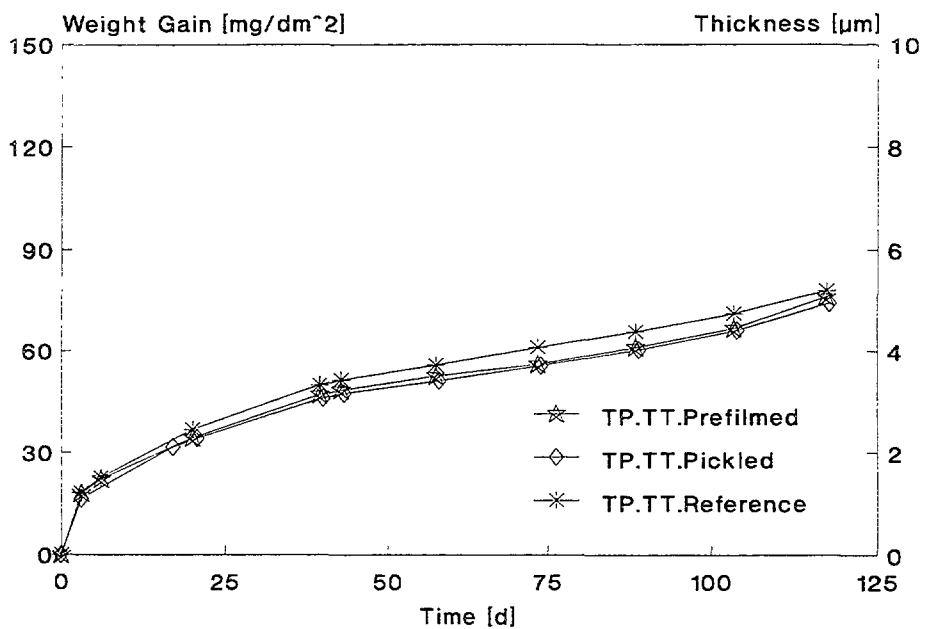


Figure 11: Corrosion kinetics in steam at 400°C of samples with heat treatment

Similar results are found with the heat-treated material, Figure 11. The samples are in the post-transition stage that started at around 105 days. These results indicate that the heat treatment improves the corrosion resistance of Zr-2.5Nb as was shown in the test performed at 435°C. Once again, no differences are detected for the samples from the simulation test.



Samples machined from pressure tube and with surface finish with 3  $\mu\text{m}$  diamond paste were used to see if the presence of resin in the medium can produce localised attack. Several marks were made in the surface of the samples in order to identify the same area. The surface of the specimens was observed before and after the simulation test with scanning electron microscopy. The inspections showed no damage as can be seen in Figures 12 a) and b).

The oxide grown on the surface of the specimens after 120 days of exposure was also inspected by scanning electron microscopy. No difference was found between the specimens from the simulation test and the reference sample, Figures 13 a) and b).

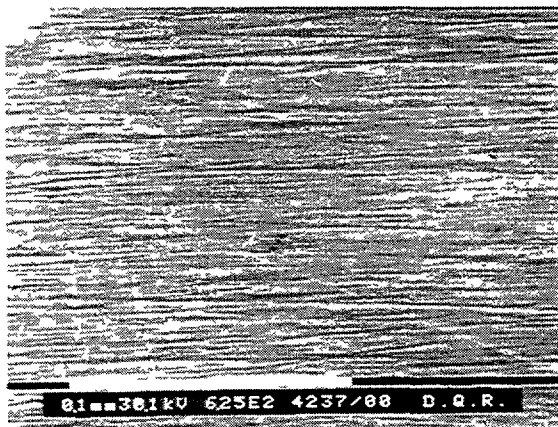


*Figure 12 a: Surface of the sample before the resin simulation test*

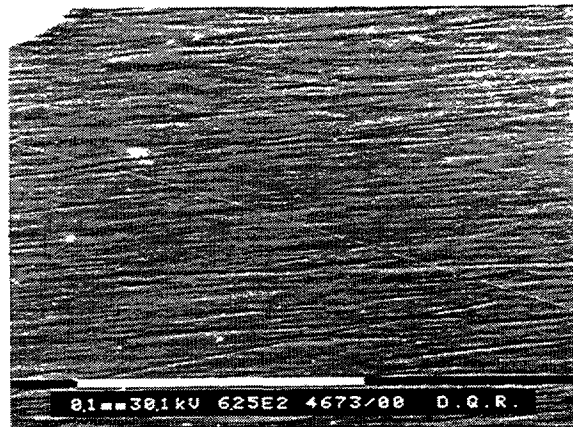


*Figure 12 b: Surface of the sample after the resin simulation test*

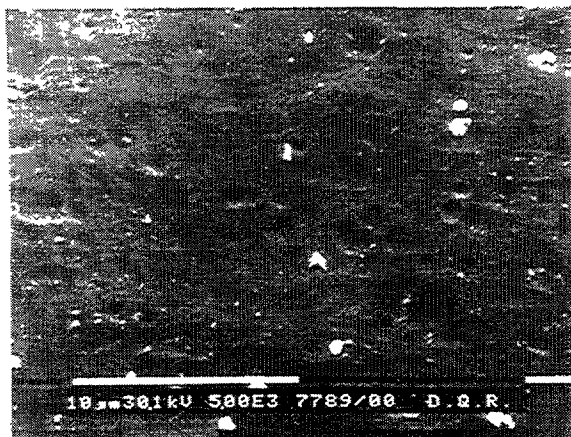


*Figure 13 a: Oxide from a sample oxidized after the resin simulation test*

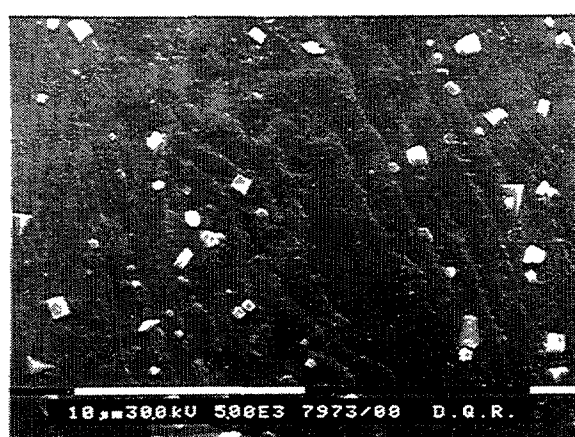


*Figure 13 b: Oxide on the surface of a reference sample*

The behaviour of the corrosion test samples inserted in the CNE autoclaves and the tests performed in the laboratory simulating the resin ingress indicate that this event has not modified the corrosion behaviour of the materials.

## 7. CONCLUSIONS

- The corrosion rate of the Zr-2.5Nb samples is larger than that of the Zry-4 specimens for our tests conditions.
- Zry-4 presents a cyclic oxidation while Zr-2.5Nb shows a two-stage or parabolic behaviour.
- Heat treatments modify significantly the corrosion rate of Zr-2.5Nb.
- The corrosion rate of both materials is controlled by the dense oxide layer at the metal/oxide interface and this dense layer decreases at the transition.
- X-ray diffraction analysis shows the difference in texture of the tetragonal phase of both materials and the relevance of taking into account the texture of the oxide when calculating the tetragonal volume fraction.
- The compressive stresses in the oxide influence the oxidation kinetics of Zry-4.
- The degradation products formed during the resin excursion, either in the actual event or in simulation tests, showed no influence in the corrosion kinetics of Zr-2.5Nb.

## REFERENCES

- [1] MAROTO, A.J.G., BORDONI, R., VILLEGAS, M., OLMEDO, A.M., BLESÁ, M.A., IGLESIAS, A., KOENIG, P., "Corrosion behaviour of zirconium alloys", *Journal of Nuclear Materials* **229** (1996) 79.
- [2] GOHR, H., SCHALLER, J., RUHMANN, H., GARZAROLLI, F., "Long-term in situ investigation of Zr alloys in simulated PWR environment by electrochemical measurements", *Zirconium in the Nuclear Industry (Proc. 11th Int. Symposium, Germany, 1995)*, ASTM, ASTM STP 1295 (1996) 181.
- [3] COX, B. "Pore structure in oxide films on irradiated and unirradiated zirconium alloys", *Journal of Nuclear Materials* **148** (1987) 332.
- [4] URBANIC, V.F., WARR, B.D., MANOLESCU, A., CHOW, C.K., SHANAHAN, "Oxidation and deuterium uptake of Zr-2.5% Nb pressure tubes in CANDU-PHW reactors", *Zirconium in the Nuclear Industry (Proc. 8th Int. Symp. San Diego, 1988)*, ASTM, ASTM STP 1023 (1989) 20.
- [5] URBANIC, V.F., GILBERT, R.W., "Effect of microstructure on the corrosion of Zr-2.5% Nb alloy", *Fundamental Aspects of Corrosion of Zirconium-Base Alloys (Proc. Mtg Portland, Oregon, USA, 1989)*, Report IEGFPT/34, IAEA, Vienna (1990) 262.
- [6] URBANIC, V.F., GRIFFITHS, M., "Microstructural aspects of corrosion and hydrogen ingress in Zr-2.5Nb", *Zirconium in the Nuclear Industry (Proc. 12th Int. Symp. Toronto, Ontario, Canada, June 1998)*, ASTM (in press).
- [7] MAROTO, A.J.G., BORDONI, R., VILLEGAS, M., OLMEDO, A.M., BLESÁ, M.A., IGLESIAS, A., RIGOTTI, G., "Growth and characterization of oxide layers on zirconium alloys", *Influence of Water Chemistry on Fuel Cladding Behaviour (Proc. Mtg, Rez, Czech Republic, October 1993)*, IAEA-TECDOC-927, Vienna (1997) 143.
- [8] WARR, B.D., VAN DER HEIDE, P.A., MAGUIRE, M.A., "Oxide characteristics and corrosion and hydrogen uptake in Zr-2.5Nb CANDU pressure tubes", *Zirconium in the Nuclear Industry (Proc. 11th Int. Symposium Germany, 1995)*, ASTM, ASTM STP 1295 (1996) 265.
- [9] WARR, B.D., RAMASUBRAMANIAN, N., ELMOSELI, M.B., GREENING, F.R., LIN, Y.P., LICHTENBERGER, P.C., Report, Ontario Hydro Research Review, N.B., August 1993.
- [10] BORDONI, R., VILLEGAS, M., OLMEDO, A.M., MIYAGUSUKU, M., KOENIG, P., Surface characterization, Modifications and Modeling, Presented at Workshop, EdeS, Buenos Aires, Argentina, July 1997.

- [11] MAROTO, A.J.G., BORDONI, R., OLMEDO, A.M., MIYAGUSUKU, M., VILLEGAS, M., in X Argentine Congress of Physical Chemistry, Tucuman, Argentine, April 1997 (in press).
- [12] BURRILL, K.A., Internal Report to the 1<sup>st</sup> Meeting of IAEA Coordinated Research Programm on Modeling of Transport of Radiactive Substances in the Primary Circuit of Water-Cooled Reactors, Ontario Hydro Head Office, Toronto, 1997, May 5-9.
- [13] MILLER, D.G., BURRILL, K.A., in CORROSION 98, PAPER N-33 5 (in press).
- [14] BOSSIS, P., LELIEVRE, G., BARBERIS, P., ILTIS, X., LEFEBVRE, F., Multi-scale characterization of the metal-oxide interface of zirconium alloys", Zirconium in the Nuclear Industry, (Proc. 12<sup>th</sup> Int. Symposium, Toronto, Ontario, Canada, June 1998), ASTM (in press).
- [15] PECHEUR, D., GODLEWSKI, J., PEYBERNES, J., FAYETTE, L., NOE, M., FRICHET, A., KERREC, O., "Contribution to the understanding of the effect of the water chemistry on the oxidation kinetics of Zircaloy-4 cladding", Zirconium in the Nuclear Industry (Proc. 12<sup>th</sup> Int. Symposium Toronto, Ontario, Canada, June 1998), ASTM (in press).
- [16] GLAVICIC, M.G., SZPUNAR, J.A., LIN, Y.P., "A method for quantative phase analysis of ZrO<sub>2</sub> film growth on Zr-2.5% Nb pressure tubes" Journal of Nuclear Materials **245** (1997) 147.
- [17] GODLEWSKI, J., BOUVIER, P., LUCAZEAU, G., FAYETTE, L., 12<sup>th</sup> Int. Symp. on Zirconium in the Nuclear Industry, Toronto, Ontario, Canada, June 1998.
- [18] GODLEWSKI, J., GROS, J.P., LAMBERTIN, M., WADIER, J.F., WEIDINGER, H., 9<sup>th</sup> Int. Symp. on Zirconium in the Nuclear Industry, ASTM STP 1132 (1991) 416.
- [19] GARZAROLLI, F., SEIDEL, H., TRICOT, R., GROS, J.P., 9<sup>th</sup> Int. Symp. on Zirconium in the Nuclear Industry, ASTM STP 1132 (1991) 395.
- [20] BARBERIS, Journal of Nuclear Materials 226 (1995) 34.
- [21] BRADHURST, D.H., HEUER, P.M., Journal of Nuclear Materials 37 (1970) 35.
- [22] GARZAROLLI, F., JUNG, W., SCHOENFELD, H., GARDE, A.M., PARRY, G.W., SMERD, P.G., EPRI NP - 2789 (1982).
- [23] HILLNER, E., Int. Symp. on Zirconium in the Nuclear Industry, ASTM STP 633 (1977) 211.
- [24] URBANIC, V.F., COX, B., FIELD, G.J., 7<sup>th</sup> Int. Symp. on Zirconium in the Nuclear Industry, ASTM STP 939 (1987) 189.
- [25] KNIGHTS, C.F., PERKINS, R., Journal of Nuclear Materials 36 (1970).

# INVESTIGATION OF LIKELY CAUSES OF WHITE PATCH FORMATION ON IRRADIATED WWER FUEL ROD CLADDINGS

YU.K.BIBILASHVILI, V.P.VELIOUKHANOV, A.Y.IOLTOUKHOVSKI, V.P.POGODIN  
A.A.Bochvar Scientific Research Institute of Inorganic Materials (VNIINM),  
Moscow, Russian Federation



XA9953299

## Abstract

The information concerning white patches observed on fuel cladding surfaces has been analytically treated. The analysis shows at least three kinds of the white patch appearance:

- bright white spots which appear to be loose corrosion product deposits disclosing corrosion pits upon spalling;
- indistinct streaks with separate pronounced spots 1-2 in dia. The spots seem to be thin superficial deposits;
- light-coloured dense uniform crud distributed over the surface of fuel claddings and fuel assembly jackets.

## 1. Experimental Results

The effect of impurities caught in the reactor water or cladding surface on the corrosion rate of Zr-based alloys (E-110, E-635) has been examined. The enhanced corrosion and a patchwork of white spots, stripes and dots are shown to develop on the alloys with any impurity resulted from various fuel handling steps or out-of-range coolant composition. The chief impurities, in order of decreasing hazard, for a fuel cladding are : fluorine, carbon and for a coolant: oxygen, LiOH, starch, graphite, mineral oil.

A number of the E-110 claddings operated in WWER-440s and WWER-1000s (Loviisa, Kozloduy, Khmelnitskaya NPPs) demonstrated white patches on their surfaces. Similar patchwork was observed after cladding exposure to fluorine, superheat or high-oxygen reactor water. Patchy claddings cause concern about the potential hazard of the oxide protective ability getting worse ,with a consequent enhanced corrosion and possible failure at the point of white patch origin.

Table 1 summarizes data on patchy fuel assemblies. Their visual appearance is illustrated by the example of the Kozloduy claddings in Fig 1. The analysis of the published information on the subject suggests that:

1. In their appearance, white patches can be classified into at least three kinds:
  - bright white spots which appear to be loose corrosion product deposits disclosing corrosion pits upon spalling;
  - indistinct streaks with separate pronounced spots 1-2 mm in dia which seem to be thin superficial deposits;
  - light-coloured dense uniform crud distributed over the surface of fuel claddings and fuel assembly jackets.
2. The white patch occurrence can be found in the literature back in 1982 but has been much more often described recently (1995-1996).
3. White patches are evidently dependent on the operating period and thermal stress of fuel elements (their amount at the fuel element centre far exceeds that at the ends). Operational and storage peculiarities can also be responsible.

TABLE I. CHARACTERISTICS OF WWER FUEL ASSEMBLIES SHOWING  
WHITE PATCHES ON THE CLADDING SURFACES

NPP Unit	Number of cycles	Operation period	Fuel Assembly	№	Enrichment	Burnup MW d/kgU	Max linear power W/cm
Lovinsaa 2 unit	4 тц 4 тц 3 тц			13601264 13604154 13607120	4,4 4,4 4,4	45,9 42,9	
Khmelnitsk 1 unit	4 тц 4 тц 3 тц 2 тц 2 тц 2 тц 1 тц 1 тц	91 - 95 92 - 96 93 - эксп 94 - эксп 94 - эксп 94 - 96 95 - эксп 95 - эксп		E2882 ЕД1312 ЕД5212 E6272 E5568 H1236 B2206 ЕД5251	4,4 4,4-3,6 4,4-3,6 4,4 4,4 1,6 3,0 4,4-3,6	43,27	
Novovoronezh 5 unit	3 тц	11 09 82 09 05 85	18 06 82	3300000007	3,3	32,65	315
Novovoronezh 5 unit	3 тц	20 06 84 25 06 87	08 1983	4436001114	4,4-3,6	44,7	
South-Ukranian 1 unit	4 тц	22 12 82 14 08 86	05 80	33000106	3,3	36,7	
Kalinin 1 unit	3 тц	05 11 85 02 07 88	04 85	33001562	3,3	32,9	
Zaporozhie 1 unit	3 тц	14 06 88 13 12 91	1988	E0328 E0329	4,4	44,0	264
Kola 3 unit	4 тц 5 тц	24 09 86 02 11 90 24 09 86 15 10 91	05 86 05 86	14422198 14422222	4,4 4,4	46,2 48,2	319 264
Novovoronezh 4 unit	4 тц	10 87 7 91	06 87	13626135	3,6	38,5	

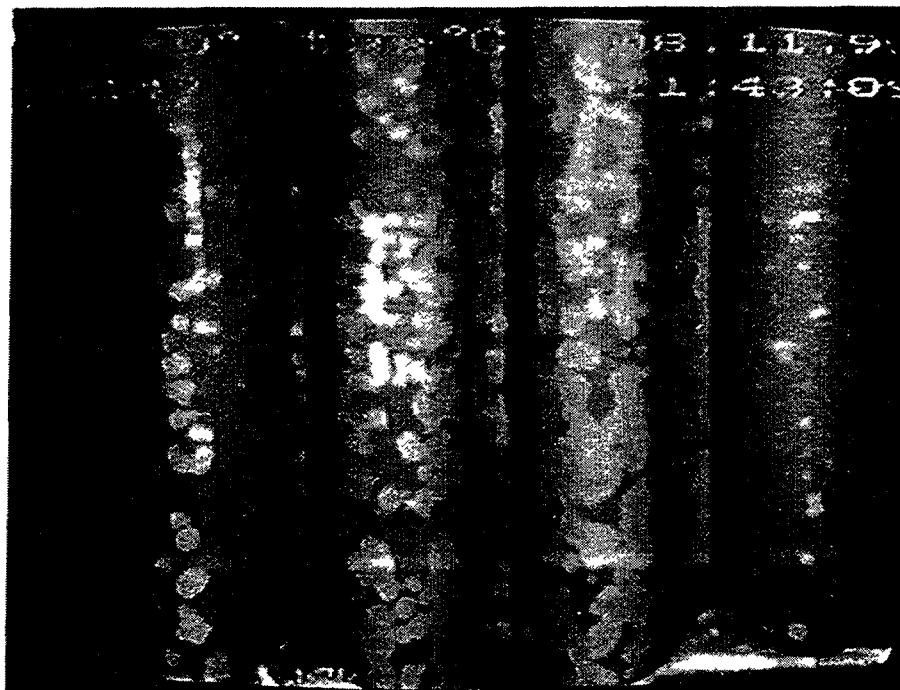


Fig.1. White patches on the Kozloduy claddings

The occurrence of white patches on E-110 and E-635 claddings as a result of their pollution by impurities has been experimentally tested. The tests were carried out in stainless steel autoclaves filled with distilled water in a sample surface area-water volume ratio of 1 cm/cm at 350°C for 3000 hr. Sections of commercial cladding tubes 20 mm long 9.15 mm in dia were used for the tests. Autoclaved samples were weighed on an analytical balance to an accuracy of  $1 \cdot 10^{-4}$  g and visually inspected with a binocular microscope at a x60 magnification.

The E-110 and E-635 samples tested were:

-as-received and oxidizing;

-exposed to fluorine (for 10 min in a 1% aqueous etching reagent solution and dried at 90-95°C);

-exposed to carbon (for 10 min in a 1% starch solution at 70-80°C, dried at 90-95°C and heated for 0.5 hr at 300°C in a nitrogen stream).

The results of the corrosion study are given in Fig.2. The data show the enhanced corrosion of the claddings by any impurity.

Exposure of Zr alloys to fluorine and carbon sharply accelerated their corrosion. Thick loose white deposits of Zr oxide covering all the fluorine-impured E-110 samples were observed as soon as 100 hours after water corrosion tests at 350°C. This was the case, to a lesser extent, for E-635: only a small oxide area remained bright grey.

The carbon pollution also considerably accelerated the corrosion in a high- temperature water environment to form a dull or bright grey deposit with whitish spots and stripes. Long autoclave tests (3000 hr) produced no spalling.

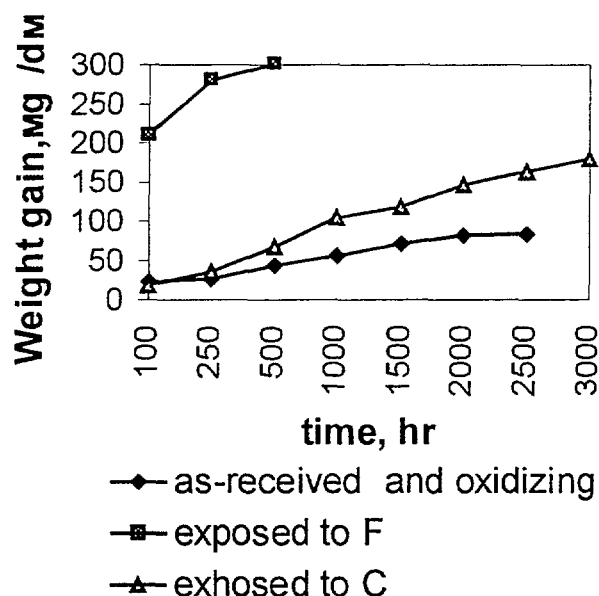


Fig.2. Weight gains for Zr-1%Nb exposed to various impurities

The data obtained suggest that that impurities like fluorine, carbon result in the enhanced corrosion and, sometimes in white patches. But spalling appears only after exposures to fluorine.

Inorganic and organic impurities and foreign particles entered into a coolant are of considerable importance in inducing an abnormal situation which can reduce the fuel assembly service life. They can be responsible for enhanced uniform corrosion, nodular corrosion, spacer grid clogging, resulting in the fuel element temperature rise and potential leakage.

The paper studies the effect of some organic impurities (oil, graphite, etc.), which can enter the reactor water, on the corrosion resistance of E-110 and E-635. The corrosion test followed the procedure described above. As-received Zr alloys were used as samples for experiments. A coolant was impured with oil (200 mg/kg), graphite (2 g/kg), starch (20 mg/kg) or LiOH (100 mg/kg) at high concentrations to get clear results soon. The results are reported in Fig 3. It follows from Fig.3 that LiOH has the most harmful corrosive effect on the E-110 cladding. The order of decreasing hazard is: LiOH, starch, graphite, oil. With all these impurities, E-635 is superior in the corrosion resistance to E-110. The surface of some samples showed white patches in 100 hours of exposure to the impure water. On longer exposures (up to 1000 hr) the white patches tended to die away.

A special feature of the effect of these organic matters in a high-temperature water is the deposition of greyish brown steel corrosion products on the alloy surfaces. High-oxygen water in the WWER primary circuit can lead to accelerated uniform corrosion and, even worse, to nodular corrosion and potential cladding leakage.

The effect of the high-oxygen reactor water was experimentally studied at 350°C and 17 MPa in stainless steel autoclaves that were filled with fresh 0.5 – 2%  $H_2O_2$  solutions just prior to placing E-110 and E-635 cladding tube segments 20 mm long 9.15 in dia into them.

The corrosion data obtained are reported in Fig.4. On long exposures the both alloys demonstrated smaller weight gains in  $H_2O_2$  –free water, although the oxide deposit formed in the  $H_2O_2$  – high water was found to be spalled off. It should be noted that the 0.5%  $H_2O_2$  – impured water makes more considerable contribution to the corrosion of both alloys than the 2%  $H_2O_2$  –containing water. At either  $H_2O_2$  concentration the corrosion of E-635 is twice as low as that of E-110.

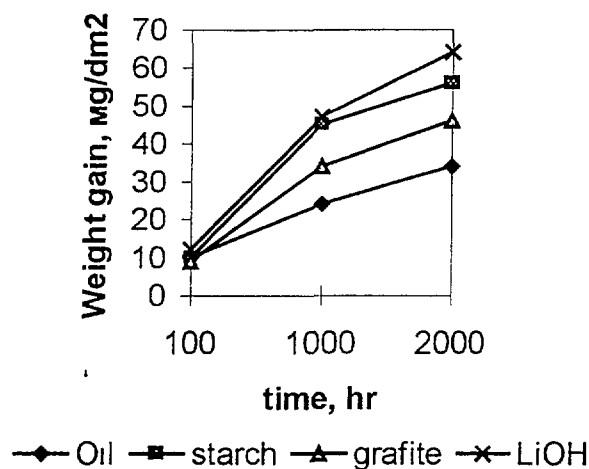


Fig 3 Weight gains for Zr-1%Nb exposed to impure water

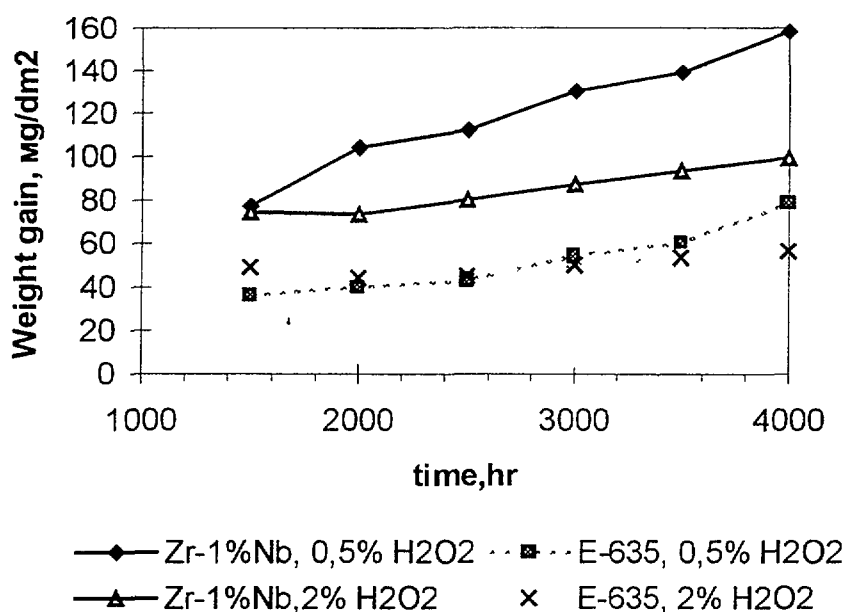


Fig 4 Weight gains for Zr-1%Nb and E-635 exposed to H<sub>2</sub>O<sub>2</sub> – impured water

Visual inspection of the samples sketches the following broad outlines. Early in the corrosion tests both E-110 and E-635 develop a glossy black oxide film with well defined white dots, spots 1-2 mm in dia or small white, grey, and greyish stripes. On longer exposures the oxide film varies considerably in its color from glassy black to dull black and dark grey, the earlier white dots, spots and stripes becoming less defined. The light-colored areas tend to spall disclosing pronounced black areas (dots, spots 1-2 mm in dia, small elongated patches).

Though the oxygen corrosion experiments showed no severely failed samples the oxygen impurity is not to be supposed to be of no concern. In actual practice thermal and neutron fluxes essentially accelerate the oxygen corrosion of these alloys. This can be illustrated by the oxygen overshoot at the Khmelnitskaya NPP (April-May 1994), resulting in a few leaky fuel assemblies with a consequent deterioration of the on-site radiation situation.



## 2. Conclusions

1. The analytical treatment of the information on white patches observed on irradiated WWER cladding surfaces has shown that:

- white patches can be seen on the claddings of both WWER-440 and WWER-1000 reactors;

- white patches can be at least of three kinds; among these are superficial deposits creating no leakage problems as judged from hot cell examination and hazardous corrosion nodules responsible for a considerable reduction in the cladding service life.

2. Autoclaved corrosion tests of F- and C-impured E-110 and E-635 cladding tube segments as well as water corrosion experiments in the presence of various impurities (oxygen, mineral oil, graphite, starch, LiOH) show the enhanced corrosion and a patchwork of white spots, dots and stripes developed with any of these substances. The chief impurities, in order of decreasing hazard, for a fuel cladding are: fluorine, carbon. The most hazard coolant impurities are oxygen, LiOH, starch, graphite, mineral oil.

3. With all these impurities, E-635 is superior in the corrosion resistance to E-110.

M. ZMÍTKO, J. KYSELA, J. ŠRANK  
Nuclear Research Institute Řež plc.



XA9953300

T. GRYGAR, J. ŠUBRT  
Institute of Inorganic Chemistry of Czech Academy of Science, Řež,

Czech Republic

## Abstract

An experimental programme was conducted at a reactor water loop RVS-3 with the intention of studying corrosion behaviour of Zr cladding materials under PWR water chemistry with a high lithium content (5 ppm Li) and subcooled boiling conditions. After completion of the first irradiation cycle, some deposits were observed on the cladding surface that led to misreading of the eddy current signal (lift-off the signal) at the Zr oxide thickness measurements. A number of analysis and investigations was then employed to identify an origin and characteristics of the deposits. It was found that deposits on the cladding surfaces originates from corrosion products of the structural materials, and was formed by precipitation mechanism from the coolant. The origin of the corrosion product deposits formation has not been fully identified and understood, but it is obvious that this process is related to a quality of the loop primary coolant, and local thermal-hydraulic conditions. Moreover, a Cr content in the corrosion products and form of presence of Cr-species indicates a corrosion attack of the loop inner surfaces via dissolution-reprecipitation mechanism which may be attributed to destabilization or even destruction of a passive film formed in the past on the loop inner surfaces.

## 1. INTRODUCTION

An experimental programme was conducted at a reactor water loop RVS-3 with the intention of studying corrosion behaviour of Zr cladding materials under PWR water chemistry with a high lithium content (5 ppm Li) and subcooled boiling conditions. A test section consisting of four electrically heated fuel rod immitators was situated in a field tube of the loop active channel located in the core of a material testing reactor LVR-15. A heated part of the fuel rod immitator matched the reactor core height, so a simultaneous effect of the water chemistry, thermal-hydraulic conditions, and irradiation could be studied.

An intermediate investigation of the cladding materials - a measurement of Zr oxide thickness by eddy current technique - was foreseen after each irradiation cycle, ie. after 21 days of the reactor operation. After completion of the first irradiation cycle, some deposits were observed on the cladding surface what led to misreading of the eddy current signal (lift-off the signal) at the Zr oxide thickness measurements. The situation was improved and more realistic oxide thickness values were measured after brushing of deposits from the cladding surface. A number of analysis and investigations was then performed to identify a nature and characteristics of the deposits on the cladding surface and a quality of the loop primary coolant.

## 2. EXPERIMENTAL CONDITIONS

A reactor water loop RVS-3 is one of the experimental facilities for conducting research projects in material testing reactor LVR-15 operated at NRI Rez. The RVS-3 loop was designed as an universal facility providing wide experimental possibilities. The loop models thermal and hydraulic parameters, and water chemistry environment of pressurized water reactors (PWRs or VVERs). The

RVS-3 loop consists of the following sub-systems: a main flow (primary) circuit with an active channel located in the reactor core, a purification system containing cation and mixed resins and mechanical filter, a make-up water system, a gas injection system, cooling systems, a sampling system including isokinetic sampling line. The loop primary circuit is a closed stainless steel system with forced circulation of the coolant. The loop volume is about 300 liters. Austenitic stainless steel 08Ch18N10T (SS 321) is used as the loop main structural material. Technological layout of the loop is shown in Fig. 1.

At this cladding corrosion experiment, the RVS-3 loop was operated at pressure 15 MPa (relevant saturation temperature 342°C). The primary coolant flow rate was 3.85 tons/hr what meant a flow velocity of 2.6 m/s at the test section outlet. Heat flux on the cladding surface was achieved by insertion of a specially designed electrically heated rod into the cladding tube. Total length of the rod was 5,100 mm with a 560 mm long heated part (section) at the rod bottom. Such design allowed to achieve heat flux of 100 W/cm<sup>2</sup> on the outer cladding surface in the heated section. Inlet and outlet coolant temperatures in the heated section were kept 325°C and 335°C, respectively. Thermal-hydraulic parameters of the experiment were chosen so that the upper region of heated section worked at subcooled boiling conditions, ie. cladding surface temperature achieved and slightly exceeded a saturation temperature at a given pressure. Calculated void fraction at the heated section outlet was about 6%. Distribution of the coolant temperature, cladding surface temperature and void fraction along the heated section are shown in Fig. 2.

Water chemistry parameters were chosen in aim to study the influence of a high lithium concentration on Zr cladding behaviour – 5 ppm Li and 650 ppm B was maintained during the

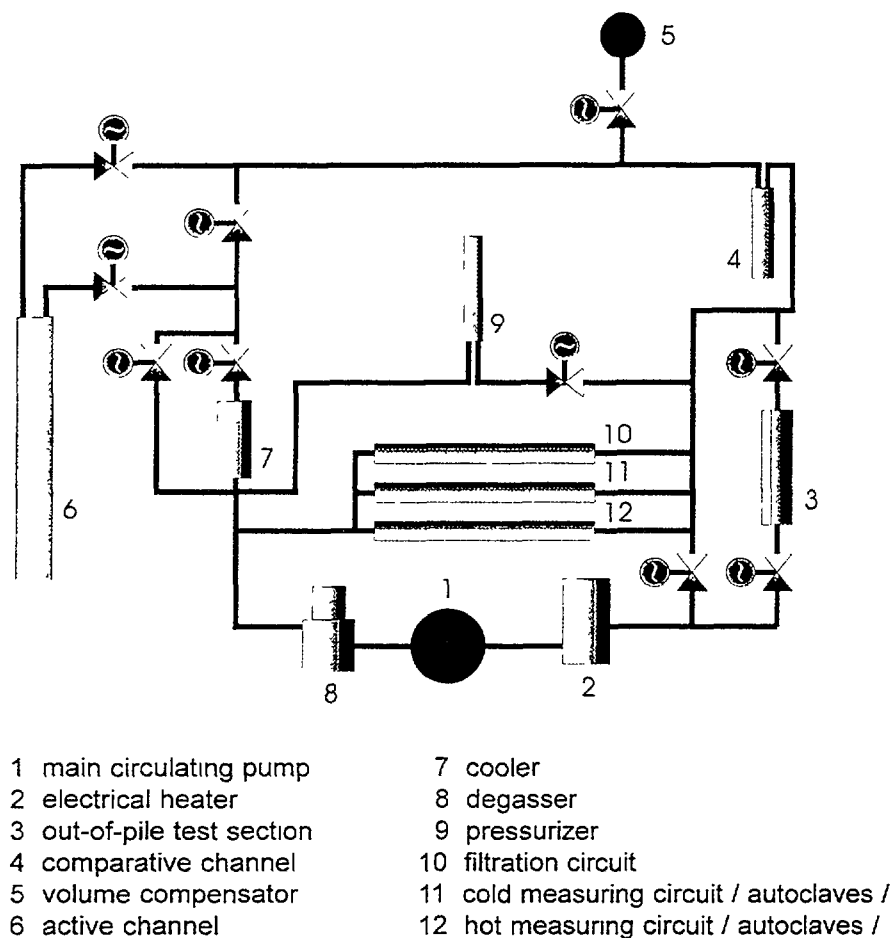


**Fig.1** Schematic layout of the reactor water loop RVS-3

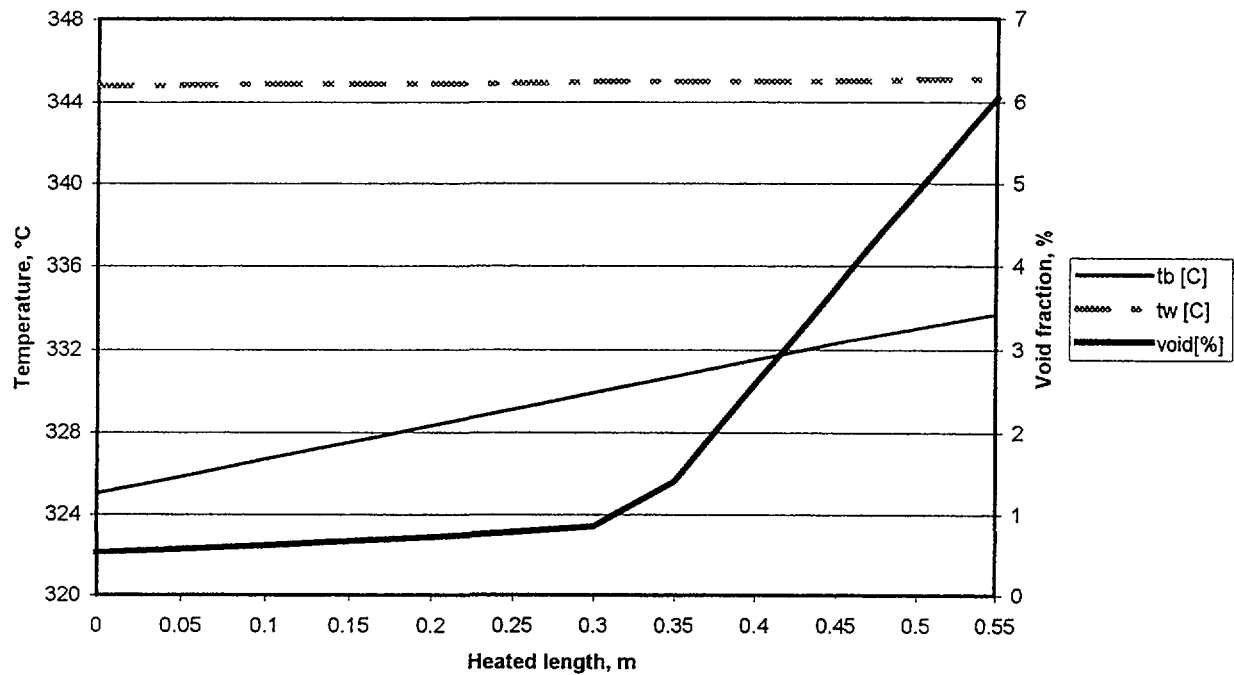


**Fig.2** Distribution of the coolant temperature ( $t_b$ ), cladding surface temperature ( $t_w$ ) and void fraction along the RVS-3 loop heated test section

experiment. Dissolved hydrogen was kept in concentration range of 20-25 ccSTP/kg. Hydrogen gas dosing was applied here to meet the specification. Calculated  $pH_{300}$  gives value of 7.58. Oxygen concentration was below 5 ppb (an on-line measurement by Orbisphere analyser).

During the experiment, a purification system worked with flow rate of 200 kg/hr, that is approximately 5% of the total primary circuit flow. The purification system consisted of one mixedbed resin that was permanently in operation, one cation resin for alkalinity control and two mechanical filters (at the inlet and outlet of the purification system).

Thermal-hydraulic parameters and water chemistry conditions in the RVS-3 loop test section during the experiment are summarized in Table 1.

**Table 1 - THERMAL-HYDRAULIC PARAMETERS AND WATER CHEMISTRY  
CONDITIONS IN RVS-3 LOOP TEST SECTION**

Parameter / Specification	Value
Pressure, MPa	15.0
Test section temperature, °C	325-335
Heat flux, W/cm <sup>2</sup>	100.0
Void fraction (calculated), %	6.0
Coolant flow rate, tons/hr	3.85
Flow velocity in test section, m/s	1.2
Test duration, hours	500
Boric acid, g/kg (Boron, ppm)	3.7 650
Lithium, ppm	5.0
Hydrogen, cc STP/kg	20 - 25
Oxygen, ppb	< 5
pH @ 300°C (calculated)	7.58

### 3. EXPERIMENTAL OBSERVATIONS AND ANALYSIS

#### 3.1 CORROSION PRODUCT DEPOSITS

Crud deposits on the Zr cladding surface were observed mainly on the heated part of the fuel rod immitator, ie. in length of 560 mm. Visual inspection showed that in the bottom region of the heated part only a black, easy removable, loose deposit was found. In the upper region, where subcooled boiling area was expected, a black heavy deposit with some “white” spots was found. More detailed investigation showed that the “white” spots are places where the deposits were spalled from the cladding surface.

Both, the loose and heavy deposits were sampled for further investigation by a various techniques and methods. A number of analysis was conducted to identify an origin and characteristics of the corrosion products deposited on cladding surfaces. The following devices were employed for analysis of solid phases: SEM - scanning electron microscopy (Tesla BS-350, Czech Republic) with Philips EDAX chemical analysis, TEM - transmission electron microscopy (Philips EM201, the Netherlands, 80 kV), XRD - X-ray diffraction (Siemens D5005, Germany, CuK $\alpha$  line emission), and Mössbauer spectroscopy (KFKI Budapest, Hungary,  $^{57}\text{Co}$  source).

#### *SEM and TEM analysis*

The loose deposits were sampled for further analysis by various techniques. A SEM picture of corrosion product deposits in the bottom region is shown in Fig. 3. It can be seen from the picture

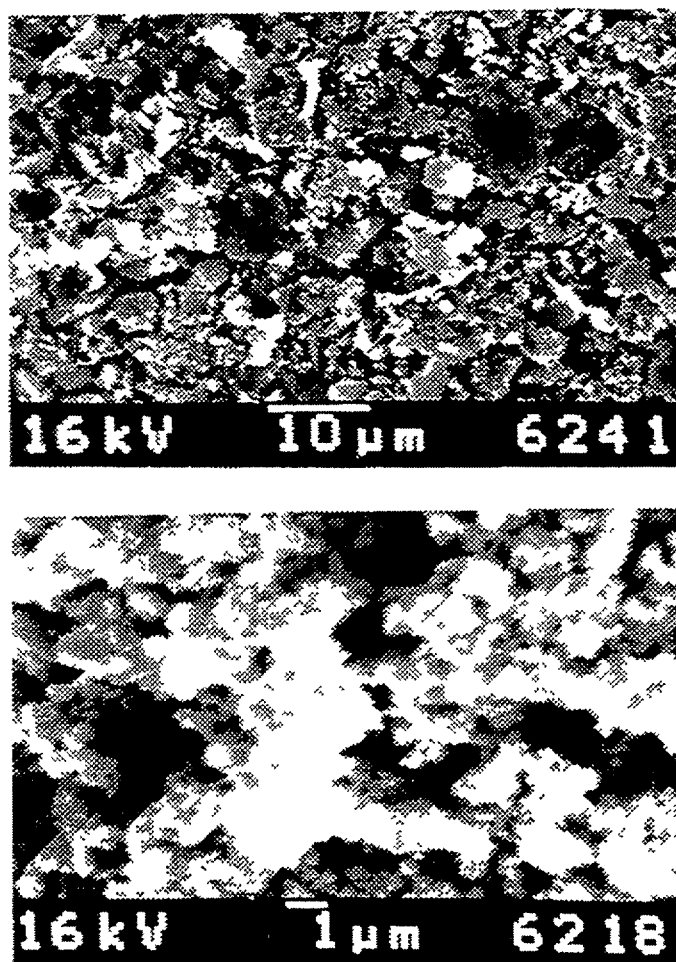


Fig.3 SEM picture of corrosion products deposited on cladding surface in RVS-3 loop - loose black deposits

that the deposit consists of fine particles with diameter of 1-5  $\mu\text{m}$ . TEM pictures of the crud deposited in the bottom region (Fig. 4) showed octahedral crystals of magnetite and some amorphous particles.

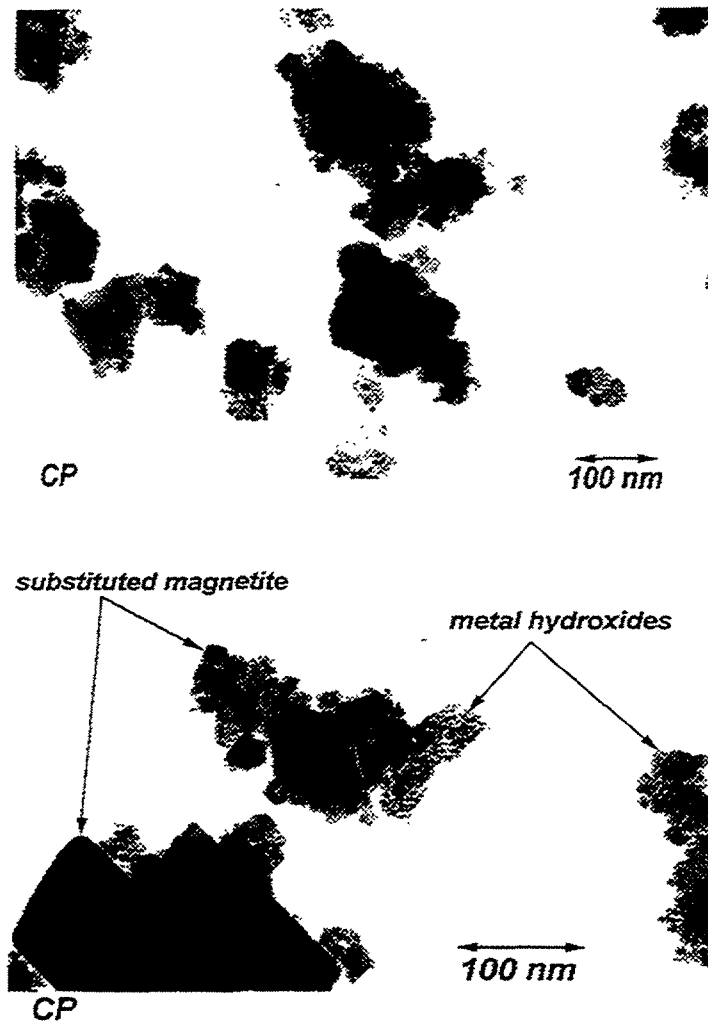


Fig.4 TEM picture of corrosion products deposited on cladding surface in RVS-3 loop

A sample of spalled deposits from the upper region was also taken and analysed. SEM pictures of the spalled layer are shown in Fig. 5. The picture No.5978 shows a “chimney” structure of the deposit which is supposed to be related to boiling phenomena. The picture No.5979 shows cross section of the spalled material. However, the orientation of the sample is not perpendicular what makes it difficult to determine thickness of the deposits (may be about 10 $\mu\text{m}$ ). The coolant/oxide interface is in the upper part of the picture.

#### EDAX analysis

Elemental composition of the deposits on the cladding surface was analysed by EDAX technique. Summary of the EDAX results and their comparison with the base material composition is given in Table 2. It is clear from the results that the deposits are enriched with chromium and depleted in nickel in comparison with the base material. Elemental composition of the loose and heavy deposits is almost the same taking into account a limited number of analysis and precision of the method. Rather higher Cr and Ni content in heavy deposits in the subcooled boiling region is

probably due to a spread of data. In some samples silica peak was identified at EDAX analysis and silica content was determined at 0.5-1.5 wt% level.

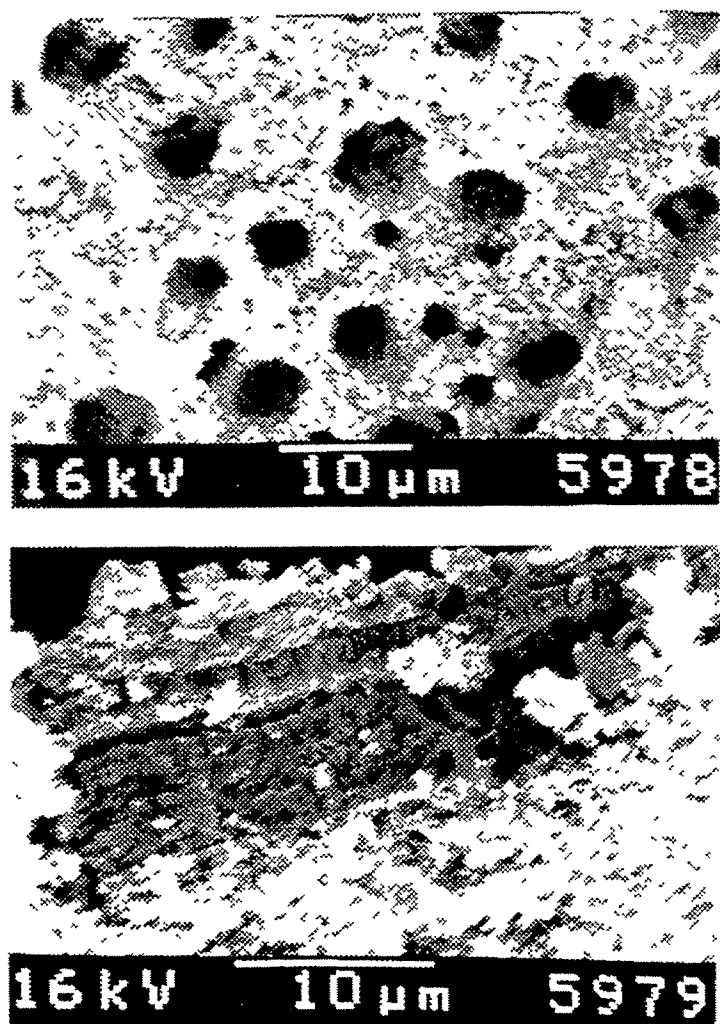


**Fig.5** SEM picture of corrosion products deposited on cladding surface in subcooled boiling area - heavy deposits

**Table 2 - ELEMENTAL COMPOSITION OF DEPOSITS  
ON CLADDING SURFACES**

Sample ID	Elemental composition, wt% (EDAX)				Sample description
	Fe	Cr	Ni	Si	
5900	70.8	24.5	4.5	n.a.	loose deposits
5901	75.6	20.8	3.5	n.a.	loose deposits
5902	81.7	13.7	4.6	n.a.	loose deposits
5903	78.6	16.0	5.4	n.a.	loose deposits
5966	65.3	26.3	8.4	n.a.	heavy deposits
5963	61.4	27.5	11.1	n.a.	heavy deposits
5978	73.3	21.7	5.0	n.a.	heavy deposits
6218	68.2	23.1	8.2	0.5	loose deposits
6219	69.2	21.5	8.2	1.1	loose deposits
6217	68.8	20.7	9.0	1.5	loose deposits
Base material	70	18-19	10-11		

## ***Mössbauer and infrared spectroscopy***

Mössbauer and infrared spectrum of the black loose deposits was analysed. Mössbauer spectroscopy identifies non-stoichiometric magnetite  $\text{Fe}_3\text{O}_4$  (sextets Ma and Mb) with some presence of normal spinel of  $\text{Fe}_x\text{Cr}_{3-x}\text{O}_4$  or  $\text{Fe}_x\text{Cr}_{2-x}(\text{Ni})\text{O}_4$  type. Infrared spectroscopy reveals non-stoichiometric spinel  $\text{Fe}_{3-x}\text{Cr}_x\text{O}_4$  ( $x < 1$ ) with a possible presence of Ni.

## ***AAS analysis***

A sufficient amount of sample of the loose black deposit was taken from the cladding surface for AAS analysis. Result of the AAS analyse confirms presence of Fe in amount of 19.6 mg of the taken sample, Cr (4.16 mg) and Ni (2.30 mg). Some small amount of lithium (only 0.022 mg) was also detected in the deposits what means that Li/Fe ratio is very low – about  $10^{-3}$ .

## ***X-ray diffraction analysis***

A sample of the black loose deposits was analysed by XRD. Three phases were revealed by XRD: a spinel ferrite, the most likely Ni-substituted magnetite,  $\text{ZrO}_2$ , and chromic hydroxide. Unlike the ferrite and  $\text{ZrO}_2$ , chromic hydroxide occurs very rarely in “normal” corrosion products. The presence of strongly hydrated Cr-species may indicate a fast corrosion attack of non-passive stainless steel surfaces in the RVS-3 loop, ie. dissolution of steel via soluble intermediates. The XRD result showing presence of chromic hydroxide in the crud deposits on the RVS-3 loop cladding surfaces confirms information obtained from TEM pictures (Fig. 4). The TEM pictures of crud deposits from the RVS-3 loop were very similar to those obtained from ageing tests of synthetic corrosion products conducted in autoclave where an amorphous phase was detected by XRD as chromic hydroxide [1].

## **3.2. CORROSION PRODUCTS IN THE COOLANT**

The primary coolant samples were taken from the RVS-3 loop by isokinetic sampling line during the experiment. A liquid sample of the loop coolant in volume of 200-500 cc was passed through a microfilter with porosity of  $0.45\ \mu\text{m}$ . Corrosion products analysed in filtrate were identified as soluble species, corrosion products collected on the microfilter as insoluble species. Soluble corrosion products were analysed by ion chromatography (IC) and ion-coupled plasma (ICP) methods. A DIONEX 500 device and ICP-OEM device were employed. Insoluble corrosion products were collected on the microfilters (SYNPOR with porosity of  $0.45\ \mu\text{m}$ ) and analysed by AAS after the microfilter dissolution. The microfilters were also dried and weighed after the sampling to determine so called “suspended solids”, ie. total amount of material collected on the microfilter.

## ***Soluble and insoluble corrosion products***

Concentrations of soluble and insoluble corrosion products circulating in the RVS-3 loop primary coolant at the experiment are given in **Table 3**. It can be seen from the table that concentration level of soluble corrosion products is influenced by coolant temperature and the loop operation conditions, ie. transient or steady state operation. Higher concentrations can be detected at transient conditions than at steady state operation. Concentration of soluble Fe in the RVS-3 loop coolant is in order of tens of ppb (hundreds ppb at transients); soluble Ni, Mn and Cr in units of ppb and soluble Co in tens of ppt. Concentration of insoluble corrosion products is similar to that of soluble species.

## ***Suspended solids***

Concentration of suspended solids in the loop coolant, ie. amount of material collected on the microfilter of  $0.45\ \mu\text{m}$  porosity, varied between 0.4 and 2.0 ppm. Again, a significant effect of the loop operation mode (transient/steady state conditions) is apparent. A discrepancy observed between



**Table 3 - CONCENTRATION LEVEL OF SOLUBLE AND INSOLUBLE  
CORROSION PRODUCTS CIRCULATING IN RVS-3 PRIMARY COOLANT**

**Soluble corrosion products**

Sample ID	Concentration of soluble CP, ppb						Note	
	Fe <sup>2+</sup>	Fe <sup>3+</sup>	Ni	Mn	Co	Cr	Temperature, °C	Method
1	24.6	1.3	1.1	1.3	0.03	-	120 (transient)	IC
2	56	34.8	20.3	1.6	0.28	-	250 (transient)	IC
3	2.6	1.8	1.0	0.2	0.03	-	250 (steady)	IC
4	65	3.6	2.9	1.8	0.05	-	250 (transient)	IC
5	4.9	2.7	13.7	1.0	0.05	-	250 (transient)	IC
6	10.1	3.1	2.4	0.2	0.06	-	330	IC
7	7.3	3.2	0.9	0.2	<0.02	-	330	IC
8	10	0.9	1.4	0.8	0.11	-	330	IC
9	6.5	1.7	0.2	0.3	0.03	-	330	IC
10 11 12 13 14	Fe		Ni	Mn	Co	Cr	100 (transient) 275 (steady) 260 (transient) 320 330	ICP
	330		35.4	-	0.04	4.2		
	18		0.4	-	<0.02	<0.1		
	93		15.6	-	0.03	4.6		
	22		6.3	-	<0.02	6.7		
	28		0.7	-	0.06	<0.1		

**Insoluble corrosion products (from microfilter)**

Sample ID	Concentration of insoluble CP, ppb					Note	
	Fe	Ni	Mn	Co	Cr	Temperature, °C	Method
1	325	33	2.7	<1	80	250 (transient)	AAS
2	27.5	1.5	<1	<1	6.7	320	AAS
3	47	5	<1	<1	12	320	AAS
4	14.5	<1	<1	<1	8.2	320	AAS

concentration of suspended solids and insoluble corrosion product species could be explained by a presence of boric acid in removed material.

### **Silica**

Silica level was also checked in the experiment. Concentration of silica was found to be in range of 0.3-1.0 ppm. In several samples even higher silica content (up to 2-5 ppm) was found. Many effort was spent to identify a source of silica in the RVS-3 loop primary circuit. We concluded that there is some silica source inside the loop primary circuit because silica content in the make-up water was found to be below 10 ppb. However, many flushes according to a special procedure did not improve the situation.

## **4. DISCUSSION OF RESULTS**

We suppose deposit on the cladding surfaces originates from corrosion products of the structural materials, and it is evident that this corrosion product deposit was formed by precipitation mechanism from the coolant. An important factor influencing mass transfer processes between a cladding surface and the coolant was found to be local thermal-hydraulic conditions - a cladding surface temperature and a void fraction. The higher surface temperature the more intensive mass transfer processes and deposit formation. A minimum amount of deposits was found on a non-heated part of the fuel rod immitator where the cladding surface temperature is equal to the coolant temperature. A sufficient heat flux in the heated part resulting in a temperature gradient between the cladding surface and the coolant led to formation of heavier corrosion product deposits. The heaviest deposit was observed in a region where subcooled boiling was supposed. This deposit was characterised by a chimney structure which is related to the vapour bubbles generation and escape from the surface.

Analysis of the deposits and corrosion products circulating in the loop coolant shows almost the same elemental composition in the both cases and confirms a hypothesis that these deposits are formed by the corrosion products from the coolant by a precipitation mechanism. The corrosion product deposits consist mainly of iron, but chromium content is surprisingly high in the both cases, even in comparison with the base material. As was identified by XRD and TEM analysis, chromium occurs in the deposits as a nanocrystalline, colloidal formation of chromic hydroxide. In the loop coolant, chromium is present mainly in insoluble form, ie. as a formation which is collected by a 0.45  $\mu\text{m}$  microfilter.

Generally, it is supposed in a classical model of stainless steels corrosion (solid state diffusion model) [2] that chromium tends to form a protective passivation film on stainless steel surfaces, ie. remains in the corrosion layer, and is minimally released into the coolant. This kind of behaviour was confirmed in a number of loop experiments where a Cr-rich passivation layer was observed on inner loop surfaces [3]. Analysis of crud deposits, which were formed on surfaces of the fuel assembly spacer grids of Loviisa 2 unit (VVER-440) by a precipitation from the coolant, showed iron as a dominant element and chromium content less than 1 wt% [4]. At the same time, the structural material used at this unit was the same as at the RVS-3 loop.

The above mentioned means that formation of the heavy corrosion product deposits on the Zr cladding surfaces in about 20 days and the higher presence of Cr in deposits and corrosion products in the coolant can be attributed to adverse corrosion behaviour of the loop itself. The presence of strongly hydrated Cr-species may indicate a fast corrosion attack of non-passive stainless steel surfaces in the RVS-3 loop, ie. dissolution of steel via soluble intermediates. Such a corrosion attack could indicate destabilization or even destroying of a passive film formed in the past on the loop inner surfaces.

A presence of silica in the coolant together with presence of magnesium, aluminium and calcium may, in some particular case, cause a formation of zeolites on the cladding surfaces [5]. In our case, except silica no other constituents were found in the deposits. Concentration of magnesium, aluminium and calcium in the loop coolant were below 10 ppb. A chemical form of silica was not determined by available analysis.

## 5. CONCLUSIONS

A reason for the crud deposit formation on Zr cladding surface has not been fully identified and understood, but it is obvious that this process relates to a quality of the loop primary coolant, and local thermal-hydraulic conditions. It is also obvious that the presence of corrosion products in the deposits (Fe, Cr, Ni-species) can be affected by a corrosion behaviour of the loop itself. Moreover, the Cr content in the corrosion products and form of presence of Cr-species may indicate a corrosion attack of the loop inner surfaces via dissolution-precipitation mechanism which is attributed to corrosion of non-passive, naked surface of stainless steel [6,7]. Such a corrosion attack could indicate to destabilization or even destruction of a passive film formed in the past on the loop inner surfaces.

A cause for a possible passive film destabilization in the loop is not unambiguously identified, but several considerations can be given:

- The RVS-3 loop is in operation for more than ten years, ie. for several thousands of operational hours. It is supposed that a protective passivation film was formed on the loop inner surfaces in this period.
- In the past, the RVS-3 loop was operated at VVER water chemistry, ie. KOH/NH<sub>3</sub> chemistry. At this experiment, the loop chemistry was changed from VVER to PWR, ie. to LiOH/H<sub>2</sub>, for the first time. However, in spite of the change of main constituents the loop water chemistry remains alkalizing-reduction in its nature.

- Severe water chemistry conditions (5 ppm Li) of this experiment resulted in high high-temperature  $\text{pH}_T$  value ( $\text{pH}_{300} = 7.6$ ) with some possible effect on corrosion rate of stainless steel. However, it is demonstrated in the literature [2] that the corrosion rate of stainless steels should not significantly change in  $\text{pH}_T$  range of 6-8.
- A possibility for oxygen ingress into the loop system was also considered and analysed mainly in relation to chromium behaviour and its presence in the coolant. But, no realistic way for the oxygen ingress was found.
- Difficulties we met at the experiment realization caused a big number of pressure and temperature transients, and loop start-ups and shut-downs. Such an unstable loop operation led to an increased level of the corrosion products in the loop coolant, and consequently acts as a source material for the deposits.
- 

Finally, it is supposed that these loop transients can be considered as the most probable explanation of the observed situation. To avoid similar crud deposit formation on the cladding surfaces in the future, an improvement of the loop purification system was proposed and realized. A main feature of this improvement consists in an increase of the volume of ion exchange resin and utilization of a mechanical filter with finer porosity.

## REFERENCES

- [1] M.ZMÍTKO, et.al., "Hydrothermal reactions of corrosion products in reactor primary conditions", Water Chemistry in Nuclear Power Plants (Proc. JAIF Int.Conf., Kashiwazaki, Japan, 1998), JAIF (1998) 707.
- [2] J.ROBERTSON, in Corrosion Science, **32** (1991) 443.
- [3] J.KYSELA et.al., "Influence of hydrazine and higher pH on the corrosion product layer of austenitic steel", Water Chemistry of Nuclear Reactor Systems (Proc. 5<sup>th</sup> Int. Conf., London, 1989),BNES (1989) 97-104.
- [4] R.ROSENBERG et.al., "Investigation of iron deposits on the fuel assemblies of the Loviisa 2 VVER-440 reactor", Water Chemistry of Nuclear Reactor Systems (Proc. 7<sup>th</sup> Int. Conf., Bournemouth, October 1996) BNES (1996) 27.
- [5] PWR Primary Water Chemistry Guidelines: Revision 3, EPRI Report TR-105714, (1995)
- [6] R.WINKLER, "Oxide film formation in high-temperature water", Interaction of Iron Based Materials with Water and Steam, (Proc. Int. Conf. Heidelberg, Germany, June 3-5, 1992), GNS (1992) 211.
- [7] B.STELLWAG, Growth mechanism of oxide films on austenitic CrNi-alloys in high-temperature water, *ibid.* 6 230.

H.P. HERMANSSON, J. CHEN  
Studsvik Material AB  
Nyköping, Sweden

### **Abstract**

A case study of fuel crud composition and morphology from three different Swedish BWRs is presented. The objectives were to investigate elemental and radiochemical composition, distribution on crystalline and amorphous phases and furthermore to describe sub-layer formation, morphology and adherence to the underlying zirconium oxide and zircaloy.

The results clearly demonstrate that part of the crud is relatively loosely adhered and can be easily removed. Another, inner fraction is tightly adherent and requires the application of an abrasive agent to be removed. In some cases a relation is observed between crud thickness and zirconium oxide thickness.

Crud always contained Fe, Ni, Cr, Mn, U and Co. In a couple of cases also Cu, Zn and Zr were found. Spinel, hematite, uranium oxide and zirconium oxide were identified. Co-60 was the dominating corrosion product radionuclide. Close to the zirconium oxide, crud morphology exhibits a very well crystallized material, which is supposed to consist of nickel spinel or trevorite. On top of this inner layer there is often an outer, consisting of finely crystalline and/or amorphous material.

It is concluded that the application of rather straightforward methods of investigation has resulted in a fairly good characterization of the crud.

## **1. INTRODUCTION**

The objectives of this work were to characterize BWR fuel crud from three Swedish BWRs and to discuss crud composition and morphology.

The work also comprised application and development of methods for sampling and analyses of crud. Those techniques were then used for the determination of elemental and radiochemical composition, studies of morphology, layer formation and adherence to underlying zirconium dioxide/Zircaloy. Furthermore, crystalline and amorphous phases present in the crud were investigated. Similar investigations were earlier performed, i. a. by Hoshi *et al.* [1].

## **2. EXPERIMENTAL**

### **2.1 Fuel pins**

Studies were carried out on a limited material of three fuel pins. One pin was taken from each of the Swedish BWRs Ringhals 1 (R1), Forsmark 2 (F2) and Forsmark 3 (F3). Fundamental data for the pins used are accounted in Table 1. Because of heavy radiation, the fuel was taken away before extracting crud samples from the pins.

All samples were extracted in the Studsvik Hot Cell Laboratory using concrete cells and manipulators for radiation protection. It was demonstrated that relatively straightforward methods for sampling and analysis of crud could be used to achieve a fairly good characterization.

TABLE I. FUNDAMENTAL DATA FOR INVESTIGATED FUEL PINS

Reactor	Water chem.	Bundle pos.	Cladd. Mtrl.	Pin nr.	Fuel type	Exp. time, y
Ringhals 1	HWC	14630/F5	LK2	120-20725	SVEA-64	7
Forsmark 2	NWC	16468/H8	LK2	166-20285	SVEA-64	6
Forsmark 3	NWC	14593/H2	LK2	119-21328	SVEA-64	3+2

According to the analytical purposes, crud was sampled in four different ways at three positions (top, middle and bottom) of the pins. See Figure 1. One method comprised cutting the sample into a cladding ring; another wiping a piece of cotton with or, the third without a grinding agent over a controlled area of the pin; and the fourth pressing a double-sided adhesive tape against the surface of the pin. The experimental details are as follows.

## 2.2 Ring samples

Ring samples were prepared for studying cross-section microstructures of crud by scanning electron microscopy (SEM). Three ring samples were cut, one from each fuel pin. Original samples were 4 mm in length and taken at 1900 mm from the bottom of the pin. See Figure 1. The rings were molded in vacuum into epoxy resin. Thereafter a thin disk was cut of which a small piece was prepared for further analyses. The samples were covered with gold before investigations. Nickel plating was not done in this case as the Fe/Ni ratio in the crud was of primary interest. In the R1 case the preparations were less successful, probably depending on previous loss of crud in the handling procedures. Ring samples from F2 and F3 were, however, successfully produced.

The strong radiation from the samples implied the above-mentioned cutting of small pieces of the rings for further investigation. One such a small piece from each ring was investigated. The intensity of the radiation nevertheless implied that the detector of the energy dispersive spectrometer (EDS) in SEM was moved to the most distant position. As a result of this, lighter elements such as oxygen could not be analyzed. However, the relative X-ray intensities of heavier elements could still be determined.

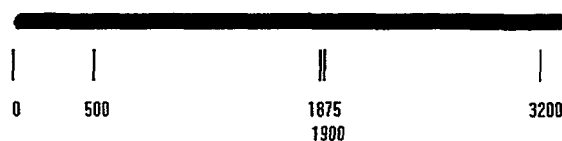


FIG. 1. Sampling positions for crud on a fuel pin. Ring samples were taken at 1900 mm from the bottom (denoted as "middle"). Wiped and taped samples at 500 ("bottom, b"), 1875 ("middle, m") and 3200 mm ("top, t"), from the 0-bottom respectively.

## 2.3 Wiped and taped samples

Wiped samples of crud were taken for both X-ray powder diffraction analyses (XRD) and elemental composition analysis with an inductively coupled argon plasma emission spectrometer (ICP). They were from the same pins as the ring samples but taken in three different places. See Figure 1. Three different methods were used: A piece of cotton impregnated with glycerol and a piece of cotton with a mixture of glycerol and  $\text{Al}_2\text{O}_3$ , respectively, were wiped over the surface by holding the piece of cotton with a manipulator against the rotating cladding cylinder.

The two different types of cotton samples were taken in order to separate loosely adhered (cotton + glycerol) and tightly adhered (cotton + mixture of glycerol and  $\text{Al}_2\text{O}_3$ ) crud in the same position on the fuel pin. The loosely adhered crud was sampled over a slightly larger area than the

tightly adhered, which was sampled within the sampling area of the loosely adhered. The area of the cylindrical sampling surfaces was estimated from photographs.

In order to study the morphology and composition of crud particles on the outer surfaces of the cladding, tape samples were made using double sided, electrically conducting tape especially suitable for SEM-investigations. Those samples were taken just outside the cotton-sampled area.

## 2.4 Analyses

Ring and taped samples were used to study morphology, layering, thickness and adhesiveness of crud in SEM.

XRD was used to elucidate the crystalline phases present in loosely adhered crud. A Guinier-camera using copper ( $\text{Cu}_{K\alpha}$ ) radiation was employed. The film was then read electro-optically using a laser scanner. Quantitative XRD was achieved with "matrix flushing" methodology. The reference data ( $I/I_{\text{Cor}}$ ) were chosen directly from the JCPDS database.

Elementary analyses were performed with SEM/EDS and ICP. SEM/EDS was performed on taped samples and ICP on wiped. It was judged that samples containing  $\text{Al}_2\text{O}_3$  (tightly adhered crud samples) could not be analyzed in ICP.

Radiochemical analyses were performed with  $\gamma$ -spectrometry using both types of wiped samples.

## 3 RESULTS

### 3.1 Ring samples

Before the ring samples were ready for SEM investigation, the fuel pins had been subjected to normal nuclear fuel handling routines, which could be hazardous for the crud integrity. This could have influenced the crud in different ways. In one example (Ringhals 1) it is quite obvious that crud has been partly detached from the fuel pin surface during this handling procedure. It should thus be kept in mind that all pins could be more or less influenced, however evident only in the R1 case.

Crud thickness was determined for all pins. The measured thickness varies from a few up to some fifty micrometers. In Figure 2, an example from F2 is given of SEM photos of the crud. It can be seen that the crud is situated outside a layer of zirconium dioxide (darker broad band) which in turn is situated outside the Zircaloy (brighter area).

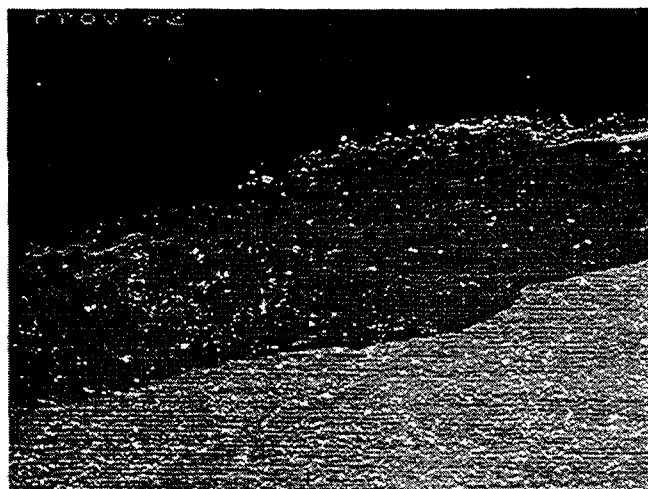


FIG. 2. Cross-section SEM photo of a ring sample from F2, 390x.

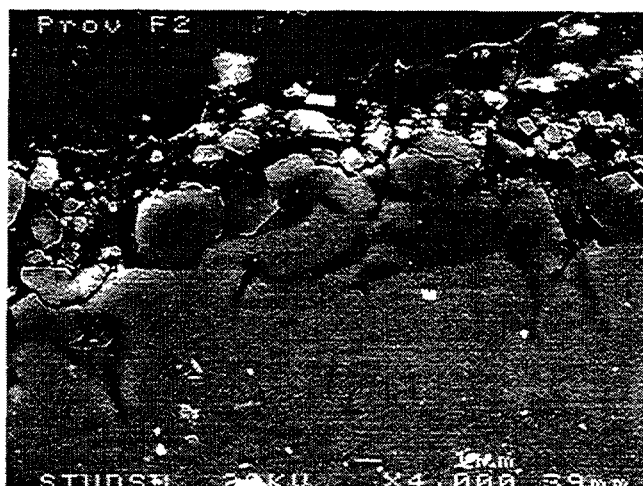


FIG. 3. Cross-section SEM photo of crud from F2, 3060x.

At higher magnifications, see Figure 3, crystals can be observed that quite well coincide in geometry and composition with the observations made on samples with loosely adhered crud. See the following. The material is well crystallized and to a mayor part composed of iron and (oxygen) with some nickel and some times also chromium present. In the F2 case there are traces of zinc and copper. See Figure 4 for an example of elementary analysis on F2 crud with SEM-EDS, performed on well-crystallized crystals in the inner sub-layer as seen in Figure 3.

No distinct layering was seen in the crud. However, layers probably of outer loosely adhered and inner tightly adhered crud can be roughly defined. In the F2 case three zones or sub-layers can be seen. See Fig. 3. There are also indications of layering in the F3 case. The inner zone in F2 comprises well-crystallized crystals containing iron and nickel. Furthermore there is zirconium, manganese and zinc present. The inner layer also seems to form a transit zone between the crud and the zirconium dioxide as deep cracks in the oxide seems to be filled with crud forming a large contact area.

In the R1 case, a part of the crud was, as already mentioned, lost probably due to previous fuel handling routines. In some cases there was, however, still some crud present and EDS-analyses indicate that the well crystallized grains normally seen contain mainly iron and nickel.

The concentration of "trace" elements such as copper and aluminum seems to increase outwards. The outermost parts of the crud-layer gives an amorphous or finely crystalline impression, in which nickel and chromium were not seen.

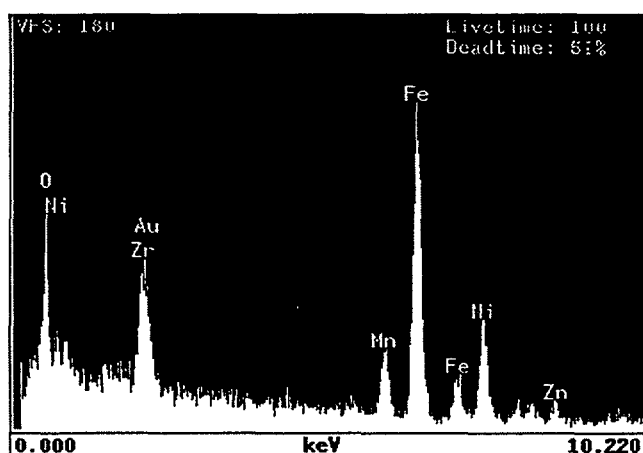


FIG. 4. EDS result on the inner layer of well-crystallized grains from F2 as shown in Fig. 3.

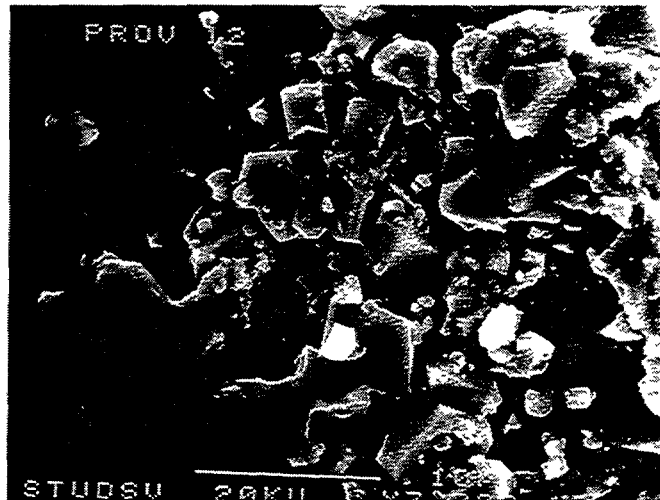


FIG. 5. Taped crud from the top of F2, 2350x.

The integrated picture of the crud would be a relatively well crystallized innermost layer, possibly containing large volumes of voids. See Figure 3. Further out, at least in the F2 crud, the outer layer seems to contain mostly iron oxide with an amorphous or very finely crystalline material crisscrossed with cracks that could originate from drying of the sample. A similar morphology could also be seen in the F3 crud.

For R1 ring samples most of the crud was probably lost during the fuel handling procedure. The crud consists mainly of scattered remains on top of the zirconium dioxide. There is no outer finely crystalline or amorphous layer at all as found in the F2 case.

### 3.2 Taped samples

In all, nine taped samples were investigated in SEM. Well formed crystals of different sizes were seen together with finely crystalline or amorphous fragments. A large part of the well-formed crystals had an octahedral-like geometry, typical for spinels [2]. See Figure 5.

EDS analyses showed that the major part of the crystals was composed of iron, often with a presence of nickel and sometimes also with chromium and manganese. See Figure 6 for an EDS analysis on an octahedrally shaped crystal from the middle of the F2 pin. Traces of uranium and silicon could also be observed in some cases. Uranium is probably a contaminant from the hot cell environment.

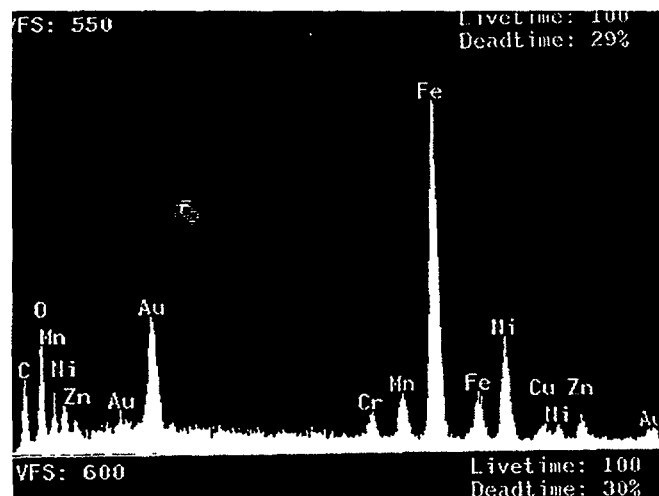


FIG. 6. EDS result on octahedrally shaped crystals from the middle of the F2 pin.



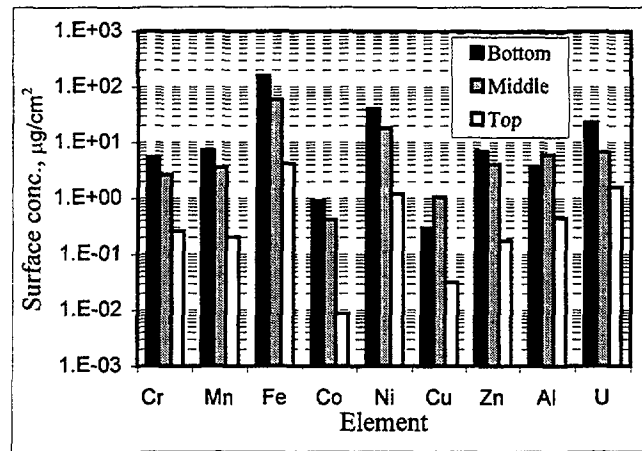


FIG. 7. Surface concentration of elements in loosely adhered crud from F2,  $\mu\text{g}/\text{cm}^2$ .

The largest deviation that could be observed in SEM between the pins is the difference in crystal size in the crud, as exemplified in Figure 5. The largest and most well formed crystals were found on the F2 pin, and crystals were of the same size on all three sampling points. On the other pins, the higher the sampling point the larger the crystals. Only the largest of those had the same crystal-size as on the F2 pin.

### 3.3 Chemical composition of loosely adhered crud

Two types of samples for chemical analysis with ICP were taken in the three positions of each pin. One type is for loosely adhered crud and the other for tightly adhered. Because of problems with the analyses of tightly adhered crud (see above) there are only data available for the loosely adhered.

Elemental iron ( $\approx 100 \mu\text{g}/\text{cm}^2$ ), nickel ( $\approx 10 \mu\text{g}/\text{cm}^2$ ) and uranium ( $\approx 10 \mu\text{g}/\text{cm}^2$ ) dominate the loosely adhered crud on all pins investigated. The noted are max-values and lower surface concentrations can also be found. For R1 the scatter is small in element concentration values between the different positions. The scatter is large for F2 and F3 and largest for F2. The element concentrations vary in different manners in the different pins and are smallest in the top part of the F2 pin. Assuming that all nickel is in the trevorite phase, the relative weight ratios of trevorite to hematite phases in crud from the top parts of R1, F2 and F3 pins are estimated to be 0.6, 1.4 and 1.5, respectively.

The relations between the different elements are similar for the different positions. This fact indicates that the composition of the loosely adhered crud seems to be about the same independently of pin position (core height). However, the element concentration varies with core height especially in F2 and F3. An example of element concentrations for F2 is shown in Figure 7.

In Figure 8 a set of elemental quotients in loosely adhered crud are shown. It can be seen that the Fe/Ni quotient in F2 and F3 is about 3 with a slight core height variation. In R1 it is higher or about 5 and there is also a slight variation with core height. The highest quotient is found in the bottom and the smallest in the top. The quotients Mn/Fe, Co/Fe and Co/Ni are relatively constant with core height in all reactors. The last two vary in parallel but the Mn/Fe quotient has a different behavior.

### 3.4 Chemical composition of tightly adhered crud

As already mentioned the tightly adhered crud was not analyzed with ICP. A simple comparison was, however, made between the tightly and loosely adhered crud, using specific activities (evaluated below). It could then be estimated that elemental iron should also dominate the tightly adhered crud ( $\approx 300 \mu\text{g}/\text{cm}^2$ ), closely followed by nickel ( $\approx 100 \mu\text{g}/\text{cm}^2$ ). Those are maximum values for all cases. It should, however, be emphasized that the values are not precise.

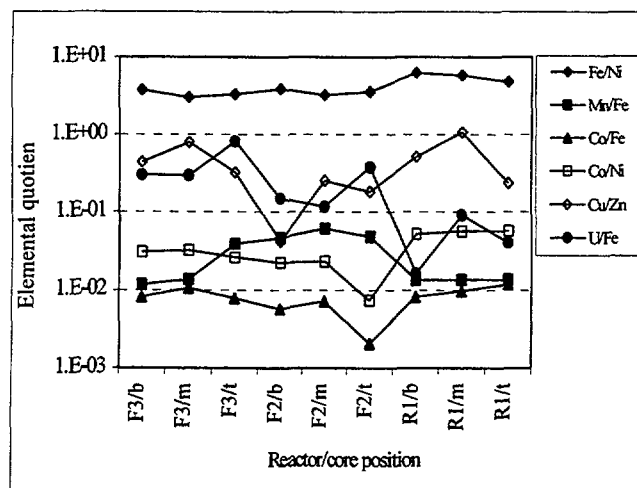


FIG. 8. Elemental quotients in loosely adhered crud. All reactors. b=bottom, m=middle, t=top.

### 3.5 Total chemical composition

Iron and nickel dominate the crud composition in the levels of about  $300 \mu\text{g}/\text{cm}^2$  for iron and  $100 \mu\text{g}/\text{cm}^2$  for nickel. In the case of F3 and R1 samples the scatter per element is small. In the case of F2 the amount of crud is smallest at the top position and larger at the middle and bottom. The tightly adhered crud may thus constitute the main part of the total crud layer.

### 3.6 X-ray diffraction

Loosely adhered crud from all positions was analyzed with XRD. Since only the crystalline phases give diffraction lines, the results could not be used to estimate the possible amorphous phases in the crud. The differences in crystallite size observed between pins in SEM did not give any significant influence in XRD pattern.

Hematite ( $\text{Fe}_2\text{O}_3$ ) and  $\text{NiFe}_2\text{O}_4$ , or more generally  $\text{Me}_x\text{Fe}_{3-x}\text{O}_4$  ( $\text{Me}=\text{Ni}, \text{Cr}, \text{Mn}, \text{Zn}, \text{etc.}$ ) are present in all samples. Varying amounts of nickel, chromium and other metal cations were found in all samples. As nickel is the second largest constituent of crud, nickel ferrite ( $\text{NiFe}_2\text{O}_4$  or  $\text{Me}_x\text{Fe}_{3-x}\text{O}_4$ ) is probably the main spinel phase in which other metal cations can form solid solution. Goetite ( $\alpha\text{-FeOOH}$ ) and lepidochrochite ( $\gamma\text{-FeOOH}$ ) or other crystalline compounds that could exist were not identified.  $\text{UO}_2$  was observed in almost all samples. However,  $\text{UO}_2$  is probably a contaminant from the hot cell environment. Three very weak diffraction lines, which might be assigned to the monoclinic  $\text{ZrO}_2$  phase, were detected separately in three crud samples from F2 and F3 pins respectively. The  $\text{ZrO}_2$  probably comes from the oxidized Zircaloy surface by wiping.

The solid solubility of ions in spinels of ferrite type is continuous and very large. However, as the cell dimensions were determined without calibration for these samples, the stoichiometry could not be settled from the XRD data.

The main difference in XRD results between the different pins is the estimated weight ratio of spinel to hematite phases. At the bottom of the F2-pin, the ratio was approximately 50:50. It was about 70:30 at both the middle and top positions. The ratio was 80:30 in all F3 positions. This means significantly less hematite than that in the F2 pin. The ratio was approximately 50:50 on all levels in R1, demonstrating a higher concentration of hematite compared with the Forsmark cases. The relative portions of hematite phase in all crud are higher than that estimated from ICP results. The general trend of both estimations is, however, similar.

It should be emphasized that the XRD results do not exclude the presence of other phases in the crud. Such phases should, however, appear in very small concentrations, as they are unable to generate visible diffraction lines.

### 3.7 Radiochemical analyses

The wiped samples were analyzed with  $\gamma$ -spectrometry. As already clarified two types of wiped samples were collected. One was on the loosely adhered and the other on the tightly adhered crud.

Analytical results were obtained as Bq/sample and nuclide. A combination of these data with measured sampling areas, and data from chemical analyses, were used to calculate the surface activity concentration per nuclide ( $\text{Bq}/\text{cm}^2$ ) in the crud. Specific activities ( $\text{Bq}/\text{g}$ ) were also calculated. Specific activities for tightly adhered crud could, however, not be calculated, as chemical analyses with ICP were not performed on such samples.

### 3.8 Radionuclides in loosely adhered crud

The specific activity of loosely adhered crud is of the order of  $10^3 - 10^7 \text{ Bq}/\mu\text{g}$ . Co-60/Co is largest, about  $10^7 \text{ Bq}/\mu\text{g}$  and Zn-65/Zn is lowest, about  $10^3 \text{ Bq}/\mu\text{g}$ . There is no main difference between sampling positions for the Forsmark cases. In the Ringhals case the specific activity is, however, larger at the top position compared with the bottom.

There is a general trend that the surface concentration of activity is the lowest at the top positions and the highest at the bottom. This is valid for Co-60 (about  $10^6 \text{ Bq}/\text{cm}^2$  at most), Co-57 and other commonly observed isotopes. The surface activity concentrations of other nuclides vary between stations. As an example, detailed data from F2 are shown in Figure 9.

### 3.9 Radionuclides in tightly adhered crud

The trends for Co-60 are the same in tightly as in loosely adhered crud. The surface concentrations are, however, higher in tightly adhered crud and in general of the order of  $8 \times 10^6 \text{ Bq}/\text{cm}^2$ . The difference between positions is minimal for F3 and R1 (all nuclides) but large for F2.

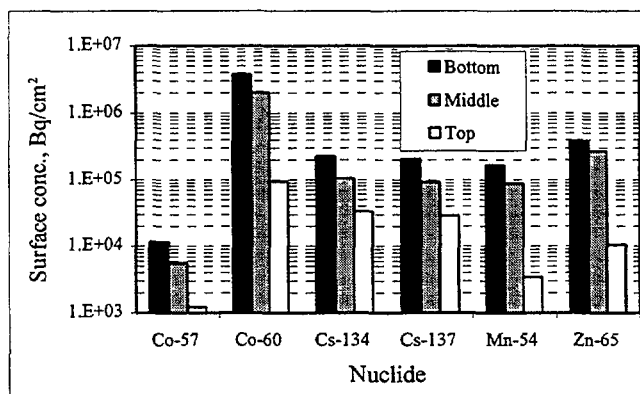


FIG. 9. Surface concentrations of radionuclides in loosely adhered crud from F2,  $\text{Bq}/\text{cm}^2$ .

## 4 DISCUSSION

### 4.1 Objectives, results and methods

The objectives, which have been well fulfilled, were to investigate elemental and radiochemical composition of the crud as well as distribution of elements on crystalline and amorphous phases.

Furthermore to describe sub-layer formation, morphology and adherence to the underlying zirconium oxide and zircaloy.

It should be kept in mind that this was a limited case study, comprising crud from three fuel pins from different Swedish BWRs. This fact of course limits the general applicability of the results, which would require data from a similar investigation on a larger fuel crud material, representing different operational backgrounds. Some specific as well as general conclusions about the crud could, however, be drawn and are discussed in the following.

One important result beside crud characterization itself is that the application of rather straightforward methods of investigation has resulted in a fairly good characterization.

## 4.2 Composition and morphology of crud

The SEM investigations show that the crud generally consists of an outer layer with very fine crystals or amorphous phase and an inner layer with relatively large, well-formed crystals. The two types can be present simultaneously, semi-separately or mixed with each other. The EDS-analyses show that the fine crystals contain largely iron and in some cases minor amounts of aluminum and copper. The well-formed crystals, on the other hand, mainly contain iron and nickel. Both hematite and spinel phases are observed by XRD. The latter means  $\approx \text{NiFe}_2\text{O}_4$  or trevorite at stoichiometric composition with the quotient  $\text{Fe/Ni} = 2$  and  $\text{FeCr}_2\text{O}_4$  or chromite at stoichiometric composition with the quotient  $\text{Cr/Fe} = 2$ . As the nickel concentration is normally 10 times larger than the chromium concentration, at least in loosely adhered crud, it is probable that the spinel phase observed by XRD is trevorite with, among others, chromium in solid solution.

A question mark remains for the tightly adhered crud, as it was not chemically analyzed with ICP. EDS analyses, however, support the assumption that the spinel observed in the tightly adhered crud to the largest extent would be trevorite. Beside the mentioned phases,  $\text{UO}_2$  and  $\text{ZrO}_2$  are also present according to XRD analyses. From several reasons it is suspected that  $\text{UO}_2$  is a chemical contaminant from the hot cell environment.

Goetite or other hydrated phases could have been formed in feed water and deposited onto the core region. They were, however, not observed by XRD. The reasons could be that 1) the relative amount of such phases is too small to be detected by XRD; 2) the phases are largely X-ray amorphous; and 3) the pins have been stored outside the reactor for several years. If present from the beginning, such phases could have transformed, for example, into hematite during the storage time. Furthermore, the transition rate into Goetite could have been rather large already during operational conditions. Goetite-like phases could also still be part of any amorphous material that could not be analyzed by the present method.

The integrated view from the analyses within the present project in combination with other information [2, 3] makes it reasonable to assume that the well-formed crystals with octahedral geometry are trevorite. The composition of the trevorite could vary within a wide range since it can form solid solution with other detected cat-ions. As hematite is one of the two main phases in crud, the fine crystals or amorphous phase may be mainly hematite. Accounted as an oxide with the formal composition  $\text{Fe}_2\text{O}_3:\text{NiFe}_2\text{O}_4 \approx 1:1$ , the analyses indicate a mean surface concentration of about  $0.4 \text{ mg/cm}^2$  of crud. This is consistent with other observation [3] on similar material.

In the case of F2, two zones or sub-layers and a transition zone can be seen in the crud. The inner zone seems to contain well-crystallized trevorite grains and contains iron and nickel. Furthermore there is manganese and probably zinc present, which is well in accordance with the ability of trevorite to add other elements in solid solution [4, 5]. The zirconium found in the inner layer may be an artifact induced by sample preparation or it may be the result of measurements near the rough crud/ $\text{ZrO}_2$  interfaces. The character of a transition state of the inner layer is evident in Figure 4. In the outer layer there are few well-crystallized crystals present but fine crystals or amorphous phase. Copper and aluminum have relatively high concentrations in the outer layer.

The presence of voids in the inner crud layer is obvious despite the compactness of the presumed trevorite crystals. The outer crud layer appears to be much more porous. The cracks in the crud could be either an artifact of sample preparation or due to drying. It is generally difficult to estimate the porosity.

Uranium and traces of silicon could be observed on all pins. Uranium probably originates from contamination from the hot cell environment. Silicon is assumed to originate from the constructional materials and the resin in the clean-up systems of the reactor. Silicon-containing phases could not, however, be identified by XRD, probably due to too low concentrations or presence in amorphous phases.

## REFERENCES

- [1] HOSHI, M., et al., "Residence time of crud on surfaces of channel box in JPDR", J. Nucl. Sci. Technol. **24(4)** (1987) 297-307.
- [2] BEVERSKOG, B., FALK, I., "Formation of large single crystals in reactor water", Rep. SKI 95:51, In Swedish.
- [3] HERMANSSON, H-P., "A model for calculation of hideout on BWR core surfaces", Rep. Studsvik/M-93/113, Studsvik Material AB, SE-61182 Nyköping, Sweden (1993), In Swedish.
- [4] BEVERSKOG, B., Studsvik Material AB, SE-61182 Nyköping, Sweden. Personal communication.
- [5] ÖSTERLUNDH, C-G., "Experimental study of cobalt up-take by trevorite and chromite with and without the presence of zinc. - Final report", Rep. Studsvik/M-95/36, Studsvik Material AB, SE-61182 Nyköping, Sweden (1995).

## ACKNOWLEDGEMENTS

Lotta Lind performed the technical work. Kurt Norrgård, Björn Claesson, Hans Bergqvist, Rikard Källström and Camilla Hansson all at Studsvik contributed with technical support and analyses. Allan Brown made part of the XRD analyses.

Barsebäck Kraft AB, Forsmarks Kraftgrupp AB, OKG Aktiebolag, Statens Kärnkraftinspektion, Vattenfall Ringhals AB and Studsvik AB raised funds for the investigations.

Individuals as well as organizations are gratefully acknowledged.



# POTENTIAL IMPACTS OF CRUD DEPOSITS ON FUEL ROD BEHAVIOR ON HIGH POWERED PWR FUEL RODS

W. WILSON, R.J. COMSTOCK  
Westinghouse Electric Company,  
Commercial Nuclear Fuel Division,  
Columbia, South Carolina,  
United States of America

## Abstract

Fuel assemblies operating with significant sub-cooled boiling are subject to deposition of surface deposits commonly referred to as crud. This crud can potentially cause concentration of chemical species within the deposits which can be detrimental to cladding performance in PWRs. In addition, these deposits on the surface of the cladding can result in power anomalies and erroneous reporting of fuel rod oxide thickness which can substantially hamper corrosion and core performance modeling efforts. Data is presented which illustrates the importance of accounting for the presence of crud on fuel cladding surfaces. Several methods used to correct for this phenomenon when collecting and analyzing zirconium alloy field oxide thickness measurements are described. Various observations related to crud characteristics and its impact on fuel rod performance are also addressed.

## 1. Introduction

Crud deposits on PWR fuel rods have been observed during visual examination of fuel assemblies. These observations contain several common features in terms of the amount and location of the deposits. Typically, the deposits are located in the upper spans of the fuel assemblies with the amount of crud being the highest in the high powered assemblies. Figure 1 shows a schematic diagram of a Westinghouse fuel assembly and the axial locations where crud deposits are typically observed.

The presence of crud impacts fuel rod performance in several ways. First, crud in the upper spans of the fuel rod interferes with eddy current probe measurement of oxide thickness on the fuel rod. The eddy current probe measures the offset from the underlying base metal and therefore provides a measure of oxide plus crud. In addition, the presence of crud can provide an additional thermal barrier resulting in an increase in the oxide-to-metal interface temperature and higher corrosion rates. Unless crud is properly account for, these effects can hamper corrosion modeling efforts. In addition, a relationship between Axial Offset Anomaly (AOA) and crud deposits has been observed.<sup>(1)</sup> The postulated mechanism is the concentration of boron within the crud due to sub-cooled boiling on high-power fuel.

Due to these impacts on fuel rod performance, Westinghouse initiated studies to characterize the nature and impact of crud deposits on fuel rod performance. The results of these studies are the subject of this paper.

## 2. Crud Characterization Studies

Characterization of crud deposits on PWR fuel rods was performed using several techniques. The simplest form of characterization was visual examination of the fuel rods to identify preferred locations on the rod where crud deposits form. Typically, a high magnification video image of the fuel rod is obtained during eddy current measurements of fuel rod oxide thickness. This video record of the fuel rod is reviewed to identify locations on the rod where crud is present and to segregate eddy current measurements which are potentially impacted by the presence of crud.

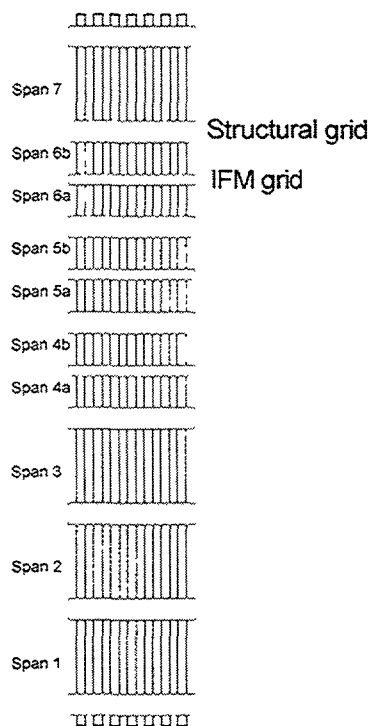


Figure 1: Schematic drawing of a Westinghouse PWR fuel assembly. Crud deposits are typically observed in spans 4 through 7.

A second means of assessing crud deposits was from crud scrapings as previously described [1, 2]. Surfaces of selected fuel rods were scraped in the spent fuel pool and particles of crud suspended in the spent fuel pool liquid were transferred into sample bottles via a vacuum system. The crud suspensions were then filtered and rinsed with de-ionized water to remove any boric acid remaining from the spent fuel pool liquid. Estimates of crud thickness were obtained from the crud mass, area of the crud scraping, and an assumed crud density of  $1.2 \text{ g/cm}^3$  [2].

Estimates of crud thickness were also obtained from measurement of the eddy current probe lift off both before and after the crud scraping. The initial measurement included the thickness of both the oxide and crud with the presence of crud confirmed visually. Following the removal of crud by scraping, the eddy current measurement of the oxide was repeated over the same area on the rod. The crud thickness was estimated by the difference between the two measurements. In addition, intact crud flakes were obtained during the scraping and sent to the hot cell for examination. Selected flakes were mounted on edge, metallographically polished, and examined in the scanning electron microscope (SEM).

A final assessment of crud and the impact of crud on corrosion was performed by sending fuel rods to the hot cell for destructive evaluation. The destructive examinations included cutting transverse cross-sections of the cladding for subsequent metallographic examinations. These examinations were performed to measure oxide thickness on the rod both in and away from crud-impacted areas on the rod. In addition, the thickness of crud was measured from the metallographic samples.

### 3. Results

Video images of crud deposits on PWR fuel rods are shown in Fig. 2. The lower magnification image in Fig. 2a shows the presence of crud in Span 6a of a fuel assembly. The higher

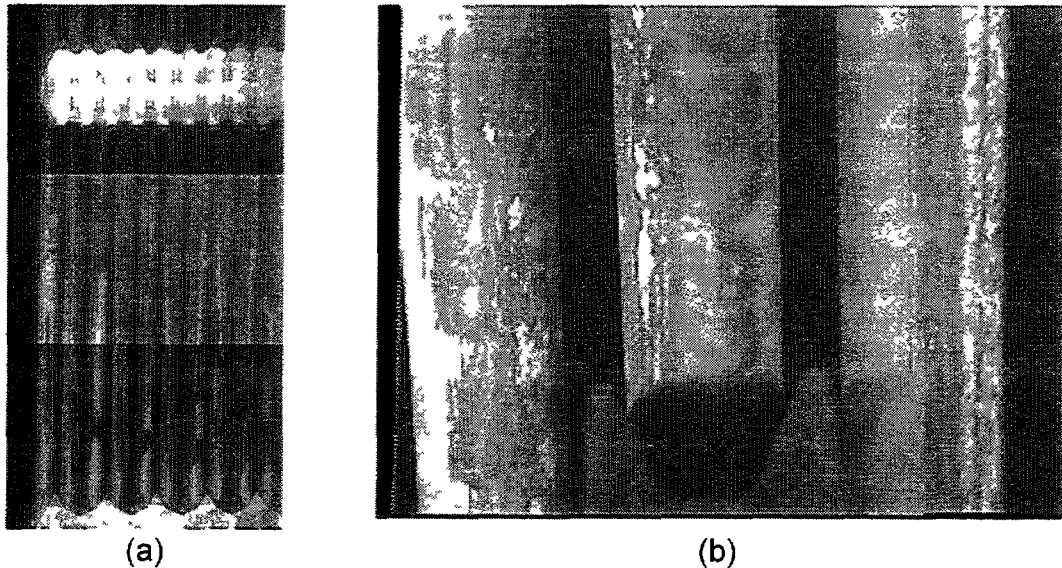


Figure 2: Video images of crud deposits in span 6a of PWR fuel.

magnification image in Fig. 2b shows the preferential deposition of crud associated with the fuel pellet height.

The visual examinations show the locations in the fuel assembly where crud is deposited but provide no information on the relative thickness of the crud. This was assessed by crud scrapings from the fuel rods in the outer rows of the assembly. Scrapings were from different axial spans as well as from both one cycle and two cycle assemblies. Estimates of the crud thickness were made as described above and are summarized in Table 1 [1].

The results reveal several trends regarding deposition of crud [1]. The thickest crud deposits were observed in Span 6 and decreased in the lower spans with no crud observed below span 4. In addition, thicker crud was observed on the higher powered rods. These observation are consistent with the thicker crud being associated with higher fuel duty. Span 6 has the highest rate of sub-cooled boiling as well as the thickest crud. For these rods, thicker crud deposits were observed on the twice-burned fuel as a result of deposition during two cycles.

Table 1  
Estimated Crud Thickness from Scrapings

Number of Cycles	Span	High Powered Rod (microns)	Avg. Powered Rod (microns)
1	6	9	2
	5	-	0.4
	4	0.4	-
2	6	20	15
	5	6	-
	4	7	3



To provide a more quantitative measure of crud thickness, eddy current measurements were performed on an improved Zircaloy-4 and ZIRLO™ fuel rod with burnups of about 45 GWD/MTU. The eddy current measurements performed along the full length of the rod are plotted in the Fig. 3. Significant increases in thickness were observed at rod elevations above 80 inches where crud was visually observed. The rods were then sectioned and four metallographic mounts were prepared from each rod corresponding to axial locations of about 15 inches, 60 inches, 77 inches and 125 inches from the bottom of the rod.

Oxide thickness measurements were made around the tube circumference along with maximum crud thickness. These data are plotted in Fig. 3. At axial elevations below 80 inches where no crud was present, there was good agreement between the eddy current measurement and metallographic measurement. In Span 6b (~125 inches), the oxide thickness from metallography was significantly lower than the eddy current measurement. A one-to-one comparison between the two techniques was not possible since the rod azimuthal orientation was not maintained during sectioning. However, reasonable agreement was obtained when comparing the eddy current data with the sum of the average oxide thickness and maximum crud thickness. Micrographs of the oxide and crud deposit are shown in Fig. 4. Apparent in the micrographs are crud deposits approximately 20 microns thick.

Another example of eddy current measurements being impacted by crud deposits is shown in Fig. 5. Axial traces were performed on a peripheral fuel rod following one cycle of irradiation with the results from Span 6b provided in the figure. The measurements were performed both before and after cleaning the fuel rod. The pre-cleaning measurements revealed a sharp increase in thickness from less than 20 microns to a maximum thickness of about 100 microns. The abrupt increase in thickness suggested the presence of crud which was confirmed by visual inspection of the rod (Fig. 6a). The eddy current measurement was repeated following mechanical cleaning and removal of the crud (Fig. 6b). The thickness measurements were about the same in the crud-free region and significantly reduced in the region previously covered by crud. The difference between the

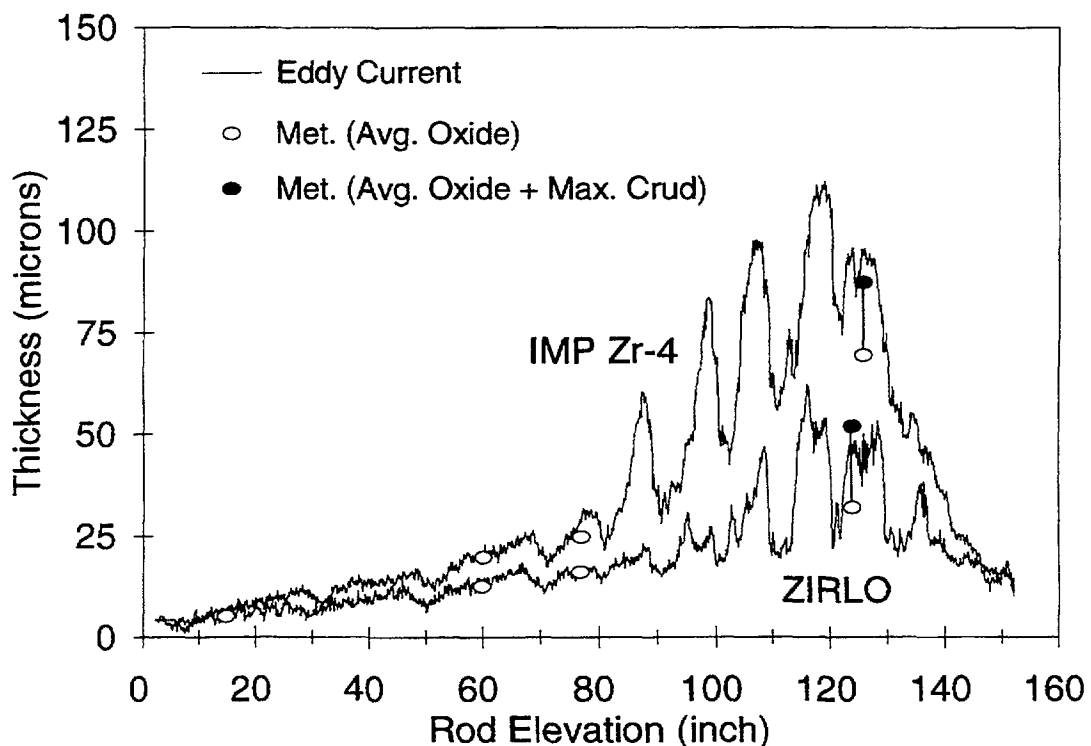


Figure 3: Eddy current and metallographic thickness measurements on improved Zircaloy-4 and ZIRLO fuel rods.

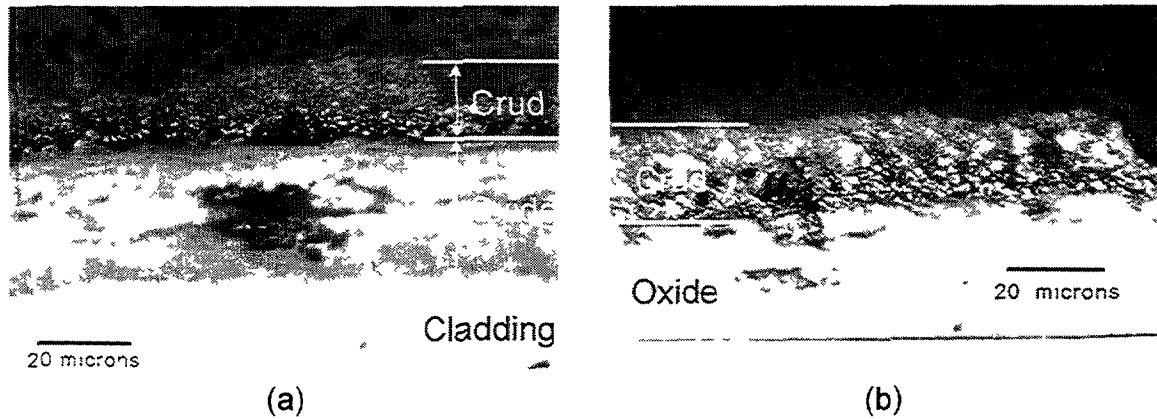


Figure 4: Metallographic cross-sections of fuel rods in crud-affected regions. (a) ZIRLO rod at axial elevation of 124 inch with 18 microns of crud and 32 micron of oxide, and (b) Zircaloy-4 rod at axial elevation of 125 inches with 20 microns of crud and 69 microns of oxide.

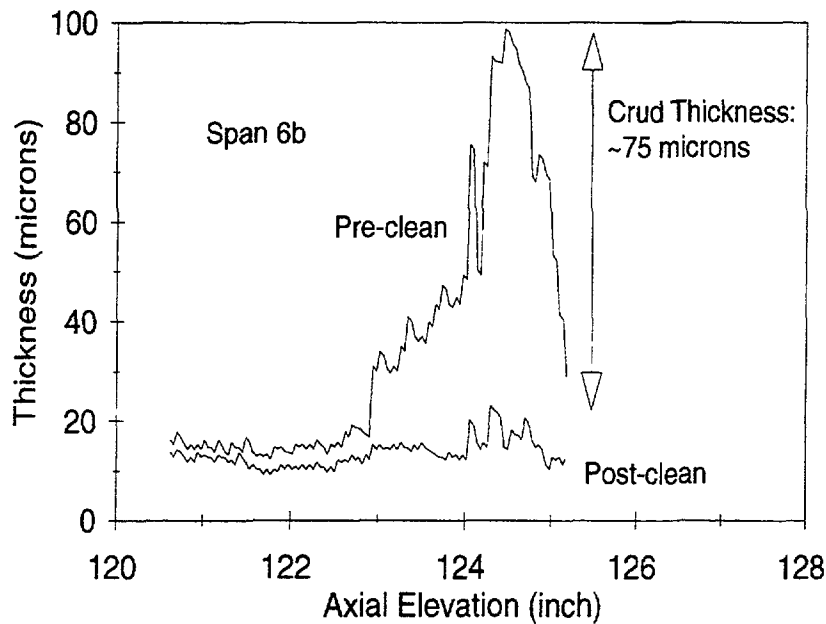


Figure 5: Eddy current probe measurement of oxide thickness in span 6b of a fuel rod before and after removal of crud deposits.

measurements before and after cleaning suggested a crud thickness as high as 75 microns. Despite the thick crud, average oxide thickness beneath the crud and in crud-free zones was similar.

This indirect measure of crud thickness was confirmed by examination of a crud flake collected during the cleaning operation. A scanning electron micrograph (SEM) of the cross-section is shown in Figure 7a where the crud thickness measured between 72 and 79 microns which was consistent with the estimated thickness from the pre- and post-cleaning eddy current measurements. Higher magnification examination of the crud flake showed the presence of boiling chimneys within the crud.

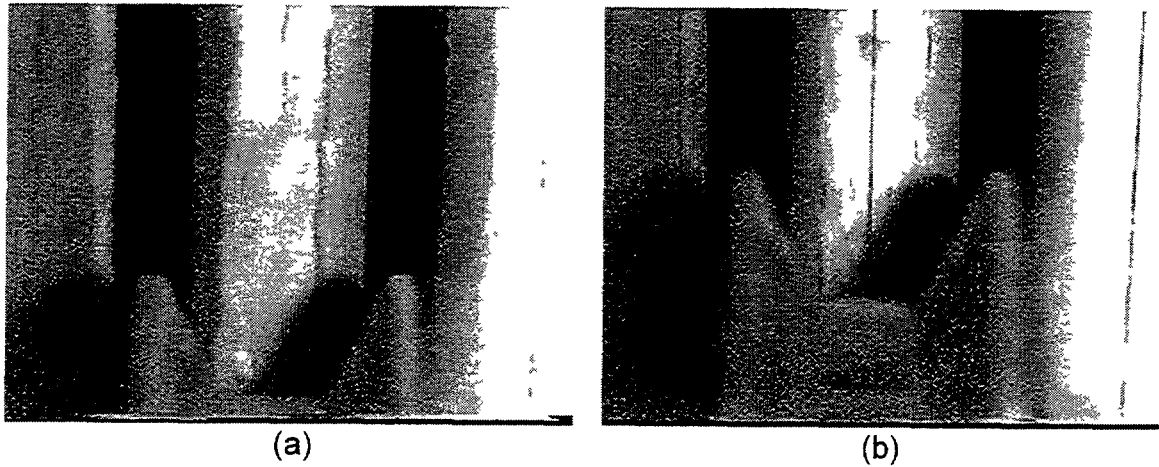


Figure 6: High magnification video image of fuel rod. (a) before removal of crud deposits and (b) after removal of crud deposit.

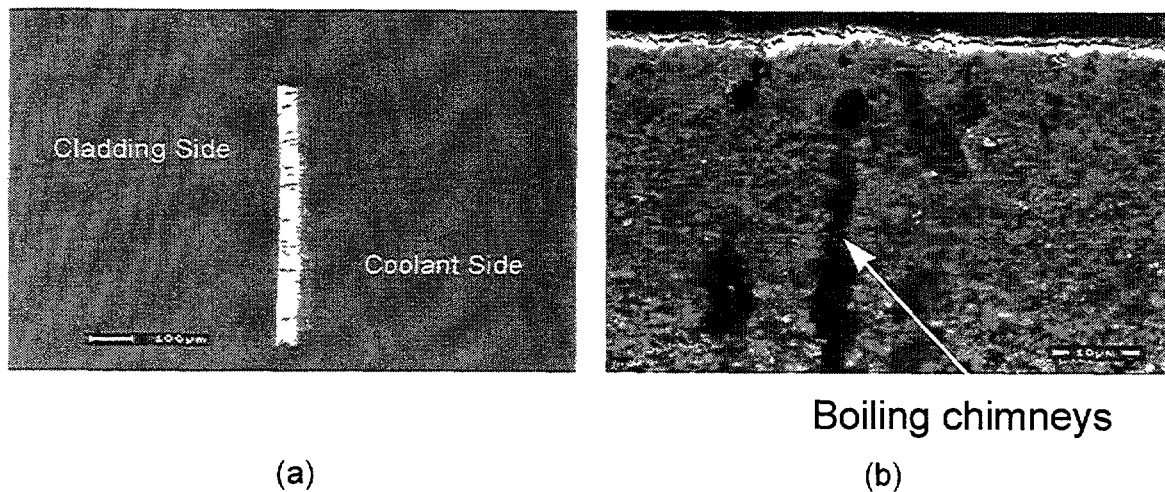


Figure 7: SEM micrograph of crud flake cross-section.

Additional rods sent to the hot cell were examined to determine the impact of crud deposits on oxide thickness. Visual examination of the rods at the reactor site showed the presence of local areas of crud on the fuel rod. The crud was not present around the entire circumference but rather appear as axial bands of crud covering only a portion of the circumference. The crud apparently flaked off during shipment to the hot cell as the crud was no longer present on the rod upon arrival at the hot cell. Even though the crud was no longer intact, the crud-free and crud-affected regions could still be visually identified. Transverse metallographic cross-sections of the rods from both the crud-free and crud-affected areas were prepared for destructive examination of the oxide thickness.

Results of the measurements from two rods are provided in Table 2. Measurements included the average oxide thickness around the circumference as well as the peak oxide thickness. The small difference between the peak and average oxide in the crud-free region of the rods indicated a rather uniform oxide around the rod circumference. Contrasted to this was the large difference between the peak and average oxide thickness at the axial locations where crud was present. The peak oxide thickness was restricted only to a portion of the rod where the crud was present. The oxide thickness around the remainder of the circumference was more typical of the oxide thickness expected at the designated elevations.

Table 2  
Impact of Crud on Cladding Corrosion

Rod	Elevation (inch)	Avg. Oxide (micron)	Peak Oxide (micron)	
1	106.9	55.3	58	No Crud
	127.9	80.8	144	Crud Present
2	96.9	49.5	54	No Crud
	105.9	62.8	118	Crud Present

#### 4. Discussion

The examinations performed on crud characterize the locations in the fuel assembly where crud can deposit as well as provide information on crud thickness and its impact on corrosion. From these studies, there is a clear correlation between crud deposits and rod power. Higher power assemblies with sub-cooled boiling are prime locations for crud deposition with the thickest crud deposits generally observed near the top of the assembly in span 6.

The impact of crud on fuel rod performance is multifaceted. In addition to complicating the interpretation of eddy current measurement of oxide thickness, crud can also result in higher local corrosion as well as provide a location for precipitation of boron resulting in a flux depression and the phenomenon known as AOA. A first step in quantifying these effects is understanding the nature of the crud which forms on high power fuel assemblies.

These initial studies quantify the crud thickness which can form on fuel rods as well as provide data regarding the effect of crud on the underlying oxide thickness. Examples have been shown where crud deposits have minimal impact on oxide thickness (i.e., Fig. 5) as well as impacting oxide thickness (i.e., Table 2). Furthermore, characterization of the cross section morphology of crud provides evidence of boiling within the crud (Fig. 7b) and supports a mechanism for AOA by precipitation of boron containing species within the crud. Additional work to understand the nature of crud and to minimize its formation is warranted so as to eliminate associated performance concerns such as corrosion and AOA.

#### 5. Conclusions

1. The presence of crud deposits impact eddy current measurement of oxide thickness and may result in local increases in oxide thickness.
2. Crud deposition is associated with sub-cooled boiling.
3. Crud deposits up to 80 microns thick have been observed.
4. Boiling chimneys were observed in thick crud flakes.
5. Thick crud and boiling can lead to precipitation of boron components within the crud resulting in axial power anomalies.

## REFERENCES

1. SABOL, G. P., SECKER, J. R., KUNISHI, H., AND CHENG, B. "Characterization of Corrosion Product Deposits on Fuel in High-Temperature Plants", Contribution of Materials Investigation to the Resolution of Problems Encountered in PWRs (Proc. IV Int. Symposium Fontevraud, France, 14-18 September, 1998), Societe Francaise d'Energie Nucleaire (1990) 45.
2. SOLOMON, Y. AND ROESMER, J. Nuclear Technology, **29** (1976) p. 166.

# CHARACTERIZATION OF THE PARAMETERS AT THE ORIGIN OF THE CHEMICAL SPECIES HIDEOUT PROCESS AT THE FUEL ROD SURFACE IN BOILING CONDITIONS

J. PEYBERNES, Ph. MARCH  
Commissariat à l'Energie Atomique,  
Cadarache, France

## Abstract

Current trends in nuclear power generation (and particularly in pressurized water reactors) are toward plant life extension and extended fuel burnup. A higher heat generation rate can induce local boiling regimes at the fuel rod surface in the hottest channels of the core, which can strongly modify the chemical environment of the cladding and influence the oxidation rate of zirconium alloys.

Tests performed in out-of-pile loops under severe chemical and thermal-hydraulic conditions (nucleate boiling, higher lithium contents compared to PWRs) reveal two important phenomena :

- an increase of the oxidation rate of Zircaloy-4 cladding materials in "high" lithiated environments,
- an enrichment of the chemical additives in the primary water (boron, lithium) at the surface of the cladding under nucleate boiling conditions.

The latter phenomenon, also called « hideout effect », is mainly controlled by some thermal hydraulic parameters such as bubble diameters and nucleation site density. These parameters strongly depend on the oxide morphology (roughness, porosity).

The lack of reliable data in high temperature water environments has led to the development of a specific instrumentation based on visualization. The fitting of windows on the REGGAE out-of-pile loop provides an optical access to the two-phase flow regime under PWR operating conditions, allowing for the characterization of the parameters at the origin of the chemical species hideout process.

These direct observations of the cladding surfaces subjected to nucleate boiling conditions provide information about the development of the boiling mechanisms in relation to the morphology of the oxide layers (porosity, thickness, roughness).

## 1. INTRODUCTION

The new operational conditions for modern nuclear power plants (and particularly in pressurized water reactors) can induce local boiling regimes at the fuel rod surface in the hottest subchannels of the core. This new trend toward higher heat generation rates and higher lithium contents for extended fuel cycles imposes a need for a fuel cladding corrosion properties enhancement.

Studies have been conducted to determine and to understand the effects of such operating conditions on the fuel cladding corrosion rate [1],[2],[3]. Some tests have been performed in experimental devices such as out-of-pile loops or autoclaves, leading to the following conclusions :

- an acceleration of the corrosion rate is observed under nucleate boiling conditions in high lithiated environments,
- the differences of behavior toward corrosion of cladding submitted to similar void fractions show that this parameter is not sufficient to evaluate the influence of nucleate boiling on corrosion,
- the effect of nucleate boiling on the corrosion rate is more pronounced for thick layers of zirconium oxide,
- some destructive analyses of the zirconium oxide layers show the existence of an interaction between the lithium enrichment under boiling condition and the oxide morphology (porosity, roughness). They also demonstrate that the presence of the vapor phase strongly modifies the chemical environment of the cladding, and leads to an enrichment of the chemical additives in the primary water (boron, lithium) at the surface of the cladding.

Based on these results, the modelling of the chemical additives enrichment under boiling conditions has been developed in order to extend the CEA/COCHISE oxidation model to the prediction of Zircaloy-4 corrosion rates under two-phase flows [2].

The enrichment phenomenon, also called the hideout effect, is extremely linked to the two-phase flow pattern near the wall (bubble diameters and density..) and also to the oxide morphology (roughness, porosity).

Nevertheless, very few data are available in the range of thermal-hydraulic parameters of PWR cores, i.e. high pressure and high heat flux. Thus, to improve our understanding of the boiling effect on corrosion kinetics, a specific instrumentation based on visualization techniques has been developed to obtain information about the flow pattern near oxidized claddings in PWR conditions.

The analysis of the images resulting from the flow visualization allows to obtain quantitative data (interfacial area concentration, granulometric properties) of great interest to evaluate the mass transfer rate between liquid and vapor for all chemical species inside the coolant [4].

## 2. MECHANISM FOR THE CHEMICAL SPECIES HIDEOUT AT THE WALL

This part is dedicated to the presentation of the hideout effect mechanism and to the analysis of the lacking experimental data which are necessary to feed the model.

In nucleate boiling conditions, the vaporization process occurs at the wall. The chemical species present in the liquid phase diffuse in the vapor phase according to their volatility. The less volatile a compound, the more it concentrates in the liquid at the base of the growing bubbles. Thus, the enrichment phenomenon occurs in a microlayer of liquid adjacent to the wall [5] (Figure 1).

From a macroscale point of view, the enrichment levels of low volatile compounds mainly depend (1) on the vaporization rate, and (2) on the liquid mass transfer from the bulk to the wall through the bubbly layer (Figure 2). The liquid mass transfer is strongly related to the two phase flow pattern near the wall (bubble diameters and density).

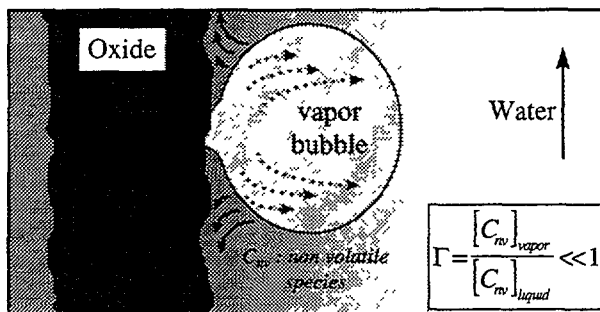


Figure 1 - The enrichment phenomenon

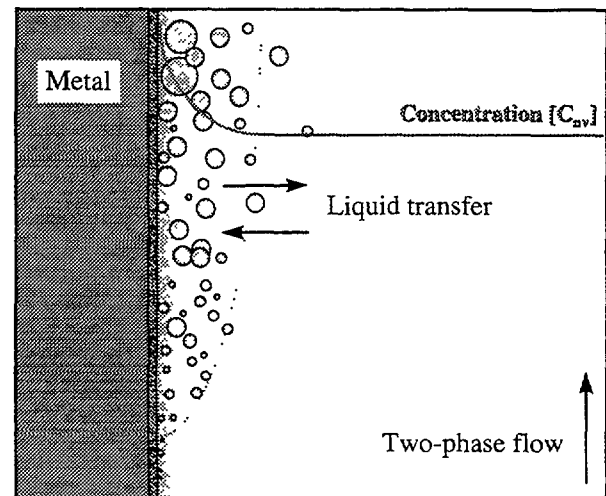


Figure 2 - The hideout effect

Based on all these considerations and thanks to a simple mass balance equation, a model for the hideout effect has been developed [2] (Figure 3) and leads to the following expression for the local enrichment factor of non volatile species  $C_{nv}$  in the liquid film at the wall :

$$F_E^\alpha = \frac{[C_{nv}]_{wall}}{[C_{nv}]_{bulk}} = \frac{G' \cdot (1 - x)}{[G' \cdot (1 - x) - \dot{m}_v] \cdot [\Gamma \cdot x + (1 - x)]}$$

with  $\dot{m}_v$  as the vaporization rate at the wall :

$$\dot{m}_v = \frac{\Phi - h \cdot \Delta T_{\text{sub}} \cdot (1 - \alpha / \alpha_d)}{\rho_v L_v + C_p \rho_L \Delta T_{\text{sub}}} \cdot \rho_v \quad (\text{kg/m}^2 \cdot \text{s})$$

with :

$x$  : true vapor weight fraction (quality)

$\Phi$  : heat flux ( $\text{W/m}^2$ )

$\Delta T_{\text{sub}}$  : liquid subcooling ( $T_{\text{sat}} - T_{\text{liq}}$ ) (K)

$L_v$  : latent heat of vaporization (J/kg)

$h$  : heat transfer coefficient ( $\text{W/m}^2 \cdot \text{K}$ )

$\rho_l, \rho_v$  : liquid and vapor densities ( $\text{kg/m}^3$ )

$C_p$  : specific heat of liquid (J/kg.K)

$\alpha$  : void fraction,  $\alpha_d$  : void fraction at the Onset of Significant Void [6]

$\Gamma$  : volatility of the chemical species (partition coefficient between the liquid and the vapor)

$G'$  : lateral mass flow rate from the bulk to the bubbly layer ( $\text{kg/m}^2 \cdot \text{s}$ ) [7]

$$G' = f(\text{Re}, D_b, G, x, \rho_l, \rho_v)$$

with :

$\text{Re}$  : Reynolds number

$D_b$  : mean diameter of the bubbles (m)

$G$  : axial mass flow rate ( $\text{kg/m}^2 \cdot \text{s}$ )

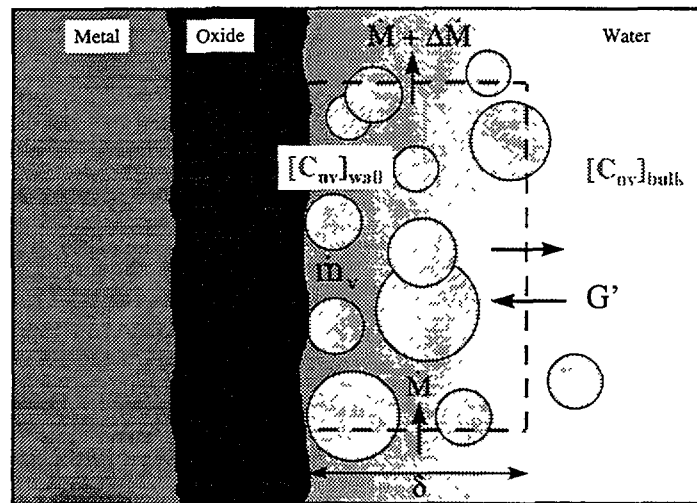


Figure 3 - Model of species enrichment

As the flow pattern is of importance, the void fraction is not sufficient to determine the local chemical environment of the cladding. Actually, the hideout process cannot be characterized properly without the knowledge of the granulometric properties of the two-phase flow. It seems obviously possible to have the same void fraction with a much higher bubble density and with a very different liquid mass transfer rate between the bubbly layer and the bulk. Furthermore, the surface condition of the cladding may strongly influence the density of the nucleation sites from which bubbles grow on the wall, as well as the bubble behavior after it leaves its nucleation site.



Unfortunately, thermal-hydraulic codes allow to calculate macroscopic parameters of the two-phase flow such as the quality or the void fraction without providing any information about the two-phase flow pattern near the wall (bubble sizes and density). Moreover, these codes do not take into account the surface condition.

Besides, very few experimental data exist concerning the characteristics of the two-phase flow near an oxidized cladding in the range of thermal-hydraulic conditions of PWR cores (high pressure and high heat flux). Then, this need for a better understanding of the interaction between the fuel cladding and its thermal hydraulic and chemical environment (hideout effect) has led to the development of a specific instrumentation based on visualization techniques.

### 3. FLOW VISUALIZATION INSTRUMENTATION

The visualization device has been adapted on the out-of-pile loop REGGAE which allows to simulate the operating conditions of the PWR except irradiation (TABLE I.). The test section includes a rod bundle with nine rods (3x3 rods in square section ) which are electrically heated with heating rods inserted inside the claddings. This test section is representative of the PWR geometry with the same mixing grids, pitch, external rod diameter, hydraulic diameters and so on.

**TABLE I. OPERATING CONDITIONS FOR PWR AND REGGAE LOOP**

<b>thermal hydraulic parameters</b>	<b>PWR</b>	<b>REGGAE</b>
Operating Pressure (MPa)	15.5	$15 < P < 19$
Maximum Wall Temperature(°C)	347	$345 < T < 363$
Mass flow rate (kg/s/m <sup>2</sup> )	$3300 < G < 4000$	$1650 < G < 3000$
Core flow velocity (m/s)	$4,7 < V < 5,7$	$2,5 < V < 5$
Wall heat flux (MW/m <sup>2</sup> )	$\Phi < 1$	$\Phi < 1.2$
Void fraction (%)	$\alpha < 5$	$\alpha < 40$

Two optical windows have been set on either side of the test section, facing each other (Figure 4). The flow can be lit from one side and observed from the other one. The windows are sapphire made to get appropriate optical and mechanical properties regarding the operating conditions (disc dimensions : 20 mm diameter, 7 mm thickness). The lighting is provided by a laser diode with 689 nm red wave length which delivers very short duration pulses (200 ns) at 25 Hz frequency. The very short duration pulses allows to freeze the bubbles on each image. The diode can also generate a double-pulse to measure the vapor phase velocity. The analogical images captured by a CCD video camera at a speed of 25 frames by second are recorded on S-VHS tapes. A macroscope fitted to the camera allows high magnification (x80) while keeping a large operating distance (20 cm).

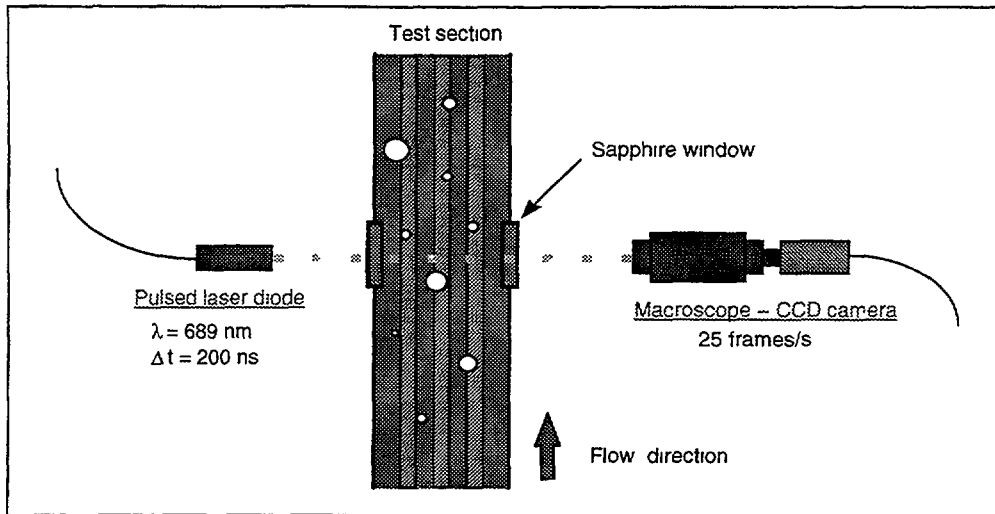


Figure 4 - Image acquisition system

For this specific visualization test, the range of thermal hydraulic parameters has been chosen as follows :

- absolute pressure : 2 stages at 2.6 and 15.5 MPa
- coolant temperature : 180 to 340°C
- core flow velocity : 3 to 4 m/s
- heat flux : 0.30 to 1 MW/m<sup>2</sup>

#### 4. EXPERIMENTAL RESULTS

The presentation of the experimental results is divided into two different parts. The first one concerns the effect of some thermal-hydraulic parameters on the two-phase flow pattern, the other part is dedicated to the effects of the surface condition on the two phase flow pattern.

Figure 5 shows an example of an image obtained thanks to the flow visualization instrumentation and its common characteristics and scale.

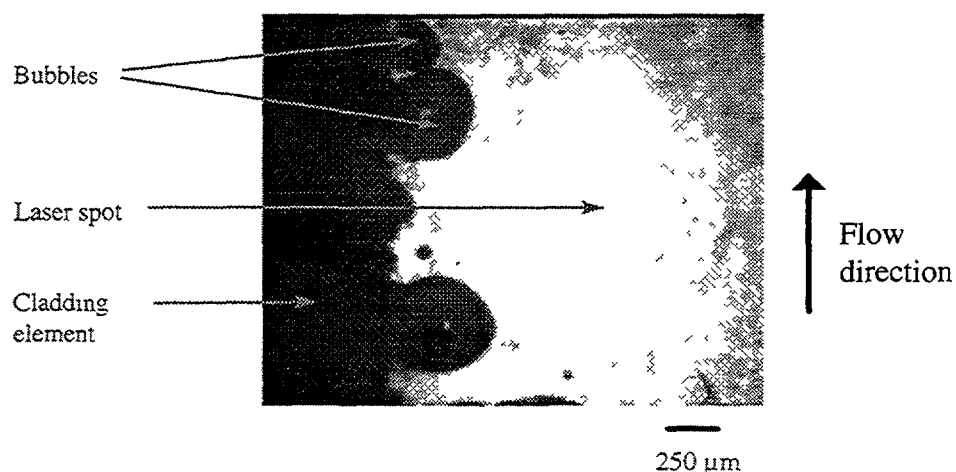


Figure 5 - Image description

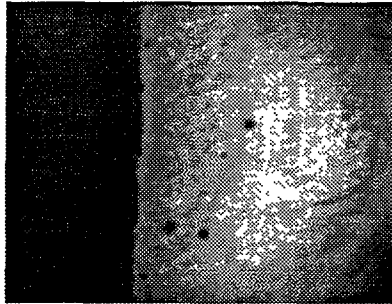
In these out-of-pile loop tests, boiling regimes at the surface of the heating rods can be obtained by increasing the fluid temperature and the power level or decreasing the axial mass flow rate.

#### 4.1 Thermal-hydraulic condition effects on the flow pattern

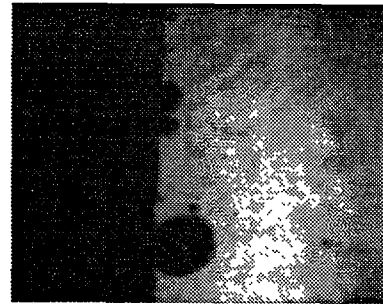
For a given pressure, three thermal hydraulic parameters are of importance concerning the two-phase flow pattern : the mass flow rate, the liquid temperature at the entrance of the test section and the heat flux at the wall.

The following images have been taken at 2.6 Mpa. The results are qualitatively the same at 15.5 Mpa, but the 2.6 Mpa images have a better quality. Below each image, the varying thermal-hydraulic parameter and the mean bubble diameter  $D$  are indicated.

- mass flow rate ( $\Phi=0.6 \text{ MW/m}^2$ ,  $T_e=201^\circ\text{C}$ )

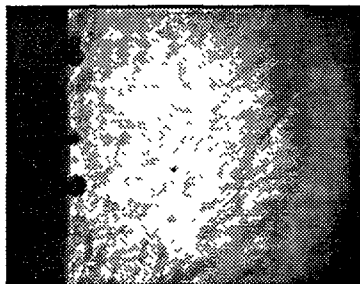


- $G=2.6 \cdot 10^3 \text{ kg/m}^2.\text{s}$   
 $D \sim 60 \mu\text{m}$

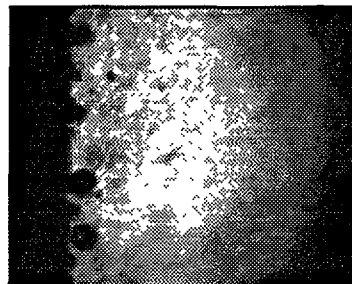


- $G=1.74 \cdot 10^3 \text{ kg/m}^2.\text{s}$   
 $D \sim 200 \mu\text{m}$

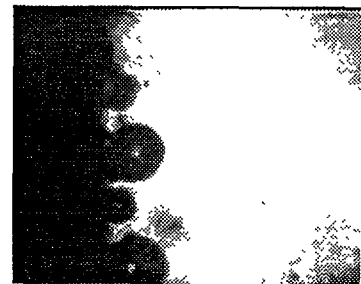
- temperature of the test section entrance ( $\Phi=0.6 \text{ MW/m}^2$ ,  $G=2.1 \cdot 10^3 \text{ kg/m}^2.\text{s}$ )



- $T_e=196^\circ\text{C}$   
 $D \sim 100 \mu\text{m}$

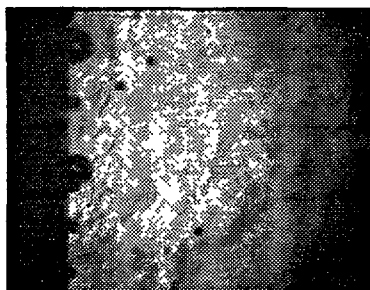


- $T_e=198^\circ\text{C}$   
 $D \sim 160 \mu\text{m}$

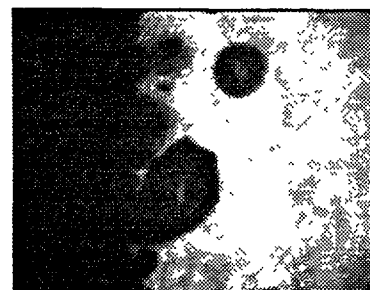


- $T_e=202^\circ\text{C}$   
 $D \sim 310 \mu\text{m}$

- heat flux ( $T_e=198^\circ\text{C}$ ,  $G=2.1 \cdot 10^3 \text{ kg/m}^2.\text{s}$ )



- $\Phi=0.6 \text{ MW/m}^2$   
 $D \sim 130 \mu\text{m}$

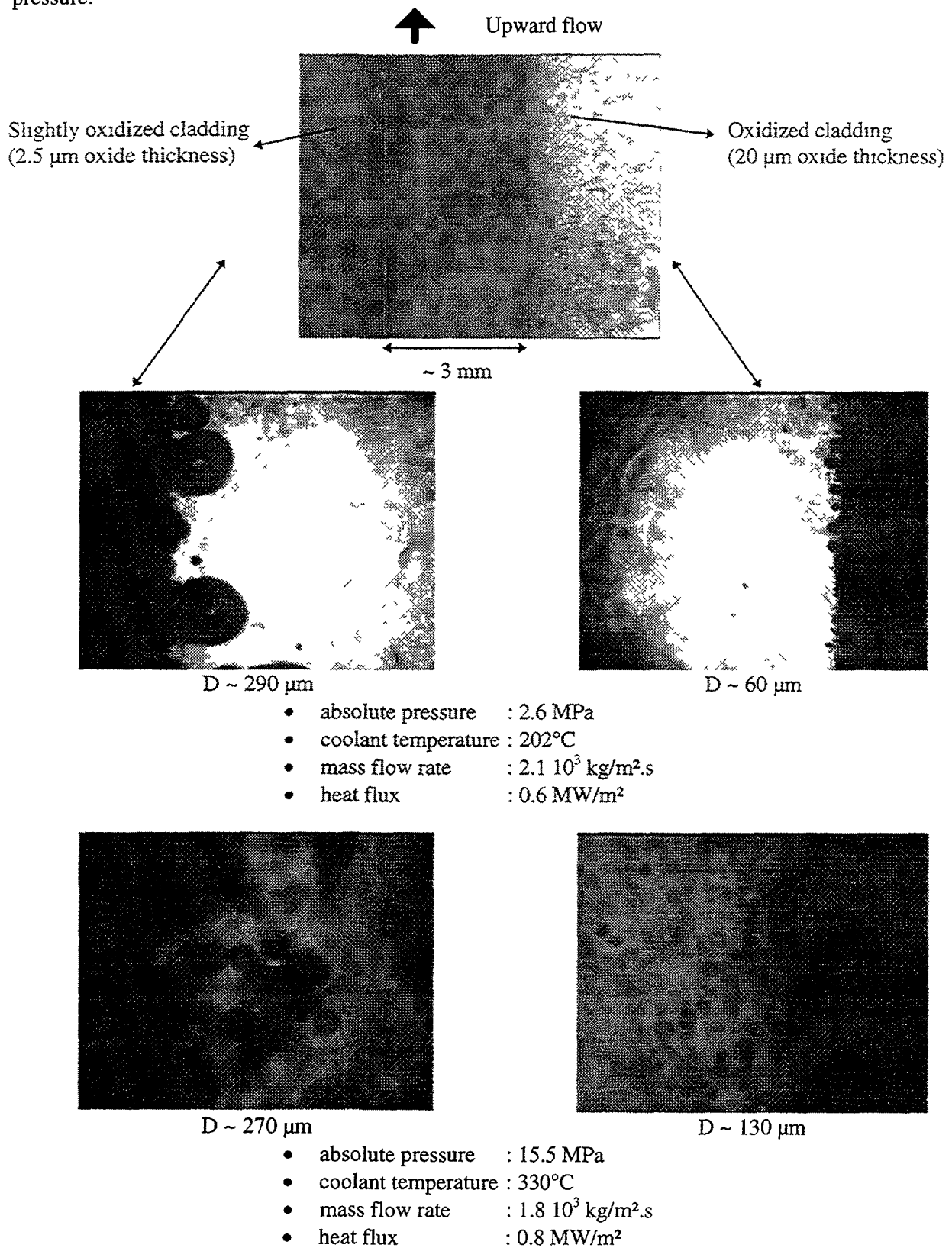


- $\Phi=0.8 \text{ MW/m}^2$   
 $D \sim 400 \mu\text{m}$

These first observations show that the flow pattern of nucleate boiling near the wall is very sensitive to the thermal-hydraulic conditions. The mean bubble size increases when the heat flux increases or the mass flow rate decreases.

## 4.2 Surface condition effects on the flow pattern

In order to reveal the impact of the cladding surface condition on the boiling process, a cladding with a low oxide layer (oxide thickness below  $3\text{ }\mu\text{m}$ ) and another one with a thicker oxide film (beyond  $20\text{ }\mu\text{m}$ ) have been observed in the same thermal-hydraulic conditions. In these tests, boiling phenomena are studied for different heat fluxes, temperatures and mass flow rates at a given pressure.



These observations reveal the same effect of the surface condition for pressures of 2.6 and 15.5 Mpa : at a given set of thermal-hydraulic conditions, the mean bubble diameter is smaller and the bubble density is higher on the thick oxide layer than on the thin one.

As a conclusion, the two phase flow pattern is extremely sensitive to the thermal hydraulic conditions and also to the surface condition of the cladding which depends on the oxidation stage.

## 5. DISCUSSION

These observations made in PWR conditions confirm that it is possible to obtain several different two-phase flow patterns for a given void fraction.

On the one hand, considering one given surface condition, the flow pattern is very sensitive to the heat flux, the mass flow rate and the temperature. This confirms that the void fraction is not sufficient to characterize the influence of nucleate boiling on the hideout effect.

On the other hand, considering one given set of constant thermal-hydraulic parameters, the flow pattern is very sensitive to the surface condition of the cladding. This observation leads to reconsider the thermal-hydraulic and chemical environment of the cladding according to the oxidation stage : the evolution of the surface condition of the fuel cladding during the corrosion process must be taken into account.

The observations are in good agreement with the enrichment model and the corrosion tests results. A decrease of the bubble mean diameter along with an increase of the bubble density can lead to a smaller turbulent intensity at the interface between the bubbly layer and the bulk. This effect minimizes the radial liquid mass transfer and increases the enrichment at the wall. Therefore, the observations confirm that the thicker the oxide layer, the higher the enrichment factor may be. According to the mechanism of chemical species hideout at the wall described beyond, the chemical species concentration at the wall could increase during the growth of the oxide layer.

Moreover, for thick oxide layers, the development of large pores and microcrack networks allows water to circulate into the oxide film. Then the liquid can be vaporized through the widest pores increasing the mass vaporization rate and the enrichment of the chemical species inside the porous oxide [8].

As an ending for this discussion, we can notice that it is difficult to account for the granulometric properties of any two-phase flow. The diameter distribution and the vapor bubble density are neither easy to measure nor easy to use for calculus. The interfacial area concentration, which is the total surface of the interface between the liquid phase and the vapor phase per unit volume, could be of interest for that aim : indeed it integrates both the diameters and the density of the vapor inclusions.

The interfacial area concentration is also very interesting because a method has been recently developed to measure it directly on the images [4]. The pictures obtained with our flow visualization instrumentation are the result of a transmitted beam through the two-phase flow. Actually, we can observe the result of the flat projection of thick slices of flow (the thickness corresponding to the microscope depth of focus). Now, we attempt to interpret quantitatively these two dimensional microscopic observations in terms of the three dimensional structure to which they are related. Some mathematical tools, so-called stereological laws, provide us with some efficient models able to deduce three dimensional data from these two dimensional microscopic observations. Actually, the local void fraction and the interfacial area concentration will soon be measured on the images and used to feed the enrichment model to characterize the effect of nucleate boiling on the cladding corrosion rate.

## 6. CONCLUSION

The water chemistry acts upon the corrosion kinetics of zirconium fuel cladding materials. As nucleate boiling can strongly modify the chemical environment of the cladding, experimental studies have been conducted showing that the void fraction is not sufficient to characterize the hideout effect, and that the knowledge of the two-phase flow pattern is necessary. Nevertheless, very few data are available in the range of thermal hydraulic parameters of PWR cores. i.e. high pressure and high heat flux.

The fitting of windows on the REGGAE out-of-pile loop provides an optical access to the two-phase flow regime under PWR operating conditions, allowing for the characterization of the size distribution of the bubbles near the cladding surface.

This visualization instrumentation is a non-intrusive and *in-situ* technique which provides us with some fundamental qualitative and quantitative data measured in PWR conditions. The void fraction and the interfacial area concentration are of particular interest for the evaluation of the effect of the two-phase flow pattern on the hideout effect.

The two main conclusions of these observations are that the void fraction is definitely not sufficient to characterize the enrichment phenomenon at the fuel rod cladding, and that the surface condition of the cladding must also be taken into account because it strongly influences the two phase flow pattern.

## REFERENCES

- [1] BILLOT, P., ROBIN J.C., GIORDANO, A., PEYBERNES, J., THOMAZET, J., AMANRICH H., "Experimental and theoretical studies of parameters that influence corrosion of Zircaloy4", Zirconium in the Nuclear Industry (Proc. 10<sup>th</sup> International Symposium Baltimore, MD, 1993), ASTM, ASTM-1245 (1994) 351.
- [2] PEYBERNES, J., Influence de l'ébullition sur la corrosion externe des gaines de crayons combustibles des réacteurs d'eau pressurisée. Thèse de Doctorat Marseille 1994.
- [3] PECHEUR, D., GODLEWSKI, J., BILLOT, P., THOMAZET, J., "Microstructure of oxide films formed during the waterside corrosion of the Zircaloy-4 cladding in lithiated environment", Zirconium in the Nuclear Industry (Proc. 11<sup>th</sup> International Symposium Garmish-Partenkirchen, 1995), ASTM, ASTM STP 1295 (1996) 94-113.
- [4] MARCH, P., PEYBERNES, J., GARNIER, J., "Visualization and flow pattern of nucleate boiling in PWR conditions: image acquisition and data treatment", Multiphase Flow (Proc. Third International Conf. Lyon, France, June 8-12, 1998)-(in press).
- [5] STYRIKOVITCH, M.A., POLONSKY, V.S., BEZRIJKOV, E.K., "A study of mass transfer in steam-generating channels by the salt method", Teplofizika Vysokikh Temperatur, Vol. 9 (1971) 583-590 (in Russian).
- [6] ROUHANI, S.Z., AXELSSON, E., "Calculation of void volume fraction in subcooled and quality boiling regimes, Int. J. Heat Mass Transfer, Vol. 13 (1970) 383-393.
- [7] YANG, J.Y., WEISMAN, J., "A phenomenological model of subcooled flow boiling in the detached bubble region", J. Multiphase Flow, Vol. 17 (1) (1991) 77-94.
- [8] STYRIKOVITCH, M., LEONTEV, A.T., MOLYSHENKO, S.P., "Transport mechanism for non-volatile impurities in boiling on surfaces coated with a porous structure", High Temperature, Vol. 14 (1976) 886-893.

# CORROSION MODELLING

(Session 4)

NEXT PAGE(S)  
10/11/11 11:11



## AMMONIA ROLE IN WWER PRIMARY CIRCUIT WATER CHEMISTRY OPTIMIZATION

V.G. KRITSKIY\*, P.S. STJAGKIN, M.N. CHVEDOVA  
VNIPIET

A.A. SLOBODOV  
Technological Institute

St. Petersburg, Russian Federation

### Abstract

Ammonia influence on iron crud's solubility at 300 °C and different relations of boric acid and alkaline cation sum are considered. Reduction of dose rate on WWER-440 steam generators at average ammonia concentration increasing is empirically explained. Practical recommendations on optimization of WWER primary circuit water chemistry are given.

### 1. Ammonia Role in WWER Primary Circuit

For WWER primary circuits of NPPs reducing boron-potassium regime, consisting in keeping boric acid concentration corresponding to fuel burn-up level, with the acid neutralizing by potassium hydroxide, is accepted [1-2]. Ammonia concentration is within limits providing reducing regime at the expense of hydrogen formation in result of ammonia decomposition at temperature > 200 °C under ionizing radiation conditions [1-3].

Because of lack of technical measuring aids,  $pH_T$  does not appear under standard control at domestic NPPs. pH of water solutions consisting of several components is a complex function of these components concentrations and dissociation constants thereof, depending on temperature. Therefore, it is difficult to judge about  $pH_{300}$  value of a solution of the same composition by  $pH_{25}$  value. In change of the component concentration relationship, first of all of  $H_3BO_3/\Sigma(K, Na, Li)$ ,  $pH_T$  value changes and corrosion products (CP), iron, nickel, cobalt solubility in different section of the circuit changes accordingly. CP solubility in the core and steam generators tube plate determines direction and intensity of mass transfer of iron CP as well as of radionuclides. Optimum relationship  $H_3BO_3/\Sigma(K, Na, Li)$  assessment in practice is not used and attending personnel can not predict current water chemistry deviation from optimum. Therefore, operating personal does not often connect these variations of relationship  $H_3BO_3/\Sigma(K, Na, Li)$  during the campaign with radiation conditions change [4].

Empirically expressed appreciable ammonia concentration effect upon dose rate build-up on steam generators (Figure 1) is not theoretically explained yet [5]. Moreover, theoretically ammonia influence upon pH value and accordingly upon mass transfer processes at temperatures > 200 °C is considered negligible. It is known that with temperature rise ammonia dissociation constant values decrease sharply (for example, comparing with alkaline metal hydroxides) and as a result it is supposed that the most part of it is in the form of  $NH_4OH$  neutral molecules [3]. The aim of our work was to find out  $NH_3$  role and importance of the primary circuit coolant with equipment interactions on the basis of  $Fe_3O_4-H_2O-H_3BO_3-KOH-NH_3-H_2$  system calculational analysis.

As there is no agreed-upon code of constants of water dissociation boric acid, potassium hydroxide and ammonia in temperature range 25-300 °C, first of all it was necessary to check up  $pH_T$

---

\* Present address: VNIPIET, Dibunovskaja 55, 197183, St.-Petersburg, , Russia



calculation correctness. There are known experimental and calculated pH values for water solutions, containing  $\text{NH}_3$ ,  $\text{LiOH}$  and  $\text{H}_3\text{BO}_3$  in different proportions [6-8]. We have calculated  $\text{pH}_T$  values for the same solutions by the model [9] using interconsistent constants of  $\text{H}_3\text{BO}_3$ ,  $\text{LiOH}$ ,  $\text{NH}_3$  dissociation.

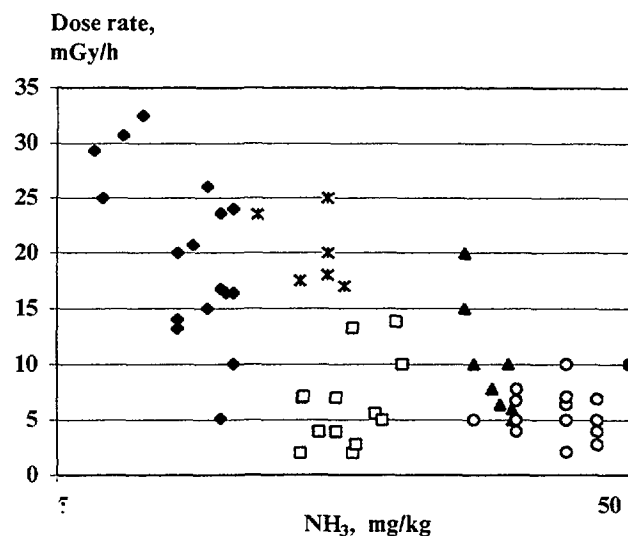


FIG. 1. Dose rate from WWER-440 steam generator collectors at different ammonia concentrations in 1 circuit water [5]

- ◆ Bohunice, unit 1,2
- Bohunice, units 3,4
- ▲ PAKS, unit 2 (standard regime)
- Kola NPP, unit 3
- × Greipph, unit 3
- PAKS unit 2 (with  $\text{N}_2\text{H}_4$ )

Absolute disagreement of experimental and calculational values of  $\text{pH}_T$  [6-8] and calculational  $\text{pH}_T$  values obtained does not exceed 0,3 (Figure 2). Advantage of calculations, we have performed, is absence of any systematical mistake as well, evidenced by discrepancy of  $\text{pH}_T$  values, we have obtained, and those of publications both in positive and negative regions (Fig. 2).

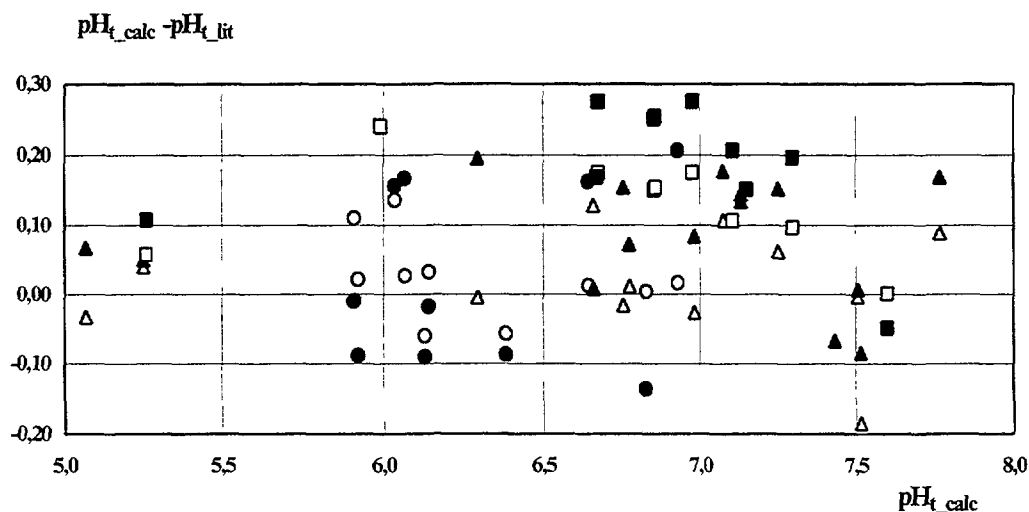


FIG. 2. Results of assessment of the calculational and experimental pH values coincidence

- calculation by [6]
- △ calculation by [7]
- calculation [8]
- experiment by [6]
- ▲ experiment by [7]
- experiment by [8]

## 2. Water Chemistry Optimization

It should be noted, that ammonia concentration effect upon  $\text{pH}_T$  values at temperatures  $> 200^\circ\text{C}$  depends on relations of boric acid and alkaline metal concentrations. Effect of ammonia concentration change upon  $\text{pH}_{300}$  value of solution with different relation  $\text{H}_3\text{BO}_3/\Sigma(\text{K}, \text{Na}, \text{Li})$  is showing Fig. 3. Figure 3 shown that with alkaline metal content decrease ammonia concentration effect rises. The least effect of ammonia is at fine-fold potassium excess comparing with required ones according to OCT [1] (Fig. 3, curve 1). With the alkaline metals content decrease at constant boric acid concentration, effect of  $\text{NH}_3$  upon  $\text{pH}_T$  value rises (Fig.3, curves 2,3,5).  $\text{pH}_T$  shift at ammonia content from 0,17 mg/kg to 53,8 mg/kg account for 0,2 unit  $\text{pH}_T$  for 0,1 mmol/kg K (Fig.3, curve 2), for 0,01 mmol/kg K - 0,9 unit  $\text{pH}_T$  (Fig.3, curve 3) and without potassium - 1,2 unit  $\text{pH}_T$  (Fig.3, curve 5).  $\text{pH}_{300}$  value change has effect upon magnetite solubility. Magnetite solubility dependence on  $\text{pH}_T$  at  $300^\circ\text{C}$  is shown in Figure 4. Magnetite solubility values in the temperature range  $25\text{--}350^\circ\text{C}$  in coordinated water chemistry at different ammonia concentration are shown in Table 1. From Figure 3, 4 and Table 1 it is evident that at optimal relation  $\text{H}_3\text{BO}_3/\text{KOH}$  corresponding to the coordinated conditions [1], boric acid and ammonia concentrations variation has practically no effect upon magnetite solubility at working temperature of operation at rated power.

Table 2 data illustrate shut-down situation and show necessity of ammonia concentration increase in shut-down according to normative documents [1,2]. Relations of alkaline metals and boric acid for coordinated and updated [2] regimes, as well as corresponding  $\text{pH}_{300}$  changes at different ammonia concentrations are shown in Figure 5 and Figure 6. At the updated regime concentrations of alkaline metals are higher and average value of  $\text{pH}_T$  for a campaign is shifted into the alkaline region and therefore an average corrosion product content is higher (Fig.2 and 6). Besides, Figure 6 shows that for a long time of the camping in the updated regime ammonia concentration variations have no effect upon  $\text{pH}_T$  value. Consequence of aforesaid is a dose expense increase being observed at maintaining of 1 circuit water chemistry according to the updated regime, comparing with the coordinated one (Figure 7).

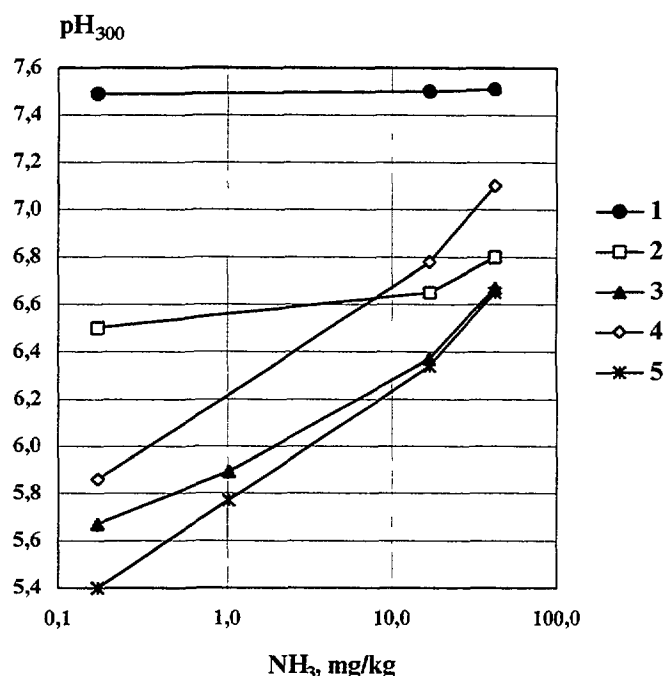


FIG. 3 Ammonia concentration effect upon  $\text{pH}_{300}$  at different relations of  $\text{H}_3\text{BO}_3$  and K

- 1 -  $\text{H}_3\text{BO}_3$  - 6,18 t/kg, K - 1 mmol/kg
- 2 -  $\text{H}_3\text{BO}_3$  - 6,18 t/kg, K - 0,1 mmol/kg
- 3 -  $\text{H}_3\text{BO}_3$  - 6,18 t/kg, K - 0,01 mmol/kg
- 4 -  $\text{H}_3\text{BO}_3$  - 0 t/kg, K - 0 mmol/kg
- 5 -  $\text{H}_3\text{BO}_3$  - 6,18 t/kg, K - 0 mmol/kg

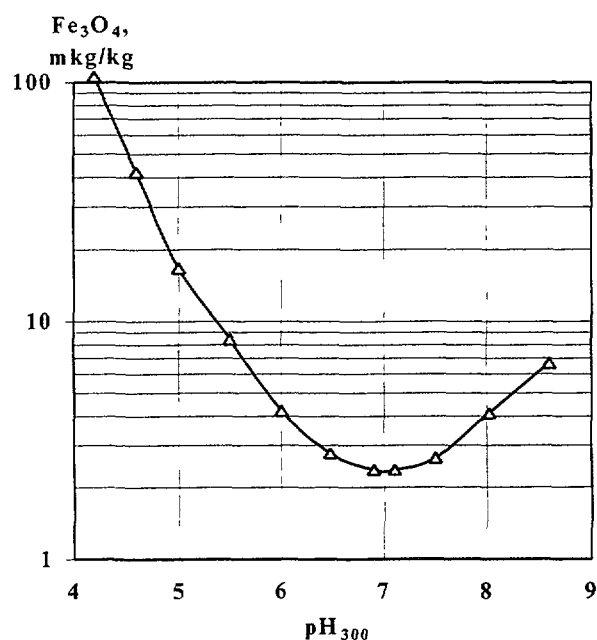


FIG. 4. Magnetite solubility dependence upon  $\text{pH}_T$  at the following relations of concentrations  
 $\text{H}_3\text{BO}_3$  - 6,18-61,8 g/kg  
 $K$  - 100-1000 mmol/kg  
 $\text{H}_2$  - 0,2 mg/kg

TABLE 1. MAGNETITE SOLUBILITY (mkg Fe/kg) IN THE SYSTEM  $\text{Fe}_3\text{O}_4\text{-H}_2\text{O-H}_2\text{-H}_3\text{BO}_3\text{-KOH-NH}_3$  at  $\text{H}_2$  CONCENTRATION 2 mg/kg

K, mmol/kg	$\text{H}_3\text{BO}_3$ g/kg	$\text{NH}_3$ , mg/kg				T, °C
		53,8	5,4	0,5	0,0	
0,22	6,18	11900	68200	82000	83900	25
0,02	0,62	136	5290	13600	14900	
0	0	0,4	1,0	1,6	1,7	
0,22	6,18	92	1130	3340	3830	100
0,02	0,62	9,2	57	226	326	
0	0,00	1,1	2,1	2,8	2,9	
0,22	6,18	18	75	153	175	150
0,02	0,62	4,5	12	20	23	
0	0	1,8	2,7	3,1	3,1	
0,22	6,18	7,7	14	17	18	200
0,02	0,62	3,7	5,4	6,1	6,2	
0	0	2,7	3,3	3,4	3,4	
0,22	6,18	5,1	5,8	5,9	5,9	250
0,02	0,62	3,8	4,2	4,3	4,3	
0	0	3,5	3,8	3,8	3,8	
0,22	6,18	5,1	4,7	4,7	4,7	300
0,02	0,62	4,8	4,5	4,5	4,5	
0	0	4,8	4,5	4,5	4,5	
0,22	6,18	5,5	4,0	3,7	3,7	350
0,02	0,62	5,5	4,0	3,7	3,7	
0	0	5,5	4,0	3,7	3,7	

TABLE 2. MAGNETITE SOLUBILITY VALUES UNDER SHUT-DOWN CONDITIONS

H <sub>3</sub> BO <sub>3</sub> , g/kg	K, mmol/kg	NH <sub>3</sub> , mg/kg	pH <sub>T</sub>	C <sub>Fe</sub> , mkg/kg	T, °C
0,5	0,07	53,8	7,2	4,8	300
		5,4	7,1	4,5	
0,5	0,07	53,8	7,2	3,6	200
		5,4	6,9	5,2	
0,5	0,07	53,8	7,9	9,2	100
		5,4	7,4	54	
0,5	0,07	53,8	8,9	136	25
		5,4	7,9	5060	
8	0,07	53,8	7,2	12420	25
		5,4	6,2	74840	

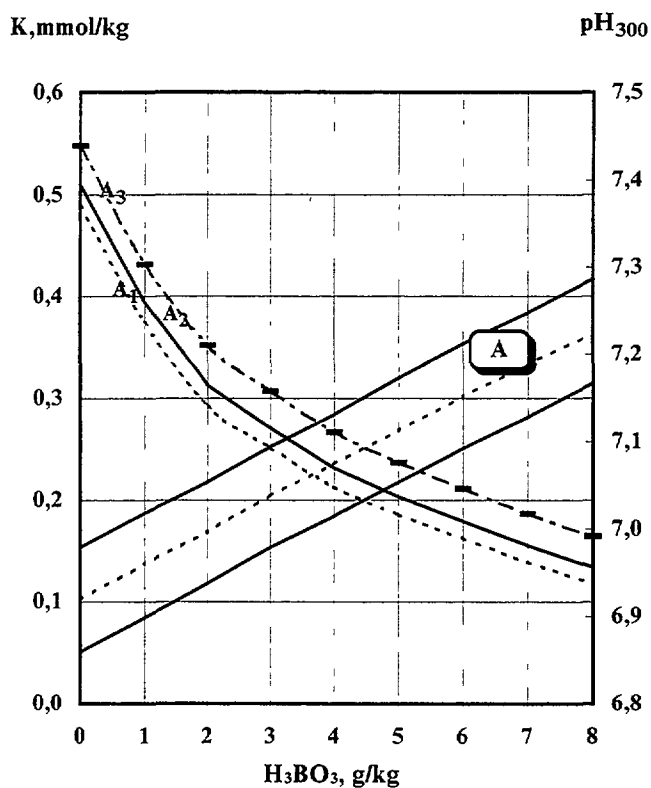


FIG. 5. Coordinated standard water chemistry by [1] and  $pH_{300}$  we have calculated for WWER-440

- ..... A1 -  $NH_3=0$  mg/kg
- A2 -  $NH_3=15$  mg/kg
- - - - A3 -  $NH_3=50$  mg/kg

At power adjustment using boric acid (for example, under emergency power decrease) immediately after injection thereof  $pH_T$  values decrease and corresponding magnetite solubility increase takes place. Then, somewhat delayed injection of potassium hydroxide solution is performed for acid neutralization. As a result, magnetite solubility change wave-like in time occurs and hence

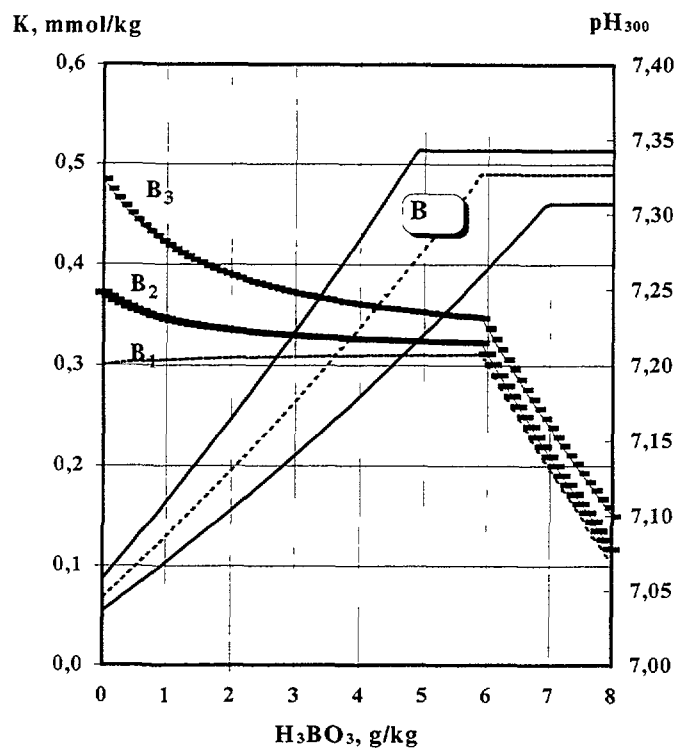


Fig. 6. Coordinated updated water chemistry by [2] and  $pH_{300}$  we have calculated for WWER-440

----- B1 - 0 mg/kg  $NH_3$   
 —■— B2 - 15 mg/kg  $NH_3$   
 —●— B3 - 50 mg/kg  $NH_3$

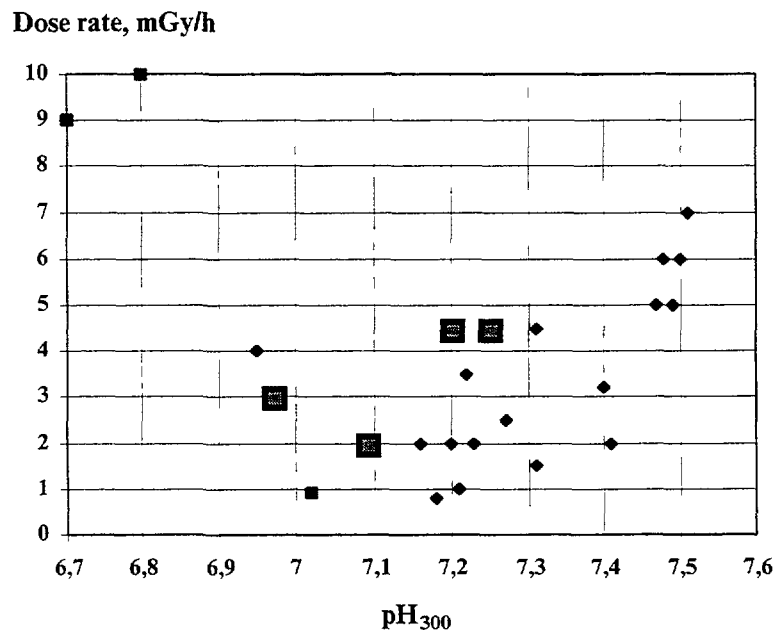


FIG. 7. Dose rate from WWER-440 steam generator collectors at different  $pH_{300}$  values [10-12]

◆ SG [10] ■ SG [12] ● SG [11]

mass transfer increases. In case of the updated regime these variations are more considerable because of higher allowable concentrations of alkaline metals. Discrepancies of current  $\text{pH}_T$  values and optimum one in the cases considered and in normal operation are caused by the procedure of the 1 circuit water chemistry control accepted at present. It does not provide stable reproduction of the relation  $\text{H}_3\text{BO}_3/\Sigma(\text{K}, \text{Na}, \text{Li})$  being normalized in coolant because of delayed alkali solution injection and lack of operative automated control over the coolant composition. As a result of pH value deviation into acidic or alkaline regions from  $\text{pH}_T$  value, corresponding to minimum CP solubility, product corrosion content and  $^{59}\text{Fe}$  activity increase [4].

Taking into account that in most cases of adjustment under emergency protection,  $\text{pH}_T$  shift into acidic region is observed because of inopportune injection of potassium hydroxide solution, ammonia begins to play role of an alkalifying agent, its importance in  $\text{pH}_T$  adjustment being increased with temperature decrease. Thus, data shown in Figure 1 can be interpreted as an effect of boric acid neutralization by ammonia, corresponding to the primary circuit water chemistry change towards conditions providing minimum magnetite solubility favoring thereby dose expenses decrease.

From Fig. 3 and Tables 1 and 2 it follows that ammonia concentration increase action is more effective at the campaign end and especially under shut-down and temperature reduction. At temperature below 200 °C (i.e. under the reactor shut-down and start-up conditions)  $\text{pH}_T$  is determined by ammonia concentration in WWER primary circuit water.

Data on activity build-up in steam generators of different loops are indirect confirmation of the proposal made - activity in different loops can differ 2-10 times, which is indicative of effect of high active water passing time via this loop under the reactor start-up and shut-down [4].

Radioactive corrosion products deposition build-up relation at two different regimes may be described by the following expression:

$$K_{\text{eff}} = C_1 \cdot D_1 \cdot \tau_1 / (C_2 \cdot D_2 \cdot \tau_2), \quad (1)$$

where

$C_{1,2}$  - magnetite solubility in regimes 1 and 2 respectively;

$D_{1,2}$  - diffusion factor in corresponding regime;

$\tau_{1,2}$  - operation duration in corresponding regime.

Operation at rated power is taken as a regime 1 and shut-down conditions - as a regime 2, corresponding values of solubility, diffusion factors and operation duration are given in Table 3.

TABLE 3. CALCULATION PARAMETERS BY EQUATION (1)

No regime	Temperature, °C	$C$ , mol/kg	$D$ , $\text{sm}^2/\text{s}$	$\tau$ , h
1	300	$10^{-7,3}$	$4 \cdot 10^{-4}$	$\sim 7 \cdot 10^3$
2	100-150	$10^{-3,5} - 10^{-4,5}$	$\sim 1,5 \cdot 10^{-4}$	10-20

Calculations for conditions, shown in Table 3, give values  $K_{\text{eff}} \approx 0,5-2$ , which confirmed validity of proposal of a great role of start-up and shut-down periods in redistribution and formation of radioactive depositions in the primary circuit.

Hence practical recommendations on primary circuit water chemistry conditioning naturally follow. The relation  $\text{H}_3\text{BO}_3/\text{KOH}$  maintaining according to OCT [1] provides minimum mass transfer processes at all operation regimes. as the main reason of water chemistry quality deviation from optimum is separate injection of boric acid and potassium hydroxide solutions, it is expedient to adjust water chemistry by a solution containing mixture of boric acid (up to 43 g/kg) and potassium hydroxide (1-2 mmol/kg) [13]. Souring in neutron poisons injection is ruled out in case the emergency protection comes into operation at the reactor shut-down and start-up.

For water conditions variation moderating it expedient to maintain ammonia concentration closer to the upper allowable limit. A degree of approximation should be chosen for each unit individually. This is connected with hydrogen formation efficiency, quantity of hydrogen returned from vents, leakage volume, processes of make-up water preparation, LWR decontamination, processing and storing.

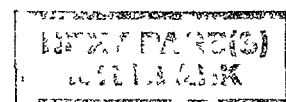
To decrease corrosion load upon the primary circuit equipment as well as radioactive curds build-up. It is expedient to use boric acid enriched in  $^{10}\text{B}$  as a neutron poison rather than that containing a natural mixture of boron isotopes. In accordance with enrichment in  $^{10}\text{B}$ , decrease of boric acid and potassium hydroxide quantity, being injected, is possible. From aforesaid it is evident, that maintaining of optimum water chemistry is simplified and possibility of disturbance thereof is decreased, besides, ammonia content as well as WWER primary circuit waste volume being processed can be decreased too.

## REFERENCES

- [1] OCT 9510301-87 (Standard). Coolant of the primary circuit of WWER-440 type nuclear power reactors with vessels without corrosion resisting hard surfacing. Technical requirements for quality. Maintaining methods, Moscow, Energoatomizdat (1988) - (in Russian).
- [2] "Temporary norms for WWER-440 power reactor primary circuits" (Standard), Moscow, Energoatomizdat (1991) - (in Russian).
- [3] COEN P. "Water technology of nuclear reactors". Trans. from English. Moscow. Energoatomizdat (1973) 328 (in Russian).
- [4] KRITSKIY V.G. "Problems of NPP corrosion and water chemistry conditions". St.-Petersburg, SINTO (1996) 136-142.
- [5] BURKLOVA I., "Corrosion of Zr-based alloys", Nucl.Eng.Int. V.36, No448 (Nov. 1991)41.
- [6] LVOV S.N., PERBONI G., BROGLIA M. "High temperature pH measurements in dilute aqueous ammonia solutions". Physical Chemistry of Aqueous Systems: Meeting the Needs of Industry on the Properties of water and Steam(Proc. the 12<sup>th</sup> International Conference Orlando, Flo.,1994) Begell House, N.-Y. (1995) 441-448.
- [7] MARTYNOVA O.I., CHARITONONOVA N.L. "Lithium metaborate solutions behaviour in steam generators under water depth-evaporation conditions". Teploenergetica, No12, (1990) 53-56 (in Russian).
- [8] SMYKOV V.B., ERMOLAEV N.P., BORTSOV I.A. "Borate-lithium water chemistry of NPP WWER-1000 PGB-1000 2 circuit". Teploenergetica, No8 (1996) 28-33 (in Russian).
- [9] HORVATH G.L., CIVIN V., ORMAI P., PINTER T. "Influence of primary circuit water chemistry on out-core surface activities". Internal progress report on the IAEA Research Agreement No4742/CF, 1988.
- [10] BURCLOVA J., "Corrosion of Zr-based alloys", Water Chemistry of Nuclear Reactor Systems (Proc. 5<sup>th</sup> Int. Conf. Bournemouth UK, Oct 23-28, 1989), BNES (1989) 78.
- [11] ZMITKO M. et all. "State-of-the art in primary water chemistry and radiation control of WWERs". Water Chemistry of Nuclear Reactor Systems (Proc. 7<sup>th</sup> Int. Conf. Bournemouth UK, 1996), BNES (1996) 451

[12] YURMANOV V.A., MAMET V.A., SHESTAKOV Yu.M., AMOSOV M.M. "Water chemistry in WWER reactors". IAEA-TECDOC-927 (Oct 4-8 1993), IAEA (1997) 433-454.

[13] SCHELIK V.G., GORIN V.D., IPATOV P.L., IVANOV V.N., KRITSKIY V.G., STJAGKIN P.S. "Pressure power reactor power boric adjustment method". Request for invention No4856404/25-084679, priority 01.08.90, positive decision 12.09.91, decision about the patent issue 19.06.92.







# MODELLING OF ZIRCONIUM ALLOYS CORROSION IN LWRs

V.G. KRITSKIY\* I.G. BEREZINA, A.V. KRITSKIY, P.S. STJAGKIN,  
VNIPIET, St. Petersburg,

Russian Federation

## Abstract

Chemical parameters, that exerted effect on Zr+1%Nb alloy corrosion and deserved consideration during reactor operation, were defined and a model was developed to describe the influence of physical and chemical parameters on zirconium alloys corrosion in nuclear power plants.

The model is based on the correlation between the zirconium oxide solubility in high-temperature water under the influence of the chemical parameters and the measured values of fuel cladding corrosion under LWR conditions. The intensity of fuel cladding corrosion in the primary circuits depends on the coolant water quality, growth of iron oxide deposits and vaporization portion.

Mathematically, the oxidation rate can be expressed as a sum of heat and radiation components. The temperature dependence on the oxidation rate can be described by the Arrenius equation.

The radiation component of Zr uniform corrosion equation is a function of several factors such as neutron fluency, the temperature the metallurgical composition and et. We assume that the main factor is the changing of water chemistry and the  $H_2O_2$  concentration play the determinative role.

Probably, the influence of  $H_2O_2$  is based on the formation of unstable compound  $ZrO_3 \cdot nH_2O$  and  $Zr(OH)_4$  with high solubility.

The validity of the used formulae was confirmed by corrosion measurements on WWER and RBMK fuel cladding. The model can be applied for calculating the reliability of nuclear fuel operation.

## 1. Physico-Chemical Fundamentals of Model

Empirical studies of numerous oxidation reactions have shown that under constant oxygen pressure in the environment the temperature dependence of the oxidation rate Zr alloys can be described by the Arrenius equation:

$$k_T = k_0 \exp [- Q/R(T+\Delta T)] \quad (1)$$

where

Q - activation energy,

R - gas constant,

T - absolute temperature at the coolant/cladding interface,

$\Delta T$  - growth of cladding temperature under corrosion deposits layer.

Experimental values of  $Q/R$  amount to  $(6,5-13) \cdot 10^3$  K [1-3]. The following experimental facts have revealed the influence of water chemistry on Zr-alloys corrosion:

- influence of water pH (Figure 1b);
- influence of  $H_2O_2$  concentration;
- diminution of corrosion film thickness in the transient stage (i.e. practically its partial dissolution [4]);

---

\* Present address: VNIPIET, Dibunovskaja 55, 197183, St.-Petersburg, , Russia

- morphology of > 3-5 mm thick films (formation of grains and pores between them of different size but the same geometric form) [4];
- crystallization of the dissolved phase in the form of fine  $\text{ZrO}_2$  powder in the water volume of the steam separator of RBMK reactor.

It is well known, that the solubility of oxides is dependent on  $T$ ,  $\text{pH}$  and the concentrations of salts and impurities in solution. The solubility was determined [5] for the systems: zirconium corrosion products ( $\text{ZrO}_2$ ,  $\text{Zr(OH)}_4$ ) - water ( $\text{H}_2\text{O}$ ) - corrective additives ( $\text{HCl}$ ,  $\text{KOH}$ ) over the temperature range of 298-623 K and the correlation between the solubility and Zr alloys corrosion rate analysed. Fig. 1a shows the calculated solubilities of zirconium corrosion products in LWR conditions. Comparing the data in Fig. 1a with Fig. 1b shows that the change of the corrosion rate with  $\text{pH}_T$  is adequate to that of the sum of  $\text{Zr(OH)}_3^+$  and  $\text{Zr(OH)}_5^-$  concentrations, which fact confirm the validity of the model adopted. According to [5], the temperature dependence of the equilibrium solubility of  $\text{ZrO}_2$  is described by an equation similar to Eq. (1), with  $Q/R = (5 \div 15)10^3 \text{ K}$  except that this depends on  $T$  and  $\text{pH}_T$ .

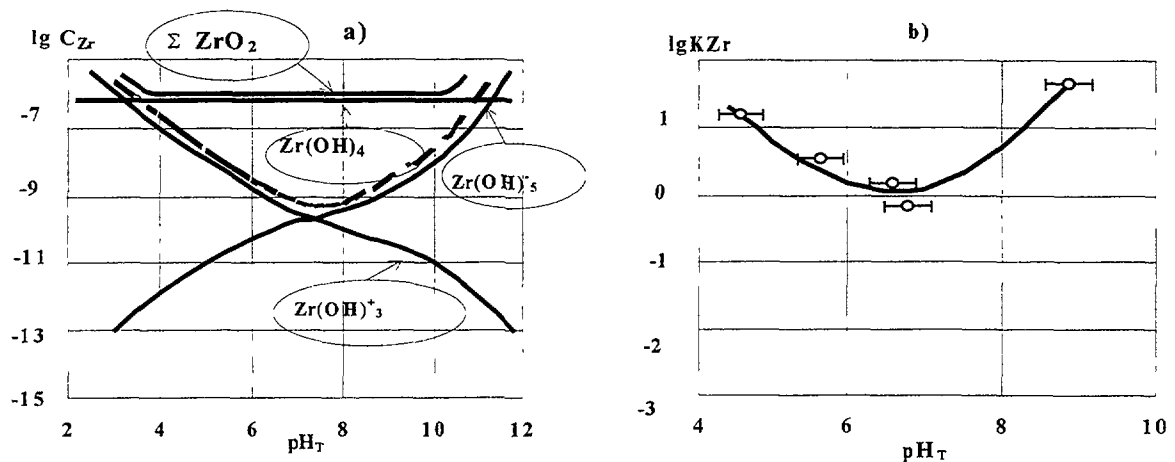


FIG. 1. The calculated solubilities of zirconium corrosion products (mole/kg) in PWR conditions [5] (a) and corrosion rate ( $\mu\text{y}^{-1}$ ) versus  $\text{pH}_T$  [6] (b)  
 ----- envelope [ $\text{Zr(OH)}_5^- + \text{Zr(OH)}_3^+$ ]

The rate of Zr alloy corrosion under reactor irradiation depends on heat flux through fuel cladding coolant chemistry (in addition to  $\text{H}_2\text{O}_2$ ,  $\text{OH}^-$ ,  $\text{O}_2^-$  concentrations one should account for the concentrations of hydrogen, ammonia, strong alkalis -  $\text{LiOH}$ ,  $\text{KOH}$ ,  $\text{pH}$ , etc.) and some other parameters.

The activation energy of radiation corrosion is very small that  $Q_F=0$ . The concentration of dissolved oxygen and products of water coolant radiolysis ( $\text{H}_2\text{O}_2$ ) is one of the important factors that influences the radiation corrosion [1]. Probably, the influence of  $\text{H}_2\text{O}_2$  is based on the formation of unstable compound  $\text{ZrO}_3 \cdot n\text{H}_2\text{O}$  and  $\text{Zr(OH)}_4$  with high solubility. It produces strong effect on the stationary concentrations of practically all products of water coolant radiolysis. In the case of two-phase flow (BWR conditions) solving we have expression (Fig. 2):

$$k_{\Phi}^{\text{BWR}} = N \frac{K_G^{\text{H}_2}}{p} F n_{\alpha}, \quad (2)$$

where

N - constant,

F - fast neutrons fluency,

$n = 0,5 - 1$ ;

$K_G^{H_2}$  - Henry constant;

p - pressure;

$\alpha$  - mass vapour content ( $\alpha = 0 \dots 1$ ).

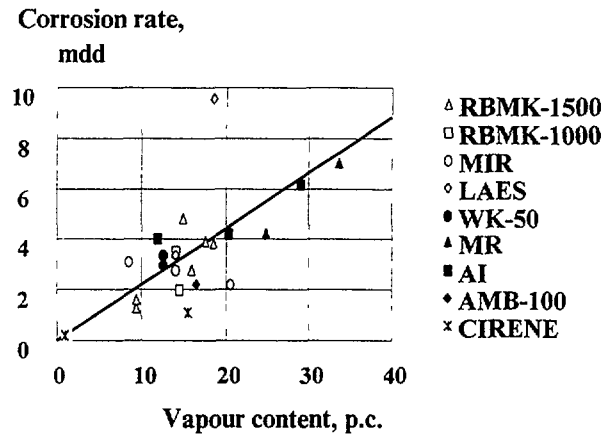


FIG. 2. The vapour content influence on linear Zr-alloy corrosion in various LWR environment

In the case of single-phase flow (PWRs) the material balance equation has another solution. The first approximation for PWRs, if  $\alpha=0$  one can assume that  $k_{\phi}^{PWR} \gg 0$ .

A system of Equations, which take into account the above-mentioned factors for producing a generalised model for calculating Zr alloys corrosion is presented in Table 1.

The Eq. (1) from Table 1 takes into account the effect of alloying components, which can be considered through the energies of mixed oxides formation by the model of ideal solutions. The energy of mixed oxide is calculating as the sum of alloy components energies with accounting of stoichiometric coefficients:  $Q_i = \sum_1^n v_i Q_i$ .

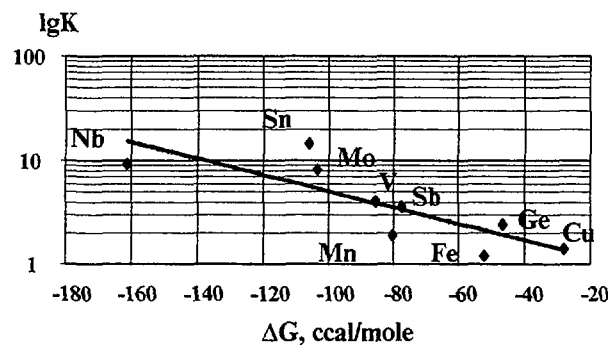


FIG. 3. Correlation between corrosion rates of Zr+1%alloys (mg/(dm<sup>2</sup>·day)) in steam at 400 °C and 17 MPa and the heat of formation of alloying component oxide. Calculations have been made with use of data from [7,8]

TABLE 1. SYSTEM OF EQUATIONS FOR GENERALISED MODEL OF Zr-ALLOYS CORROSION AND FUEL FAILURE INTENSITY

No	Parameter	Equation
1	Composition of alloy	$\ln K_i \sim \frac{\sum v Q_{Me_n O_n}}{RT}$
2	Temperature, heat flow	$K_i \sim K_{io} \exp[-Q_i/(R(T+\Delta T))]$ $\Delta T \sim \Delta x q / \lambda$
3	Radiation, vapour content	$K_j \sim K_{jo} \alpha F^n$
4	Water chemistry, coolant impurities	$pH_T \rightarrow C_{Zr(OH)_n^{4-n}}$ $K_i \sim K_{il} [C_{Zr(OH)_n^{4-n}} + C_{H_2O_2}]$ $K_1 \sim C_x (RT/h) \exp(\sum v Q_i / RT)$
5	General corrosion equation	$K = k_1 e^{-\frac{\sum v Q_i}{R(T+\Delta T)}} + k_2 \frac{1}{1 - \alpha + \beta} F^n$ $vQ_i$ is energy contributions of alloying components and water impurities to oxide formation

TABLE 2. SPECIFICATION FOR Zr ALLOYS IN CORROSION TESTS

Alloy type	Mark	Nb, %	Sn, %	TRM, %			O, ppm	C, ppm	Si, ppm	N, ppm	Refer.
				Fe	Ni	Cr					
Zr-Nb-Sn-Fe	E-635	0,95-1,05	1,20-1,30	0,34-0,40	-	-	500-700	50-100	50-100	30-60	[10]
	ZIRLO	1	1	0,1	-	-	-	-	-	-	[10]
Zr-Nb	E-110	0,95-1,05	-	0,006-0,012	-	-	500-700	50-100	50-100	30-60	[10]
Zr-Sn-TRM	Zr-4	-	1,2-1,7	0,18-0,24	0,007	0,07	-	-	-	-	[9]
	A-1		1,4		0,33		-	-	-	-	[9]
	A-3		0,8		0,8		-	-	-	-	[9]
Zr-Sn-Nb-TRM	B-1	0,3	0,8		0,5		-	-	-	-	[9]
	B-2	0,8	0,8		0,3		-	-	-	-	[9]

Fig.3 represents the influence of alloying components on Zr-alloy corrosion (data from [7,8] have been used specification for Zr alloys see Table 2). Fig.4 gives a correlation between the corrosion rates for various Zr-based alloys in Li-ion containing water and the free energy of mixed oxides formation (calculated with the data from Ref. [8,9,10]). Fig.5 shows a correlation between E-110 alloy corrosion and the ion hydration energy ( $\Delta H_i$ ) in solution at various water coolant chemistries. The effect of the solution composition was considered by similar way with using the quasi-binary model of the energy of an ideal mixed oxide formation:  $Q_2 = \sum_i^n v_i \Delta H_i$ .

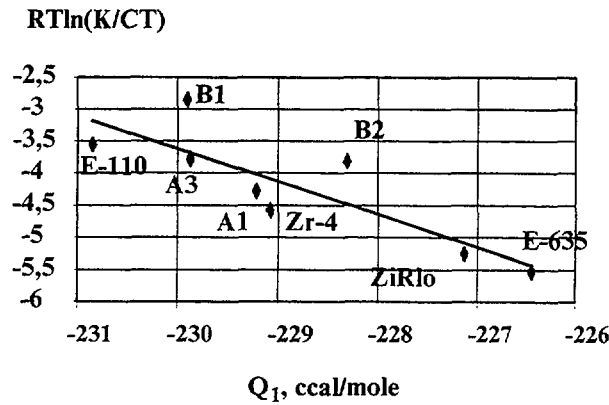


FIG. 4. Dependence of Zr alloys (alloying components: Nb, Sn, Fe, Cr) corrosion in LiOH solutions on  $Q_1$  (calculations have been made with the use of data [8,9,10])

This equations describe the uniform and nodular corrosion of E-110 alloy under LWR's operation conditions. The correlation analysis has proved the applicability of the before developed model [3] which include the Eqs (2) and (3) from Table 1 and derived equations for describing the experimental data.

The success of such approach makes possible to propose a generalised model for calculating the corrosion of Zr-alloys.

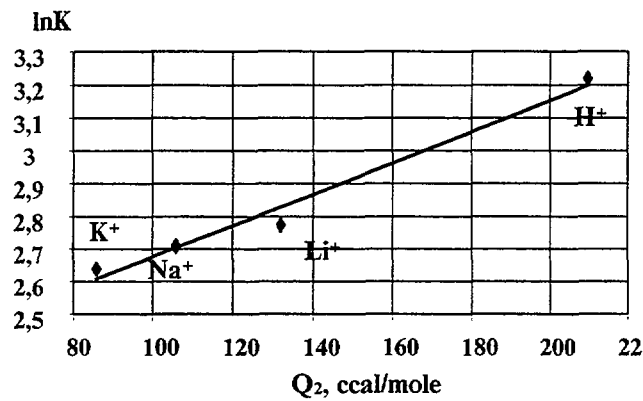


FIG. 5. Correlation between corrosion of E-110 alloy and energy of ion hydration ( $Q_2$ ) with  $\sim 10^{-5}$  mole concentration (autoclave testing at  $360^\circ\text{C}$ ) (Calculations have been made with the use of data from [10])

## 1. Model for Estimating the Number of Fuel Failures

During operation of LWR's fuel integrity can be deteriorated by a series of factors and corrosion is only one of them. To describe the situation we have chosen a model of proportional risks used in the reliability theory. For every set of data this model offers an equation to define the impact of an additional parameter on the failure intensity, and then

$$n_i = n_0 \exp \sum_{a=1}^K b_a V_a \quad (3)$$

where

$n$  is a nominal number of failures at LWRs;

$n_i$  is a number of failures at LWRs,

$V_a = K_T + K_\Phi$  is variation of the corrosion parameter year of observation, examination in the series observed (surveyed);

- $b_a$  is a coefficient to define the extent of corrosion impact on the fuel failure in the series observed;
- $K$  is a number of parameters considered (corrosion included).

The approach described is supported by the data of Table 3.

TABLE 3. DEPENDENCE OF FUEL FAILURE INTENSIVITY ON FUEL CLADDING CORROSION

No	Reactor type	Fuel Failure intensity $\times 10^5 \cdot \text{F} \cdot \text{y}^{-1}$	Max. cladding cor. rate, $\mu \cdot \text{y}^{-1}$
1	WWER-440	6	1-2
2	WWER-1000	8	3-5
3	RBMK-1000	110	40-60
4	RBMK-1500	80	30-50

For calculations we've obtained a corrosion rate equation accounting for Fe-oxides deposition and probable radiolysis suppression (by  $\text{H}_2$  and Cu impurities in water) and used this in our computer calculations Eq. (4):

$$V_a = \frac{dh}{dt} \Big|_{t=0} = A_1 \left( \frac{1}{1-\alpha} \exp \frac{B}{T+\gamma M_{Fe}} \right) + A_2 \left( \frac{F}{1-\alpha+\beta} \right) \quad (4)$$

where

$A_1$  and  $A_2$  are coefficients depending on water chemistry regime;

$B=Q/R$ ,

$T$  is the coolant temperature;

$\alpha$  is mass vapour content;

$F$  - neutron flux;

$M_{Fe} = \sum c \tau$  is a quantity of iron entered into the core during fuel operation;

$\gamma=q/\lambda$ ;

$q$  - heat flux;

$\lambda$  - coefficient of thermal conductivity for oxide layers;

$\beta$  is a coefficient accounting for the extent of radiolysis suppression impurities.

In result calculations for WWER and RBMK reactors the coefficient of the correlation between observed and calculated fuel failures per year ranges from 0,63 to 0,77 (Fig. 6). The effect of water chemistry is most pronounced evident at the early stage of Zr+1%Nb clad fuel operation.

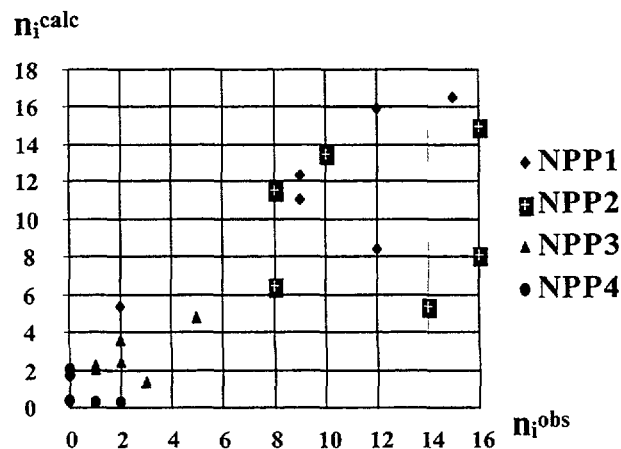


FIG. 6. Correlation between observed ( $n_i^{obs}$ ) and calculated ( $n_i^{calc}$ ) fuel failures per year ranges for RBMK reactors

It follows from mathematical analyses, that optimal water chemistry control results in the decrease of  $n_i(t)$ . At some power units the intensity of fuel failure can be reduced at least by a factor from two to five.

## Conclusions

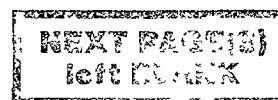
1. A model was developed to describe the effect of physical and chemical parameters of Zr alloys under LWR conditions. The choice was made of chemical parameters which influence Zr corrosion and can be considered during reactor operation.

2. The activation energy of oxidation process is calculating on the base of ideal mixed oxide formation model. The calculation formulae were verified on the base of experimental data on fuel cladding corrosion in the loops and NPPs LWR reactors.

3. Fuel failure intensity at NPPs with WWERs and RBMKs has been shown to depend on coolant quality namely on the growth of Fe-oxide deposits and local vaporisation. At some power units optimal water quality control can reduce the fuel failure intensity at least by half.

## REFERENCES

- [1] "Corrosion of Zirconium alloys in nuclear power plants". IAEA, Vienna (1993). IAEA-TECDOC 684.
- [2] PYECHA, T.D., BAIN, G.M., McINTEER, W.A., PHAM, C.H., "External cladding corrosion of B&W-designed PWR fuel rods through burnups of 50 GWD/MTU", IAEA Technical Committee on External Cladding Corrosion in Water Power Reactors, Cadarache, France, Oct. 14-18 (1985).
- [3] KRITSKIY, V.G., PETRIK, N.G., BEREZINA, I.G., DOILNITSINA, V.V., "Effect of Water Chemistry and Fuel Operation Parameters on Zr+1%Nb Cladding Corrosion", IAEA Meeting on Influence of Water Chemistry on Fuel Cladding Behaviour. Rez, Czech Republic, Oct. 04-08 (1993). Vienna, 1997, February, IAEA-TECDOC-927, p.23-43.
- [4] MAROTO, A.J.G., et al., "Growth and characterisation of oxide layers on zirconium alloys", IAEA Meeting on Influence of Water Chemistry on Fuel Cladding Behaviour. Rez, Czech Republic, Oct. 04-08 (1993).
- [5] KRITSKIY, A.V., "Rastvorimost produktov korrozii zirkoniya i hroma v vodnih rastvorah pri 298-623 K", Avtoreferat dissertatsii na soiskanie uchyonoy stepeni kandidata himicheskikh nauk. S.-Petersburg (1992).
- [6] AMAEV, A.D. et al., "Obosnovanie vybora zirkonievogo splava dl'a obolochek tvelov seriynykh energeticheskikh reaktorov WWER-440", Trudy nauchno-tehnicheskoy konferentsii "Atomnaya energetika, toplivnye tsikly, radiatsionnoe materialovedenie". Ul'yanovsk, Russia, Oct. 05-10 (1970).
- [7] PARFENOV, B.G., GERASIMOV, V.V., VENEDICTOVA, G.I. "Corrosion of zirconium and its alloys". M.: Atomizdat, 1967, 257 pp.
- [8] "Thermodynamic properties of inorganic substances". Guidebook. Editor A.P.Zefirova, Ph.D., M.: Atomizdat, 1965, 460 pp.
- [9] JEONG, Y.H., RUHMANN, H., GARZAROLLI, F., "Influence of Alkali Metal Hydroxides on Corrosion of Zr-based Alloys". IAEA Influence of water chemistry on fuel cladding behaviour. Proceeding of a Technical Committee meeting held in Rez, Czech Republic, 4-8 October 1993. Vienna, 1997 February, IAEA-TECDOC-927, p.193-206.
- [10] NIKULINA, V. et. al. "Zirconium Alloy E635 as a Material for Fuel Rod Cladding and Other Components of WWER and RBMK Cores". Eleventh International Symposium on Zirconium in the Nuclear Industry, 1994, Pal Alto, USA.



# SUBCOOLED BOILING EFFECT ON DISSOLVED GASES BEHAVIOUR

M. ZMÍTKO

Nuclear Research Institute Řež plc.



XA9953306

J. SINKULE<sup>†</sup>, V. LINEK

Institute of Chemical Technology

Prague, Czech Republic

## Abstract

A model describing dissolved gasses (hydrogen, nitrogen) and ammonia behaviour in subcooled boiling conditions of VVERs was developed. Main objective of the study was to analyse conditions and mechanisms leading to formation of a zone with different concentration of dissolved gases, eg. a zone depleted in dissolved hydrogen in relation to the bulk of coolant. Both, an equilibrium and dynamic approaches were used to describe a depletion of the liquid surrounding a steam bubble in the gas components. The obtained results show that locally different water chemistry conditions can be met in the subcooled boiling conditions, especially, in the developed subcooled boiling regime. For example, a 70% hydrogen depletion in relation to the bulk of coolant takes about 1 ms and concerns a liquid layer of 1  $\mu\text{m}$  surrounding the steam bubble. The locally different concentration of dissolved gases can influence physico-chemical and radiolytical processes in the reactor system, eg. Zr cladding corrosion, radioactivity transport and determination of the critical hydrogen concentration.

## 1. Introduction

A primary water chemistry of the pressurized water reactors is controlled with respect to assure an integrity of the primary pressure boundary, the fuel cladding integrity, and minimization of the radiation fields and occupational radiation exposure. For this reason, weak-alkaline, reduction conditions are kept in the primary coolant. The reduction conditions are maintained by an overpressure of hydrogen which suppresses a generation of oxidizing species by radiolytical processes in the reactor core.

In the WWER units, the hydrogen overpressure is maintained by ammonia dosing into the primary coolant where hydrogen and nitrogen is generated by its subsequent radiolytical and thermolytical decomposition. During a normal operation, concentration of dissolved hydrogen and nitrogen is in range of 25-35 ccSTP  $\text{H}_2/\text{kg}$  and 10-15 ccSTP  $\text{N}_2/\text{kg}$ , respectively. Ammonia concentration varies from plant to plant, typically between 10 and 40 ppm. Such level of dissolved hydrogen guarantees the oxygen concentration in the VVER and PWR units below 5-10 ppb.

However, a zone can be found in the reactor core where the fuel cladding temperature may exceed a saturation temperature at given pressure and where a subcooled boiling occurs. An existence of the subcooled boiling can influence a behaviour of the dissolved gases and be responsible for a formation of their locally different concentration levels. It is considered that a local depletion in a dissolved gas in relation to the bulk of coolant can occur by eg. hydrogen stripping into the steam bubbles that subsequently escape from the surface into the bulk flow where condensate. Because of a depletion in dissolved hydrogen, a shift of radiochemical reactions can follow in favour of the oxidizing species production in such zone, and finally a different water chemistry conditions can be established. In this connection, a critical hydrogen concentration is considered. This concentration is defined as a concentration of hydrogen that is still able to suppress radiolytical production of the oxidizing species.



A phenomenon of the formation of locally different water chemistry conditions due to a subcooled boiling effect is considered mainly with respect to a possible acceleration of zirconium cladding corrosion and an effect on corrosion product behaviour and radioactivity build-up on the primary system surfaces.

So, the main objective of this study was to analyse conditions and mechanisms leading to formation of a zone with different concentration of dissolved gases, eg. the zones depleted in dissolved hydrogen in relation to the bulk of coolant.

## 2. Thermal-Hydraulic Assessment

A WWER-1000 unit was chosen for detail analysis of the dissolved gases behaviour. The first of all, thermal-hydraulic conditions of the WWER-1000 unit were analysed with respect to a possible formation of locations in the reactor core working in subcooled boiling regime, an extent and intensity of the subcooled boiling process. The thermal-hydraulic assessment was based on a simplified model of the fuel channel where a surface heat flux  $q_w$ , the coolant temperature  $T$  and cladding surface temperature  $T_w$  were determined. The assessment was performed for the following parameters:

Primary system pressure (saturation temperature),  $P$ : 15.7 MPa ( $T_s$ : 345.8°C)

Core inlet temperature,  $T_i$ : 289 °

Average linear heat rate of the fuel rod,  $q_{la}$ : 15.8 kW/m

Average heat flux on the cladding surface,  $q_{wa}$ : 550 kW/m<sup>2</sup>

Fuel rod outer diameter,  $d$ : 9.144 mm

Fuel rod length,  $L$ : 3.5 m

Coolant flow velocity in the core (considered as input data),  $v_L$ : 4 m/s

Radial coefficient of the power distribution in the core,  $K_r$ : 1.2

Axial coefficient of the power distribution in the core,  $K_z$ : 1.45

Results of the thermal-hydraulic assessment show that there is a number of the fuel channels working in the subcooled boiling regime, ie. where the cladding temperature is reaching saturation temperature ( $T_w = T_s$ ). Temperature distribution in the reactor core is shown in Fig.1 in form of isotherms for the coolant and cladding surface temperatures. Distribution of the heat flux, and the coolant and cladding surface temperatures in the axial fuel channel ( $r = 0$ ) is given in Fig.2.

## 3. Modelling of Dissolved Gases Behaviour

Two different approaches were considered in development of a model of dissolved gases behaviour. An *equilibrium model* describes a process of saturation of the steam bubbles by dissolved gases or ammonia as an equilibrium process where the equilibrium concentration of the gas in steam (ie. its solubility level) is reached. In the opposite, a *dynamic model* describes the saturation process with respect to its dynamics. A reaching of the chemical equilibrium state is considered as a time-dependant process where the final equilibrium state need not to be reached.

### 3.1 Equilibrium model

A depletion of the coolant in dissolved gases can occur at steam phase generation. If steam bubbles are equilibrationally saturated with a dissolved gas the following balance and equilibrium state is valid:

$$\begin{aligned} V_{L0} \rho_L &= V_L \rho_L + V_G \rho_G \\ V_{L0} c_{L0i} &= V_L c_{Li} + V_G c_{Gi} \\ c_{Gi} &= \psi_i c_{Li} \end{aligned} \quad (1)$$

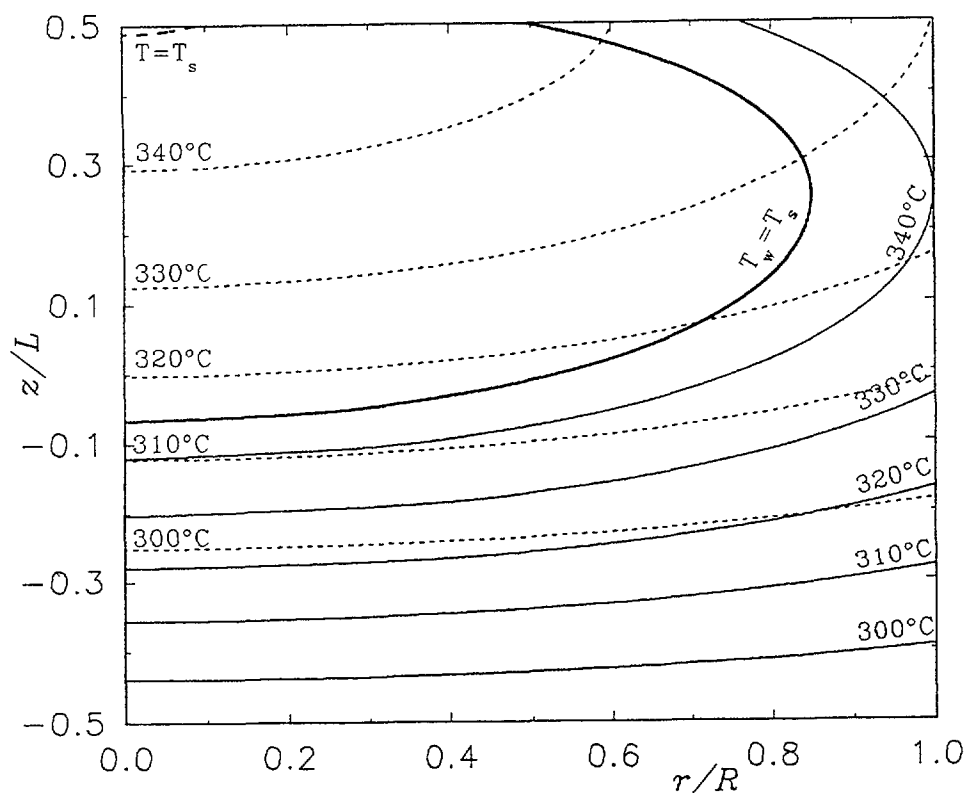


**Fig.1** Thermal-hydraulic assessment of VVER-1000 Temperature distribution in the reactor core – isotherms for constant coolant ( $T$ ) and cladding surface ( $T_w$ ) temperature ( $K_z = 1.45$ ,  $K_r = 1.2$ )

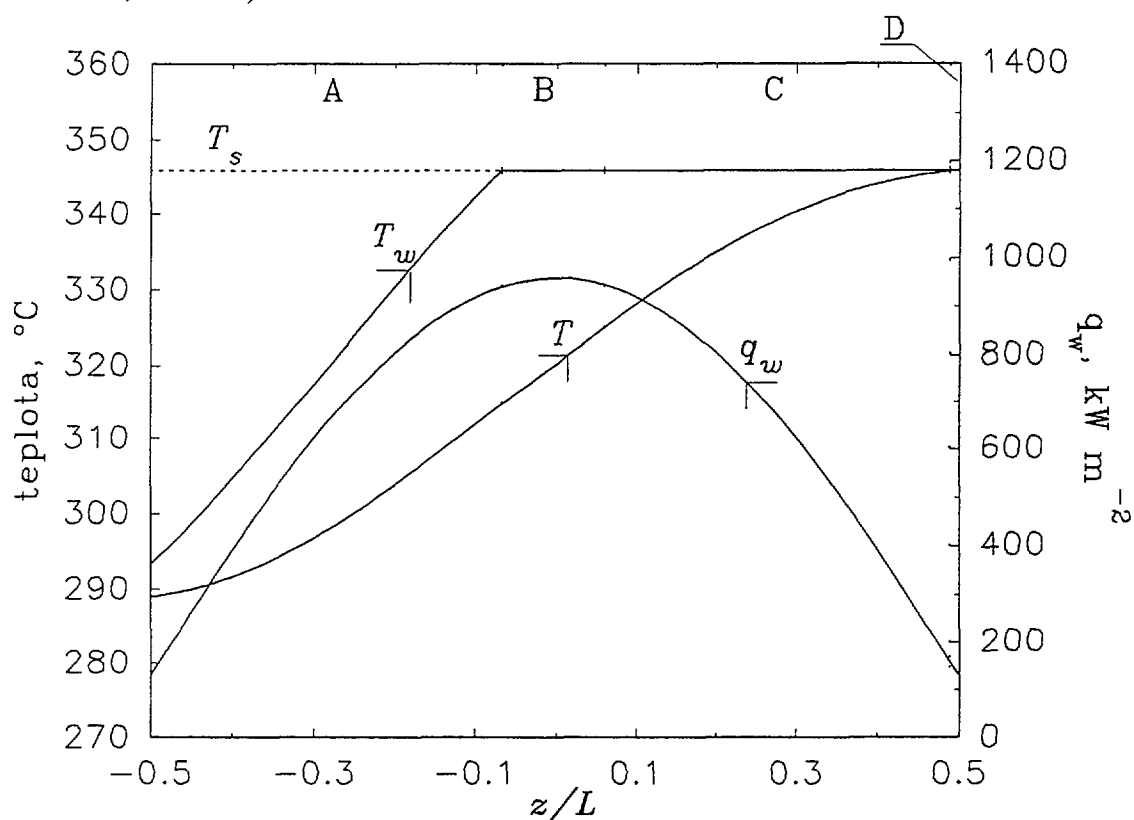


**Fig.2** Thermal-hydraulic assessment of VVER-1000: Distribution of heat flux ( $q_w$ ), the coolant ( $T$ ) and cladding surface ( $T_w$ ) temperature in the axial fuel channel ( $r=0$ ), A – convective heat transfer, B – non-developed subcooled boiling, C – developed subcooled boiling, D – boiling

A distribution coefficient  $\Psi_i$  is calculated from the gas solubility values [2,3] as:

$$\Psi_i = \frac{22400 \rho_G}{He_i P M_{H_2O} \rho_L} \quad i = H_2, N_2, NH_3 \quad (2)$$

The index 0 in the equation (1) indicates an initial state of the liquid phase before the steam phase generation. A relative drop of concentration of the gas component  $i$  dissolved in the coolant  $c_{Li}/c_{Li0}$  can be expressed in dependance on the steam phase fraction (ie. void fraction)  $e = V_G/(V_G + V_L)$  as:

$$\frac{c_{Li}}{c_{Li0}} = \frac{\varepsilon \rho_G + (1 - \varepsilon) \rho_L}{\rho_L (\varepsilon \Psi_i + 1 - \varepsilon)} \quad (3)$$

An effect of the void fraction on a relative drop of concentration of dissolved nitrogen, hydrogen and ammonia is shown in Fig.3 for the given thermal-hydraulic conditions. It is evident that some significant depletion of the coolant in dissolved hydrogen and nitrogen occurs at the void fraction  $e > 0.05$  (5%), ie. at relatively high steam phase fraction. This effect is caused by a high solubility of the both gases at given temperature in comparison with ambient temperature – the difference in 10-12 times. Hydrogen solubility is higher than nitrogen solubility so that the depletion in nitrogen is higher. On the other hand, the depletion in ammonia is negligible due to its very high solubility in water.

It was shown by calculations that the steam phase fraction in the subcooled boiling regime can reach as maximum 2.5%, at the same time an average void fraction is less than 0.5%. At such conditions, the equilibrium model of the dissolved gases behaviour gives maximum depletion in hydrogen and nitrogen about 10%, and the average depletion only 2.5%.

### 3.2. Dynamic model

A depletion of the coolant in dissolved gases can also occur due to a steam flow inside the bubble or at the steam bubble growth process. Such a depletion has a local character, ie. it is related to the liquid surrounding the steam bubble, and is limited in time.

#### *Subcooled boiling mechanisms*

A heat removal from the fuel rods can proceed in qualitatively different mechanisms in dependance on the local heat flux  $q_w$  and local coolant temperature  $T$ . A **convection heat transfer mechanism** takes place when the fuel cladding surface temperature is below the saturation temperature at given pressure. If the convective transfer is not sufficient to remove the generated heat, a surface temperature exceeds the saturation temperature and steam bubbles are formed by nucleation, ie. a **subcooled boiling mechanism** is taking place.

Bubbles are predominantly formed on places with a proper geometrical microstructure. It is supposed that the steam generated on the fuel cladding surface flows through a stagnant bubble and re-condensates at a top of the bubble. The condensation heat is taken through a thinner boundary layer from here into the bulk of coolant. Because of a relatively big difference between the cladding surface and bulk coolant temperatures in this area ( $T_s - T$ ), the bubbles have a small diameter and are sitting on the surface. This kind of subcooled boiling mechanism is called as a **non-developed subcooled boiling**. The bubbles are not escaping from the surface because a hydrodynamic drag force of the coolant flow is lower than a surface tension force keeping a bubble on the surface. A critical radius of the bubble, ie. a distance between a top of the bubble and the cladding surface at moment of an escape, can be expressed from a balance of the forces as follows [1]:

$$Y_b = 0,015 \sqrt{\frac{\sigma_L d_e}{\tau_w}} \quad \text{kde} \quad \tau_w = \frac{1}{2} f \rho_L v_L^2 \quad (4)$$

The critical bubble radius for the given thermal-hydraulic conditions is  $Y_b = 1,14 \times 10^{-5}$  m.

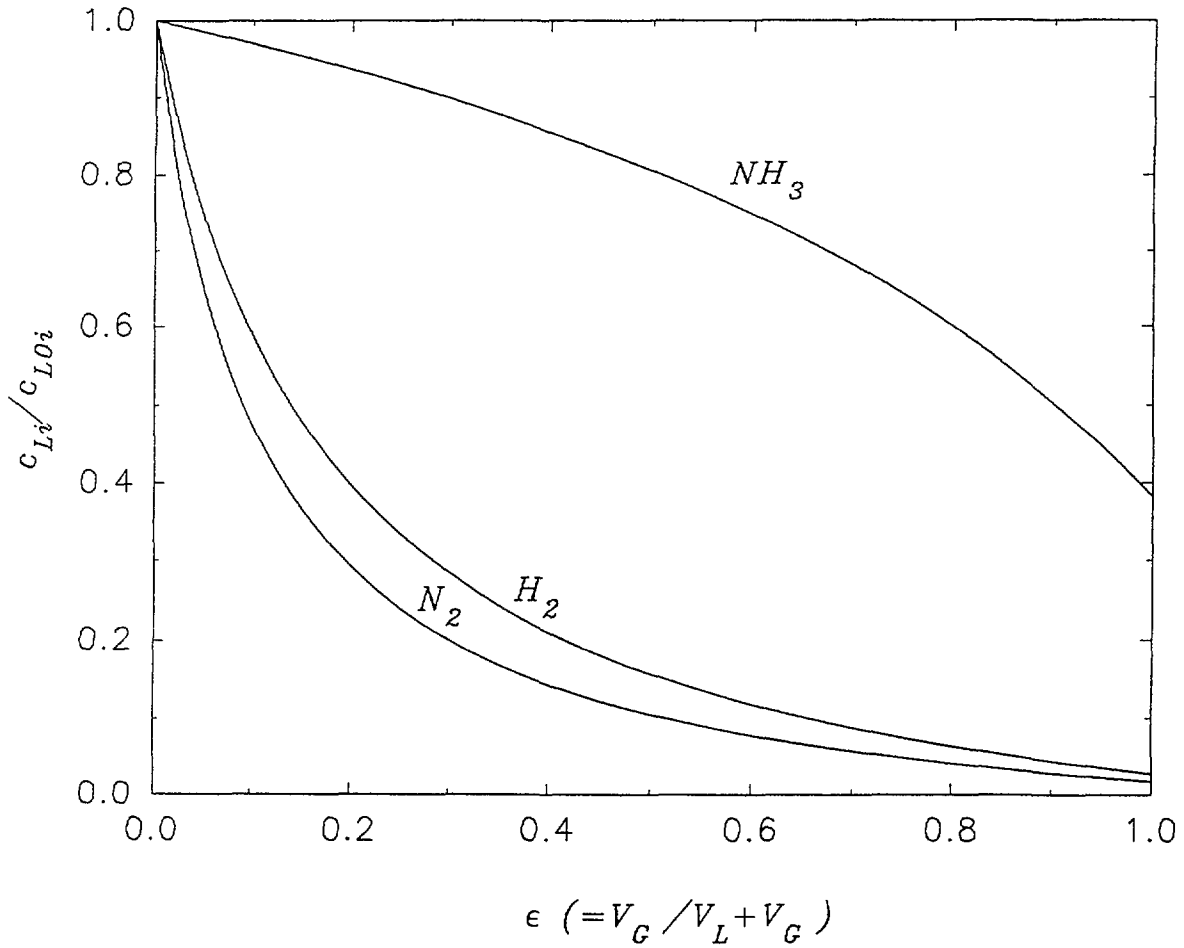


**Fig.3** Effect of void fraction on relative drop of concentration of dissolved nitrogen, hydrogen and ammonia (results of calculations by the equilibrium model)

If an intensity of the steam generation is higher than its rate of condensation in the top of bubble, a bubble is growing and the bubble radius exceeds the critical bubble radius. In this case, the bubble escapes from the surface into the bulk of coolant where it condensates. Such state of the process is called as a **developed subcooled boiling**.

#### *Non-developed subcooled boiling*

A model used for analysis of a possible local depletion of the coolant in dissolved gases in surrounding of the stagnant bubbles is shown in Fig.4. A cylinder with height and diameter of  $Y_b$  is considered as a model stagnant bubble. Water evaporated on the surface ( $y = 0$ ) flows through the bubble and condensates in the top of bubble ( $y = Y_b$ ). Condensation heat is taken into the bulk of coolant through a boundary layer with thickness of  $(d - Y_b)$ . Thickness of the thermal boundary layer is expressed as  $d = l_f / \alpha$ . Dissolved gases diffuse into the steam bubble from the surrounding liquid through sides of the cylinder. Inside the bubble, the gases are flushed by steam toward the top of bubble and then diffuse through the boundary layer into the bulk of coolant. Numerical analysis showed that because of a low concentration of the gases in steam, a flow velocity of the steam-gases mixture in the bubble is practically the same as the flow velocity of the steam itself. Thus, a model for description of dissolved gases behaviour at the non-developed subcooled boiling conditions can be formulated as follows:

$$D_{G_i} \frac{d^2 c_{G_i}}{dy^2} - v_G \frac{dc_{G_i}}{dy} + k_{L R i} \frac{2}{Y_b} (c_{L i} - c_{G_i} / \psi_i) = 0 \quad (5)$$

$$v_G = q_b / \rho_G \Delta H_{vyp} \quad q_b = k_T (T_s - T)$$

with boundary conditions:

$$y = 0: \quad D_{G_i} \frac{dc_{G_i}}{dy} - v_G c_{G_i} = 0 \quad (6)$$

$$y = Y_b: \quad D_{G_i} \frac{dc_{G_i}}{dy} - v_G c_{G_i} = k_{L_i} (C_{L_i} - c_{G_i} / \psi_i)$$

The heat and mass transfer coefficients from the top of bubble  $k_T$  and  $k_{L_i}$ , and the side diffusion coefficient  $k_{L_{Ri}}$  were calculated taking into account more realistic shape of the steam bubble – hemisphere (see Fig.5):

$$k_T = \frac{\lambda_L}{\delta} f(Y_b) = \alpha f(Y_b) \quad k_{L_i} = \frac{D_{L_i}}{\delta} f(Y_b) \quad k_{L_{Ri}} = \frac{D_{L_i}}{Y_b} \quad (7)$$

where a correction factor  $f(Y_b)$  expresses a changing distance of the bubble top from a border of the thermal boundary layer  $d$  at an one-way heat transfer or diffusion process in  $y$ -direction:

$$f(Y_b) = -\frac{2\delta}{Y_b} \left[ 1 + \frac{\delta}{Y_b} \ln \left( 1 - \frac{Y_b}{\delta} \right) \right] \quad (8)$$

Results of calculations for a part of the fuel channel working in the non-developed subcooled boiling conditions are given in Fig.6. Concentration of hydrogen, nitrogen and ammonia in the liquid surrounding the stagnant steam bubbles is shown for the bubbles of maximum hydraulic stable radius at the given conditions ( $Y_b = 1,14 \times 10^{-5}$  m). It can be seen that the difference of the dissolved gases concentration in comparison with their concentration in the bulk of coolant depends on temperature gradient between the cladding surface and the coolant ( $T_s - T$ ) which determines the steam flow velocity through a bubble. Maximum depletion in the dissolved gases occurs at the beginning of the non-developed subcooled boiling when a number of bubbles on the cladding surface is relatively low.

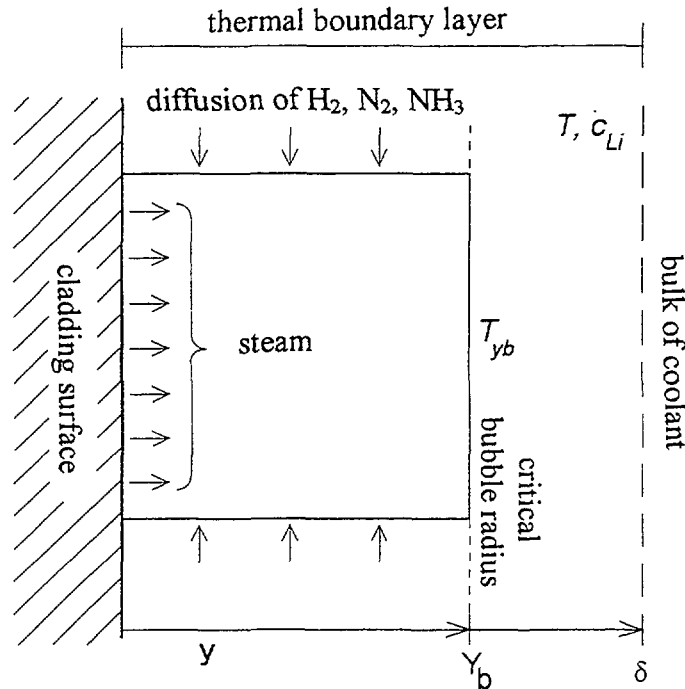


**Fig.4** Model of a stagnant steam bubble used for analysis of local depletion of the coolant in dissolved gases in surrounding of the bubble (the dynamic model – non-developed subcooled boiling regime)

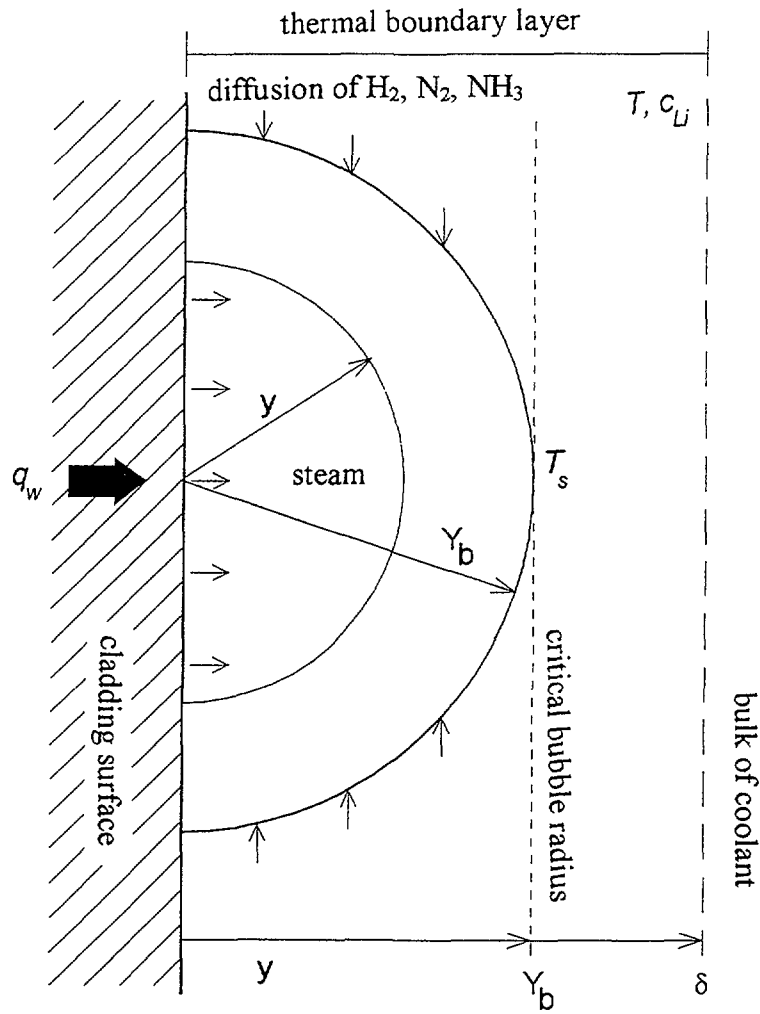


**Fig.5** Model of a growing steam bubble with the critical bubble radius used for analysis of local depletion of the coolant in dissolved gases in surrounding of the bubble (the dynamic model – developed subcooled boiling regime)

The maximum depletion in relation to the bulk concentration can reach 15% for hydrogen, 35% for nitrogen and 27% for ammonia. Such depletion occurs in a 5  $\mu\text{m}$  thick liquid layer surrounding the steam bubble and is not limited in time.

#### *Developed subcooled boiling*

A heat transfer mechanism connected with a development subcooled boiling starts play a role when the stagnant steam bubbles are not able to take away a generated heat. In this case, a volume of the steam bubble is growing until its radius reaches the critical one. Then, the bubble escapes from the surface into the bulk of coolant and condensates. Because of the low concentration of dissolved gases in the coolant, their effect on the rate of heat and steam transfer in the bubble is negligible. Then, the steam bubble growth can be modelled independently from a diffusion saturation of the bubble by dissolved gases. A schema of the model is shown in Fig.5.

A balance of steam in the bubble is described by an equation

$$\frac{d}{dt} \left( \frac{2}{3} \pi y^3 \right) = \frac{(2Y_b)^2 q_w}{\rho_G \Delta H_{vyp}} - \frac{\pi y^2 k_T (T_s - T)}{\rho_G \Delta H_{vyp}} \quad (9)$$

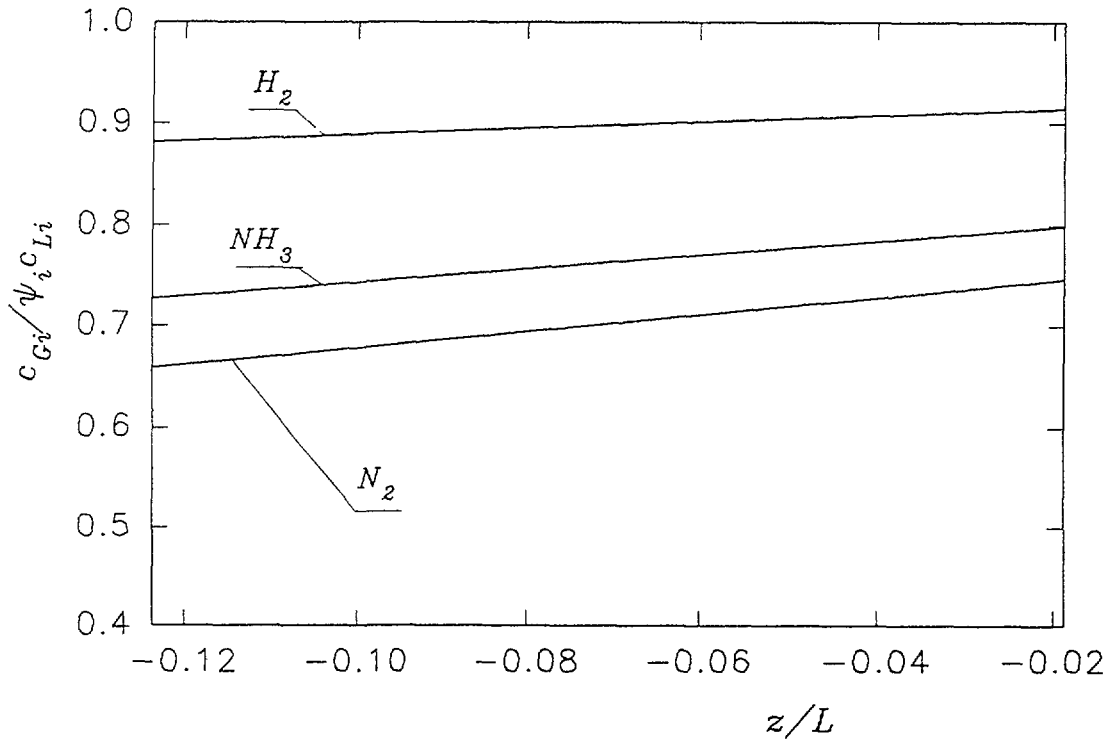


**Fig.6** Calculated axial profile of concentration of dissolved nitrogen, hydrogen and ammonia related to its concentration in the bulk of coolant  $c_{Gi}/\psi_i c_{Li}$  (the dynamic model – non-developed subcooled boiling area)

where the term on the left side of the equation (9) expresses the bubble volume growth rate. The first term on the right side is a volume flow rate of generated steam which is proportional to the heat flux through a square with side of  $2Y_b$ . The second term expresses a volume flow rate of the steam which is condensated on a bubble-coolant interface. An initial condition is:

$$t = 0: \quad y = 0 \quad (10)$$

A period of the bubble growth  $t_b$ , ie. time of the bubble existence before its escape from the surface, can be obtained by integration of the equation (9) with upper limit of  $y = Y_b$ . During this growth period, the bubble is continuously saturated with dissolved gases from the surrounding liquid by a diffusion process. Formulation and solution of a problem with a moving phase boundary is difficult, therefore a simplified model for description of the bubble saturation process was used. According to this simplification, it is considered that the bubble with critical radius  $Y_b$  is saturated by diffusion during the bubble growth period  $t_b$ . The following equations describe the bubble saturation process by diffusion:

A balance of the gas  $i$  ( $H_2$ ,  $N_2$ ,  $NH_3$ ) in the bubble

$$\frac{2}{3} \pi Y_b^3 \frac{dc_{Gi}}{dt} = 2 \pi Y_b^2 D_{Li} \left[ \frac{\partial c_{Lbi}}{\partial y} \right]_{y=Y_b} \quad (11)$$

where  $c_{Gi}$  is a gas concentration in the bubble, and  $c_{Lbi}$  is a concentration of dissolved gas in the liquid surrounding the bubble.

A balance of the gas  $i$  in the liquid

$$\frac{\partial c_{Lbi}}{\partial y} = D_{Li} \frac{\partial^2 c_{Lbi}}{\partial y^2} \quad (12)$$

with boundary and initial conditions:

$$\begin{aligned} y = Y_b: \quad c_{Lbi} &= c_{Gi} / \psi_i \\ y = \infty: \quad c_{Lbi} &= c_{Li} \\ t = 0: \quad c_{Lbi} &= c_{Li} \quad c_{Gi} = 0 \end{aligned} \quad (13)$$

An analytical solution of the equation system (11)-(13) can be found in the following form:

$$\begin{aligned} \frac{c_{Gi}(t)}{\psi_i c_{Li}} &= 1 - \exp(\beta t) \operatorname{erfc}(\sqrt{\beta t}) \\ \frac{c_{Lbi}(t, y)}{c_{Li}} &= 1 - \exp\left[\beta t + (y - Y_b) \sqrt{\beta / D_{Li}}\right] \operatorname{erfc}\left(\sqrt{\beta t} + \frac{y - Y_b}{2\sqrt{D_{Li} t}}\right) \\ \beta &= D_{Li} \left(\frac{3}{Y_b \psi_i}\right)^2 \end{aligned} \quad (14)$$

A term  $c_{Gi}(t)/\psi_i c_{Li}$  in the equations (14) expresses a level of saturation of the growing bubble by gas  $i$  in relation to its equilibrium concentration (ie. solubility) in the bulk of coolant. In a similar way, the term  $c_{Lbi}(t, y)/c_{Li}$  expresses a concentration of dissolved gas  $i$  in the liquid surrounding the steam bubble in relation to its equilibrium concentration (ie. solubility) in the bulk of coolant. Then, a relative depletion of the liquid in dissolved gas  $i$  is expressed as a supplement to 1.

Results of the calculations are demonstrated in Fig.7 and Fig.8. The Fig.7 shows a concentration profiles of hydrogen, nitrogen and ammonia in the liquid surrounding the bubble in period of its growth. The bubble growth period  $\tau_b$  calculated for the given thermal-hydraulic conditions is in range of 1-2 ms. Therefore, the calculated concentration profiles are valid only for times  $t < \tau_b$ . It can be seen from the figure that a deep depletion in dissolved hydrogen and nitrogen in liquid surrounding the bubble can occur in times below 1 ms, what is in the most cases the bubble growth period. Such a depleted layer of the liquid is very thin, units of  $\mu\text{m}$ . Moreover, the bubble growth process is a periodic one and the situation will repeat itself. A frequency of the steam bubble arising on the surface is in order of 1,000 times per a second, ie. 1 kHz.

A sense of the depletion extension and time period can be apparent from Fig.8. Here is shown a thickness of the liquid layer surrounding the bubble,  $l_0$ , as a function of time for a different level of dissolved gas depletion. For example, it can be found from the figure that a liquid layer with 70% depletion in dissolved hydrogen (in average) will exist for 0.95 ms and its thickness will be maximally  $l_0/Y_b = 0.11$ , ie.  $l_0 = 0.11 \cdot 1.14 \cdot 10^{-5} = 1.3 \cdot 10^{-6} \text{ m} = 1.3 \mu\text{m}$ .

A similar picture as shown for dissolved hydrogen behaviour can be also found for dissolved nitrogen. Ammonia behaviour is different from that because of its high solubility, ie. ammonia depletion level in the surrounding liquid will be much lower. In the case of hydrogen and nitrogen, which are less soluble in the liquid, the time of a bubble growth is not sufficient for its saturation and the bubble contains only a part of the achievable equilibrium concentration at the moment of its escape from the surface.



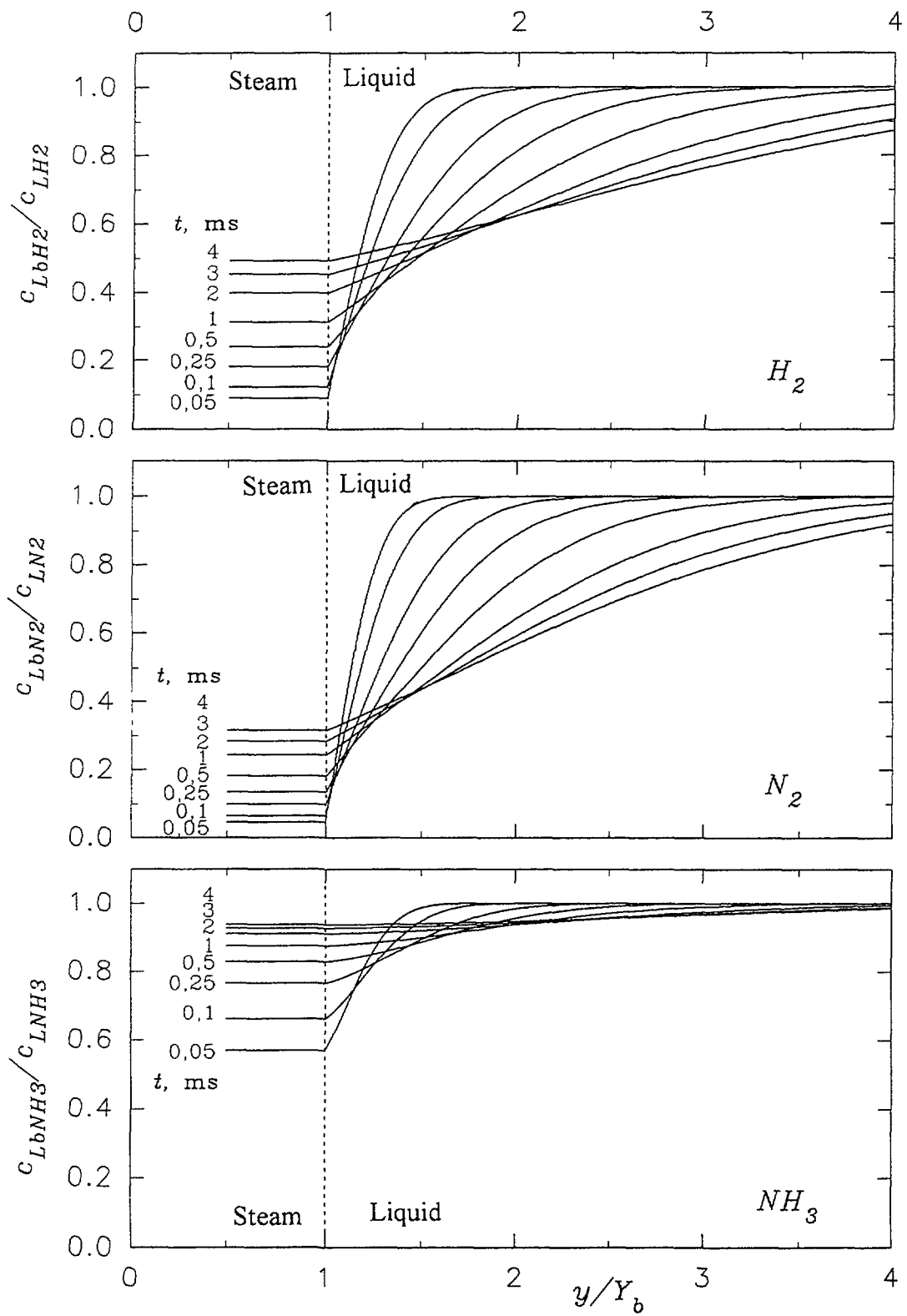


**Fig.7** Calculated concentration profile of dissolved hydrogen, nitrogen and ammonia in the liquid surrounding a steam bubble in period of its growth  $c_{Lb}/c_{Li}$  (the dynamic model – developed subcooled boiling regime)

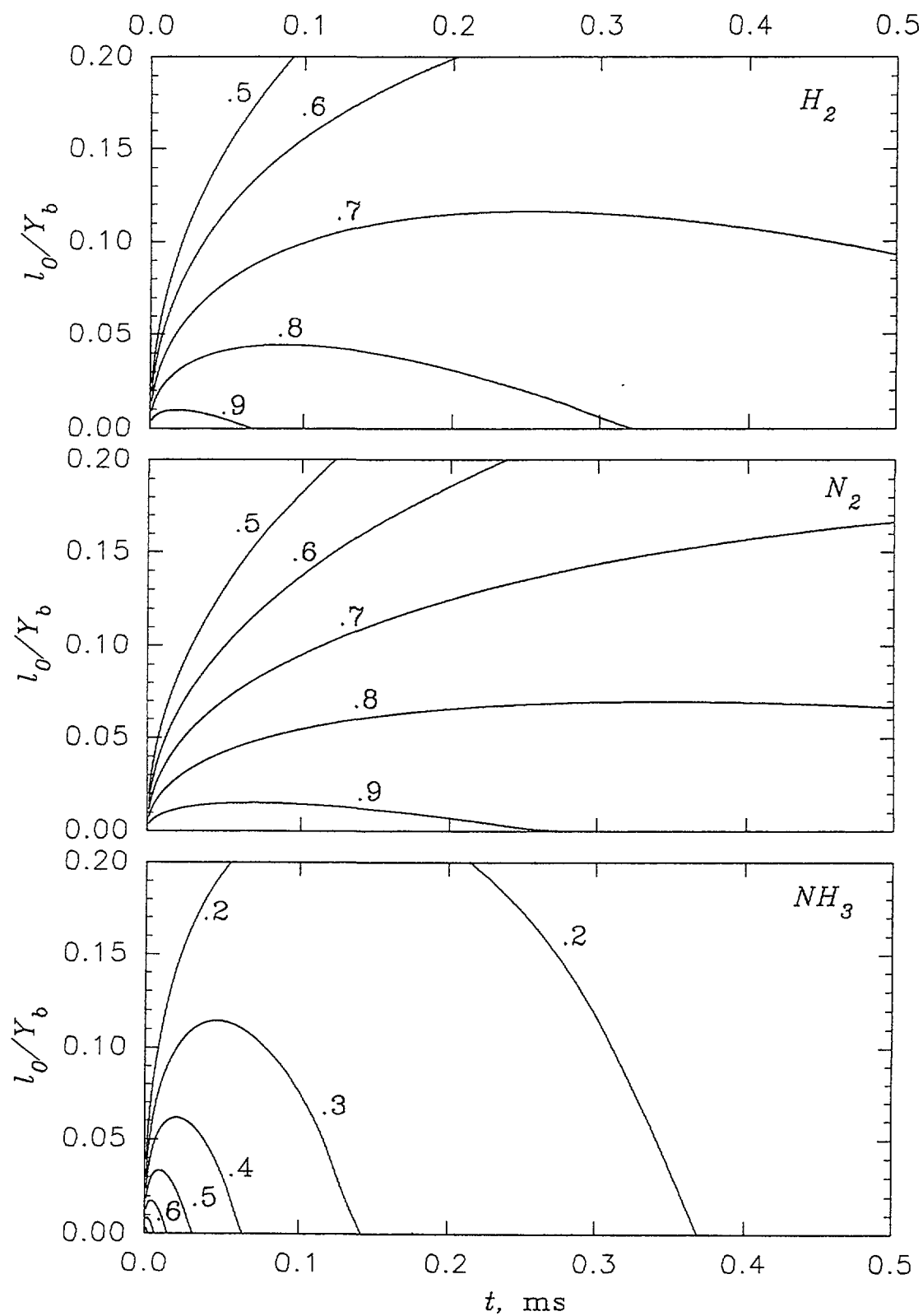


**Fig.8** Thickness of the liquid layer surrounding a steam bubble ( $l_0$ ) as a function of time for different level of dissolved gas depletion (the dynamic model – developed subcooled boiling regime)

## Conclusions

The physic-chemical models describing behaviour of the dissolved gases (hydrogen, nitrogen) and ammonia in the subcooled boiling conditions of the pressurized water reactors were developed. Both, an equilibrium and dynamic approaches were used to describe a depletion of the liquid surrounding a steam bubble in the gas components. This depletion phenomenon is a consequence of the gas diffusion into the steam bubbles.

Results obtained by the equilibrium model indicate that a steam phase fraction in the subcooled boiling regime can reach max. 2.5%. For this condition, the general equilibrium depletion in dissolved hydrogen and nitrogen can be max. 10% that is not sufficient level from point of view of some significant change of the water chemistry conditions.

The dynamic model describes two different mechanisms of the subcooled boiling process - non-developed and developed subcooled boiling. In the case of non-developed subcooled boiling, stagnant bubbles are formed on the cladding surface. These bubbles are flushed by steam which is generated on the surface and re-condensates at a top of the bubble. A depletion of liquid in dissolved gases has a local character and is caused by a limited diffusion rate of the gases from surrounding into the bubble. It was found by calculations that the maximum depletion in dissolved hydrogen can reach 15%, in dissolved nitrogen 35%, and in ammonia 27%. The liquid layer surrounding the bubble affected by such depletion level is approx. 5  $\mu\text{m}$ .

In the case of developed subcooled boiling, the gas depletion in the liquid phase has a local character and is a space and time limited. In principle, the level of depletion is not limited, but the deeper gas depletion the shorter period and smaller liquid volume is affected. The bubble generation, growth and escape from the surface is a periodic process which is repeated with a frequency in order of thousand times per a second. A significant gas depletion (eg. 70% hydrogen depletion in relation to the bulk of coolant) takes about 1 ms and concerns a liquid layer of 1  $\mu\text{m}$  surrounding the steam bubble.

The obtained results show that locally different water chemistry conditions can be met in the subcooled boiling conditions, especially, in the developed subcooled boiling regime. An extension and duration of such locally different conditions is in range of micrometers and milliseconds, respectively. On the other hand, the radiolytical processes and reactions, causing a formation of oxidizing species and radicals, proceed in spurs of 1-2 nm that are formed by a high energy radiation, and take much shorter time. From the above, the locally different water chemistry conditions (dissolved gases concentration) can influence physic-chemical and radiolytical processes in the reactor system, eg. Zr cladding corrosion, radioactivity transport, and determination of the critical hydrogen concentration.

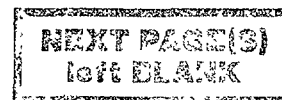
## LIST OF SYMBOLS

$c_{L,i}$ , $c_{G,i}$	molar volume concentration of component $i$ in bulk of coolant and in steam, $\text{mol}/\text{m}^3$
$c_{Lb,i}$	molar volume conc. of component $i$ in liquid surrounding a steam bubble, $\text{mol}/\text{m}^3$
$d_e$	ekivalent hydrodynamic diameter, m
$D_{G,i}$	molecular diffusivity of component $i$ in steam, $\text{m}^2/\text{s}$
$D_{L,i}$	molecular diffusivity of component $i$ in liquid, $\text{m}^2/\text{s}$
$\text{erfc}$	complementary error function
$f$	friction factor, -
$He_i$	solubility of gas component $i$ , $\text{Nml } i/\text{kg Pa}$ (or $\text{ccSTP } i/\text{kg Pa}$ )
$DH_{\text{vyp}}$	evaporation heat of liquid, $\text{J}/\text{kg}$
$k_{LR,i}$	mass transfer coefficient of component $i$ by a side diffusion, $\text{m}/\text{s}$
$k_{L,i}$	mass transfer coefficient of component $i$ , $\text{m}/\text{s}$
$k_T$	heat transfer coefficient, $\text{W}/\text{m}^2 \text{ K}$
$l_0$	thickness of liquid layer surrounding a steam bubble, m

$M_i$	molar weight of component $i$ , kg/mol
$P$	total pressure in the system, Pa
$r$	radial axis, m
$q_w$	heat flux on the fuel rod surface, W/m <sup>2</sup>
$q_{wa}$	average heat flux on the fuel rod surface, W/m <sup>2</sup>
$q_b$	heat flux through a bubble, W/m <sup>2</sup>
$t$	time, s
$T, T_w$	coolant and cladding surface temperature, °C
$T_s$	saturation temperature at given pressure, °C
$V_L, V_G$	liquid and steam volume, m <sup>3</sup>
$v_G, v_L$	steam and liquid (coolant) flow velocity, m/s
$y$	an axis, perpendicular distance from the cladding surface, m
$Y_b$	critical bubble radius, m
$z$	axial axis, m
$a$	convective heat transfer coefficient, W/m <sup>2</sup> K
$d$	thickness of thermal boundary layer, m
$e$	steam phase fraction in liquid (void fraction), -
$l_L$	thermal conductivity of liquid, W/mK
$\rho_L, \rho_G$	liquid and steam density, kg/m <sup>3</sup>
$\sigma_L$	liquid surface tension, N/m
$t_b$	time of a bubble growth, s
$\tau_w$	tangential forces on the surface, Pa
$\Psi_i$	distribution coefficient of gas $i$ ( $= c_{Gi}/c_{Li}$ ), -

## REFERENCES

- [1] LEVY, S., "Forced Convection Subcooled Boiling Prediction of Vapour Volumetric Fraction", Int. Heat Mass Transfer, **10** (1967) 951.
- [2] HEITMANN, H.-G., "Praxis der Kraftwerk-Chemie", Vulkan Verlag, Essen 1986.
- [3] LANDOLD-BÖRNSTEIN, "Zahlenwerte und Funktionen", IV. Band, 4. Teil", Springer Verlag, New York 1976.
- [4] COLLIER, J.G., "Convective boiling and condensation", McGraw-Hill, London 1972.



# THE POSSIBLE INFLUENCES OF FUEL CRUD BUILD-UP AND WATER CHEMISTRY ON WATERSIDE CORROSION OF ZIRCONIUM ALLOYS

J. CHEN, B. ROSBORG  
Studsvik Material AB,  
Nyköping, Sweden



## Abstract

The possible effects of fuel crud build-up and water chemistry on waterside corrosion of zirconium alloys have drawn a certain attention in fuel integrity evaluation programs. This article is an attempt to explore the possible causes for such effects, based on the presumption that diffusion of oxygen vacancies in the oxide barrier layer is the rate limiting process for corrosion in reactor water environments. It is shown that fuel crud build-up and water chemistry may influence corrosion through changing the chemical reactivity at the metal/oxide and oxide/water interfaces, the oxygen vacancy concentration and the diffusivity through the oxide layer. In particular, crud build-up may increase corrosion by enhancing, for example, the oxygen content of reactor water by radiolysis at the crud/water interface and the cladding surface temperature. The presence of fuel crud may also affect  $\text{ZrO}_2$  grain growth and its phase transformation, which are also closely related to the corrosion kinetics.

## 1. INTRODUCTION

The effect of fuel crud build-up on the fuel integrity has rarely been explored in any detail [1]. The early investigations on fuel crud were focused on the radioactivity transport caused by the crud deposition and release in the nuclear power plants and on the water chemistry control. It has been observed [2] that fuel crud of up to 50  $\mu\text{m}$  were built-up even in the BWRs with extremely low crud concentration in the reactor water. Since no scientific ground and evidence can exclude the possible impact of fuel crud build-up on fuel integrity, this issue remains to be explored.

Water chemistry, which is closely related to the behavior of fuel crud build-up, can influence the corrosion behavior of zirconium alloys. However, the mechanism for such an impact is largely unclear. In fact, the major obstacle has been that many influencing factors are seen to play a role in the corrosion process and that it has been difficult to study each factor more closely and relate it to some basic corrosion process.

This article is by no means an attempt to review the status of the corrosion research which has been well treated recently [1], but to discuss the possible influences of fuel crud and water chemistry based on a much simplified corrosion model. The idea is to relate the effects of fuel crud and water chemistry to some fundamental processes occurring during corrosion of zirconium alloys.

## 2. CORROSION KINETICS OF ZIRCONIUM ALLOYS

### 2.1. The linear oxide growth kinetics

The weight gains (or oxide growth) for in-pile corrosion of zirconium alloys are commonly described to follow the linear rate law. Such a treatment may be acceptable for the sake of

---

<sup>1</sup> Present address: VNIPIET, Dibunovskaja 55, 197183, St.-Petersburg, , Russia

<sup>2</sup> Present address: VNIPIET, Dibunovskaja 55, 197183, St.-Petersburg, , Russia

convenience, but it is highly unreliable to be used for any mechanistic interpretation of corrosion behavior. This is because:

- The oxide thickness data are normally too scattered and too few to be suitable for the corrosion kinetics evaluation;
- The time intervals for data collection are usually large, during which the oxide growth may involve repetitive continuous and breakaway growth, as observed in the out-of-pile corrosion studies [3].

If a linear rate law is implied in the description of corrosion kinetics, the rate-limiting process may be

- The probably slow reaction occurring at the metal/oxide or oxide/water interface;
- The diffusion through a coherent oxide layer, or the oxide barrier layer, whose thickness is kept constant as the result of mechanical failure of the film under the stresses generated during oxidation, as proposed by Greenbank and Harper [4] for dry oxidation of a zirconium metal;
- The cumulative generation of porosity in the oxide layer resulting from the preferential dissolution of primary knock-on spikes induced by fast-neutron collision, as proposed by Cox [5].

These hypotheses have not yet been verified experimentally.

## **2.2. The non-linear oxide growth kinetics**

For the similar reasons described above, the weight gains (or oxide growth) for in-pile corrosion of zirconium alloys may also be described to follow two types of non-linear rate laws, namely, that the growth rate decreases with exposure time (passivation) and *vice versa* (accelerated corrosion). These two mechanisms may occur repetitively at different corrosion stages, *i.e.* pre-transition period and post-transition period. For the accelerated corrosion, the formation of microcracks in the metal matrix may occur, which can lead to the exposure of a large fresh metal surface to the oxidant. No analytical approach has so far been developed to characterize this type of corrosion.

The passivation mechanisms for corrosion of zirconium alloys in high temperature water have not been examined in detail using an analytical approach. The defect chemistry of the zirconium oxide formed on zirconium alloys is still poorly understood. Moreover, there has been some hesitation to apply the Wagner oxidation theory, as it was suspected that the complex corrosion processes may not meet the pre-requisites for this theory [1].

In out-of-pile corrosion studies, the numerical approach is often used. The result with such a method is no more than a well fitted weight gain (or oxide thickness) curve by a chosen mathematical expression. Such a numerical approach is only useful in finding the missing data between the measured data points. For the mechanistic analysis, it provides hardly any insight to the corrosion mechanism. Moreover, some mathematical practices would reveal that it is indeed not uncommon that a set of weight gain data (or oxide thickness) could be nicely fitted by several equations. Therefore, an analytical approach for modeling the corrosion kinetics should be preferred whenever it is possible.

## **2.3. A kinetic model for the oxide growth**

One possible growth model may be stated as the following. The oxide growth is governed by diffusion of oxygen vacancies through the oxide barrier layer which may be broken down upon reaching some critical thickness due to the stresses developed in the layer. The oxygen vacancies are

produced through the substitution of  $Zr^{4+}$  cations by other impurity metal cations, such as  $Fe^{3+}$  and  $Ni^{2+}$  present in the oxide layer.

According to this model, the number of  $ZrO_2$  molecules formed per unit area per unit time is given by the Wagner oxidation theory as

$$\frac{dn}{dt} = \left( \frac{c_0}{2} \int_{\mu'}^{\mu^0} D_o d\mu_o \right) \frac{1}{x} \quad (1)$$

where  $c_0$  is the oxygen concentration;  $D_o$  the oxygen diffusion coefficient;  $x$  the thickness of the  $ZrO_2$  layer;  $\mu^0$  and  $\mu'$  the chemical potentials of oxygen at the  $ZrO_2$ /water (outer) and  $Zr/ZrO_2$  (inner) interfaces, respectively. Further exploration of Eq. 1 is not available at present for corrosion in high temperature water.

For oxidation of zirconium alloys in  $O_2$  gas, the following parabolic growth equation is derived [6]

$$x^2 = \frac{1}{4} \left[ Mf_{Zr}'' \right] D_{V_o} \left( \ln p_{O_2}^0 - \ln p_{O_2}' \right) \cdot t \quad (2)$$

where  $\left[ Mf_{Zr}'' \right]$  is the concentration of impurity cations ( $Mf^{2+}$ ) which substitute zirconium cations;  $D_{V_o}$  the diffusion coefficient of oxygen vacancies;  $p_{O_2}^0$  and  $p_{O_2}'$  the  $O_2$  partial pressure at the outer and inner interfaces, respectively. It can be seen from Eq. 2 that the oxide growth is influenced by the following three factors: (1) the partial pressures of oxygen at the interfaces,  $p_{O_2}^0$  and  $p_{O_2}'$ ; (2) the diffusivity of oxygen vacancies in the oxide layer,  $D_{V_o}$ , and (3) the concentration of the impurity cations which substitute zirconium cations in the oxide layer,  $\left[ Mf_{Zr}'' \right]$ .

For wet corrosion an expression with the similar nature to that of Eq. 2 may presumably be derived. In the following, the possible influences of fuel crud and water chemistry on the above three major factors are discussed.

### 3. THE INFLUENCES OF FUEL CRUD

Fuel crud mainly consists of iron and nickel oxides, in addition to a small amount of other metal oxides of various kinds depending on the types of materials with which high temperature water reacts. In phase compositions, PWR fuel crud mainly consists of nickel ferrite while BWR fuel crud mainly of both nickel ferrite and hematite. Some other metal oxides usually form solid solution with nickel ferrite. The influence of fuel crud on the major factors involved in corrosion of zirconium alloys may be discussed as follows.

#### 3.1. The effect on $ZrO_2$ phase stability

The  $ZrO_2$  phase newly formed in the oxide/metal interface region during corrosion in reactor water environments is thought to be either cubic or tetragonal phase [1]. With the growth of the oxide layer it is converted into monoclinic phase, which is accompanied by a large volume change. Since the phase transformation deteriorates the integrity of the oxide layer by forming microcracks in the layer, the phase stability of the oxide may directly influence the material corrosion resistance. It is known [6] that the cubic fluorite structure of  $ZrO_2$  may be stabilized at high temperatures (usually at

above 1100°C) by addition of many di- and trivalent metal oxides. This yields corresponding fluorite type solid solutions of the oxides. If the crud constituents react with  $\text{ZrO}_2$  and stabilize the cubic or tetragonal phase, it may lead to fewer cracks and therefore more protective oxide barrier layer. However, there has been no evidence which suggests that this occur in the reactor water environments.

### **3.2. The effect on the oxygen vacancy concentration**

The oxygen vacancy concentration is in the level of the concentration of the impurity cations which substitute zirconium cations in the oxide [6]. The impurity ions come partly from the dissolved and oxidized secondary phase particles (SPPs) in the oxide and other impurities introduced in the alloy production, and partly from the crud constituents which deposit and diffuse in the  $\text{ZrO}_2$  grain boundary region. It is possible that crud constituents in the  $\text{ZrO}_2$  grain boundaries interact with  $\text{ZrO}_2$  to form more oxygen vacancies in the oxide and therefore increase the corrosion rate.

### **3.3. The effect on the diffusivity of oxygen vacancies**

The diffusion of oxygen vacancies in the oxide layer should be conducted largely through  $\text{ZrO}_2$  grain boundaries. The diffusion rate is therefore dependent on the composition and structures of the grain boundaries. The presence of crud constituents in the grain boundaries may increase the diffusivity of oxygen vacancies, leading to corrosion enhancement.

### **3.4. The effect on the chemical potentials of oxygen at the interfaces**

According to Eq. 1 the corrosion rate is partly determined by the chemical potentials of oxygen at the oxide/crud and metal/oxide interfaces. The presence of fuel crud on the oxide surface may drastically increase the concentrations of some ion species locally [7, 8]. It is possible that the production rate of oxygen and hydrogen peroxide by the radiolysis processes under irradiation may be affected, which is known to have a profound impact on the corrosion rate of zirconium alloys [9].

### **3.5. The effect on cladding surface temperature**

Fuel crud is a poor thermal conductor. In the absence of boiling, conduction through the crud layer is the principal mode of heat transfer, leading to temperature gradients of the order of 1°C per micrometer of deposit thickness at a heat flux of about 1MW/m<sup>2</sup> [10]. An increase in cladding surface temperature would affect almost every physical and chemical process involved in corrosion. For example, at 360°C an increase in temperature of 10°C would increase the oxygen vacancy diffusion coefficient by 42%, while at 285°C by 57% [6]. According to Eq. 2 it would correspond to an increase in oxide thickness by 19% and 25%, respectively.

## **4. THE INFLUENCES OF WATER CHEMISTRY**

Water chemistry can influence the corrosion rate of zirconium alloys no matter if fuel crud would be present on the cladding surface or not [1]. Some chemical species such as  $\text{F}^-$  and  $\text{Cl}^-$  in reactor water may have potential effect on corrosion. Among the various parameters concerned, lithium hydroxide, oxygen and hydrogen contents of the reactor water may be particularly important for waterside corrosion of zirconium alloys. In the following, the influences of some water chemistry parameters on the above-mentioned three major factors are discussed.

### **4.1. The effect on the chemical potential of oxygen at the oxide/water interface**

The oxygen, hydrogen peroxide and hydrogen contents of reactor water are probably most relevant to the chemical potential of oxygen at the oxide/crud interface. The oxygen content was



found to have a profound impact on the corrosion rate of zirconium alloys [9]. Since a part of oxygen in reactor water comes from the radiolysis reactions and the irradiation impact on different parts of fuel rods are not homogeneous, the oxygen contents at the different parts of fuel rods should be different.

In order to understand the mechanism of the oxygen effect, a knowledge of defect chemistry of the oxide under the reactor water conditions may be required.

#### **4.2. The effect on the concentration and diffusivity of oxygen vacancies**

The concentration and diffusivity of oxygen vacancies in the oxide barrier layer depend largely on the impurity level and the microstructure of the oxide layer. In PWR reactor water, the lithium concentration may have a certain effect on the concentration of oxygen vacancies in the oxide, provided that some lithium cations substitute zirconium cations in the oxide and increase the oxygen vacancy concentration. Another possible effect of lithium is an increase in the porosity of the oxide layer [5], which creates fast paths for the permeation of oxidants.

#### **4.3. The effect on the chemical potential of oxygen at the oxide/metal interface**

The chemical potential of oxygen at the oxide/metal interface may be influenced by (1) the amount of oxidized SPP at the oxide/metal interface, which subsequently react with the oxide to form oxygen vacancies, and (2) the hydrogen content of the zirconium metal at the oxide/metal interface. During oxidation the hydrogen gas produced at the oxide/metal interface may diffuse towards both metal and oxide. With the metal hydrogen reacts to form hydrides, while in the oxide hydrogen diffuses as molecule either through pores or grain boundaries or through the oxide lattices in which self-diffusion of oxygen vacancies is involved [11]. If the oxide barrier layer grows and breaks periodically during corrosion, the chemical potential of hydrogen at the oxide/metal interface should vary accordingly, which would in turn affect the equilibrium for oxidation reaction at the interface.

Table 1 summarizes the relationships between some corrosion processes and crud build-up as well as water chemistry.

It is obvious that the above descriptions about the corrosion and the influencing factors are much simplified and focused mainly on some aspects of corrosion chemistry. Some other important processes involved in the corrosion, such as crack propagation in the oxide barrier layer and in the underlying metal matrix, have not been properly treated. It is, however, our opinion that any discussion about the corrosion kinetics should be referred to the basic physical and chemical parameters as partly described above.

### **5. SUMMARY**

The complexity of corrosion of zirconium alloys in reactor water environments lies in the fact that a number of physical and chemical processes occur simultaneously and the importance of each process may change with the structural evolution of corrosion scale. Since many important factors, such as irradiation, microstructure of the corrosion products, the cladding surface temperature and oxygen content of the reactor water, are interrelated, it would be difficult to study the effect of a chosen factor on the overall corrosion.

In this paper the corrosion rate of zirconium alloys is assumed to be governed both by the solid-state diffusion through an inner barrier layer of the corrosion scale, and by the breakdown of the growing barrier layer when a critical mechanical stress is reached. Based on this assumption, the role of crud build-up and water chemistry is highlighted with respect to some important parameters for the corrosion process. These parameters include the chemical potentials of oxygen at the oxide/metal and

water/oxide interfaces and the concentration and diffusivity of the oxygen vacancies in the oxide barrier layer, to which the possible influences of fuel crud and water chemistry could be referred and interpreted.

TABLE 1. THE RELATIONSHIPS BETWEEN ZIRCALOY CORROSION AND CRUD BUILD-UP AS WELL AS SOME WATER CHEMISTRY PARAMETERS (DIFFUSION-CONTROLLED CORROSION MECHANISM).

Independent processes	Influencing factors	Crud build-up	Water chemistry
Surface reaction (on the surface of the barrier layer) ▲	<ul style="list-style-type: none"> <li>◦ Oxygen activity ▲</li> <li>◦ Irradiation ▲</li> <li>◦ T ▲</li> </ul>	<ul style="list-style-type: none"> <li>◦ Affect interfacial oxygen activity?</li> <li>◦ Enhance local radiolysis?</li> <li>◦ Increase cladding temperature ▲</li> </ul>	<ul style="list-style-type: none"> <li>◦ Radiolysis ▲</li> <li>◦ <math>pO_2</math> ▲</li> <li>◦ T ▲</li> <li>◦ <math>pH_2</math> ▼</li> <li>◦ <math>[Li^+]</math> (PWR)?</li> </ul>
Diffusion (in the barrier layer) ▲	<ul style="list-style-type: none"> <li>◦ <math>[Mf_{Zr}]</math> ▲</li> <li>◦ SPP and its size distribution ▼▲</li> <li>◦ <math>ZrO_2</math> grain size ▼</li> <li>◦ Structural defects ▲</li> <li>◦ Phase transformation ▲</li> <li>◦ T ▲</li> <li>◦ Irradiation ▲</li> </ul>	<ul style="list-style-type: none"> <li>◦ Increase <math>[Mf_{Zr}]</math>?</li> <li>◦ Affect <math>ZrO_2</math> grain growth?</li> <li>◦ Enhance phase transformation?</li> <li>◦ Increase cladding temperature ▲</li> </ul>	<ul style="list-style-type: none"> <li>◦ <math>[Li^+]</math> (PWR) ▲</li> <li>◦ T ▲</li> </ul>
Interfacial reaction (at the oxide/ metal interface or metal/water interface) ▲	<ul style="list-style-type: none"> <li>◦ Hydrides ▼▲</li> <li>◦ <math>pO_2</math> ▼</li> <li>◦ Structural defects ▲</li> <li>◦ T ▲</li> <li>◦ Irradiation ▲</li> </ul>	<ul style="list-style-type: none"> <li>◦ Increase cladding temperature ▲</li> <li>◦ Enhance local radiolysis?</li> </ul>	<ul style="list-style-type: none"> <li>◦ T ▲</li> <li>In contact with water through pores and cracks</li> <li>◦ Radiolysis ▲</li> <li>◦ <math>pO_2</math> ▲</li> <li>◦ <math>pH_2</math> ▼▲</li> </ul>

The symbols (▼), (▲) and (?) denote the negative, positive and probable effects of the factors on the corresponding independent processes, respectively.

## ACKNOWLEDGEMENT

Financial support from the Swedish nuclear power utilities is gratefully acknowledged.

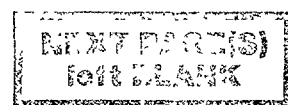
## REFERENCES

- [1] INTERNATIONAL ATOMIC ENERGY AGENCY, Waterside corrosion of zirconium alloys in nuclear power plants, IAEA-TECDOC-996, Vienna (1998).
- [2] HERMANSSON, H-P. and CHEN, J. "Microstructural investigation of Swedish fuel crud", these Proceedings.

- [3] PETERS, H R, Improved characterisation of aqueous corrosion kinetics of Zircaloy-4. Rep. (ASTM-STD-824) ASTM, Philadelphia, PA (1984).
- [4] GREEBANK, J. C. and HARPER, S. The mechanism of breakaway oxidation in zirconium alloys. *Electrochem. Technol.* **4** (1966) 88-95.
- [5] COX, B, "A new model for the in-reactor corrosion of zirconium alloys", *Influence of Water Chemistry on Fuel Cladding Behaviour* (Proc., Rez, Czech, 1993) IAEA, Vienna (1997) 91-110.
- [6] KOFSTAD, P, *Nonstoichiometry, diffusion and electrical conductivity in binary metal oxides*, John Wiley & Sons, Inc., New York (1972) 382 pp.
- [7] PAN, C, JONES, B. G., et al., Concentration levels of solutes in porous deposits with chimneys under wick boiling conditions. *Nuclear Engineering and Design* **99** (1987) 317-327.
- [8] PAN, C., JONES, B. G. et al., "Concentration levels of solutes in porous deposits with chimneys under wick boiling conditions". *Reactor Thermal Hydraulics* (Proc. Newport, RI, USA, 1985). American Nuclear Society. (1985) 21C1-21C9.
- [9] COX, B., "An assessment of irradiation corrosion mechanisms for zirconium alloys in high temperature water". *Influence of Radiation on Corrosion of Structural Materials* (IAEA CS, Vienna, Austria, 1989). See figure 2 on page 27 of the same proceedings as for Ref. 5.
- [10] MACBETH, R. V., TRENBERTH, R. et al. An Investigation into the Effect of 'Crud' Deposits on Surface Temperature, Dry-Out and Pressure Drop, with Forced Convection Boiling of Water at 69 bar in an Annular Test Section. UKAEA Reactor Group, Winfrith. Atomic Energy Establishment (1971).
- [11] SMITH, T. Kinetics and mechanism of hydrogen permeation of oxide films on Zircaloy. *J. Nucl. Mater.* **18** (1966) 323-336.

# IN SITU MEASUREMENT, LOOP FACILITIES

(Session 5)





## SHADOW CORROSION TESTING IN THE INCA FACILITY IN THE STUDSVIK R2 REACTOR

A.C. Nystrand, A. Lassing  
Studsvik AB,  
Nyköping, Sweden

### Abstract

Shadow corrosion is a phenomenon which occurs when zirconium alloys are in contact with or in proximity to other metallic objects in a boiling water reactor environment (BWR, RBMK, SGHWR etc.). An enhanced corrosion occurs on the zirconium alloy with the appearance of a "shadow" of the metallic object. The magnitude of the shadow corrosion can be significant, and is potentially limiting for the lifetime of certain zirconium alloy components in BWRs and other reactors with a similar water chemistry. In order to evaluate the suitability of the In-Core Autoclave (INCA) in the Studsvik R2 materials testing reactor as an experimental facility for studying shadow corrosion, a demonstration test has been performed. A number of test specimens consisting of Zircaloy-2 tubing in contact with Inconel were exposed in an oxidising water chemistry. Some of the specimens were placed within the reactor core and some above the core. The conclusion of this experiment after post irradiation examination is that it is possible to use the INCA facility in the Studsvik R2 reactor to develop a significant level of shadow corrosion after only 800 hours of irradiation.

### 1. INTRODUCTION

In reactors with oxidising water chemistry enhanced corrosion has been seen on zirconium alloys in contact with or in proximity to other metallic objects appearing as a "shadow" of the metallic object [1,2]. The shadow effect in the area of a spacer cell on a BWR fuel rod cladding is illustrated in Figure 1 (this measurement has been performed at the Studsvik Hot Cell Laboratory). The magnitude of the shadow corrosion can be significant and is potentially limiting for the lifetime of certain zirconium alloy components in BWRs and other reactors where this phenomenon occurs. In order to evaluate the suitability of the In-Core Autoclave (INCA) in the Studsvik R2 materials testing reactor as an experimental facility for studying shadow corrosion, a demonstration experiment has been performed.

### 2. EXPERIMENTAL CONDITIONS

#### 2.1 The Studsvik R2 test reactor

The Studsvik R2 test reactor is a 50 MW tank-in-pool reactor, see Figure 2. It has been in operation since 1960. Today it is used for fuel and materials testing, silicon doping, radio-isotope production and basic research. The reactor is in operation 11 cycles a year. Each cycle is about 17 days long with a one week stop between the cycles. The reactor is equipped with a number of facilities in order to perform different types of experiment. For instance it has two in-pile loops in which BWR and PWR conditions are simulated.

#### 2.2 The INCA-facility

The INCA-loop is a test facility for water chemistry and materials research in the Studsvik R2 reactor. INCA is especially designed for experiments under well controlled water chemistry conditions. It consists of two major parts: the external water supply with control and water analysis

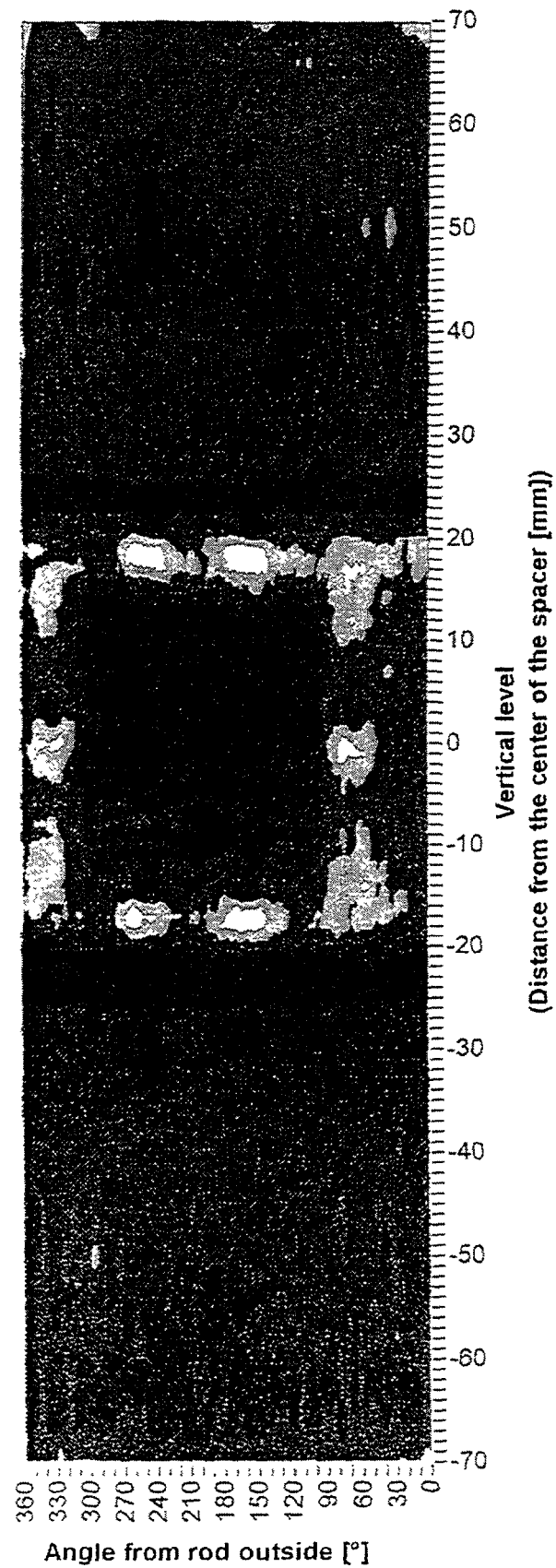
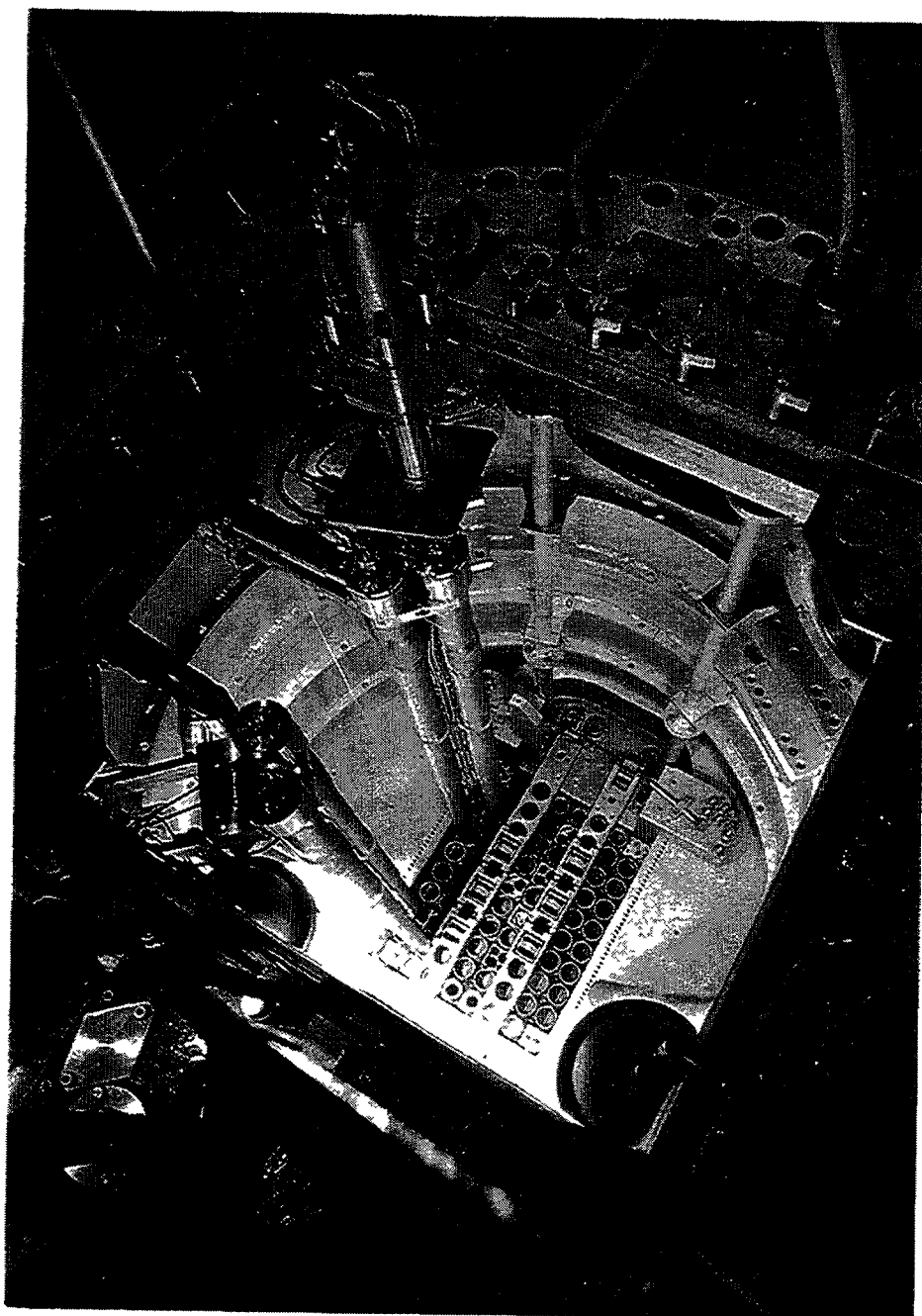


Figure 1. Oxide thickness map (from eddy current measurements) in the area of a spacer cell on a BWR fuel rod cladding. The oxide thickness decreases with the grey scale in the order  $\bigcirc > \cdot > \bullet > \bullet$ .



*Figure 2. General view into the R2 reactor tank.*

systems and the in-core rig. Degassed, high-purity water feeds the INCA-loop with a variable flow-rate. Injections of additives and impurities can be performed either before the water enters the rig or just above the in-core section of the rig. Both the inlet and outlet water can be analysed (content of oxygen, hydrogen, hydrogen peroxide, ions, conductivity etc.).

The INCA rig is illustrated in Figure 3 in its once-through operation mode where the water is drained after it has passed the in-core section. It is installed within one of the LWR loops in the R2 reactor. The water of the main loop serves as a heating or cooling medium for the INCA-rig. The two main parts of the INCA rig are the rig tube and the insert. The test specimens are installed on the test specimen rod. The rod can easily be changed between two cycles of operation. The INCA-loop can be operated from ambient conditions up to 15 MPa and 325°C.

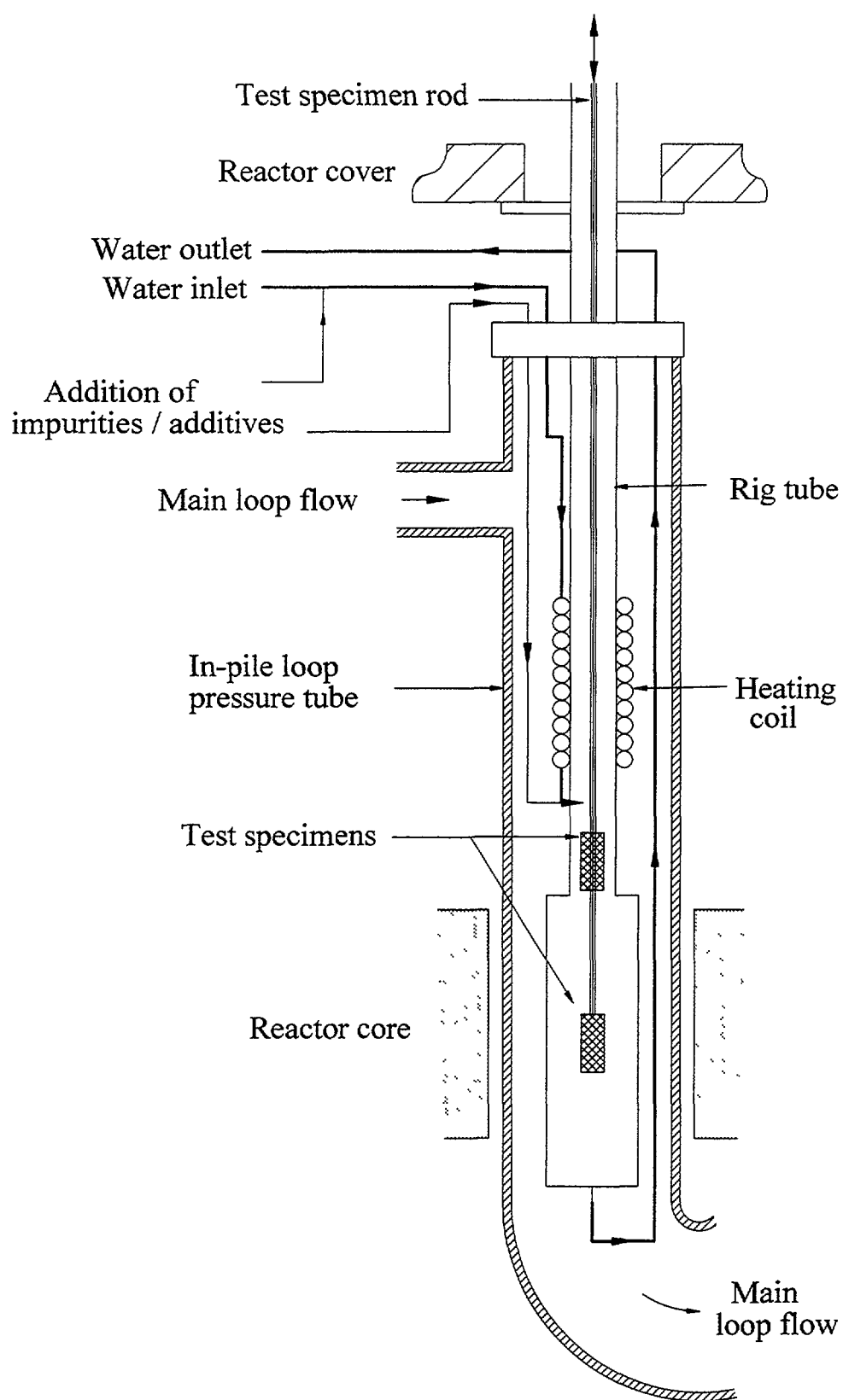


Figure 3. The in-core part of the INCA loop.



The INCA facility was used for this experiment. Earlier it has also been used for in-core electrochemical potential measurements [3,4]

### 2.3 The demonstration test

In this shadow corrosion demonstration test the water inlet temperature was 275°C at 8.5 MPa, (no boiling). The oxidising water chemistry typical of BWRs and other reactors where shadow corrosion has been observed, was created by adding 200 ppb of oxygen to the inlet water. The irradiation lasted for about 800 hours (two cycles of about 17 days each with a shutdown period in between the two cycles).

A number of test specimens were supplied by ABB Atom, and assembled on a stringer (the test specimen rod) in such a way that some of the specimens were within the reactor core, while some of them were above the core. The water flowed downwards through the rig which means that it passed the out-of-core specimens first and then the in-core specimens. This means that the changes of the water chemistry caused by the irradiation only affected the in-core specimens. Each test specimen consisted of a 35 mm long piece of Zircaloy-2 tubing in contact with Inconel.

The water chemistry was analysed during the test (average values by weight):

O <sub>2</sub> measured at inlet	200 ppb
O <sub>2</sub> measured at outlet	270 ppb
H <sub>2</sub> measured at inlet	0 ppb
H <sub>2</sub> measured at outlet	25 ppb

The neutron flux plus the gamma and neutron intensities were calculated after the test.

The fast neutron flux was 0,7-0,9 10<sup>14</sup> n/cm<sup>2</sup>,s (>1MeV)

The thermal flux was 1,4-2,0 10<sup>14</sup> n/cm<sup>2</sup>,s (<0,625 eV)

The dose rate from gamma radiation was 3,4-4,6 W/gH<sub>2</sub>O

The dose rate from neutron radiation was 3,7-4,9 W/gH<sub>2</sub>O

### 3. OXIDE MEASUREMENTS

Following the irradiation, two of the specimens, consisting of exactly the same types of materials in the same geometry, were examined by optical microscopy at 825X magnification in order to measure the oxide thickness. One of the specimens had been in the out-of-core location during the test, while the other specimens had been in-core. The specimens were embedded in epoxy prior to sectioning and polishing, so that the Inconel and Zircaloy were kept in contact. No oxide could be detected anywhere on the test specimen located outside the core illustrated in Figure 4, so the oxide thickness was concluded to be less than 0,5 µm (the microscope resolution). The test specimen exposed inside the core, see Figure 5, was generally covered with a 1-2 µm thick oxide layer, with local areas of accelerated corrosion at, and in proximity to, the points of contact between the Inconel and Zircaloy. The oxide thickness was about 10 µm in these areas, which were a few millimetres in extent.

### 4. CONCLUSION

The conclusion of this experiment is that it is possible to use the INCA facility in the Studsvik R2 Reactor to develop a significant level of shadow corrosion after only 800 hours of irradiation. Standard Post Irradiation Examination techniques can be used to evaluate the shadow corrosion. Since local accelerated corrosion was not observed on the specimens tested outside the core, shadow corrosion was shown to be an in-core reactor phenomenon.

## 5 . FUTURE PLANS

The specimen in-core and out-of-core was exposed to the same conditions except the irradiation. Future experiments are planned to be performed in the INCA-loop. The objectives of future tests are to find the parameters that will influence shadow corrosion and to determine the mechanism of shadow corrosion. Parameters that will be /can be tested are type of material, irradiation time, dose and fluence, water chemistry, geometrical aspects etc.

## REFERENCES

- [1] SUMERILING, R, et al., Further Evidence of Zircaloy corrosion in fuel elements irradiated in a steam generating heavy water reactor., Proc. 5<sup>th</sup> Conf. On Zirconium in the Nuclear Industry, ASTM-STP 681, p 107 (1979).
- [2] CHEN J-S F, ADAMSON R B, Observations of shadow phenomena on zirconium alloys. Int. Topical Meeting on Light Water Reactor Fuel Performance, W. Palm Beach, Florida, April 17-21, 1994.
- [3] MOLANDER A, CHRISTENSEN H, et al., Experimental studies of radiolysis in an in-core loop in the Studsvik R2 reactor, Eurocorr 96, vol IX OR30, Nice 1996.
- [4] CHRISTENSEN H, MOLANDER A, Experimental studies of radiolysis in an in-core loop in the Studsvik R2 reactor, Water Chemistry of Nuclear Reactor Systems 7 BNES, 1996, p 138-40.



# ON-LINE MONITORING OF RESISTANCE OF AQUEOUS SOLUTIONS AT HIGH TEMPERATURE

HU SHILIN, ZHANG PINGZHU, ZHANG WEIGUO  
China Institute of Atomic Energy,  
Beijing, China

## Abstract

The coulstatic measurement is a fast speed electrochemical test method. By this technology, analyzing  $\Delta E(t) - T$  curves recorded under coulstatic perturbation, the solution resistance  $R_s$ , resistance of coated film  $R_f$ , capacity of coated film  $C_f$ , Polarization resistance  $R_p$  and double layer capacity  $C_d$  are obtained. The resistance variety of 0.05N KCl is measured from room temperature up to 255 °C under saturation steam pressure.

## 1. INTRODUCTION

On-line monitoring refers to the continuous ( or near-continuous ) real-time measurement of water chemistry parameters or corrosion data in an operating power plant system. Both water chemistry monitoring and corrosion monitoring are extremely useful. Utility personnel use real-time monitoring of water chemistry parameters or corrosion to assure water quality, provide a warning of plant equipment malfunction or failure, facilitate process control, optimize maintenance and repair schedules, and improve corrosion control in nuclear power plants, reduce costs, and increase efficiency, assure safety operating of nuclear power plants. High temperature on-line monitoring of conductivity is one technology of chemistry monitoring and corrosion monitoring. In nuclear power plants, a lot of corrosion problems of construction materials depend strongly on water chemistry, such as pH, conductivity(or resistance of solution aqueous), oxygen content and impurity concentration. In general, the conductivity is measured, but the sampled water must be cooled down to room temperature under lower pressure, and the measurement might be continuous, but this method is very difficult to accurately measure electrical conductivity of high temperature solution aqueous.

The theory of strong electrolyte conductance was first developed by Debye and Huckel , Onsager perfected the kinetic theory to obtain the limiting conductance equation in 1927. It is known that the equation of electric conductivity of low concentration solution has the form :

$$\Lambda = \Lambda_0 - SC^{1/2} + E\ln C + \text{higher order terms}$$

where C is solution concentration,  $\Lambda_0$  is the limiting equivalent conductance, S and E are coefficients depending on dielectric constant D, temperature T, viscosity  $\eta$ , electric charges Q and mobilities  $\omega$  of the solvent. For some simple electrolytes, the conductance was computed by Pitts , Fuoss and Onsager , Fuoss and Accascina . For the aqueous solution with more chemical compositions, it will be very difficult to compute the conductance of electrolyte.

The facts in our work have confirmed that on-line monitoring of the conductance of high temperature solution aqueous is useful. By on-line monitoring of electric conductivity of solution, the

water qualities can accurately be determined, and the effect of impurities on corrosion of material can well be estimated. At present, there are mainly two methods for on-line monitoring of electric conductivity, one is on-line monitoring of voltage at elevated temperature up to 150 °C and the other is the measurement of alternating current resistance by electrochemical technology at elevated temperature up to 300 °C.

The coulometric technology is also a fast speed electrochemical measurement method, it can be used in the measurement of high temperature conductivity of solution aqueous.

## 2. THEORETICAL

The coulometric method is that a small amount of charge is supplied to double layer capacity of the electrical conductivity electrodes, the aqueous solution resistance can be obtained by recording and analyzing  $E(t)$ - $T$  attenuation curve under coulometric perturbation, it is a fast, sensitive electrochemical method, it is especially fit to measure higher aqueous solution resistance, In this on-line monitoring test, a general equivalent circuit used for measurement of aqueous solution resistance is shown in Figure 1.

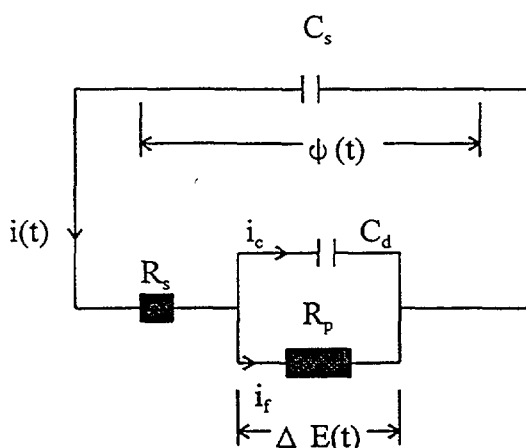


Figure 1. The general equivalent circuit for aqueous solution resistance.

in the above Figure 1, those parameters mean:

- $R_p$ : Polarization resistance
- $C_d$ : Double layer capacity
- $C_s$ : Standard capacity
- $R_s$ : aqueous solution resistance
- $i_f$ : Faraday current
- $i_c$ : Charging current

The whole current in the circuit is

$$i(t) = -C_s \frac{d\phi(t)}{dt} = C_d \frac{d\Delta E(t)}{dt} + i_f$$

To active-polarized systems, there is an equation as follow

$$i_f = i_{\text{corr}} \exp[2.303 \Delta E(t)/b_a] - i_{\text{corr}} \exp[-2.303 \Delta E(t)/b_c]$$

where  $i_{\text{corr}}$  is corrosion current density,  $b_a$  and  $b_c$  are Tafel slopes for anodic and cathodic reactions, respectively, and  $\Delta E(t)$  is the over-voltage.

In accordance with Kirchhoff's law,  $\phi(t)$ , overvoltage at time  $t$  is

$$\phi(t) = \Delta E(t) + R_s[-C_s d(t)/dt]$$

when  $t = 0$ ,  $\phi(0) = V_s$ ,  $\Delta E(0) = 0$ .

$V_s$  is overvoltage within capacity  $C_s$  before the test. For a system in which the electrode is passivated, the equivalent circuit is more complex than Figure 1, the resistance of coated film  $R_{FD}$  and capacity of coated film  $C_f$  must be considered.

### 3. EXPERIMENTAL AND RESULTS

Figure 2 is coulstatic test circuit. It includes three parts, one part is a high quality charge, composed of direct current power and high steady capacity; one is cell (or electrochemical autoclave),

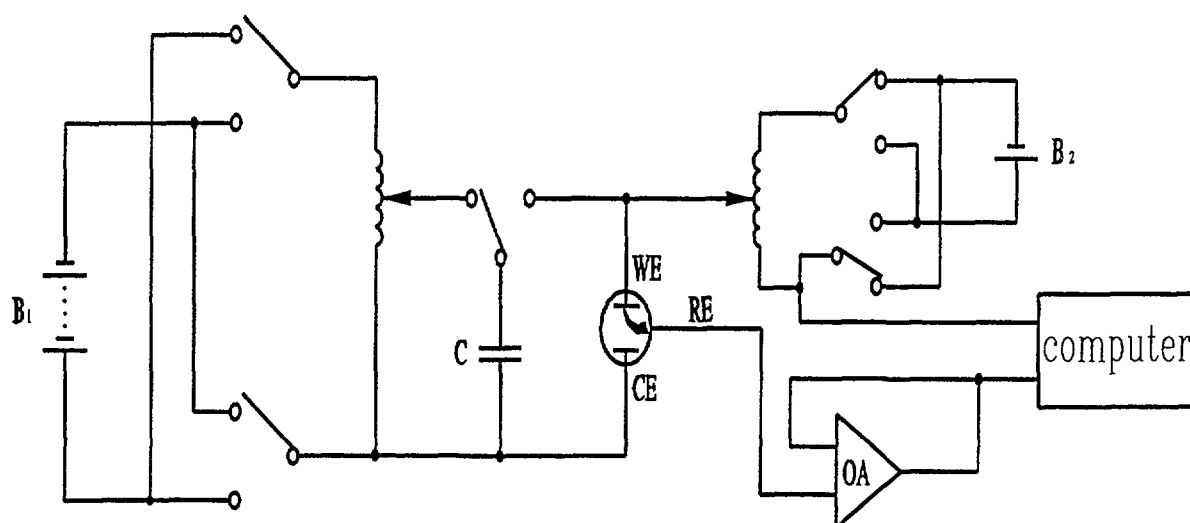


Figure 2. A simple coulstatic test circuit for monitoring of conductance. WE, working electrode; RE, reference electrode; CE, counter electrode; C, high steady capacity; OA, operational amplifier.

the working electrode and reference electrode is both platinum, counter electrode is Inconel-690; third part test signal amplifier, and test data recorder and data treatment.

In the monitoring of solution aqueous conductivity, it is necessary that a interface-friend software have compiled. There are a fit software and A/D D/A transfer interface, these are installed in a microcomputer (586). The monitoring for conductivity of aqueous solution is convenient and simple, and the measurement time is sometimes shorter than 1 second. When the conductivity is measured, it is not necessary to add electrical signal between both of the conductivity electrodes as potential, so the outer signal disturbance is reduced. Although the equations will get more for passived electrode system, it is yet convenient and fast to on-line monitoring of electric conductivity of solution aqueous by micro-computer.

By this coulstatic electrochemical measurement method, we have monitored the resistance of KCl, its concentration is 0.05N at elevated temperature from 25 °C up to 255 °C with saturation oxygen in autoclave. The experiment results at 25 °C are as follow

When the test temperature is elevated, the resistance value of solution aqueous is shown in Figure 4. The resistance of KCl solution straightly drops with temperature going up, and the electric conductivity will directly rise. When the test of monitoring of solution conductance known is finished, or by

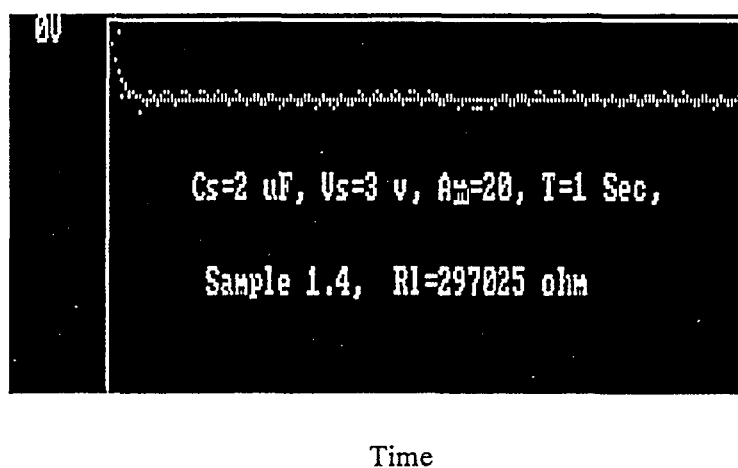


Figure 3. Polarization potential  $\eta(t)$ — $t$  curve for platinum electrode at 25 °C

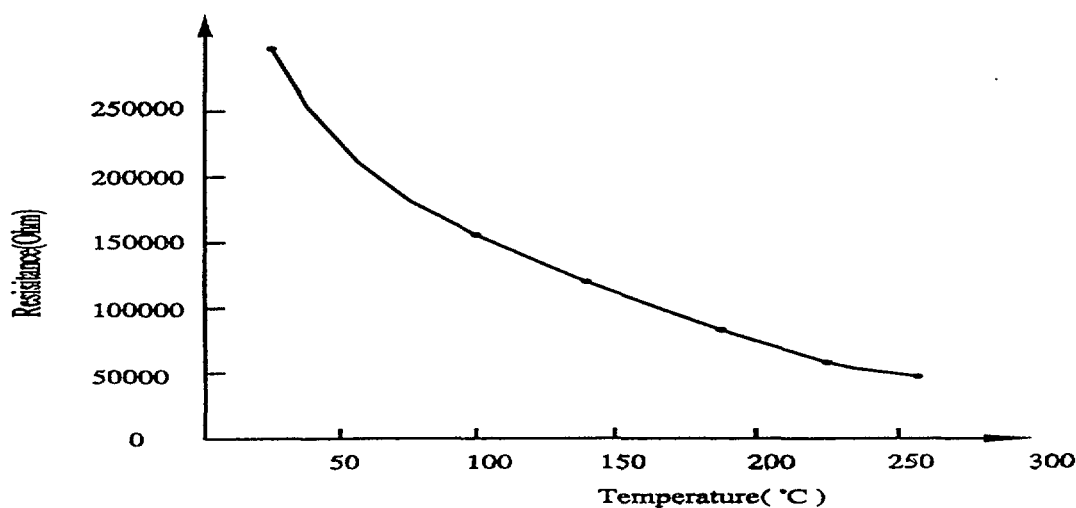
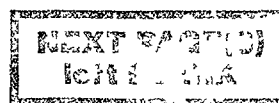


Figure 4. Temperature dependent of lower concentration KCl

calculating the conductance value measured, the conductivity cell constant will be obtained. Using a standard electric conductivity cell which cell constant is known, the on-line monitoring of electric conductivity can be carried out. Because the test is finished in no-flowing loop, the dissolved oxygen content affects the resistance of test solution aqueous.

#### 4- CONCLUSION

An on-line monitor to determine electrical resistance of aqueous solution at elevated temperature up to 255 °C was developed. The electrical resistance of KCl is reduced with test temperature elevation. The coulstatic technology is a fast speed electrochemical test method, during the measurement, it is not necessary to add between both of electrodes. It is entirely possible to be used to on-line monitor the electrical conductivity of aqueous solution.





## ADVANCED IN-SITU CHARACTERISATION OF CORROSION PROPERTIES OF LWR FUEL CLADDING MATERIALS

E. ARILAHTI, B. BEVERSKOG\*, M. BOJNOV, L. HANSSON-LYYRA,  
T. LAITINEN, J.F.W. MARKGRAF\*\*, P. MOILANEN, K. MÄKELÄ,  
M. MÄKELÄ, T. SAARIO, P. SIRKIÄ  
VTT Manufacturing Technology, Finland

\*OECD Halden Reactor Project, Halden, Norway

\*\*JRC, IAM, HFR Unit, Petten N.H., The Netherlands

### Abstract

The trend towards higher fuel burnups imposes a demand for better corrosion and hydriding resistance of cladding materials. Development of new and improved cladding materials is a long process. There is a lack of fast and reliable in-situ techniques to investigate zirconium alloys in simulated or in-core LWR coolant conditions. This paper describes a Thin Layer Electrode (TLE) arrangement suitable for in-situ characterization of oxide films formed on fuel cladding materials. This arrangement enables us to carry out:

- Versatile Thin Layer Electrochemical measurements, including:
  - ◊ Thin Layer Electrochemical Impedance Spectroscopic (TLEIS) measurements to characterize the oxidation kinetics and mechanisms of metals and the properties of their oxide films in aqueous environments. These measurements can also be performed in low conductivity electrolytes.
  - ◊ Thin-Layer Wall-Jet (TLWJ) measurements, which give the possibility to detect soluble reaction products and to evaluate the influence of novel water chemistry additions on their release.
- Solid Contact measurements:
  - ◊ Contact Electric Resistance (CER) measurements to investigate the electronic properties of surface films on the basis of d.c. resistance measurements.
  - ◊ Contact Electric Impedance (CEI) measurements to study the electronic properties of surface films using a.c. perturbation.

All the above listed measurements can be performed using one single measurement device developed at VTT. This device can be conveniently inserted into an autoclave. Its geometry is currently being optimized in cooperation with the OECD Halden Reactor Project. In addition, the applicability of the device for in-core measurements has been investigated in a joint feasibility study performed by VTT and JRC Petten. Results of some autoclave studies of the effect of LiOH concentration on the stability of fuel cladding oxide films are presented in this paper.

## 1. INTRODUCTION

The structural integrity of the construction materials in the heat transfer system of a nuclear power plant is of major importance as far as their safe and economical operation is concerned. The trend towards higher burn-ups imposes demands for better corrosion resistance of cladding materials of the fuel rods. The corrosion resistance is greatly influenced by the electrical and electrochemical properties of the surface oxide films formed on cladding materials during normal operation conditions.

Electrochemical research on the corrosion behaviour of a zirconium alloy / oxide film / high-temperature aqueous electrolyte systems, such as boiling water reactor (BWR) coolant conditions, is limited by the low conductivity of such an electrolyte. This restricts the use of a conventional electrochemical cell set-up. There is a call for fast and reliable in-situ techniques to investigate the corrosion behavior of zirconium alloys in simulated or in-core light water reactor coolant conditions.

## 2. THIN LAYER ELECTRODE ARRANGEMENT

In conventional three-electrode measurements the potential of a specimen in an electrolyte is controlled and measured by a reference electrode while the current flows through a working electrode (specimen) and a counter electrode. In the case of poorly conductive electrolytes, such as Boiling Water Reactor (BWR) coolants, the control of the potential is inaccurate due to the ohmic drop in the electrolyte between the working electrode and the reference electrode. Moreover, the power output of



several commercial potentiostats may not be large enough to pass the required current between the working electrode and the counter electrode.

The Thin Layer Electrode (TLE) arrangement has been developed to overcome such problems. Figure 1 shows a scheme of the TLE arrangement to carry out electrochemical measurements at high temperatures and pressures.

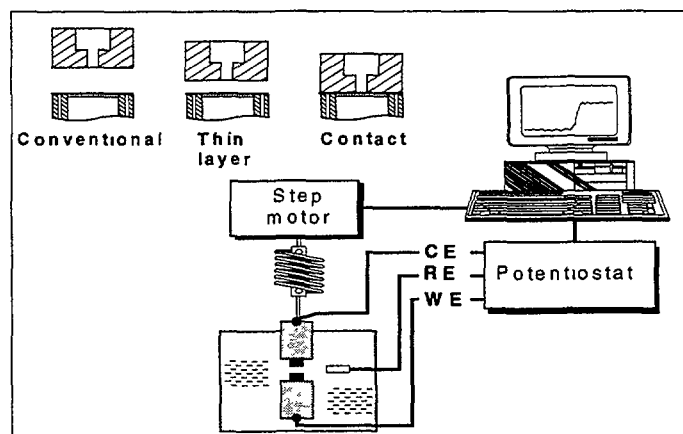


FIG. 1. A scheme of the experimental set-up for the thin-layer electrochemical measurements.

To study the corrosion phenomena in aqueous environments the TLE measurement system can be conveniently inserted into a high-temperature re-circulation loop simulating the desired LWR conditions. The TLE arrangement is designed to operate in electrolytes at pressures up to 20 MPa and at temperatures up to 360°C [1].

## 2.1. Thin Layer Electrochemical Measurements

In the Thin Layer Electrochemical (TLEC) measurements the working electrode made of the material to be studied and the counter electrode are constructed as two small-diameter rods with their end surfaces parallel to each other. The distance between the electrodes can be adjusted with an accuracy of  $10^{-9}$  m up to about  $10^{-4}$  m as shown in Figure 2. A low resistance reference electrode is placed beside the working electrode.

The current flows across a tiny gap between the specimen and the counter electrode. The effect of the ohmic drop in the electrolyte is overruled since the potential is measured at the side of the specimen where the electric field is negligible.

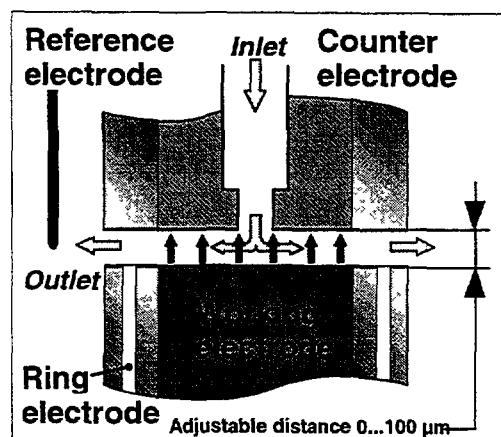


FIG. 2. The principle of the thin-layer electrode arrangement developed for electrochemical measurements in low-conductivity media.

### *2.1.1. Thin Layer Electrochemical Impedance Spectroscopy (TLEIS)*

In the conventional electrochemical impedance spectroscopy (EIS) different frequencies of a.c. perturbations are applied to the working electrode. The different processes can be distinguished from each other on the basis of their ability to reach a steady state after the a.c. perturbation. The processes taking place in the oxide film and in the coolant may be interfacial reactions and electron and ion transfer, i.e. diffusion and migration.

In poorly conductive solutions these measurements can be carried out by using the TLE arrangement, in which the gap between the working electrode and the counter electrode is typically few micrometers [1].

### *2.1.2. Other Thin Layer Electrochemical Measurements*

#### *2.1.2.1. Controlled Potential and Current measurements*

Conventional controlled potential and controlled current measurements provide the basis for understanding the electrochemical behaviour of metals in specific environments at specified potentials. These measurements can be carried out in poorly conductive electrolytes using the TLE arrangement. In BWR coolant conditions current-voltage curves have successfully been obtained for example with AISI 316 L specimens [2].

#### *2.1.2.2. Thin Layer Wall-Jet (TLWJ) Measurements*

Electrochemical detection of soluble species in a flowing system can be performed by maintaining the potential of the detecting electrode at a specified value and monitoring the oxidation or reduction current as a function of time. The most widely used amperometric detectors are based on the thin-layer and wall-jet configurations.

The thin layer electrochemical arrangement shown in Figure 2 can also be used to detect soluble products of the specimen at open circuit or during polarisation at high temperatures and pressures simulating PWR and BWR coolant conditions. In the Thin Layer Wall-Jet design, the test solution is pumped through the counter electrode onto the working electrode surface. As the corrosion reaction takes place on the working electrode surface, the dissolved reaction products are transported with the test solution stream to the ring/detecting electrode. Depending on the ring potential, the reaction products are oxidised or reduced and the resulting current is measured [3].

As the potential of the ring electrode is changed, different soluble species can be detected in the solution. By changing the pumping rate or the distance between the working electrode and the counter electrode, it is possible to change the flow rate of the test solution on the working electrode surface [3].

## **2.2. Solid Contact Measurements**

An additional benefit of the TLE arrangement is that the working electrode and the counter electrode can be brought into contact with each other thus enabling the Contact Electric Resistance (CER, using direct current) and Contact Electric Impedance measurements (CEI, using alternating current). When comparing the solid contact measurement with the thin layer electrochemical measurements, in the solid contact measurements the contribution of the electrolyte to the measured resistance or impedance value can be virtually overruled. That is, the measured resistance value or impedance spectrum can be related to the properties of the oxide film alone.

### *2.2.1. Contact Electric Resistance (CER) Measurements*

In the CER technique the counter electrode and the working electrode used in the TLE arrangement are connected and disconnected at a certain frequency to expose the specimen to the

environment. A small current is passed through the contact surfaces. The electric resistance of the contact surface of the working electrode generates a voltage signal which is amplified and recorded. Thus, changes in the electronic resistance of the surface film of the specimen can be measured. The counter electrode can be made of a noble metal, e.g. Iridium, which does not have a surface film in the electrolyte and in the potential range used in the measurement. The contact area is typically 0.015 cm<sup>2</sup> [2].

The maximum measurement frequency is roughly 1Hz, which enables us to follow the kinetics of several surface related processes, such as adsorption, passivation and growth of oxide film. The technique can also be used to distinguish the changes in the film resistance due to structural changes or changes in electron transport in the film [4]. The TLE arrangement shown in Figure 1 is applicable for the CER measurements in the high temperature and high pressure environments.

### 2.2.2. Contact Electric Impedance (CEI) Measurements

The contact electric impedance measurements are carried out by using the same experimental TLE set-up as for the CER measurements. The specimen and the counter electrode are brought to mechanical contact with each other but in this case an a.c. perturbation is applied to the system.

CEI can be used to investigate in-situ the mechanism of electronic conductivity of the oxide layers formed [5]. The CEI measurements carried out at low ac frequencies approach direct current conditions. In such measurements the impedance values approach the resistance values of the oxide films, respectively.

## 2.3. Corrosion Tests of Zirconium Alloys Using the CER Technique

The contact electric resistance (CER) technique has been applied in different fields of technology, e.g. in research on the effect of LiOH on the stability of oxides of Zirconium alloys [4]. The growth of the oxide layers of three different zirconium alloys was measured in-situ using the CER method in static autoclaves in simulated PWR coolant conditions at 300 °C. The water contained 350 ppm of B added as boric acid. 1M LiOH solution was injected at high temperatures using a liquid chromatography pump. Nitrogen bubbling was used to remove oxygen from the water before starting the test [6].

### 2.3.1. Materials and electrodes

The composition of the three fuel cladding materials used in this CER experiment is presented in Table I.

TABLE I. COMPOSITION OF THE ZIRCONIUM ALLOYS (WT %) [6].

	Sn	Fe	Cr	Ni	Nb
ZrNb1	1.0	0.1	0.015	0.001	1.0
Zircaloy-4	1.34	0.2	0.10	-	-
Zircaloy-2	1.33	0.17	0.10	0.05	-

Each CER specimen was a 20 mm long piece of cladding tube and the other CER tip was made of Iridium. Before starting the tests the contact surfaces were polished to remove any air borne oxides. After polishing the contact surfaces were rinsed with de-mineralised water and the specimens were assembled into the specimen holder for the CER measurements [6].

The potential was measured both with an external 0.1 M Ag/AgCl reference electrode and with a reversible H<sup>+</sup>/ H<sub>2</sub> electrode by polarizing a Pd wire cathodically [6].

### 2.3.2. Experimental results

Zirconium alloy oxides formed during their exposure to high temperature coolant conditions are considered to be insulators. The electric resistance of the oxides of three different Zirconium alloys as a function of exposure time in simulated PWR coolant conditions is shown in Fig. 4.

The results of the CER measurements indicated that all three alloys behaved in a similar manner [4]. There was first a period of instability after which the film resistance started to grow up steadily. After reaching a specific value the film resistance of each alloy appeared to remain rather stable. However, the time required for each alloy to reach the more or less stable level of film resistance varied from alloy to alloy.

After removing the specimens from the autoclave the oxide thickness of all specimens was analysed. The measured oxide thickness ranged from 0.6 to 0.8  $\mu\text{m}$ . The measured hydrogen and lithium concentrations in the oxide films of all three alloys were within the same order of magnitude.

The difference in the time required to reach a stable level of resistance or the absolute value of this level was obviously not caused by the variation of the oxide thickness or by the incorporation of impurities into the oxide layers, but to be due to the characteristic resistive properties of each specific oxide layer.

The initial growth of the oxide layers of zirconium and zirconium alloys follows a cubic or parabolic time relation. When the 'transition point', corresponding to the weight gain of 30  $\text{mg}/\text{dm}^3$ , is attained the rate of oxidation becomes linear with a rate constant higher than the slope at the end of cubic period. Since the volume of  $\text{ZrO}_2$  is 1.56 times the volume of Zr, the oxide scale is under compression. In the cubic regime for oxide layer thickness higher than approximately 1  $\mu\text{m}$ , lateral cracks appear to relieve the stresses. The linear rate after the transition point is caused by the vertical cracking outside of the still intact barrier layer adjacent to the metal surface [7]. The broken oxide layer on the barrier layer exhibits no transport resistance.

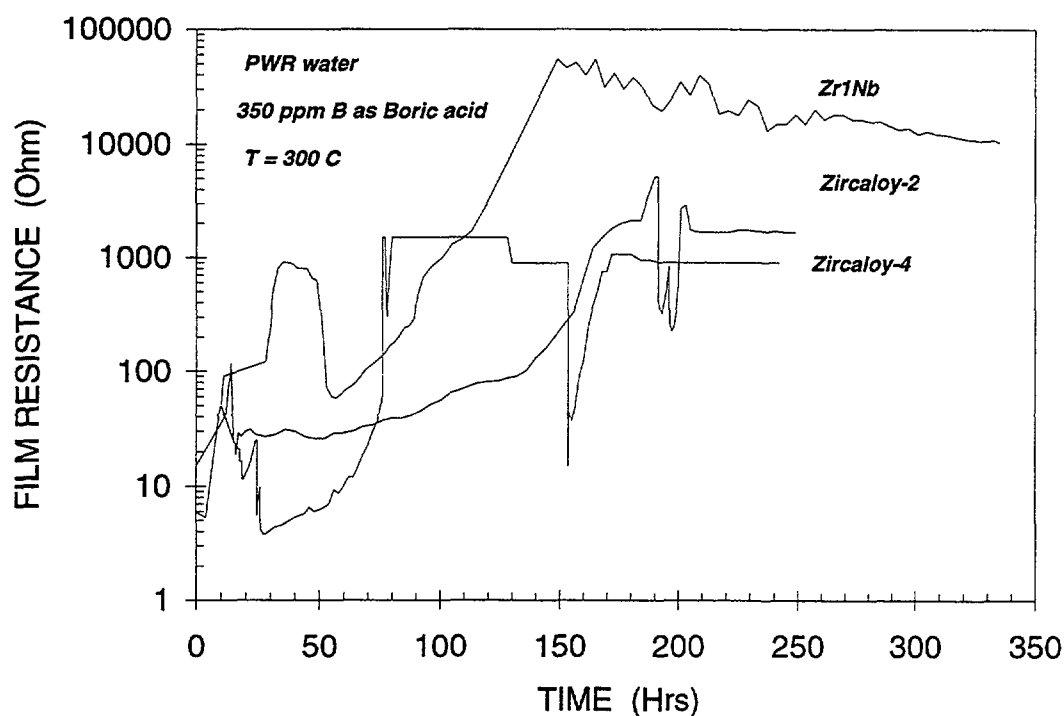


FIG. 4. Resistance of surface films of Zircaloy-2, Zircaloy-4 and Zr1Nb alloys as a function of time in PWR water environment (2000 ppm  $\text{H}_3\text{BO}_3$ , 300°C) [4].

The period of steady growth of resistance, shown in Fig. 4 is proposed to result from the growth of the barrier layer. In general, the growth of zirconium oxide layer takes place by diffusion of oxygen ions through vacancies in the oxide lattice, from outside of the layer to the metal-oxide interface. In this case the growth rates of the oxides are proposed to be limited by the diffusion rate of the oxygen anion vacancies. The time required to reach a stable level of resistance (so called 'incubation' time) is a measure for the diffusion rate of oxygen anions. The longer the time, the better the corrosion properties of the alloy and the smaller the weight gain in a long-term exposure [4].

After the stable level of resistance has been reached, the transfer of electrons may become a rate limiting process for the oxide growth. In such a case it is probable that the zirconium alloy having the highest electronic resistance of the surface film also exhibits the lowest weight gain.

In Table II Zircaloy-2, Zircaloy-4 and ZrNb1 are compared with each other based either on the time required to reach the stable level of resistance ('incubation' time) or based on the absolute level of resistance reached in the CER measurements. The order of the weight gain measurements of the same alloys based on in-reactor data are shown in the same table.

The results of the CER measurements are analogous to the results of in-reactor weight gain measurements [4]. The highest value of resistance for ZrNb1 correlates with the lowest value of weight gain of the same alloy. A similar type of correlation applies to Zircaloy-2 and Zircaloy-4. An additional benefit related to the CER measurements is the saving in testing time. The CER tests required roughly 10 days, whereas the conventional weight gain tests generally require 150 to 700 days.

TABLE II. COMPARISON OF CORROSION PROPERTIES OF Zircaloy-2, Zircaloy-4 AND ZrNb1 BASED ON IN-REACTOR WEIGHT GAIN DATA (BURNUP FROM 42 - 68 MWD/KGU) [8, 9] AND RESISTANCE MEASUREMENTS BY CER TECHNIQUE.

Alloy	In-reactor weight gain, Ref. [8], [9]	Electronic resistance of oxide film	'Incubation' time
Zircaloy-2	2 <sup>nd</sup> lowest weight gain value	2 <sup>nd</sup> highest resistance	longer
Zircaloy-4	3 <sup>rd</sup> lowest weight gain value	3 <sup>rd</sup> highest resistance	shortest
ZrNb1	lowest weight gain value	highest resistance	longer

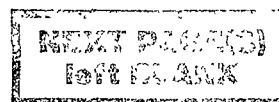
### 3. CONCLUSIONS

All the electrochemical measurements discussed in this paper can be performed by using a single measurement device, the thin layer electrode (TLE) arrangement, developed at VTT. A typical procedure to carry out corrosion tests using the TLE arrangement is to start with CER measurements of the material to be studied. The changes in the resistance of the oxide film as well as the corrosion potential of the material are monitored simultaneously during the first stages of exposure. The possibility to distinguish changes in the oxide film resistance due to structural changes and changes in charge carrier density of an oxide is one of the main advantages of the CER technique. After the growth of the oxide film has been stabilised the electronic conductivity of the oxide film can be further studied by means of contact impedance spectroscopic measurements.

Understanding and modeling of the corrosion mechanisms taking place on oxide surfaces and within oxide films requires far more experimental data. The TLE arrangement has been developed to overcome this deficiency, especially when performing electrochemical measurements in low conductivity media at high temperatures and pressures. The small size of the specimens makes the TLE arrangement especially suitable for research on irradiated materials.

## REFERENCES

- [1] BOJINOV, M., et al., "A novel technique for electrochemical measurements in low conductivity environments", EUROCORR'98, Utrecht, The Netherlands (1998) (in press).
- [2] BOJINOV, M., et al., "Development of electrochemical techniques to study oxide films on construction materials in high temperature water", Water Chemistry in Nuclear Power Plants (Proc. 1998 JAIF Int. Conf. Kashiwasaki, Japan, 1998), JAIF (1998) 111.
- [3] BOJINOV, M., et al., "Characterisation of material behaviour in high temperature aqueous environments by means of electrochemical techniques", Presented at the Enlarged Halden Program Group Meeting, Lillehammer, Norway (1998).
- [4] SAARIO, T., PIIPPO, J., "A new electrochemical technique for in situ measurements of electric resistance and semiconductor characteristics of surface films on metals", Materials Science Forum Vols. 185-188 (1995) 621-628.
- [5] BOJINOV, M., et al., "A combination of ac impedance and dc resistance techniques to study corrosion in high temperature aqueous environments", Electrochemical Impedance Spectroscopy (Proc. 4th International Symp., Rio de Janeiro, Brazil, 1998), NACE, (1998) 393-395.
- [6] SAARIO, T., TÄHTINEN, S., "In-situ measurement of the effect of LiOH on the stability of fuel cladding oxide film in simulated PWR primary water environment" (Proc. 12th International Corrosion Congress, 1993), Vol. 6, NACE (1993) 4325-4336.
- [7] OLANDER, D., Department of Nuclear Engineering, University of California, Berkeley, personal communication, 1986.
- [8] LIMBÄCK, M., et al., "Corrosion and hydriding performance of Zircaloy-2 and Zircaloy-4 cladding materials in PWRs, LWR Fuel Performance (Proc. ANS Int. Topical Meeting West Palm Beach, FL, USA, 17-21 April, 1994), ANS (1994) 286.
- [9] SABOL, G.P., et al., "In-reactor fuel cladding corrosion performance at higher burnups and higher coolant temperatures", LWR Fuel Performance (Proc. ANS Int. Topical Meeting Portland, Oregon, 1997), ANS (1997) 397.



**MODEL EXPERIMENTS ON SIMULATION OF  
THE VVER WATER-CHEMICAL CONDITIONS  
AT LOOP FACILITIES OF THE MIR REACTOR\***



XA9953311

O.S. BENDERSKAYA\*\*, E.A. ZOTOV, V.A. KUPRIENKO, V.A. OVCHINNIKOV

State Scientific Center of the Russian Federation,

Research Institute of Atomic Reactors,

Dimitrovgrad, Russian Federation

**Abstract**

The experiments on simulation of the VVER type reactors water-chemical conditions have been started at the State Scientific Center RIAR. These experiments are being conducted at the multi-loop research MIR reactor at the PVK-2 loop facility. The dosage stand was created. It allows introduction of boric acid, potassium and lithium hydroxides, ammonia solutions and gaseous hydrogen. Corrosion tests of the Russian E-635 and E-110 alloys are being conducted at the PVK-2 loop under the VVER water-chemical conditions. If necessary, fuel elements are periodically extracted from the reactor to perform visual examination, to measure their length, diameter, to remove the deposits from the claddings, to measure the burnup and to distribute the fission products over the fuel element by gamma-spectrometry. The chemical analytical "on line" equipment produced by the ORBISPHERE Laboratory (Switzerland) will be commissioned in the nearest future to measure concentration of the dissolved hydrogen and oxygen as well as pH and specific conductivity. The objective of the report is to familiarize the participants of the IAEA Technical Committee with the capabilities of performing the model water-chemical experiments under the MIR reactor loop facility conditions.

**1. INTRODUCTION**

The material science MIR reactor is operating at the State Scientific Center of Russian Federation "Research Institute of Atomic Reactors" situated in the town of Dimitrovgrad [1]. Its experimental loop facilities having irradiation channels in the reactor core are closed circuits with different coolants equipped with circulation pumps, heat exchangers and other technological equipment.

These loops are oriented to perform quite different tests of model and full-size fuel elements and FA of the operating and designed reactors for atomic stations and other nuclear-power facilities. Long-time simulation of the nominal operating conditions of pilot fuel elements (service-life tests) is carried out in the experiments. The transient conditions and power ramps are investigated. Different emergency situations typical for the power reactors fuel elements are simulated.

In the last few years owing to the necessity of providing the increased corrosion resistance of FA materials (due to the growing duration of the fuel cycle and other causes) there was need in greater attention to the simulation items in the water-chemical conditions (WCC) loops of the coolant. The works are aimed at further improvement of WCC, at revealing the consequences of particular deviations from the adopted regulations, at selection of the most prospective structural materials and their experimental substantiation, etc.

The present paper considers the capabilities of performing such works at the MIR reactor.

---

\*Work performed within the framework of the IAEA TCM on Water Chemistry and Corrosion Control of Cladding and Primary Circuit Components.

\*\*Present address: 433510, Ulyanovsk region, Dimitrovgrad-10, Russia. SSC RF RIAR

## 2. GENERAL

The main characteristics of the MIR reactor are presented in Tab.1, and the cartogram of its core is shown in Fig.1. In the core beryllium stack consisting of hexagonal blocks there are the reactor fuel channels, experimental loop channels and various CPS bodies including the combined absorber rods with fuel additional charge.

TABLE I MAIN CHARACTERISTICS OF THE MIR REACTOR

Characteristic	Value
Power, MW	up to 100
Maximum neutron flux, $1/\text{cm}^2\cdot\text{s}$ :	
E < 0.68 eV	$5 \times 10^{14}$
E > 0.1 MeV	$2 \times 10^{14}$
Moderator	Be, H <sub>2</sub> O
Reflector	Be
Coolant	H <sub>2</sub> O
Coolant pressure, Mpa	1.24
Coolant temperature, °C	40 – 83
Campaign, d	30 – 40
FA fuel	UO <sub>2</sub> – Al
Quantity of FA	48
Quantity of shim rods	29
Quantity of rods with fuel additional charge	12
Quantity of loop channels	11
Height of core, m	1

Good physical characteristics of the core, sufficient control means of the energy release level allow realization of a wide range of thermal loads on pilot fuel elements in every loop channel providing compliance of the required operating conditions of all loop channels at the specified reactor power level. The reactor operates, as a rule, at the power of 40–60% of the nominal one, and only in separate experiments (power ramps) it uses its potential capabilities.

Table 2 presents the main characteristics of the water coolant loop facilities.



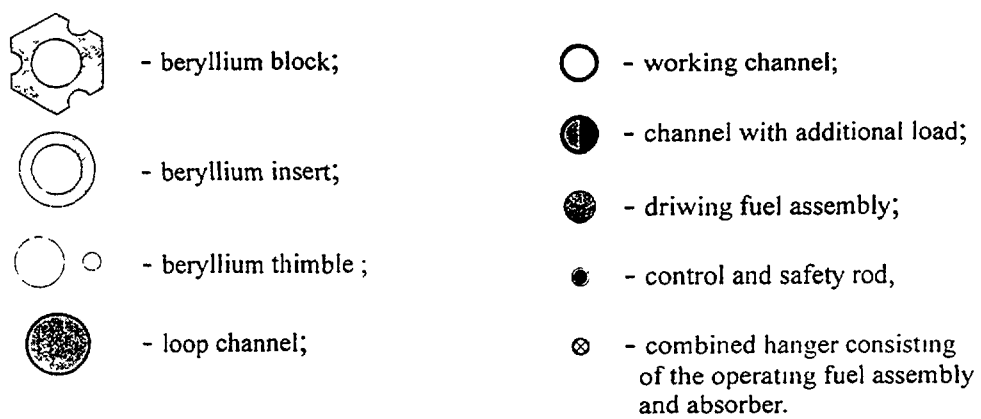
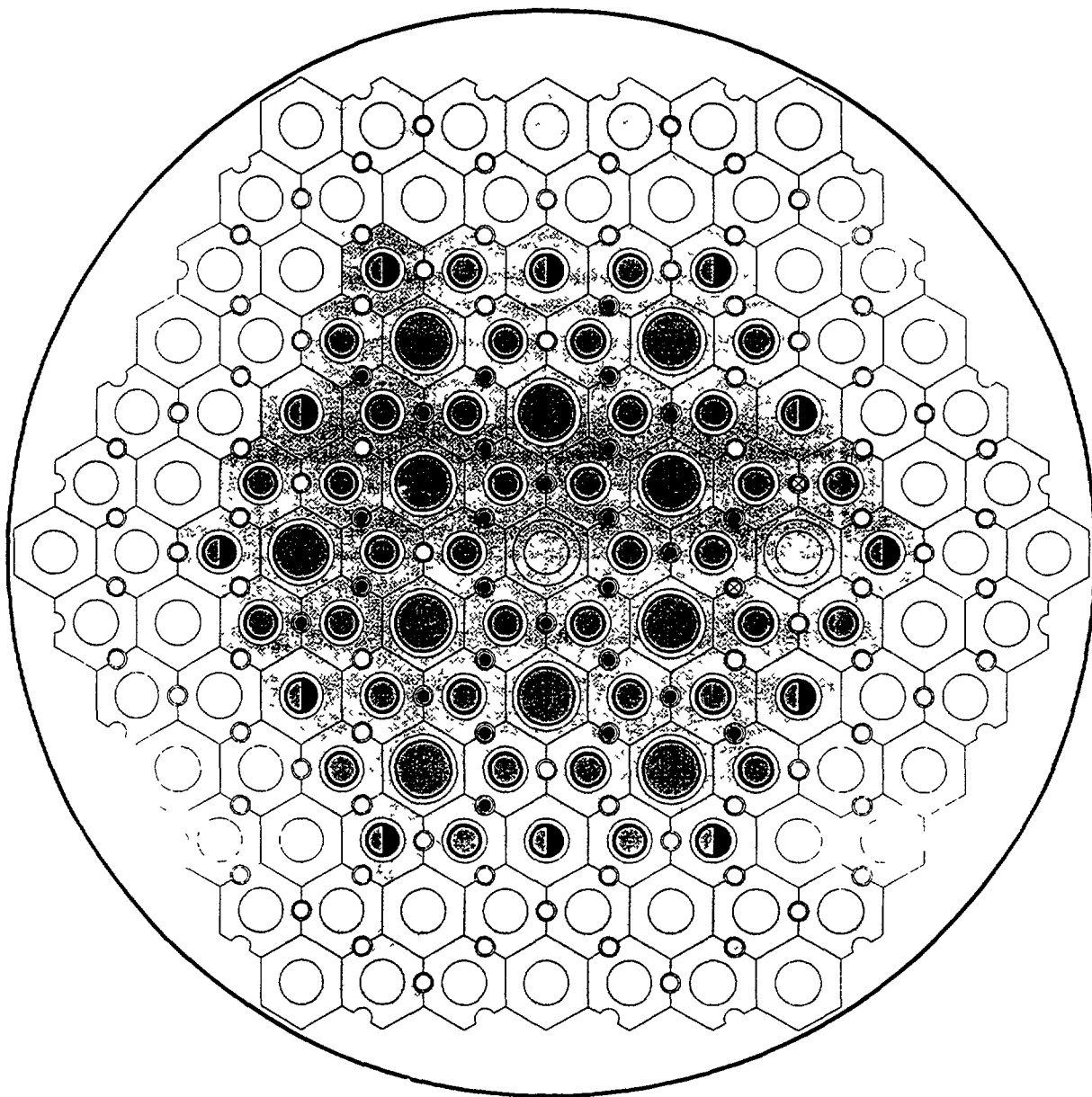


Fig.1 . Cartogram of the MIR reactor core.

TABLE II. MAIN CHARACTERISTICS OF THE WATER COOLANT LOPP FACILITIES

Name of loop facility	PV-1 PV-2	PVK-1 PVK-2	PVP-1	PVP-2
Coolant	water	water, steam	water, steam	water, steam
Pressure, MPa	20.0	20.0	8.5	20.0
Power, kW	2000	2000	100	2000
Temperature, °C	340	340	500	500
Flowrate via the loop channel, kg/h	16000	14000	675	1000
Maximum permissible activity of the coolant, Bq/kg	$3.7 \times 10^7$	$3.7 \times 10^7$	$3.7 \times 10^7$	$3.7 \times 10^{10}$

The WCC provision scheme at the loop facilities, designed to create the neutral correction-free conditions, is similar for all loops. It includes: make-up tanks with water distillate prepared in the specialized subdivision of the Institute, ion-exchange filters filled with domestic resins KU-2-8 (cationite) and AV-17-8 (anionite) for purifying the coolant in the loop circuit.

Special measures in 3 of the enumerated loop facilities (PV-2, PVK-2, PVP-2) are provided to realize different WCC and to conduct the relevant experiments. Let's consider these capabilities by a specific example of the PVK-2 loop.

### 3. EXPERIMENTAL CAPABILITIES OF THE PVK-2 LOOP IN ORGANIZATION OF WATER-CHEMICAL EXPERIMENTS

Inert gas (nitrogen) supplied to different vessels is also prepared in the specialized subdivision of the Institute.

The general design of the loop channel, with 2 channels in the loop, is shown in Fig.2. The schematic diagram of the PVK-2 loop facility of the MIR reactor with the correction unit is presented in Fig.3, and the control block of water-chemical conditions - in Fig.4. The entire loop facility is made of stainless steel.

Fuel elements and materials specimens of different configuration can be installed into the central cavity of the channel. There are standard devices, into which fuel elements specimens, either 200 mm long (4 floors along the core height) or 1 m long, are loaded. It is also possible to install in the channel both the refabricated fuel elements produced from FA components spent in the reactors cores of atomic power plants and the full-size fuel elements themselves. In this case only their lower part, 1 m long, will be in the research reactor core.

It should be noted that in the loop thermal scheme there is no electric heater. So in the case of irradiating the devices with structural materials there must simultaneously be some fuel elements

sufficient to provide the required temperature conditions in the channels of this loop. In another PVP-2 loop there is the relevant heater.

If it is necessary to place the control specimens beyond the irradiation area, they can be installed in both the loop channel itself (above the core) and in the special witness-channels being in the loop room (not indicated in the scheme).

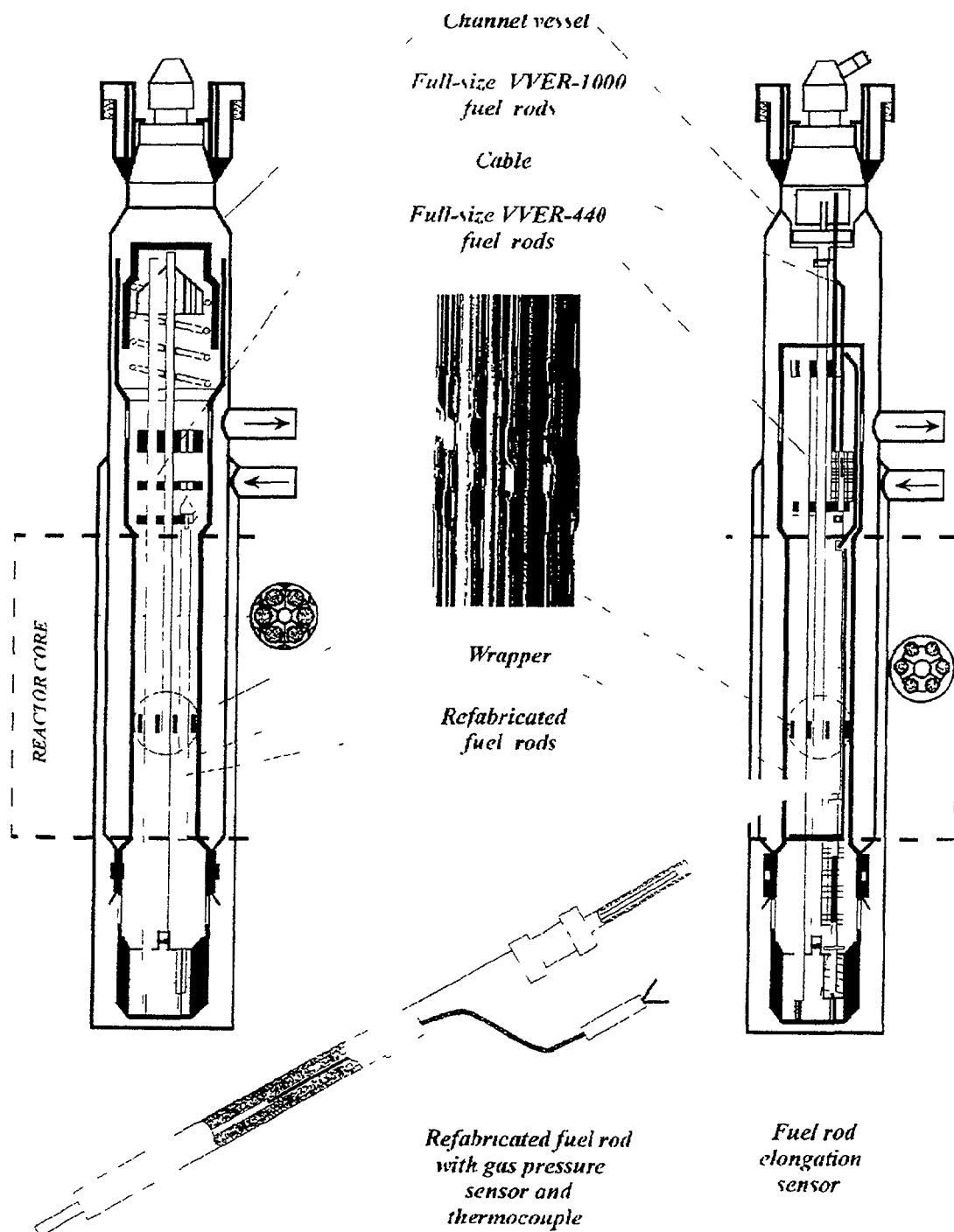


Fig. 2 Dismountable experimental devices for testing full-size and refabricated VVER fuel rods

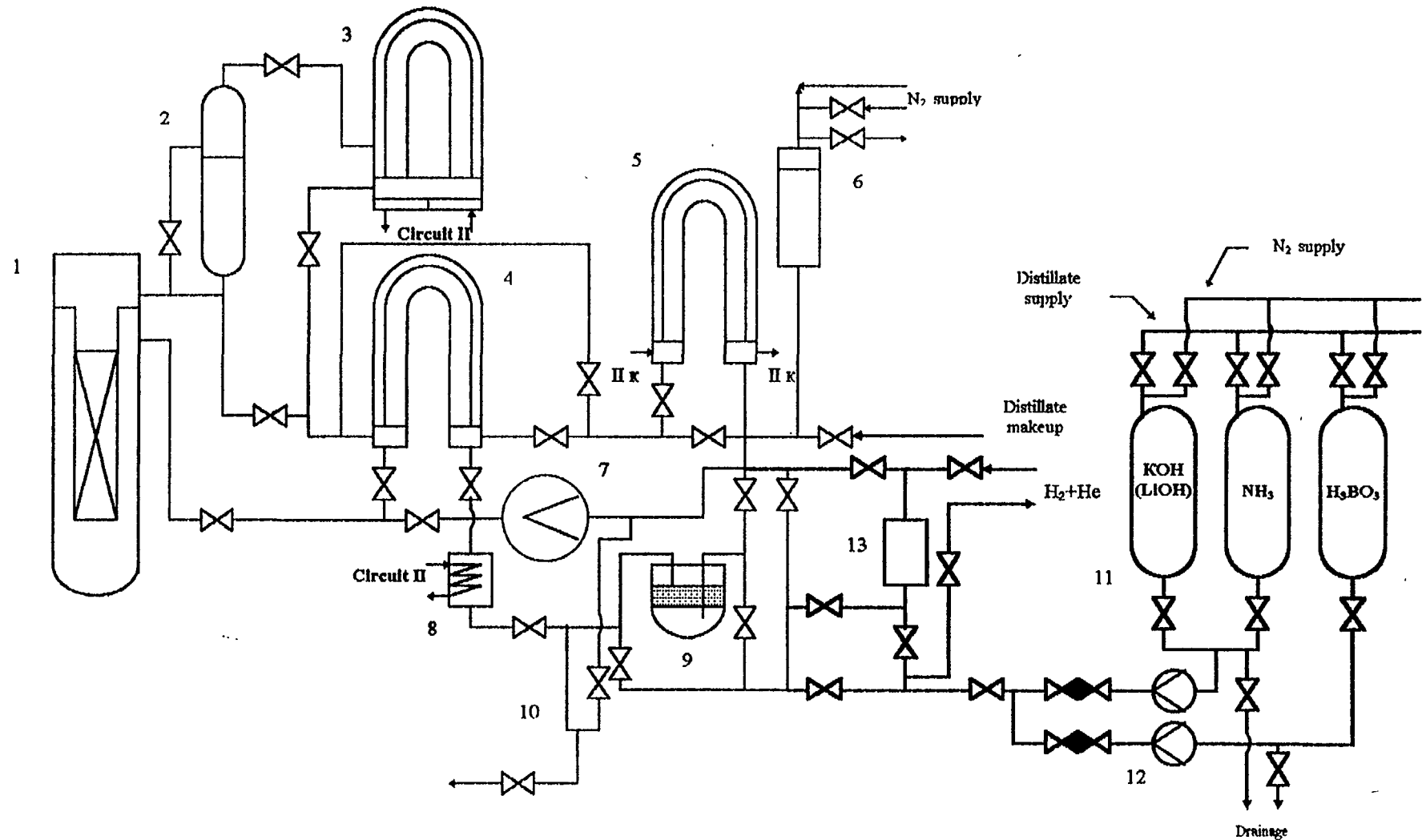


FIG.3. Schematic diagram of the primary circuit of the MIR reactor PVK-2 loop facility with the correction unit of water-chemical conditions (in bold type):  
 1 – loop channel; 2 – separator; 3,4,5 – heat exchangers; 6 – pressure compensator of the makeup pump; 7 – main circulation pump; 8 – IEF heat exchanger;  
 9 – ion-exchange filter; 10 – sampling system of loop coolant; 11 – dosage vessels for chemical reagents; 12 – dosage pumps; 13 – gas dosage vessel.

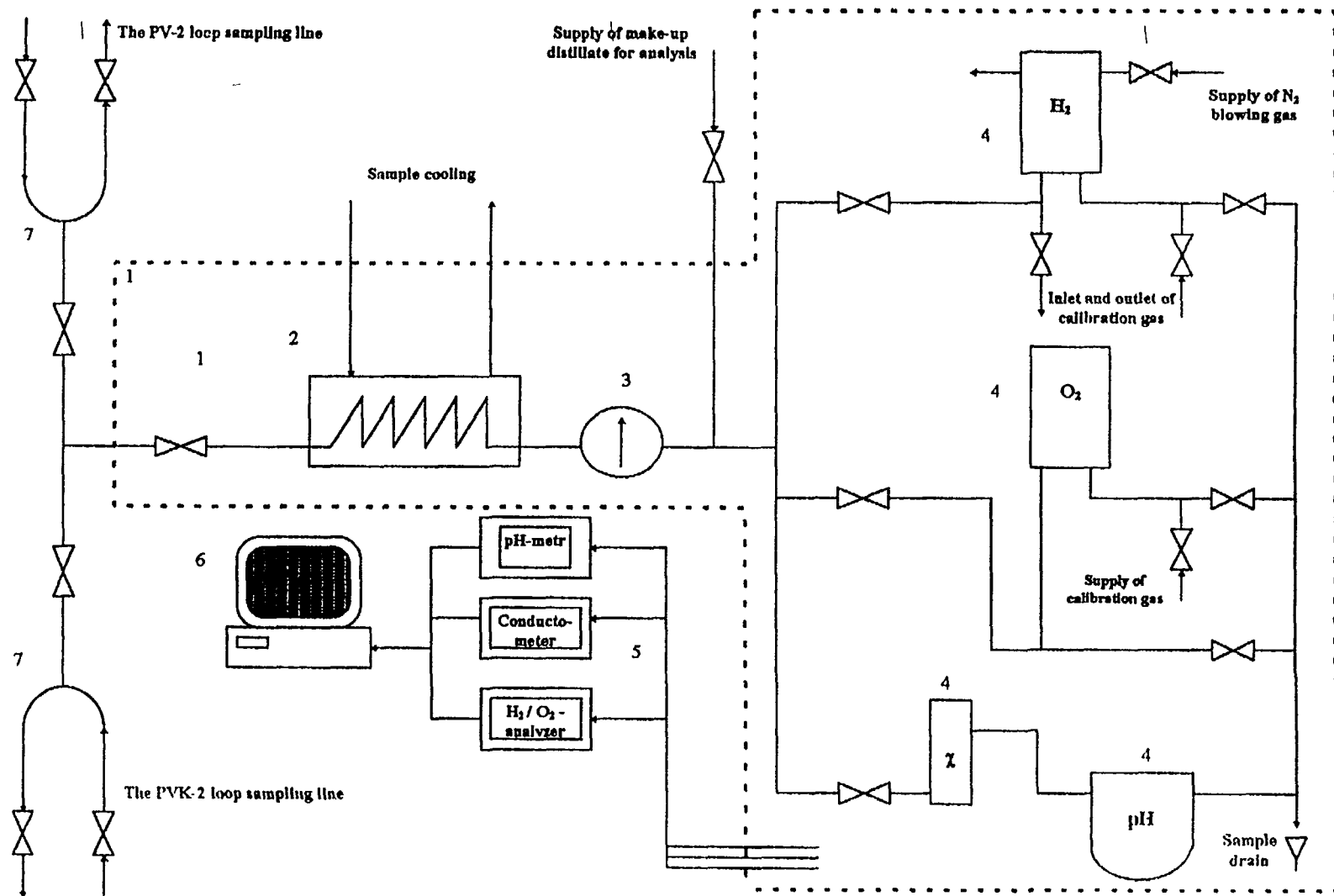


FIG.4. Installation of the automatic chemical control sensors at the primary circuits of the PV-2 and PVK-2 loops of the MIR reactor:  
 1 – coolant samples preparation system with the installed sensors; 2 – sample cooler; 3 – temperature and pressure control sensors; 4 – measuring sensors of hydrogen, oxygen content, specific conductivity and pH value; 5 – secondary devices: pH-meter, conductometer, gas analyzer of H<sub>2</sub> and O<sub>2</sub>; 6 – computer data acquisition; 7 – connecting to the sampling lines of the loops primary circuits.

The maximum internal diameter of the loop channels (depending on the type) is 74 mm and 60 mm. The nominal neutron flux density in empty channels is as follows:

- $E < 0.68 \text{ eV} - (3-5) \times 10^{14} \text{ cm}^{-2} \text{ s}^{-1}$
- $E > 0.1 \text{ MeV} - (2-4) \times 10^{13} \text{ cm}^{-2} \text{ s}^{-1}$ .

10–20 sensors registering the irradiation parameters and test conditions are installed in the loop channel, if necessary, included in the device under irradiation.

The loop thermal scheme allows operation with the parameters indicated in Tab.2 under the “pressurized water” conditions and under the steam formation conditions at the less pressure.

Under the correction-free water-chemical conditions (under long operation) the standard coolant quality indices are characterized by the values presented in Tab.3.

TABLE III. COOLANT QUALITY INDICES UNDER THE CORRECTION-FREE NEUTRAL WCC

Parameter	Value
Specific conductivity, $\mu\text{Sm/cm}$	up to 1.5
pH at 25°C	6.5–7.0
Mass concentration of chloride-ions, $\mu\text{g/kg}$ , no more	50
Mass concentration of ferrum ions, $\mu\text{g/kg}$ , no more	50
Mass concentration of copper ions, $\mu\text{g/kg}$ , no more	50
Mass concentration of aluminum ions, $\mu\text{g/kg}$	50

Such parameters of the coolant in the loop circuit are maintained with the constantly operating system of ion-exchange purification and the flowrate of 0.2 – 0.5 m<sup>3</sup>/h (at the total loop volume 1.8 m<sup>3</sup>). The total volume of the loaded ion-exchange resin makes up 70 l with 1:1 ratio).

For possible simulation of other water-chemical conditions (different from the correction-free ones), there is a correction unit common for 3 loop facilities including:

- vessels, 10 l in volume each, for chemical reagents solutions (boric acid, potassium or lithium hydroxides, ammonia, etc.);
- dosage pumps to bring the acid and alkaline solutions to the primary circuit of the loop;
- vessel for dosing the required gas (hydrogen, nitrogen, helium), 3 l in volume, for preliminary gas dissolving in water before introduction to the primary circuit.

The automatic chemical coolant control system equipped with the devices produced in Switzerland (ORBISPHERE) is also common for 3 loop facilities (Fig.4). It allows analysis of the dissolved gases (hydrogen and oxygen), pH and specific conductivity. The remaining parameters (content of boric acid, ions of alkaline metals, ammonia, etc.) are controlled by the laboratory methods.

The ion-exchange purification unit of the coolant for every loop facility provides hydro-loading and hydro-unloading of the resin. Depending on the maintained WCC, the resins before loading to the columns can be preliminarily converted to one or another ion form.

The experimental equipment complex described above allows tests of fuel elements and structural materials under the necessary neutron-physical, thermo-hydraulic and water-chemical conditions.

It should be noted that use of boric acid in the loop facility circuit stipulates the necessity of additional analysis of safety aspects under normal operating conditions and emergency situations in the loop. The MIR reactor is equipped with the critical stand – physical model of the core, where experimental investigations on this problem can be conducted in addition to the neutron-physical calculations of the particular irradiation device cooled by the coolant with the specified concentration of boric acid. The final material science investigations are performed in the specialized Laboratory of the Institute.

Interim examinations of the elements under irradiation are of great importance in performing the water-chemical experiments. At the MIR reactor it is carried out using the hot cell, where, if necessary, the fuel elements or structural materials specimens, that are periodically extracted from the loop channel, are visually examined. Their length, diameter are measured, the deposits are removed, the burnup in fuel elements is measured, and fission products are distributed by gamma-spectrometry.

If one of the objectives of the experiment under the specified WCC is to study the features of distributing fission products and activated corrosion products over the loop circuit, then apart from the standard control systems (for delayed neutrons at the channel outlet, the total gamma-activity in different points of the circuit), use is made of the gamma-spectrometric analysis system.

#### 4. SOME RESULTS OF WCC SIMULATION METHODOLOGICAL EXPERIMENTS

One of the first tasks on simulation of the VVER primary circuit water-chemical conditions was to determine the possibility of reliable long (a month and more) maintaining the relatively low level of concentration of boric acid and, respectively, of alkaline metals cations in the coolant with allowance for the structural and technological features of the loop:

- broad circuit scheme with availability of stagnant sections;
- periodical organized samplings of the coolant and some unorganized leakages stipulated by large quantity of drainages and air drainages;
- necessity of periodical seal failure of the loop circuit (refuelling of the loop channels and other operations).

The conditions with constant concentrations of boric acids: 100, 300 and 1000 mg/kg were investigated (Fig.5). It is established that maintaining the specified concentration levels can be provided in the range of  $\pm 15\%$  of the specified value. The concentration of boric acid is measured by the laboratory flame photometry method. Table 4 presents the comparative data on the modeled coolant composition in the final methodical experiments.

As follows from Tab.5, in the primary circuit of the loop the quality parameters of the VVER coolant except content of the dissolved oxygen were satisfactorily realized. High concentrations of oxygen are observed after seal failure of the primary circuit (loss of integrity of the loop channels for refueling or examination of the specimens, repair and preventive works). On the whole, maintaining this parameter is a problem to be improved.

At present in the PVK-2 loop channels there is irradiation of model fuel elements with the E-110 and E-635 zirconium alloys claddings and of model FA with the "soft" zirconium space grids under the VVER water-chemical conditions with different content of boric acid changing due to the program. The comparative corrosion experiment program commenced in 1997 is intended for several years.

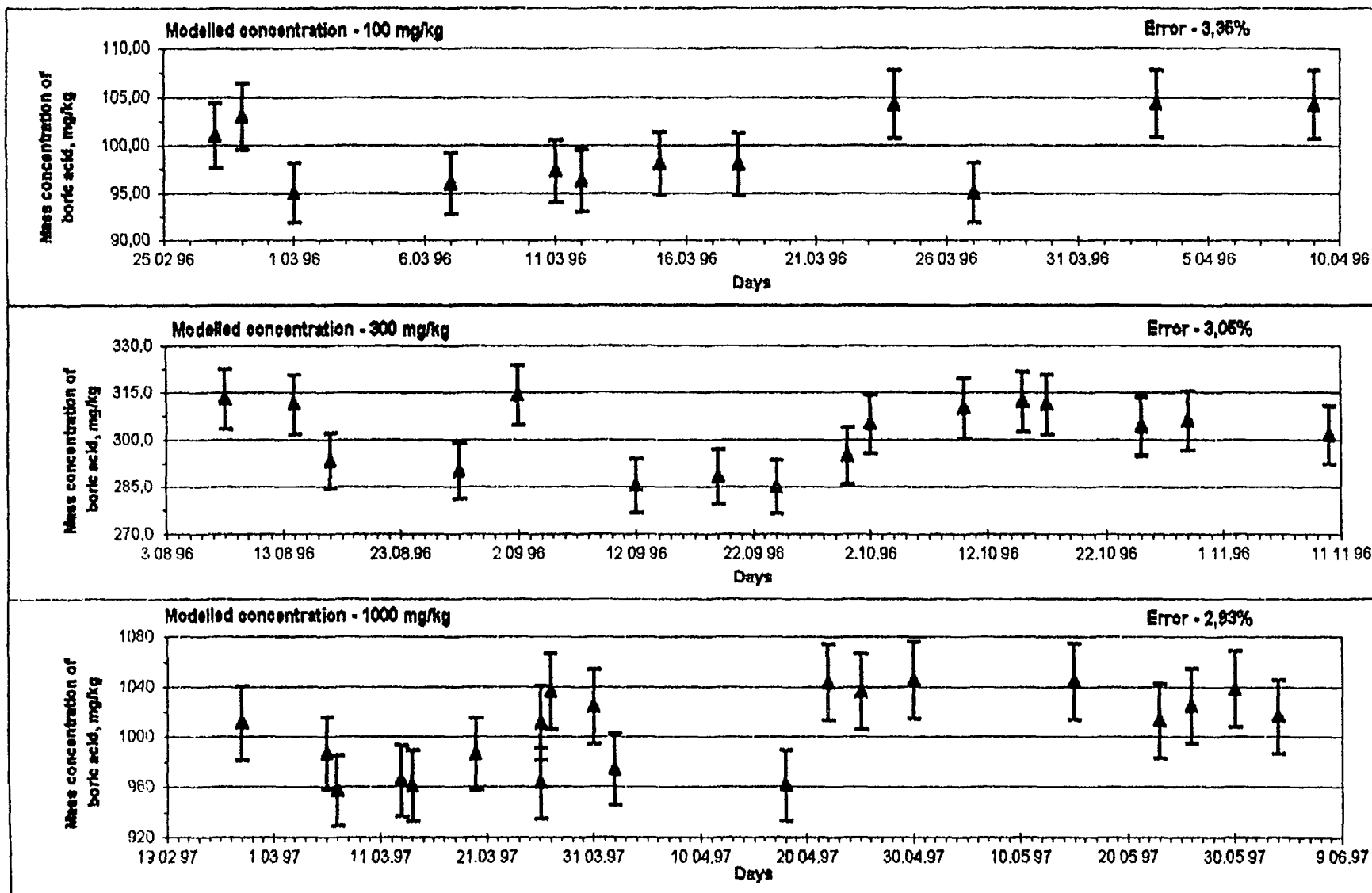


Fig.5. Experimental results on boric acid concentration measurements under different set values in primary coolant of the PVK-2 loop facility in MIR reactor during VVER water chemistry condition simulation

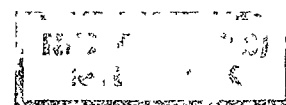


Table IV. COMPOSITION OF THE VVER MODELED COLLANT IN THE PVK-2 LOOP

Normalized index	Values in PVK-2	Values due to the VVER norms
pH at 25°C	8.5 – 8.3	7.5 – 10.5
Mass concentration of boric acid, g/kg	1.0 – 1.06	up to 12.0
Mass concentration of potassium ions, mmol/kg	0.13 – 0.14	0.02 – 0.50
Mass concentration of ammonium ions, mg/kg	40 – 50	> 5.0
Mass concentration of ferrum ions, µg/kg	10 – 20	< 50
Mass concentration of copper ions, µg/kg	5 – 10	< 20
Content of dissolved hydrogen, ncm <sup>3</sup> /kg	30 – 35	30 – 60
Content of dissolved oxygen, ncm <sup>3</sup> /kg	up to 0.07	< 0.0035

## REFERENCES

- [1] KUPRIENKO, V.A., KLINOV, A.V., SVYATKIN, M.N. and SHAMARDIN, V.K.,  
 "The SM and MIR Reactors Experience" Topical Seminar on "Management of Ageing of  
 Research Reactors", Geesthacht/Hamburg, Germany, 8–12 May, 1995. IAEA-SR-190/49.



# LOOP CAPABILITIES IN REZ FOR WATER CHEMISTRY AND CORROSION CONTROL OF CLADDING AND IN-CORE COMPONENTS

J. KYSELA, M. ZMÍTOKO, J. ŠRANK, R. VŠOLÁK  
Nuclear Research Institute Rez plc, Czech Republic



XA9953312

## Abstract

Main characteristics of LVR-15 research reactor and its irradiation facilities are presented. For testing of cladding, internals and RPV materials specialised loop are used. There are now five high pressure loops modelling PWR, VVER or BWR water environment and chemistry. Loops can be connected with instrumented in-pile channels enable slow strain rate testing, 1CT or 2CT specimens loading and electrically heated rods exposition. Reactor dosimetry including neutronic parameters measurements and calculations and mock-up experiments are used. Water chemistry control involves gas ( $O_2$ ,  $H_2$ ) dosing system, Orbisphere  $H_2/O_2$  measurement, electrochemical potential (ECP) measurements and specialised analytical chemistry laboratory.

For cladding corrosion studies in-pile channels with four electrically heated rods with heat flux up to  $100 \text{ W/cm}^2$ , void fraction 5 % at the outlet, inlet temperature  $320^\circ\text{C}$  and flow velocity 3 m/s were development and tested. For corrosion layer investigation there is eddy current measurements and PIE techniques which use crud thickness measurement, chemical analyses of the crud, optical metallography, hydrogen analysis, SEM and TEM.

## 1. Introduction

Main characteristics of LVR-15 research reactor and its irradiation facilities are presented. For testing of cladding, internals and RPV materials specialised loop are used. There are now five high pressure loops modelling PWR, VVER or BWR water environment and chemistry. Loops can be connected with instrumented in-pile channels enable slow strain rate testing, 1CT or 2CT specimens loading and electrically heated rods exposition. Reactor dosimetry including neutronic parameters measurements and calculations and mock-up experiments are used. Water chemistry control involves gas ( $O_2$ ,  $H_2$ ) dosing system, Orbisphere  $H_2/O_2$  measurement, electrochemical potential (ECP) measurements and specialised analytical chemistry laboratory.

For cladding corrosion studies in-pile channels with four electrically heated rods with heat flux up to  $100 \text{ W/cm}^2$ , void fraction 5 % at the outlet, inlet temperature  $320^\circ\text{C}$  and flow velocity 3 m/s were development and tested. For corrosion layer investigation there is eddy current measurements and PIE techniques which use crud thickness measurement, chemical analyses of the crud, optical metallography, hydrogen analysis, SEM and TEM.

## 2. Reactor LVR-15

The LVR-15 is a light-water moderated and cooled tank nuclear reactor with forced cooling. The maximum reactor power is 10 MWth. The fuel type IRT-2M enriched to 80 % or 36 % and a combined water-beryllium reflector are used. The reactor core is composed of IRT-2M type fuel assemblies made in Russia with enrichment of 80 %  $^{235}\text{U}$ . This fuel has been changed for fuel with an enrichment of 36 %  $^{235}\text{U}$ . The reactor core grid has a pitch of 71,5 mm and 80 cells. In the basic operation configuration, 28-34 cells contain fuel elements, 2-4 of the fuel cells are dedicated to channels for experimental probes and 3-6 cells in the reflector and core periphery are dedicated to vertical irradiation channels.

The reactor core is situated in the reactor vessel (outer diameter 2 300 mm, total height of the vessel 6 235 mm), which is made of stainless steel, the internal parts of the reactor are made of an aluminium alloy. The reactor has a forced circulation of the coolant. The generated heat is transported via three cooling circuits to Vltava river.

The primary circuit contains 5 main circulation pumps and 2 emergency pumps which provide the circulation of the coolant through the reactor core and 2 heat exchanges. The emergency pumps are connected with an emergency battery source and a diesel generator, which secure their operation when the electrical network in the reactor site fails. The coolant flows through the core downwards, with the maximum coolant temperature at the reactor output of 51 ° C. The nominal flow is 2 100 m<sup>3</sup>/hour. The coolant is light demineralised water.

### 3. Light Water Loops

At present five loops are used to perform tests in core. Parameters and type of water chemistry are presented in Table 1.

#### 3.1. RVS-3 Loop

The loop is designed for material and radioactivity transport investigation under PWR/VVER conditions. The RVS-3 loop facility enables to perform irradiation experiments in wide range of operational parameters limited by following maximum parameters: pressure 16,5 MPa, temperature 345 ° C, water flow rate 10 000 kg/hr.

Table 1 High pressure loop parametrs

Loop	Water chemistry	Temper. (° C)	Pressure (MPa)	Flow rate (t/h)
RVS-3	VVER/PWR	345	16,5	3-10
BWR-1	BWR	300	10	2
BWR-2	BWR	300	12	8
ZINC	PWR	320	15,5	0,8-1
RVS-4	VVER	322	15,7	2

The loop is a closed stainless piping system with usual technological auxiliary systems. The experimental equipment of the loop consists of:

- active (in-pile) channels situated in the reactor core for irradiation of materials samples;
- out-of-pile test section; provides the same thermal-hydraulic parameters as in-pile channel;
- electrically heated rod immitators for corrosion tests of fuel cladding materials (heat flux up to 100 W/cm<sup>2</sup> in the core region of 560 mm);
- loading facility for investigation of corrosion fatigue at low-cycle load and SSRT test;
- filtration system equipped with mechanical and ion exchange filters;
- make-up water system for water environment preparation and dosing into the loop system;
- sampling system (including isokinetic) for water sampling from different points of the loop;
- high-temperature sensors for water chemistry monitoring (conductivity, pH<sub>T</sub>, ECP).

The RVS-3 loop can provide experimental services in wide area of interest, e.g.:

- investigation of structural materials mechanical properties degradation and corrosion behaviour under irradiation and PWR/VVER water chemistry and thermal-hydraulic conditions;
- investigation of behaviour (corrosion, hydriding) of fuel cladding materials under influence of irradiation, thermal flux and water chemistry conditions;

- investigation of radioactivity transport and behaviour under PWR/VVER conditions (e.g. influence of water chemistry, pH<sub>T</sub> regime, zinc injection ammonia);
- testing of high-temperature, high-pressure sensors for water chemistry monitoring.

### 3.2. BWR-1 Loop

The loop is designed for investigation of structural materials behaviour and radioactivity transport under BWR conditions. The BWR-1 loop facility enables to perform irradiation experiments in wide range of operational parameters limited by the following maximum parameters: pressure 10 MPa, temperature 300°C, water flow rate 2,000 kg/hr.

The loop is a closed stainless steel piping system usual technological auxiliary systems. Main features of the loop from point of view of experimental utilisation are:

- ion exchange purification system with flow rate 200 kg/hr (i.e. 10% of the primary flow);
- oxygen and hydrogen gas dosing system for maintaining normal or hydrogen water chemistry;
- active (in-pile) channels situated in the reactor core for irradiation of material samples;
- sampling system (including isokinetic) for water sampling from different points of the loop;
- on-line monitoring of dissolved gases O<sub>2</sub>/H<sub>2</sub> concentration and specific conductivity.

The BWR-1 loop can be used for the following purposes:

- investigation of materials mechanical properties degradation and corrosion behaviour under irradiation and BWR water chemistry conditions;
- investigation of radioactivity transport and behaviour under BWR conditions (e.g. hydrogen water chemistry, zinc injection, etc.);
- testing of high-temperature, high-pressure sensors for water chemistry monitoring.

### 3.3. BWR-2 Loop

The experimental water loop shall be used for the material research of BWR reactors under conditions simulating the operation of BWR reactors (pressure, temperature, radiation, fluid analysis).

The loop consists of closed pressurized circuit with forced water circulation in the generation channel K1 located inside the active core, test irradiation channel K2 located next to the LVR-15 reactor core and in-out-of-pile channel K3 outside the neutron radiation field in the machine hall. In the K2 irradiation channel two 50 CT specimens provided with a notch and loaded with a cyclic stress of 151,7 kN in periods taking 28 to 32 hours are placed. During mechanical load the specimen is exposed to the effects of neutron flux and water flow. Physical and chemical conditions of the specimen exposure in the channel are close to operational conditions inside the boiling water reactors where the tested materials will be used. During the experiment, the size of developing crack and its spreading is measured continuously.

The K3 reference channel where the two 50 CT specimens are located is connected to the loop. The above specimens are exposed to the same mechanical load as the specimens inside the K2 irradiation channel. The above specimens, however, are not exposed to the effects of radioactive radiation and the content of H<sub>2</sub>O<sub>2</sub> is lower than in the K2 channel. The remaining physical and chemical parameters are the same in both channels. By comparison of measured results of the specimens in both channels, the effect of irradiation on the corrosion process and crack propagation can be evaluated.

The primary circuit of BWR-2 loop, two sampling lines for measuring H<sub>2</sub>O<sub>2</sub> concentration and the sampling point for measuring H<sub>2</sub>, O<sub>2</sub> concentration are given schematically in Fig.1. The length of primary circuit is about 95 m, the lengths of sampling lines: Line2- 16,2 m (the volume is about  $3,25 \cdot 10^{-4} \text{ m}^3$ ), Line3 - 16,1 m (the volume is about  $3,05 \cdot 10^{-4} \text{ m}^3$ ). Flow rate in the loop is 8 t / hr and flow rate in the sampling lines, when the sample is taking, about  $1,67 \cdot 10^{-5} \text{ m}^3 / \text{s}$ .

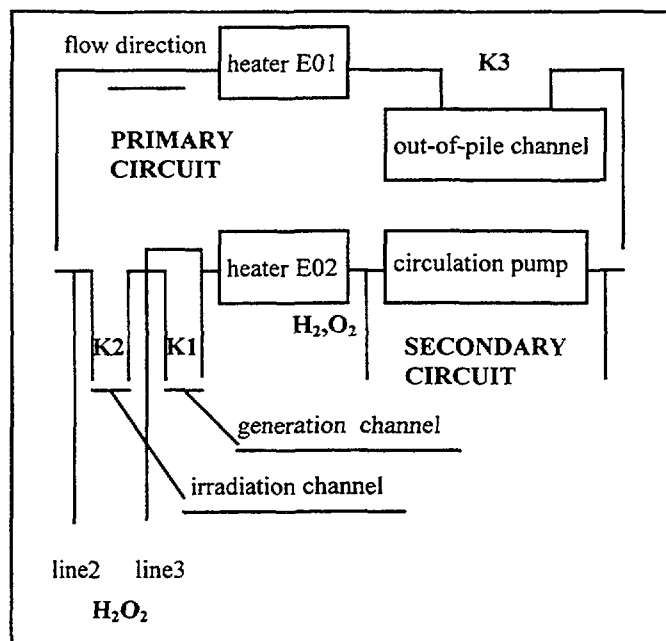


Fig. 1. Primary Circiut of BWR-2 Loop

### 3.4. Modelling of Water Radiolysis

The program for the calculations of water radiolysis product concentration [1] profiles under the mixed g and fast neutron irradiation in NRI Øe□ experimental BWR-2 loop employs the reaction mechanism of water radiolysis suggested by [2]. The  $G_r$ -values for fast neutrons and g -irradiation recommended by these authors were also used. In addition, the catalytic decomposition on the stainless steel tubing wall was incorporated into the model as well as the loop surface corrosion by the diluted oxygen.

The hydrogen peroxide decomposition in the loop was considered both the hommogeneous and the catalytic one. The values of kinetic constants for homogeneous and catalytic decomposition were obtained by regression of the experimental data on the decomposition inside stainless steel tubes from [3]. The value of kinetic constant which is necessary for the oxygen consumption due to the loop surface corrosion modelling was estimated from  $O_2$  dosage frequency required in the BWR-2 loop. Radicals and molecules productions were calculated by  $G_r$ -values and irradiation intensities in LWR-15 research reactor.

$H_2O_2$  behaviour in the loop and measuring of  $H_2O_2$  concentration in the vicinity of the specimens located in channel K2 is proved by experimental measuring of  $H_2O_2$ ,  $H_2$  and  $O_2$  concentration and comparison with calculations. Measured concentrations (under temperature 288°C with corrosion) were:  $H_2$ = 10-16 ppb,  $O_2$ = 150-200 ppb,  $H_2O_2$  (Line2)= 10-16 ppb,  $H_2O_2$  (Line3)= 30-60 ppb. Calculated values agreed well with experimental values ( $H_2O_2$  concentration in the vicinity of the specimens is about 210-240 ppb) (see Fig. 2).

### 3.5. ZINC Loop

This experimental facility is designed to be used in a programme of neutron irradiation testing to investigate the effect of zinc addition on activity transport in PWRs. A series of in-pile loop experiments will be carried out with different levels of zinc addition to obtain basic data on radioactive material generation, migration and deposition within PWR. Two identical mini loops were manufactured , installed and subsequently irradiated in the research reactor. Each loop will be dismantled on removal from the reactor and parts will be examined in post-irradiation examination cells.

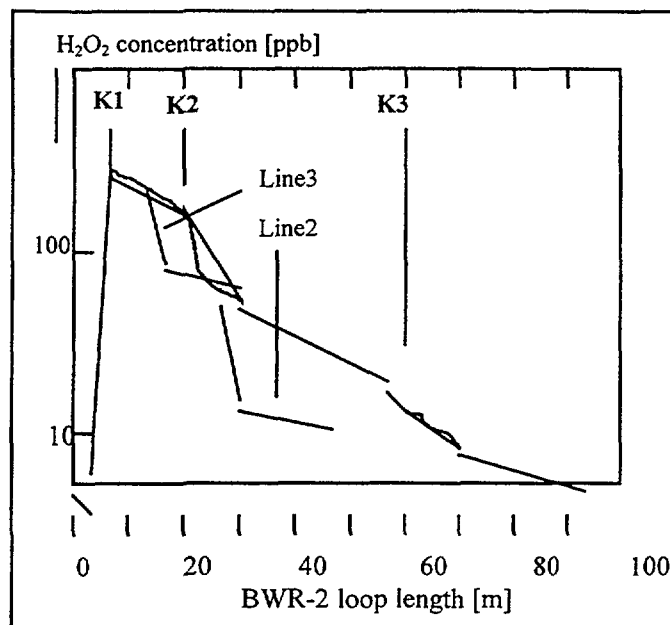


Fig. 2. Concentration of Dissolved Hydrogen Peroxide along the Primary Circuit of BWR-2 Loop

The facility consists of an in-pile mini loop and out-of-pile water conditioning, injection, bleed and analysis circuits. The in-pile rig comprises three regions which model main material and parameter features of PWRs, as follows:

- a heated in-core region consisting of small diameter Zircaloy tubing; the Zircaloy tubing is heated externally via a liquid lead filled bath contained within an electrically heated capsule;
- a cooled out-of-core region comprising Inconel MA 600 tubing; cooling is provided by a flow of secondary water;
- a section made up of stainless steel (SS) tubing.

The out-of-pile system is used for the loop feed and bleed to ensure representative PWR conditions, water chemistry monitoring and other experiment and operational requirements, eg. the loop pressure control. The feed and bleed flow is typically 100 cc/hr, ie.  $1 \times 10^{-4}$  of the main flow. The system also serves for oxygen removal from make-up water and creating of specified hydrogen overpressure.

### 3.6. RVS-4 Loop

The loop is designed to perform an experimental programme focused on a study of corrosion product radionuclides behaviour and radioactivity build-up at different VVER/PWR water chemistries. An investigation of ammonia (low and high concentration level), hydrogen and hydrazine primary water chemistry is considered. A study of Zircaloy cladding corrosion behaviour at these water chemistries is another subject of the experimental programme.

The loop RVS-4 is closed stainless steel system which models main thermal-hydraulic, material and irradiation conditions of VVER-1000 units. The integral high-pressure loop consists of following main component and systems:

- an in-pile rig consists of pressure channel with field tube for flow division inside the channel;
- an in-pile test section comprises four electrically heated fuel rod immitators with designed heat flux up to  $60 \text{ W/cm}^2$  in the core region of 560 mm; electrically heated rod with SS sheath is inserted into the zirconium cladding tube;
- primary circulation system comprising of the main circulation pump, primary piping and a primary cooler;

- pressurizer and volume compensating system;
- make-up water preparation and dosing system with continual feed and bleed of 100 cc/hr;
- primary coolant sampling system.

#### 4. In-Pile Channels

The special in-pile instrumented channels and irradiation rigs are used. The neutron irradiation of specimens is performed in CHOUCA irradiation (see Fig.3). It enables full temperature control of irradiated specimen. Basically, four types of specimens can be irradiated: tensile specimen, CT specimen, round CTs and Charpy-V specimens. At present time, new irradiation rigs are operated for the irradiation of 2T CTs and 1T CTs. After preirradiation the specimen can be loaded to SSRT channel (see Fig.4) or 2CT (1CT) channel for constant or cyclic SCC tests (see Fig.5). For corrosion of fuel cladding material under influence of irradiation, heat flux and water chemistry a channel with electrically heated rods is operated (see Fig.6). Thermohydraulic parameters of test section of this channels are shown in Fig.7 which involves inlet and outlet temperature, flow rate, surface temperature and void fraction. In presence of subcooled boiling (about 10% of void fraction) a typical 'chimney' structure of corrosion product deposits is developed on the zirconium cladding surfaces (see Fig.8).

#### 5. Water Chemistry

Water chemistry control in all of the loop consists in the following items: special make-up water preparation, water purification, O<sub>2</sub> or H<sub>2</sub> direct gas dosing for both BWR and PWR chemistries, Orbisphere gases high pressure measurements and analytical chemistry using top Dionex ion-chromatography.

Changes of oxygen and hydrogen concentration in the BWR-2 loop during reactor start up are presented in Fig.9.

#### 6. IN-CORE DOSIMETRY

The power and neutron group flux densities distribution in the core are calculated with the NODER 4 groups diffusion code developed in the NRI. The macroscopic constants for this code are prepared with the use of WIMSD4 and WIMSD4-M codes. The neutron spectrum is determined using the DORT transport code. Monte-Carlo transport codes KENO and MCNP were also tried for these purposes. The DORT code is also used for the determination of gamma field parameters.

Sets of self-powered neutron detectors situated near the irradiation channels of irradiation devices are used for the neutron flux densities distribution along the reactor core height monitoring and for the obtained neutron fluence determination and prediction. Sets of reactor calorimeters can be also used. Final total fluences are determined after the end of irradiation with the use of sets of activation fluence monitors situated inside the irradiation channels.

When a new type of irradiation experiment shall be carried out, or when the irradiation channel position in the reactor core shall be completely different than those used during the preceeding experiments, a mock up experiment is carried out. For this experiment a model of irradiation assembly is produced and it contains an appropriate amount of activation monitors situated in the places of interest. In this experiment the calculated neutron spectrum is verified, neutron flux densities distribution in the irradiation assembly and relations to the outer self-powered neutron detectors signals are determined.

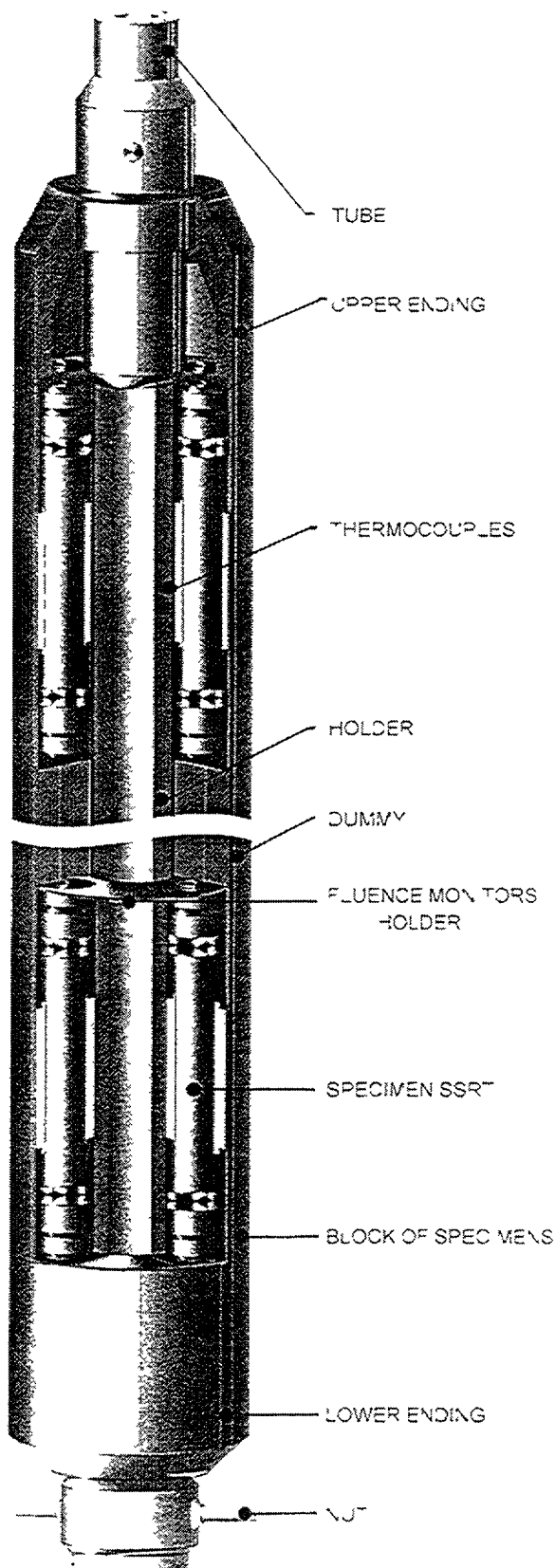


Fig. 3  
IRRADIATION RIG  
CHOUCA-MT  
SPECIMENS CARRIER

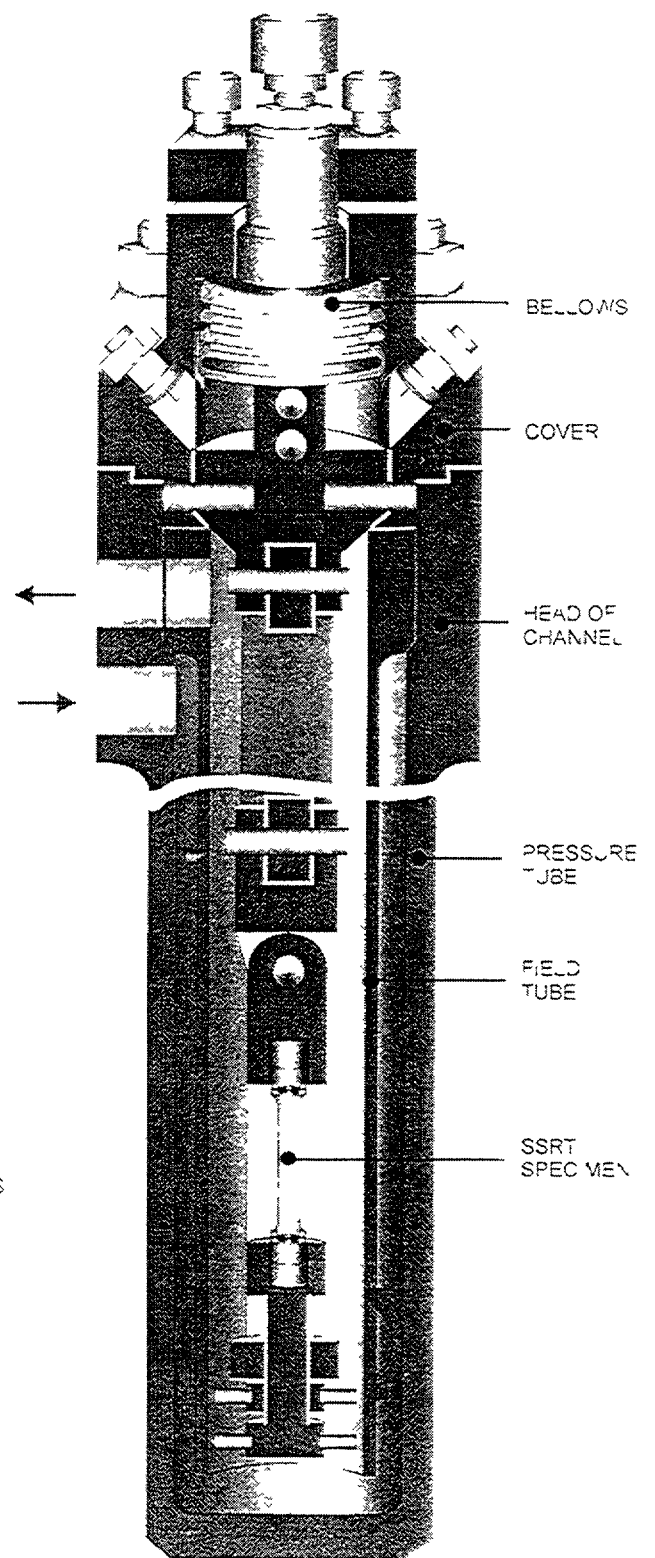
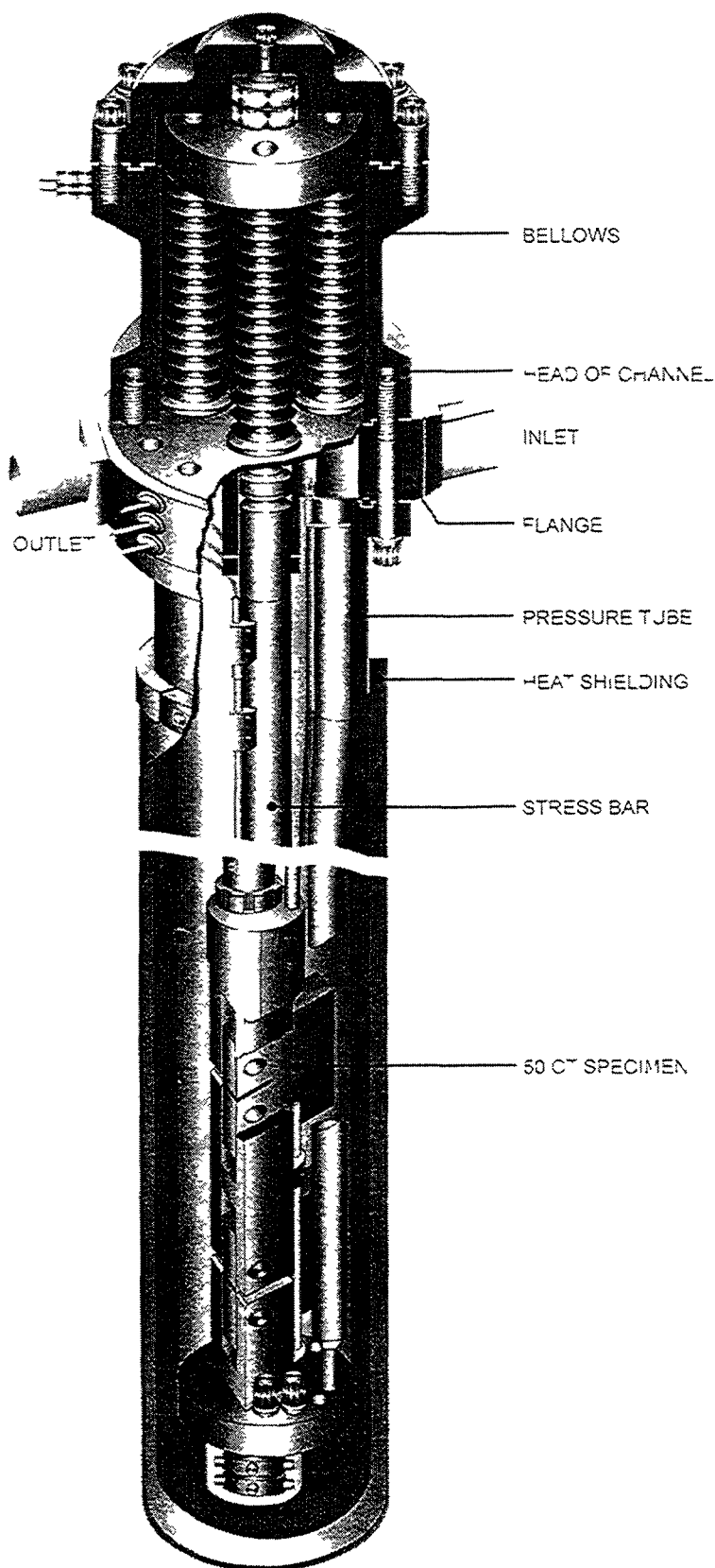
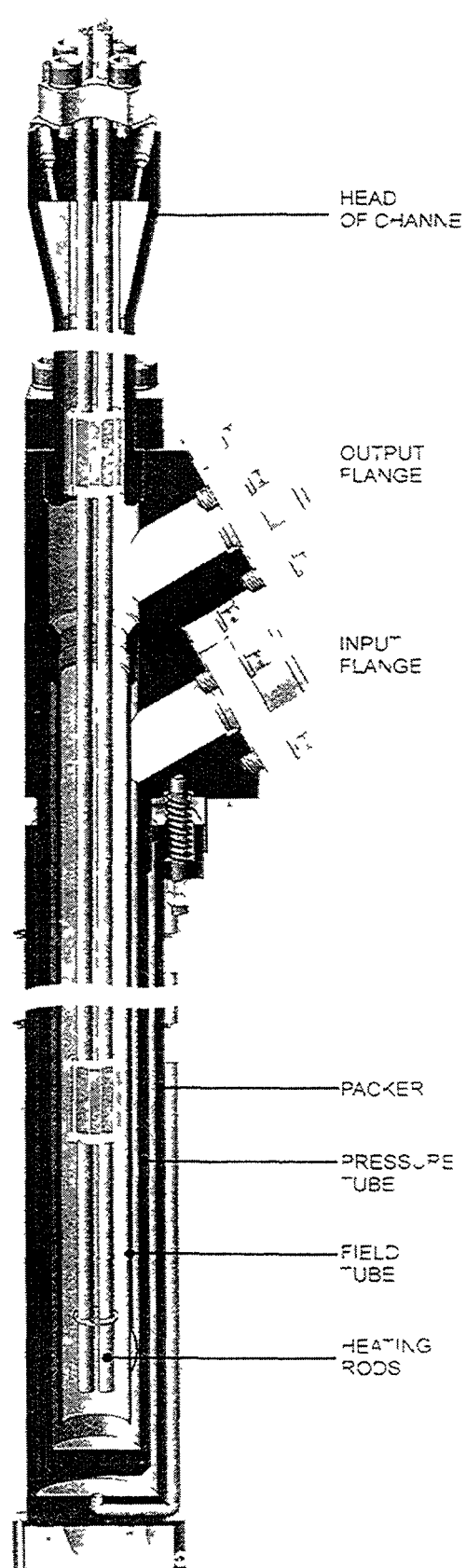


Fig. 4  
IRRADIATION CHANNEL  
WITH SSRT SPECIMEN





**Fig.5**  
BWR - 2 LOOP  
IRRADIATION  
CHANNEL



**Fig.6**  
RVS - 3 LOOP  
IRRADIATION  
CHANNEL

Thermal-hydraulic parameters along the active channel

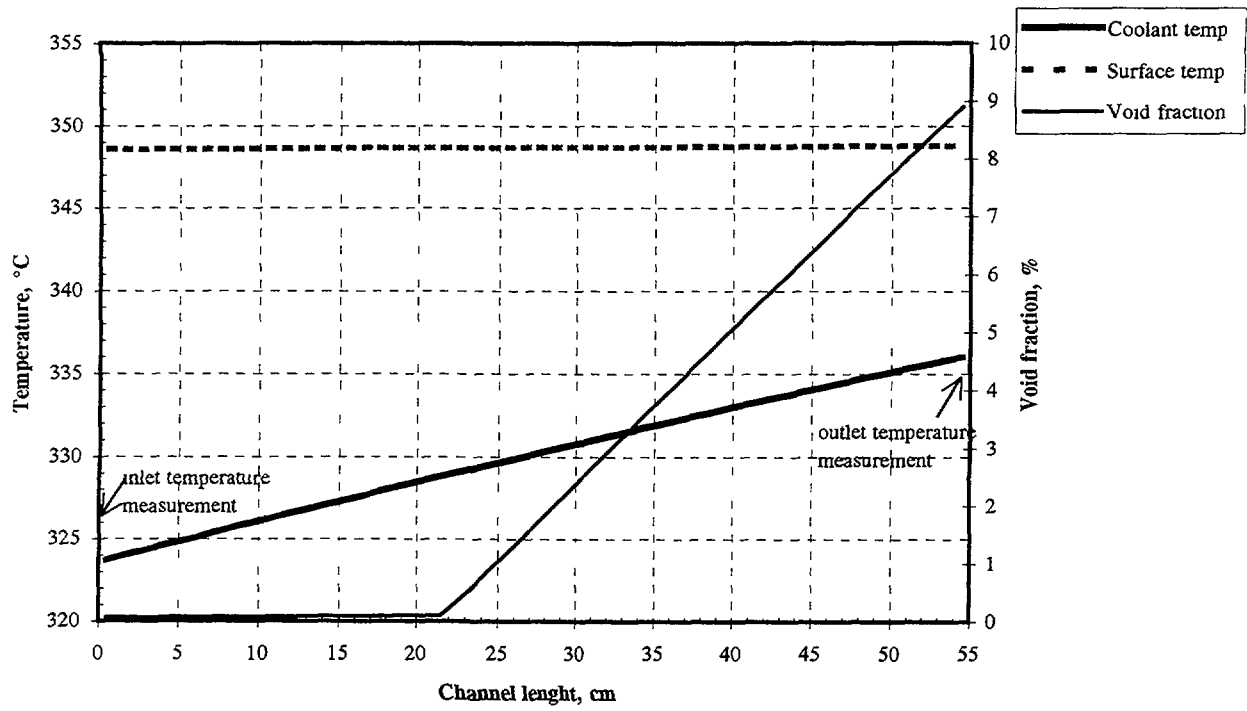


Fig. 7 Distribution of thermal-hydraulic parameters along the active channel situated in the reactor core.

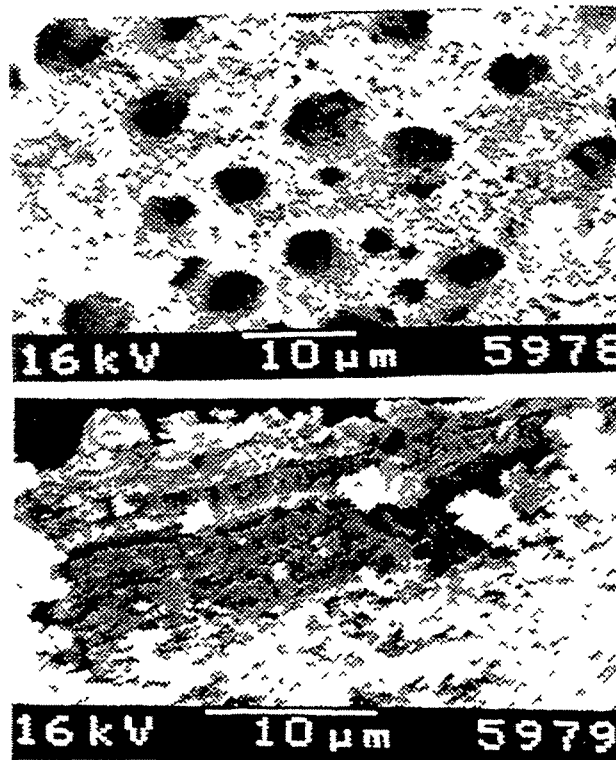


Fig.8 An example of corrosion product on the zirconium cladding surface

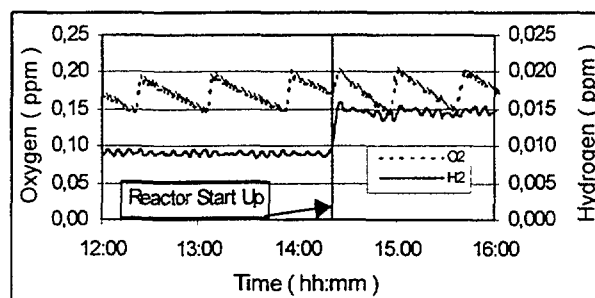


Fig.9 Concentration of O<sub>2</sub> and H<sub>2</sub> in the BWR-2 loop

## REFERENCES

- [1] MOUCHA T., LINEK V., "Modelling of water radiolysis in the BWR-2 experimental loop in NRI Rez", Inst. Chem. Technology-ICT), Dep. Chem. Engineering, Prague, ICT (July 1998).
- [2] CHRISTENSEN, H., LUNDGREN, G., "Model calculations of water radiolysis in the primary coolant circuit of the Barseback-1 BWR", Water Chemistry of Nuclear Reactor Systems (Prec. 7.Int. Conf. Bornemouth, 1996), BNES, (1996) 214-221.
- [3] LIN C. C., SMITH F. R.: Project 2295-3, EPRI NP-6733, Interim Report, March 1990



## HALDEN RESEARCH ON ZIRCALOY CLADDING CORROSION

T.M. KARLSEN, M. McGRATH, E. KOLSTAD  
OECD Halden Reactor Project,  
Halden, Norway

### Abstract

Light water loop systems simulating both BWR and PWR environments have been used for fuel and materials investigations at the Halden Project for a number of years. One series of studies is aimed at addressing the effects of water chemistry and high burnup on the corrosion behaviour of Zircaloy cladding under PWR conditions. The studies have included an evaluation of the effect of high lithium on the corrosion behaviour of pre-irradiated standard Zircaloy-4, and assessments of the effects of parameters such as stress condition, hydriding, fluence and heat flux on standard and low tin Zircaloy-4 as well as more modern cladding variants. In this report, the objectives and main results from some of these investigations are presented. Plans for possible future studies, which include exploration of the separate effects of local radiation fields on shadow corrosion, and a study aimed at addressing the effects of water chemistry and local heat flux on cladding crud deposition, are outlined.

## 1. INTRODUCTION

One of the experimental programmes at Halden addresses the effects of PWR water chemistry and operating parameters on the corrosion behaviour of Zircaloy cladding materials. The deterioration of cladding properties due to waterside corrosion, irradiation damage and hydrogen pick-up and migration is a potential performance / life limiting factor when going to higher discharge burn-ups. Data from commercial plants show that the growth rates of oxide layers increase considerably at burn-ups in excess of 30-40 MWd/kgUO<sub>2</sub>. While this phenomenon is partly explained by higher metal / oxide interface temperatures created by the oxide layer itself, other processes (irradiation damage and hydrogen effects which produce changes in the cladding properties) may also contribute to accelerated corrosion.

Studies aimed at assessing, separately, the factors affecting cladding corrosion make use of test facilities in which the coolant chemistry and operating variables may be altered to suit experimental needs. The studies have made use of unirradiated and pre-irradiated test segments prepared from standard and modern PWR cladding materials. Typical examples of loop systems and the in-core test arrangements that have been used in the PWR programme are outlined below.

## 2. GENERAL DESCRIPTION OF A PWR LOOP SYSTEM

In-pile investigations on the effects of operating parameters and water chemistry on the corrosion behaviour of Zircaloy cladding have been performed in facilities operating under representative PWR thermal-hydraulic, neutronic and water chemistry parameters. The in-core test rigs, which are described in the sections which follow, are connected to recirculating loop systems (Fig. 1) with temperature, pressure and flow conditions typical of those found in commercial reactors. The loops comprise a main circulating system, a water analysis and sampling system, and a purification plant. Ion exchange beds in the anionic and cationic form are used to regulate the lithium and boron levels while a mixed bed ion exchange unit removes impurities. The loops may be operated with range of lithium and boron concentrations, according to the requirements of the experiment. Further, chemical species (for example zinc) may be added, via an injection system, in studies where the effects of chemical additives or impurities are to be investigated.

In addition to the studies performed in the in-pile test sections, use is also made of the external loop systems for studies on the effects of water chemistry on the Co deposition and activation of primary circuit component materials. In the past, a series of such studies were conducted in order to examine the effects of zinc addition on Co uptake. The tests were conducted by installing a series of coupon specimens prepared from primary circuit constructional materials such as 304L SS, VVER SS and Inconel alloys, in out-of-pile autoclaves. At regular intervals, coupons were removed from the autoclaves and subjected to detailed characterisation of the oxide layers. Results from these investigations are reported in detail elsewhere [1,2].

### 3. DESCRIPTIONS OF IN-CORE TEST SECTIONS

#### 3.1 Effects of increased lithium contents on standard Zr-4 corrosion behaviour

In an early study, a PWR test facility was used to assess the effects of an increased lithium concentration in the coolant on the corrosion behaviour of standard Zircaloy-4 [3]. The test rig (Fig. 2) contained four PWR rod segments which had been pre-irradiated in a commercial reactor to an average burn-up of 28.5 MWd/kgUO<sub>2</sub>. The two lower rod segments were cooled by one-phase flow and the upper two rod segments were subjected to nucleate boiling conditions. The loop was operated with 1000 ppm boron and 4-4.5 ppm lithium, resulting in a pH<sub>300</sub> of 7.2-7.4, respectively.

The four test segments, which had initial oxide thicknesses of 10, 20 and 40 µm, were irradiated in the Halden reactor for a total of 10 200 full power hours, reaching a final burn-up accumulation of 45 MWd/kgUO<sub>2</sub> and average oxide thickness increases of 30 to 55 µm. Pre-test, as well as interim and final oxide layer thickness measurements were made on the test segments and the results were compared with model predictions based on the EPRI/C-E/KWU post transition corrosion equation.

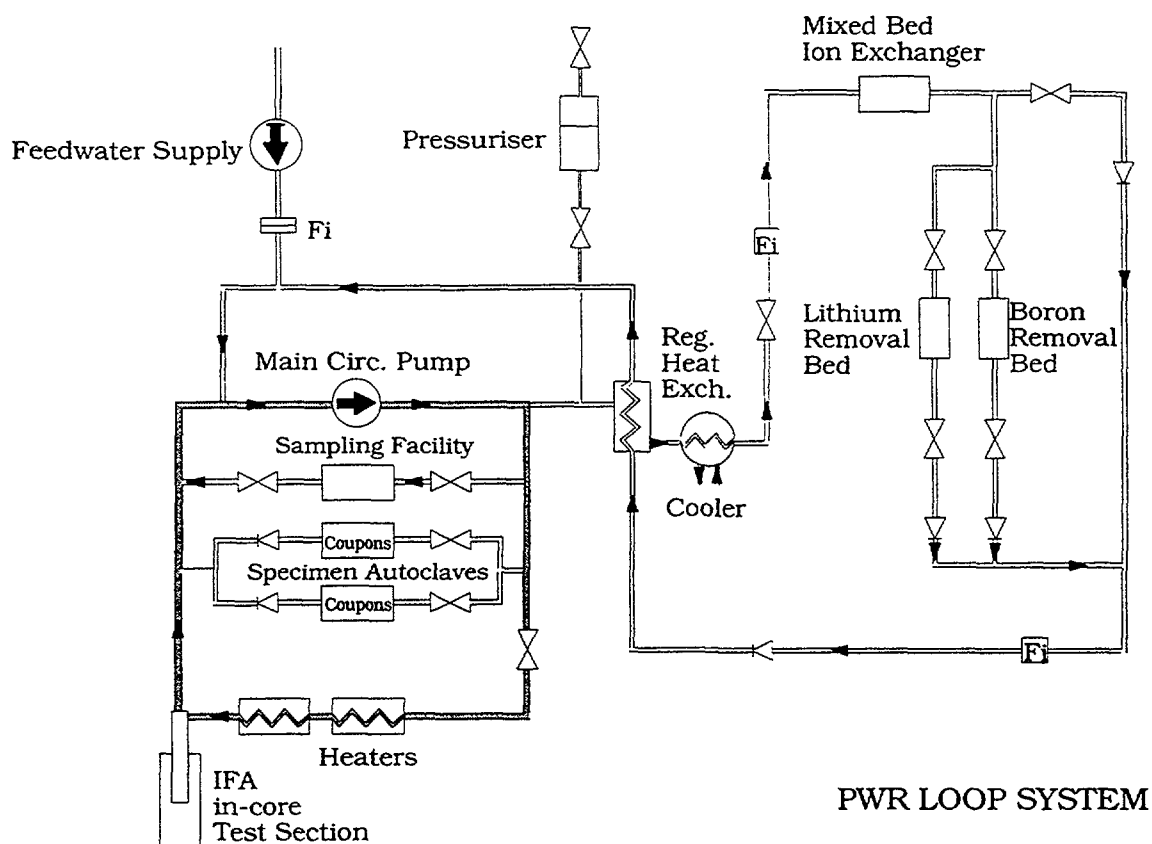


FIG. 1. A schematic illustration of a typical PWR loop system. One or more in-core test sections may be connected to the loop and autoclaves may be installed in the outer loop system.

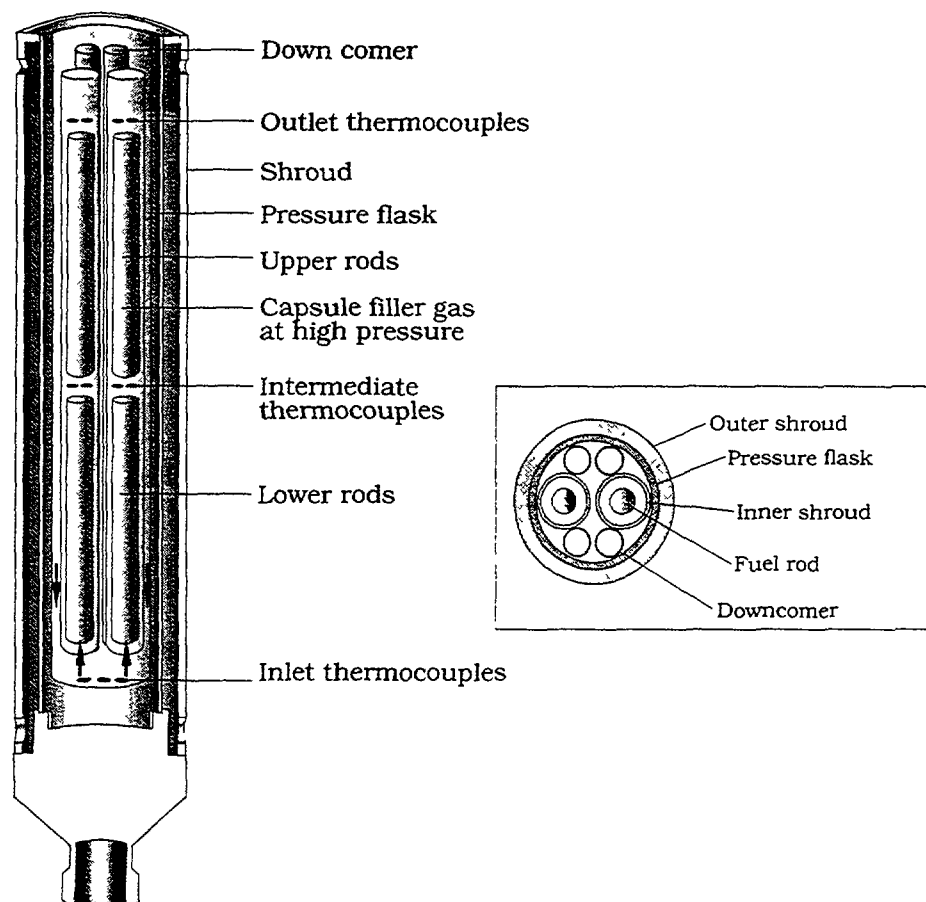


FIG. 2. Illustration of the test rig used to study the effects of elevated pH (high lithium) on the corrosion behaviour of four pre-irradiated cladding segments located in two coolant subchannels.

The experimental data were found to agree favourably with the model predictions and while the model tended to slightly underestimate the average oxide thicknesses of the fuelled region of the rods, the results were within the scatterband of the data used in development of the model. It was concluded that an aggravating effect of mild nucleate boiling / lithium concentrations in the range 4-4.5 ppm was not clearly apparent under the conditions of this study.

### 3.2 Corrosion and hydriding behaviour of standard and low tin Zr-4

In a recently completed study, designed to assess the separate effects of various parameters on oxidation rate of high and low tin cladding materials exposed to representative PWR operating conditions and water chemistry, a total of eight test rods with different features were utilised. The test rod designs were varied (with different fuel enrichments, rod internal pressures and cladding hydrogen contents) in order to study the effects of the variables stress, heat flux and hydriding on corrosion rate. The effects of fluence and material were also addressed by utilising rods prepared from fresh or pre-irradiated Zr-4 with standard or low tin contents, respectively. As an example, the design features of five of the test segments that were used in the investigation are outlined below:

- Two of the test rods were prepared from standard Zr-4 cladding. One of the rods was in the unirradiated state and the other in an irradiated condition (with a maximum oxide thickness of  $37\text{ }\mu\text{m}$  and an accumulated fluence of  $1.2 \times 10^{22}\text{ n/cm}^2$ ). Both rods were fabricated with fresh fuel with 6 % enrichment. Included in the fuel stacks of both rods were two regions filled with  $\text{Al}_2\text{O}_3$  pellets and the centre section of each fuel stack contained larger diameter pellets, in order to produce strong local ridging and PCMI.

- Two unirradiated low tin cladding segments were designed to incorporate several different features. In one rod, there were two different hoop stresses created by means of different rod internal pressures. The second rod was designed with three different fuel regions, including a high enrichment region and a no-heated region with an Al<sub>2</sub>O<sub>3</sub> pellet stack.
- The upper cladding region of a fifth rod was pre-charged with hydrogen by electrolysis, followed by a heat treatment to homogenise the distribution. The rod was ground to re-establish normal surface conditions and one section of the rod was ground further to remove the hydrided rim at the outer surface. Mean hydrogen concentrations measured over cross-sections of the cladding were 915 ppm in the hydrided zone with rim and 230 ppm in the hydrided zone without rim.

During irradiation the loop was operated with 3 ppm Li and 1000 ppm B, and with a hydrogen content in the range 2-4 ppm. The low tin and the standard Zr-4 rods were irradiated for a total of ~5900 hours while the pre-hydrided rod was exposed for 2400 hours and replaced with a rod of different design in subsequent cycles. The oxide layer thicknesses on each of the cladding segments were measured with an eddy current proximity probe during reactor outages. The measurements were made at axial orientations of 0 / 360°, 60°, 120°, 180° 240° and 300° and the results were compared with oxide thicknesses calculated with the EPRI/C-E/KWU post transition corrosion model:

- the oxide thickness data recorded for the pre- and unirradiated standard Zircaloy 4 rods are presented in Figs 3 and 4. For the pre-irradiated cladding, the rates of corrosion were found to increase with increasing exposure time, indicating a thermal feedback effect and a deleterious influence on oxidation behaviour as a consequence of the radiation damage accumulated during the pre-irradiation phase.
- in the case of the fresh rods with low tin, little effect of cladding hoop stress or heat flux in the range 25-30 kW/m was observed, while, as expected, unfuelled sections of cladding corroded significantly less than fuelled regions. Improved corrosion resistance of the low tin material was indicated by over estimations of oxide thickness increases as determined by the corrosion model (Fig. 5).
- enhanced corrosion was clearly observed for the pre-hydrided rod (Fig. 6) although atypical surface conditions, produced as a result of the grinding, may have introduced some inaccuracy in the measured oxide data. An average oxide layer thickness of ~7 µm was measured over the axial region with a hydride concentration of 230 ppm while ~3 µm was measured for the non-hydrided region. In the zone with 915 ppm hydride, oxide thicknesses of ~20 µm were recorded, while the thickness in the hydrided plenum (lower clad temperature region) was ~10 µm.

### 3.3 Mechanisms affecting the corrosion behaviour of modern cladding materials

In a second cladding corrosion study, which is presently in progress, the test matrix comprises a range of modern cladding materials in the pre and unirradiated condition which have been fabricated with fresh 8% enriched UO<sub>2</sub> fuel. The test segments are arranged in three rods each comprising four segments as illustrated schematically in Fig. 7. In order to create representative fast neutron flux conditions, the test section is surrounded by a ring of 12 highly enriched “booster” fuel rods. In addition to the fuelled test segments, which include standard and low tin Zr-4, Zirlo, M4, M5, Alloy A and Alloy E635 with burn-ups ranging from 20 to 52 MWd / kgUO<sub>2</sub>, 36 unfuelled coupons are also installed in the high flux region of the facility. The coupons have different compositions, and some have been pre-oxidised or pre-hydrided. The study is scheduled to continue for several reactor cycles, with the rig being operated with nucleate boiling and high heat rates. As in the previous investigation, the loop is being operated with 3 ppm Li and 1000 ppm B, corresponding to a pH<sub>300</sub> of ~7.1.

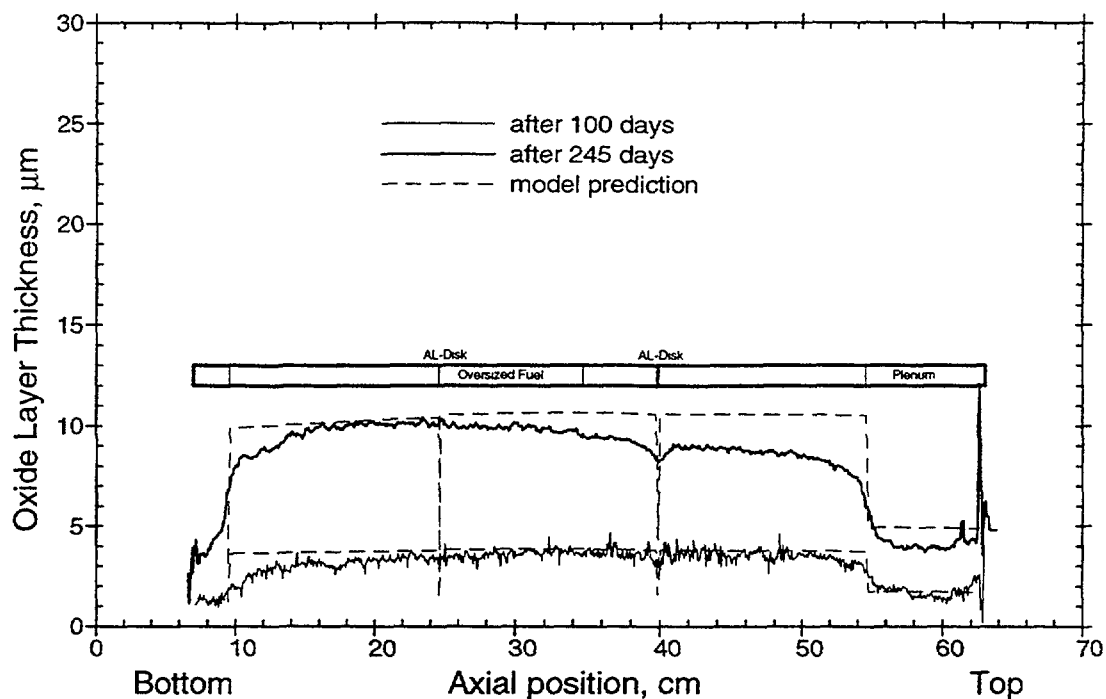


FIG. 3. Comparison of the measured and predicted oxide thicknesses on a standard Zr-4 test rod with a fuel stack comprising 6 % enriched fuel, two  $\text{Al}_2\text{O}_3$  regions and a centre stack of slightly oversized pellets.

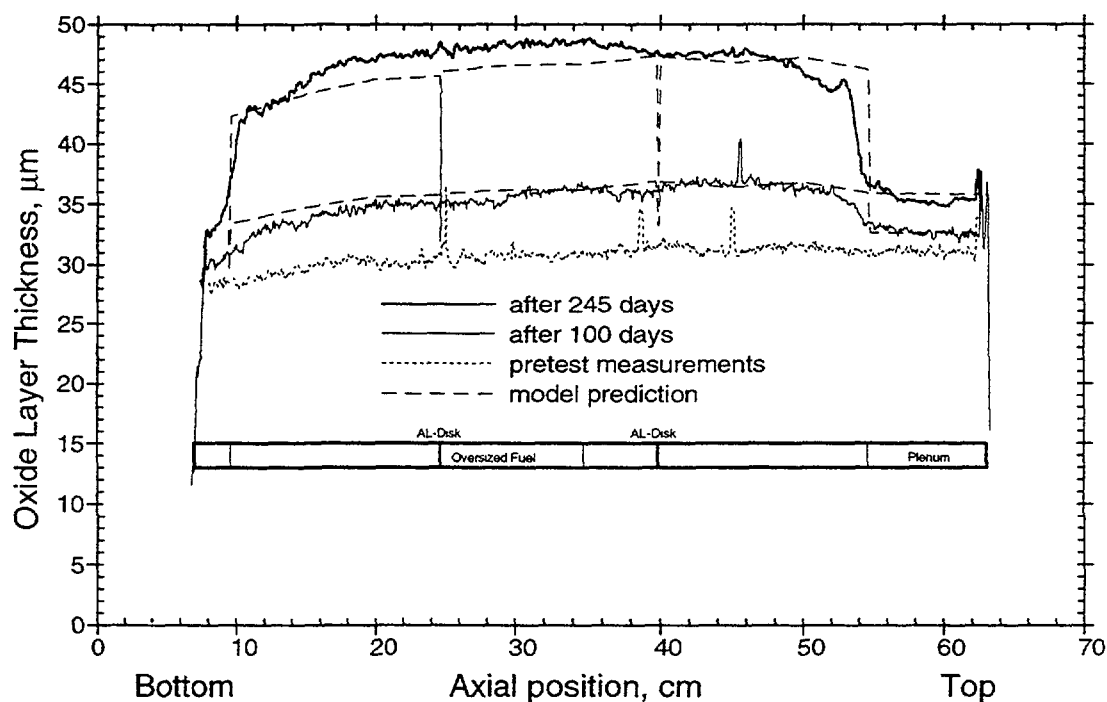


FIG. 4. Comparison of the measured and predicted oxide thicknesses on a standard Zr-4 test rod which had been pre-irradiated to a fluence of  $1.2 \times 10^{22} \text{ n/cm}^2$  (oxide thickness  $\sim 37 \mu\text{m}$ ) before testing in the Halden reactor. The design of the fuel stack is the same as that of the test segment appearing in FIG. 3.



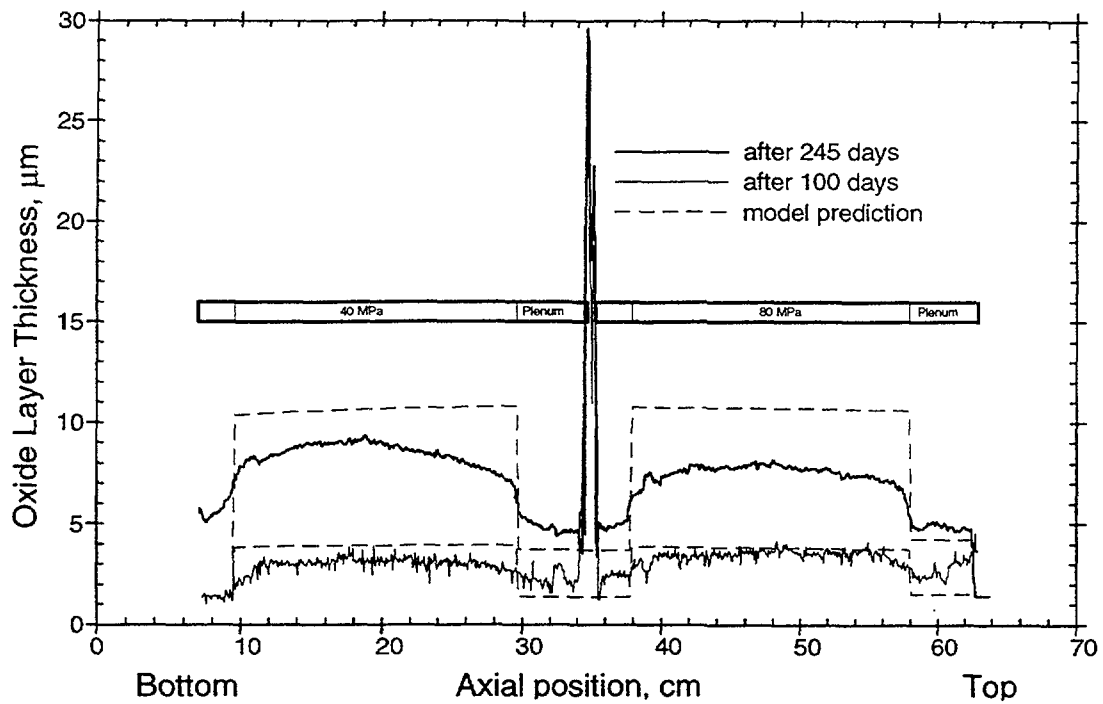


FIG. 5. Comparison of the measured and predicted oxide thicknesses on a low Sn Zr-4 test rod having two different hoop stresses.

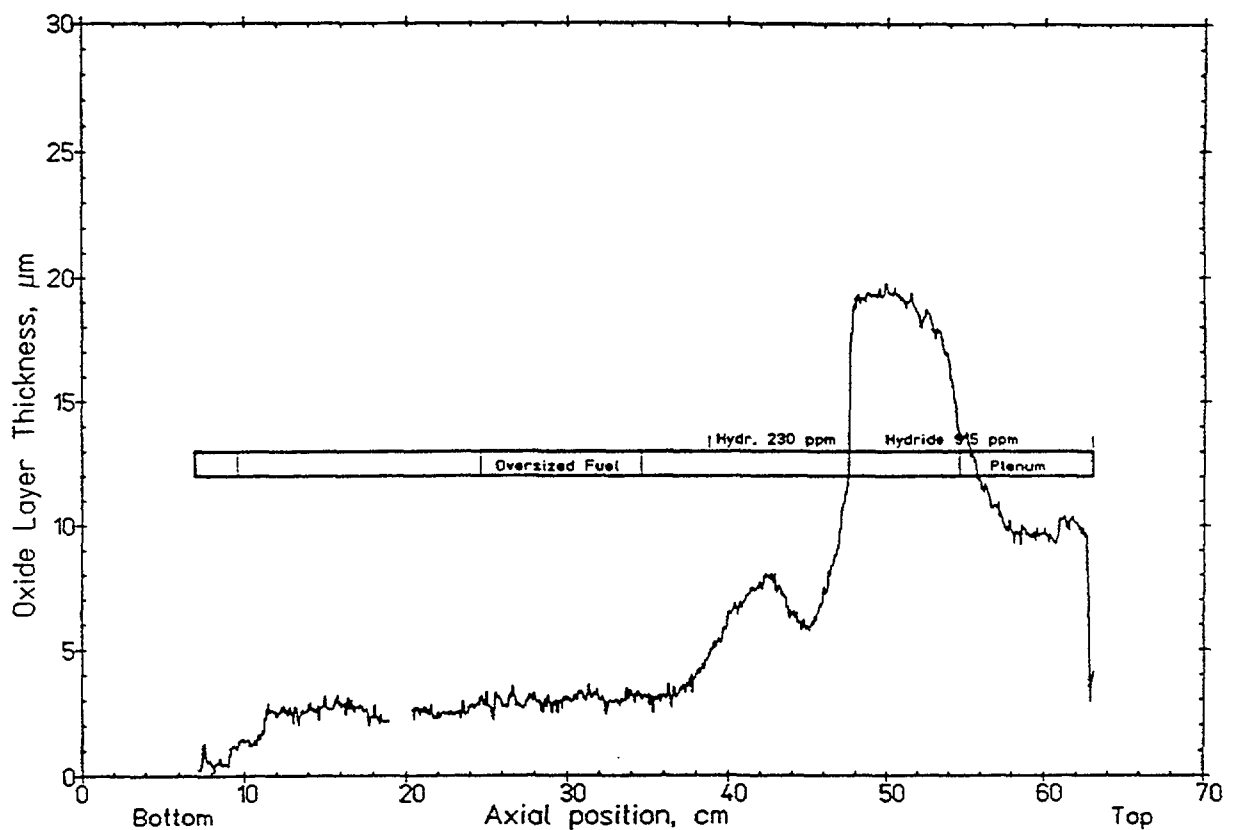
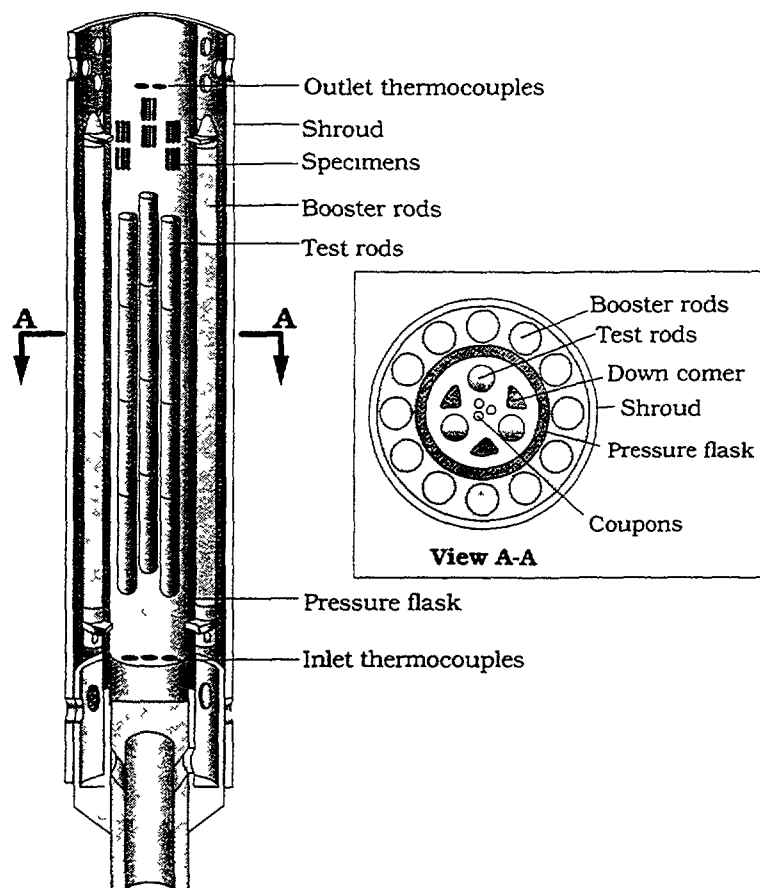


FIG. 6. The measured oxide thicknesses on a low Sn Zr-4 test rod in which sections of the rod had been pre-hydrated. A clear corrosion enhancement was apparent for the pre-hydrated regions of the rod.



*FIG. 7. Illustration of the arrangement of test segments in a cladding corrosion study that is currently in progress. Each of the three test rods consists of two unirradiated and two irradiated subsegments.*

The progress of corrosion will be determined out-of-pile during reactor outages when the coupons will be weighed and oxide thickness measurements will be made on the fuel segments by means of the eddy current method. The oxide thickness data will, as in previous experiments, be compared with the EPRI/C-E/KWU model post transition equation. Both the coupons and the fuelled segments are removable and may be replaced with other samples or test segments as required during the course of the study.

Four pre-irradiated cladding segments of the same type as those used in the corrosion study have been included in a follow-on creep experiment. In this manner, the corrosion behaviour of the modern cladding variants are complemented by valuable additional information on the in-pile cladding creep properties of the same materials. Creep-down, recovery effects, stress reversal and tensile creep behaviour are to be addressed in the study.

#### 4. PLANS FOR FUTURE INVESTIGATIONS

A pilot study has shown that diameter scanning gauges fitted to fuel rods may prove to be a valuable tool for the study of crud deposition and dissolution during in-reactor service. In the pre-study, which was designed primarily as an investigation of creep behaviour in Zircaloy cladding, diameter gauges were fitted to an unfuelled test rod and a fuelled test rod (divided into two subsegments) in order to record the in-reactor axial profiles of the rod diameters at regular intervals (Fig. 8).

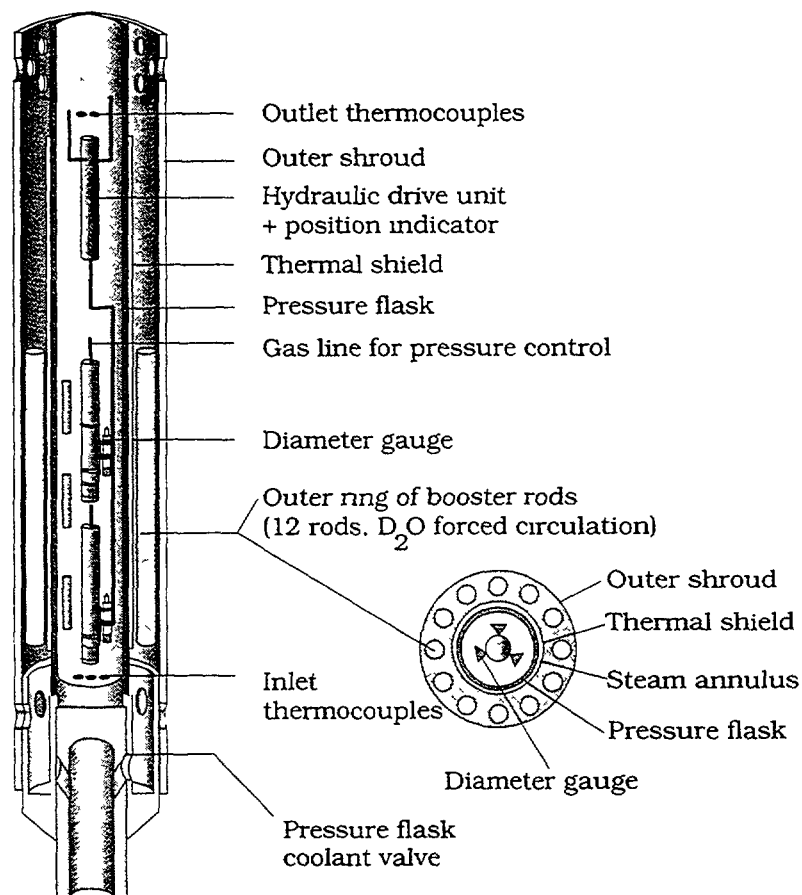


FIG. 8. Illustration of the rod arrangement that was used in an earlier cladding creep study. The lower, unfuelled rod and the upper, fuelled subsegments were fitted with in-pile diameter gauges.

The diameter measurements were made on the outer surfaces of the rods, which were located in a test rig operating under PWR pressure and temperature conditions. During the first phase of investigation the loop was operated with 2 - 4 ppm lithium and 1000 ppm boron and gradual changes in rod diameter, occurring through creep deformation of the cladding were recorded with the diameter gauges. In the final phase of the study, zinc was introduced to the coolant and two transient increases in zinc concentration were accompanied by marked increases (Figs 9 (a) and 9 (b)) in the measured rod diameter of the fuelled test rod, while the diameter of the unfuelled test segment remained relatively unaffected. A pronounced decrease in the diameter of the fuelled subsegments (Fig. 9 (c)) was observed during low temperature operation of the loop during a reactor shutdown ~2000 hours after the excursions in zinc content.

The diameter increases (and subsequent decrease) are attributed to the formation (and later dissolution) of a thick deposit of zinc rich "crud" on the outer surface of the cladding subsegments. From the profiles presented in Figs 9 (a) through (c) it appears that crud deposition rate is strongly affected by local heat rating, with the thickest deposits being recorded for the lower subsegment which, in this study, was located in a peak axial flux position. A heat rate dependency is also supported by the fact that only minor diameter changes were recorded for the unfuelled rod.

Overall, the results from the pre-, or pilot, study suggest that the use of in-pile diameter measurements will serve as a useful technique with which to measure crud deposition as affected by water chemistry and operational variables and plans for a future investigation of this nature are currently being discussed.

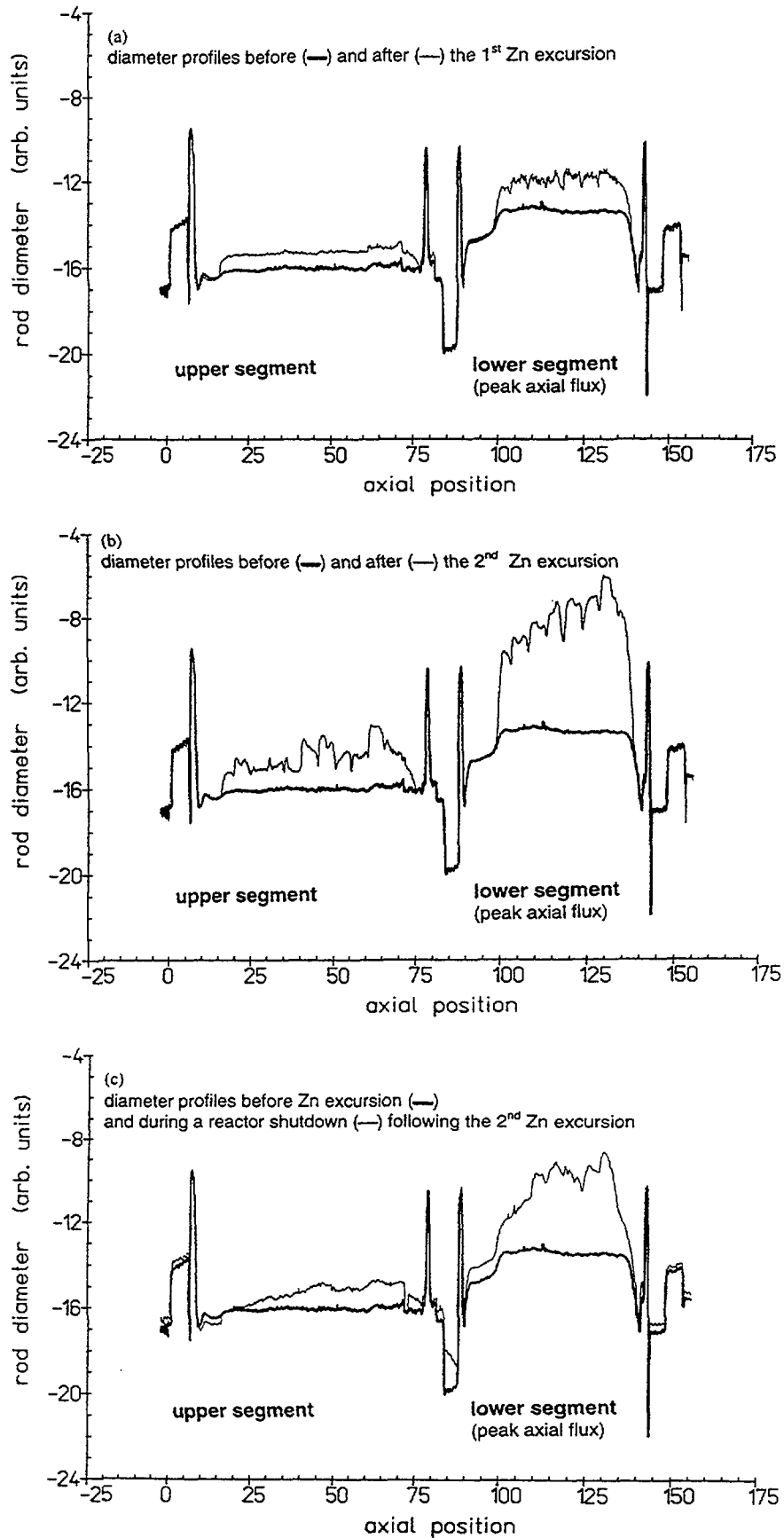


Fig. 9 Comparison of rod diameter measured immediately prior to two excursions in zinc concentration, with the diameter measured (a) after the first excursion, (b) the second excursion and (c) during low temperature operation of the loop at a shutdown.

A second study under consideration for a future experimental series is that of shadow corrosion. Possibilities for an experimental arrangement include the installation of materials acting as  $\beta$  sources either in the wall of the pressure flask in which the cladding specimens are situated or a more localised arrangement where the source is placed in close proximity to the test section or cladding segments under evaluation. Enhanced localised corrosion would be determined by means of oxide thickness measurements. Investigations on shadow corrosion have already been conducted at Halden in a separately sponsored test programme undertaken on behalf of participating organisations. Results from these investigations are described in detail elsewhere [4,5], while for illustrative purposes, a typical example of a shadow corrosion effect as detected by oxide measurements in these studies is shown schematically in Fig.10.

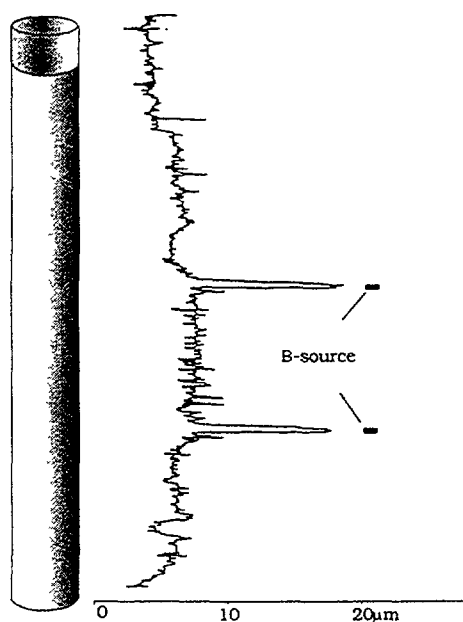


FIG. 10. Example of the effects of Pt ( $\beta$  emitter) sources on oxide thickness.

#### REFERENCES

- [1] W.J SYMONS, T.M. KARLSEN and P. GUNNERUD, "Materials Degradation and Activity Transport Studies at Halden", Activity Transport in Water Cooled Nuclear Power Reactors, (Proc. Int. Symposium Ottawa, Canada, 24-26 October 1994), CNS, (1994) 76.
- [2] P.J. BENNETT, P. GUNNERUD, H. LONER, J.K. PETTERSEN and A. HARPER, "The Effects of Zinc Addition on Cobalt Deposition in PWRs", Water Chemistry of Nuclear Reactor Systems (Proc. 7<sup>th</sup> Int. Conf. Bornemouth, 1996), BNES (1996) 189.
- [3] T. KARLSEN and C. VITANZA, "Effects of Pressurised Water Reactor (PWR) Coolant Chemistry on Zircaloy Corrosion Behaviour", Zirconium in the Nuclear Industry (Proc. Tenth Int. Symposium Baltimore, MD, 1993), ASTM, ASTM STP 1245 (1994) 779-769.
- [4] Y. ETOH et al, "Study of Environmental Effects on Water-Side Corrosion of Zircaloy-2 Fuel Cladding", Journal of Nuclear Materials **248** (1997) 299-305.
- [5] S. SHIMADA et al, "Evaluation of Zircaloy-2 Cladding Corrosion Characteristics by Simulated BWR Corrosion Loop Test", Zirconium in the Nuclear Industry (Proc. 12<sup>th</sup> Int. Symposium Toronto, Canada, 15-18 June 1998) ASTM (in press).

## LIST OF PARTICIPANTS

Arkhyenko, O.	Ministry of Energy, Kreshchatyk Str. 30, 1252601 Kiev-1, Ukraine
Benderskaia, O.S.	Research Institute of Atomic Reactors, 43350 Dimitrovgrad, Ulyanovsk Region, Russian Federation
Bogáncs, J.	PAKS Nuclear Power Plant, P.O. Box 71, H-7031 Paks, Hungary
Boydens, P.	SCK/CEN Dept. TCH, Boeretang 200, B-2400 Mol, Belgium
Comstock, R.J.	Westinghouse Electric Company, 1310 Benlah Road, Pittsburgh, PA 15235, United States of America
El-Sayed, A.E.A.	Atomic Energy Authority, Dept. of Metallurgy, Nuclear Research Centre, P.O.B. 13759, Cairo, Egypt
Gebhardt, O.	Paul Scherrer Institut, CH-5232 Villigen PSI, Switzerland
Gilbert, C.	CEA/SACLAY, DMT/SEMI/LECM, Bldg. 605, France
Hansson-Lyyra, L.K.	VTT Manufacturing Technology, P.O. Box 1704, Kemistintie 3, 02150 Espoo, Finland
Hermannsson, H.P.	Studsvik Material AB, S-611 82 Nyköping, Sweden
Hu, Shilin	China Institute of Atomic Energy, P.O. Box 275 (53), 102413 Beijing, China
Iourmanov, V.	VNIIAES, Ferganskaya 25, 109507 Moscow, Russian Federation
Jeong, Y.H.	Korea Advanced Institute of Science and Technology, P.O. Box 105, Yusung, Taejon, Republic of Korea
Kamimura, K.	Nuclear Fuel Department, Nuclear Power Engineering Corp., Fujita Kanko Toramonon Bldg., 6F, 3-17-1, Toranomom, Minato-ku, Tokyo 105, Japan
Karlsen, T.M.	Institut for Energiteknikk, OECD Halden Reactor Project, P.O. Box 173, Norway
Khokhunova, T.N.	All-Russian Scientific Research, Institute of Inorganic Materials (VNIINM), Rogova 5, 123060 Moscow, Russian Federation

Kovyrshin, V.G.	State Scientific and Technical Centre on Nuclear and Radiation Safety, 35/37 Radgospna, 252142 Kiev, Ukraine
Kritskij, V.G.	VNIPIET', Dibunovskaya Street 55, 197183 St. Petersburg, Russian Federation
Kysela, J.	Nuclear Research Institute Rez, Reactor Services Division, 250 68 Rez, Czech Republic
Lassing, S.A.	Studsvik Nuclear AB, S-611 82 Nyköping, Sweden
Lovincic, D.	Slovenian Nuclear Safety Administration, Vojkova 59, 1000 Ljubljana, Slovenia
Makela, K.	VTT Manufacturing Technology, P.O. Box 1704, Kemistintie 3, 02150 Espoo, Finland
Maroto, A.	Argentine Atomic Energy Commission, Av. del Libertador 8250, 1429 Buenos Aires
Nystrand, A.C.	Studsvik Nuclear AB, S-611 82 Nyköping, Sweden
Onoufrieu, V.	International Atomic Energy Agency , Division of Nuclear Fuel Cycle and Waste Technology, Wagramer Strasse 5, P0 Box 100, A-1400 Vienna
Peev, P.	Natsionalna Elektricheska Kompania, 5, Vesletz Str., 1040 Sofia, Bulgaria
Pimenov, Y.V.	Joint Stock Company "TVEL,"24/26 Bolshaya Ordynka, 101000 Moscow, Russian Federation
Pippo, J.	Cornet Ltd, P.O. Box 35, Fin-00411, Finland
Rosborg, B.	Studsvik Nuclear AB, S-611 82 Nyköping, Sweden
Ruhmann, H.	Siemens AG, KWU, NBTW, P.O. Box 3220, D-91058 Erlangen, Germany
Saxena, A.K.	Nuclear Power Corporation, Vikram Sarabhai Bhavan, 12 <sup>th</sup> Floor, Central Avenue, Anushaktinagar, Mumbai 400 094, India
Schunk, J.	PAKS Nuclear Power Plant, P.O. Box 71, H-7031 Paks, Hungary
Serna, J.J.	ENUSA, Santiago Rusinol 12, 28040 Madrid, Spain

Shishov, V.N.	All-Russian Scientific Research, Institute of Inorganic Materials (VNIINM), Rogova 5, 123060 Moscow, Russian Federation
Smiesko, I.	Slovak Power Plants a.s., Nuclear Power Plants Bohunice, Department of Chemistry, 91931 Jaslovske Bohunice, Russian Federation
Starkie, H.	HM Nuclear Installations Inspectorate, Nuclear Safety Directorate, RM 501, St. Peters House, Balliot Road, Bootle, Merseyside L20 3QY, United Kingdom
Thomazet, J.	FRAMATOME, Nuclear Fuel, 10 Rue Juliette Récamier, France
Tomani, H.	Studsvik Nuclear AB, S-61182 Nyköping, Sweden
Urbanic, V.F.	Atomic Energy of Canada Ltd, Chalk River Laboratories, Chalk River, Ontario, K0J 1J0, Canada
Van Nieuwenhove, R.	SCK/CEN Belgian Nuclear Research Centre, Boeretang 200, B-2400 Mol, Belgium
Veliokhanov, V.P.	All-Russian Scientific Research, Institute of Inorganic Materials (VNIINM), Rogov 5, 123060 Moscow, Russian Federation
Vrtílková, V.	DIAMO, Uranová 379, 15610 Prague 5, Czech Republic
Walters, W.S.	AEA Technology, Chemistry Services Department, 220, Harwell Business Centre, Didcot, Oxfordshire, OX11 0RA, United Kingdom
Zmítko, M..	Nuclear Research Institute Rez, Reactor Services Division, 250 68 Rez, Czech Republic
Zotica, D.	Cernavoda NPP Romania, Medgidiei 1, P.O. Box 42, 8625 Cernavoda, Romania

#### **List of Observers**

Čmakal, J.	ŠKODA - ÚJP Praha a.s., Nad Kamínkou 1345, Prague 156 10, Czech Republic
Ernst, D.	NPP Temelín, 37305 Temelín, Czech Republic



Hamouz, V.	ŠKODA -ÚJP Praha a.s., Nad Kamínkou 1345, Prague 156 10, Czech Republic
Hanus, V.	NPP Temelín, 37305 Temelín, Czech Republic
Janešík, J.	NPP Temelín, 37305 Temelín, Czech Republic
Maláč, M.	NPP Dukovany, 675 56 Dukovany, Czech Republic
Neubauer, J.	NPP Temelín, 37305 Temelín, Czech Republic
Petrecký, I.	NPP Dukovany, 675 56 Dukovany, Czech Republic
Pišťelka, M.	NPP Temelín, 37305 Temelín, Czech Republic
Urbančík, L.	State Office of Nuclear Safety, Senovážné náměstí 19, 110 00 Prague 1, Czech Republic
Valach, M.	NRI Řež plc, 250 68 Řež, Czech Republic